

ABSTRACT

Title of dissertation: ANALYSIS OF THE STOCHASTIC
STABILITY AND ASYMPTOTICALLY
STATIONARY STATISTICS FOR
A CLASS OF NONLINEAR
ATTITUDE ESTIMATION ALGORITHMS

Joseph M. Galante
Doctor of Philosophy, 2018

Dissertation directed by: Professor Robert M. Sanner
Department of Aerospace Engineering

Attitude estimation algorithms are critical components of satellite control systems, aircraft autopilots, and other applications. Attitude estimation systems perform their task by fusing attitude and gyroscope measurements; however, such measurements are typically corrupted by random noise and gyroscopes may have significant bias. Variations of the extended Kalman filter are commonly used, but this technique relies on instantaneous linearization of the underlying nonlinear dynamics and global stability cannot be guaranteed. Nonlinear attitude observers with guaranteed global stability have been derived and experimentally demonstrated, but only for the deterministic setting where no stochastic effects are present.

The first part of this thesis extends a deterministic nonlinear attitude estimator by introducing additional dynamics that allow learning variations of gyro bias as a function of operating temperature, a common source of bias variation in rate gyro readings. The remainder of the thesis formally addresses the problem of stochastic

stability and asymptotic performance for this family of estimators when the measurements contain random noise. Analysis tools from stochastic differential equation theory and stochastic Lyapunov analysis are used together to demonstrate convergence of the filter states to a stationary distribution, and to bound the associated steady-state statistics as a function of filter gains and sensor parameters.

In many cases these bounds are conservative, but solutions have been found for the associated stationary Fokker-Planck PDEs for two cases. When only the gyro measurement contains noise, the attitude estimation errors are shown to converge to a bipolar Bingham distribution. When the gyro measurement is further assumed to have constant bias, the estimation errors are shown to converge to a joint bipolar Bingham and multivariate Gaussian distribution. Knowledge of the stationary distributions allow for exact computation of steady-state statistics. Further, the analysis suggests a method for modeling a continuous quaternion noise process with specified statistics on $SO(3)$; this model is used for analyzing estimator performance when both the gyro and the attitude measurements contain noise. Bounds and exact predictions for the different noise models are validated using a high fidelity numerical integration method for nonlinear stochastic differential equations.

ANALYSIS OF THE STOCHASTIC STABILITY
AND
ASYMPTOTICALLY STATIONARY STATISTICS
FOR A CLASS OF
NONLINEAR ATTITUDE ESTIMATION ALGORITHMS

by

Joseph M. Galante

Dissertation submitted to the Faculty of the Graduate School of the
University of Maryland, College Park in partial fulfillment
of the requirements for the degree of
Doctor of Philosophy
2018

Advisory Committee:
Professor Robert M. Sanner, Chair/Advisor
Professor Christine M. Hartzell
Professor Nuno C. Martins
Professor Derek A. Paley
Professor Raymond J. Sedwick

© Copyright by
Joseph M Galante
2018

Dedication

To my Aunt Chris and Uncle John,

for inspiring me to look to the horizon.

To my mother and father,

for teaching me the tenacity to seek it.

To my loving wife,

for helping me take the journey.

Acknowledgments

During my time as a graduate student at the University of Maryland, I have been incredibly fortunate to receive academic, financial, and emotional support from numerous people and agencies. I owe immense gratitude to all the people who have enabled me to write this thesis.

I would first and foremost like to thank my advisor, Dr. Robert M Sanner. He provided intellectual and academic support from my first year as a student in his nonlinear control systems course through my final preparations to finish this document. He taught amazing classes, opened my eyes to numerous fields of research, and never let me settle for anything but my very best work.

I would also like to thank the faculty who took the time and effort to serve on my examining committee: Dr. Christine Hartzell, Dr. Nuno Martins, Dr. Derek Paley, and Dr. Ray Sedwick. The Robotics@Maryland club was fortunate to have Dr. Nuno Martins as a faculty advisor, and he quickly became a personal mentor. Dr. Derek Paley made several insightful suggestions for the direction of my research at the pre-defense; pursuit of those directions eventually led to some of the main contributions of this thesis.

Other professors have provided guidance and support over my time in graduate school. I started out my graduate career under an assistantship with Dr. David Akin of the Space Systems Lab, and he generously furnished me with a desk in his graduate student office as well as lab space in the Neutral Buoyancy Research Facility (NBRF) during my Masters work. I had the pleasure of learning from professors from

the Aerospace Engineering, Mathematics, and Electrical Engineering departments. Additionally, many professors from my undergraduate studies at the Rose-Hulman Institute of Technology (RHIT), such as Dr. Robert Throne and Dr. Jeffery Leader, gave me invaluable career advice and support.

I have many colleagues to thank as well. My manager, Dr. James O'Donnell, has been incredibly supportive of my seemingly never-ending pursuit of higher education. My mentor John Van Eepoel has also been of instrumental support over the years. My project management in the Space Servicing Projects Division (SSPD) and the Plankton Aerosol Cloud ocean Ecosystem (PACE) mission management have been very flexible to allow me to finish my studies, and have provided me work assignments that dovetail well with my research interests. I am very thankful for my many friends and co-workers on both projects that have entertained my numerous academic discussions.

I received several sources of financial support. Dr. David Akin's Space Systems Lab (SSL) provided me with a research assistantship my first year. I was fortunate to be awarded a National Defense Science and Engineering Graduate (NDSEG) Fellowship that funded my studies for another three years. The American Institute of Aeronautics and Astronautics (AIAA) Orville and Wilbur Wright Graduate Award funded my tuition for some time. The NASA GSFC Academic Investments for Mission Success (AIMS) program also provided significant support for my studies over many years through the Part Time Graduate Student Fellowship (PTGSF) Program and the Study Fellowship Program (SFP).

The friendship, technical discourse, and life discussions with my many friends

and co-workers over the years have been of enormous help. Many who started near the time I did at the SSL remain as good friends, such as Barrett Bedford-Dillow, Dr. Sharon Singer-Barnard, Kate McBryan, and Nick Limparis. My professional development also received substantive benefit from my friends of the Robotics@Maryland team, such as Joe Lisee and Dr. Leo Singer. My colleagues at work have also helped me through the years, notably Dr. Andrew Hyslop (now at ESA), Bryan Patrick, Cinnamon Wright, Dr. Chris D'Souza, and Dr. Russell Carpenter.

Finally, I would like to thank my family. My Aunt Chris and Uncle John have been an unwaivering source of inspiration and encouragement, from gifting me science fiction novels as a boy, to giving me science and mathematics texts as a teen, to continually cheering me on through my graduate work. My sister Emilie has always believed in me, and her fervent belief and supportive phone calls have helped me immensely. Of course my parents have done an incredible job getting me to this point. Mother wouldn't let me out to play as a boy until I had finished my math flash cards. Father suggested I study the physics of light for my elementary school science fair. Their enthusiasm for learning would be difficult not to internalize, and they made their top priority when raising me to instill in me an unquenchable passion for learning. Last but certainly not least, I thank my wife Amanda whose unconditional love, support, and incredible patience have made this possible. The many years full of late nights and long weekends have at last paid off.

My gratitude also goes to the many unnamed others who have helped me over the years. It would be impossible to list them all, but I apologize to those who I have inadvertently omitted.

Table of Contents

Abstract	i
Dedication	ii
Acknowledgements	iii
Table of Contents	vi
List of Tables	ix
List of Figures	x
List of Abbreviations	xviii
1 Introduction	1
1.1 State of the Art	3
1.2 Contributions	8
1.3 Dissertation Outline	11
2 Background	16
2.1 Nonlinear Stochastic Differential Equations and Stability	16
2.1.1 Deterministic Ordinary Differential Equations	17
2.1.2 Deterministic Stability Analysis	20
2.1.3 Stochastic Differential Equations	26
2.1.4 Stochastic Stability Analysis	39
2.1.4.1 LTI State Observer Example	43
2.1.4.2 Stochastic Logistic Population Model Example	50
2.1.5 Stationary Fokker-Planck Analysis	58
2.2 Numerical Integration of Nonlinear SDEs	64
2.2.1 Runge-Kutta fixed-step Integration Scheme	65
2.2.2 Euler-Maruyama Integration Scheme	67
2.2.3 Kloeden-Platen Explicit Weak 2.0 Integration Scheme	68
2.2.4 Numerical Integration Performance Comparison	70

2.3	Attitude Kinematics Overview	74
2.3.1	Attitude Kinematics in $SO(3)$	74
2.3.2	Attitude Kinematics in $SO(2)$	79
2.4	A Class of Nonlinear Attitude Observers	82
3	Deterministic Gyro Thermal Bias Observer	85
3.1	Gyro Constant Bias Observer (CBO) Formulation	87
3.2	Gyro Thermal Bias Model	90
3.3	CBO Deterministic Simulation Study	95
3.4	Function Approximation	102
3.5	Gyro Thermal Bias Observer (TBO) Formulation	115
3.6	Gyro Thermal Bias Observer (TBO) Function Learning Simulations	121
3.7	Gyro CBO and TBO Stochastic Simulation Models	147
3.8	Gyro CBO and TBO Stochastic Simulations	153
3.9	Gyro CBO and TBO Gain Search	160
4	Attitude Estimation Filter for Noisy Gyro Measurements	166
4.1	Attitude Filter Formulation in $SO(3)$	168
4.2	Stochastic Lyapunov Analysis in $SO(3)$	171
4.3	Numerical Simulation of $SO(3)$ Stochastic Lyapunov Bounds	175
4.4	Fokker-Planck PDE in $SO(3)$	177
4.5	Attitude Filter Formulation in $SO(2)$	179
4.6	Stochastic Lyapunov Analysis in $SO(2)$	181
4.7	Numerical Simulation of Stochastic $SO(2)$ Lyapunov Bounds	185
4.8	Fokker-Planck Analysis in $SO(2)$	187
4.9	Numerical Simulation of Stochastic $SO(2)$ Analytic Results	192
4.10	An $SO(3)$ Upper Bound	196
4.11	Exact Solution to the Stationary $SO(3)$ Fokker-Planck PDE	200
4.12	Numerical Simulation of Stochastic $SO(3)$ Analytic Results	213
5	Gyro Bias Filter for Gyro with Constant Bias and Additive Noise	214
5.1	Gyro Bias Filter Formulation in $SO(3)$	216
5.2	Stochastic Stability Analysis in $SO(3)$	220
5.3	Fokker-Planck PDE in $SO(3)$	223
5.4	Attitude Filter Formulation in $SO(2)$	225
5.5	Fokker-Planck Analysis in $SO(2)$	228
5.6	Numerical Simulation of Stochastic $SO(2)$ Analytic Results	234
5.7	An $SO(3)$ Upper Bound	241
5.8	Exact Solution to the Stationary $SO(3)$ Fokker-Planck PDE	252
5.9	Numerical Simulation of Stochastic $SO(3)$ Analytic Results	256
6	Attitude Measurement Noise	262
6.1	Quaternion Measurement Noise Model	264
6.2	Attitude Estimation Filter for Gyro Additive Noise and Attitude Measurement Noise	269

6.2.1	Filter Formulation in SO(3)	270
6.2.2	Stochastic Lyapunov Analysis in SO(3)	274
6.2.3	Numerical Simulation of SO(3) Stochastic Lyapunov Bounds	280
6.2.4	Filter Formulation in SO(2)	286
6.2.5	Stochastic Lyapunov Analysis in SO(2)	289
6.2.6	Numerical Simulation Verification of Stochastic SO(2) Lyapunov Bounds	296
6.2.7	Fokker-Planck Analysis in SO(2)	299
6.2.8	Numerical Simulation of Stochastic SO(2) Analytic Results	307
6.2.9	SO(3) Bound Extrapolated from SO(2) Analytic Solution	318
6.3	Gyro Constant Bias Filter for Gyro Additive Noise and Attitude Measurement Noise	324
6.3.1	Gyro Constant Bias Filter Formulation in SO(3)	326
6.3.2	Gyro Constant Bias Filter Formulation in SO(2)	332
6.3.3	Fokker-Planck Analysis in SO(2)	335
6.3.4	Numerical Simulation of Stochastic SO(2) Analytic Results	341
6.3.5	SO(3) Bound Extrapolated from SO(2) Analytic Solution	348
7	Future Directions and Concluding Remarks	365
7.1	Future Directions	369
7.1.1	Non-axis-symmetric Gyro Additive Noise	370
7.1.2	Gyro Random Walk Bias	371
7.1.3	Augment Attitude Estimation Filter State to Estimate Non-White Attitude Measurement Noise	373
7.1.4	Closed Loop Attitude Control Analysis	376
7.2	Final Remarks	381
	Bibliography	384

List of Tables

1.1	Thesis Contributions	10
2.1	Comparison of the performance of the SDE numerical integration schemes of Kloeden-Platen Explicit Weak 2.0 of Equation 2.61, the Euler-Maruyama scheme of Equation 2.58, the fixed-step ad-hoc Runge-Kutta algorithm of Equation 2.57, and MATLAB's <code>ode45</code> utility for simulating the stochastic logistic population model of SDE 2.23 to the stochastic Lyapunov upper bounds of Corollaries 2.1.6.1 and 2.1.6.2 and the analytic ultimate expectations of Theorem 2.1.7.	71
3.1	Comparison of the steady-state bias estimate error for the CBO, box-car TBO, hat TBO, and Gaussian TBO; error statistics are the ergodic average of the last 100 orbits' worth of bias estimate errors from 1000 orbit long simulations.	146

List of Figures

2.1	The two interpretations of the Langevin form differential equation lead, in general, to two distinct stochastic processes.	34
2.2	SDEs and PDEs associated with the two interpretations of the Langevin form differential equation for the stochastic logistic population model.	63
3.1	Measurement of gyro bias as a function of operating temperature for a specific MEMS gyro unit by Aggarwal, Syed, and El-Sheimy [6].	90
3.2	The first order gyro thermal bias function of Equation 3.7.	93
3.3	The third order gyro thermal bias function of Equation 3.8.	94
3.4	The CBO demonstrates sinusoidal tracking error for the first order gyro thermal bias model of Equation 3.7 as the gyro operating temperature heats and cools once every orbit of 90 minutes. The CBO gains were set to $k_e = 1$ and $\alpha = 0.1$	97
3.5	The CBO demonstrates sinusoidal tracking error for the third order gyro thermal bias model of Equation 3.8 as the gyro operating temperature heats and cools once every orbit of 90 minutes. The CBO gains were set to $k_e = 1$ and $\alpha = 0.1$	98
3.6	The CBO demonstrates sinusoidal tracking error for the first order gyro thermal bias model of Equation 3.7 as the gyro operating temperature heats and cools once every orbit of 90 minutes. The CBO gains were set to $k_e = 1$ and $\alpha = 0.1$	100
3.7	The CBO demonstrates sinusoidal tracking error for the third order gyro thermal bias model of Equation 3.8 as the gyro operating temperature heats and cools once every orbit of 90 minutes. The CBO gains were set to $k_e = 1$ and $\alpha = 0.1$	101
3.8	Radial basis functions (left) can be horizontally scaled and shifted (right) via composition with a linear function as in Equation 3.14.	104
3.9	Boxcar RBF approximation of a first order polynomial.	107
3.10	Hat RBF approximation of a first order polynomial.	108
3.11	Gaussian RBF approximation of a first order polynomial.	110
3.12	Boxcar RBF approximation of a third order polynomial.	111
3.13	Hat RBF approximation of a third order polynomial.	113

3.14	Gaussian RBF approximation of a third order polynomial.	114
3.15	The boxcar TBO estimates the first order gyro thermal bias function of Equation 3.7.	124
3.16	Time series plots of the attitude and estimate error for the boxcar TBO as it estimates the first order gyro thermal bias function of Equation 3.7.	125
3.17	The hat TBO estimates the first order gyro thermal bias function of Equation 3.7.	127
3.18	Time series plots of the attitude and estimate error for the hat TBO as it estimates the first order gyro thermal bias function of Equation 3.7.	128
3.19	The Gaussian TBO estimates the first order gyro thermal bias function of Equation 3.7.	130
3.20	Time series plots of the attitude and estimate error for the Gaussian TBO as it estimates the first order gyro thermal bias function of Equation 3.7.	131
3.21	The Gaussian TBO estimates the first order gyro thermal bias function of Equation 3.7.	132
3.22	The boxcar TBO estimates the third order gyro thermal bias function of Equation 3.8.	134
3.23	Time series plots of the attitude and estimate error for the boxcar TBO as it estimates the third order gyro thermal bias function of Equation 3.8.	135
3.24	The hat TBO estimates the third order gyro thermal bias function of Equation 3.8.	137
3.25	Time series plots of the attitude and estimate error for the hat TBO as it estimates the third order gyro thermal bias function of Equation 3.8.	138
3.26	The Gaussian TBO estimates the third order gyro thermal bias function of Equation 3.8.	140
3.27	Time series plots of the attitude and bias estimate error for the Gaussian TBO as it estimates the third order gyro thermal bias function of Equation 3.8.	141
3.28	The Gaussian TBO estimates the third order gyro thermal bias function of Equation 3.8.	142
3.29	Comparison of the observer's bias estimate error time series for the third order gyro thermal bias function of Equation 3.8.	144
3.30	Time series plots of the estimate estimate error for the Gaussian TBO as it estimates the third order gyro thermal bias function of Equation 3.8. In the top plot $k_e = 1$ and $\alpha = 0.1$; in the bottom plot $k_e = 1$ and $\alpha = 1$	145
3.31	Simulation run bias estimate errors (LEO)	154
3.32	Simulation run (LEO)	155

3.33	Bias and attitude estimate errors for the CBO, boxcar TBO, hat TBO, and Gaussian TBO for a range of thermal oscillation periods τ for the first order true gyro thermal bias function model of Equation 3.7.	158
3.34	Bias and attitude estimate errors for the CBO, boxcar TBO, hat TBO, and Gaussian TBO for a range of thermal oscillation periods τ for the third order true gyro thermal bias function model of Equation 3.8.	159
3.35	Error statistics over a subset of the gain parameter space for the CBO as obtained via numerical simulation for the linear gyro thermal bias model of Equation 3.7.	162
3.36	Error statistics over a subset of the gain parameter space for the boxcar TBO as obtained via numerical simulation for the linear gyro thermal bias model of Equation 3.7.	163
3.37	Error statistics over a subset of the gain parameter space for the hat TBO as obtained via numerical simulation for the linear gyro thermal bias model of Equation 3.7.	164
3.38	Error statistics over a subset of the gain parameter space for the Gaussian TBO as obtained via numerical simulation for the linear gyro thermal bias model of Equation 3.7.	165
4.1	Comparison of simulation realizations of attitude estimate errors of the SO(3) error dynamics Itô SDE of Equation 4.6 to the stochastic Lyapunov upper bound from Theorem 4.2.1 in red, the lower bound of Corollary 4.2.1.1 in blue, and the upper bound of Corollary 4.2.1.2 in yellow.	176
4.2	Comparison of simulation realizations of attitude estimate errors of the SO(2) error dynamics Itô SDE of Equation 4.24 to the stochastic Lyapunov upper bound from Theorem 4.6.1 in red, the lower bound of Corollary 4.6.1.1 in blue, and the upper bound of Corollary 4.6.1.2 in yellow.	186
4.3	PDFs for the Itô SDE 4.24 computed from an ensemble of 100 realizations for four gyro noise levels agree with the von Mises PDF of Equation 4.44; depicted in SO(2) quaternion space (top) and Euler angle space (bottom).	193
4.4	Comparison of simulation realizations of attitude estimate errors of the SO(2) error dynamics Itô SDE of Equation 4.24 to the ultimate variance given by the analytic solution from Corollary 4.8.1.2.	195
4.5	Comparison of simulation realizations of the attitude estimate error and the notional bound of Equation 4.49 for several choices of ξ and for various gyro measurement noise levels	197
4.6	Comparison of simulation realizations of the SO(3) attitude estimate error for the Itô SDE 4.6 and the ultimate upper bound of Equation 4.50 for various gyro measurement noise levels	199

4.7	The analytic ultimate attitude estimate error of Equation 4.57 exactly matches simulation realizations of the SO(3) attitude estimate error for the Itô SDE 4.6.	213
5.1	Comparison of the ultimate attitude estimate error variance of Corollary 5.5.1.2 to simulation realizations for a range of values of the tracking gain k_e	236
5.2	Comparison of the ultimate gyro bias estimate error variance of Equation 5.25 to simulation realizations for a range of values of the tracking gain k_e	237
5.3	Comparison of the ultimate attitude estimate error variance of Corollary 5.5.1.2 to simulation realizations for a range of values of the adaptation gain α	239
5.4	Comparison of the ultimate gyro bias estimate error variance of Equation 5.25 to simulation realizations for a range of values of the adaptation gain α	240
5.5	Comparison of simulation realizations of the attitude estimate error variance and the notional bound of Equation 5.26 for several choices of ξ over a range of tracking gains k_e	243
5.6	Comparison of simulation realizations of the bias estimate error variance and the notional bound of Equation 5.26 for several choices of ξ over a range of tracking gains k_e	244
5.7	Comparison of simulation realizations of the attitude estimate error variance and the notional bound of Equation 5.26 for several choices of ξ over a range of adaptation gains α	246
5.8	Comparison of simulation realizations of the bias estimate error variance and the notional bound of Equation 5.26 for several choices of ξ over a range of adaptation gains α	247
5.9	Comparison of simulation realizations of the attitude estimate error variance and the notional bound of Equation 5.28 for a range of tracking gain parameters k_e	248
5.10	Comparison of simulation realizations of the bias estimate error variance and the notional bound of Equation 5.29 for a range of tracking gain parameters k_e	249
5.11	Comparison of simulation realizations of the attitude estimate error variance and the notional bound of Equation 5.28 for a range of adaptation gain parameters α	250
5.12	Comparison of simulation realizations of the bias estimate error variance and the notional bound of Equation 5.29 for a range of adaptation gain parameters α	251
5.13	Comparison of simulation realizations of the attitude estimate error variance with the analytic solution for a range of tracking gain parameters k_e	257

5.14	Comparison of simulation realizations of the bias estimate error variance with the analytic solution for a range of tracking gain parameters k_e	258
5.15	Comparison of simulation realizations of the attitude estimate error variance with the analytic solution for a range of adaptation gain parameters α	260
5.16	Comparison of simulation realizations of the bias estimate error variance with the analytic solution for a range of adaptation gain parameters α	261
6.1	Comparison of simulation realizations of the general moment of Equation 6.11 and the associated bound for the case of a vehicle spinning at 5 revolutions per minute about the vehicle body's $[1\ 2\ 3]^T$ axis.	282
6.2	Comparison of simulation realizations of the general moment of Equation 6.11 and the associated bound for the case of a vehicle inertially fixed (not spinning).	283
6.3	Comparison of simulation realizations of the attitude estimate error and the bound of Equation 6.13 for the case of a vehicle spinning at 5 revolutions per minute about the vehicle body's $[1\ 2\ 3]^T$ axis.	284
6.4	Comparison of simulation realizations of the attitude estimate error and the bound of Equation 6.13 for the case of a vehicle inertially fixed (not spinning).	285
6.5	Comparison of simulation realizations of attitude estimate errors of the SO(2) error dynamics Itô SDE of Equation 6.16 to the stochastic Lyapunov upper bound of Equation 6.19 in blue, the stochastic Lyapunov lower bound of Equation 6.23 in red, and the stochastic Lyapunov upper bound of Equation 6.25 in yellow.	298
6.6	The analytic ultimate expectation of $\tilde{\varepsilon}(t)$, provided in Equation 6.39, converges to simulation realizations of attitude estimate errors of the SO(2) error dynamics Itô SDE of Equation 6.16 as $\gamma \rightarrow 0$	308
6.7	The analytic ultimate expectation of Corollary 6.2.3.1 matches the simulation realizations of attitude estimate errors of the SO(2) error dynamics Itô SDE of Equation 6.16.	309
6.8	Varying the individual values of k_m and σ_m^2 while holding the ratio $\frac{k_m}{\sigma_m^2}$ constant yields the same performance curve from both the analytic expectation of Corollary 6.2.3.1 and the simulation realizations.	311
6.9	Plots of the ultimate expectation from Corollary 6.2.3.1 for various attitude measurement noise levels $\frac{\sigma_m^2}{k_m}$; as the attitude measurement noise level $\frac{\sigma_m^2}{k_m}$ decreases (as $\frac{k_m}{\sigma_m^2}$ increases), the high filter gain limit of the attitude estimate errors decrease.	312
6.10	Plots of the ultimate expectation from Corollary 6.2.3.1 for various angular measurement noise levels σ_w . The effect of increasing σ_w is to shift the filter's attitude estimate performance curve to the right.	313

6.11	Comparison of simulation realizations of the attitude estimate error and the notional bound of Equation 6.46 for several choices of ξ and for the case of a vehicle spinning at 5 revolutions per minute about the vehicle body's $[1\ 2\ 3]^T$ axis.	320
6.12	Comparison of simulation realizations of the attitude estimate error and the notional bound of Equation 6.46 for several choices of ξ and for the case of a vehicle inertially fixed (not spinning).	321
6.13	Comparison of simulation realizations of the attitude estimate error and the heuristic bound of Equation 6.47 for the case of a vehicle spinning at 5 revolutions per minute about the vehicle body's $[1\ 2\ 3]^T$ axis.	322
6.14	Comparison of simulation realizations of the attitude estimate error and the heuristic bound of Equation 6.47 for the case of a vehicle inertially fixed (not spinning).	323
6.15	Comparison of the ultimate attitude estimate error variance of Corollary 6.3.1.1 to simulation realizations for a range of values of the tracking gain k_e	343
6.16	Comparison of the ultimate gyro bias estimate error variance of Equation 6.71 to simulation realizations for a range of values of the tracking gain k_e	344
6.17	Comparison of the ultimate attitude estimate error variance of Corollary 6.3.1.1 to simulation realizations for a range of values of the adaptation gain α	346
6.18	Comparison of the ultimate gyro bias estimate error variance of Equation 6.71 to simulation realizations for a range of values of the adaptation gain α	347
6.19	Comparison of simulation realizations of the attitude estimate error variance and the notional bound of Equation 6.72 for several choices of ξ for a range of tracking gains k_e for an inertially fixed vehicle (not spinning).	350
6.20	Comparison of simulation realizations of the bias estimate error variance and the notional bound of Equation 6.73 for several choices of ξ for a range of tracking gains k_e for an inertially fixed vehicle (not spinning).	351
6.21	Comparison of simulation realizations of the attitude estimate error variance and the notional bound of Equation 6.72 for several choices of ξ for a range of tracking gains k_e for a vehicle spinning at 5 revolutions per minute about the vehicle body's $[1\ 2\ 3]^T$ axis.	352
6.22	Comparison of simulation realizations of the bias estimate error variance and the notional bound of Equation 6.73 for several choices of ξ for a range of tracking gains k_e for a vehicle spinning at 5 revolutions per minute about the vehicle body's $[1\ 2\ 3]^T$ axis.	352

6.23	Comparison of simulation realizations of the attitude estimate error variance and the notional bound of Equation 6.72 for several choices of ξ for a range of adaptation gains α for an inertially fixed vehicle (not spinning).	353
6.24	Comparison of simulation realizations of the bias estimate error variance and the notional bound of Equation 6.73 for several choices of ξ for a range of adaptation gains α for an inertially fixed vehicle (not spinning).	354
6.25	Comparison of simulation realizations of the attitude estimate error variance and the notional bound of Equation 6.72 for several choices of ξ for a range of adaptation gains α for a vehicle spinning at 5 revolutions per minute about the vehicle body's $[1\ 2\ 3]^T$ axis.	355
6.26	Comparison of simulation realizations of the bias estimate error variance and the notional bound of Equation 6.73 for several choices of ξ for a range of adaptation gains α for a vehicle spinning at 5 revolutions per minute about the vehicle body's $[1\ 2\ 3]^T$ axis.	356
6.27	Comparison of simulation realizations of the attitude estimate error variance and the notional bound of Equation 6.74 for a range of tracking gains k_e for an inertially fixed vehicle (not spinning).	358
6.28	Comparison of simulation realizations of the bias estimate error variance and the notional bound of Equation 6.73 for a range of tracking gains k_e for an inertially fixed vehicle (not spinning).	359
6.29	Comparison of simulation realizations of the bias estimate error variance and the notional bound of Equation 6.75 for a range of tracking gains k_e for a vehicle spinning at 5 revolutions per minute about the vehicle body's $[1\ 2\ 3]^T$ axis.	360
6.30	Comparison of simulation realizations of the bias estimate error variance and the notional bound of Equation 6.75 for a range of tracking gains k_e for a vehicle spinning at 5 revolutions per minute about the vehicle body's $[1\ 2\ 3]^T$ axis.	360
6.31	Comparison of simulation realizations of the attitude estimate error variance and the notional bound of Equation 6.74 for a range of adaptation gains α for an inertially fixed vehicle (not spinning).	361
6.32	Comparison of simulation realizations of the bias estimate error variance and the notional bound of Equation 6.75 for a range of adaptation gains α for an inertially fixed vehicle (not spinning).	362
6.33	Comparison of simulation realizations of the attitude estimate error variance and the notional bound of Equation 6.74 for a range of adaptation gains α for a vehicle spinning at 5 revolutions per minute about the vehicle body's $[1\ 2\ 3]^T$ axis.	363
6.34	Comparison of simulation realizations of the bias estimate error variance and the notional bound of Equation 6.75 for a range of adaptation gains α for a vehicle spinning at 5 revolutions per minute about the vehicle body's $[1\ 2\ 3]^T$ axis.	364

7.1 Comparison of numerical simulations of the closed-loop attitude controller error Itô SDE 7.2 with the ultimate error upper bound of Equation 7.3. 379

List of Abbreviations

BIBO	Bounded-Input Bounded-Output
BVM	Bivariate von Mises (distribution)
CARE	Continuous Algebraic Riccati Equation
CBO	Constant Bias Observer
EKF	Extended Kalman Filter
FOGM	First Order Gauss Markov
GAS	Globally Asymptotically Stable
GES	Globally Exponentially Stable
GSFC	Goddard Space Flight Center
i.i.d.	independent identically distributed
iff	if and only if
LEO	Low Earth Orbit
LTI	Linear Time Invariant
MEKF	Multiplicative Extended Kalman Filter
MEMS	Micro-Electrical-Mechanical System(s)
NASA	National Aeronautics and Space Administration
ODE	Ordinary Differential Equation
PDE	Partial Differential Equation
PDF	Probability Density Function
RBF	Radial Basis Function
SDE	Stochastic Differential Equation
SO(2)	Special Orthogonal Group in 2 dimensions
SO(3)	Special Orthogonal Group in 3 dimensions
S.O.S.	Sum of Squares
SPD	Symmetric and Positive Definite
TBO	Thermal Bias Observer

UUB Uniformly Ultimately Bounded

VM Von Mises (distribution)

Chapter 1: Introduction

Attitude and angular rate estimation are critical systems for a great many applications. For example, NASA routinely utilizes spacecraft as a platform for hosting scientific observatories above the atmosphere; precise attitude and angular rate estimates of the spacecraft are needed to ensure the science instruments point in the appropriate direction with minimal error. Aircraft autopilots rely on attitude and angular rate estimates to achieve appropriate conditions to maintain smooth flight. Autonomous underwater vehicles (AUVs) rely on attitude and angular rate estimates to similarly maintain appropriate conditions to dive and maneuver underwater. Other recent applications for attitude and angular rate estimation include personnel tracking in unstructured environments [24], fitness tracking [55], and virtual reality systems [63]. It is typical to need both attitude and angular rate estimates; as attitude measurements inherently have noise differentiating the attitude measurements to provide angular rate estimates is often insufficient for closed loop attitude control, estimating body motion, etc.

In many applications, it is challenging to model the system dynamics. In the spacecraft attitude estimation problem, disturbance torques induced by bending modes in solar panels, variation in aerodynamic drag as the atmosphere expands

and contracts, variation in solar radiation pressure due to sun spots or solar flares, liquid propellant slosh, jitter due to rotating instruments onboard the spacecraft, and other effects are common examples [31, 66]. Aircraft may be subjected to wind gusts and variation in mass properties as payload shifts and passengers move about. AUVs are similarly often exposed to changing water currents, unexpected shifts to their center of mass, and unexpected changes to their center of buoyancy [23]. Even rigid body vehicles in an environment with negligible disturbance can prove challenging to model as a system's inertia tensor may be hard to measure or estimate.

In applications where the system dynamics are difficult to model with sufficient fidelity, it is common to instead rely on a sensor fusion approach based on a kinematic model [51, 56] driven by angular rate gyro measurements. As orientation kinematics are known [31] precisely, an angular rate gyro can be used to measure the effect of dynamics and drive the kinematic equations; thus the challenge shifts from modeling the dynamics of the underlying system to modeling the gyro sensor itself. This technique is sometimes referred to as dynamic model replacement.

One of the main sources of error with the dynamics model replacement technique is error in the gyro measurements. Gyro sensors are characterized by the magnitude of bias in their measurements and how the bias might vary. High end gyros have better (smaller) bias characteristics, but come at substantial expense in addition to size, weight, and power requirements; note that even the highest grade of gyros commercially available still have noticeable bias for many applications. Of course, size, weight, power, and financial constraints often dictate lower quality gyro sensors are required for a particular application. The emergence of micro-electrical-

mechanical system (MEMS) gyros has enabled attitude estimation for entirely new classes of problems as well as providing a useful alternative to traditional gyros, but MEMS gyros in particular are known for having large bias that varies over time. A critical idea behind the dynamics model replacement technique is to estimate the gyro bias; the gyro bias estimate is then subtracted from the gyro measurement to attempt to cancel the impact of the underlying gyro bias. The “corrected” gyro measurement is then used to drive the attitude kinematics equation of the estimation algorithm.

1.1 State of the Art

Many of the early advances in attitude estimation theory came from the space industry. As many of the first developments were in the interest of rocket and missile development during the beginning of the Cold War, an accurate and complete history is difficult to assemble as the work was kept classified [102].

The importance of Kalman’s work [39] in the estimation of linear stochastic systems was immediately recognized by Schmidt and his collaborators [69, 82, 83].

Kalman filter techniques were soon applied to attitude estimation. One of the first published works is by Farrell [18, 19] who used a Kalman filter to fuse sun sensor and magnetometer sensors to provide an attitude estimate. Potter and Velde [76] used a Kalman filter to combine star tracker data with gyro measurements. However, as noted by [79] many of these early applications did not have sufficient performance; an inability to model the underlying system dynamics with enough fidelity was a

major setback.

The dynamic model replacement technique met this challenge with great success. The technique appears to have originated with the Space Precision Attitude Reference System (SPARS) described in an Euler angle formulation by Paulson, Jackson, and Brown [74] and a quaternion and error angle formulation by Toda, Heiss, and Schlee [97]. These formulations both estimated gyro bias which was subsequently used to correct the gyro measurements used in their filter's attitude kinematics equations. The Multiplicative Extended Kalman Filter (MEKF) introduced by Lefferts, Markley, and Shuster [51, 64] improved on the work by Toda et al. by formulating new attitude measurement information as a quaternion for measurement updates. The MEKF was employed for the Space Shuttle, is currently employed on the Hubble Space Telescope, the International Space Station, and numerous other current missions. It is the current industry standard and is incorporated in designs for the James Webb Space Telescope and Orion Crew Exploration Vehicle.

Research in attitude estimation filters continues. An Unscented Kalman Filter by Crassidis [14] has been employed to attempt to address the highly nonlinear attitude kinematics. Particle Filters have been developed by Cheng and Crassidis [12] and Oshman and Carmi [73] for attitude estimation problems to relax the typical Kalman filter assumption of Gaussian measurement noise. Unfortunately these techniques come with considerable computational cost compared to the classic MEKF. Other recent work includes the construction of an assumed density Bayesian filter by Glover and Kaelbling [27] based on the assumption that the attitude estimate obeys a Bingham distribution, a type of probability distribution on the unit quaternion hy-

persphere. This same probability density is used in a recursive filter implementation by Kurz et al [48].

Kalman filter techniques have enjoyed considerable success for attitude estimation, but their use is not without criticism as they require instantaneous linearization of the highly nonlinear attitude kinematics equation. It is known [9] that extended Kalman filters based on instantaneous linearization are not guaranteed to be globally stable. With improper tuning or inappropriate initialization it is possible for divergence to occur. Even with appropriate tuning and initialization, the region of stability for an extended Kalman filter can be difficult to establish. Additionally, Kalman filter techniques can be computationally expensive, requiring matrix inverses and propagation of a covariance matrix in addition to the filter state.

Application of nonlinear state observers to the attitude estimation problem has provided an appealing alternative to filter techniques based on instantaneous linearization. Several nonlinear attitude observers have been developed with global stability guarantees derived via Lyapunov analysis. The use of Lyapunov analysis to establish stability for quaternion feedback was first demonstrated for attitude control algorithms. Wie and Barba [105] and Wie, Weiss, and Arapostathis [106] proposed a set of Lyapunov functions that were used to show global asymptotic stability of a class of spacecraft attitude regulators. Egeland and Godhavn [17] extended one of the Wie et al. controllers for attitude tracking control, and showed stability with an augmentation to adaptively learn mass parameters such as the inertia matrix. Fjellstad and Fossen [21] considered a number of various quaternion feedback control schemes for attitude regulation and list associated Lyapunov functions used to show

stability.

Following the successful application of Lyapunov stability analysis to the attitude control problem, several authors have utilized similar Lyapunov candidate functions to demonstrate global stability for nonlinear attitude observers. Salcudean [80] introduced a nonlinear observer for rigid body attitude and angular rate; using deterministic Lyapunov stability theory the observer was shown to eventually converge exponentially fast. Vik, Shiriaev, and Fossen [101] extended this nonlinear observer to also estimate exponentially decaying gyro bias. Thienel and Sanner [94, 95] showed that the gyro bias observer of [101] is exponentially stable even when the biases are constant (persistent); additionally, they show the observer, when combined with a passivity-based attitude controller from [17], exhibits a nonlinear version of the separation principle. Mahony, Hamel, and Pflimlin [56] extended the analysis to consider line-of-sight attitude measurements (e.g. a magnetometer or sun sensor) in addition to estimating persistent gyro bias online; their analysis is provided in both quaternion space and rotation matrix space.

In all of the above nonlinear observer studies, the analysis was performed in a deterministic Lyapunov framework. Thienel and Sanner [94, 95] point out that exponential stability guarantees the stability of the observers in the presence of bounded additive gyro noise, but the deterministic analysis does not provide a means to quantify the stochastic performance of the system. Thus deterministic Lyapunov theory is unable to provide criteria for selection of observer gains based on sensor noise specifications. Choukroun [13] demonstrated how to perturb quaternion kinematics by Brownian motion angular rate noise and analyzed stability using a result from

linear stochastic differential equation theory, but the result does not generalize to nonlinear drift terms that arise in the nonlinear attitude observers of [80, 95, 101] and no explicit stationary performance metric is provided.

The theory of stochastic differential equations (SDEs) are the natural setting for considering measurement noise in the highly nonlinear attitude estimation problem. The rigorous foundation for SDEs dates back to Wiener [16, 107] for linear SDEs and Itô for nonlinear SDEs [33–35, 67]. While the linear SDE work of Wiener provided the basis for the celebrated work of Kalman, the lack of a readily available estimation framework suitable for application appears to have prevented the nonlinear SDE case from finding as much utility. The development of the time evolution of probability densities goes back further to the work of Fokker [22], Planck [75], and Komolgorov [46]. Unfortunately, the time evolution of probability densities is given by a second order parabolic partial differential equation (PDE) which can be challenging to solve.

Several results provide a stochastic analog to the deterministic theory of Lyapunov, referred to as stochastic Lyapunov analysis [43, 96, 112–114], but do not appear to be widely used in the literature. Some of these results allow for the direct computation of bounds of statistics on certain statistics of a nonlinear Itô SDE. For example, this theory has been used to optimize gains in a nonlinear angular rate regulator [52]. Additionally, several results of stochastic Lyapunov theory allow for the determination of various definitions of stochastic stability. This can be a powerful tool as weak stochastic stability implies that the system converges in the infinite time limit to a stationary state (where the probability distribution for the

system states remains constant); thus the complication of solving the time varying Fokker Planck PDE, a second order parabolic PDE, can be reduced to the simpler stationary Fokker-Planck PDE, which is a second order elliptic PDE. If the underlying system is one-dimensional, then the stationary Fokker-Planck PDE reduces to a second order ODE. These simplifications and reductions may make the solution of a Fokker-Planck PDE tractable.

1.2 Contributions

The first contribution of the thesis is the extension of a nonlinear gyro bias observer to allow for the learning of gyro bias as a function of operating temperature. Provided the underlying gyro thermal bias function is sufficiently smooth, the gyro thermal bias observer is able to learn an approximation to gyro thermal bias of arbitrary shape by using an adaptation law to update weighting coefficients of a collection of radial basis functions (RBFs). Simulation studies demonstrate the performance of the observer.

The remaining contributions of this thesis are directed at the formal understanding of the stochastic stability and stationary statistics of several nonlinear attitude observers when provided measurements with noise. The analyses conducted in this thesis are summarized in Table 1.1. Each row depicts the analysis of a nonlinear attitude observer (or attitude and gyro bias observer) with progressively more complicated measurement noise and error models. The columns are broken into SO(2) and SO(3) results for weak stochastic stability, ultimate bounds on perfor-

mance statistics derived via stochastic Lyapunov analysis, and the solution to the corresponding stationary Fokker-Planck PDE. For many measurement models, weak stochastic stability guarantees were found via stochastic Lyapunov analysis. For the gyro additive noise and gyro constant bias measurement model case, weak stochastic stability was found via an appeal to a converse Lyapunov theorem. In the cases where the $SO(3)$ solutions remain unknown to the author, the analysis proceeded to the corresponding $SO(2)$ analogs which were shown to have tractable solutions to their stationary Fokker-Planck PDEs. Ultimate statistics from the solution to the stationary Fokker-Planck PDE for the $SO(2)$ analogs were then extrapolated as heuristic bounds for the $SO(3)$ case; the heuristic bounds were subsequently verified by numerical simulation.

Another significant contribution of the thesis is the development of a Itô SDE quaternion measurement noise model. Prior work has utilized an additive noise model which does not obey the unit norm constraint for quaternions parameterizing rotation. Other work has generated a noise quaternion via a nonlinear mapping from a Gaussian distribution, but this nonlinear mapping precludes the possibility of modeling the noise as a specific type of Itô SDE referred to as an Itô diffusion. By formulating the quaternion measurement noise model as a continuous time Itô diffusion, high fidelity stochastic numerical integration tools may be utilized for simulation studies. Further, the ultimate statistics of the quaternion measurement noise model presented in this thesis were found in the full $SO(3)$ case, allowing for specification of the measurement noise level for simulation and analysis purposes.

Table 1.1: Thesis Contributions

Measurement Model	SO(2)			SO(3)		
	Weak	Stochastic	Fokker	Weak	Stochastic	Fokker
	Stochastic	Lyapunov	Planck	Stochastic	Lyapunov	Planck
	Stability	Bounds	Solution	Stability	Bounds	Solution
Gyro Noise	yes	yes	yes	yes	yes	yes
Gyro Noise & Const	via		yes	via		yes
Gyro Bias	lyap			lyap		
Gyro & Attitude Noise	yes	yes	asymptotic	yes		SO(2) extrap
Gyro Noise, Const Gyro Bias, & Attitude Noise			asymptotic			SO(2) extrap

1.3 Dissertation Outline

Chapter 2 provides an overview of the mathematical theory and analysis tools used throughout the thesis. The chapter begins with a brief review of nonlinear deterministic differential equations and analysis tools to provide a basis for comparison. The chapter then details important concepts from nonlinear stochastic differential equation theory with a detailed discussion of modeling aspects. Stochastic stability concepts are introduced and several results from stochastic Lyapunov theory are presented. The Fokker-Planck PDE is also discussed with an example demonstrating its utility. Numerical SDE simulation techniques are described which are used throughout the thesis to provide validation of the analytical results. Quaternion arithmetic and attitude kinematics are then presented to familiarize the reader with notation used throughout the document. Finally, the structure of several deterministic observers is discussed providing a more detailed description of the remaining chapters.

Chapter 3 provides an extension to the deterministic observer of Thienel and Sanner [95] to account for gyro bias as a function of operating temperature. A brief review of the phenomena of gyro thermal bias from the literature is presented and a pair of notional gyro thermal bias models are provided. Some techniques from function approximation theory are presented, providing a mechanism by which an adaptive observer can encode an estimate of a gyro thermal bias function. The function approximation techniques are then combined with the nonlinear adaptive observer of Thienel and Sanner to formulate a deterministic gyro thermal bias ob-

server. Deterministic simulations demonstrate that the observer is able to “learn” an approximation to the gyro thermal bias function. The deterministic observer of Thienel and Sanner, as well as the new gyro thermal bias observer, are then placed in a stochastic setting by including additive gyro noise and attitude measurement noise. The performance of the observers is compared. Finally, a number of simulations are conducted to sample the gain parameter space in an attempt to find the gain selection criteria for the performance of the filters. The inexact nature of the study and excessive computational cost to perform the work provide motivation for analytic criteria for gain parameter selection.

Chapter 4 details a rigorous analysis of the simple case of a nonlinear attitude observer with additive gyro noise; as the analysis is done in a stochastic setting the terminology changes to a nonlinear attitude filter. The error dynamics are formulated as an Itô SDE and the filter is determined to be weakly stochastically stable. Stochastic Lyapunov theory is used to find performance bounds for the system, but the bounds are shown to be conservative compared to simulation realizations. The $SO(3)$ Fokker-Planck PDE is derived but the complicated structure does not appear to immediately suggest a solution. To gain further understanding of the problem, the analysis is restricted to the $SO(2)$ (single axis) case. The stochastic Lyapunov analysis is repeated there and found to still be conservative, but analysis of the Fokker-Planck PDE proves to be tractable; the solution is given by a von Mises distribution. The solution of the $SO(2)$ stationary Fokker-Planck PDE allows for analytic computation of stationary statistics of the filter which agree with numerical simulation. Intuition gained from the $SO(2)$ case provides motivation for

a proposed solution to the $SO(3)$ Fokker-Planck PDE which fits numerical simulation data. Finally, the insight gained from the $SO(2)$ case suggests a solution to the $SO(3)$ stationary Fokker-Planck PDE which is found as a bipolar Bingham distribution; the solution is used to derive exact analytic expressions for the ultimate statistics of the $SO(3)$ process which agree with numerical simulation. The $SO(3)$ stationary Fokker-Planck solution is subsequently used to compute the entire ultimate covariance matrix for the attitude estimate errors.

Chapter 5 extends the results of the fourth chapter by considering constant gyro bias. The error dynamics for the filter are found to be weakly stochastically stable via an appeal to a converse Lyapunov theorem. While the converse Lyapunov theorem is successfully used in combination with stochastic Lyapunov analysis to demonstrate stability, no explicit formulation of the Lyapunov function is available to find performance bounds for the filter using stochastic Lyapunov analysis. The $SO(3)$ Fokker-Planck PDE is found but again has complicated structure. As before, the analysis focuses on the restricted $SO(2)$ case for further insight. The stochastic Lyapunov analysis is repeated there and found to still be conservative, but analysis of the Fokker-Planck PDE proves to be tractable; the solution is given by a joint von Mises and Gaussian distribution. The solution of the $SO(2)$ stationary Fokker-Planck PDE allows for analytic computation of stationary statistics of the filter which agree with numerical simulation. Intuition gained from the $SO(2)$ case provides motivation for a proposed solution to the $SO(3)$ Fokker-Planck PDE which fits numerical simulation data. Finally, the insight gained from the $SO(2)$ case suggests a solution to the $SO(3)$ stationary Fokker-Planck PDE which is found as a

joint bipolar Bingham and multivariate Gaussian distribution; the solution is used to derive exact analytic expressions for the ultimate statistics of the $SO(3)$ process which agree with numerical simulation.

Chapter 6 introduces attitude measurement noise to the analysis. As the analysis tools used in this thesis require the error dynamics be formulated as an Ito SDE, the filter error dynamics are augmented by a separate process to generate quaternion measurement noise with specified noise density; the filter dynamics from Chapter 4 provide such a mathematical process. The first section begins with additive gyro noise and attitude measurement noise only, no gyro bias is considered. Weak stochastic stability is demonstrated using Lyapunov analysis. Ultimate performance bounds are found using stochastic Lyapunov analysis; however, numerical simulation shows the performance bounds are very conservative and not indicative of actual performance. Following the analysis strategy of previous chapters, the system is reduced to the $SO(2)$ case. An asymptotic solution to the stationary Fokker-Planck PDE is found as a bivariate von Mises distribution; the solution is used to compute stationary statistics for the filter which agree with numerical simulation. Intuition gained from the $SO(2)$ case provides a suggestion for a heuristic upper bound for the $SO(3)$ case which correctly envelopes numerical simulation data. The next section repeats the analysis for the case of additive gyro noise, gyro constant bias, and attitude measurement noise. A stability result for this case eludes the author, but as in the previous section an asymptotic solution to the $SO(2)$ stationary Fokker-Planck PDE is found as a joint bivariate von Mises and Gaussian distribution which agrees with simulation realizations. The $SO(s)$ solution is again extrapolated to the $SO(3)$

case as a heuristic bound which is found to agree with extensive simulation data.

Chapter 7 provides a summary of the dissertation and discusses directions for future research. Aside from filling in the gaps in Table 1.1, other important gyro noise models are discussed; particularly non-axis-symmetric additive gyro noise and bias random walk. An extension of the filters of Chapter 6 is proposed to filter the non-white attitude noise present in the attitude measurement noise model from that chapter. Additionally, the subject of closed-loop attitude control is mentioned along with a preliminary stability and performance result. The chapter concludes with final remarks on the stochastic tools and analysis approach used in the thesis.

Chapter 2: Background

This chapter provides an overview of relevant background material used in this thesis. First, Section 2.1 covers stochastic differential equations (SDEs) and methods of analyzing stability; it begins with a brief review of ODEs in Section 2.1.1 and deterministic Lyapunov stability theory 2.1.2 to provide a basis for the overview of SDEs in Section 2.1.3 and stochastic Lyapunov stability theory presented in Section 2.1.4, and concludes with a discussion of Fokker-Planck analysis in Section 2.1.5. Next, Section 2.2 reviews numerical integration methods useful for validating analytical results. Quaternion arithmetic and attitude kinematics are presented in Section 2.3. Finally, Section 2.4 discusses the structure of the deterministic observers that serve as the basis for the attitude filters analyzed in this thesis.

2.1 Nonlinear Stochastic Differential Equations and Stability

This section reviews several key concepts from deterministic ordinary differential equations (ODEs) along with methods of establishing stability via Lyapunov analysis. Next, the stochastic analog of these concepts are presented, including a rigorous definition of stochastic differential equations (SDEs), practical stochastic modeling issues, and stochastic Lyapunov analysis techniques for determining

stability and performance. An alternative analysis technique utilizing partial differential equations (PDEs) via stationary Fokker-Planck analysis is discussed. Several examples are used to illustrate the theoretical concepts.

2.1.1 Deterministic Ordinary Differential Equations

Consider the deterministic Ordinary Differential Equation (ODE)

$$\dot{\mathbf{x}}(t) = \mathbf{f}(\mathbf{x}(t)) + G(\mathbf{x}(t)) \mathbf{u}(t) \quad \mathbf{x}(t_a) = \mathbf{x}_a \quad (2.1)$$

where $\mathbf{x}(t) \in \mathbb{R}^{n \times 1}$ is the system state evaluated at time t and the input $\mathbf{u}(t)$ is some deterministic known function of time.

The ODE is interpreted by its integral

$$\mathbf{x}(t_b) - \mathbf{x}(t_a) = \int_{t_a}^{t_b} \mathbf{f}(\mathbf{x}(t)) dt + \int_{t_a}^{t_b} G(\mathbf{x}(t)) \mathbf{u}(t) dt \quad (2.2)$$

The integrals in Equation 2.2 are the ordinary Riemann integrals of elementary calculus, defined as

$$\int_{t_a}^{t_b} \mathbf{f}(\mathbf{x}(t)) dt = \lim_{\delta \rightarrow 0} \sum_{i=0}^{N-1} \mathbf{f}(\mathbf{x}(\tau_i)) [t_{i+1} - t_i] \quad (2.3)$$

where $t_a = t_0 < t_1 \dots t_N = t_b$ is a partition of the integration interval $[t_a, t_b]$, $\delta = \max_i(t_{i+1} - t_i)$, and each $\tau_i \in (t_i, t_{i+1})$. If the limit does not exist, the integral is said to not exist or not converge.

Of course, the integral Equation 2.2 does not directly yield the solution of the system as $x(t)$ appears on both sides of the equation. The linear time invariant (LTI) system, a special case of Equation 2.1, is given as

$$\dot{\mathbf{x}}(t) = A\mathbf{x}(t) + B\mathbf{u}(t) \quad \mathbf{x}(t_a) = \mathbf{x}_a \quad (2.4)$$

The solution to the LTI ODE is a well known result from elementary calculus [11]

$$\mathbf{x}(t_b) = e^{(t_b-t_a)A}\mathbf{x}(t_a) + \int_{t_a}^{t_b} e^{(t_b-\tau)A}B\mathbf{u}(\tau)d\tau$$

This solution may be used to determine the properties and behavior of the system. The solution to certain classes of linear time varying (LTV) systems that are periodic can be found via a time varying coordinate change that transforms the periodic system into an LTI system using Floquet theory [11].

The situation is less well understood for the general nonlinear ODE of Equation 2.1. Closed-form solutions to the general nonlinear ODE may be very challenging to find, or even impossible. Tenenbaum and Pollard [93] state “It is unfortunately true that only very special types of first order differential equations possess solutions which can be expressed in terms of elementary functions. Most first order differential equations, in fact, one could say almost all, cannot be thus expressed.”

While closed-form solutions to the general nonlinear ODE of Equation 2.1 may be difficult or impossible to find, it may be possible to find a more general solution or at least determine if a unique solution exists. The existence of a solution, and uniqueness of that solution, can be established by the Picard-Lindelof Theorem which has Lipschitz continuity conditions that ensure the integral of the ODE converges [42, 93]. Assuming a unique solution exists, the solution can then always be found via successive Picard iterations; however, this solution technique may yield the solution as an infinite series of nested integrals.

For design and analysis purposes, however, an explicit closed form solution often isn’t needed. As long as a unique solution exists, it may be sufficient to assess

qualitative properties of a system such as system stability or boundedness. The following section presents ODE analysis techniques that do not require the explicit solution.

2.1.2 Deterministic Stability Analysis

Some highlights of Lyapunov stability analysis are reviewed in this section. The discussion here provides a basis for understanding the stochastic Lyapunov results presented in the upcoming stochastic stability analysis overview of Section [2.1.4](#).

Consider a system described by the ODE

$$\dot{\mathbf{x}}(t) = \mathbf{f}(\mathbf{x}(t)) \quad \mathbf{x}(t_a) = \mathbf{x}_a \quad (2.5)$$

The system of Equation [2.5](#) is said [\[42\]](#) to be

- stable if, for each $\epsilon > 0$ there exists a $\delta = \delta(\epsilon) > 0$ such that

$$\|\mathbf{x}_a\| < \delta \implies \|\mathbf{x}(t)\| < \epsilon \quad \forall t \geq t_a$$

- Globally Asymptotically Stable (GAS) if

$$\lim_{t \rightarrow \infty} \mathbf{x}(t) = \mathbf{0} \quad \forall \mathbf{x}(t_a) = \mathbf{x}_a$$

- Globally Exponentially Stable (GES) if there exist positive constants c, k , and λ such that

$$\|\mathbf{x}(t)\| \leq k \|\mathbf{x}(t_a)\|^{-\lambda(t-t_a)} \quad \forall \mathbf{x}(t_a) = \mathbf{x}_a$$

In words, a system is stable if for any ball of arbitrary radius centered at the origin, the system states remain within that ball for any initial condition inside some initial condition set (a ball centered at the origin with radius dependent on the first ball). A system is GAS if, for any initial condition, the state asymptotically approaches

the origin. A system is GES if, for any initial condition, the state approaches the origin exponentially fast. These types of stability may be assessed via the analysis techniques pioneered by Lyapunov.

Theorem 2.1.1 (Lyapunov's Direct Method [42]). *Let $\mathbf{x} = \mathbf{0}$ be an equilibrium point for Equation 2.5 and $V : \mathbb{R}^{n \times 1} \rightarrow \mathbb{R}$ be a continuously differentiable function such that*

$$V(\mathbf{0}) = 0 \quad \text{and} \quad V(\mathbf{x}) > 0 \quad \forall \mathbf{x} \neq \mathbf{0}$$

If

$$\dot{V}(\mathbf{x}(t)) \leq 0 \quad \forall \mathbf{x}(t)$$

then the system described by Equation 2.5 is stable.

Moreover, if

$$\dot{V}(\mathbf{x}(t)) < 0 \quad \forall \mathbf{x}(t) \neq \mathbf{0}$$

then the system described by Equation 2.5 is Globally Asymptotically Stable (GAS).

Consider the LTI system of Equation 2.4 in the unforced case (when the input is $\mathbf{u}(t) = \mathbf{0} \forall t$). Then Equation 2.4 reduces to

$$\dot{\mathbf{x}}(t) = A\mathbf{x}(t) \tag{2.6}$$

The choice of Lyapunov function $V(\mathbf{x}(t)) = \mathbf{x}^T(t)P\mathbf{x}(t)$ with P symmetric and positive definite (SPD) leads to

$$\begin{aligned} \dot{V}(t) &= \mathbf{x}^T(t) \left(A^T P + P A \right) \mathbf{x}(t) \\ &= -\mathbf{x}^T(t) Q \mathbf{x}(t) < 0 \quad \forall \mathbf{x}(t) \neq \mathbf{0} \quad \text{iff } Q \text{ is SPD} \end{aligned}$$

This is of course an abbreviated derivation of the well known stability Lyapunov equation for LTI systems given in the following corollary.

Corollary 2.1.1.1 (Lyapunov Asymptotic Stability for LTI Systems). *The LTI system of Equation 2.6 is Globally Asymptotically Stable iff there exists SPD matrices P, Q such that*

$$A^T P + P A = -Q$$

Other types of stability exist. The system of Equation 2.5 is said to be Globally Uniformly Ultimately Bounded (globally UUB) [42] if there exists a $T < \infty$ and a positive scalar k such that

$$\|\mathbf{x}(t)\| < k < \infty \quad \forall t \geq t_a + T, \forall \mathbf{x}(t_a) = \mathbf{x}_a \quad (2.7)$$

Note the distinction between stability in the sense of Theorem 2.1.1 and UUB. Theorem 2.1.1 requires a system to be such that the states remain within a ball of *any* size (centered on the origin) to be deemed stable. UUB relaxes this notion as a system is UUB if its states remain within any finite bound; a system may rapidly diverge from the origin and still be UUB provided its states remain within *some* ball centered on the origin. A classic example is the Van der Pol oscillator which, for positive damping coefficient, is unstable but UUB as the system trajectory converges to a stable limit cycle [42]. The following Lyapunov theorem may be used to assess if a particular system is UUB. First recall that a continuous function $\alpha(\cdot)$ is said to belong to class \mathcal{K} if it is strictly increasing and $\alpha(0) = 0$.

Theorem 2.1.2 (Uniformly Ultimately Bounded Lyapunov Theorem [42]). *Let*

$V : \mathbb{R}^n \rightarrow \mathbb{R}$ be a continuously differentiable function such that

$$\alpha_1 (\|\mathbf{x}(t)\|) \leq V(\mathbf{x}(t)) \leq \alpha_2 (\|\mathbf{x}(t)\|)$$

where $\alpha_1(\cdot)$ and $\alpha_2(\cdot)$ are class \mathcal{K} functions and $\alpha_1(\|\mathbf{x}(t)\|) \rightarrow \infty$ as $\|\mathbf{x}(t)\| \rightarrow \infty$.

If

$$\dot{V}(\mathbf{x}(t)) = \left(\frac{\partial V}{\partial \mathbf{x}} \right)^T \mathbf{f}(\mathbf{x}(t)) \leq W(\mathbf{x}(t)) < 0 \quad \forall \|\mathbf{x}(t)\| \geq \mu > 0 \quad \forall t \geq t_a$$

for some continuous positive definite function $W(\cdot)$, then the system described by Equation 2.5 is Uniformly Ultimately Bounded (UUB). If the above holds for any initial condition $\mathbf{x}(t_a) = \mathbf{x}_a$, the system is globally UUB.

Furthermore, for any $r > 0$ satisfying $\mu < \alpha_2^{-1}(\alpha_1(r))$, there exists a $T \geq 0$ (dependent on $\mathbf{x}(t_a)$ and μ) such that

$$\|\mathbf{x}(t)\| \leq \alpha_1^{-1}(\alpha_2(\mu)), \quad \forall t \geq t_a + T$$

To illustrate the utility of the UUB theorem, consider the logistic population model given by the scalar nonlinear ODE

$$\dot{x}(t) = rx(t) \left(1 - \frac{x(t)}{k} \right) \quad x(t_0) = x_0 > 0 \quad (2.8)$$

In the model, $x(t)$ is some population that can be modeled with a continuous variable (a large group of individual animals, or perhaps bacteria). The parameter r models the growth and decay (birth and death) in the population while k models the environmental carrying capacity. Note that the population can never become

negative; the population begins with a positive value. As the solution is continuous, and $\dot{x}(t) = 0$ for $x(t) = 0$, the solution must remain positive semidefinite; if the population ever drops to zero, it remains zero forever after.

The logistic population model of Equation 2.20 is UUB. Choose $V = \frac{1}{2}x^2(t)$.

Then

$$\dot{V}(t) = rx^2(t) \left(1 - \frac{x(t)}{k}\right) < 0 \quad \forall x(t) > k$$

Application of Theorem 2.1.2 shows the desired result.

The above theorems used a Lyapunov function to demonstrate a stability property of a given system. There will be use in this thesis for converse Lyapunov theorems as well. These theorems allow one to use the fact that a system is GES to infer the existence of a Lyapunov function that has certain properties without finding the explicit form of the Lyapunov function. In Chapter 6, the fact that a deterministic system is known to be GES will be used with the following converse Lyapunov theorem to generate a Lyapunov function that will in turn be used to show a stochastic extension of the system is weakly stochastically stable using a stochastic Lyapunov theorem.

Theorem 2.1.3 (Converse Lyapunov [42]). *Let $\mathbf{x} = \mathbf{0}$ be an equilibrium point for Equation 2.5 with $\mathbf{f}(\cdot) : \mathbb{R}^n \rightarrow \mathbb{R}^n$ continuously differentiable and $\frac{\partial \mathbf{f}}{\partial \mathbf{x}}$ be bounded. If there exist positive constants k, λ such that trajectories of the system satisfy*

$$\|\mathbf{x}(t)\| \leq k\|\mathbf{x}(t_a)\|e^{-\lambda(t-t_a)}, \quad \forall t \geq t_a$$

then there is a function $V : \mathbb{R}^n \rightarrow \mathbb{R}$ that satisfies the inequalities

$$\begin{aligned}c_1 \|\mathbf{x}\|^2 &\leq V(\mathbf{x}) \leq c_2 \|\mathbf{x}\|^2 \\ \frac{\partial V}{\partial \mathbf{x}} \mathbf{f}(\mathbf{x}(t)) &\leq -c_3 \|\mathbf{x}\|^2 \\ \left\| \frac{\partial V}{\partial \mathbf{x}} \right\| &\leq c_4 \|\mathbf{x}\|\end{aligned}\tag{2.9}$$

for some positive constants c_1, c_2, c_3 , and c_4 .

2.1.3 Stochastic Differential Equations

Extending the model of Equation 2.1 to include the effects of random noise is of great interest for modeling disturbance forces and torques, measurement noise, and other phenomena [9, 37, 68]. Inclusion of random noise will require considerably more mathematical theory than was used to define ODEs; this section presents a rigorous definition of a stochastic differential equation (SDE).

A common approach to formulating an SDE [9, 26, 84, 109] is to perturb an ODE by a Gaussian white noise process $\mathbf{n}(\cdot)$ where at each time t the process is an independent identically distributed (iid) sample from a zero mean unit variance Gaussian noise distribution: $\mathbf{n}(t) \sim \mathcal{N}(\mathbf{0}, I)$.

$$\dot{\mathbf{x}}(t) = \mathbf{f}(\mathbf{x}(t)) + G(\mathbf{x}(t))\mathbf{n}(t) \quad (2.10)$$

In this thesis an ODE perturbed by a Gaussian white noise process will be referred to as a Langevin form differential equation.

The scalar white noise process $n(\cdot)$ is so named since at each time instant $n(t)$ is drawn from an independent identically distributed normal distribution, $n(t) \sim \mathcal{N}(0, 1)$, thus the autocorrelation is necessarily $E[n(t)n(\tau)] = \delta(t - \tau)$. This is how the noise process gets its name as the Fourier transform of the autocorrelation function, the spectral density, is flat for this process. That is, the spectral density contains content at all frequencies, similar to how white light contains content of all visible light frequencies. Of course, a dirac-delta autocorrelated process is not continuous [72], the process is nonphysical as a signal would require infinite energy to be truly white [109],

and the process is difficult to interpret rigorously [44, 67].

A closely related process is the Brownian motion process, also called a Wiener process, which will be denoted as $\beta(\cdot)$. Brownian motion is defined as a process with the following properties [44]:

- **Independent Increments** $\beta(t) - \beta(s)$ for $t > s$ is independent of the past, meaning independent of $\beta(u)$ for $0 \leq u \leq s$
- **Normal Increments** $\beta(t) - \beta(s)$ for $t > s$ has a normal distribution with mean 0 and variance $t - s$; symbolically, $E[\beta(t) - \beta(s)] = 0$ and $E\{[\beta(t) - \beta(s)]^2\} = t - s$
- **Continuous Paths** $\beta(t), t \geq 0$ are continuous functions of t .

In fact, the third property, that the Brownian motion process has continuous paths, can be deduced from the first two defining properties [44].

Wiener [67, 107] rigorously derived his integral using the Brownian motion process:

$$\int_{t_a}^{t_b} G(t) d\beta(t) = l.i.m._{\delta \rightarrow 0} \sum_{i=0}^{N-1} G(t_i) [\beta(t_{i+1}) - \beta(t_i)]$$

where $t_a = t_0 < t_1 < \dots < t_N = t_b$ and $\delta = \max_i (t_{i+1} - t_i)$. The limit is taken as the limit in the mean, or the mean square limit, and *l.i.m.* is shorthand for

$$l.i.m._{\delta \rightarrow 0} x_\delta = x \quad \Leftrightarrow \quad \lim_{\delta \rightarrow 0} E[(x_\delta - x)^2] = 0$$

In the definition of the Wiener integral, the integrand $G(t)$ is restricted to be deterministic; it must in no way depend on the Brownian motion process $\beta(\cdot)$. Since the state is dependent on the Brownian motion process, the Wiener integral is not

defined for integrands that are a function of the state [67]. Note that in the sum, the integrand is evaluated at the left end of the integration interval, t_i .

With this in hand, the stochastic differential equation

$$d\mathbf{x}(t) = \mathbf{f}(\mathbf{x}(t))dt + G(t)d\boldsymbol{\beta}(t) \quad \mathbf{x}(t_a) = \mathbf{x}_a \quad (2.11)$$

can now be associated with the integral equation

$$\mathbf{x}(t_b) - \mathbf{x}(t_a) = \int_{t_a}^{t_b} \mathbf{f}(\mathbf{x}(t))dt + \int_{t_a}^{t_b} G(t)d\boldsymbol{\beta}(t) \quad (2.12)$$

where the first integral is an ordinary Riemann integral and the second integral is a Wiener integral.

Wiener calculus serves as the rigorous basis for interpreting Langevin form differential equations of the type

$$\dot{\mathbf{x}}(t) = \mathbf{f}(\mathbf{x}(t)) + G(t)\mathbf{n}(t) \quad (2.13)$$

by replacing the problematic $\mathbf{n}(\cdot)$ white noise process with the Brownian increment $d\boldsymbol{\beta}(\cdot)$. The white noise process $n(\cdot)$ can be thought of [37, 44, 67, 72], informally, as the “derivative” of the Brownian motion process $\beta(\cdot)$, symbolically “ $\dot{\beta}(t) = n(t)$ ”. However, the Brownian motion process is nowhere differentiable. Hence the pathological nature of white noise; it is the derivative of a process that has no derivative. This can seem to be a subtle distinction and is of little consequence for working with Langevin form differential equations when G is independent of the state like in Equation 2.13; however, when the diffusion matrix G is state dependent, the Brownian increment is no longer independent of the diffusion matrix as the state is itself dependent on the Brownian increment.

Wiener calculus shares many of the same fundamental mechanics as ordinary calculus, such as the chain rule. Again it should be stressed that the Wiener integral does not allow for $G(t)$ to be dependent on the state. The Wiener integral is the type of integral used in the derivation of an extended Kalman filter, which addresses the issue by instantaneously linearizing the system dynamics at every time step and thus assuming the $G(t)$ matrix is only time varying. The region of validity of this assumption is difficult to assess.

Most of the stochastic differential equations (SDEs) encountered in this thesis are such that the G matrix does indeed depend on the state, which in turn depends on previous values of the Brownian motion process. The Wiener integral was extended by Itô [33, 34, 37, 67] as

$$\int_{t_a}^{t_b} G(\mathbf{x}(t))d\boldsymbol{\beta}(t) = \underset{\delta \rightarrow 0}{l.i.m.} \sum_{i=0}^{N-1} G(\mathbf{x}(t_i)) [\boldsymbol{\beta}(t_{i+1}) - \boldsymbol{\beta}(t_i)]$$

Note carefully that the integrand is again evaluated at the left side of the integration interval. Since the Brownian motion process has increments independent of its prior values it follows that for each term in the summation $G(\mathbf{x}(t_i))$ and $\boldsymbol{\beta}(t_{i+1}) - \boldsymbol{\beta}(t_i)$ are independent.

Observe that the Wiener integral is a special case of the Itô integral. Similarly, the Itô stochastic differential equation (SDE)

$$d\mathbf{x}(t) = \mathbf{f}(\mathbf{x}(t))dt + G(\mathbf{x}(t))d\boldsymbol{\beta}(t) \quad \mathbf{x}(t_a) = \mathbf{x}_a \quad (2.14)$$

is interpreted as

$$\mathbf{x}(t_b) - \mathbf{x}(t_a) = \int_{t_a}^{t_b} \mathbf{f}(\mathbf{x}(t))dt + \int_{t_a}^{t_b} G(\mathbf{x}(t))d\boldsymbol{\beta}(t) \quad (2.15)$$

In Equation 2.15, the first integral is interpreted as an ordinary Riemann integral and the second is an Itô integral. The $\mathbf{f}(\mathbf{x}(t))$ term is often referred to as the drift term and $G(\mathbf{x}(t))$ as the diffusion matrix. By construction of the Itô integral, the solution to $\mathbf{x}(t)$ is a Markov process [44, 67]. This thesis only considers a specific type of SDE called an Itô diffusion; that is, an SDE that can be written in the form of Equation 2.14 which is affine in the driving noise.

While the Wiener integral and the Itô integral appear to be very similar, Wiener calculus follows the same rules as ordinary calculus while the more general Itô integral and its attendant calculus do not. Specifically, the chain rule of ordinary calculus does not hold. Consider the twice continuously differentiable function $V(\mathbf{x}(t))$. Its derivative with respect to the SDE of Equation 2.14 is given by Itô's Lemma, which is the chain rule for Itô calculus [67]:

$$\begin{aligned}
dV(\mathbf{x}(t)) &= \left(\frac{\partial V}{\partial \mathbf{x}}\right)^T d\mathbf{x}(t) + \frac{1}{2} \text{tr} \left(G^T(\mathbf{x}(t)) \frac{\partial^2 V}{\partial \mathbf{x}^2} G(\mathbf{x}(t)) \right) dt \\
&= \left[\left(\frac{\partial V}{\partial \mathbf{x}}\right)^T \mathbf{f}(\mathbf{x}(t)) + \frac{1}{2} \text{tr} \left(G^T(\mathbf{x}(t)) \frac{\partial^2 V}{\partial \mathbf{x}^2} G(\mathbf{x}(t)) \right) \right] dt \\
&\quad + \left(\frac{\partial V}{\partial \mathbf{x}}\right)^T G(\mathbf{x}(t)) d\boldsymbol{\beta}(t) \\
&= \mathcal{L}V(\mathbf{x}(t)) dt + \left(\frac{\partial V}{\partial \mathbf{x}}\right)^T G(\mathbf{x}(t)) d\boldsymbol{\beta}(t)
\end{aligned} \tag{2.16}$$

where the $\mathcal{L}\cdot$ operator is given by

$$\mathcal{L}V(\mathbf{x}(t)) = \left(\frac{\partial V}{\partial \mathbf{x}}\right)^T \mathbf{f}(\mathbf{x}(t)) + \frac{1}{2} \text{tr} \left(G^T(\mathbf{x}(t)) \frac{\partial^2 V}{\partial \mathbf{x}^2} G(\mathbf{x}(t)) \right) \tag{2.17}$$

The operator is known as the differential generator [67] [96], the differential operator [114], and the generator [44] [43]; it will be referred to as a differential generator in this thesis and will be used extensively. The differential generator is such that

$\mathcal{L}V = E[dV]$; that is, it is the expectation of the Itô derivative along sample paths of the associated SDE [67].

Alternative integrals exist for handling state dependent G matrices. A popular alternative is the Stratonovich [37, 67, 91, 92] integral, defined as

$$\int_{t_a}^{t_b} G(\mathbf{x}(t)) \circ d\boldsymbol{\beta}(t) = \lim_{\delta \rightarrow 0} \sum_{i=0}^{N-1} G\left(\mathbf{x}\left(\frac{t_{i+1} - t_i}{2}\right)\right) [\boldsymbol{\beta}(t_{i+1}) - \boldsymbol{\beta}(t_i)]$$

where the \oint and $\circ d\boldsymbol{\beta}(t)$ are used to distinguish a Stratonovich integral from a Wiener or Itô integral. Note that in this definition the integrand is evaluated in the middle of the integration interval.

The Stratonovich integral allows for Stratonovich SDEs of the form

$$d\mathbf{x}(t) = \mathbf{f}(\mathbf{x}(t))dt + G(\mathbf{x}(t)) \circ d\boldsymbol{\beta}(t), \quad \mathbf{x}(t_a) = \mathbf{x}_a \quad (2.18)$$

to be interpreted as

$$\mathbf{x}(t_b) - \mathbf{x}(t_a) = \int_{t_a}^{t_b} \mathbf{f}(\mathbf{x}(t))dt + \int_{t_a}^{t_b} G(\mathbf{x}(t)) \circ d\boldsymbol{\beta}(t) \quad (2.19)$$

where the first integral is an ordinary Riemann integral and the second is a Stratonovich integral.

The Stratonovich and Itô integrals differ in several fundamental ways. As noted earlier, the Itô integral and its attendant calculus utilize their own special chain rule which differs from that of ordinary calculus. The Stratonovich integral and its attendant calculus utilizes the same chain rule as that of ordinary calculus. While this might make it more attractive, it has its own drawbacks. The Stratonovich integral is not a martingale while the Itô integral is [72]; the martingale property makes the Itô integral easier to work with in proofs so Itô calculus is more prevalent

in the literature. Additionally, the Stratonovich integral is only defined for explicit functions of $\beta(t)$ while the Itô integral is defined for functionals on $\{\beta(\tau), \tau \leq t\}$, so Itô integrals are applicable to a wider class of systems [37, 58].

Note that for the restricted class of functions for which the Stratonovich integral can be defined, there is a one-to-one correspondence between an Itô SDE and a Stratonovich SDE [26, 67]. The same process $\mathbf{y}(t)$ may be represented as the Itô SDE

$$d\mathbf{y}(t) = \mathbf{f}_{ito,\mathbf{y}}(\mathbf{y}(t))dt + G(\mathbf{y}(t))d\beta(t)$$

or the Stratonovich SDE

$$d\mathbf{y}(t) = \left[\mathbf{f}_{ito,\mathbf{y}}(\mathbf{y}(t)) - \frac{1}{2} \sum_j \frac{\partial \mathbf{g}_j}{\partial \mathbf{y}} \mathbf{g}_j \right] dt + G(\mathbf{y}(t)) \circ d\beta(t)$$

where \mathbf{g}_j is the j^{th} column of $G(\mathbf{y}(t)) \in \mathbb{R}^{n \times m}$ and for any $\mathbf{v} \in \mathbb{R}^{m \times 1}$

$$\frac{\partial \mathbf{v}}{\partial \mathbf{y}} = \begin{bmatrix} \frac{\partial v_1}{\partial y_1} & \dots & \frac{\partial v_1}{\partial y_n} \\ \vdots & \ddots & \vdots \\ \frac{\partial v_m}{\partial y_1} & \dots & \frac{\partial v_m}{\partial y_n} \end{bmatrix}$$

Conversely, the same process $\mathbf{z}(t)$ may be represented as the Stratonovich SDE

$$d\mathbf{z}(t) = \mathbf{f}_{strat,\mathbf{z}}(\mathbf{z}(t))dt + G(\mathbf{z}(t)) \circ d\beta(t)$$

or the Itô SDE

$$d\mathbf{z}(t) = \left[\mathbf{f}_{strat,\mathbf{z}}(\mathbf{z}(t)) + \frac{1}{2} \sum_j \frac{\partial \mathbf{g}_j}{\partial \mathbf{y}} \mathbf{g}_j \right] dt + G(\mathbf{y}(t))d\beta(t)$$

The question remains, how does one interpret a Langevin form differential equation such as Equation 2.10? Or, as eloquently stated in [71], “which kind of

calculus does nature use?” Opinions differ [70, 87, 89, 98, 100, 104], although there is agreement that both Itô calculus and Stratonovich calculus are both self-consistent and the correspondence between Itô and Stratonovich SDEs may be utilized to freely transform a system description as needed [37, 67, 71]. Note that *the two different interpretations of the Langevin form differential equation lead, in general, to two distinct stochastic processes*. Each process can be described by an Itô SDE, a Stratonovich SDE, or a Fokker-Planck PDE (which will be discussed in Section 2.1.5). The situation is illustrated in Figure 2.1.

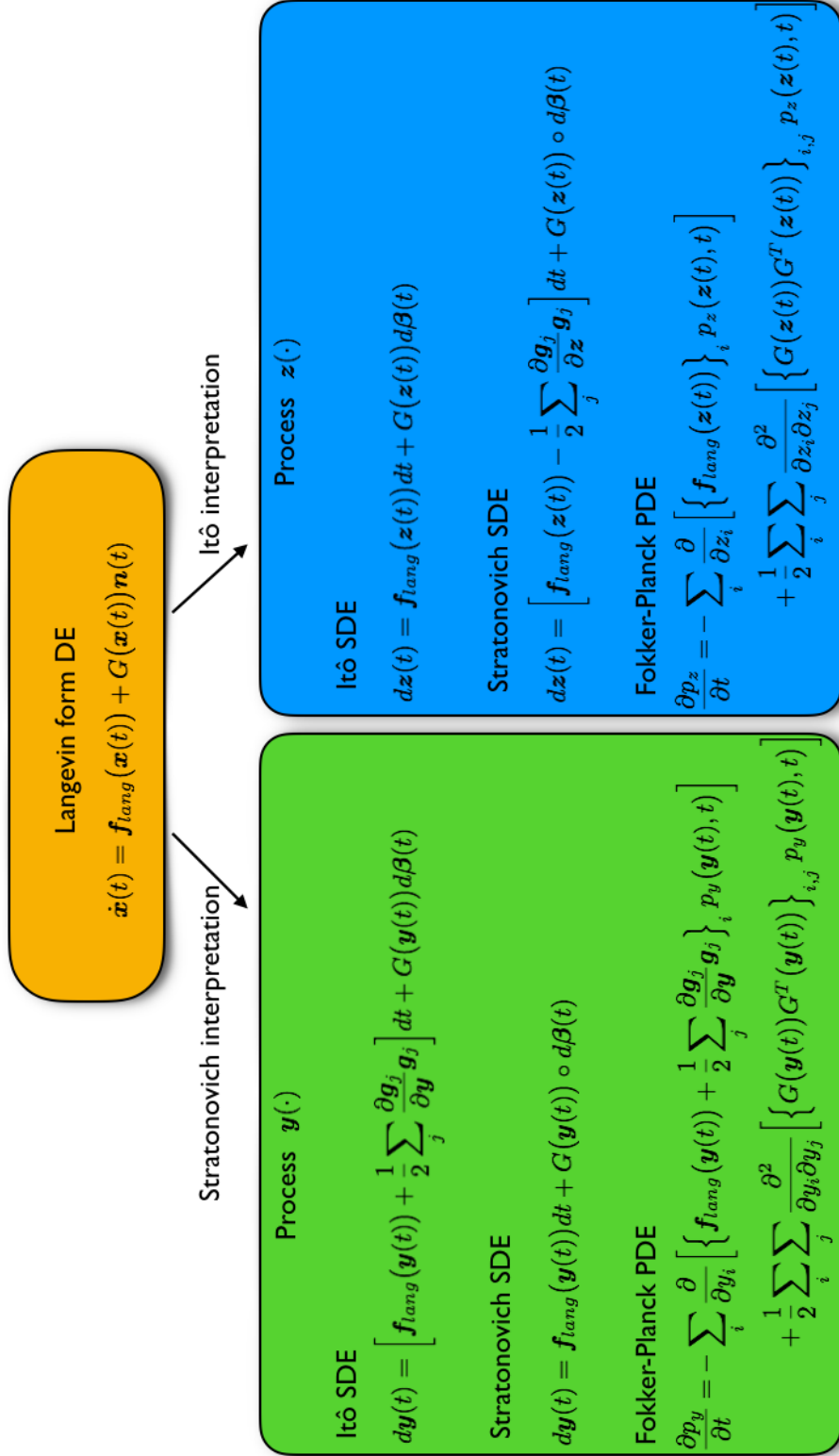


Figure 2.1: The two interpretations of the Langevin form differential equation lead, in general, to two distinct stochastic processes.

Some authors, particularly in mathematics [44, 72] and chemistry [98–100], argue that the non-rigorous definition and construction of the white noise process, evidenced by the possibility of distinct interpretations of the Langevin form differential equation, means the Langevin form differential equation itself should be discarded and the modeling process should begin with an Itô SDE, a Stratonovich SDE, or a Fokker-Planck PDE (or the more generalized Master Equation). Other authors [87, 104] argue unequivocally that Langevin form differential equations should be interpreted as Stratonovich SDEs (by replacing the white noise term with the Brownian increment) based on analytical analysis and experimental data. All cited authors agree that the Stratonovich interpretation of a Langevin form differential equation is appropriate when the noise being modeled is a so called “external force”, such as a disturbance force, disturbance torque, a disturbance due to an external thermal source (aka dark current), and shot noise. Examples of “internal forces” in this context are typically due to chemical reactions. As this thesis is concerned with modeling gyro noise and attitude measurement sensor noise, which would be considered due to “external forces”, the Stratonovich interpretation appears appropriate.

Analyses conducted by Wong and Zakai [110, 111] attempted to address this issue. They studied a sequence of ODEs driven by continuous piecewise linear approximations to Brownian motion process where the approximations converge to actual Brownian motion processes in the limit. They found that the sequence of solutions to the ODEs converged in the limit to the Stratonovich interpretation of the Langevin form differential equation, not the Itô interpretation. This interpretation

has been quite influential and is recommended by prominent texts by mathematicians [40, 45], physicists [26], and engineers [37]. Following these recommendations, in this thesis first principles will be used to derive Langevin form differential equations which will be interpreted as Stratonovich SDEs. However, since the results from stochastic stability theory (to be presented in Section 2.1.4) and high fidelity numerical integration algorithms (to be presented in Section 2.2) are given for Itô SDEs, the Stratonovich SDEs will subsequently be converted into Itô SDEs for analysis and numerical simulation.

In summary, in this thesis Langevin form differential equations such as

$$\dot{\mathbf{x}}(t) = \mathbf{f}_{lang}(\mathbf{x}(t)) + G(\mathbf{x}(t))\mathbf{n}(t)$$

will be interpreted as a Stratonovich SDE

$$d\mathbf{x}(t) = \mathbf{f}_{lang}(\mathbf{x}(t))dt + G(\mathbf{x}(t)) \circ d\boldsymbol{\beta}(t)$$

which will in turn be converted to an Itô SDE given by

$$d\mathbf{x}(t) = \left[\mathbf{f}_{lang}(\mathbf{x}(t))dt + \frac{1}{2} \sum_j \frac{\partial \mathbf{g}_j}{\partial \mathbf{x}} \mathbf{g}_j \right] dt + G(\mathbf{x}(t))d\boldsymbol{\beta}(t)$$

These concepts will now be illustrated using, as an example, a stochastic version of the logistic population model. The deterministic logistic population model is given by the scalar nonlinear ODE

$$\dot{x}(t) = rx(t) \left(1 - \frac{x(t)}{k} \right) \quad x(t_0) = x_0 > 0 \quad (2.20)$$

In the model, $x(t)$ is some population that can be modeled with a continuous variable (a large group of individual animals, or bacteria, or the concentration of a chemical

species in a reaction). The parameter r models the growth and decay (birth and death) in the population while k models the environmental carrying capacity. Note that the population can never become negative; the population begins with a positive value. As the solution is continuous, and $\dot{x}(t) = 0$ for $x(t) = 0$, the solution must remain positive semidefinite; if the population ever drops to zero, it remains zero forever after.

Assume now that there are random effects on the rate of change of the population level due to variation in the environment that would be proportional to the population level. A Langevin form differential equation for the system could then be written as

$$\dot{x}(t) = rx(t) \left(1 - \frac{x(t)}{k}\right) + \sigma x(t)n(t), \quad x(t_0) = x_0 > 0 \quad (2.21)$$

where the volatility of the random effect is parameterized by σ and $n(t)$ is a zero mean unit variance Gaussian white noise process. This system is of interest in biology, microbiology, chemistry, mathematical modeling, and risk assessment [10, 54, 88].

If the Langevin form differential equation 2.21 is interpreted as a Stratonovich SDE, the interpretation that will be used in later chapters of this thesis, it is then written as

$$dx(t) = rx(t) \left(1 - \frac{x(t)}{k}\right) dt + \sigma x(t) \circ d\beta(t) \quad (2.22)$$

which can be converted to Itô form, yielding

$$dx(t) = rx(t) \left(1 - \frac{x(t)}{k} + \frac{\sigma^2}{2r}\right) dt + \sigma x(t) d\beta(t) \quad (2.23)$$

Alternatively, the Langevin form differential equation [2.21](#) may be interpreted as an Itô SDE, and would be written as

$$dx(t) = rx(t) \left(1 - \frac{x(t)}{k} \right) dt + \sigma x(t) d\beta(t) \quad (2.24)$$

which can be converted to Stratonovich form, yielding

$$dx(t) = rx(t) \left(1 - \frac{x(t)}{k} - \frac{\sigma^2}{2r} \right) dt + \sigma x(t) \circ d\beta(t) \quad (2.25)$$

Note that the Stratonovich interpretation of the Langevin form differential equation given by the Stratonovich SDE [2.22](#) and Itô SDE [2.23](#) are consistent with each other, but differ from the Itô interpretation of the Langevin form differential equation given by the Stratonovich SDE [2.25](#) and Itô SDE [2.24](#). The two interpretations yield distinct stochastic processes. Later sections will show these distinct stochastic processes have different stationary statistics, only one of which is physically meaningful for all possible r , k , and σ .

2.1.4 Stochastic Stability Analysis

This section discusses stability of stochastic differential equations. First, the concept of weak stochastic stability introduced by Wonham [113] is presented. Next, two Lyapunov-like theorems are discussed; these theorems will be the primary tool used in this thesis to assess stochastic stability. This section concludes with two demonstrations of the application of these stochastic Lyapunov-like theorems. First, the stochastic Lyapunov-like theorems are used to evaluate the performance of the classic LTI state observer; the resulting analysis is used to optimize the LTI state observer gain and a comparison is made to the classical analysis. Next, the stochastic logistic population model is investigated as it is an example nonlinear stochastic differential equation.

There are many notions of stability for stochastic differential equations. If one examines the origin as an equilibrium point, there are a substantial number of Lyapunov-like theorems similar in spirit to Theorem 2.1.1 available to assess the stochastic analog of asymptotic and exponential stability [43, 96] of Equation 2.14. Of course for this type of stability, it is necessary that the diffusion matrix $G(\cdot)$ be such that $G(\mathbf{x}) \rightarrow 0$ as $\mathbf{x} \rightarrow \mathbf{0}$; while this is true for the examples of Equations 2.23 and 2.24 it does not hold for any of the nonlinear attitude filters considered in this thesis.

Alternatively, there are a number of sample path boundedness Lyapunov-like theorems similar in spirit to Theorem 2.1.2. These theorems guarantee that the actual realization of the process remains within some bound with probability one

[43]. Unfortunately, even the conclusion of sample path boundedness excludes many stochastic models, even some for which all ultimate moments $\lim_{t \rightarrow \infty} E [\|\mathbf{x}(t)\|^n]$ are bounded [113].

Instead this thesis will utilize much less restrictive notions of stability, specifically the notion coined “weakly stochastically stable” by Wonham [113]. By Wonham’s definition, a process (such as the solution $\mathbf{x}(\cdot)$ of the SDE 2.14) that is weakly stochastically stable is one that admits a unique invariant probability distribution. Provided that the drift and diffusion coefficients are respectively once and twice continuously differentiable (as they will be for all systems considered in this thesis), the invariant probability distribution corresponds to a stationary (joint) probability density function $p_s(\mathbf{x})$. Symbolically, if the solution $\mathbf{x}(\cdot) = \{\mathbf{x}(t) \forall t \geq t_0\}$ to SDE 2.14 has the (instantaneous) joint probability density function $p(\mathbf{x}(t), t)$, then the statement that the SDE admits a unique invariant probability density means that $p_s(\mathbf{x})$ exists, is such that

$$\lim_{t \rightarrow \infty} p(\mathbf{x}(t), t) = p_s(\mathbf{x}) \tag{2.26}$$

and, further, that $p_s(\mathbf{x})$ is the solution to the stationary Fokker Planck PDE for the system which will be discussed in the next section. Note carefully that Wonham’s notion of weak stochastic stability differs from Khasminskii’s weak stochastic stability in probability [43] which is stronger but more restrictive.

In this thesis weak stochastic stability is established using a Lyapunov-like theorem from Zakai [114], a version of Wonham’s [113] that relaxes Wonham’s restriction on the diffusion matrix having full rank.

Theorem 2.1.4 (Zakai Stability [114]). *Let $\mathbf{x}(\cdot)$ be the solution to the Itô SDE 2.14 and $V : \mathbb{R}^n \rightarrow \mathbb{R}$ be a twice continuously differentiable function such that*

$$\alpha_1(\|\mathbf{x}(t)\|) \leq V(\mathbf{x}(t)) \leq \alpha_2(\|\mathbf{x}(t)\|) \quad (2.27)$$

where $\alpha_1(\cdot)$ and $\alpha_2(\cdot)$ are class \mathcal{K} functions and $\alpha_1(\|\mathbf{x}(t)\|) \rightarrow \infty$ as $\|\mathbf{x}(t)\| \rightarrow \infty$.

If there exist positive numbers $R_0 < \infty$ and k such that

$$\mathcal{L}V(\mathbf{x}(t)) \leq -k < 0 \quad \forall \|\mathbf{x}\| > R_0$$

then the process defined by the SDE 2.14 admits an invariant probability distribution.

If the solution to an SDE is weakly stochastically stable, it is often of interest to compute bounds on various stationary averages when they exist. The next theorem was originally derived and named by Wonham [112]. Zakai [114] later relaxed the conditions of the theorem. The theorem allows one to compute bounds on various stationary averages, also referred to as ultimate (general) moments, provided the SDE is weakly stochastically stable.

Theorem 2.1.5 (Zakai Ultimate Moment Bound [114]). *Let $\mathbf{x}(\cdot)$ be the solution to SDE 2.14 known to be weakly stochastically stable and $V : \mathbb{R}^n \rightarrow \mathbb{R}$ be a twice continuously differentiable function such that*

$$\alpha_1(\|\mathbf{x}(t)\|) \leq V(\mathbf{x}(t)) \leq \alpha_2(\|\mathbf{x}(t)\|) \quad (2.28)$$

where $\alpha_1(\cdot)$ and $\alpha_2(\cdot)$ are class \mathcal{K} functions and $\alpha_1(\|\mathbf{x}(t)\|) \rightarrow \infty$ as $\|\mathbf{x}(t)\| \rightarrow \infty$.

If there exists a positive number k and a nonnegative function $L(\mathbf{x}) : \mathbb{R}^n \rightarrow \mathbb{R}$ such that

$$\mathcal{L}V(\mathbf{x}(t)) \leq k - L(\mathbf{x}(t)) \quad \forall \mathbf{x} \in \mathbb{R}^n$$

then

$$\lim_{t \rightarrow \infty} E[L(\mathbf{x}(t))] \leq k$$

Theorem 2.1.5 can be considered as a stochastic analog of the deterministic uniform ultimate boundedness theorem of Theorem 2.1.2. Here the ultimate bound is not on the sample path, but merely on the expectation of some nonnegative function of the process, sometimes referred to as a generalized moment bound.

2.1.4.1 LTI State Observer Example

This section demonstrates the utility of stochastic Lyapunov theory for the LTI state observer. First the mathematical model of the system is presented. Then the optimal filter gain is found using classical analysis. Finally, stochastic Lyapunov analysis is applied to optimize the gain; the result from the stochastic Lyapunov analysis is compared to the result from the classical approach.

Consider the Linear Time-Invariant (LTI) system

$$\begin{aligned}\dot{\mathbf{x}}(t) &= A\mathbf{x}(t) + D\mathbf{n}_d(t) \\ \mathbf{y}(t) &= C\mathbf{x}(t) + M\mathbf{n}_m(t)\end{aligned}\tag{2.29}$$

where $\mathbf{x}(t)$ is the system state evaluated at time t , A is a matrix such that $A\mathbf{x}(t)$ describes the homogeneous dynamics of the system, and the disturbance noise $\mathbf{n}_d(\cdot)$ is a zero mean unit variance Gaussian white noise process with $E[D\mathbf{n}_d(t)\mathbf{n}_d^T(\tau)D^T] = DD^T\delta(t - \tau)$ where $\delta(t - \tau)$ is the Dirac delta function. Measurements $\mathbf{y}(t)$ of the state are assumed to be continuously available where the measurement matrix C describes the extent to which each component of the state is included in each component of the measurement, while the measurement noise $\mathbf{n}_m(\cdot)$ is a zero mean unit variance Gaussian white noise process with $E[M\mathbf{n}_m(t)\mathbf{n}_m^T(\tau)M^T] = MM^T\delta(t - \tau)$. The disturbance noise and measurement noise are assumed to be independent, $E[\mathbf{n}_d(t)\mathbf{n}_m^T(\tau)] = 0$. Further assume the usual conditions, that the pair (A, C) is detectable, the pair (A, D) is stabilizable, that MM^T is positive definite, and that DD^T is positive definite.

A fixed structure LTI state observer for the system of Equation 2.29 is given as

$$\begin{aligned}\dot{\hat{\mathbf{x}}}(t) &= A\hat{\mathbf{x}}(t) + L(\mathbf{y}(t) - \hat{\mathbf{y}}(t)) \\ &= A\hat{\mathbf{x}}(t) + L(\mathbf{y}(t) - C\hat{\mathbf{x}}(t))\end{aligned}$$

where $\hat{\mathbf{x}}(t)$ is the observer estimate of the state $\mathbf{x}(t)$ at time t and the matrix L is a gain matrix.

Defining the filter error as $\tilde{\mathbf{x}}(t) = \mathbf{x}(t) - \hat{\mathbf{x}}(t)$ yields the observer error dynamics

$$\begin{aligned}\dot{\tilde{\mathbf{x}}}(t) &= \dot{\mathbf{x}}(t) - \dot{\hat{\mathbf{x}}}(t) \\ &= (A - LC)\tilde{\mathbf{x}}(t) + D\mathbf{n}_d(t) - LM\mathbf{n}_m(t) \\ &= F\tilde{\mathbf{x}}(t) + \begin{bmatrix} D & -LM \end{bmatrix} \begin{bmatrix} \mathbf{n}_d(t) \\ \mathbf{n}_m(t) \end{bmatrix} \\ &= F\tilde{\mathbf{x}}(t) + G\mathbf{n}(t)\end{aligned}\tag{2.30}$$

where by inspection $F = A - LC$, $G = \begin{bmatrix} D & -LM \end{bmatrix}$, and $\mathbf{n}(t) = \begin{bmatrix} \mathbf{n}_d(t) \\ \mathbf{n}_m(t) \end{bmatrix}$.

Denote the estimate error covariance matrix as $P(t) = E[\tilde{\mathbf{x}}(t)\tilde{\mathbf{x}}^T(t)]$. The design goal is to choose the gain matrix L to minimize the trace of the steady state estimate error covariance matrix $P_s = \lim_{t \rightarrow \infty} P(t)$.

The classic approach to this problem is to solve the covariance matrix evolution equation in the infinite time limit. Specifically, for the LTI system of Equation 2.30 the time derivative of the covariance matrix $P(t)$ can be found by differentiating the expectation integral (including differentiating the expectation integral limits)

resulting in

$$\dot{P}(t) = FP(t) + P(t)F^T + GG^T \quad (2.31)$$

If L is chosen such that $F = A - LC$ is Hurwitz, then $\lim_{t \rightarrow \infty} \dot{P}(t) = 0$ and there exists a unique symmetric positive definite matrix $P_s = \lim_{t \rightarrow \infty} P(t)$ that solves

$$FP_s + P_sF^T = -GG^T \quad (2.32)$$

which is in the form of a stability Lyapunov equation. This specific stability Lyapunov equation is sometimes called a covariance Lyapunov equation.

So in the classical analysis the design goal of minimizing $\text{tr} \{P_s\}$ is subject to the constraint given in Equation 2.32, which can be adjoined via the Lagrange multiplier matrix Z to formulate the cost function

$$\begin{aligned} J &= \text{tr} \left\{ P_s + Z \left(FP_s + P_sF^T + GG^T \right) \right\} \\ &= \text{tr} \left\{ P_s + Z \left((A - LC)P_s + P_s(A - LC)^T + DD^T + LMM^T L^T \right) \right\} \end{aligned}$$

To minimize the cost function with respect to the filter gain L , impose the extremal conditions. The first is

$$0 = \frac{\partial J}{\partial P_s} = I + ZF + F^T Z \quad (2.33)$$

which is another stability Lyapunov equation. Since by assumption L was chosen such that $F = A - LC$ is Hurwitz, the stability Lyapunov equation guarantees the Lagrange multiplier matrix Z is symmetric and positive definite. The second extremal condition is

$$\begin{aligned} 0 &= \frac{\partial J}{\partial L} = -ZP_sC^T - Z^T P_sC^T + Z^T LMM^T + ZLMM^T \\ &= 2Z(LMM^T - P_sC^T) \end{aligned}$$

which must hold for all possible Z . Solving yields

$$L = P_s C^T (M M^T)^{-1} \quad (2.34)$$

which is the steady-state LTI Kalman filter gain. Further, substituting the optimal gain back into Equation 2.32 yields the Continuous Algebraic Riccati Equation (CARE)

$$\begin{aligned} 0 &= F P_s + P_s F^T + G G^T \\ &= (A - LC) P_s + P_s (A - LC)^T + D D^T + L M M^T L^T \\ &= A P_s + P_s A^T + D D^T - P_s C^T (M M^T)^{-1} C P_s \end{aligned}$$

The classical analysis approach required the derivation of the time evolution equation for the covariance matrix, given in Equation 2.31. In the LTI case with $F = A - LC$ Hurwitz the system is known to be weakly stochastically stable and the covariance evolution equation simplified to the covariance Lyapunov Equation 2.32. For general Itô SDEs, determination of weak stochastic stability is more involved and the time evolution of the covariance matrix may not be given as a simple matrix differential equation that is a function of the covariance matrix. For general Itô SDEs, the time evolution of the probability density function, which is given by the Fokker-Planck PDE, can be used to find the time evolution of the covariance matrix, but the Fokker-Planck PDE can be challenging to solve. More on this topic will be discussed in Section 2.1.5.

Now consider the same design goal, but utilize stochastic Lyapunov analysis. As the diffusion matrix (noise input matrix) G of Equation 2.30 is independent of the state, conversion to an Itô SDE trivially results in

$$\begin{aligned}\dot{\tilde{\mathbf{x}}}(t) &= F\tilde{\mathbf{x}}(t)dt + G\mathbf{n}(t) \\ &= \mathbf{f}(\tilde{\mathbf{x}}(t))dt + G\mathbf{n}(t)\end{aligned}\tag{2.35}$$

Let S be a symmetric positive definite matrix satisfying the stability Lyapunov equation

$$F^T S + S F = -I\tag{2.36}$$

Choose the Lyapunov function $V = \tilde{\mathbf{x}}^T(t)S\tilde{\mathbf{x}}(t)$. Then applying the differential generator with respect to the Itô SDE 2.35 yields

$$\begin{aligned}\mathcal{L}V &= \left(\frac{\partial V}{\partial \tilde{\mathbf{x}}}\right)^T \mathbf{f}(\tilde{\mathbf{x}}(t)) + \frac{1}{2} \text{tr}\left(G^T \frac{\partial^2 V}{\partial \tilde{\mathbf{x}}^2} G\right) \\ &= \tilde{\mathbf{x}}^T(t) (F^T S + S F) \tilde{\mathbf{x}}(t) + \text{tr}(G^T S G) \\ &= -\tilde{\mathbf{x}}^T(t)\tilde{\mathbf{x}}(t) + \text{tr}(D^T S D) + \text{tr}(M^T L^T S L M)\end{aligned}$$

thus application of the Zakai Stability Theorem 2.1.4 shows the system is weakly stochastically stable. Further, Zakai Ultimate Moment Bound Theorem 2.1.5 implies

$$\lim_{t \rightarrow \infty} E [\tilde{\mathbf{x}}^T(t)\tilde{\mathbf{x}}(t)] = \text{tr}(G^T S G) = \text{tr}(D^T S D) + \text{tr}(M^T L^T S L M)\tag{2.37}$$

where $\lim_{t \rightarrow \infty} E [\tilde{\mathbf{x}}^T(t)\tilde{\mathbf{x}}(t)] = \text{tr}\{P_s\}$ is the design objective to be minimized. As in the classical analysis approach, a constraint was used that must be adjoined to

the cost function for minimization

$$\begin{aligned} J &= \text{tr} \left\{ G^T S G + Z(FS + SF^T + I) \right\} \\ &= \text{tr} \left\{ D^T S D \right\} + \text{tr} \left\{ M^T L^T S L M \right\} + \text{tr} \left\{ Z((A - LC)S + S(A - LC)^T + I) \right\} \end{aligned}$$

where again Z is a Lagrange multiplier matrix. Note that in contrast to the classical analysis approach where the adjoined constraint was the covariance Lyapunov Equation 2.32, here the constraint to be adjoined is merely the stability Lyapunov Equation 2.36.

To minimize the cost function with respect to the filter gain L , impose the extremal conditions. The first is

$$\begin{aligned} 0 &= \frac{\partial J}{\partial S} = FZ + ZF^T + GG^T \\ &= (A - LC)Z + Z(A - LC)^T + DD^T + LMM^T L^T \end{aligned} \quad (2.38)$$

which recovers the covariance Lyapunov Equation 2.32 when $Z = P_s$.

The second extremal condition is

$$0 = \frac{\partial J}{\partial L} = 2S(LMM^T - ZC^T)$$

which must hold for all S . Solving for L and using $Z = P_s$ yields $L = P_s C^T (MM^T)^{-1}$ which exactly matches the result from the classical analysis technique. Further, substituting the optimal result into the extremal constraint of Equation 2.38 recovers the CARE.

Both the classical analysis and the stochastic Lyapunov analysis produced the same optimal LTI filter gain, which is the steady state Kalman filter gain. The classical analysis required L to be such that $F = A - LC$ was Hurwitz in order

to use the covariance Lyapunov Equation as a constraint in the optimization. In the stochastic Lyapunov analysis approach, the requirement that L be such that $F = A - LC$ was Hurwitz was the only condition needed to proceed with the Lyapunov analysis; the covariance Lyapunov equation was recovered as a result from the extremal condition during optimization. Note further that the stochastic Lyapunov analysis approach provided a single framework to assess weak stochastic stability as well as find the stationary statistic $\lim_{t \rightarrow \infty} E [\tilde{\mathbf{x}}^T(t)\tilde{\mathbf{x}}(t)] = \text{tr}(G^T SG)$. Finally, the stochastic Lyapunov analysis approach is applicable to nonlinear Itô SDEs. Since the stochastic Lyapunov analysis approach was able to find the Kalman filter gain for the LTI observer, this thesis will explore if the stochastic Lyapunov analysis tools can be used to find optimal “Kalman filter like” optimality results for the nonlinear attitude observer and gyro bias observer.

2.1.4.2 Stochastic Logistic Population Model Example

Consider again the stochastic logistic population model developed at the end of Section 2.1.3. The Zakai Lyapunov-like analysis techniques allow for the determination of stability of the model, as well as provide a means to bound ultimate statistics. Since the Zakai Lyapunov-like theorems are written for Itô SDEs, the following theorem will be applied to the Itô SDE 2.23 that corresponds to the Stratonovich SDE 2.22. The application of stochastic Lyapunov theory to the stochastic logistic population model appears to be unreported in the literature.

Theorem 2.1.6. *The stochastic logistic population model SDE 2.23 is weakly stochastically stable.*

Proof. Choose as a Lyapunov function $V(x(t)) = \frac{1}{2}x^2(t)$. Then

$$\begin{aligned} \mathcal{L}V(x(t)) &= -\frac{r}{k}x^3(t) + (r + \sigma^2)x^2(t) \\ &< 0 \quad \forall x(t) > \frac{k}{r}(r + \sigma^2) \end{aligned} \tag{2.39}$$

Weak stochastic stability follows from application of Theorem 2.1.4.

□

Corollary 2.1.6.1. *The stochastic logistic population model SDE 2.23 has the ultimate first moment bound*

$$\lim_{t \rightarrow \infty} E[x(t)] \leq k + \frac{k\sigma^2}{r} \tag{2.40}$$

Proof. Consider again the differential generator applied to the Lyapunov function $V(x(t)) = \frac{1}{2}x^2(t)$ in Equation 2.39. If one could find $\mathcal{L}V \leq -p_1x(t) + p_0$ for

constant p_0 and positive constant p_1 , then Theorem 2.1.5 could be used to deduce $\lim_{t \rightarrow \infty} E[x(t)] \leq \frac{p_0}{p_1}$. Thus the problem has been reduced to finding constants $p_1 > 0$ and p_0 such that $e(x(t)) \geq 0$ where

$$\begin{aligned} 0 \leq e(x(t)) &= -p_1 x(t) + p_0 - \mathcal{L}V(x(t)) \\ &= -p_1 x(t) + p_0 + \frac{r}{k} x^3(t) - (r + \sigma^2) x^2(t) \quad x(t) \geq 0 \quad \forall t > t_0 \end{aligned} \quad (2.41)$$

Lasserre [50, Thm. 2.5,p. 20] provides the sum of squares (S.O.S.) result (for a polynomial of degree 3) that $e(x) \geq 0 \quad \forall x \geq 0$ iff it can be written as

$$\begin{aligned} e(x) &= \begin{bmatrix} 1 & x \end{bmatrix} \begin{bmatrix} u_{11} & u_{12} \\ u_{12} & u_{22} \end{bmatrix} \begin{bmatrix} 1 \\ x \end{bmatrix} + x \begin{bmatrix} 1 & x \end{bmatrix} \begin{bmatrix} w_{11} & w_{12} \\ w_{12} & w_{22} \end{bmatrix} \begin{bmatrix} 1 \\ x \end{bmatrix} \\ &= \begin{bmatrix} 1 & x \end{bmatrix} U \begin{bmatrix} 1 \\ x \end{bmatrix} + x \begin{bmatrix} 1 & x \end{bmatrix} W \begin{bmatrix} 1 \\ x \end{bmatrix} \end{aligned} \quad (2.42)$$

with U, W symmetric and positive semidefinite.

Equating the two expressions from Equation 2.41 and Equation 2.42 for $e(t)$ lead to

$$w_{22} = \frac{r}{k} \quad u_{22} + 2w_{12} = -(r + \sigma^2) \quad w_{11} + 2u_{12} = -p_1 \quad u_{11} = p_0$$

Of course U is symmetric and positive semidefinite if and only if

$$u_{11} \geq 0 \quad u_{22} \geq 0 \quad u_{11}u_{22} - u_{12}^2 \geq 0$$

Similarly, W is symmetric and positive semidefinite if and only if

$$w_{11} \geq 0 \quad w_{22} \geq 0 \quad w_{11}w_{22} - w_{12}^2 \geq 0$$

Observe that actually $w_{22} > 0$ since $w_{22} = \frac{r}{k}$ and $r, k > 0$.

Combining the constraints $p_1 > 0$, $-p_{11} = w_{11} + 2u_{12}$, and $w_{11} \geq 0$ leads to the requirement

$$u_{12} < \frac{-w_{11}}{2}$$

so choose

$$u_{12} = \frac{-\phi w_{11}}{2}$$

where $\phi > 1$ is to be determined.

Combining the constraints $w_{11}w_{22} - w_{12}^2 \geq 0$, $u_{22} + 2w_{12} = -(r + \sigma^2)$, and $w_{22} = \frac{r}{k}$ leads to the requirement

$$w_{11} \geq \frac{\left(u_{22} + (r + \sigma^2)\right)^2}{4\frac{r}{k}}$$

so choose

$$w_{11} = \frac{\gamma\left(u_{22} + (r + \sigma^2)\right)^2}{4\frac{r}{k}}$$

where $\gamma \geq 1$ is to be determined.

Finally, combining the constraints $u_{11}u_{22} - u_{12}^2 \geq 0$ and $u_{11} = p_0$, and noting that $u_{22} \geq 0$ by requirement, leads to the combined requirement

$$p_0 \geq \frac{u_{12}^2}{u_{22}}$$

so choose

$$p_0 = \frac{\psi u_{12}^2}{u_{22}}$$

where $\psi \geq 1$ is to be determined.

Solving for p_0 in terms of u_{22} , ϕ , γ , and ψ results in

$$p_0 = \frac{\psi\phi^2\gamma^2\left(u_{22} + (r + \sigma^2)\right)^4}{64\frac{r^2}{k^2}u_{22}}$$

Similarly, solving for p_1 yields

$$p_1 = \frac{\gamma(\phi - 1) \left(u_{22} + (r + \sigma^2) \right)^2}{4 \frac{r}{k}}$$

By construction, if $u_{22} > 0, \phi > 0, \psi \geq 1$, and $\gamma \geq 1$ then U and W will be symmetric and positive semidefinite. This in turn implies, by Lasserre [50, Thm. 2.5,p. 20], that $e(x) \geq 0 \forall x \geq 0$. Thus by Zakai's ultimate moment bound theorem of Theorem 2.1.5

$$\lim_{t \rightarrow \infty} E[x(t)] \leq \frac{p_0}{p_1} = \frac{\psi \gamma}{16 \frac{r}{k}} \frac{\phi^2}{\phi - 1} \frac{\left(u_{22} + (r + \sigma^2) \right)^2}{u_{22}} = M(u_{22}, \phi, \psi, \gamma)$$

where $u_{22} > 0, \phi > 0, \psi \geq 1$, and $\gamma \geq 1$.

Now minimize the parameterized bound $M(u_{22}, \phi, \psi, \gamma)$ over the valid domain of the parameters. Obviously choose $\psi = \gamma = 1$ to minimize M . Taking the partial derivative with respect to ϕ reveals

$$\frac{\partial M}{\partial \phi} = \frac{\psi \gamma}{16 \frac{r}{k}} \frac{\left(u_{22} + (r + \sigma^2) \right)^2}{u_{22}} \frac{\phi(\phi - 2)}{(\phi - 1)^2}$$

The critical point $\phi = 2$ minimizes M with respect to ϕ . Taking the partial derivative with respect to u_{22} yields

$$\frac{\partial M}{\partial u_{22}} = \frac{\psi \gamma}{16 \frac{r}{k}} \frac{\phi^2}{\phi - 1} \frac{u_{22}^2 - (r + \sigma^2)^2}{u_{22}}$$

The critical point $u_{22} = r + \sigma^2$ minimizes M with respect to u_{22} .

Substituting the minimizers into the bound $M(u_{22}, \phi, \psi, \gamma)$ results in the optimal stochastic Lyapunov bound, given the choice of Lyapunov function used and SOS bounding technique employed, as

$$\lim_{t \rightarrow \infty} E[x(t)] \leq k + \frac{k}{r} \sigma^2$$

□

Corollary 2.1.6.2. *The stochastic logistic population model SDE 2.23 has the ultimate noncentral second moment bound*

$$\lim_{t \rightarrow \infty} E[x^2(t)] \leq k^2 + \frac{2k^2\sigma^2}{r} + \frac{\sigma^4 k^2}{r^2} \quad (2.43)$$

Proof. Consider again the differential generator applied to the Lyapunov function $V(x(t)) = \frac{1}{2}x^2(t)$ in Equation 2.39. If one could find $\mathcal{L}V \leq -s_2x^2(t) + s_0$ for constant s_0 and positive constant s_1 , then Theorem 2.1.5 could be used to deduce $\lim_{t \rightarrow \infty} E[x^2(t)] \leq \frac{s_0}{s_2}$. Thus the problem has been reduced to finding constants $s_2 > 0$ and s_0 such that $e(x(t)) \geq 0$ where

$$\begin{aligned} 0 \leq e(x(t)) &= -s_2x^2(t) + s_0 - \mathcal{L}V(x(t)) \\ &= -s_2x^2(t) + s_0 + \frac{r}{k}x^3(t) - (r + \sigma^2)x^2(t) \quad x(t) \geq 0 \quad \forall t > t_0 \end{aligned} \quad (2.44)$$

Again utilize the theorem from Lasserre [50, Thm. 2.5,p. 20] that the sum of squares (S.O.S.) result (for a polynomial of degree 3) that $e(x) \geq 0 \quad \forall x \geq 0$ if and only if it can be written in the form of Equation 2.42 with U, W symmetric and positive semidefinite. Equating the two expressions for $e(t)$ from Equation 2.42 and Equation 2.44 lead to

$$w_{22} = \frac{r}{k} \quad u_{22} + 2w_{12} = -\left(s_2 + (r + \sigma^2)\right) \quad w_{11} + 2u_{12} = 0 \quad u_{11} = s_0$$

As before, U is symmetric and positive semidefinite if and only if

$$u_{11} \geq 0 \quad u_{22} \geq 0 \quad u_{11}u_{22} - u_{12}^2 \geq 0$$

and W is symmetric and positive semidefinite if and only if

$$w_{11} \geq 0 \quad w_{22} \geq 0 \quad w_{11}w_{22} - w_{12}^2 \geq 0$$

where in fact $w_{22} \geq 0$ is immediately satisfied since $w_{22} > 0$ as $w_{22} = \frac{r}{k}$ and $r, k > 0$.

Combining the constraints $u_{22} + 2w_{12} = -\left(s_2 + (r + \sigma^2)\right)$ and $s_2 > 0$ leads to the requirement

$$w_{12} < \frac{-\left(u_{22} + (r + \sigma^2)\right)}{2}$$

so choose

$$w_{12} = \frac{-\gamma\left(u_{22} + (r + \sigma^2)\right)}{2}$$

where $\gamma > 1$ is to be determined.

The constraint $w_{11}w_{22} - w_{12}^2 \geq 0$, combined with the fact $w_{22} = \frac{r}{k} > 0$, implies the requirement

$$w_{11} \geq \frac{w_{12}^2}{w_{22}}$$

so choose

$$w_{11} = \frac{\phi w_{12}^2}{w_{22}}$$

where $\phi \geq 1$ is to be determined.

Impose the constraint $u_{22} > 0$; this combined with the constraint $u_{11}u_{22} - u_{12}^2 \geq 0$ implies the requirement

$$u_{11} \geq \frac{u_{12}^2}{u_{22}}$$

so choose

$$u_{11} = \frac{\psi u_{12}^2}{u_{22}}$$

where $\psi \geq 1$ is to be determined.

Solving for s_0 in terms of u_{22} , ϕ , γ , and ψ results in

$$s_0 = \frac{\psi\phi^2\gamma^4\left(u_{22} + (r + \sigma^2)\right)^4}{64u_{22}\frac{r^2}{k^2}}$$

Similarly, solving for s_2 yields

$$s_2 = (\gamma - 1)\left(u_{22} + (r + \sigma^2)\right)$$

By construction, if $u_{22} > 0$, $\gamma > 1$, $\phi \geq 1$, and $\psi \geq 1$ then U and W will be symmetric and positive semidefinite. This in turn implies, by Lasserre [50, Thm. 2.5,p. 20], that $e(x) \geq 0 \forall x \geq 0$. Thus by Zakai's ultimate moment bound theorem of Theorem 2.1.5

$$\lim_{t \rightarrow \infty} E[x(t)] \leq \frac{s_0}{s_2} = \frac{\psi\phi^2}{64\frac{r^2}{k^2}} \frac{\left(u_{22} + (r + \sigma^2)\right)^3}{u_{22}} \frac{\gamma^4}{\gamma - 1} = M(u_{22}, \phi, \psi, \gamma) \quad (2.45)$$

where $u_{22} > 0$, $\gamma > 1$, $\phi \geq 1$, and $\psi \geq 1$.

Now minimize the parameterized bound $M(u_{22}, \phi, \psi, \gamma)$ over the valid domain of the parameters. Obviously choose $\psi = \phi = 1$ to minimize M . Taking the derivative with respect to u_{22} yields

$$\frac{\partial M}{\partial u_{22}} = \frac{\psi\phi^2}{64\frac{r^2}{k^2}} \frac{\gamma^4}{\gamma - 1} \frac{2u_{22}^3 + 3(r + \sigma^2)u_{22}^2 - (r + \sigma^2)^3}{u_{22}^2}$$

The critical point $u_{22} = \frac{1}{2}(r + \sigma^2)$ minimizes M with respect to u_{22} . Taking the derivative with respect to γ results in

$$\frac{\partial M}{\partial \gamma} = \frac{\psi\phi^2}{64\frac{r^2}{k^2}} \frac{\left(u_{22} + (r + \sigma^2)\right)^3}{u_{22}} \frac{\gamma^3(3\gamma - 4)}{(\gamma - 1)^2}$$

The critical point $\gamma = \frac{4}{3}$ minimizes M with respect to γ .

Substituting the minimizers into the bound $M(u_{22}, \phi, \psi, \gamma)$ results in the optimal stochastic Lyapunov bound, given the choice of Lyapunov function used and SOS bounding technique employed, as

$$\lim_{t \rightarrow \infty} E[x^2(t)] \leq k^2 + \frac{2k^2\sigma^2}{r} + \frac{\sigma^4 k^2}{r^2}$$

□

Note that the choice of the form of the bound $\mathcal{L}V \leq -p_1x(t) + p_0$ may not result in the least upper bound for $\lim_{t \rightarrow \infty} E[x(t)]$; this choice may introduce some conservatism. Likewise, the choice of the form of the bound $\mathcal{L}V \leq -p_1x(t) + p_0$ may not result in the least upper bound for $\lim_{t \rightarrow \infty} E[x^2(t)]$. Of course, the Theorem 2.1.5 makes no claim to provide the *least* upper bound on the ultimate moment $\lim_{t \rightarrow \infty} E[L(\mathbf{x}(t))]$.

In this thesis, many of the stochastic Lyapunov moment bounds will prove to be conservative compared to other analysis techniques considered in the next section and numerical simulation results. On the other hand, for some systems considered in this thesis stochastic Lyapunov theory is the only analysis technique that has yet yielded tractable rigorous performance bounds; a conservative performance bound is more informative than no bound at all.

2.1.5 Stationary Fokker-Planck Analysis

Provided the drift and diffusion coefficients are respectively once and twice continuously differentiable, the process described by any Itô SDE of the form SDE 2.14 may also be described by the time evolution of its (joint) probability density function (pdf) notated $p(\mathbf{x}(t), t)$. The time evolution of a stochastic process's pdf is described by the Fokker-Planck equation, also known as the forward Kolmogorov equation, a second order parabolic partial differential equation (PDE). The PDE associated with SDE 2.14 is

$$\begin{aligned} \frac{\partial}{\partial t} p(\mathbf{x}(t), t) = & - \sum_i \frac{\partial}{\partial x_i} [f_i(\mathbf{x}(t)) p(\mathbf{x}(t), t)] \\ & + \frac{1}{2} \sum_i \sum_j \frac{\partial^2}{\partial x_i \partial x_j} \left[\{G(\mathbf{x}(t)) G^T(\mathbf{x}(t))\}_{ij} p(\mathbf{x}(t), t) \right] \end{aligned} \quad (2.46)$$

where $f_i(\mathbf{x}(t))$ is the i^{th} element of $\mathbf{f}(\mathbf{x}(t))$ and $\{G(\mathbf{x}(t)) G^T(\mathbf{x}(t))\}_{ij}$ is the element in the i^{th} row and the j^{th} column of the matrix $G(\mathbf{x}(t)) G^T(\mathbf{x}(t))$.

The Fokker-Planck PDE can be very challenging to solve even for very simple systems. However, if one can establish that a process is weakly stochastically stable, such as by using Theorem 2.1.4, then there exists a stationary pdf $p_s(\mathbf{x})$ such that

$$\lim_{t \rightarrow \infty} p(\mathbf{x}(t), t) = p_s(\mathbf{x}) \quad (2.47)$$

where the stationary pdf satisfies the stationary Fokker-Planck PDE

$$0 = - \sum_i \frac{\partial}{\partial x_i} [f_i(\mathbf{x}) p_s(\mathbf{x})] + \frac{1}{2} \sum_i \sum_j \frac{\partial^2}{\partial x_i \partial x_j} \left[\{G(\mathbf{x}) G^T(\mathbf{x})\}_{ij} p_s(\mathbf{x}) \right] \quad (2.48)$$

which is a simpler second order elliptic PDE. If the system is one-dimensional, the stationary Fokker-Planck PDE reduces to a second order ODE.

Even the stationary Fokker-Planck PDE can be challenging to solve. If a solution $p_s(\mathbf{x})$ can be found, however, it can be used to compute any (instantaneous) ultimate moment of the underlying process. Once again the stochastic logistic population model of SDE 2.23 will be used as an example.

Theorem 2.1.7. *The stationary Fokker-Planck PDE associated with the stochastic logistic population model described by SDE 2.23 is solved by a Gamma distribution*

$$p_s(x) = \frac{1}{\Gamma(\alpha)\theta^\alpha} x^{\alpha-1} e^{-\frac{x}{\theta}} \quad (2.49)$$

with shape parameter $\alpha = \frac{2r}{\sigma^2}$ and scale parameter $\theta = \frac{k\sigma^2}{2r}$. The ultimate distribution has the following ultimate moments

$$\lim_{t \rightarrow \infty} E[x(t)] = k \quad (2.50)$$

$$\lim_{t \rightarrow \infty} Var[x(t)] = \frac{k^2 \sigma^2}{2r} \quad (2.51)$$

Comparing the ultimate mean of Equation 2.50 from the stationary Fokker-Planck analysis with the ultimate mean bound of Equation 2.40 from the stochastic Lyapunov analysis demonstrates that while the Lyapunov analysis did provide a valid bound, there is indeed conservatism in the bound. Similarly, the ultimate variance of Equation 2.51 from the stationary Fokker-Planck analysis can be considerably less than the ultimate variance bound of Equation 2.43 from the stochastic Lyapunov analysis. However, as will be seen for many systems under consideration in this thesis, stochastic Lyapunov bounds are readily obtainable for some systems while solutions to the stationary Fokker-Planck equation may remain unknown.

The proof follows almost directly from [54], however the proof in [54] is for the Itô interpretation of the logistic population model of SDE 2.24 resulting in a slightly different Gamma distribution with

$$\begin{aligned}\lim_{t \rightarrow \infty} E[x(t)] &= k \frac{2r - \sigma^2}{2r} \\ \lim_{t \rightarrow \infty} Var[x(t)] &= \frac{k^2 \sigma^2}{2r} \frac{2r - \sigma^2}{2r}\end{aligned}\tag{2.52}$$

Note that these ultimate moments from [54] can be nonphysical as the ultimate mean can be negative if $\sigma^2 > 2r$, but the solution $x(t)$ to the SDE 2.24 is non-negative. Additionally, the ultimate variance from [54] can be negative if $\sigma^2 > 2r$, a violation of the definition of variance. These insights provide further evidence that the Stratonovich interpretation of the Langevin form differential equation is more physically meaningful. As the proof provides an demonstration of a stationary Fokker-Planck analysis and differs from [54], it is included below.

Proof. Noting that the system described by SDE 2.23 was shown to be weakly stochastically stable in Theorem 2.1.6, there exists an ultimate probability density function (stationary PDF) $p_s(x)$ such that

$$\lim_{t \rightarrow \infty} p(x(t), t) = p_s(x)$$

where $p(x(t), t)$ is the (nonstationary) pdf of the process. Furthermore, weak stochastic stability implies $p_s(x)$ solves the stationary Fokker-Planck PDE 2.46 which in the single dimension case reduces to

$$0 = -\frac{\partial}{\partial x} (f(x)p_s(x)) + \frac{1}{2} \frac{\partial^2}{\partial x^2} (G^2(x)p_s(x))$$

where $f(x) = rx \left(1 - \frac{x}{k} + \frac{\sigma^2}{2r}\right)$ and $G(x) = \sigma x$.

Integrating the stationary Fokker-Planck equation once yields

$$c = -f(x)p_s(x) + \frac{1}{2} \frac{\partial}{\partial x} (G^2(x)p_s(x))$$

where c is a constant of integration. Since $p_s(x)$ is a pdf, it obeys the normalization constraint $\int_{-\infty}^{\infty} p_s(x)dx = 1$. The normalization constraint implies that $p_s(x) \rightarrow 0$ as $x \rightarrow \infty$, which in turn implies $c = 0$. Thus

$$f(x)p_s(x) = \frac{1}{2} \frac{\partial}{\partial x} (G^2(x)p_s(x))$$

Substituting in the expressions for $f(x)$, $G(x)$, taking the partial derivative, and rearranging to separate variables yields

$$\frac{dp_s}{p_s} = \left(\frac{2r - \sigma^2}{\sigma^2} \frac{1}{x} - \frac{2r}{k\sigma^2} \right) dx$$

Integrating yields

$$\ln(p_s(x)) = \frac{2r - \sigma^2}{\sigma^2} \ln(x) - \frac{2r}{k\sigma^2} x + c_2$$

where c_2 is another constant of integration. Exponentiating yields

$$p_s(x) = c_3 x^{\frac{2r - \sigma^2}{\sigma^2}} e^{-\frac{2r}{k\sigma^2} x}$$

where $c_3 = e^{c_2}$. By choosing $\alpha = \frac{2r}{\sigma^2}$, $\theta = \frac{k\sigma^2}{2r}$, and $c_3 = \frac{1}{\Gamma(\alpha)\theta^\alpha}$ the stationary PDF can be rewritten as

$$p_s(x) = \frac{1}{\Gamma(\alpha)\theta^\alpha} x^{\alpha-1} e^{-\frac{x}{\theta}}$$

which is a Gamma distribution with shape parameter α and scale parameter θ .

The mean of the Gamma distribution is given by $\alpha\theta$, so

$$\lim_{t \rightarrow \infty} E[x(t)] = \int_0^{\infty} xp_s(x)dx = \alpha\theta = k$$

Similarly, the variance of the Gamma distribution is given by $\alpha\theta^2$, resulting in

$$\lim_{t \rightarrow \infty} Var[x(t)] = \alpha\theta^2 = \frac{k^2\sigma^2}{2r}$$

□

The key descriptions associated with the stochastic logistic population model are collected in Figure 2.2. Note carefully that the two interpretations of the Langevin form differential equation lead to distinct stochastic processes. The two stochastic processes may each be described by an Itô SDE, a Stratonovich SDE, or a Fokker-Planck PDE. For the stochastic logistic population model, stochastic Lyapunov analysis was able to establish weak stochastic stability and provide ultimate bounds on the mean and variance of the process(es), though these bounds are conservative. A stationary Fokker-Planck analysis led to the analytic stationary probability density function which was used to calculate the precise ultimate mean and variance of the process(es). The values differ for the different processes.

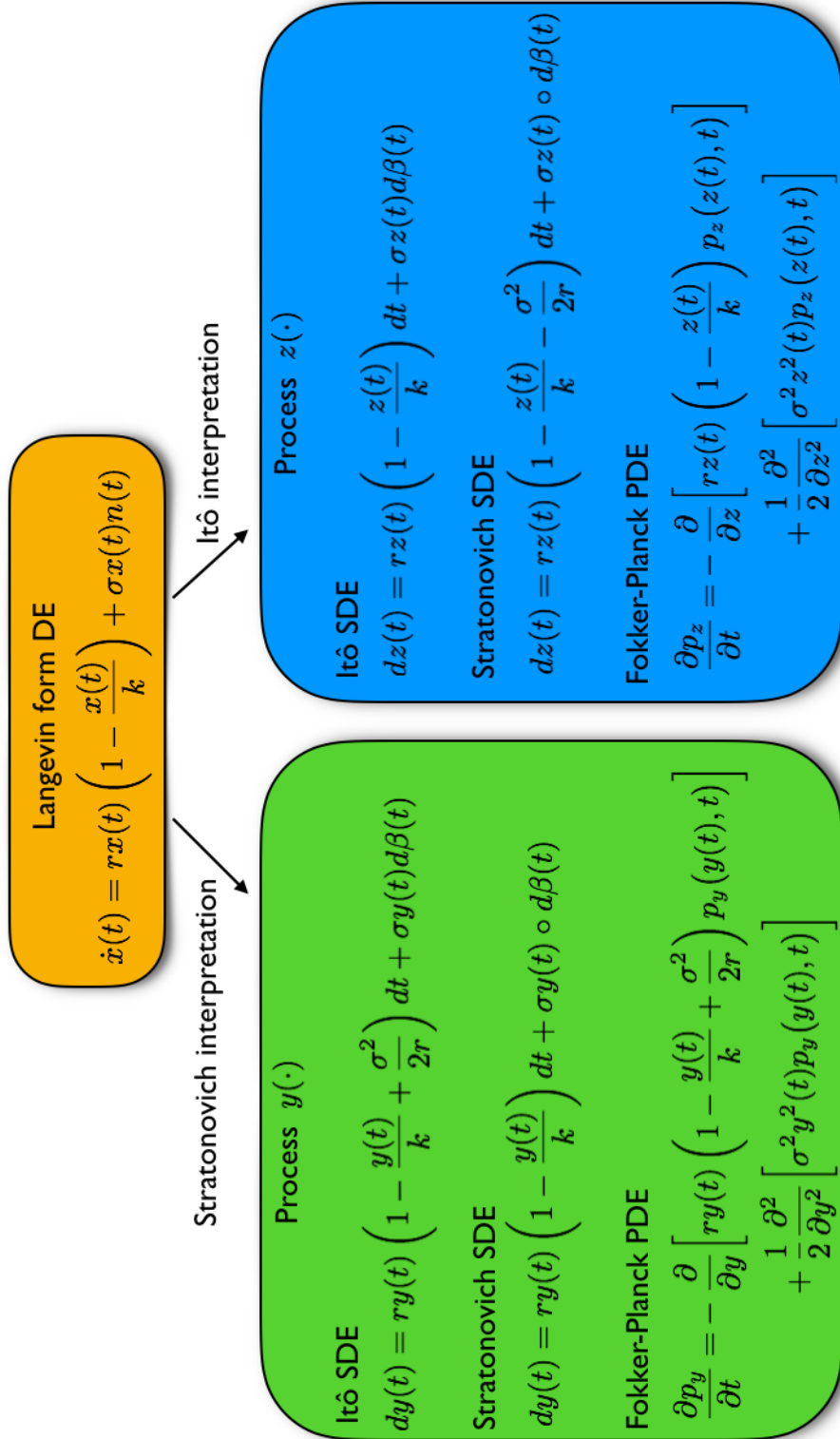


Figure 2.2: SDEs and PDEs associated with the two interpretations of the Langevin form differential equation for the stochastic logistic population model.

2.2 Numerical Integration of Nonlinear SDEs

Numerical simulation can be used to validate analytical results from a stochastic Lyapunov analysis or stationary Fokker-Planck analysis. In this context, the numerical integration of an SDE for a given noise realization is a simulation of the stochastic process. By repeating the simulation many times with distinct noise realizations (by, for example, changing the seed of the random number generator), one can perform a Monte Carlo analysis. Statistics over the ensemble of simulation realizations can then be compared to analytical predictions.

This section briefly reviews several numerical integration techniques to integrate a general multidimensional nonlinear Itô stochastic differential equation [2.14](#) repeated here for convenience:

$$d\mathbf{x}(t) = \mathbf{f}(\mathbf{x}(t))dt + G(\mathbf{x}(t))d\boldsymbol{\beta}(t) \quad (2.53)$$

with the initial condition $\mathbf{x}(t_a) = \mathbf{x}_a$ over a time interval $t_a \leq t \leq t_b$. All the numerical integration techniques that are considered in this section are fixed step, meaning the time interval $t_a \leq t \leq t_b$ is divided into a regular partition

$$\begin{aligned} & \left\{ t_0, t_1, t_2, \dots, t_i, \dots, t_N \right\} \\ & = \left\{ t_a, t_a + \Delta t, t_a + 2\Delta t, \dots, t_a + i\Delta t, \dots, t_a + N\Delta t \right\} \end{aligned} \quad (2.54)$$

with time increments $\Delta t = \frac{t_i - t_{i-1}}{N}$ and $t_N = t_b$.

The section concludes with a comparison of the performance of the techniques using the logistic population SDE of Equation [2.23](#).

2.2.1 Runge-Kutta fixed-step Integration Scheme

The fixed-step 4th order Runge-Kutta numerical integration scheme, often referred to as simply *the* Runge-Kutta numerical integration algorithm, is widely used and works well for many ordinary differential equations (ODEs). For the deterministic multivariate ODE

$$\dot{\mathbf{x}}(t) = \mathbf{h}(\mathbf{x}(t), t) \quad \mathbf{x}(t_0) = \mathbf{x}_0 \quad (2.55)$$

the fixed-step 4th order Runge-Kutta numerical integration scheme approximates the solution $\mathbf{x}(t_i)$ with \mathbf{y}_i using the recursive rule

$$\mathbf{y}_{i+1} = \mathbf{y}_i + \frac{\Delta t}{6} (\mathbf{k}_1 + 2\mathbf{k}_2 + 2\mathbf{k}_3 + \mathbf{k}_4) \quad (2.56)$$

where

$$\begin{aligned} \mathbf{k}_1 &= \mathbf{h}(t_i, \mathbf{y}_i) \\ \mathbf{k}_2 &= \mathbf{h}\left(\mathbf{y}_i + \frac{\Delta t}{2}\mathbf{k}_1, t_i + \frac{\Delta t}{2}\right) \\ \mathbf{k}_3 &= \mathbf{h}\left(\mathbf{y}_i + \frac{\Delta t}{2}\mathbf{k}_2, t_i + \frac{\Delta t}{2}\right) \\ \mathbf{k}_4 &= \mathbf{h}(t_i + \Delta t, \mathbf{y}_i + \Delta t\mathbf{k}_3) \end{aligned}$$

and $\mathbf{y}_a = \mathbf{x}(t_a)$. The algorithm gets its name as it is a 4th order method, meaning that $\mathbf{y}_N - \mathbf{x}(t_N) = O((\Delta t)^4)$ [90].

It can be tempting to utilize the 4th order Runge-Kutta numerical integration scheme for the numerical integration of SDEs by treating the Brownian noise increment as simply a time varying input to a deterministic ODE. This heuristic scheme could be implemented as follows.

First generate a standard Brownian motion process over a refined partition of solution approximation's time partition 2.54 by setting $\beta(t_a) = \mathbf{0}$ and computing values of

$$\left\{ \beta(t_a), \beta\left(t_a + \frac{\Delta t}{2}\right), \beta(t_a + \Delta t), \beta\left(t_a + \frac{3\Delta t}{2}\right), \dots, \beta(t_b) \right\}$$

according to

$$\begin{aligned} \beta\left(t_i + \frac{\Delta t}{2}\right) &= \beta(t_i) + \mathbf{n}_i \\ \beta(t_{i+1}) &= \beta\left(t_i + \frac{\Delta t}{2}\right) + \mathbf{n}_{i+\frac{1}{2}} \end{aligned}$$

where \mathbf{n}_i and $\mathbf{n}_{i+\frac{1}{2}}$ are independent identically distributed Gaussian random variables with zero mean and variance $\Delta t I$.

One might then apply a fixed-step 4th order Runge-Kutta numerical integration technique to the SDE 2.53 by setting $\mathbf{y}_0 = \mathbf{x}_a$ and using the recursive rule

$$\mathbf{y}_{i+1} = \mathbf{y}_i + \frac{\Delta t}{6} (\mathbf{k}_1 + 2\mathbf{k}_2 + 2\mathbf{k}_3 + \mathbf{k}_4) \quad (2.57)$$

where

$$\begin{aligned} \mathbf{k}_1 &= \mathbf{f}(\mathbf{y}_i) \\ \mathbf{k}_2 &= \mathbf{f}\left(\mathbf{y}_i + \frac{\Delta t}{2}\mathbf{k}_1\right) + \beta\left(t_i + \frac{\Delta t}{2}\right) - \beta(t_i) \\ \mathbf{k}_3 &= \mathbf{f}\left(\mathbf{y}_i + \frac{\Delta t}{2}\mathbf{k}_2\right) + \beta\left(t_i + \frac{\Delta t}{2}\right) - \beta(t_i) \\ \mathbf{k}_4 &= \mathbf{f}(\mathbf{y}_i + \Delta t\mathbf{k}_3) + \beta(t_i + \Delta t) - \beta(t_i) \end{aligned}$$

As explained in [45, p. 150] however, heuristic generalizations of Runge-Kutta algorithms are not consistent with Itô calculus and in general their approximations \mathbf{y}_i

do not converge to the true process $\mathbf{x}(t_a+i\Delta t)$ as step size Δt is reduced. As will soon be demonstrated for a test problem, even the simple yet rigorously justified Euler-Maruyama integration scheme outperforms this heuristic Runge-Kutta algorithm for many systems.

2.2.2 Euler-Maruyama Integration Scheme

The Euler-Maruyama numerical integration scheme is given by the simple rule

$$\mathbf{y}_{i+1} = \mathbf{y}_i + \Delta t \mathbf{f}(\mathbf{y}_i, t_i) + G(\mathbf{y}_i, t_i) \mathbf{n}_i \quad (2.58)$$

where \mathbf{n}_i is a collection of independent identically distributed Gaussian random variables with zero mean and variance matrix $\Delta t I$. The scheme works directly for nonautonomous SDEs [45].

This scheme has strong convergence of order 0.5, meaning there exists a positive constant c_1 such that for all i

$$E\left[|\mathbf{x}(t_i) - \mathbf{y}_i|\right] \leq c_1 (\Delta t)^{0.5} \quad (2.59)$$

where $t_i = t_0 + i\Delta t$. In words, this quantifies the rate of convergence of the numerical approximation to the true process (also known as the rate of pathwise convergence).

Further, assuming $\mathbf{f}(\cdot)$ and $G(\cdot)$ are sufficiently smooth, the Euler-Maruyama scheme has weak convergence of order 1.0, meaning there exists a positive constant c_2 such that for all i

$$\left|E[p(\mathbf{x}(t_i))] - E[p(\mathbf{y}_i)]\right| \leq c_2 (\Delta t)^{1.0} \quad (2.60)$$

for any polynomial $p(\cdot) : \mathbb{R}^n \rightarrow \mathbb{R}$. Weak convergence is in the sense that the numerical approximation may not exactly match the sample path of the true process, but since the definition requires the bound to hold for any polynomial $p(\cdot)$ it is implied that all moments of the numerical approximation converge to all moments of the sample path of the true process [45, p. 128].

2.2.3 Kloeden-Platen Explicit Weak 2.0 Integration Scheme

The Kloeden-Platen Explicit Weak 2.0 [45, p. 186] integration scheme is one of the few schemes available for obtaining higher order statistics for nonlinear autonomous SDEs without requiring the computation of derivatives of the drift and diffusion terms of the SDE. The integration rule is given by

$$\begin{aligned}
\mathbf{y}_{i+1} = & \mathbf{y}_i + \frac{1}{2} \left(\mathbf{f}(\mathbf{\Upsilon}) + \mathbf{f}(\mathbf{y}_i) \right) \Delta t \\
& + \frac{1}{4} \sum_{j=1}^m \left[\left(G^j(\mathbf{r}_+^j) + G^j(\mathbf{r}_-^j) + 2G^j(\mathbf{y}_i) \right) \Delta w_i^j \right. \\
& \quad \left. + \sum_{k=1, k \neq j}^m \left(G^j(\mathbf{u}_+^k) + G^j(\mathbf{u}_-^k) - 2G^j(\mathbf{y}_i) \right) \Delta w_i^j \frac{1}{\sqrt{\Delta t}} \right] \\
& + \frac{1}{4} \sum_{j=1}^m \left[\left(G^j(\mathbf{r}_+^j) - G^j(\mathbf{r}_-^j) \right) \left\{ (\Delta w_i^j)^2 - \Delta t \right\} \right. \\
& \quad \left. + \sum_{k=1, k \neq j}^m \left(G^j(\mathbf{u}_+^k) - G^j(\mathbf{u}_-^k) \right) \left\{ \Delta w_i^j \Delta w_i^k + V_{k,j} \right\} \right] \frac{1}{\sqrt{\Delta t}} \quad (2.61)
\end{aligned}$$

where

$$\mathbf{\Upsilon} = \mathbf{y}_i + \mathbf{f}(\mathbf{y}_i) \Delta t + \sum_{j=1}^m G^j(\mathbf{y}_i) \Delta w_i^j$$

$$\mathbf{r}_\pm^j = \mathbf{y}_i + \mathbf{f}(\mathbf{y}_i) \Delta t \pm G^j(\mathbf{y}_i) \sqrt{\Delta t}$$

$$\mathbf{u}_\pm^j = \mathbf{y}_i \pm G^j(\mathbf{y}_i) \sqrt{\Delta t}$$

and m is the spatial dimension of $d\boldsymbol{\beta}$ or, equivalently, the number of columns of $G(\cdot)$. In the above equations, $G^j(\cdot)$ denotes the j^{th} column of $G(\cdot)$.

At every time step i , the column matrix $\Delta\boldsymbol{w}_i = [\Delta w_i^1 \quad \Delta w_i^2 \quad \dots \quad \Delta w_i^m]^T$ consists of m independent identically distributed random variables Δw_i^j drawn from a three point distribution with

$$P(\Delta w_i^j = \sqrt{3\Delta t}) = \frac{1}{6} \quad P(\Delta w_i^j = -\sqrt{3\Delta t}) = \frac{1}{6} \quad P(\Delta w_i^j = 0) = \frac{2}{3}$$

Also at every time step i , the V_{j_1, j_2} are independent two point distributed random variables with

$$P(V_{j_1, j_2} = \Delta t) = \frac{1}{2} \quad P(V_{j_1, j_2} = -\Delta t) = \frac{1}{2}$$

for $j_2 = 1, 2, \dots, j_1 - 1$,

$$V_{j_1, j_1} = -\Delta t$$

and

$$V_{j_1, j_2} = -V_{j_2, j_1}$$

for $j_2 = j_1 + 1, \dots, m$ and $j_1 = 1, 2, \dots, m$.

While this numerical integration scheme is not strongly convergent, it has weak convergence of order 2.0, meaning there exists a positive constant c_3 such that for all i

$$\left| E[p(\boldsymbol{x}(t_i))] - E[p(\boldsymbol{y}_i)] \right| \leq c_3 (\Delta t)^{2.0} \quad (2.62)$$

Therefore the statistical properties of the approximation from this scheme converge much faster to the statistical properties of the true system than the approximation from the Euler-Maruyama integration scheme.

2.2.4 Numerical Integration Performance Comparison

This section features a comparison of the performance of the ad hoc Runge-Kutta 4th order scheme of Equation 2.57, the Euler-Maruyama scheme of Equation 2.58, the Kloeden-Platen Explicit Weak 2.0 scheme of Equation 2.61, and MATLAB's `ode45` command using default options for the stochastic logistic population model of SDE 2.23. The performance of these numerical integration schemes are further compared against analytic stochastic Lyapunov bounds of Corollaries 2.1.6.1 and 2.1.6.2 and the known analytic ultimate expectations of Theorem 2.1.7. These results provide context on performance and will provide a rationale for the selection of the numerical methods employed in this thesis.

Specifically, 100 distinct realizations of the process were numerically simulated with each of the numerical integration schemes. Each simulation realization is computed with 1,000,000 steps with a step size of $\Delta t = 0.001s$ for a 1,000 second simulation. The mean, variance, and second noncentral moment of the last 100 seconds are then computed. Finally, the ensemble mean for each integration scheme is computed by averaging the means and variances of each realization for the given integration scheme. All simulations used the parameters $r = 6$, $k = 20$, $\sigma = 2$, and initial condition $x(t_0) = 5$. The results are reported in Table 2.1.

First note the significant conservatism in the stochastic Lyapunov bounds compared to the analytic values from the stationary Fokker-Planck analysis. There is no guarantee that the bounds from a stochastic Lyapunov analysis will be “tight”, and various choices of Lyapunov functions and bounds on the expectation of the

Table 2.1: Comparison of the performance of the SDE numerical integration schemes of Kloeden-Platen Explicit Weak 2.0 of Equation 2.61, the Euler-Maruyama scheme of Equation 2.58, the fixed-step ad-hoc Runge-Kutta algorithm of Equation 2.57, and MATLAB's ode45 utility for simulating the stochastic logistic population model of SDE 2.23 to the stochastic Lyapunov upper bounds of Corollaries 2.1.6.1 and 2.1.6.2 and the analytic ultimate expectations of Theorem 2.1.7.

	$\lim_{t \rightarrow \infty} E[x(t)]$	$\lim_{t \rightarrow \infty} Var[x(t)]$	$\lim_{t \rightarrow \infty} E[x^2(t)]$
Lyap UB	33.333	-	1111.111
Analytic Sol	20.000	133.333	533.333
	$\text{Mean}_{sims} \left[\text{Mean}_{t_i \in T_{ss}} [x(t_i)] \right]$	$\text{Mean}_{sims} \left[\text{Var}_{t_i \in T_{ss}} [x(t_i)] \right]$	$\text{Mean}_{sims} \left[\text{Mean}_{t_i \in T_{ss}} [x^2(t_i)] \right]$
Kloeden-Platen	19.979	133.307	532.921
Euler-Maruyama	20.014	133.772	534.624
Runge-Kutta	25.466	93.491	742.302
MATLAB ode45	26.635	0.471	709.878

stochastic derivative will yield different ultimate moment bounds.

The Kloeden-Platen Explicit Weak 2.0 scheme and the Euler-Maruyama scheme have very similar performance and have excellent agreement with the analytic ultimate statistics. It is tempting to suggest the Euler-Maruyama approach over the Kloeden-Platen scheme, but this table does not indicate the performance as the step size Δt is increased. In practice the Euler-Maruyama scheme is not as numerically robust to large step sizes and rapidly diverges. When comparing the two approaches, there is a tradeoff between the computational complexity of the Kloeden-Platen scheme and the worse step size robustness of the Euler-Maruyama scheme. It is common to require step sizes that are several orders of magnitude smaller for the Euler-Maruyama scheme to remain numerically stable compared to the Kloeden-Platen scheme.

Finally, observe the poor performance of the ad hoc Runge-Kutta scheme of Equation 2.57 and MATLAB's `ode45` utility. These algorithms did manage to produce estimates of the stationary mean that were within 30% of the analytic expectation, but that is far worse than the SDE numerical integrators' performances. The Runge-Kutta algorithms were off dramatically for the stationary variance, a 2^{nd} order statistic. The ad hoc Runge-Kutta's stationary variance estimate was off by 50% while MATLAB's `ode45` was off by several orders of magnitude.

Throughout the remainder of this thesis, any simulation results are the product of a C implementation of the Kloeden-Platen Explicit Weak 2.0 integration scheme. The implementation utilizes the GNU scientific library (GSL [2]) which has optimized basic linear algebra routines (through BLAS [1] and LAPACK [3]). Data

is output to `.mat` files using the `matio` library [4]. All simulations were validated via comparison with MATLAB implementations of both the Kloeden-Platen Explicit Weak 2.0 and the Euler-Maruyama schemes.

2.3 Attitude Kinematics Overview

This section reviews basic spacecraft attitude kinematics. The presentation begins with rotational motion in three spatial dimensions, referred to as the SO(3) case, which is fundamental to the mathematical description of the systems considered in this thesis. Then the SO(2) case is discussed, in which motion will be restricted to a single spin axis.

2.3.1 Attitude Kinematics in SO(3)

The attitude of a rigid body can be represented by a unit quaternion \mathbf{q} , consisting of a unit vector \mathbf{a} known as the Euler axis and a rotation ϕ about that axis, which is such that

$$\mathbf{q} = \begin{bmatrix} \mathbf{a} \sin\left(\frac{\phi}{2}\right) \\ \cos\left(\frac{\phi}{2}\right) \end{bmatrix} = \begin{bmatrix} \boldsymbol{\varepsilon} \\ \eta \end{bmatrix} = \begin{bmatrix} \varepsilon_x \\ \varepsilon_y \\ \varepsilon_z \\ \eta \end{bmatrix} \quad (2.63)$$

It is typical in spacecraft attitude applications for the quaternion \mathbf{q} to represent the orientation of the spacecraft's body-fixed reference frame relative to an inertially-fixed reference frame. Specifically, the unit quaternion \mathbf{q} parameterizes the attitude rotation matrix via

$$\begin{aligned} R(\mathbf{q}) &= (\eta^2 - \boldsymbol{\varepsilon}^T \boldsymbol{\varepsilon}) I - 2\eta [\boldsymbol{\varepsilon} \times] + 2\boldsymbol{\varepsilon} \boldsymbol{\varepsilon}^T \\ &= \eta^2 I - 2\eta [\boldsymbol{\varepsilon} \times] + \boldsymbol{\varepsilon} \boldsymbol{\varepsilon}^T + [\boldsymbol{\varepsilon} \times] [\boldsymbol{\varepsilon} \times] \end{aligned} \quad (2.64)$$

where I is the identity matrix and the skew-symmetric cross product matrix is given as

$$[\boldsymbol{\varepsilon} \times] = \begin{bmatrix} 0 & -\varepsilon_z & \varepsilon_y \\ \varepsilon_z & 0 & -\varepsilon_x \\ -\varepsilon_y & \varepsilon_x & 0 \end{bmatrix}$$

The inverse relationship, which is rather more involved, is given in [65]. The attitude rotation matrix $R(\mathbf{q})$ is such that a vector expressed in inertial frame coordinates \mathbf{v}_n and the same vector in body frame coordinates \mathbf{v}_b are related via $\mathbf{v}_b = R(\mathbf{q}) \mathbf{v}_n$. While the space of unit quaternions is a global non-singular covering of the space of rotations in $SO(3)$, there is a well known 2-to-1 mapping between unit quaternions and rotations. Specifically, $R(\mathbf{q}) = R(-\mathbf{q})$. Note that the identity rotation matrix is parameterized by $\mathbf{q}_{Identity} = [0 \ 0 \ 0 \ \pm 1]^T$ which is called the identity quaternion.

The quaternion inverse, given by

$$\mathbf{q}^{-1} = \begin{bmatrix} -\boldsymbol{\varepsilon} \\ \eta \end{bmatrix} \quad (2.65)$$

is such that

$$R(\mathbf{q}) R(\mathbf{q}^{-1}) = R(\mathbf{q}) R^{-1}(\mathbf{q}) = I = R^{-1}(\mathbf{q}) R(\mathbf{q}) = R(\mathbf{q}^{-1}) R(\mathbf{q})$$

For any two quaternions \mathbf{q}_1 and \mathbf{q}_2 , the quaternion product operation is defined

[66] as

$$\begin{aligned} \mathbf{q}_1 \otimes \mathbf{q}_2 &= \begin{bmatrix} \boldsymbol{\varepsilon}_1 \\ \eta_1 \end{bmatrix} \otimes \begin{bmatrix} \boldsymbol{\varepsilon}_2 \\ \eta_2 \end{bmatrix} \\ &= \begin{bmatrix} \eta_2 \boldsymbol{\varepsilon}_1 + \eta_1 \boldsymbol{\varepsilon}_2 + \boldsymbol{\varepsilon}_1 \times \boldsymbol{\varepsilon}_2 \\ \eta_1 \eta_2 - \boldsymbol{\varepsilon}_1^T \boldsymbol{\varepsilon}_2 \end{bmatrix} = \begin{bmatrix} \eta_1 I + [\boldsymbol{\varepsilon}_1 \times] & \boldsymbol{\varepsilon}_1 \\ -\boldsymbol{\varepsilon}_1^T & \eta_1 \end{bmatrix} \begin{bmatrix} \boldsymbol{\varepsilon}_2 \\ \eta_2 \end{bmatrix} \end{aligned} \quad (2.66)$$

Note that this quaternion product is adopted from [51, 66] where the quaternions are multiplied in the same order as rotation matrix multiplication; this definition is in contrast to the original quaternion product established by Hamilton [30]. The quaternion product may be used to compute the relative orientation $\tilde{\mathbf{q}}$ between the coordinate frames represented by \mathbf{q} and $\hat{\mathbf{q}}$

$$\tilde{\mathbf{q}} = \begin{bmatrix} \tilde{\boldsymbol{\varepsilon}} \\ \tilde{\eta} \end{bmatrix} = \mathbf{q} \otimes \hat{\mathbf{q}}^{-1} = \begin{bmatrix} \boldsymbol{\varepsilon} \\ \eta \end{bmatrix} \otimes \begin{bmatrix} -\hat{\boldsymbol{\varepsilon}} \\ \hat{\eta} \end{bmatrix}$$

The quaternion product operation is not restricted to unit quaternions [66].

It will frequently be used to compute the product between angular rate vectors and quaternions:

$$\boldsymbol{\omega} \otimes \mathbf{q} = \begin{bmatrix} \boldsymbol{\omega} \\ 0 \end{bmatrix} \otimes \mathbf{q} = \begin{bmatrix} \boldsymbol{\omega} \\ 0 \end{bmatrix} \otimes \begin{bmatrix} \boldsymbol{\varepsilon} \\ \eta \end{bmatrix} = \begin{bmatrix} \eta \boldsymbol{\omega} - \boldsymbol{\omega} \times \boldsymbol{\varepsilon} \\ -\boldsymbol{\omega}^T \boldsymbol{\varepsilon} \end{bmatrix}$$

and similarly $\mathbf{q} \otimes \boldsymbol{\omega} = \mathbf{q} \otimes \begin{bmatrix} \boldsymbol{\omega} \\ 0 \end{bmatrix}$. The quaternion product is also useful for changing the coordinate frame of expression for a vector:

$$\begin{bmatrix} \mathbf{v}_b \\ 0 \end{bmatrix} = \begin{bmatrix} R(\mathbf{q}) \mathbf{v}_n \\ 0 \end{bmatrix} = \mathbf{q} \otimes \begin{bmatrix} \mathbf{v}_n \\ 0 \end{bmatrix} \otimes \mathbf{q}^{-1} = \mathbf{q} \otimes \mathbf{v}_n \otimes \mathbf{q}^{-1}$$

Orientation kinematics, such as that of a rigid body spacecraft, are known [103]

to obey

$$\begin{aligned}\dot{\mathbf{q}}(t) &= \frac{1}{2}\boldsymbol{\omega}(t) \otimes \mathbf{q}(t) = \begin{bmatrix} \frac{1}{2}\eta(t)\boldsymbol{\omega}(t) - \frac{1}{2}\boldsymbol{\omega}(t) \times \boldsymbol{\varepsilon}(t) \\ -\frac{1}{2}\boldsymbol{\omega}^T(t)\boldsymbol{\varepsilon}(t) \end{bmatrix} \\ &= \begin{bmatrix} \frac{1}{2}\left\{\eta(t)I + [\boldsymbol{\varepsilon}(t) \times]\right\} \\ -\frac{1}{2}\boldsymbol{\varepsilon}^T(t) \end{bmatrix} \boldsymbol{\omega}(t) = \begin{bmatrix} -\frac{1}{2}[\boldsymbol{\omega}(t) \times] & \frac{1}{2}\boldsymbol{\omega}(t) \\ -\frac{1}{2}\boldsymbol{\omega}^T(t) & 0 \end{bmatrix} \mathbf{q}(t) \end{aligned} \quad (2.67)$$

where $\boldsymbol{\omega}(t)$ is the body's angular rate expressed in body frame coordinates.

This thesis will consider several attitude estimation observers and filters. These algorithms will utilize estimates $\hat{\mathbf{q}}(t)$ of the true attitude $\mathbf{q}(t)$ which are driven by their own kinematic relationship

$$\dot{\hat{\mathbf{q}}}(t) = \frac{1}{2}\hat{\boldsymbol{\omega}}(t) \otimes \hat{\mathbf{q}}(t) \quad (2.68)$$

Noting that $\hat{\mathbf{q}}(t) \otimes \hat{\mathbf{q}}^{-1}(t) = \mathbf{q}_{Identity} \forall t$, one can take the derivative to find

$$0 = \dot{\hat{\mathbf{q}}}(t) \otimes \hat{\mathbf{q}}^{-1}(t) + \hat{\mathbf{q}}(t) \otimes \frac{d}{dt}(\hat{\mathbf{q}}^{-1}(t))$$

which can be rearranged to solve for $\frac{d}{dt}(\hat{\mathbf{q}}^{-1}(t))$

$$\begin{aligned}\frac{d}{dt}(\hat{\mathbf{q}}^{-1}(t)) &= -\hat{\mathbf{q}}^{-1}(t) \otimes \dot{\hat{\mathbf{q}}}(t) \otimes \hat{\mathbf{q}}^{-1}(t) \\ &= -\frac{1}{2}\hat{\mathbf{q}}^{-1}(t) \otimes \hat{\boldsymbol{\omega}}(t) \end{aligned} \quad (2.69)$$

The attitude observer or filter error, denoted $\tilde{\mathbf{q}}(t)$, is computed as

$$\tilde{\mathbf{q}}(t) = \mathbf{q}(t) \otimes \hat{\mathbf{q}}^{-1}(t) \quad (2.70)$$

The error kinematics are then given by

$$\begin{aligned}
\dot{\hat{\mathbf{q}}}(t) &= \dot{\mathbf{q}}(t) \otimes \hat{\mathbf{q}}^{-1}(t) + \mathbf{q}(t) \otimes \frac{d}{dt} \left(\hat{\mathbf{q}}^{-1}(t) \right) \\
&= \frac{1}{2} \boldsymbol{\omega}(t) \otimes \mathbf{q}(t) \otimes \hat{\mathbf{q}}^{-1}(t) - \frac{1}{2} \mathbf{q}(t) \otimes \hat{\mathbf{q}}^{-1}(t) \otimes \hat{\boldsymbol{\omega}}(t) \\
&= \frac{1}{2} \boldsymbol{\omega}(t) \otimes \tilde{\mathbf{q}}(t) - \frac{1}{2} \tilde{\mathbf{q}}(t) \otimes \hat{\boldsymbol{\omega}}(t) \otimes \tilde{\mathbf{q}}^{-1}(t) \otimes \tilde{\mathbf{q}}(t) \\
&= \frac{1}{2} \boldsymbol{\omega}(t) \otimes \tilde{\mathbf{q}}(t) - \frac{1}{2} \left\{ R(\tilde{\mathbf{q}}(t)) \hat{\boldsymbol{\omega}}(t) \right\} \otimes \tilde{\mathbf{q}}(t) \\
&= \frac{1}{2} \left\{ \boldsymbol{\omega}(t) - R(\tilde{\mathbf{q}}(t)) \hat{\boldsymbol{\omega}}(t) \right\} \otimes \tilde{\mathbf{q}}(t) \tag{2.71}
\end{aligned}$$

As shown in [31], orientation kinematics may also be expressed directly in the Euler axis and angle parameterization, providing an alternative (yet equivalent) formulation to Equation 2.67. Recalling from Equation 2.63 that the Euler axis is denoted $\mathbf{a}(t)$ and the Euler angle is $\phi(t)$, the kinematics may be written as

$$\begin{aligned}
\dot{\mathbf{a}}(t) &= \frac{1}{2} \left[[\mathbf{a}(t) \times] - \cot \left(\frac{\phi(t)}{2} \right) [\mathbf{a}(t) \times] [\mathbf{a}(t) \times] \right] \boldsymbol{\omega}(t) \\
\dot{\phi}(t) &= \mathbf{a}^T(t) \boldsymbol{\omega}(t) \tag{2.72}
\end{aligned}$$

2.3.2 Attitude Kinematics in SO(2)

Many of the analyses in this thesis will be restricted to rotational motion about a single axis. Without loss of generality, the attitude of a single axis rigid body can be parameterized via the quaternion

$$\mathbf{q} = \begin{bmatrix} \sin\left(\frac{\phi}{2}\right) \\ 0 \\ 0 \\ \cos\left(\frac{\phi}{2}\right) \end{bmatrix} = \begin{bmatrix} \varepsilon \\ 0 \\ 0 \\ \eta \end{bmatrix}$$

which is simply Equation 2.63 with the y and z components zeroed out. Similarly, other multidimensional quantities will be restricted as

$$\hat{\mathbf{q}} = \begin{bmatrix} \hat{\varepsilon} \\ 0 \\ 0 \\ \hat{\eta} \end{bmatrix} \quad \boldsymbol{\omega} = \begin{bmatrix} \omega \\ 0 \\ 0 \end{bmatrix} \quad \hat{\boldsymbol{\omega}} = \begin{bmatrix} \hat{\omega} \\ 0 \\ 0 \end{bmatrix}$$

and so on. Note that as a consequence

$$\tilde{\mathbf{q}} = \begin{bmatrix} \tilde{\varepsilon} \\ 0 \\ 0 \\ \tilde{\eta} \end{bmatrix} \quad \dot{\mathbf{q}}(t) = \begin{bmatrix} \dot{\varepsilon}(t) \\ 0 \\ 0 \\ \dot{\eta}(t) \end{bmatrix} \quad \dot{\hat{\mathbf{q}}}(t) = \begin{bmatrix} \dot{\hat{\varepsilon}}(t) \\ 0 \\ 0 \\ \dot{\hat{\eta}}(t) \end{bmatrix} \quad \dot{\tilde{\mathbf{q}}}(t) = \begin{bmatrix} \dot{\tilde{\varepsilon}}(t) \\ 0 \\ 0 \\ \dot{\tilde{\eta}}(t) \end{bmatrix}$$

where the fact that, for any SO(2) quaternion $\mathbf{q} = [\varepsilon \ 0 \ 0 \ \eta]^T$, that

$$R(\mathbf{q}) = \begin{bmatrix} 1 & 0 & 0 \\ 0 & \eta^2 - \varepsilon^2 & 2\eta\varepsilon \\ 0 & -2\eta\varepsilon & \eta^2 - \varepsilon^2 \end{bmatrix}$$

was used.

Since by construction the y and z elements of every SO(2) unit quaternion will always be zero, SO(2) unit quaternions will be written as simply

$$\mathbf{q} = \begin{bmatrix} \sin\left(\frac{\phi}{2}\right) \\ \cos\left(\frac{\phi}{2}\right) \end{bmatrix} = \begin{bmatrix} \varepsilon \\ \eta \end{bmatrix}$$

For any two SO(2) quaternions \mathbf{q}_1 and \mathbf{q}_2 , the quaternion product operation of Equation 2.66 simplifies to

$$\mathbf{q}_1 \otimes \mathbf{q}_2 = \begin{bmatrix} \varepsilon_1 \\ \eta_1 \end{bmatrix} \otimes \begin{bmatrix} \varepsilon_2 \\ \eta_2 \end{bmatrix} = \begin{bmatrix} \eta_2\varepsilon_1 + \eta_1\varepsilon_2 \\ \eta_1\eta_2 - \varepsilon_1\varepsilon_2 \end{bmatrix}$$

Similarly, the quaternion kinematics of Equation 2.67 simplify in SO(2) to

$$\dot{\mathbf{q}}(t) = \frac{1}{2}\omega(t) \otimes \mathbf{q}(t) = \begin{bmatrix} \frac{1}{2}\eta(t)\omega(t) \\ -\frac{1}{2}\varepsilon(t)\omega(t) \end{bmatrix}$$

and the filter error dynamics of Equation 2.71 simplify in SO(2) to

$$\dot{\tilde{\mathbf{q}}}(t) = \frac{1}{2}\left\{\omega(t) - \hat{\omega}(t)\right\} \otimes \tilde{\mathbf{q}}(t) \quad (2.73)$$

In SO(2), the Euler axis and angle parameterization of the spacecraft kinematics of Equation 2.72 simplifies considerably to

$$\dot{a}(t) = 0$$

$$\dot{\phi}(t) = \omega(t)$$

where, without loss of generality, the Euler axis is assumed to be $a(t) = 1 \forall t$.

2.4 A Class of Nonlinear Attitude Observers

Salcudean [80] introduced a nonlinear observer for rigid body attitude and angular rate; using deterministic Lyapunov stability theory the observer was shown to eventually converge exponentially fast. The observer is given by

$$\begin{aligned}\dot{\hat{\mathbf{q}}}(t) &= \frac{1}{2}\hat{\boldsymbol{\omega}}(t) \otimes \hat{\mathbf{q}}(t) \\ &= \frac{1}{2}\left[R(\tilde{\mathbf{q}}^{-1}(t))\left(\boldsymbol{\omega}_{meas}(t) + k \operatorname{sign}(\tilde{\eta}(t))\tilde{\boldsymbol{\varepsilon}}(t)\right)\right] \otimes \hat{\mathbf{q}}(t)\end{aligned}\quad (2.74)$$

where $0 < k \in \mathbb{R}$ is a constant gain and the observer has access to the true vehicle attitude (via measurements with negligible error) allowing online computation of the attitude error $\tilde{\mathbf{q}}(t) = \mathbf{q}(t) \otimes \hat{\mathbf{q}}^{-1}(t)$. The observer also has access to noise-corrupted measurements of the vehicle's angular rate notated as $\boldsymbol{\omega}_{meas}(t)$. The noise was not explicitly modeled as the stability analysis was done entirely in a deterministic setting. Under this assumption, the tracking feedback term $k \operatorname{sign}(\tilde{\eta}(t))\tilde{\boldsymbol{\varepsilon}}(t)$ was shown to enable the observer error to converge exponentially fast to zero.

Vik, Shiriaev, and Fossen [101] extended this nonlinear observer to consider the case when the vehicle's angular rate is measured via an angular rate gyro with bias:

$$\boldsymbol{\omega}_g(t) = \boldsymbol{\omega}(t) + \mathbf{b}(t)\quad (2.75)$$

where the gyro bias $\mathbf{b}(t)$ was assumed to decay exponentially fast. Again, as this work was done in a deterministic setting gyro noise was not explicitly modeled. They augmented the observer state to include a gyro bias estimate, leading to the

observer dynamics

$$\begin{aligned}
\dot{\hat{\mathbf{q}}}(t) &= \frac{1}{2} \hat{\boldsymbol{\omega}}(t) \otimes \hat{\mathbf{q}}(t) \\
&= \frac{1}{2} \left[R(\tilde{\mathbf{q}}^{-1}(t)) \left(\boldsymbol{\omega}_g(t) - \hat{\mathbf{b}}(t) + k \operatorname{sign}(\tilde{\eta}(t)) \tilde{\boldsymbol{\varepsilon}}(t) \right) \right] \otimes \hat{\mathbf{q}}(t) \\
\dot{\hat{\mathbf{b}}}(t) &= -\alpha \operatorname{sign}(\tilde{\eta}(t)) \tilde{\boldsymbol{\varepsilon}}(t)
\end{aligned} \tag{2.76}$$

where $\hat{\mathbf{b}}(t)$ is the observer's estimate of the gyro bias and $0 < \alpha \in \mathbb{R}$ is again an observer gain. Under the deterministic assumptions and requirement that the gyro bias decays exponentially fast, they show the observer to be exponentially stable.

Thienel and Sanner [94, 95] showed that the gyro bias observer of [101] is exponentially stable even when the biases are constant (persistent); additionally, they show the observer, when combined with a passivity-based attitude controller from [17], exhibits a nonlinear version of the separation principle. Finally, they showed that if the gyro is further subjected to bounded stochastic measurement noise, the bias estimates converge exponentially fast to an error bound that is a function of the noise parameters and that the attitude tracking errors converge asymptotically to an error bound that is also a function of the noise parameters. Mahony, Hamel, and Pflimlin [56] extended the analysis to consider line-of-sight attitude measurements (e.g. a magnetometer or sun sensor) in addition to estimating persistent gyro bias online; their analysis is provided in both quaternion space and rotation matrix space however their analysis does not consider noise.

Chapter 3 of this thesis will consider a deterministic extension of the observer of Equation 2.76 to include gyro biases that are a function of temperature assuming that the gyro bias function of temperature remains constant and that the gyro's

temperature is available with negligible error.

In Chapters 4, 5, and 6 of this thesis will analyze observer structures like that of Equation 2.76 in a stochastic setting. This will allow for the explicit consideration of stability and performance when the gyro is subjected to unbounded “white” measurement noise (Chapter 4), when the attitude measurements are also corrupted by noise (Chapter 5), and when the gyro bias also drifts according to a constant bias or first-order Gauss Markov process (Chapter 6).

In the deterministic work to date, stability results were generated using Lyapunov analysis. Specifically, Lyapunov functions of the kind

$$V(\mathbf{x}(t)) = \frac{1}{2} \tilde{\mathbf{b}}^T(t) \tilde{\mathbf{b}}(t) + \frac{1}{2} \begin{cases} (\tilde{\eta}(t) - 1)^2 + \tilde{\boldsymbol{\varepsilon}}^T(t) \tilde{\boldsymbol{\varepsilon}}(t) & \tilde{\eta} \geq 0 \\ (\tilde{\eta}(t) + 1)^2 + \tilde{\boldsymbol{\varepsilon}}^T(t) \tilde{\boldsymbol{\varepsilon}}(t) & \tilde{\eta} < 0 \end{cases} \quad (2.77)$$

were used. While the Lyapunov function of Equation 2.77 is once continuously differentiable which met the conditions of the Lyapunov stability theorems utilized, it is not twice continuously differentiable. In order to satisfy the conditions of the stochastic Lyapunov Theorems 2.1.4 and 2.1.5, later chapters in this thesis will instead consider attitude *filters* (as the system models shift from a deterministic to a stochastic setting) with the structure

$$\begin{aligned} \dot{\hat{\mathbf{q}}}(t) &= \frac{1}{2} \hat{\boldsymbol{\omega}}(t) \otimes \hat{\mathbf{q}}(t) \\ &= \frac{1}{2} \left[R(\tilde{\mathbf{q}}^{-1}(t)) \left(\boldsymbol{\omega}_{meas}(t) + k\tilde{\eta}(t)\tilde{\boldsymbol{\varepsilon}}(t) \right) \right] \otimes \hat{\mathbf{q}}(t) \end{aligned} \quad (2.78)$$

where the feedback term $k\tilde{\eta}(t)\tilde{\boldsymbol{\varepsilon}}(t)$ retains the same direction as the feedback term $k \text{sign}(\tilde{\eta}(t))\tilde{\boldsymbol{\varepsilon}}(t)$ of Salcudean’s observer but is twice continuously differentiable (and further is smooth).

Chapter 3: Deterministic Gyro Thermal Bias Observer

This chapter considers the impact of deterministic gyro bias that are time-invariant functions of gyro temperature on the performance of several nonlinear adaptive attitude observers. The first section 3.1 introduces the nonlinear adaptive gyro constant bias observer from Thienel and Sanner [95] which is referred to as a Constant Bias Observer (CBO) in this thesis. The next section 3.2 presents a pair of notional gyro thermal bias function models; the functions are assumed to be time-invariant but as gyro temperature varies the gyro thermal bias evaluated at a specific time will vary when these models are employed. Deterministic numerical simulation shown in Section 3.3 show the CBO bias estimates “chase” the time varying gyro bias resulting in an attitude estimate error.

Section 3.4 presents techniques from function approximation theory, providing a mechanism by which sufficiently smooth gyro bias functions of arbitrary shape can be represented. These techniques are then used to extend the CBO to adaptively estimate (“learn”) gyro thermal bias functions in real time in Section 3.5 in an extension referred to here as a Thermal Bias Observer (TBO). Deterministic numerical simulations in Section 3.6 demonstrate several variations of the TBO learning gyro thermal bias functions.

Section 3.7 considers the CBO and TBO when measurements are no longer deterministic; additive unbounded gyro measurement noise and attitude measurement noise are combined with the CBO and TBO dynamics to formulate Itô SDEs for both systems. Stochastic numerical simulations of the observers are described in Section 3.8 to understand performance in the stochastic setting. Finally, an attempt to understand performance as a function of observer tuning parameters is conducted via stochastic numerical simulation in Section 3.9. The computational expense and imprecise nature of this technique provide significant motivation to find analytic expressions for observer performance as a function of gain parameters and measurement noise specifications which are the subject of the remainder of the thesis.

3.1 Gyro Constant Bias Observer (CBO) Formulation

This section presents an overview of the gyro bias observer from [95], which in this thesis is referred to as the gyro Constant Bias Observer (CBO). The structure of the CBO is used as the basis of all attitude observers and filters considered in the thesis.

The CBO is assumed to be provided with angular rate gyro measurements that are corrupted by a constant bias

$$\boldsymbol{\omega}_g(t) = \boldsymbol{\omega}(t) + \mathbf{b} \quad (3.1)$$

where $\boldsymbol{\omega}_g(t)$ is the gyro measurement at time t , $\boldsymbol{\omega}(t)$ is the true angular rate at time t , and the bias is denoted \mathbf{b} . As the bias is assumed to be constant, $\dot{\mathbf{b}}(t) = 0$.

It is further assumed that the CBO has access to perfect (noise free and unbiased) attitude measurements $\mathbf{q}_m(t)$ of the true attitude $\mathbf{q}(t)$

$$\mathbf{q}_m(t) = \mathbf{q}(t) = \begin{bmatrix} \boldsymbol{\varepsilon}(t) \\ \eta(t) \end{bmatrix} = \begin{bmatrix} \varepsilon_x(t) \\ \varepsilon_y(t) \\ \varepsilon_z(t) \\ \eta(t) \end{bmatrix} \quad (3.2)$$

The true attitude $\mathbf{q}(t)$ evolves according to the usual kinematics equation

$$\dot{\mathbf{q}}(t) = \frac{1}{2} \boldsymbol{\omega}(t) \otimes \mathbf{q}(t)$$

The CBO of Thienel and Sanner [95] is given as

$$\dot{\hat{\mathbf{q}}}(t) = \frac{1}{2} \left\{ R(\tilde{\mathbf{q}}^{-1}(t)) \left[\boldsymbol{\omega}_g(t) - \hat{\mathbf{b}}(t) + k_e \tilde{\eta}(t) \tilde{\boldsymbol{\varepsilon}}(t) \right] \right\} \otimes \hat{\mathbf{q}}(t) \quad (3.3)$$

$$\dot{\hat{\mathbf{b}}}(t) = -\alpha \tilde{\eta}(t) \tilde{\boldsymbol{\varepsilon}}(t) \quad (3.4)$$

where $k_e > 0$ is an observer (estimator) gain parameter and $\alpha > 0$ is an adaptation gain parameter. The observer's estimate $\hat{\mathbf{q}}(t)$ at time t of the true attitude $\mathbf{q}(t)$ is obtained by propagating the attitude kinematic equation using the measured angular rate corrected by a bias estimate along with the feedback term $k_e \tilde{\eta}(t) \tilde{\boldsymbol{\varepsilon}}(t)$ in Equation 3.3. The feedback term is a measure of the observer's attitude estimate error, given by

$$\tilde{\mathbf{q}}(t) = \begin{bmatrix} \tilde{\boldsymbol{\varepsilon}}(t) \\ \tilde{\eta}(t) \end{bmatrix} = \mathbf{q}(t) \otimes \hat{\mathbf{q}}^{-1}(t)$$

which is available to the observer in real time as the attitude measurements are assumed to be perfect. The feedback term is also used in the observer's gyro bias adaptation law of Equation 3.4 where $\hat{\mathbf{b}}(t)$ is the observer's estimate at time t of the gyro bias \mathbf{b} . The observer's bias estimate error $\tilde{\mathbf{b}}(t)$ is given as

$$\tilde{\mathbf{b}}(t) = \mathbf{b} - \hat{\mathbf{b}}(t) \quad (3.5)$$

When there is no attitude error, the feedback term goes to zero and thus the bias estimate stops changing. If there is error in the bias estimate, however, the bias estimate will divert the observer attitude estimate through the observer attitude kinematics. This in turn will increase the attitude estimate error, providing the feedback loop.

Thienel and Sanner [95] show that in the deterministic setting that the CBO is not only stable, but that it is Globally Exponentially Stable (GES). This means that not only does the observer’s bias estimate error remain bounded, it goes to zero exponentially fast. As the CBO was shown to be GES, it is furthermore BIBO (bounded-input bounded-output) stable [42]. Thienel and Sanner show that this implies that for *bounded* gyro noise the CBO estimate errors are bounded. They further find the bound as a function of the bound on the noise.

Section 3.2 will consider time-varying deterministic gyro bias. The CBO is not GES in this situation, but provided the gyro bias is bounded the CBO estimate errors are still bounded. Sections 3.4 and 3.5 will provide a technique to extend the CBO to learn gyro bias functions provided the gyro bias is a constant function of some other readily available signal, specifically gyro temperature. The remaining sections of the chapter will consider unbounded gyro noise and attitude measurement noise via numerical simulation. A rigorous stochastic analysis of the CBO will be presented in Chapter 6.

As explained in Section 2.4, the CBO considered in this thesis is actually a slightly modified version than that of [95]; the feedback term $k \text{sign}(\tilde{\eta}(t))\tilde{\epsilon}(t)$ has been altered to $k\tilde{\eta}(t)\tilde{\epsilon}(t)$ for the CBO here. This modification results in a smoother observer dynamics equation as the $\text{sign}(\cdot)$ function is not continuously differentiable. The results of [95] can similarly be established for the CBO given here.

3.2 Gyro Thermal Bias Model

The Constant Bias Observer (CBO) of Section 3.1 made the modeling assumption that the angular rate gyro measurements are corrupted by a constant gyro bias, or at least that the gyro bias is constant relative to the time scales of the dynamics of the CBO. This is a common modeling assumption amongst the attitude filter literature as well [20, 51, 64].

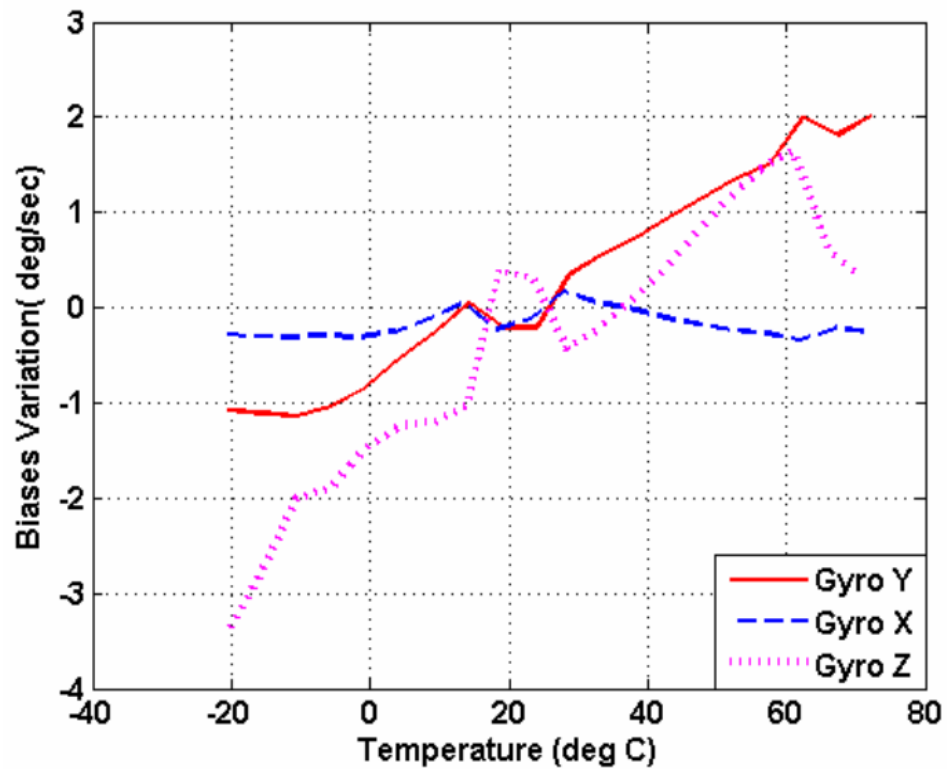


Figure 3.1: Measurement of gyro bias as a function of operating temperature for a specific

MEMS gyro unit by Aggarwal, Syed, and El-Sheimy [6].

One of the predominate deterministic factors behind gyro bias variation is due to change in the operating temperature of the gyro. It has been reported in

the literature that this is a particularly important phenomena for micro-electrical-mechanical system (MEMS) gyros [6, 78]. A commonly reported mechanism for this phenomena is that despite their various designs, all MEMS gyros use some sort of a vibrating proof mass or structure made of silicon which expands and contracts with temperature. Several studies fit linear functions to measured gyro bias as a function of temperature [7, 41, 78]. Other studies fit second and third order functions to measured gyro bias as a function of temperature [29, 38]. The magnitude of the gyro bias as a function of temperature is specific to the particular design of the MEMS elements; over a range of 100° C, the bias varied by as much as 5 $\frac{deg}{sec}$ for some MEMS gyros [6] and as little as $0.0056 \frac{deg}{sec} \approx 97 \frac{\mu rad}{sec}$ for other gyro units [85]. An example of a measurements of gyro bias as a function of operating temperature for a specific MEMS gyro (an orthogonally-mounted triad of ADXRS150 MEMS gyros made by Analog Devices Inc) by Aggarwal, Syed, and El-Sheimy [6] is repeated here in Figure 3.1. Note carefully that while a pre-flight calibration campaign may be utilized to attempt to characterize gyro thermal bias, the gyro thermal model has been known to vary (slowly) over the life of the sensor as the moving components age.

In this chapter, two gyro thermal bias models are considered. In both cases, the gyro measurement model is given by the equation

$$\boldsymbol{\omega}_g(t) = \boldsymbol{\omega}(t) + \mathbf{b}(T(t)) \quad (3.6)$$

where $\boldsymbol{\omega}_g(t)$ is the angular rate gyro measurement at time t , $\boldsymbol{\omega}(t)$ is the true vehicle angular rate in $\frac{rad}{sec}$, and the gyro bias $\mathbf{b}(T(t))$ is a function of the time-varying gyro

temperature $T(t)$ given in degrees Celsius. For simplicity, in this thesis the gyro temperature is assumed to be homogeneous; that is, each gyro sensing element is the same temperature at any given time. For real world applications, many MEMS gyro designs have an independent temperature sensing element for each motion axis and can provide distinct temperature measurement for each sensing element.

The first gyro thermal bias model considered in this chapter is linear in gyro temperature. The model is given by

$$\mathbf{b}(T(t)) = \begin{bmatrix} 0.02 \\ 0.02 \\ 0.011 \end{bmatrix} T(t) + \begin{bmatrix} -1 \\ 0 \\ -1 \end{bmatrix} \quad (3.7)$$

in units of degree/second and visualized in Figure 3.2. This notional model is of the same shape and magnitude as that measured by Aggarwal et al [6] for a low cost MEMS gyro unit. This type and quality of gyro is common for cubesats and hosted payloads for space applications, as well as being representative of the type of gyros used in consumer electronics like cell phones, consumer UAVs, and virtual reality equipment.

The second gyro thermal bias model considered in this chapter is a third order function of gyro temperature. The model is given by

$$\mathbf{b}(T(t)) = \begin{bmatrix} 0.000015 \\ 0.000008 \\ 0.000008 \end{bmatrix} T^3(t) + \begin{bmatrix} -0.002 \\ -0.0007 \\ -0.001 \end{bmatrix} T^2(t) + \begin{bmatrix} 0.07 \\ 0.012 \\ 0.039 \end{bmatrix} T(t) + \begin{bmatrix} -1 \\ 0 \\ -0.1 \end{bmatrix} \quad (3.8)$$

in units of degree/second and displayed in Figure 3.3. This notional model has a shape similar to that studied in [29] and ongoing gyro modeling work at NASA. The

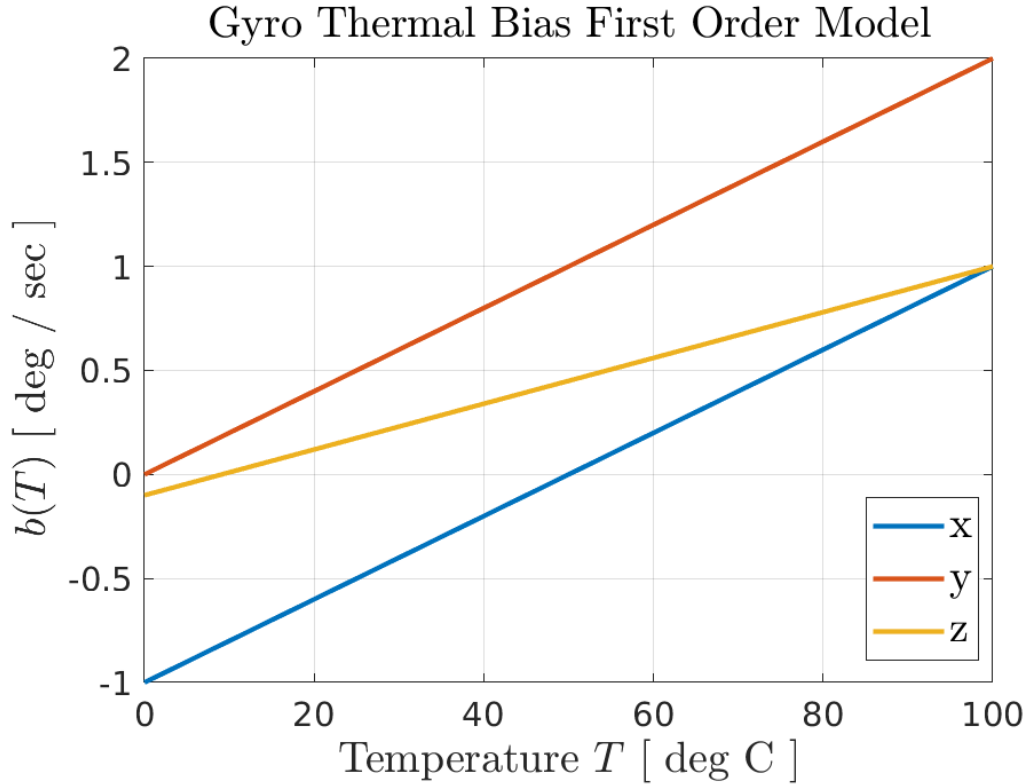


Figure 3.2: The first order gyro thermal bias function of Equation 3.7.

magnitude of the thermal bias is again consistent with low cost MEMS gyro units commonly used in cubesats.

For a satellite in orbit utilizing a gyro to rate measurement, the impact of a gyro thermal bias can lead to a failure to meet pointing requirements. It is not uncommon for a Low Earth Orbiting (LEO) satellite in an orbit passing in and out of Earth’s shadow to experience temperature variation of 100° C over each orbit. Other satellites are spin stabilized with spin rates of 5 revolutions per minute being common, and can experience temperature variation oscillating with the spin rate. Due to cost, complexity, and other thermal design considerations it too is common for gyro instruments aboard satellites to experience the full range of the vehicle’s

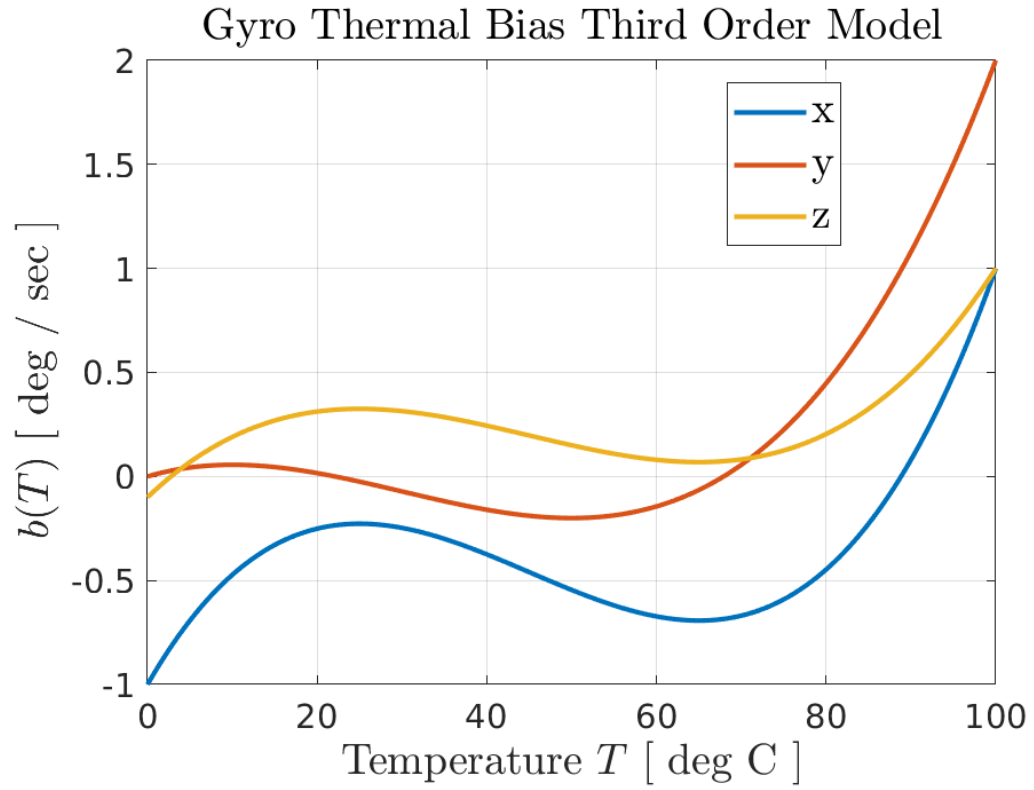


Figure 3.3: The third order gyro thermal bias function of Equation 3.8.

thermal variation.

3.3 CBO Deterministic Simulation Study

This section features simulation studies of the CBO of Section 3.1 when the gyro measurements are corrupted by bias as a function of operating temperature.

In the simulations, the gyro's operating temperature varies sinusoidally according to

$$T(t) = \frac{100}{2} \cos\left(\frac{2\pi t}{\tau} + \pi\right) + \frac{100}{2} \quad (3.9)$$

in degrees Celsius. The amplitude is 100°C with a phase angle chosen so the simulation starts at the coldest temperature. The thermal oscillation period τ is chosen as 5400 seconds, providing a thermal profile representative of a satellite in Low Earth Orbit (LEO) passing through Earth's shadow every 90 minutes.

The gyro measurement model is now given by

$$\boldsymbol{\omega}_g(t) = \boldsymbol{\omega}(t) + \mathbf{b}(T(t)) \quad (3.10)$$

where as before $\boldsymbol{\omega}_g(t)$ is the gyro measurement at time t and $\boldsymbol{\omega}(t)$ is the true angular rate at time t . The bias, denoted $\mathbf{b}(T(\cdot))$, is given by the notional gyro bias thermal function models of Section 3.2. While the gyro thermal bias function $\mathbf{b}(T(\cdot))$ is assumed to be time-invariant function of temperature, the value of the gyro bias in general varies between time t_1 to time t_2 , from $\mathbf{b}(T(t_1))$ to $\mathbf{b}(T(t_2))$, as the temperature $T(t)$ varies with time. If the temperature is constant, or the gyro bias function of temperature is a constant, the model of Equation 3.10 reverts to the gyro constant bias model of Equation 3.1.

Figure 3.4 shows time series plots for the CBO attitude estimate error and bias

estimate error. In this figure, the gyro thermal bias is modeled as the first order thermal bias function of Equation 3.7. After an initial transient, the bias estimates lag behind the true gyro bias. As the gyro bias varies sinusoidally (since it is a linear function of gyro operating temperature which is sinusoidally varying), the bias estimate error passes through zero once every time the derivative of the gyro bias changes sign. Essentially the gyro bias estimate “crosses paths” with the true gyro bias, but can never keep up.

The study is repeated in Figure 3.5 for the third order thermal bias function of Equation 3.8. Now as the temperature varies continuously from 0 to 100 degrees Celsius over half an orbit, the derivative of the true thermal bias changes sign three times. Accordingly, the CBO bias estimate error passes through zero three times every half orbit.

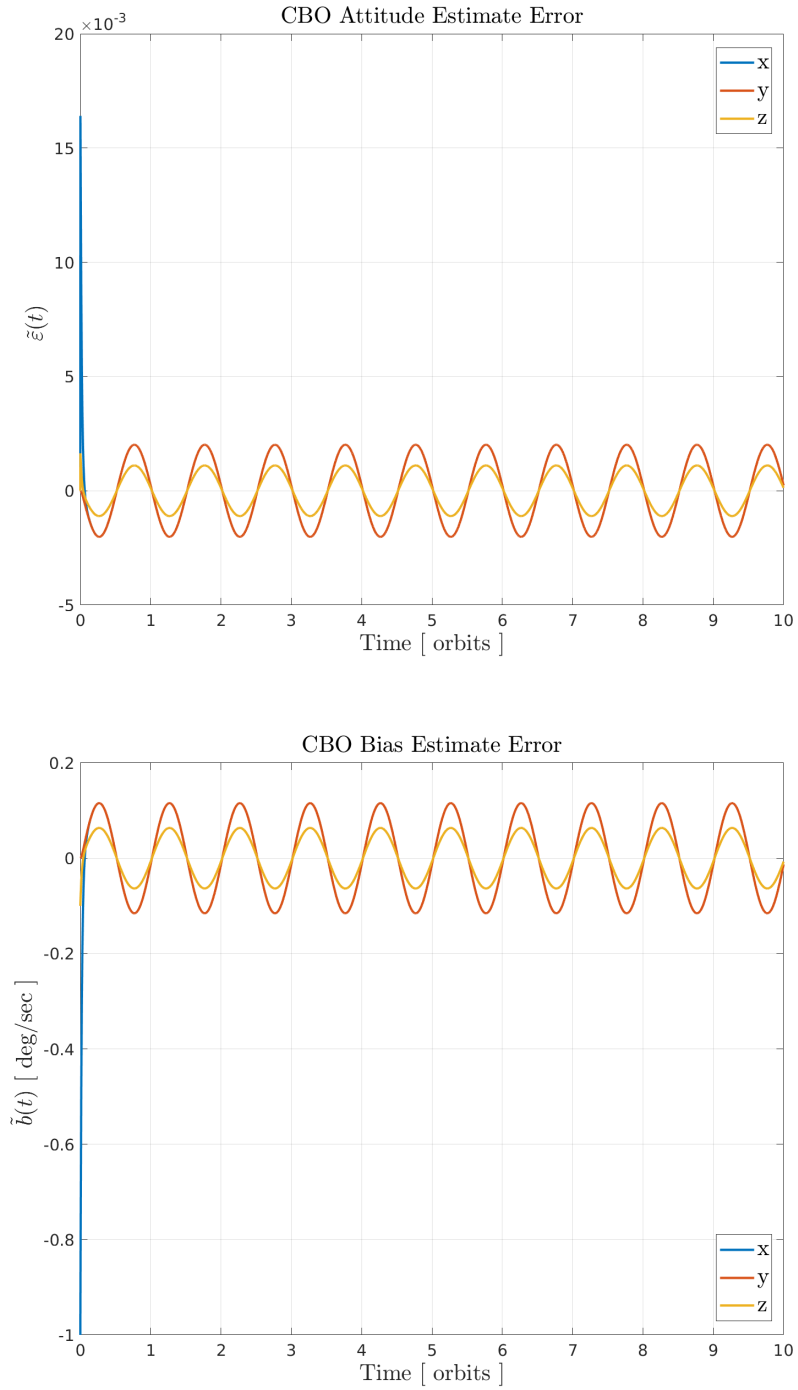


Figure 3.4: The CBO demonstrates sinusoidal tracking error for the first order gyro thermal bias model of Equation 3.7 as the gyro operating temperature heats and cools once every orbit of 90 minutes. The CBO gains were set to $k_e = 1$ and $\alpha = 0.1$.

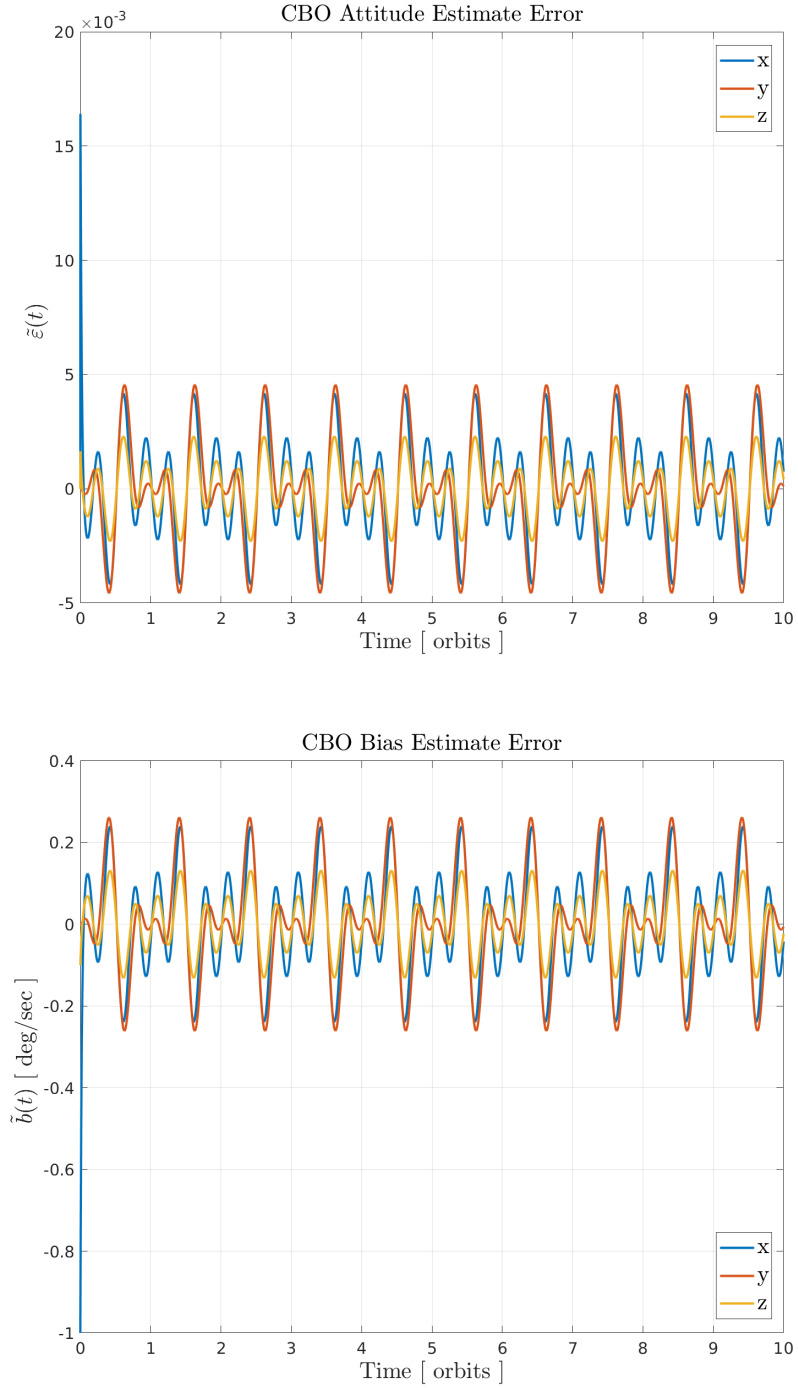


Figure 3.5: The CBO demonstrates sinusoidal tracking error for the third order gyro thermal bias model of Equation 3.8 as the gyro operating temperature heats and cools once every orbit of 90 minutes. The CBO gains were set to $k_e = 1$ and $\alpha = 0.1$.

The next simulation study explores the variation of the estimate error as a function of the thermal oscillation period. The gyro operating temperature is again given by the sinusoidal model of Equation 3.9, but now the thermal oscillation period τ is varied. The smallest (fastest) thermal oscillation period considered is $\tau = 60$ seconds. This period is consistent with a 1 rpm spin stabilized satellite, although the thermal amplitude of the oscillation is unrealistic for this frequency. The largest (slowest) thermal oscillation period considered is $\tau = 2$ hours which is representative with a spacecraft in LEO. The thermal variation amplitude of components in a LEO spacecraft coming into and out of the Earth's shadow are commonly on the order of 100°C .

Figure 3.6 shows the estimate errors as a function of gyro operating temperature oscillation period τ for the first order gyro thermal bias model; Figure 3.7 repeats the analysis for the third order gyro thermal bias model. In both cases, the estimate error rapidly drops off with increasing τ which is to be expected. As the thermal oscillation period τ increases, the gyro thermal bias better matches a constant gyro bias which the CBO is capable of tracking exponentially fast. However, in many applications the bias estimate error of the CBO may still exceed requirements and an algorithm capable of estimating the gyro thermal bias might be necessary.

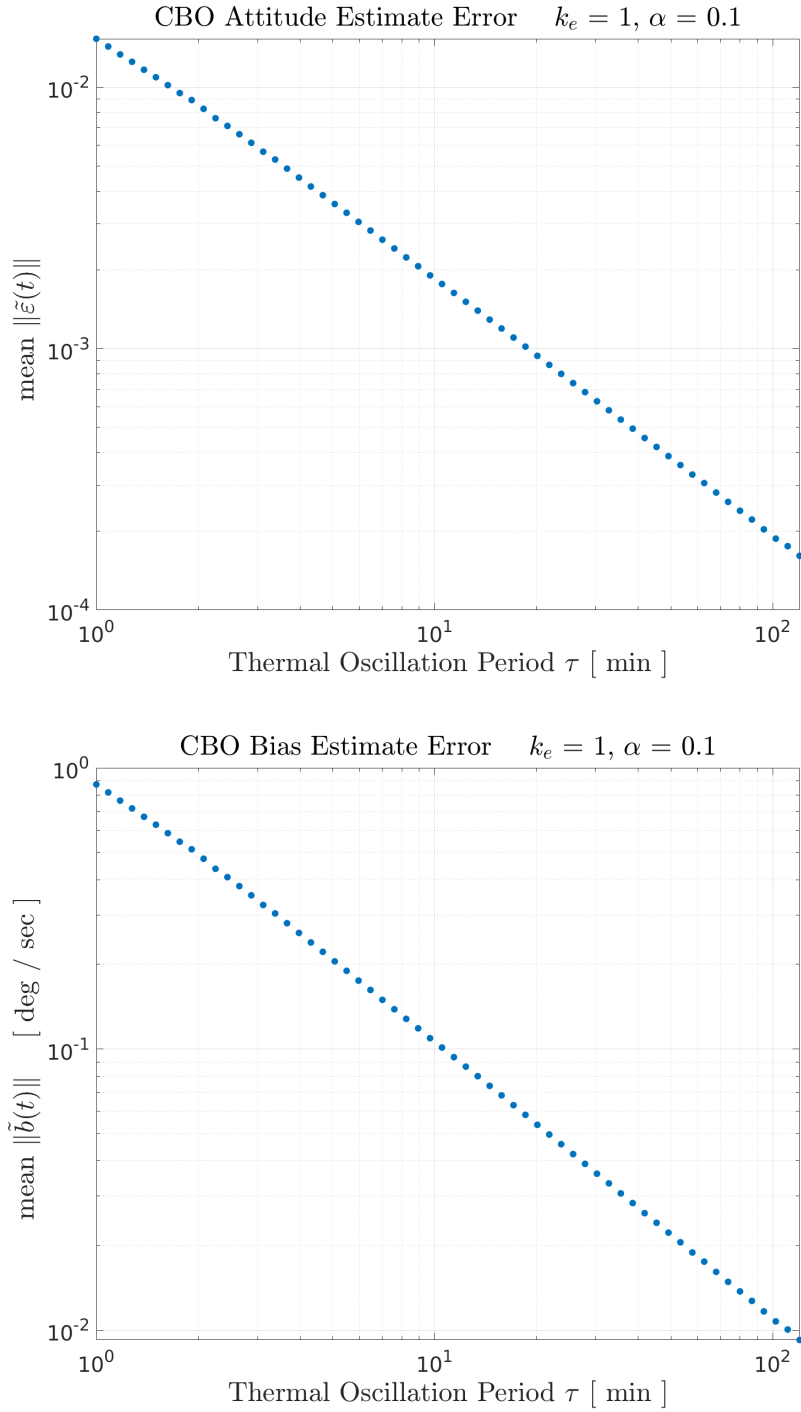


Figure 3.6: The CBO demonstrates sinusoidal tracking error for the first order gyro thermal bias model of Equation 3.7 as the gyro operating temperature heats and cools once every orbit of 90 minutes. The CBO gains were set to $k_e = 1$ and $\alpha = 0.1$.

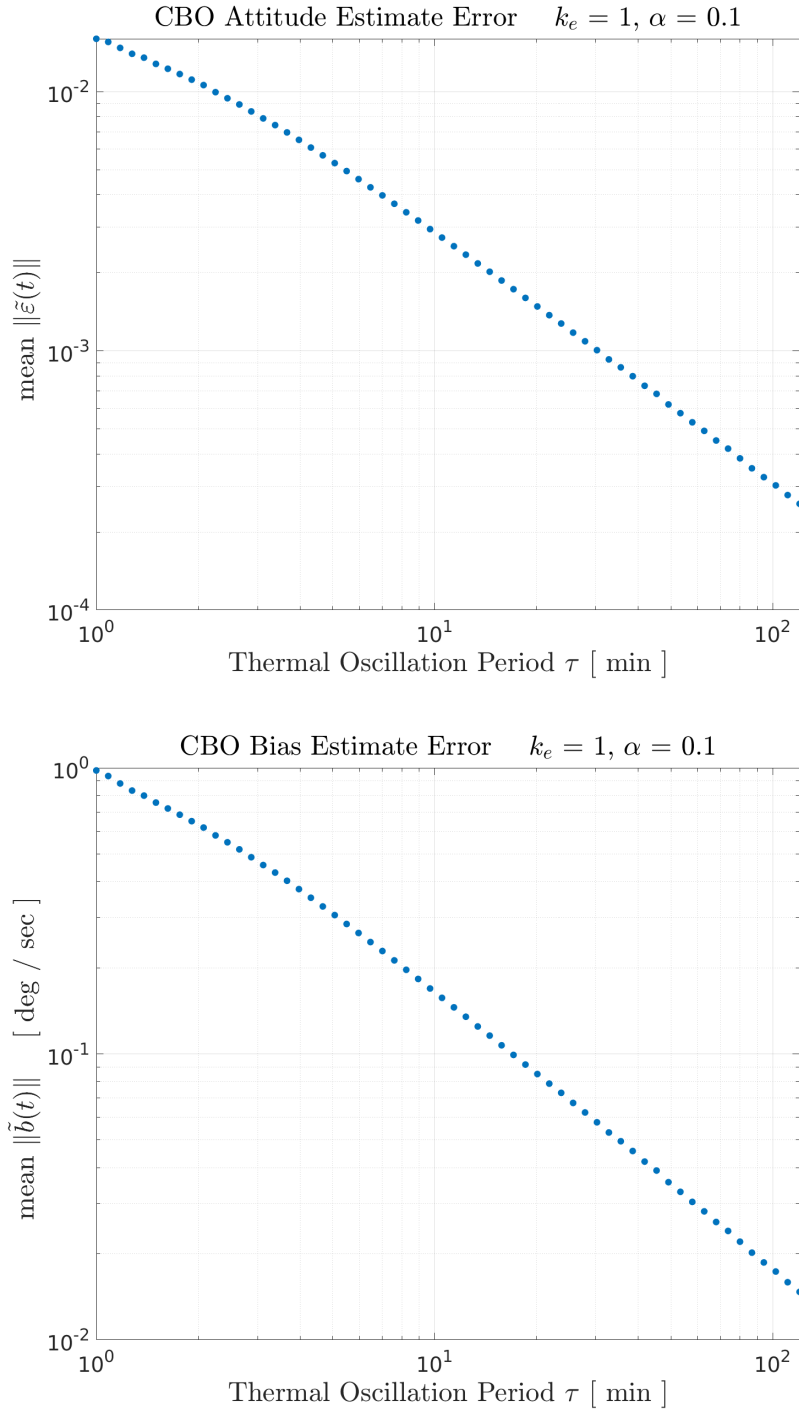


Figure 3.7: The CBO demonstrates sinusoidal tracking error for the third order gyro thermal bias model of Equation 3.8 as the gyro operating temperature heats and cools once every orbit of 90 minutes. The CBO gains were set to $k_e = 1$ and $\alpha = 0.1$.

3.4 Function Approximation

This section is a brief overview of some basic concepts of function approximation theory. With an appropriate parameterization, the CBO of Section 3.1 may be extended to estimate not merely a constant gyro bias, but parameters of an approximation to the gyro thermal bias function of temperature.

The fundamental idea behind function approximation is to use a set of canonical functions as a basis for a class of functions one wishes to approximate. Assuming the class of functions to be approximated is sufficiently smooth, weighted linear combinations of scaled and shifted collections of the basis functions serve as the approximation. The approximation gets better as more basis functions are used.

Many types of functions may be used to form a basis. For example, sinusoids of differing frequency constitute the well-known Fourier basis, Chebyshev polynomials constitute a Chebyshev basis, and so on. For many practical applications, however, these bases require a great number of distinct basis functions in the linear combination to achieve a suitable function approximation. Many applications instead use radial basis functions (RBFs), such as the boxcar radial basis function:

$$g(x) = \begin{cases} 1 & |x| \leq 0.5 \\ 0 & |x| > 0.5 \end{cases} \quad (3.11)$$

the hat radial basis function:

$$g(x) = \begin{cases} 1 - |x| & |x| \leq 1 \\ 0 & |x| > 1 \end{cases} \quad (3.12)$$

or the Gaussian radial basis function

$$g(x) = \exp \left\{ -x^2 \right\} \quad (3.13)$$

These standard radial basis functions are depicted graphically in Figure 3.8. The left images in the figure depict the RBFs of Equation 3.11 (Boxcar RBF, top left), Equation 3.12 (Hat RBF, middle left), and Equation 3.13 (Gaussian RBF, bottom left). These RBF can be horizontally scaled and shifted by composing the RBF with a linear function, such as

$$g(hx - k) = g \left(\frac{1}{w}x - \frac{\lambda_k}{w} \right) \quad (3.14)$$

where w is the basis function width and λ_k is the basis function's center location (also called a knot point); note that $k = \frac{\lambda_k}{w}$ is an integer. The right side of the figure has a plot of the RBFs of Equation 3.11 (Boxcar RBF, top right), Equation 3.12 (Hat RBF, middle right), and Equation 3.13 (Gaussian RBF, bottom right) each scaled to have a width of 10 and a center location of 40.

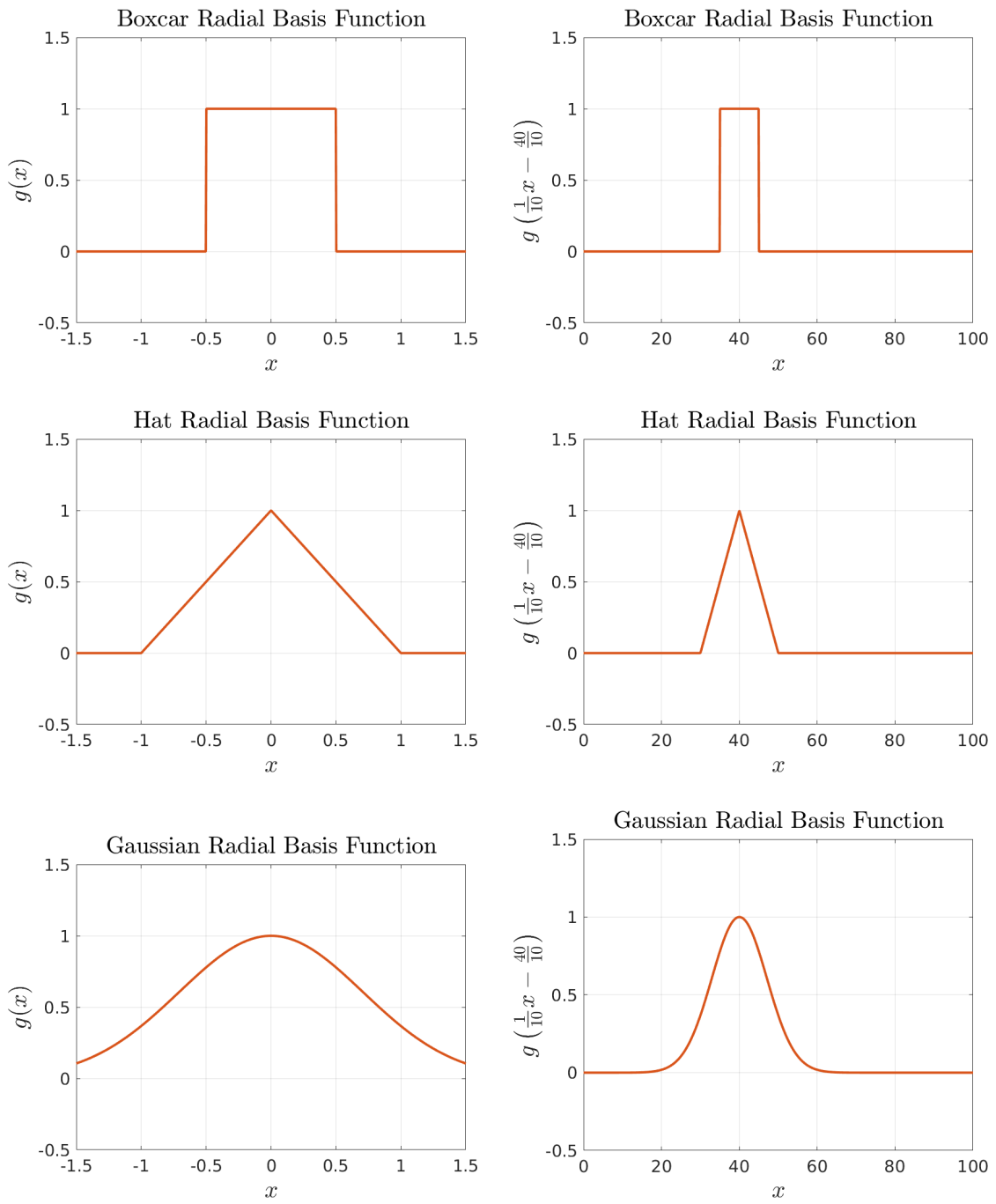


Figure 3.8: Radial basis functions (left) can be horizontally scaled and shifted (right) via composition with a linear function as in Equation 3.14.

Now consider the task of approximating a known function. The top left image of Figure 3.9 depicts a first order polynomial gyro thermal bias function. The top right image of the same figure depicts a collection of boxcar RBFs of Equation 3.11, each of width $10^\circ C$. The boxcar RBFs have center locations of $\lambda_0 = 0^\circ C$, $\lambda_1 = 10^\circ C$, ..., $\lambda_{11} = 100^\circ C$ spanning the domain of $0^\circ C$ to $100^\circ C$. These RBFs form a basis for functions that are piecewise constant over the domain. The bottom left image of the same figure shows the function to be approximated in a thick blue line, the weighted individual RBFs in thin red lines, and the sum of all weighted RBFs in a thick red line. The sum of the weighted RBFs is the bias function approximation, given by the equation

$$\hat{b}(T) = \sum_{k=1}^{11} c_k g(hT - k) = \sum_{k=1}^{11} c_k g\left(\frac{1}{w}T - \frac{\lambda_k}{w}\right) \quad (3.15)$$

where $\hat{b}(T)$ is the approximation of the thermal bias function $b(T)$ evaluated at temperature T . The bias function approximation weights c_i were found by sampling the true gyro thermal bias function at 1000 points along the domain (0,100) and performing a least squares fit. Thus a given weighting coefficient, say c_7 , is the least squares best fit piecewise constant value of the function to be approximated over the interval $(\lambda_7 - \frac{w}{2}, \lambda_7 + \frac{w}{2})$. Finally, the bottom right of the same figure depicts the bias function approximation error $\tilde{b}(T) = b(t) - \hat{b}(T)$. Note that as boxcar RBFs are piecewise constant, a function approximation using them will fail to capture the slope of the true thermal bias function.

If the domain were partitioned by more boxcar RBFs of smaller width, the function approximation would better match the true function. This notion is made

precise for spline approximations in Theorem 20.3 of Powell [77] where, for sufficiently smooth thermal bias function $b(\cdot)$ a j^{th} order spline approximation $\hat{b}(T)$ is such that

$$\|b(\cdot) - \hat{b}(\cdot)\|_\infty \leq c \left(\frac{w}{2}\right)^{j+1} \|b^{(j+1)}(\cdot)\|_\infty \quad (3.16)$$

In the inequality, w is the knot spacing (space between RBF centers), $b^{(j)}$ is the j^{th} derivative of the gyro thermal bias, and c is a positive constant. Note that a boxcar RBF is a 0^{th} order spline and a hat RBF is a 1^{st} order spline. A Gaussian RBF is in some sense the infinite limit of the sequence of splines [81].

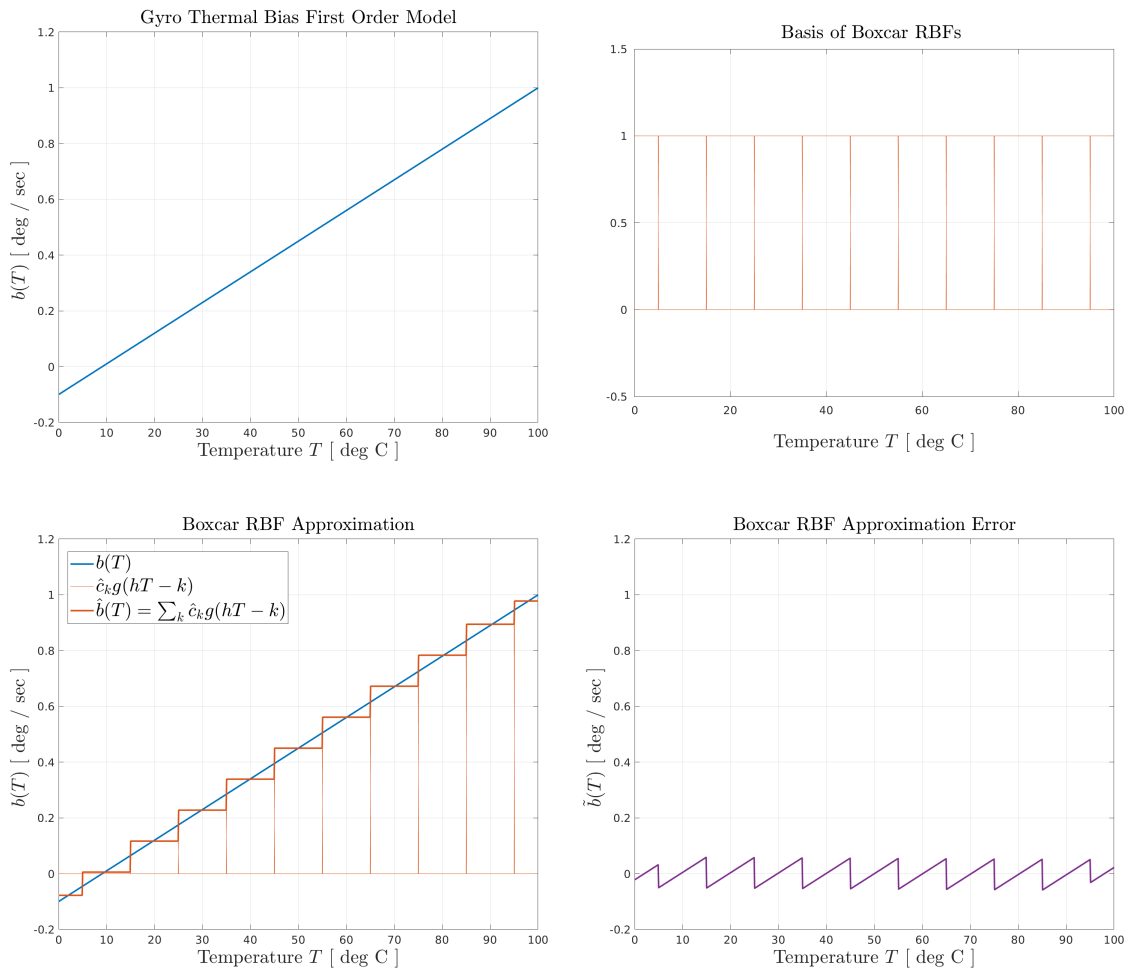


Figure 3.9: Boxcar RBF approximation of a first order polynomial.

A function approximation using hat RBFs is able to capture slope information. Figure 3.10 demonstrates the performance of hat RBF function approximation for the same first order gyro thermal bias function depicted in the top left plot. The top right plot shows a collection of hat RBFs forming a basis over the interval for approximation. The bottom left plot compares the hat RBF function approximation with the true gyro thermal bias which is perfectly covered by the approximation. The function approximation error is the constant zero function.

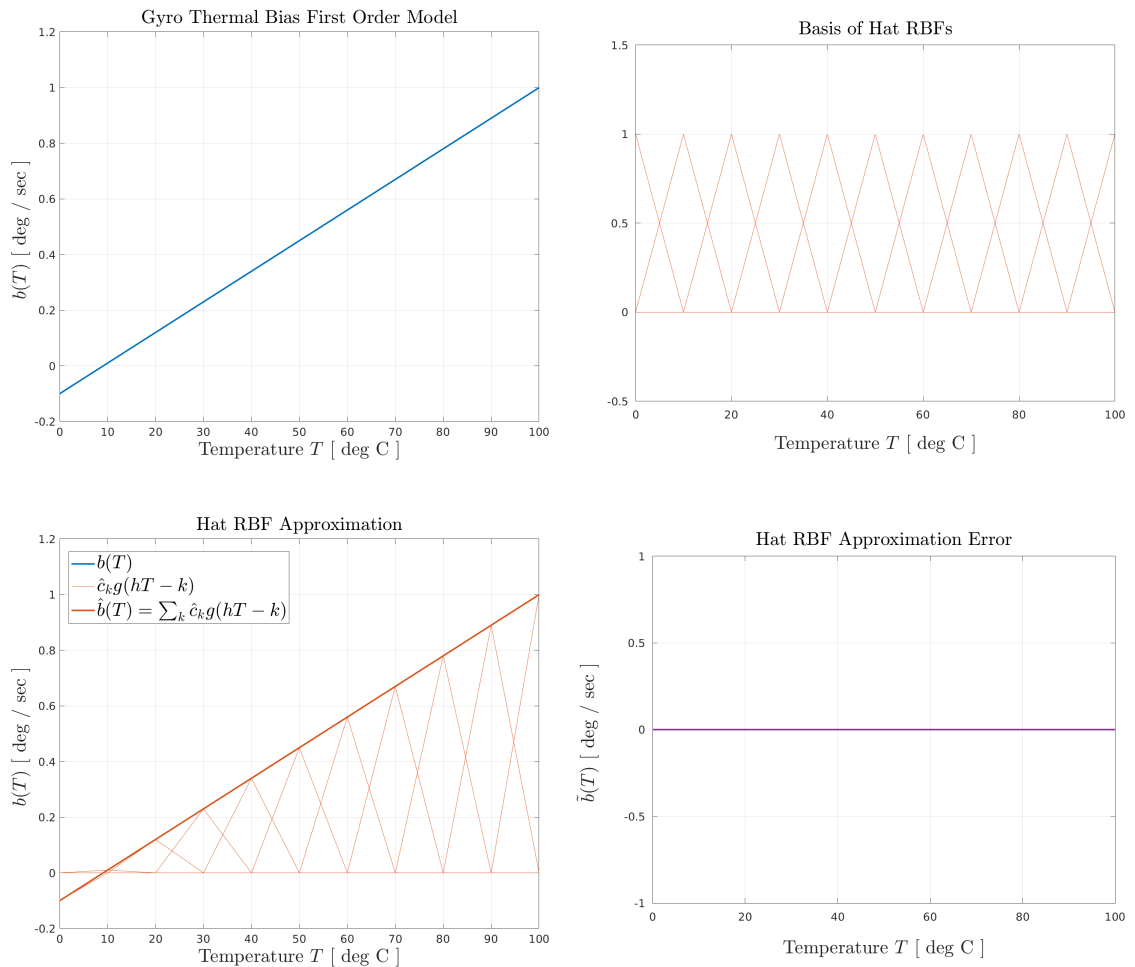


Figure 3.10: Hat RBF approximation of a first order polynomial.

A function approximation using Gaussian RBFs is theoretically able to capture arbitrary order functions; however, as noted in Sanner and Slotine [81] to approximate functions on a bounded interval many Gaussian RBFs well outside the interval may be needed. The Gaussian RBFs for this problem were chosen to have center locations of $\lambda_0 = -100^\circ C$, $\lambda_1 = -90^\circ C$, ..., $\lambda_N = 200^\circ C$. Figure 3.11 demonstrates Gaussian RBF function approximation for the same first order gyro thermal bias function depicted in the top left plot. The top right plot shows a collection of Gaussian RBFs forming a basis over the interval for approximation. The bottom left plot compares the Gaussian RBF function approximation with the true gyro thermal bias which is covered by the approximation. The function approximation error is negligibly small.

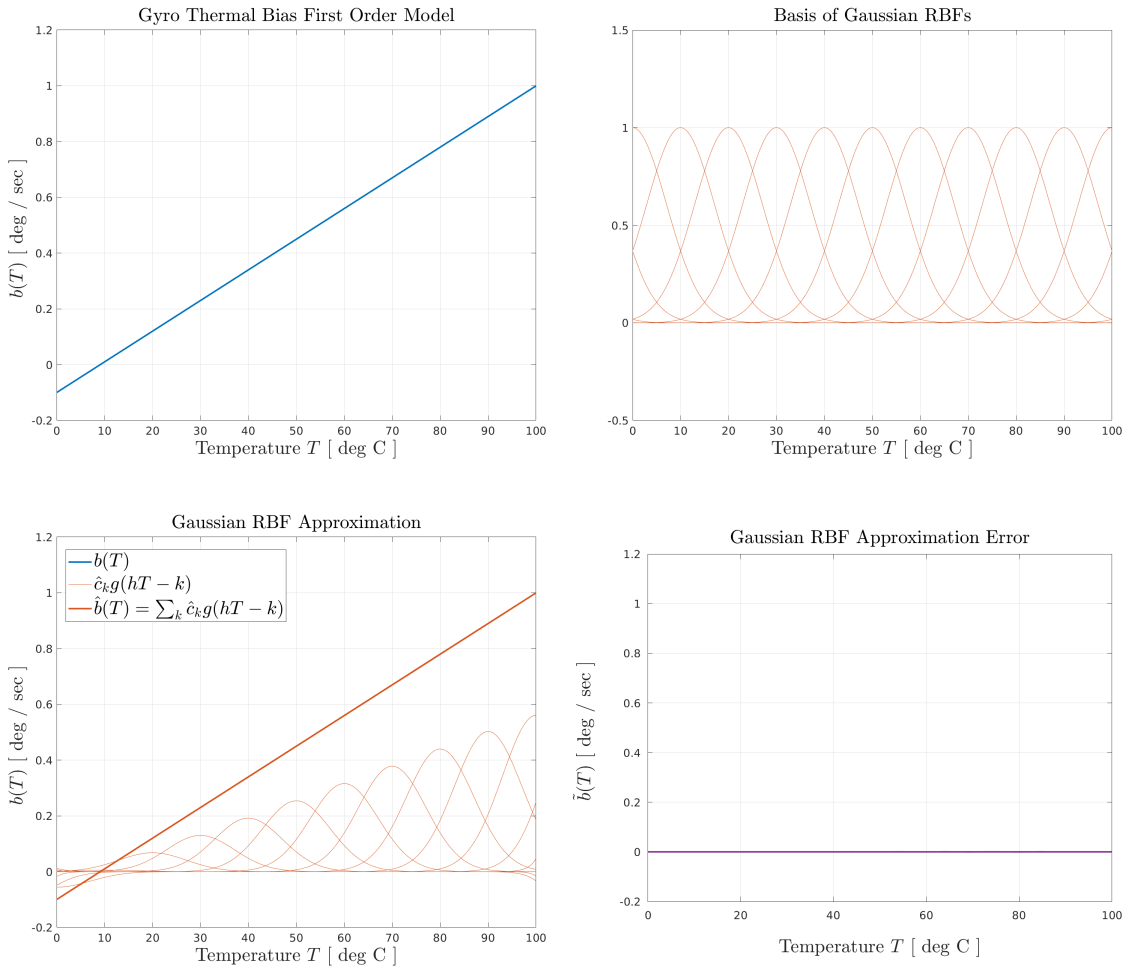


Figure 3.11: Gaussian RBF approximation of a first order polynomial.

Figure 3.12 depicts function approximation via boxcar RBFs for a third order gyro thermal bias which is shown in the top left plot. The bottom left plot compares the function approximation to the true gyro thermal bias. The bottom right plot shows the bias function approximation error which is significant, as in the first order boxcar RBF function approximation case.

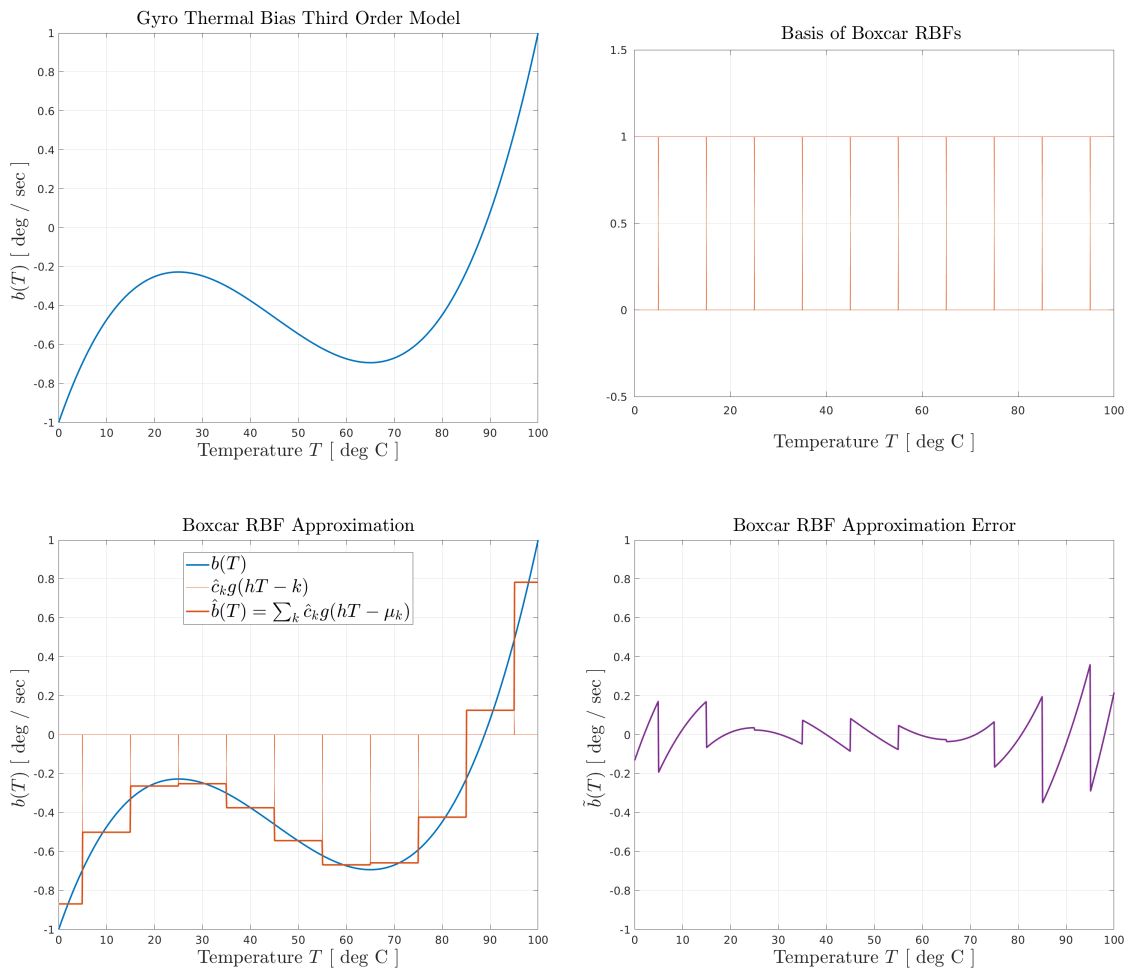


Figure 3.12: Boxcar RBF approximation of a third order polynomial.

The third order gyro thermal bias is approximated via hat RBFs in Figure 3.13. As opposed to the first order thermal bias case where the hat RBFs were able to capture the highest order of the true bias function, in this case with a third order bias function the piecewise linear hat RBFs are unable to capture the highest order components of the true bias function. The approximation error in the bottom right plot is still far smaller than the boxcar RBF approximation for this gyro thermal bias function as predicted by the function approximation error criterion of Equation 3.16 from Powell [77].

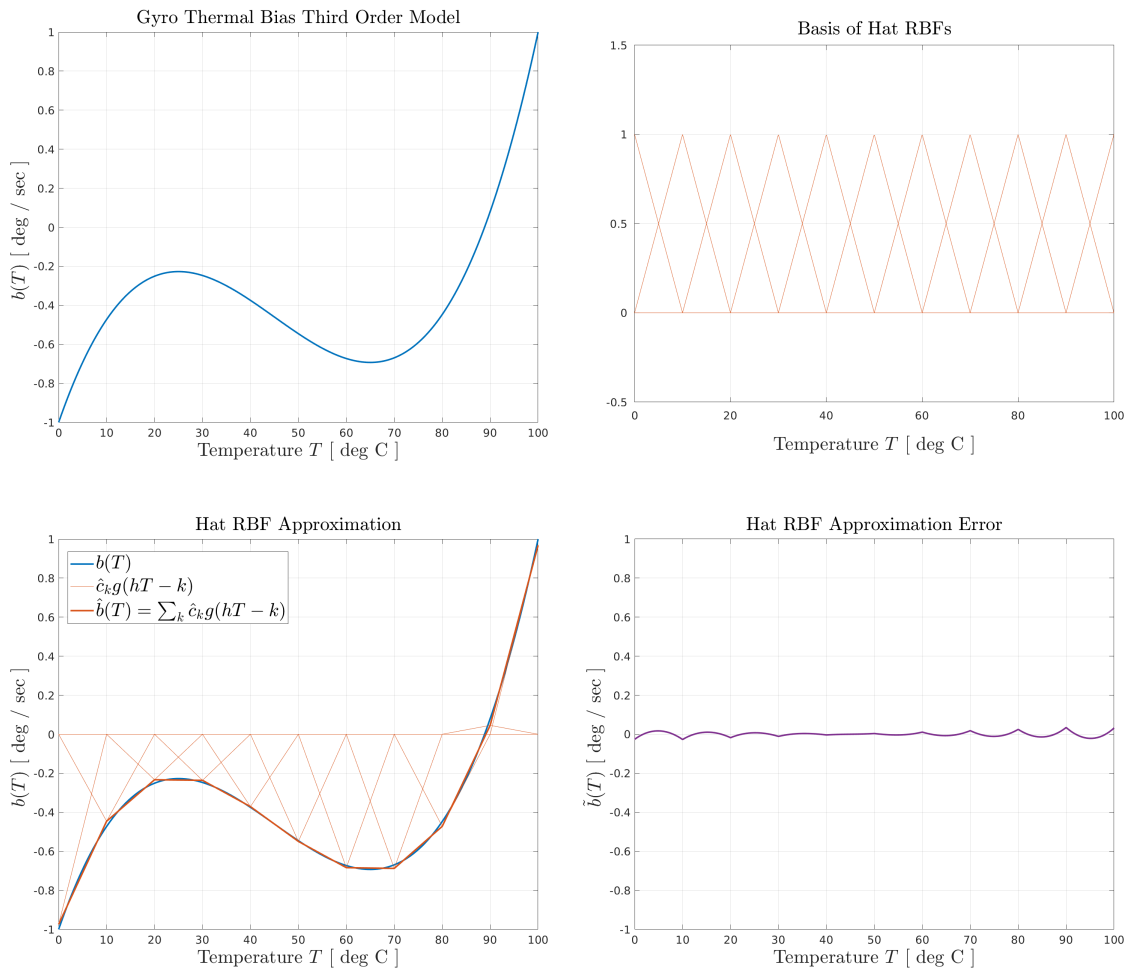


Figure 3.13: Hat RBF approximation of a third order polynomial.

Finally, the third order gyro thermal bias is approximated via Gaussian RBFs in Figure 3.14. As in the previous Gaussian RBF function approximation case, the Gaussian RBFs were chosen to have center locations of $\lambda_0 = -100^\circ C$, $\lambda_1 = -90^\circ C$, ..., $\lambda_N = 200^\circ C$ to ensure suitable coverage over the interval of approximation. The Gaussian RBF function approximation covers the true gyro thermal bias function in the bottom left plot. The corresponding error function in the bottom right plot is negligibly small.

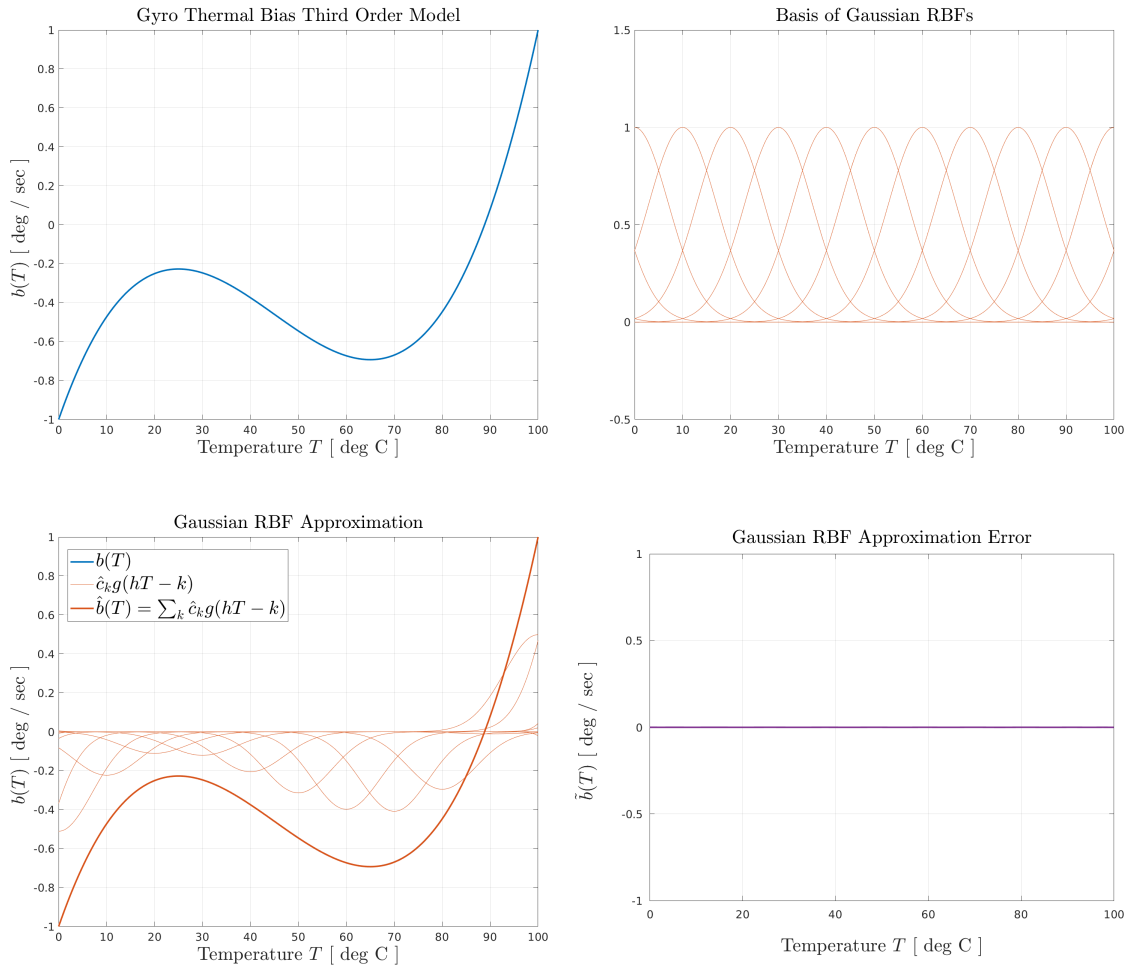


Figure 3.14: Gaussian RBF approximation of a third order polynomial.

3.5 Gyro Thermal Bias Observer (TBO) Formulation

This section extends the gyro constant bias observer of Section 3.1 to estimate gyro bias as a function of temperature. This extended version is referred to in this thesis as a gyro Thermal Bias Observer (TBO).

As in Equation 3.10, the gyro measurement model is given by

$$\boldsymbol{\omega}_g(t) = \boldsymbol{\omega}(t) + \mathbf{b}(T(t)) \quad (3.17)$$

where as before $\boldsymbol{\omega}_g(t)$ is the gyro measurement at time t and $\boldsymbol{\omega}(t)$ is the true angular rate at time t . Now the gyro thermal bias, denoted $\mathbf{b}(T(\cdot))$, is assumed to be a time-invariant, continuous, yet unknown function of the gyro temperature. As in the previous section, while the gyro thermal bias function $\mathbf{b}(T(\cdot))$ is assumed to be time-invariant function of temperature, the value of the gyro bias in general varies between time t_1 to time t_2 from $\mathbf{b}(T(t_1))$ to $\mathbf{b}(T(t_2))$ as the temperature $T(t)$ varies with time. The gyro temperature is assumed to be available to the observer.

The TBO, presented by Galante and Sanner in [25], is given by

$$\dot{\hat{\mathbf{q}}}(t) = \frac{1}{2} \left\{ R(\tilde{\mathbf{q}}^{-1}(t)) \left[\boldsymbol{\omega}_g(t) - \hat{\mathbf{b}}(T(t)) + k_e \tilde{\eta}(t) \tilde{\boldsymbol{\varepsilon}}(t) \right] \right\} \otimes \hat{\mathbf{q}}(t) \quad (3.18)$$

$$\dot{\hat{\mathbf{c}}}_k(t) = -\alpha \tilde{\eta}(t) \tilde{\boldsymbol{\varepsilon}}(t) g(hT(t) - k) \quad (3.19)$$

where, as for the CBO, the $k_e > 0$ is a tracking gain and $\alpha > 0$ is an adaptation gain. The observer's attitude kinematic equation 3.18 is similar to that of the CBO in Equation 3.3; however, in the TBO case the gyro bias estimate is computed using

a weighted sum of RBFs

$$\hat{\mathbf{b}}(T(t)) = \sum_k \hat{\mathbf{c}}_k(t) g(hT(t) - k) \quad (3.20)$$

where $g(\cdot)$ is a radial basis function, $h = \frac{1}{w}$ encodes the knot spacing w , and $k = \frac{\lambda_k}{w}$ is an integer specifying the center location λ_k of k^{th} RBF. The weighting coefficients are updated via the adaptation law of Equation 3.19, which is the same law used for the CBO in Equation 3.4 but scaled by the RBF evaluated at the current gyro temperature. The TBO is parameterized not only by a feedback gain k_e and an adaptation gain α , but also the choice of RBF basis, the RBF spacing (knot spacing) encoded in h , and the RBF center locations (knot locations) k .

As before, the observer attitude estimate error is given by

$$\tilde{\mathbf{q}}(t) = \begin{bmatrix} \tilde{\boldsymbol{\varepsilon}}(t) \\ \tilde{\boldsymbol{\eta}}(t) \end{bmatrix} = \mathbf{q}(t) \otimes \hat{\mathbf{q}}^{-1}(t)$$

which is available to the observer in real time as the attitude measurements are assumed to be perfect. The bias estimate error at time t is given by

$$\tilde{\mathbf{b}}(T(t)) = \mathbf{b}(T(t)) - \hat{\mathbf{b}}(T(t))$$

which is of course not available to the observer in real time.

In this formulation, the CBO can be viewed as a special case of the TBO using a single constant basis function $g(T) = 1$. Conversely, if the TBO RBFs are chosen to be boxcar RBFs, referred to as a boxcar TBO, then the observer is similar to utilizing a bank of CBOs. In this analogy, the temperature range is divided into partitions (the domain of each boxcar RBF) with a CBO i is assigned

to each partition. Then each CBO is “responsible” for the gyro bias estimate in its temperature partition. If the gyro temperature remains within one boxcar RBF’s temperature partition, then the boxcar RBF TBO behaves precisely the same as the CBO. Naturally, if the gyro temperature does not reach the domain of a particular RBF, the corresponding coefficient will never update as the true gyro thermal bias model has not been excited at that temperature. Essentially, the boxcar TBO uses the CBO’s gyro bias persistent excitation guarantee to learn the gyro thermal bias function at any experienced temperature.

Note that the TBO does not have an a priori model of the true thermal bias function. The TBO estimates coefficients of RBFs that serve as an *approximation* to a suitable basis for representing the thermal bias function. The performance of this approximation depends on the number of RBFs used and their relative spacing, the choice of RBF used, and the smoothness of the true gyro thermal bias function.

Assume the true gyro thermal bias function can be written as

$$\mathbf{b}(T) = \sum_k \mathbf{c}_k g(hT - k) \quad (3.21)$$

allowing one to write the bias estimate error as

$$\begin{aligned} \tilde{\mathbf{b}}(T(t)) &= \mathbf{b}(T(t)) - \hat{\mathbf{b}}(T(t)) \\ &= \sum_i (\mathbf{c}_i - \hat{\mathbf{c}}_i(t)) g(hT(t) - k) \\ &= \sum_i \tilde{\mathbf{c}}_i g(hT(t) - k) \end{aligned} \quad (3.22)$$

Then the attitude observer dynamics given by Equations 3.18, 3.19, and 3.20 can be combined with the quaternion error kinematics of Equation 2.71 and the perfect

(noise free) attitude measurement model 3.27 to find the observer's estimate error dynamics:

$$\begin{aligned}\dot{\tilde{\mathbf{x}}}(t) &= \begin{bmatrix} \dot{\tilde{\mathbf{q}}}(t) \\ \dot{\tilde{\mathbf{c}}}_i(t) \end{bmatrix} \\ &= \begin{bmatrix} \frac{1}{2} \left\{ \boldsymbol{\omega}(t) - R(\tilde{\mathbf{q}}(t))R(\tilde{\mathbf{q}}^{-1}(t)) \left[\boldsymbol{\omega}_g(t) - \hat{\mathbf{b}}(T(t)) + k_e \tilde{\boldsymbol{\eta}}(t) \tilde{\boldsymbol{\varepsilon}}(t) \right] \right\} \otimes \tilde{\mathbf{q}}(t) \\ -\dot{\tilde{\mathbf{c}}}_k(t)g(hT(t) - k) \end{bmatrix}\end{aligned}$$

Subtracting the bias estimate from the gyro measurement model of Equation 3.10 leads to

$$\begin{aligned}\boldsymbol{\omega}_g(t) - \hat{\mathbf{b}}(T(t)) &= \\ &= \boldsymbol{\omega}(t) + \sum_k \mathbf{c}_k g(hT(t) - k) - \sum_k \hat{\mathbf{c}}_k(t)g(hT(t) - k) \\ &= \boldsymbol{\omega}(t) + \sum_k \tilde{\mathbf{c}}_k g(hT(t) - k)\end{aligned}$$

Substituting back into the error dynamics, and substituting in the bias adaptation law, resolves as

$$\begin{aligned}\dot{\tilde{\mathbf{x}}}(t) &= \begin{bmatrix} \dot{\tilde{\mathbf{q}}}(t) \\ \dot{\tilde{\mathbf{c}}}_k(t) \end{bmatrix} \\ &= \begin{bmatrix} \frac{1}{2} \left\{ -k_e \tilde{\boldsymbol{\eta}}(t) \tilde{\boldsymbol{\varepsilon}}(t) - \sum_k \tilde{\mathbf{c}}_k g(hT(t) - k) \right\} \otimes \tilde{\mathbf{q}}(t) \\ \alpha \tilde{\boldsymbol{\eta}}(t) \tilde{\boldsymbol{\varepsilon}}(t) g(hT(t) - k) \end{bmatrix} \quad (3.23)\end{aligned}$$

where the attitude estimate error dynamics can be broken into the quaternion vector and scalar components as

$$\dot{\tilde{\mathbf{q}}}(t) = \begin{bmatrix} \dot{\tilde{\boldsymbol{\varepsilon}}}(t) \\ \dot{\tilde{\boldsymbol{\eta}}}(t) \end{bmatrix} = \begin{bmatrix} -\frac{1}{2}k_e \tilde{\boldsymbol{\eta}}^2(t) \tilde{\boldsymbol{\varepsilon}}(t) - \frac{1}{2} \left[\tilde{\boldsymbol{\eta}}(t)I + [\tilde{\boldsymbol{\varepsilon}} \times] \right] \sum_k \tilde{\mathbf{c}}_k g(hT(t) - k) \\ \frac{1}{2}k_e \tilde{\boldsymbol{\eta}}(t) \tilde{\boldsymbol{\varepsilon}}^T(t) \tilde{\boldsymbol{\varepsilon}}(t) + \frac{1}{2} \tilde{\boldsymbol{\varepsilon}}^T(t) \sum_k \tilde{\mathbf{c}}_k g(hT(t) - k) \end{bmatrix}$$

The stability of the TBO is provided in the following theorem.

Theorem 3.5.1. *Assume the gyro measurement model of Equation 3.10 has a thermal bias function that can be expressed as in Equation 3.20. Then the thermal bias observer error dynamics of Equation 3.23 are stable. Further,*

$$\lim_{t \rightarrow \infty} \tilde{\boldsymbol{\varepsilon}}^T(t) \tilde{\boldsymbol{\varepsilon}}(t) = 0$$

Proof. Choose the Lyapunov function $V(t) = \frac{1}{2} \tilde{\boldsymbol{\varepsilon}}^T(t) \tilde{\boldsymbol{\varepsilon}}(t) + \frac{1}{4\alpha} \sum_k \tilde{\boldsymbol{c}}_k^T(t) \tilde{\boldsymbol{c}}_k(t)$. Taking the derivative yields

$$\begin{aligned} \dot{V}(t) &= -\frac{1}{2} k_e \tilde{\eta}^2(t) \tilde{\boldsymbol{\varepsilon}}^T(t) \tilde{\boldsymbol{\varepsilon}}(t) \\ &\quad - \frac{1}{2} \tilde{\eta}(t) \tilde{\boldsymbol{\varepsilon}}^T(t) \sum_k \tilde{\boldsymbol{c}}_k(t) g(hT(t) - k) + \frac{1}{2} \tilde{\eta}(t) \sum_k \tilde{\boldsymbol{c}}_k^T(t) \tilde{\boldsymbol{\varepsilon}}(t) g(hT(t) - k) \\ &= -\frac{1}{2} k_e \tilde{\eta}^2(t) \tilde{\boldsymbol{\varepsilon}}^T(t) \tilde{\boldsymbol{\varepsilon}}(t) \quad \forall t \end{aligned}$$

This establishes that $\tilde{\boldsymbol{c}}_k(t)$, $\tilde{\boldsymbol{\varepsilon}}(t)$, and $\tilde{\eta}(t)$ are globally uniformly bounded.

Differentiating again results in

$$\ddot{V}(t) = \frac{1}{2} k_e^2 (\tilde{\eta}^2(t) - 1) \tilde{\eta}^2(t) \tilde{\boldsymbol{\varepsilon}}^T(t) \tilde{\boldsymbol{\varepsilon}}(t) + \frac{1}{2} k_e \tilde{\eta}(t) (\tilde{\eta}^2(t) - \tilde{\boldsymbol{\varepsilon}}^T(t) \tilde{\boldsymbol{\varepsilon}}(t)) \tilde{\boldsymbol{\varepsilon}}^T(t) \tilde{\boldsymbol{b}}(t)$$

which is bounded as $\tilde{\boldsymbol{c}}_k(t)$, $\tilde{\boldsymbol{\varepsilon}}(t)$, and $\tilde{\eta}(t)$ are bounded. Barbalat's Lemma [42] then shows that

$$\lim_{t \rightarrow \infty} \tilde{\boldsymbol{\varepsilon}}^T(t) \tilde{\boldsymbol{\varepsilon}}(t) = 0$$

□

The proof comes almost directly from Thienel and Sanner [95] for the CBO. Note however, that in Thienel and Sanner's proof for the CBO they were able to show that the gyro constant bias is *always* persistently exciting. In the TBO case, the adaptation law for weighting coefficient $\hat{\boldsymbol{c}}_k$ is not activated if $g(hT - k) = 0$. For the

boxcar TBO this has the consequence that if the gyro temperature remains constant only the weighting coefficient associated with the measured gyro temperature will ever change. In this case the problem can be modeled precisely as in the CBO case and the weighting coefficient will converge to the true bias exponentially fast as shown by Thienel and Sanner. For the constant temperature case, the gyro bias estimates of the hat TBO and Gaussian TBO will converge to the true bias exponentially fast according to the proof from Thienel and Sanner, but the RBF weighting coefficients $\hat{\mathbf{c}}_k(t)$ may not converge to the RBF weighting coefficients \mathbf{c}_k for the true gyro thermal model.

3.6 Gyro Thermal Bias Observer (TBO) Function Learning Simulations

This section presents a number of numerical simulations of the TBO of Section 3.5 to demonstrate its function estimation ability. These deterministic simulations are performed using MATLAB's `ode45` numerical integrator with default arguments. In each simulation study, the TBO has no initial knowledge of the true gyro thermal bias function. The simulation study is conducted for each RBF discussed in Section 3.4 and both gyro thermal bias models of Section 3.2 for a total of six simulations.

The TBO has the same parameters for each simulation (aside from the choice of RBF). The TBO tracking gain is set to $k = 1$ and the adaptation gain is set to $\alpha = 0.1$. The RBF knot spacing (center location spacing) is set uniformly to $w = \frac{1}{h} = 10^\circ\text{C}$. Knot locations (center locations) are chosen as -0°C , 10°C , ..., 100°C for the boxcar and hat RBFs, but the knot locations for the Gaussian RBFs are chosen as -100°C , -90°C , ..., 200°C . Note that these choices of parameters are not optimized according to any criteria, they are merely chosen for demonstration purposes.

As before, the gyro's operating temperature varies sinusoidally according to

$$T(t) = \frac{100}{2} \cos\left(\frac{2\pi t}{\tau} + \pi\right) + \frac{100}{2} \quad (3.24)$$

in degrees Celsius. The amplitude is 100°C with a phase angle chosen so the simulation starts at the coldest temperature. The thermal oscillation period τ is chosen as 5400 seconds for the simulations of this section, providing a thermal profile repre-

sentative of a notional satellite in Low Earth Orbit (LEO) passing through Earth’s shadow every 90 minutes.

Figure 3.15 contains a collection of plots detailing the TBO using boxcar RBFs over the course of a simulation. The true first order gyro thermal bias function of Equation 3.7 is depicted in the upper left plot, but is unknown to the TBO which starts with an initial estimate of zero bias at all temperatures. After $\frac{1}{8}$ orbit, the gyro temperature has warmed from $0^{\circ}C$ to just over $15^{\circ}C$; the TBO gyro thermal bias function estimate $\hat{\mathbf{b}}(T)$ shifts to a piecewise linear approximation of the true gyro bias for the temperatures observed by the TBO up to that point. After $\frac{1}{4}$ orbit the gyro temperature has increased to $50^{\circ}C$ and the TBO has accordingly adjusted its gyro thermal bias function estimate over the range of temperatures experienced thusfar. After half an orbit, the TBO has sampled the gyro thermal bias function over the entire range of the temperature profile. The TBO continues to refine its gyro thermal bias estimate as the simulation continues. After one full orbit, the temperature has returned to $0^{\circ}C$. The bottom right plot shows the TBO gyro thermal bias estimate error. As the true gyro thermal bias in this simulation is linear, the boxcar function approximation error is off by a linear function. Notice that since the most recent temperature experienced in the domain of each boxcar RBF was on the leftmost (coldest) side, so the thermal bias function estimate is most accurate on the leftmost side of each temperature partition creating a sawtooth error shape.

Time series of the bias estimate and attitude estimate errors for the boxcar TBO during this simulation are shown in Figure 3.16. There is significant error dur-

ing the first half orbit as the TBO's weighting coefficients each in turn experience a transient as the gyro operating temperature increases from the coldest to warmest values of its thermal profile. After the entire temperature range has been experienced, the observer's bias estimate error settles to a lower level consistent with the error of using boxcar RBFs to approximate a line.

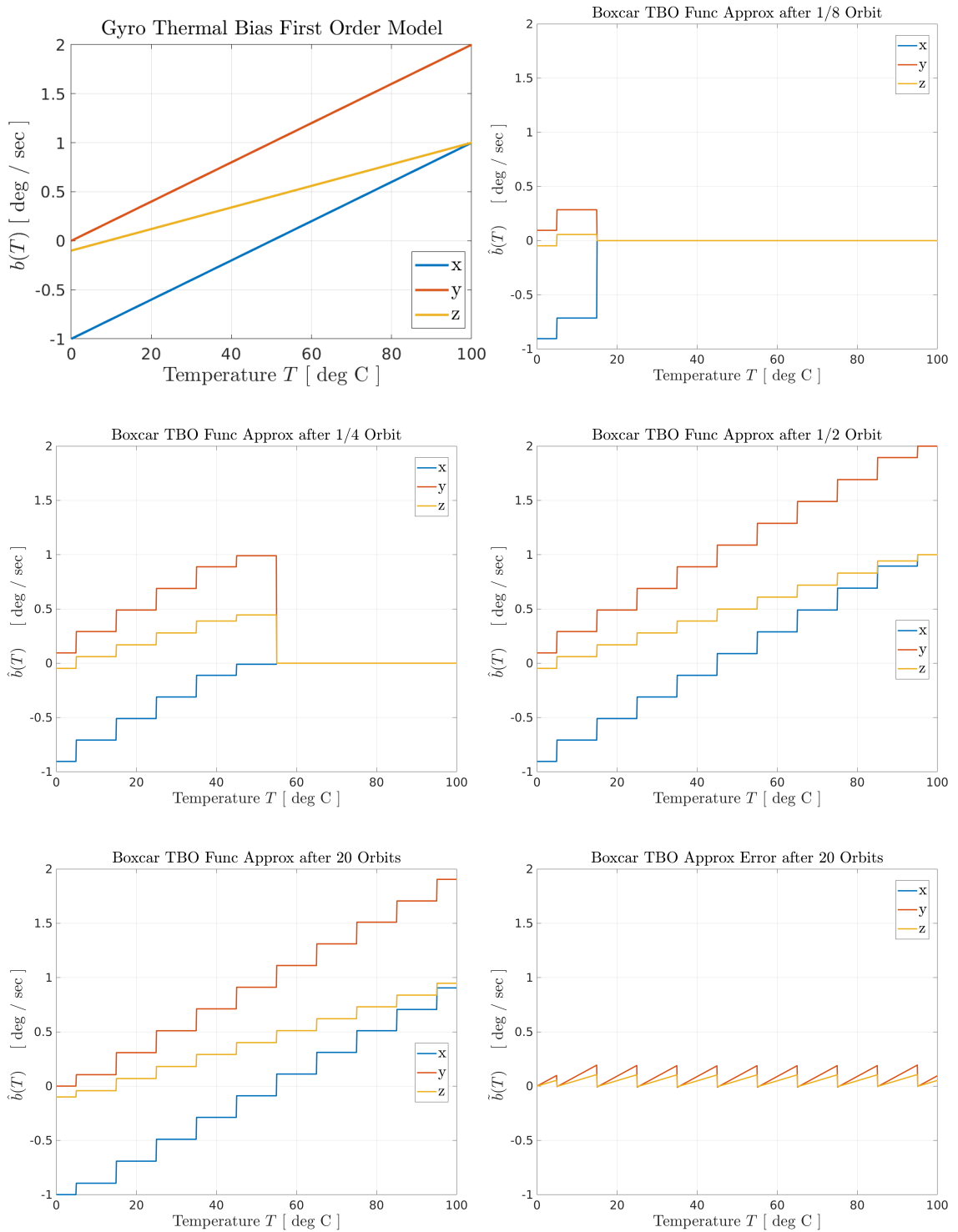


Figure 3.15: The boxcar TBO estimates the first order gyro thermal bias function of Equation 3.7.

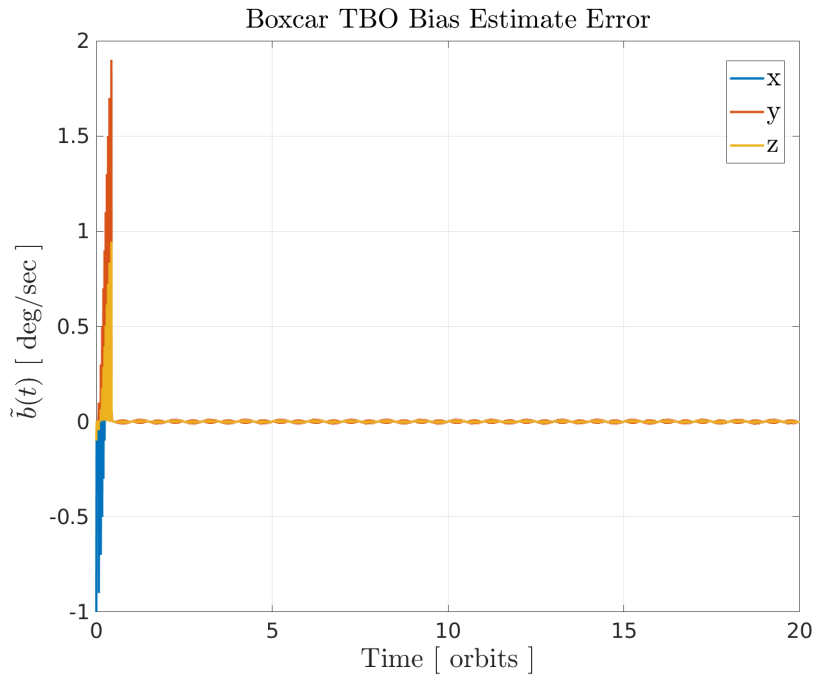
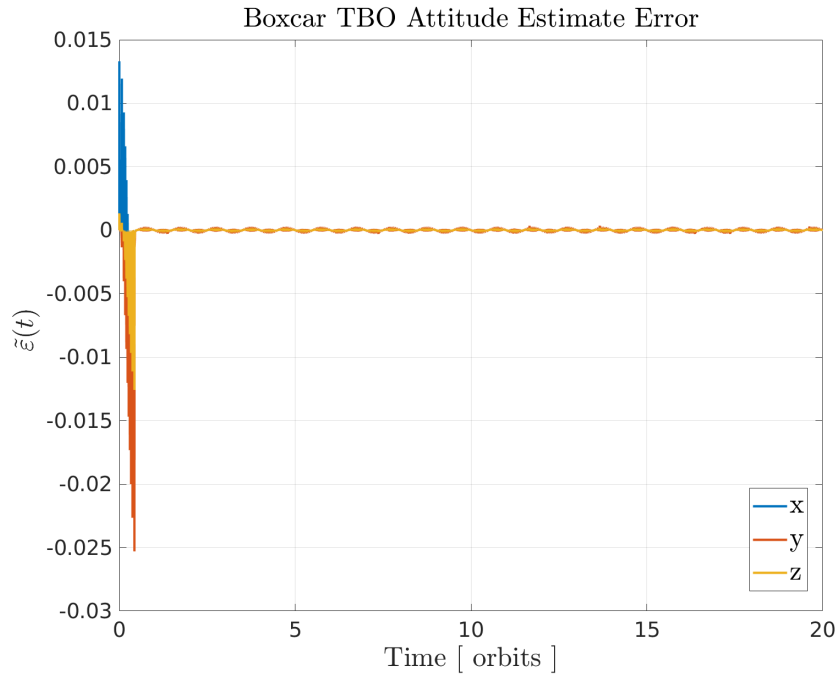


Figure 3.16: Time series plots of the attitude and estimate error for the boxcar TBO as it estimates the first order gyro thermal bias function of Equation 3.7.

The hat TBO is considered next. Figure 3.17 depicts the estimated thermal bias function at the same simulation time as the boxcar TBO previously considered. The thermal bias function approximation has significant error after the first orbit, incorrectly approximating both the value and the slope of the true bias function. After 20 orbits, however, the transient has settled and the thermal bias function approximation has little error. The time series plots of the attitude and bias estimate errors in Figure 3.18 show the error decays to zero.

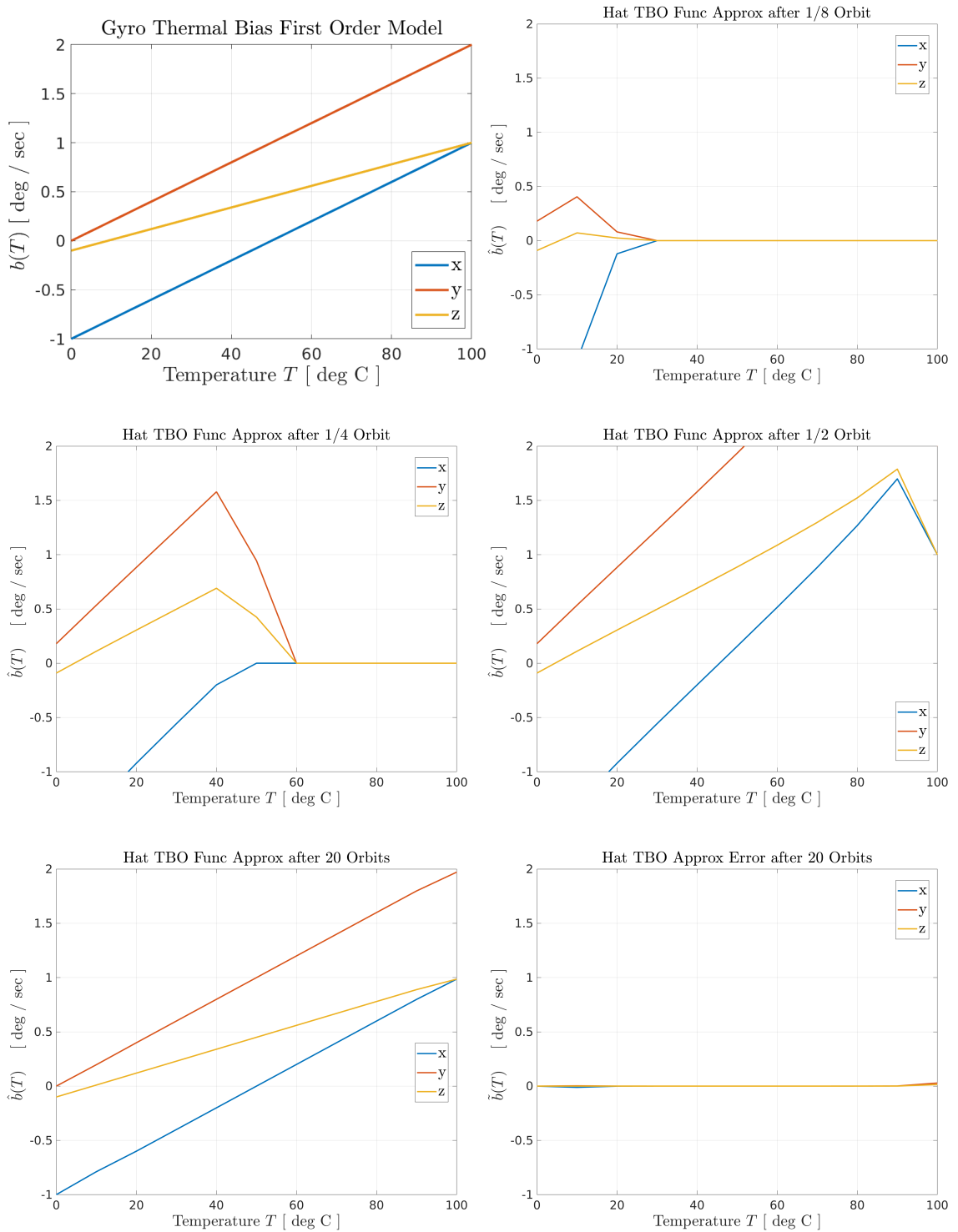


Figure 3.17: The hat TBO estimates the first order gyro thermal bias function of Equation

3.7.

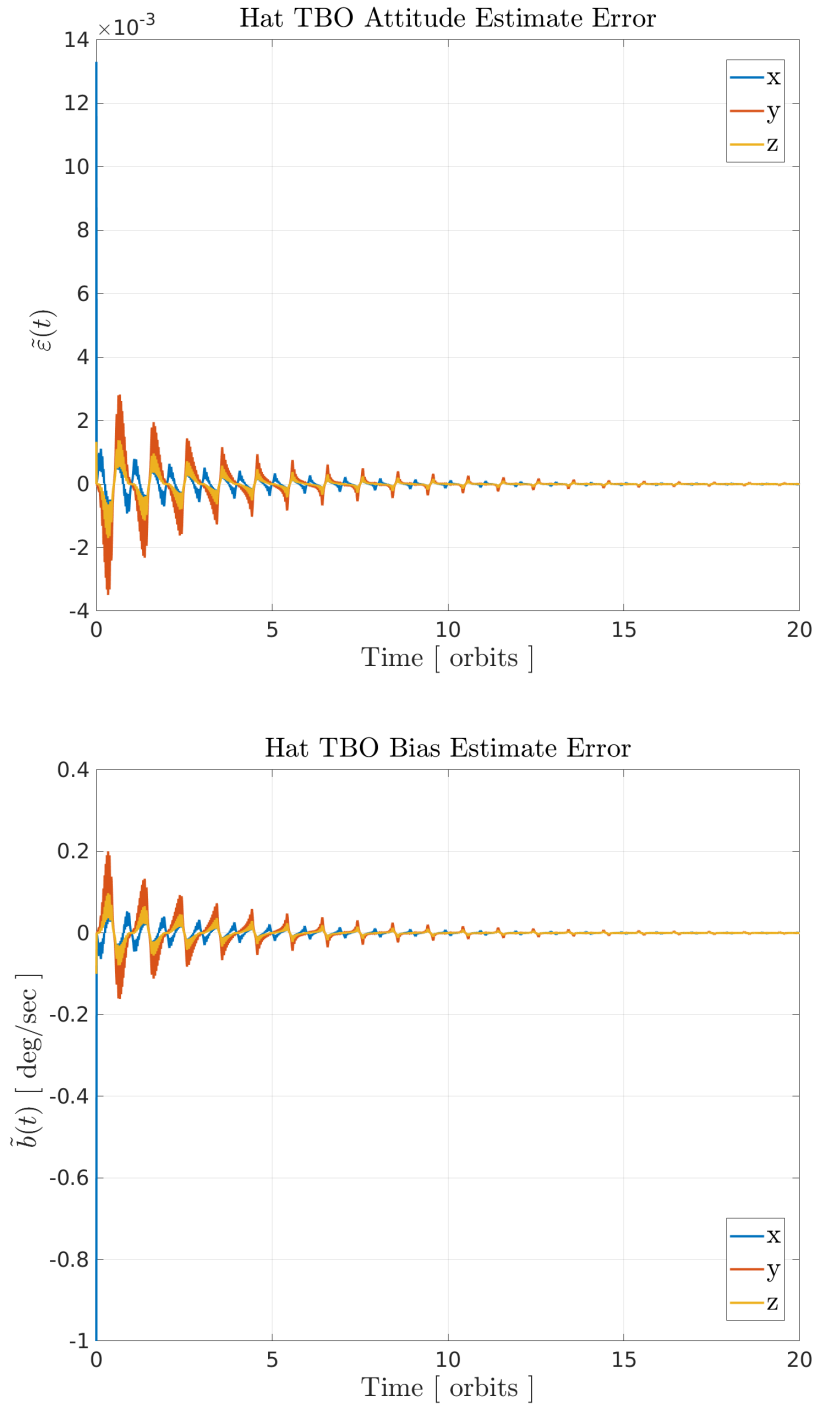


Figure 3.18: Time series plots of the attitude and estimate error for the hat TBO as it estimates the first order gyro thermal bias function of Equation 3.7.

The Gaussian TBO, parameterized by the same tracking gain k and adaptation gain α , experiences a significantly longer transient than the boxcar or hat TBOs. Figure 3.19 depicts the gyro thermal bias function estimate at the same simulation times as the boxcar and hat TBOs, but after 20 orbits the Gaussian TBO has yet to capture the linear shape of the true gyro thermal bias function, particularly at the edges of the temperature interval. The time series plots in Figure 3.20 confirm that the Gaussian TBO has not yet reached steady state after 20 orbits. Figure 3.21 displays the Gaussian TBO thermal bias function estimate at 10 orbits, 100 orbits, and 1000 orbits, where the Gaussian TBO's bias function estimate error finally reaches the level of the Hat TBO's function error estimate after just 20 orbits.

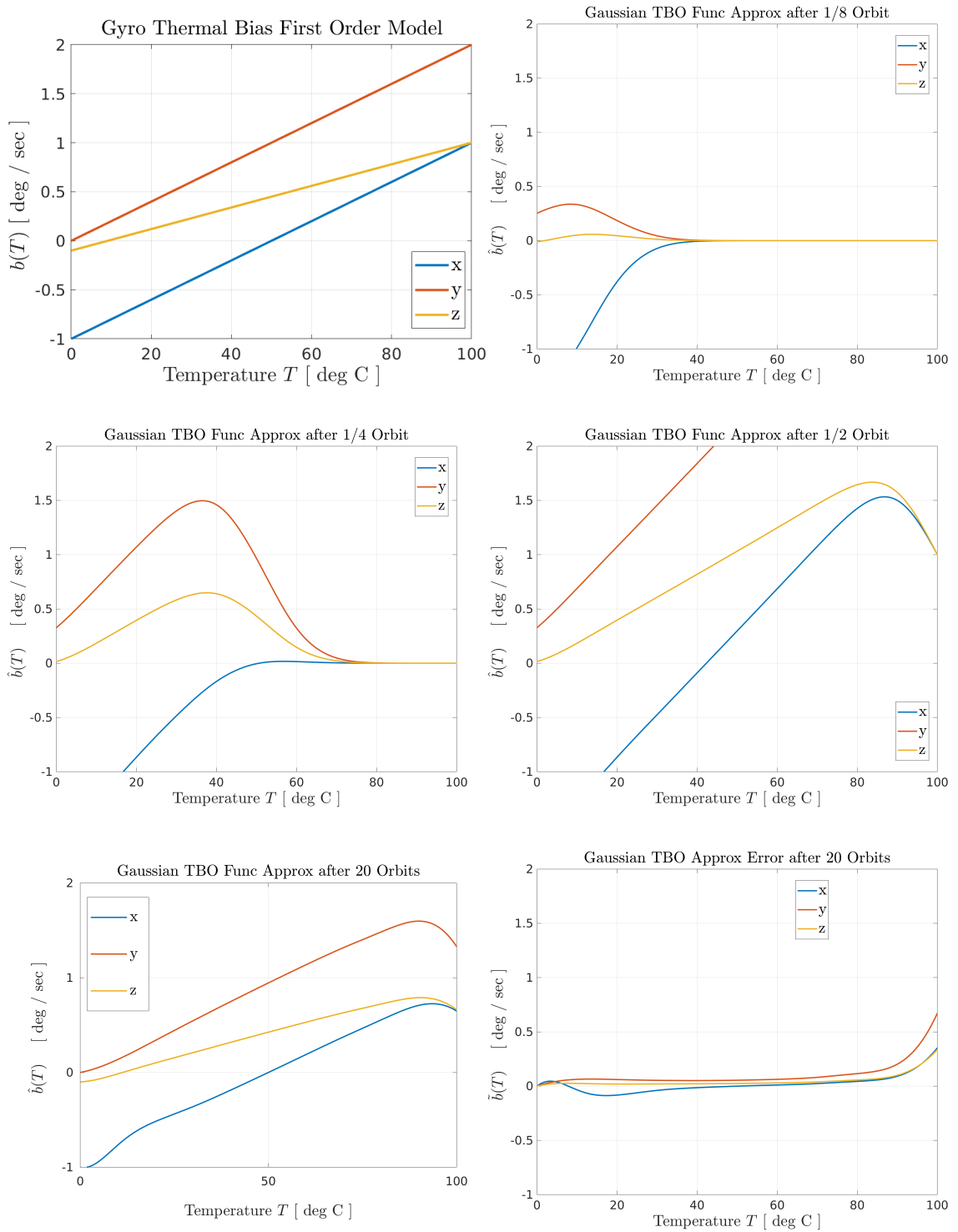


Figure 3.19: The Gaussian TBO estimates the first order gyro thermal bias function of Equation 3.7.

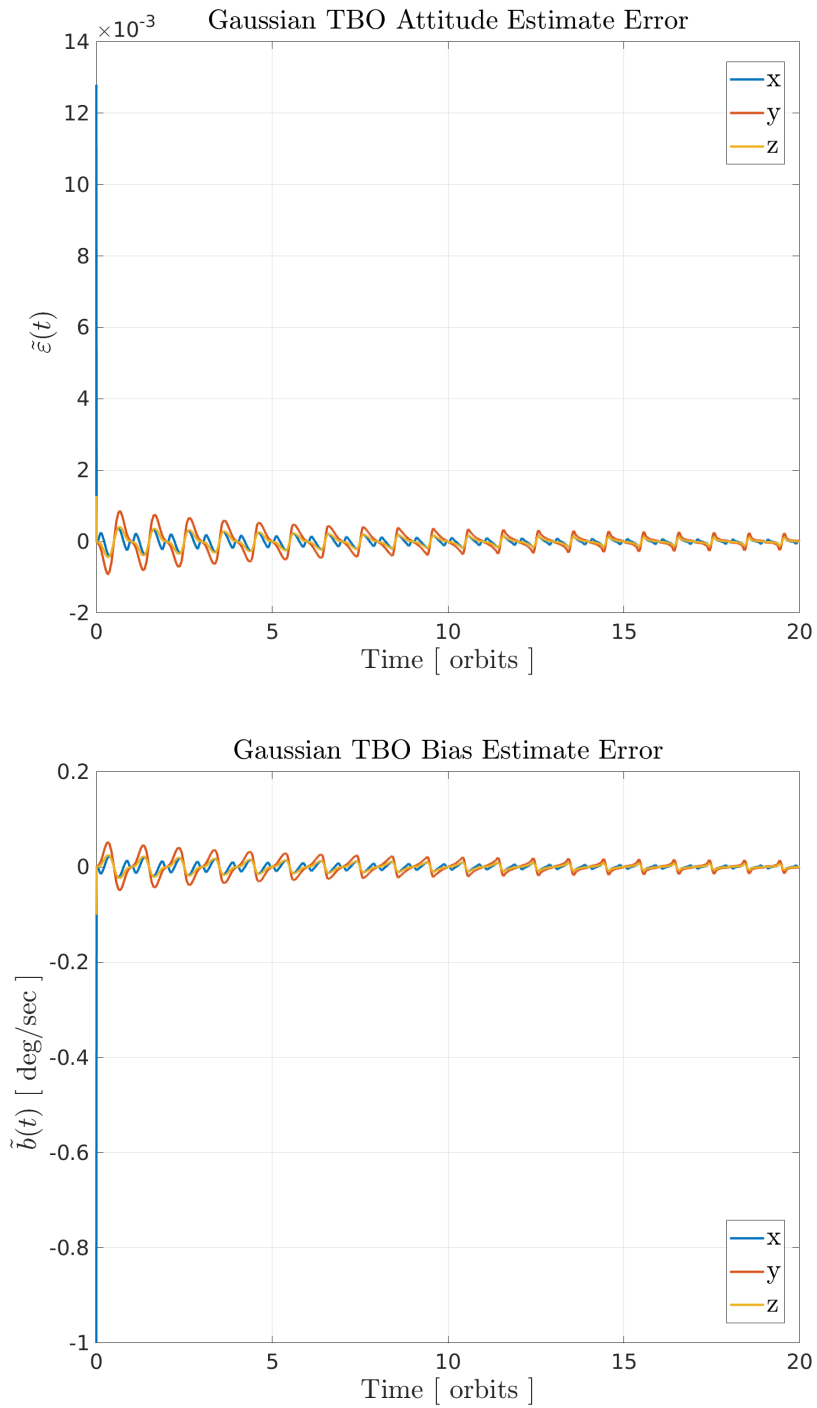


Figure 3.20: Time series plots of the attitude and estimate error for the Gaussian TBO as it estimates the first order gyro thermal bias function of Equation 3.7.

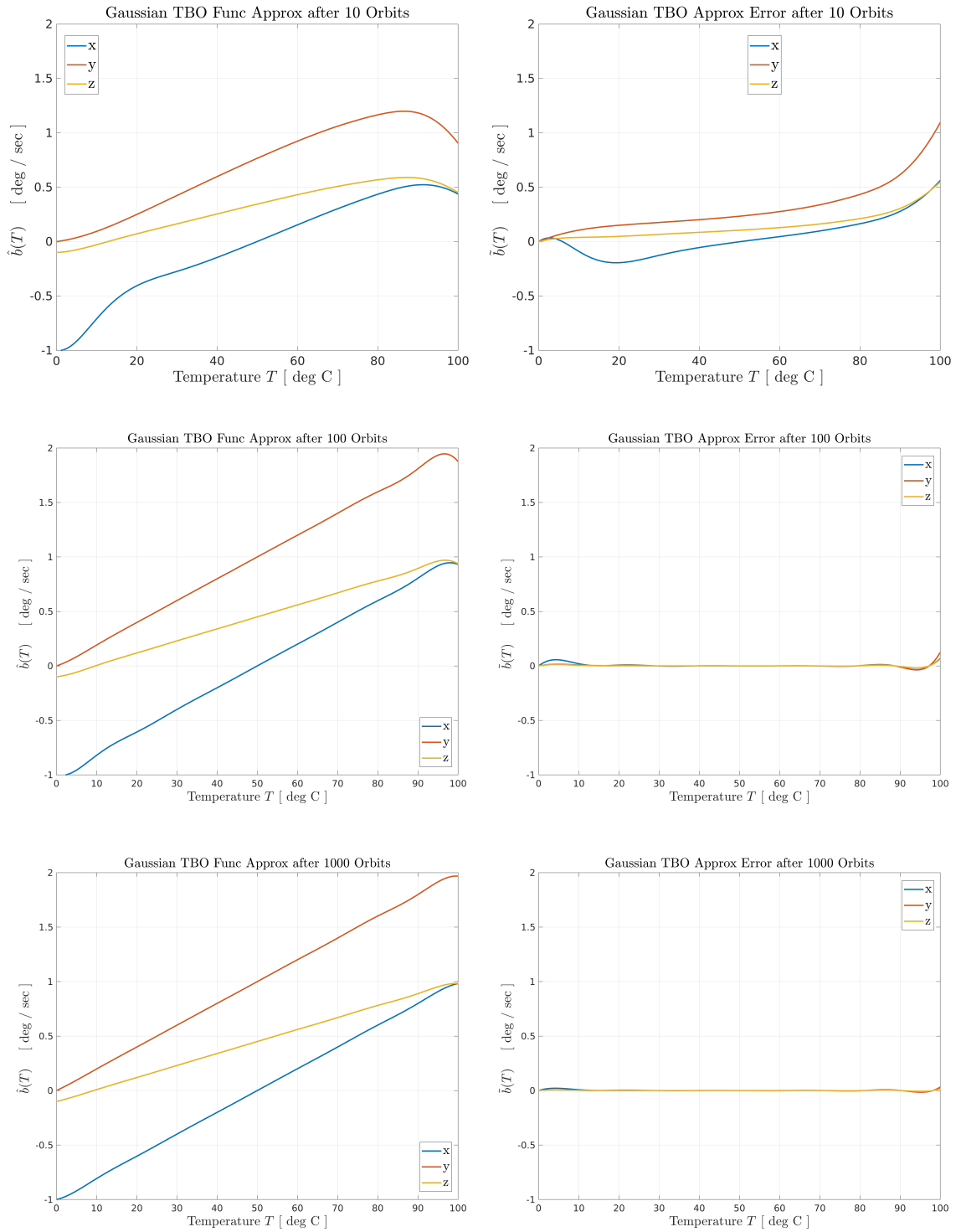


Figure 3.21: The Gaussian TBO estimates the first order gyro thermal bias function of Equation 3.7.

Figure 3.22 shows the boxcar TBO estimating the third order gyro thermal bias function of Equation 3.8. The bias estimate error for the boxcar TBO is more pronounced for this model than the first order model, which is to be expected as higher order information is harder for the boxcar approximation to capture. The transient response is similar to the first order thermal model case however, needing only half an orbit (the ability to experience the full gyro operating temperature range) to reach a steady state performance level.

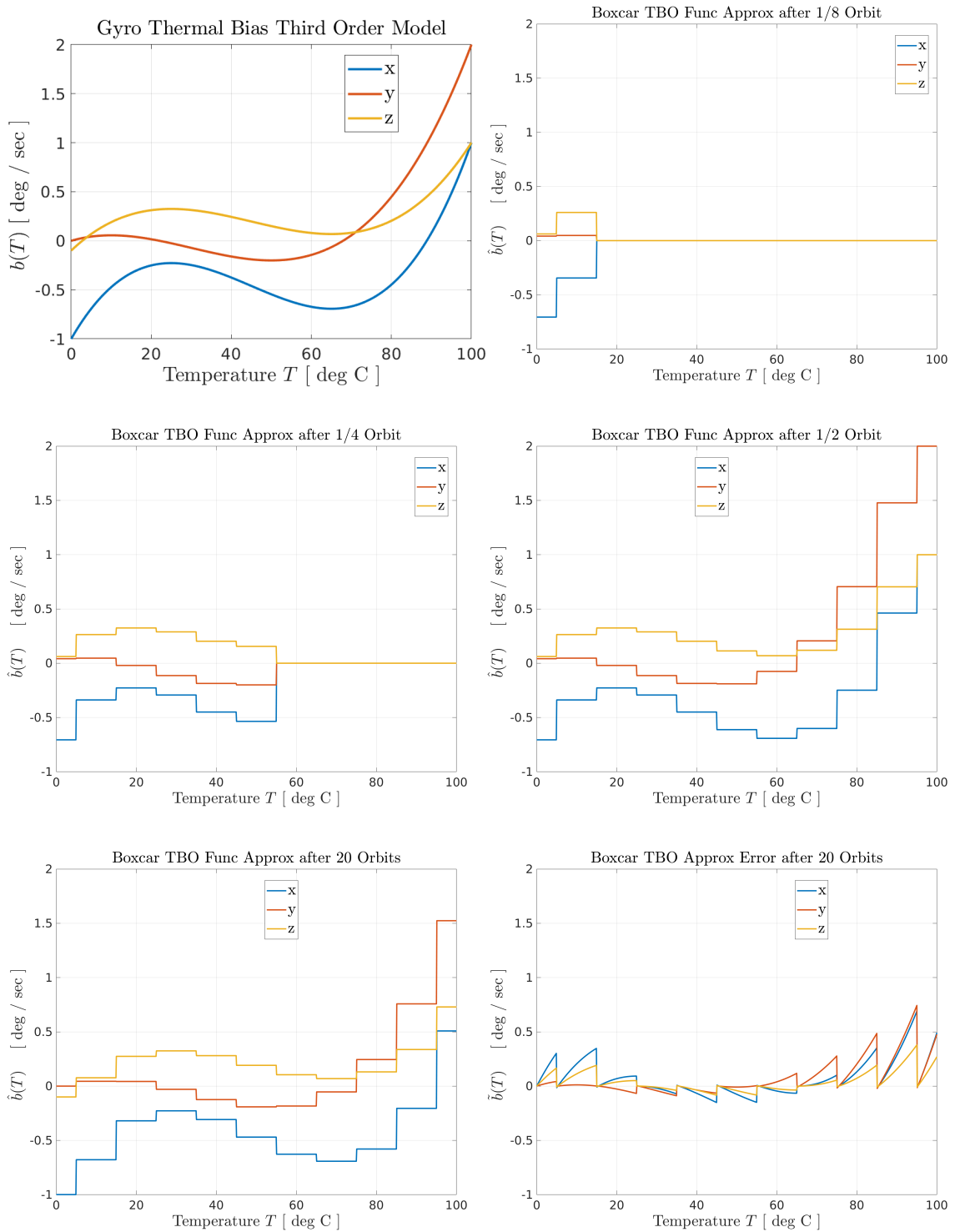


Figure 3.22: The boxcar TBO estimates the third order gyro thermal bias function of Equation 3.8.

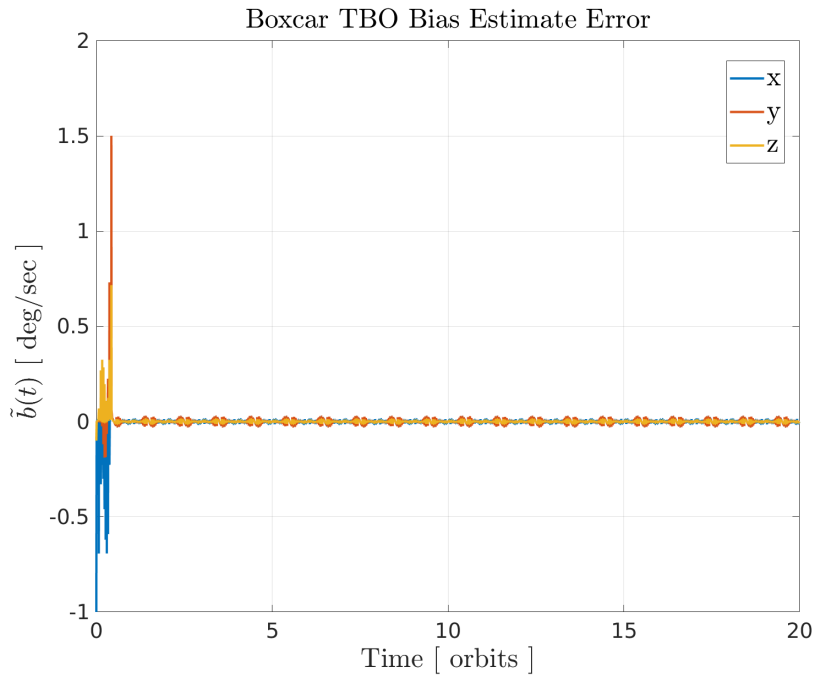
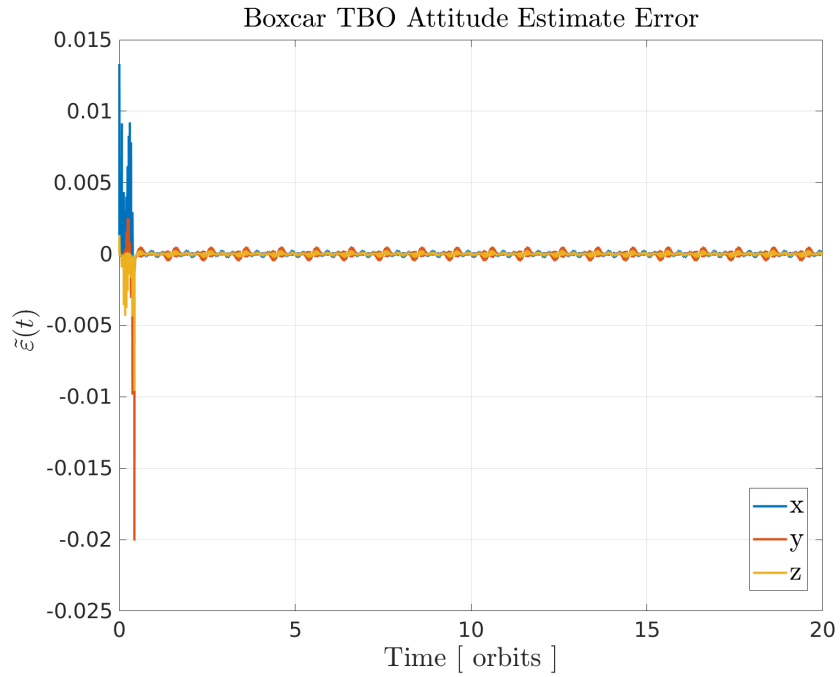


Figure 3.23: Time series plots of the attitude and estimate error for the boxcar TBO as it estimates the third order gyro thermal bias function of Equation 3.8.

The hat TBO bias function estimation process for the third order gyro thermal bias function of Equation 3.8 is depicted in Figure 3.24. The corresponding time series plots are included in Figure 3.25. The estimate error settling time for the third order gyro thermal bias model case as for the first order gyro thermal bias model case. Note that in this case, as opposed to the case of the first order gyro thermal bias model, that there is significant bias function estimate error. This is to be expected as the order of the true gyro thermal bias function now exceeds what can be encoded by a first order spline (hat RBF).

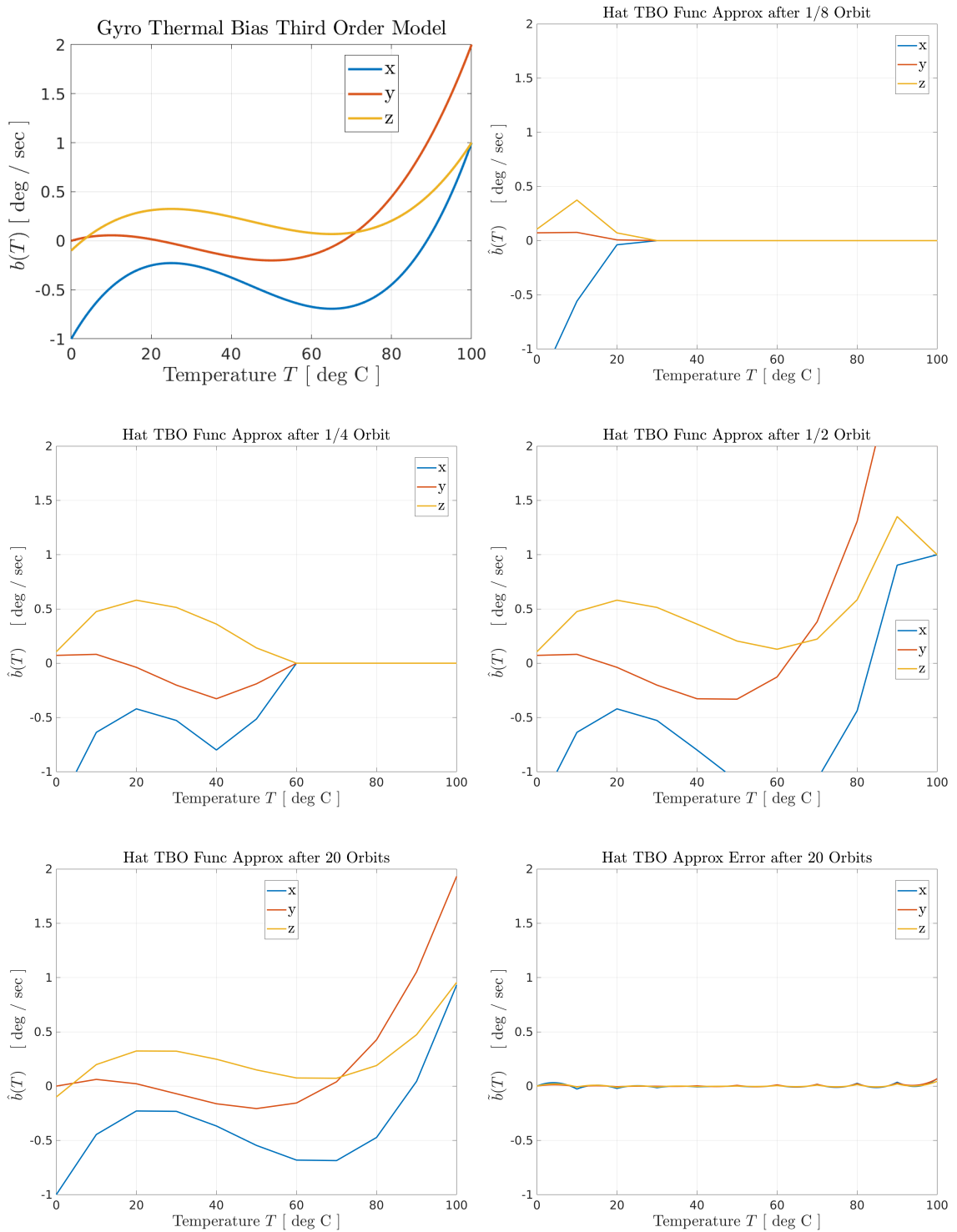


Figure 3.24: The hat TBO estimates the third order gyro thermal bias function of Equation 3.8.

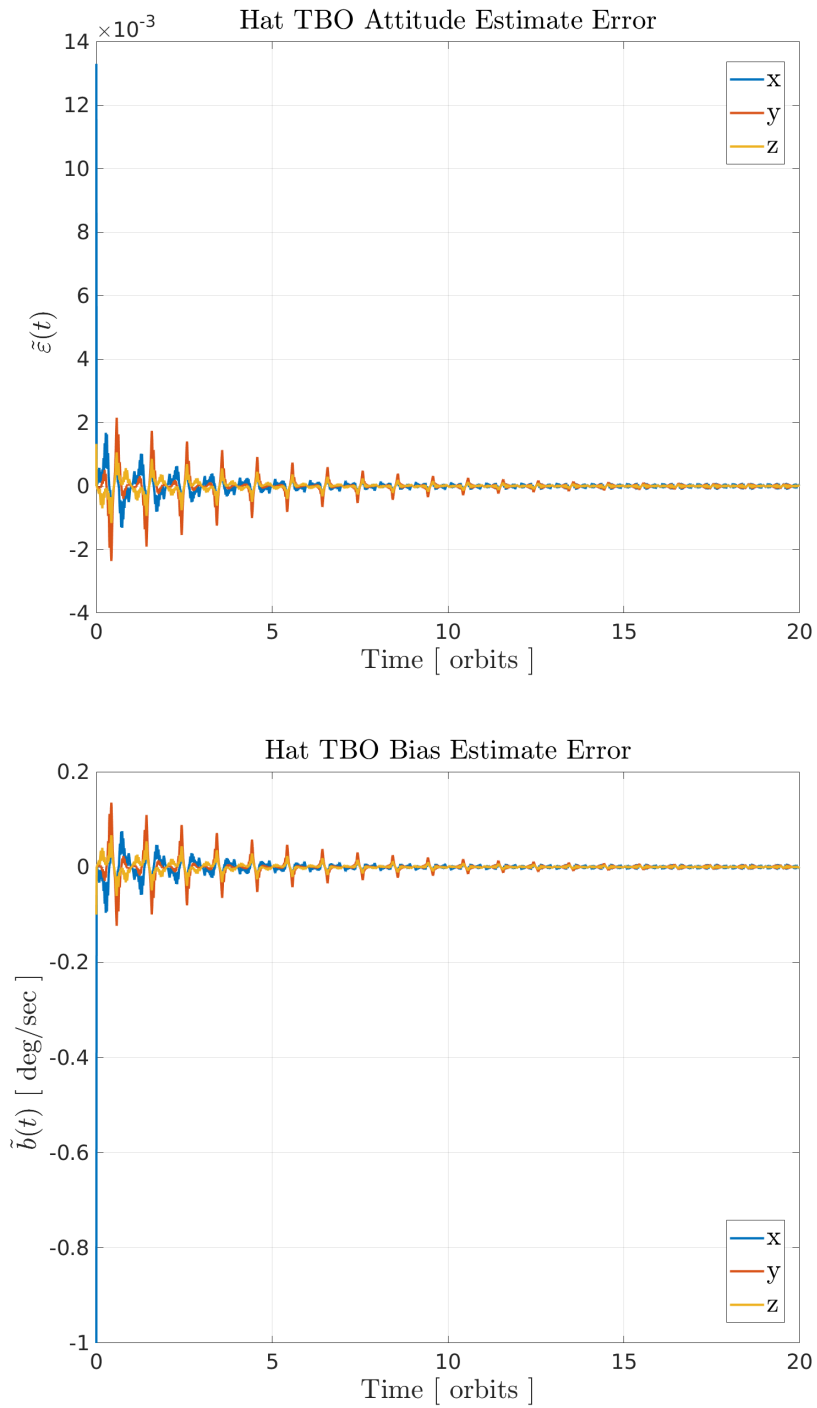


Figure 3.25: Time series plots of the attitude and estimate error for the hat TBO as it estimates the third order gyro thermal bias function of Equation 3.8.

The last permutation to consider is the Gaussian TBO estimating a third order gyro thermal bias function of temperature. The bias function estimates are depicted in Figure 3.26. As in the case of the Gaussian TBO estimating a first order gyro thermal bias, the Gaussian TBO takes significantly longer than the boxcar or hat TBOs to reach a steady state. Again, the Gaussian TBO's estimates of the gyro thermal bias function are worst at the edges of the experienced temperature range. The time series plots of Figure 3.27 show that by 20 orbits the observer's estimates still haven't converged. Figure 3.28 compares the Gaussian TBO's thermal bias function estimation performance at 10, 100, and 1000 orbits. After 1000 orbits have elapsed, the Gaussian TBO's thermal bias function estimate error near 0 and 100 degrees Celsius is finally of the same order of magnitude as the hat TBO was after 20 orbits. However, in this third order gyro thermal bias function case the smoothness of the Gaussian function approximation leads to significantly less bias function estimation error once the transient has settled.

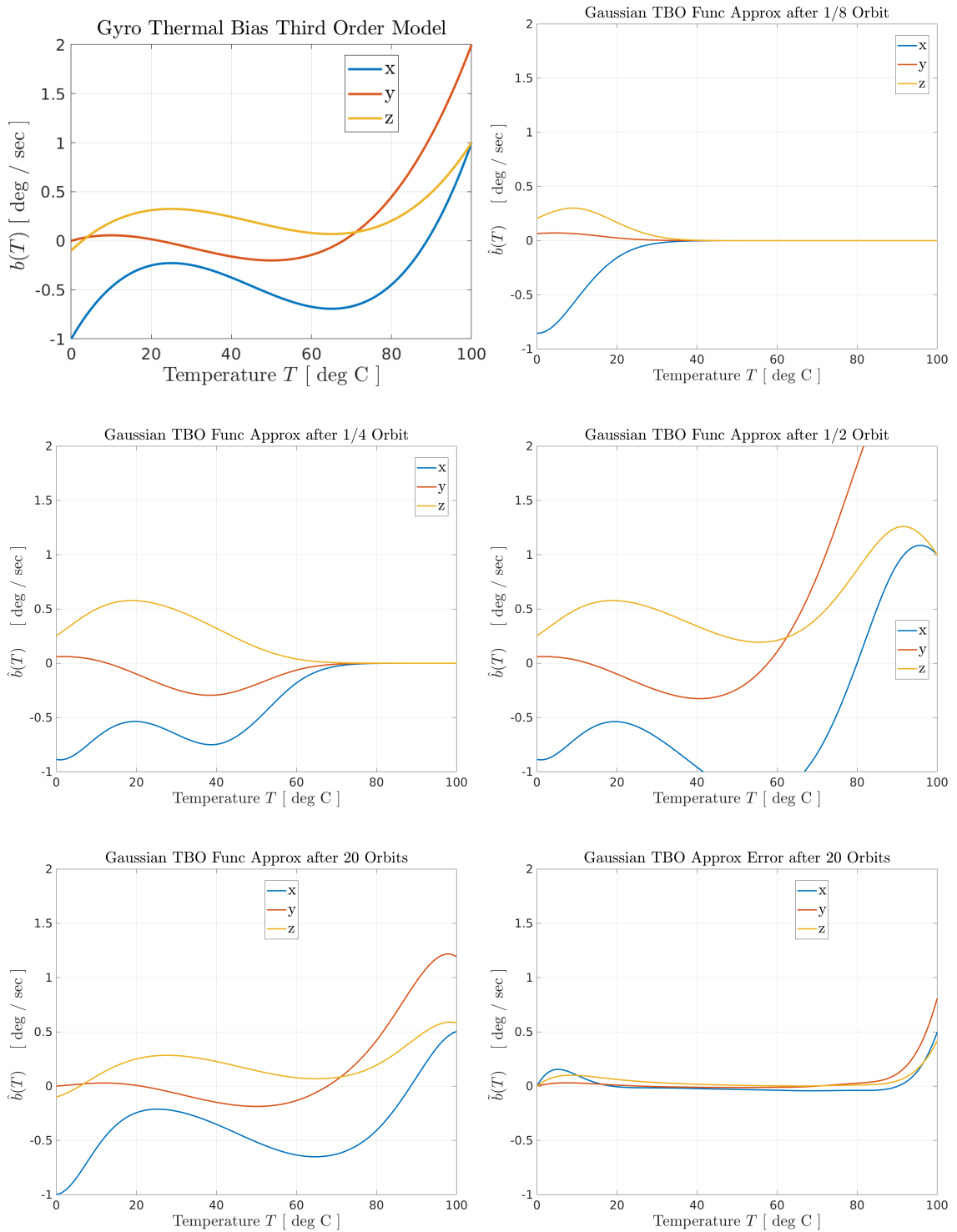


Figure 3.26: The Gaussian TBO estimates the third order gyro thermal bias function of Equation 3.8.

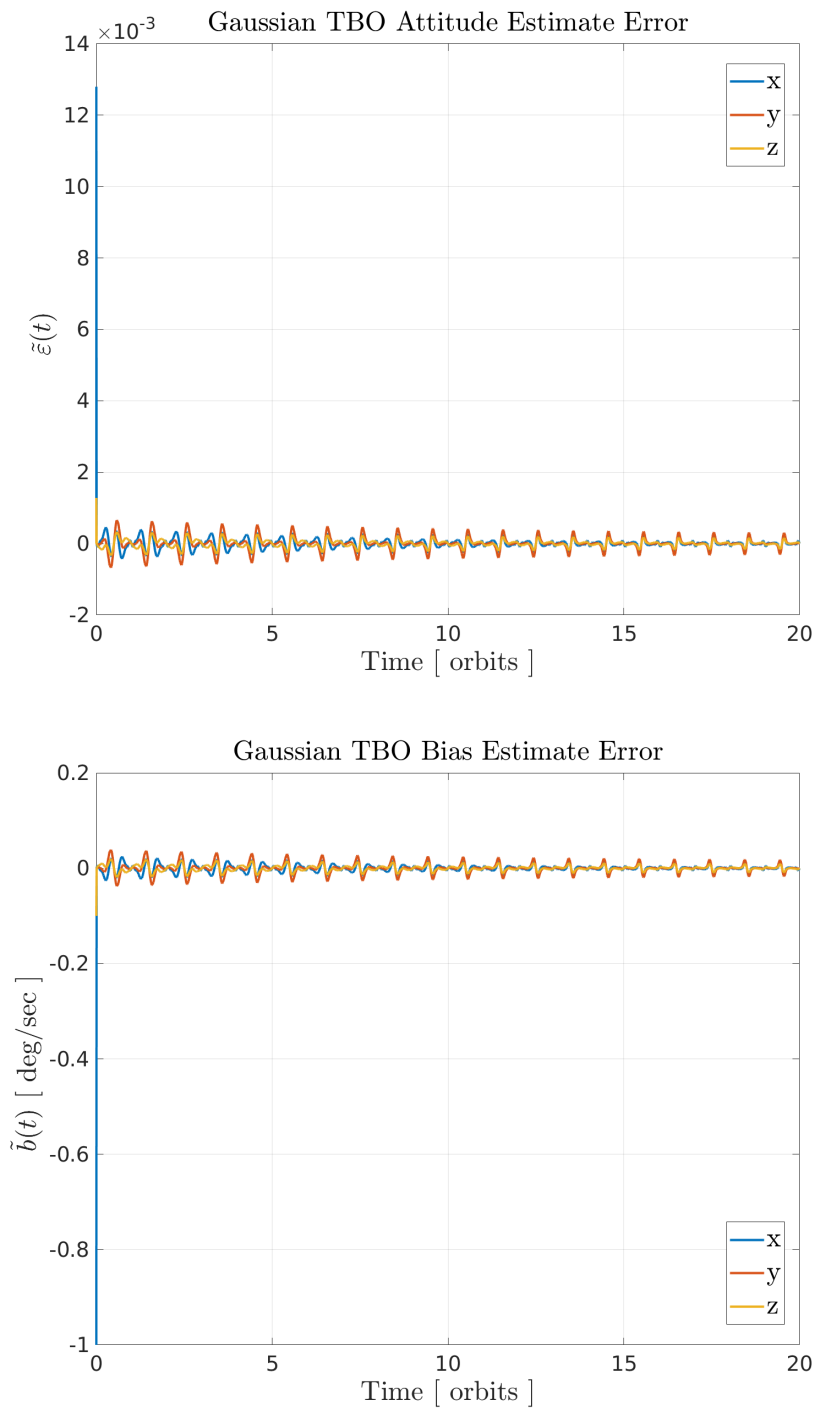


Figure 3.27: Time series plots of the attitude and bias estimate error for the Gaussian TBO as it estimates the third order gyro thermal bias function of Equation 3.8.

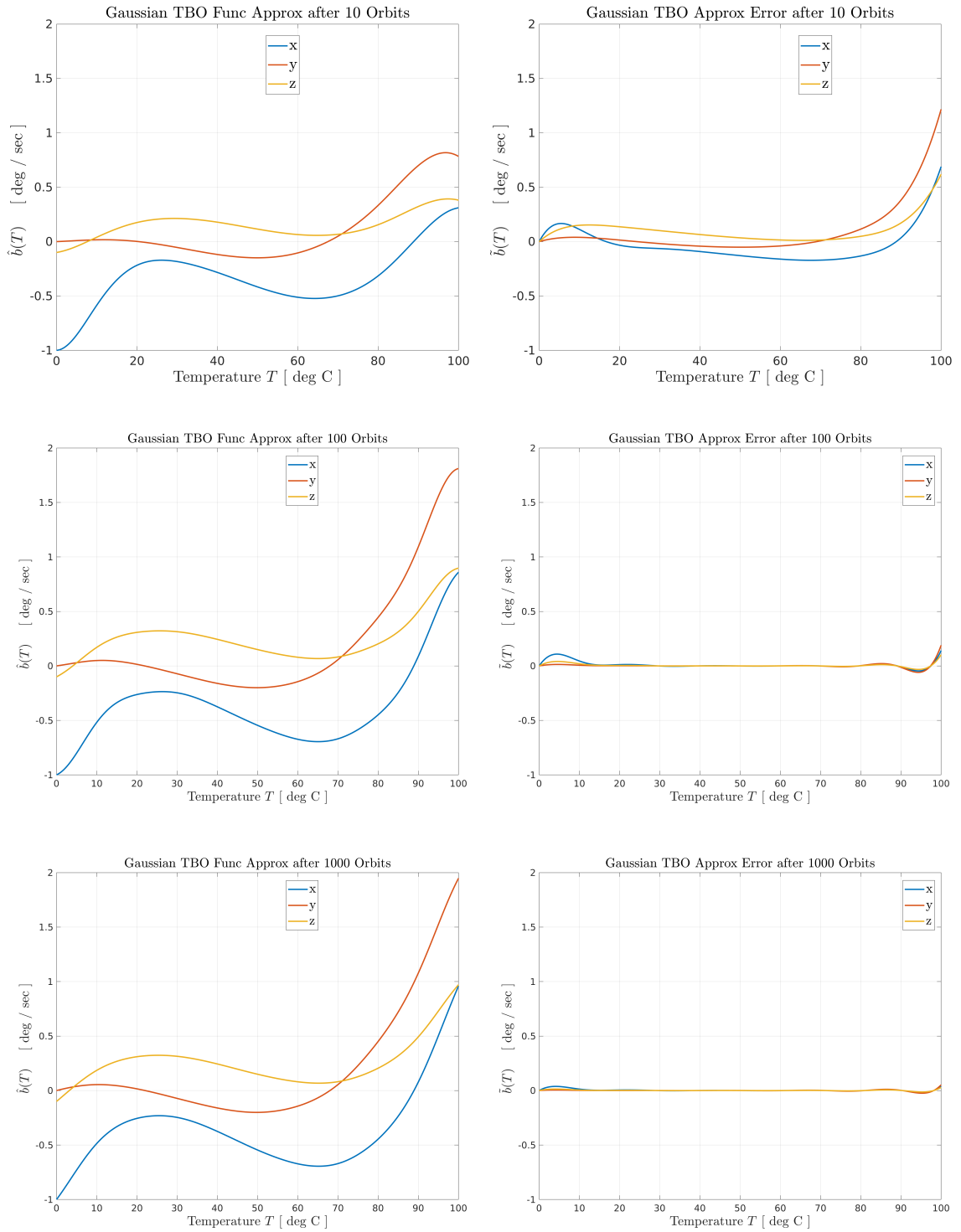


Figure 3.28: The Gaussian TBO estimates the third order gyro thermal bias function of Equation 3.8.

Figure 3.29 shows the transient response for the CBO, boxcar TBO, hat TBO, and Gaussian TBO for the third order gyro thermal bias function of Equation 3.8. As before, the gyro operating temperature sinusoidally oscillates with a period of 90 minutes and all observers have tracking gain $k_e = 1$ and adaptation gain $\alpha = 0.1$ with no observer having any initial knowledge of the gyro bias. The CBO and boxcar TBO experience very short transients (less than an orbit), but have the worst gyro bias estimate performance in steady state. The hat TBO takes approximately 15 orbits to converge, but its steady state error is less than the CBO and boxcar TBO. The Gaussian TBO takes much longer to converge than 20 orbits as noted before. The top plot of Figure 3.30 shows that the Gaussian TBO converges after approximately 1000 orbits, but the steady state performance has again improved. The convergence rate can be reduced by increasing the adaptation gain; the bottom plot in Figure 3.30 has an order-of-magnitude larger adaptation gain of $\alpha = 1$ and the convergence time is approximately 500 orbits.

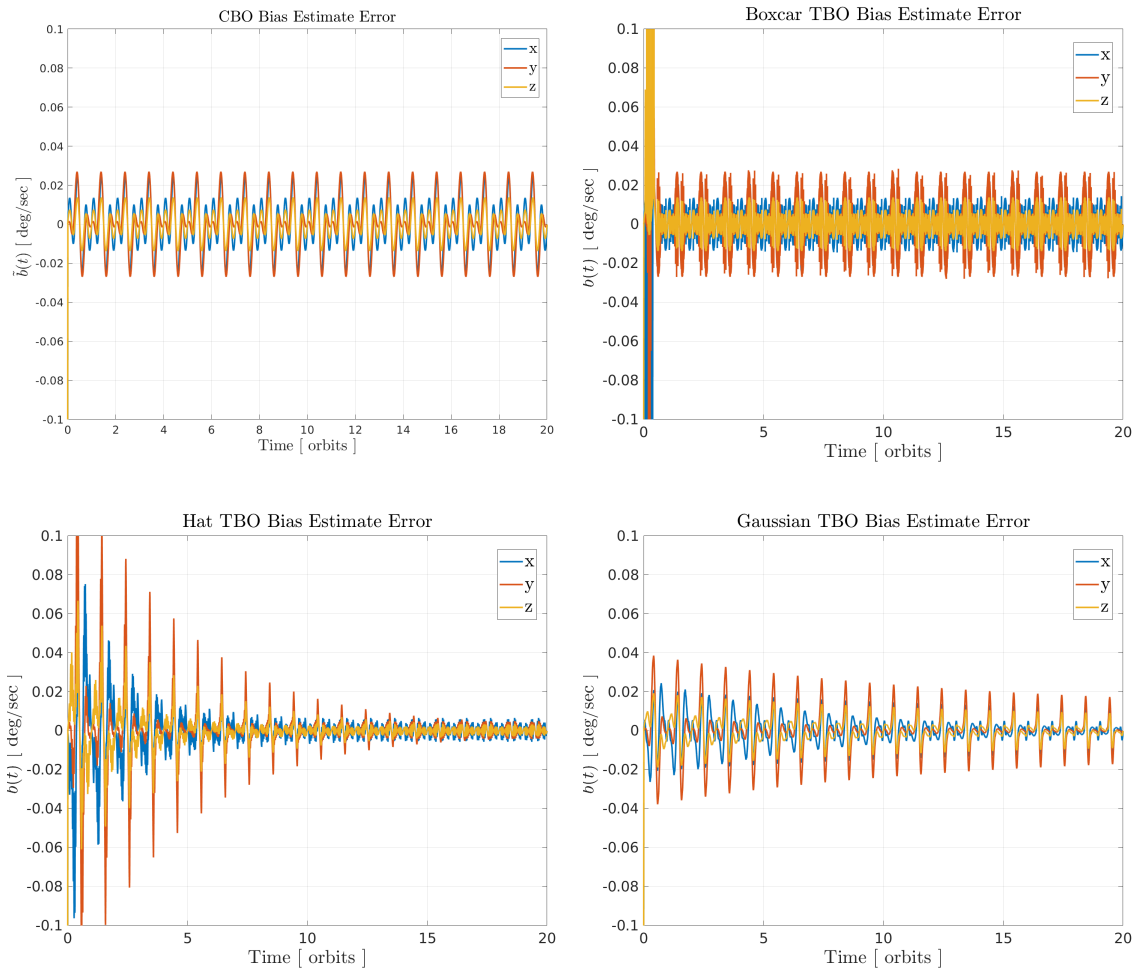


Figure 3.29: Comparison of the observer's bias estimate error time series for the third order gyro thermal bias function of Equation 3.8.

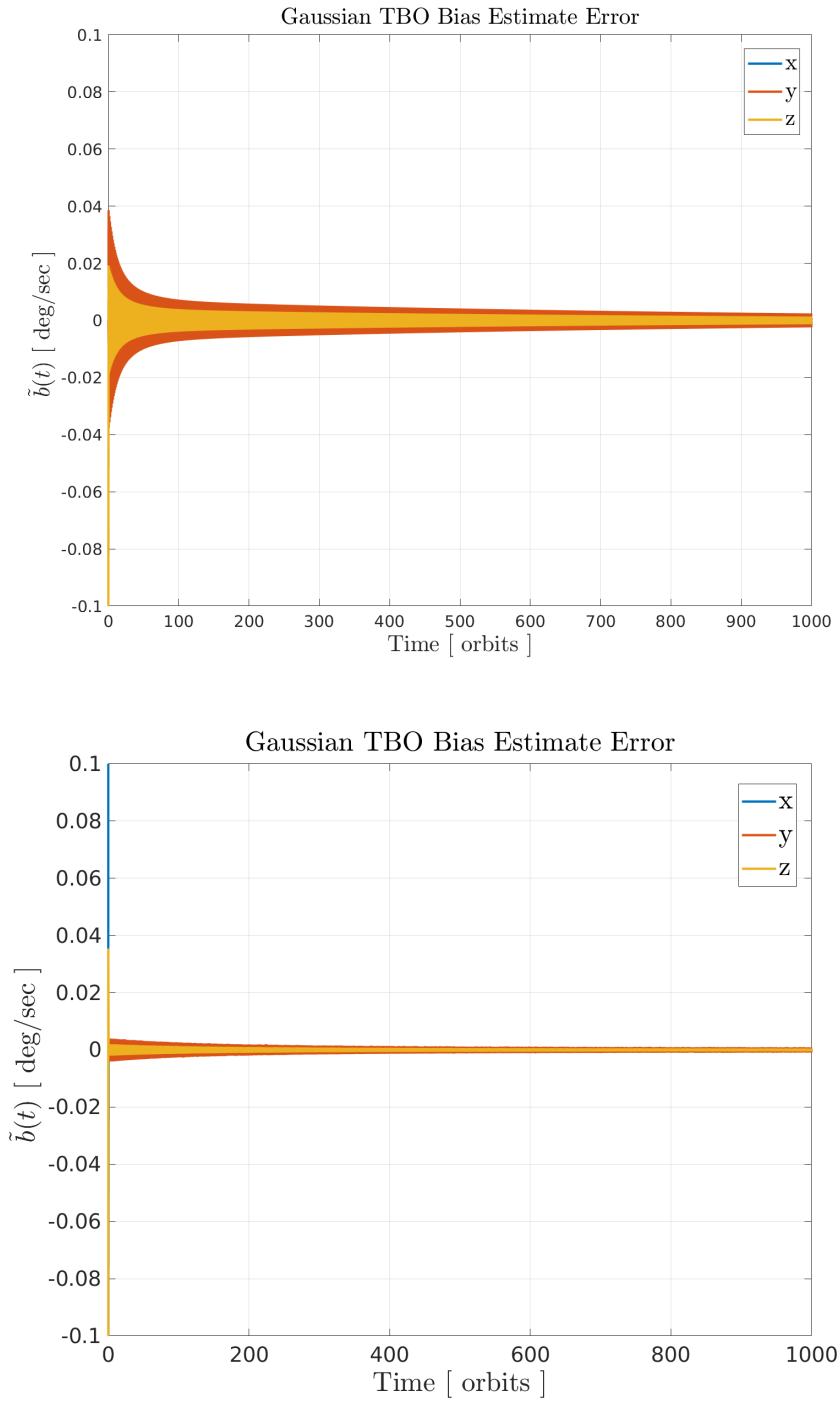


Figure 3.30: Time series plots of the estimate estimate error for the Gaussian TBO as it estimates the third order gyro thermal bias function of Equation 3.8. In the top plot $k_e = 1$ and $\alpha = 0.1$; in the bottom plot $k_e = 1$ and $\alpha = 1$.

Table 3.1: Comparison of the steady-state bias estimate error for the CBO, boxcar TBO, hat TBO, and Gaussian TBO; error statistics are the ergodic average of the last 100 orbits' worth of bias estimate errors from 1000 orbit long simulations.

Observer	Mean $\left[\ \tilde{\mathbf{b}}(t_i)\ \right]$ in $\frac{\text{deg}}{\text{sec}}$
CBO	0.01634
Boxcar TBO	0.01523
Hat TBO	0.00316
Gaussian TBO	0.00086

The steady-state performance of the CBO, boxcar TBO, hat TBO, and Gaussian TBO are compared in Table 3.1. For each entry in the table, the indicated observer was simulated for 1000 orbits with the tracking gain $k_e = 1$ and adaptation gain $\alpha = 0.1$. The ergodic mean was computed from the time series of the bias estimate error $\tilde{\mathbf{b}}(t) = \mathbf{b}(T(t)) - \hat{\mathbf{b}}(T(t))$ over the final 100 orbits. As noted previously, the CBO and boxcar TBO have very similar performance as the boxcar TBO's gyro thermal bias function approximation is little better than the CBO's. The hat TBO has nearly an order of magnitude improvement in bias estimate error as the hat basis provides a more useful gyro thermal bias function approximation. Finally, the Gaussian TBO's bias estimate error is nearly an order of magnitude better than the hat TBO's as the Gaussian basis is capable of perfectly approximating third order polynomial functions.

3.7 Gyro CBO and TBO Stochastic Simulation Models

The CBO of Thienel and Sanner [95] and the TBO were developed in a deterministic setting. Global exponential stability (GES) of the CBO is guaranteed by the work of Thienel and Sanner for a constant gyro bias. They also point out that the GES property implies the CBO estimate error is bounded for bounded gyro noise; they provide a bound on the estimate error as a function of a bound on the noise. In Section 3.5 the TBO was found to be stable for sufficiently smooth time-invariant gyro thermal bias models. In neither sets of analyses was *unbounded* additive gyro noise considered, nor was attitude measurement noise considered. Neither sets of analyses provided insight on how to choose the observer gain parameters.

Of course the attitude estimation performance of the observers is affected by sensor noise and choice of gain parameters. In this section, stochastic differential equations will be developed to model the impact of attitude measurement noise and gyro noise on the observers. Subsequent sections of this chapter will then use stochastic integration techniques to explore how measurement noise influences the estimate errors of the observers.

In the stochastic setting, the gyro measurement model of Equation 3.10 is now augmented with additive noise as

$$\boldsymbol{\omega}_g(t) = \boldsymbol{\omega}(t) + \mathbf{b}(T(t)) + \sigma_w \mathbf{n}_w(t) \quad (3.25)$$

where σ_w is a positive scaling constant and $\mathbf{n}_w(\cdot)$ is a zero mean unit variance Gaussian white noise process.

In addition to gyro measurement noise, the observers are also assumed to have attitude measurements with noise. The attitude measurement $\mathbf{q}_m(t)$, possibly from a quaternion output star tracker, is a noise corrupted version of the true vehicle attitude $\mathbf{q}(t)$

$$\mathbf{q}_m(t) = \begin{bmatrix} \boldsymbol{\varepsilon}_m(t) \\ \eta_m(t) \end{bmatrix} = \check{\mathbf{q}}^{-1}(t) \otimes \mathbf{q}(t) \quad (3.26)$$

where $\check{\mathbf{q}}(\cdot)$ is “quaternion noise”. Note that the stochastic numerical integration methods presented in Section 2.2 are defined only for Itô diffusions, a specific class of SDEs that are affine in the driving noise.

As will be explained in detail in Section 5.1, an Itô SDE that is useful for generating quaternion measurement noise is given by the Langevin form differential equation

$$\dot{\mathbf{q}}_m(t) = \frac{1}{2} \{ R(\check{\mathbf{q}}^{-1}(t)) [\boldsymbol{\omega}(t) + \sigma_m \mathbf{n}_m(t) + k_m \check{\eta}(t) \check{\boldsymbol{\varepsilon}}(t)] \} \otimes \mathbf{q}_m(t) \quad (3.27)$$

where k_m and σ_m are positive scalars that parameterize the attitude measurement noise statistics, $\mathbf{n}_m(\cdot)$ is a collection of independent identically distributed zero mean unit variance Gaussian white noise processes independent of $\mathbf{n}_w(\cdot)$, and $\check{\mathbf{q}}(t)$ compares the attitude measurement process to the true attitude

$$\check{\mathbf{q}}(t) = \mathbf{q}(t) \otimes \mathbf{q}_m^{-1}(t) = \begin{bmatrix} \check{\boldsymbol{\varepsilon}}(t) \\ \check{\eta}(t) \end{bmatrix} \quad (3.28)$$

In Chapter 4.10 the attitude measurement noise process $\check{\mathbf{q}}(t)$ will be shown to have the heuristic upper bound on its ultimate noise statistics

$$\lim_{t \rightarrow \infty} E \left[\check{\boldsymbol{\varepsilon}}^T(t) \check{\boldsymbol{\varepsilon}}(t) \right] \leq \frac{3}{4} \left(1 - \frac{I_1 \left(\frac{k_m}{3\sigma_m^2} \right)}{I_0 \left(\frac{k_m}{3\sigma_m^2} \right)} \right) \quad (3.29)$$

where $I_0(\cdot)$ and $I_1(\cdot)$ are the 0^{th} and 1^{st} modified Bessel functions of the first kind. The bound 3.29 provides a way to parameterize the attitude measurement noise by selection of the ratio $\frac{k_m}{\sigma_m^2}$.

In the forthcoming stochastic models for the CBO and TBO, the observers will no longer have access to the true attitude to compute the attitude estimate error $\tilde{\mathbf{q}}(t)$ for use in their feedback term $\tilde{\eta}(t)\tilde{\boldsymbol{\epsilon}}(t)$. Instead, the observers will be provided the noise corrupted attitude measurement $\mathbf{q}_m(t)$ generated from the model of Equation 3.27, so they instead compute a corrupted attitude estimate error

$$\begin{aligned}\tilde{\mathbf{q}}_m(t) &= \begin{bmatrix} \tilde{\boldsymbol{\epsilon}}_m(t) \\ \tilde{\eta}_m(t) \end{bmatrix} = \mathbf{q}_m(t) \otimes \hat{\mathbf{q}}^{-1}(t) \\ &= \check{\mathbf{q}}^{-1}(t) \otimes \mathbf{q}(t) \otimes \hat{\mathbf{q}}^{-1}(t) \\ &= \check{\mathbf{q}}^{-1}(t) \otimes \tilde{\mathbf{q}}(t)\end{aligned}$$

which results in the corrupted feedback term

$$\tilde{\eta}_m(t)\tilde{\boldsymbol{\epsilon}}_m(t) = \left(\check{\eta}(t)\tilde{\eta} + \check{\boldsymbol{\epsilon}}^T(t)\tilde{\boldsymbol{\epsilon}}(t) \right) \left[-\tilde{\eta}(t)\check{\boldsymbol{\epsilon}}(t) + \check{\eta}(t)\tilde{\boldsymbol{\epsilon}}(t) + \check{\boldsymbol{\epsilon}}(t) \times \tilde{\boldsymbol{\epsilon}}(t) \right] \quad (3.30)$$

Combining the CBO dynamics equations 3.3 and 3.4 with the gyro measurement model of Equation 3.25 and the attitude measurement model from Equation

3.27 results in the Langevin form differential equation for the CBO

$$\begin{aligned}
\begin{bmatrix} \dot{\hat{\mathbf{e}}}_m \\ \dot{\hat{\eta}}_m \\ \dot{\hat{\boldsymbol{\epsilon}}}_m \\ \dot{\hat{\eta}} \\ \dot{\hat{\mathbf{b}}} \end{bmatrix} &= \begin{bmatrix} \frac{1}{2} [\eta_m I + [\boldsymbol{\epsilon}_m \times]] R(\mathbf{q}^{-1}) [\boldsymbol{\omega} + k_m \check{\eta} \check{\boldsymbol{\epsilon}}] \\ -\frac{1}{2} \boldsymbol{\epsilon}_m^T R(\mathbf{q}^{-1}) [\boldsymbol{\omega} + k_m \check{\eta} \check{\boldsymbol{\epsilon}}] \\ \frac{1}{2} [\hat{\eta} I + [\hat{\boldsymbol{\epsilon}} \times]] R(\mathbf{q}_m^{-1}) [\boldsymbol{\omega} + \mathbf{b}(T) - \hat{\mathbf{b}} + k_e \tilde{\eta}_m \tilde{\boldsymbol{\epsilon}}_m] \\ -\frac{1}{2} \hat{\boldsymbol{\epsilon}}^T R(\mathbf{q}_m^{-1}) [\boldsymbol{\omega} + \mathbf{b}(T) - \hat{\mathbf{b}} + k_e \tilde{\eta}_m \tilde{\boldsymbol{\epsilon}}_m] \\ -\alpha \tilde{\eta}_m \tilde{\boldsymbol{\epsilon}}_m \end{bmatrix} \\
&+ \begin{bmatrix} \frac{1}{2} [\eta_m I + [\boldsymbol{\epsilon}_m \times]] R(\mathbf{q}^{-1}) \sigma_m & 0 \\ -\frac{1}{2} \boldsymbol{\epsilon}_m^T R(\mathbf{q}^{-1}) \sigma_m & 0 \\ 0 & \frac{1}{2} [\hat{\eta} I + [\hat{\boldsymbol{\epsilon}} \times]] R(\mathbf{q}_m^{-1}) \sigma_w \\ 0 & -\frac{1}{2} \hat{\boldsymbol{\epsilon}}^T R(\mathbf{q}_m^{-1}) \sigma_w \\ 0 & 0 \end{bmatrix} \begin{bmatrix} \mathbf{n}_m \\ \mathbf{n}_w \end{bmatrix}
\end{aligned} \tag{3.31}$$

where function of time notation has been suppressed for brevity. The quaternion rotation matrix identities $[\eta I + [\boldsymbol{\epsilon} \times]] R(\mathbf{q}) = [\eta I + [\boldsymbol{\epsilon} \times]]$ and $\boldsymbol{\epsilon}^T R(\mathbf{q}) = \boldsymbol{\epsilon}^T$ were used to further simplify the expression.

Per Section 2.1.3, the Langevin form error dynamics differential equation 3.31

is interpreted as a Stratonovich SDE. Converting to an Itô SDE yields

$$\begin{aligned}
\begin{bmatrix} d\boldsymbol{\varepsilon}_m \\ d\eta_m \\ d\hat{\boldsymbol{\varepsilon}} \\ d\hat{\eta} \\ d\hat{\boldsymbol{b}} \end{bmatrix} &= \begin{bmatrix} \frac{1}{2} \left[\eta_m I + [\boldsymbol{\varepsilon}_m \times] \right] R(\mathbf{q}^{-1}) \left[\boldsymbol{\omega} + k_m \check{\eta} \check{\boldsymbol{\varepsilon}} \right] - \frac{3}{8} \sigma_m^2 \boldsymbol{\varepsilon}_m \\ -\frac{1}{2} \boldsymbol{\varepsilon}_m^T R(\mathbf{q}^{-1}) \left[\boldsymbol{\omega} + k_m \check{\eta} \check{\boldsymbol{\varepsilon}} \right] - \frac{3}{8} \sigma_m^2 \eta_m \\ \frac{1}{2} \left[\hat{\eta} I + [\hat{\boldsymbol{\varepsilon}} \times] \right] R(\mathbf{q}_m^{-1}) \left[\boldsymbol{\omega} + \mathbf{b}(T) - \hat{\boldsymbol{b}} + k_e \tilde{\eta}_m \tilde{\boldsymbol{\varepsilon}}_m \right] - \frac{3}{8} \sigma_w^2 \hat{\boldsymbol{\varepsilon}} \\ -\frac{1}{2} \hat{\boldsymbol{\varepsilon}}^T R(\mathbf{q}_m^{-1}) \left[\boldsymbol{\omega} + \mathbf{b}(T) - \hat{\boldsymbol{b}} + k_e \tilde{\eta}_m \tilde{\boldsymbol{\varepsilon}}_m \right] - \frac{3}{8} \sigma_w^2 \hat{\eta} \\ -\alpha \tilde{\eta}_m \tilde{\boldsymbol{\varepsilon}}_m \end{bmatrix} dt \\
&+ \begin{bmatrix} \frac{1}{2} \left[\eta_m I + [\boldsymbol{\varepsilon}_m \times] \right] R(\mathbf{q}^{-1}) \sigma_m & 0 \\ -\frac{1}{2} \boldsymbol{\varepsilon}_m^T R(\mathbf{q}^{-1}) \sigma_m & 0 \\ 0 & \frac{1}{2} \left[\hat{\eta} I + [\hat{\boldsymbol{\varepsilon}} \times] \right] R(\mathbf{q}_m^{-1}) \sigma_w \\ 0 & -\frac{1}{2} \hat{\boldsymbol{\varepsilon}}^T R(\mathbf{q}_m^{-1}) \sigma_w \\ 0 & 0 \end{bmatrix} \begin{bmatrix} d\boldsymbol{\beta}_m \\ d\boldsymbol{\beta}_w \end{bmatrix}
\end{aligned} \tag{3.32}$$

where $\tilde{\eta}_m(t) \tilde{\boldsymbol{\varepsilon}}_m(t)$ is expanded in Equation 3.30.

The process is similar for the TBO, resulting in the Itô SDE

$$\begin{aligned}
\begin{bmatrix} d\boldsymbol{\varepsilon}_m \\ d\eta_m \\ d\hat{\boldsymbol{\varepsilon}} \\ d\hat{\eta} \\ d\hat{\mathbf{c}}_0 \\ \vdots \\ d\hat{\mathbf{c}}_N \end{bmatrix} &= \begin{bmatrix} \frac{1}{2} \left[\eta_m I + [\boldsymbol{\varepsilon}_m \times] \right] R(\mathbf{q}^{-1}) \left[\boldsymbol{\omega} + k_m \check{\eta} \check{\boldsymbol{\varepsilon}} \right] - \frac{3}{8} \sigma_m^2 \boldsymbol{\varepsilon}_m \\ -\frac{1}{2} \boldsymbol{\varepsilon}_m^T R(\mathbf{q}^{-1}) \left[\boldsymbol{\omega} + k_m \check{\eta} \check{\boldsymbol{\varepsilon}} \right] - \frac{3}{8} \sigma_m^2 \eta_m \\ \frac{1}{2} \left[\hat{\eta} I + [\hat{\boldsymbol{\varepsilon}} \times] \right] R(\mathbf{q}_m^{-1}) \left[\boldsymbol{\omega} + \mathbf{b}(T) - \hat{\mathbf{b}}(T) + k_e \tilde{\eta}_m \tilde{\boldsymbol{\varepsilon}}_m \right] - \frac{3}{8} \sigma_w^2 \hat{\boldsymbol{\varepsilon}} \\ -\frac{1}{2} \hat{\boldsymbol{\varepsilon}}^T R(\mathbf{q}_m^{-1}) \left[\boldsymbol{\omega} + \mathbf{b}(T) - \hat{\mathbf{b}}(T) + k_e \tilde{\eta}_m \tilde{\boldsymbol{\varepsilon}}_m \right] - \frac{3}{8} \sigma_w^2 \hat{\eta} \\ -\alpha \tilde{\eta}_m \tilde{\boldsymbol{\varepsilon}}_m g(hT - \mu_0) \\ \vdots \\ -\alpha \tilde{\eta}_m \tilde{\boldsymbol{\varepsilon}}_m g(hT - \mu_N) \end{bmatrix} dt \\
&+ \begin{bmatrix} \frac{1}{2} \left[\eta_m I + [\boldsymbol{\varepsilon}_m \times] \right] R(\mathbf{q}^{-1}) \sigma_m & 0 \\ -\frac{1}{2} \boldsymbol{\varepsilon}_m^T R(\mathbf{q}^{-1}) \sigma_m & 0 \\ 0 & \frac{1}{2} \left[\hat{\eta} I + [\hat{\boldsymbol{\varepsilon}} \times] \right] R(\mathbf{q}_m^{-1}) \sigma_w \\ 0 & -\frac{1}{2} \hat{\boldsymbol{\varepsilon}}^T R(\mathbf{q}_m^{-1}) \sigma_w \\ 0 & 0 \\ \vdots & \vdots \\ 0 & 0 \end{bmatrix} \begin{bmatrix} d\boldsymbol{\beta}_m \\ d\boldsymbol{\beta}_w \end{bmatrix}
\end{aligned} \tag{3.33}$$

3.8 Gyro CBO and TBO Stochastic Simulations

Stochastic simulation of the CBO and TBO were performed using the Euler-Maruyama method detailed in Section 2.2. Note that the Kloeden-Platen Explicit Weak 2.0 scheme, used for all other stochastic simulations in this thesis, is not applicable here as the system is nonautonomous [45, p. 186]. Specifically, the gyro bias is a function of temperature which, in turn, is an explicit function of time. Simulation step size was set to $\Delta t = 0.1\text{s}$.

The first simulation study consists of a comparison of a single realization of both the TBO and CBO. In the simulation, the gyro experiences a thermal oscillation of period 90 minutes, again representative of a spacecraft in LEO going into and out of the Earth's shadow. The gyro noise level was set to $\sigma_w = 0.01$ and the attitude measurement noise level set to $\frac{k_m}{\sigma_m^2} = 10^4$. The TBO tracking gain is set to $k = 1$ and the adaptation gain is set to $\alpha = 0.01$.

Plots of the instantaneous bias estimate error are given in Figure 3.31. Both observers experience a transient of similar magnitude, but the CBO transient dies out within seconds. The TBO transient is significantly longer, taking nearly half an orbit. Of course this is to be expected; the TBO has no internal model of the gyro thermal bias and must experience the effect of temperature variation in order to estimate the corresponding portion of the bias thermal function. Once the TBO has sampled enough of the temperature range, its bias estimate error is driven largely by noise. The CBO, on the other hand, has a consistent bias estimate error as its estimate attempts to keep up with the true gyro bias that is time varying. A plot

of the TBO's gyro thermal bias function estimate from the end of the simulation is given in Figure 3.32.

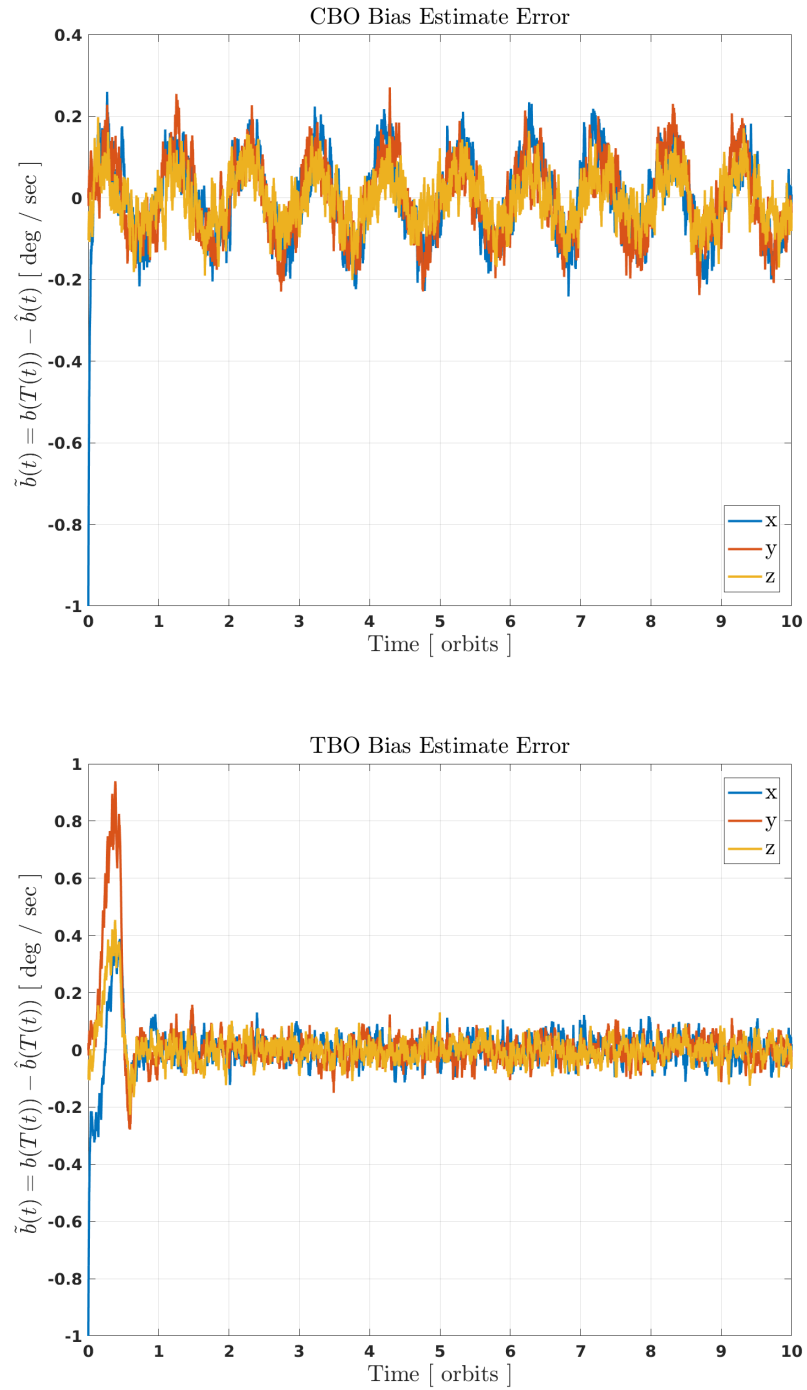


Figure 3.31: Simulation run bias estimate errors (LEO)

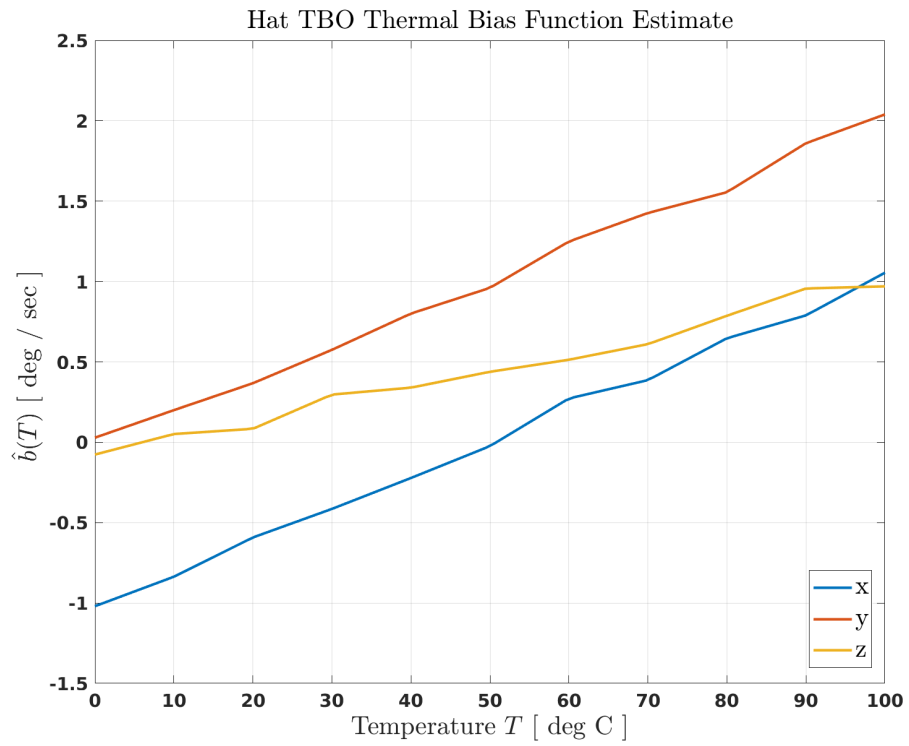


Figure 3.32: Simulation run (LEO)

The next simulation study varies the thermal oscillation period τ similar to the deterministic simulation study of the CBO in Section 3.3. The thermal profile still assumes the form of Equation 3.9, repeated here for convenience

$$T(t) = \frac{100}{2} \cos\left(\frac{2\pi t}{\tau} + \pi\right) + \frac{100}{2} \quad (3.34)$$

with the same amplitude of 100°C , but 60 distinct simulations were conducted, each with a different value of the thermal oscillation period τ . As in Section 3.3, the smallest (fastest) thermal oscillation period considered is $\tau = 60$ seconds, consistent with a 1 rpm spin stabilized satellite. The largest (slowest) thermal oscillation period considered is $\tau = 2$ hours which is representative with a spacecraft in LEO. The simulations were performed with the Euler-Maruyama scheme with a step size of $\Delta t = 0.1s$ for 10^6 steps, for a total simulation time of just under 28 hours. In each simulation realization, the observers had no initial bias knowledge.

A plot of the bias estimate error and the attitude estimate error for the CBO and the TBO with each RBF choice is given in Figures 3.33 and 3.34. The true gyro thermal bias function was modeled as the first order function of Equation 3.7 in Figure 3.33 and the third order function of Equation 3.8 in Figure 3.34.

The CBO estimate error performance approaches the TBO estimate error performance for large τ , which is when the temperature varies so slowly that the gyro thermal bias acts almost like a constant. The CBO performs the worst of all observers considered for rapid thermal variation (small τ) as expected. It is interesting to note that the attitude estimate errors for all TBOs were nearly the same for the first order gyro thermal bias model in Figure 3.33, however the attitude estimate

errors for the boxcar TBO are slightly worse than the other TBOs for the third order gyro thermal bias model in Figure 3.34.

The relative performance of the TBOs was more distinct in the bias estimate error plots. The hat TBO had the lowest bias estimate error for all cases considered, followed by the Gaussian TBO, and then the hat TBO. Given that the total simulation time was only 28 hours the Gaussian TBO has not reached steady state in any of the plots.

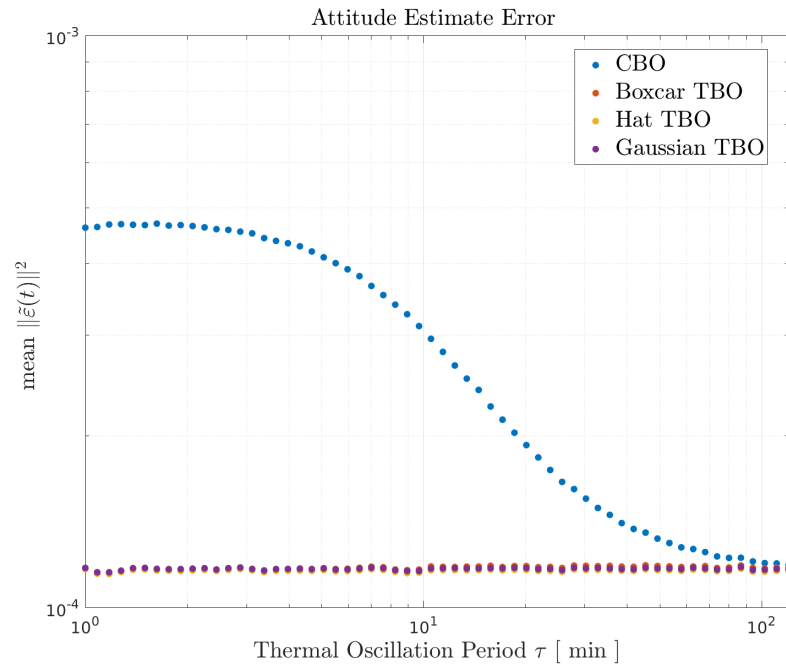
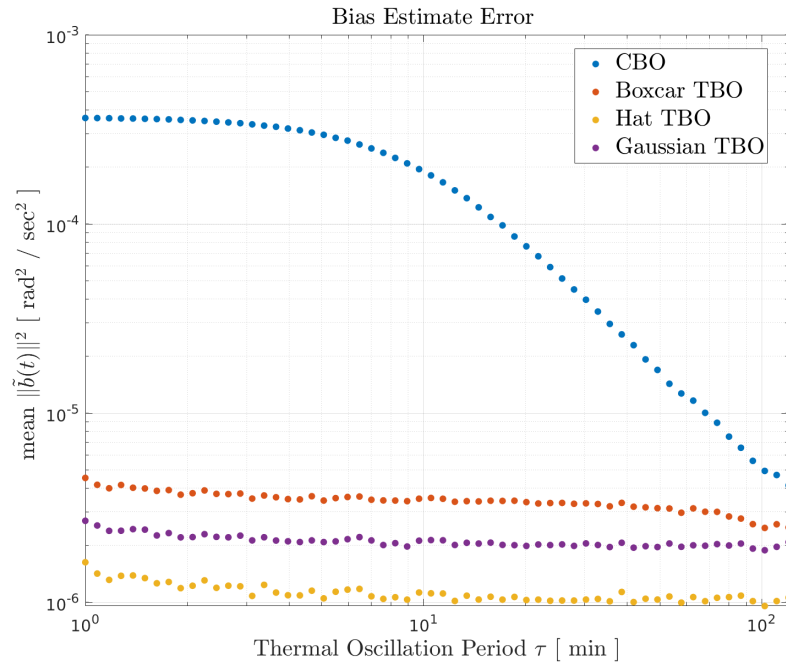


Figure 3.33: Bias and attitude estimate errors for the CBO, boxcar TBO, hat TBO, and Gaussian TBO for a range of thermal oscillation periods τ for the first order true gyro thermal bias function model of Equation 3.7.

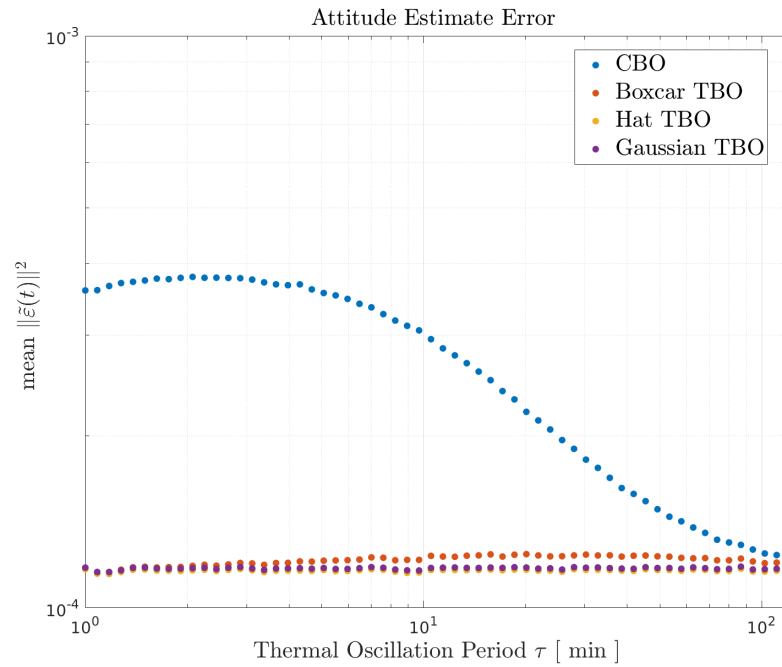
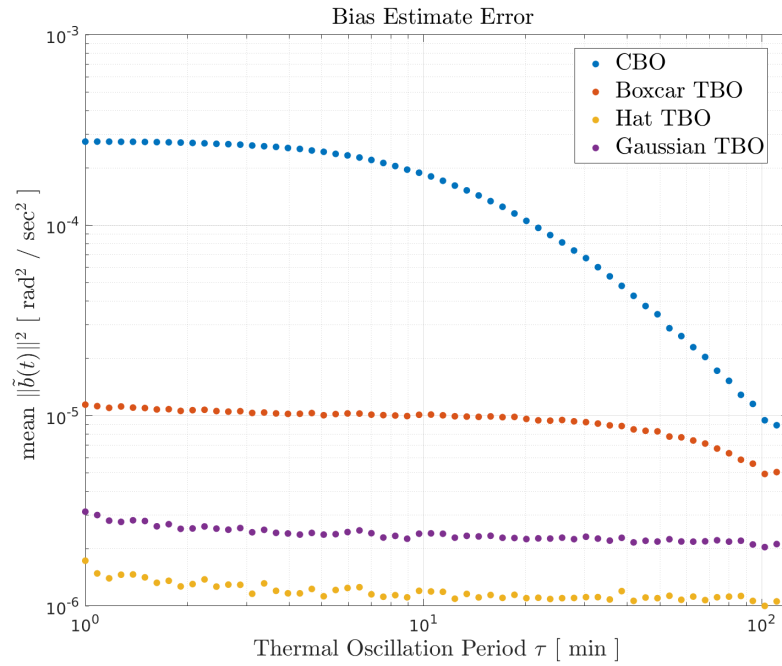


Figure 3.34: Bias and attitude estimate errors for the CBO, boxcar TBO, hat TBO, and Gaussian TBO for a range of thermal oscillation periods τ for the third order true gyro thermal bias function model of Equation 3.8.

3.9 Gyro CBO and TBO Gain Search

While the work of Thienel and Sanner [95] proved the CBO was GES for constant gyro bias, the deterministic Lyapunov theory and subsequent analysis used was unable to provide any notion for how to select the tracking gain k and adaptation gain α other than both must be positive. In this section, a search is conducted by performing simulations for a number of choices of these parameters. Error statistics from each simulation realization can be then used to form an understanding of the observer performance as a function of the gain.

As before, in each simulation the gyro experiences a thermal oscillation of period 90 minutes, again representative of a spacecraft in LEO going into and out of the Earth's shadow. The gyro noise level was set to $\sigma_w = 0.01$ and the attitude measurement noise level set to $\frac{k_m}{\sigma_m^2} = 10^4$. Each simulation was run for 10^5 seconds of simulation time (which is just over 18 orbits). The TBO had no initial knowledge of the true gyro bias thermal function. For both observers, simulations were run for every permutation of a choice of 20 different tracking gains k and 20 different adaptation gains α for a total of 400 simulations.

The results of the search of the gain space are shown in Figure 3.35 for the CBO, Figure 3.7 for the boxcar TBO, Figure 3.7 for the hat TBO, and Figure 3.7 for the Gaussian TBO. A black dot represents a choice of gains α and k where a simulation was actually performed. MATLAB's `contourf` utility was then used to plot a surface generated from the numerical data for visualization purposes. The numerical data suggest the underlying estimate error for the observers as a function

of the gains may be a smooth function.

Of course the true underlying estimate error function may be of any shape. The surfaces drawn in the figures are merely fits to a small sampling of the space. Note also the computational expense required to generate these simulation surfaces and the dependence on numerical integration techniques which may have numerical stability issues. Additionally, this simulation study is representative of a single gyro noise level, a single attitude measurement noise level, thermal oscillation period, and so on.

The remainder of this thesis will pursue an analytic treatment of this problem. The hope is to find analytic expressions for the estimation error as a function of the gain and noise level parameters. If these analytic expressions exist, they can be used to predict performance without the expense of running numerous simulations to generate performance surfaces like those of the plots. Analytic expressions for estimation error performance may even exist that could allow one to compute an analytic optimum gain choice for a given set of sensor noise level parameters.

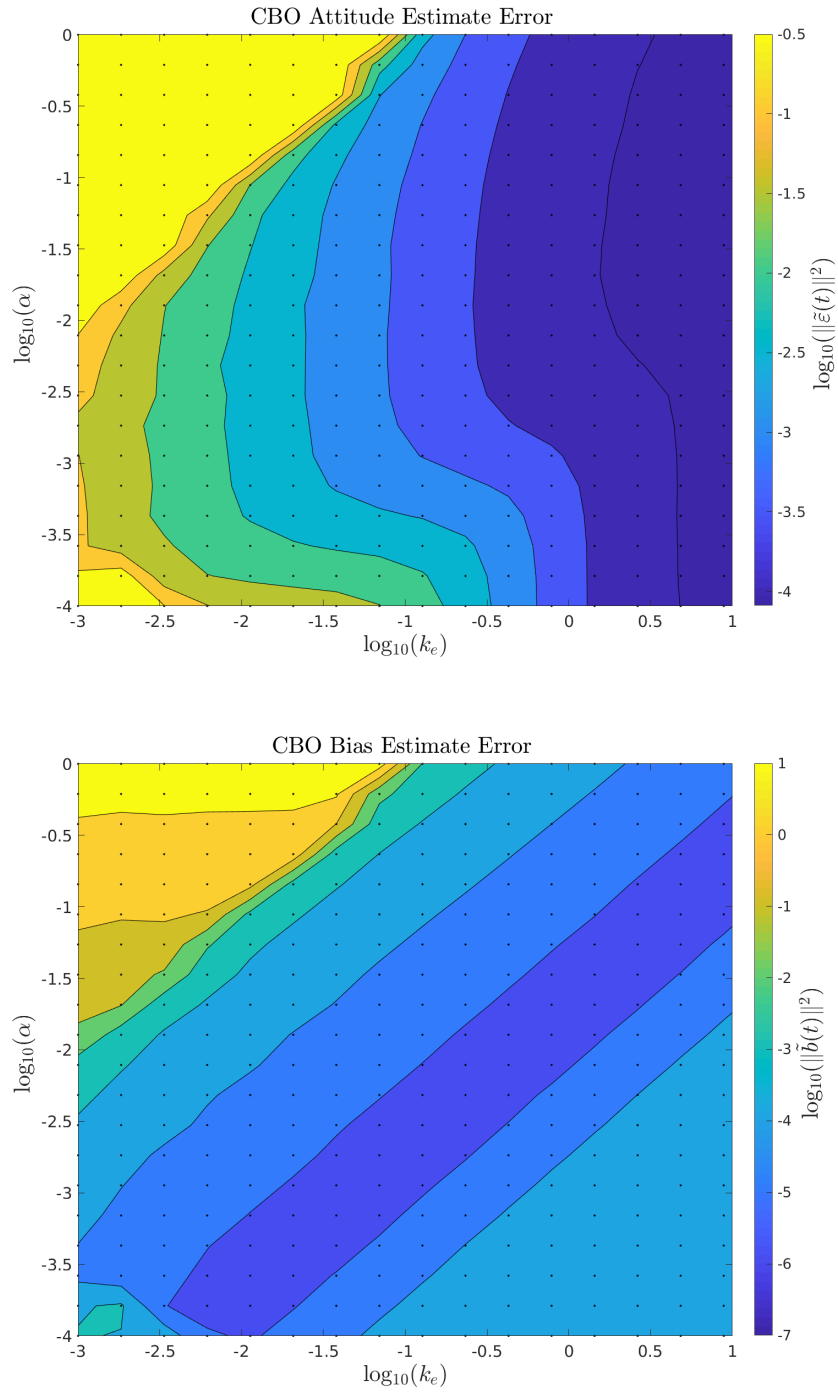


Figure 3.35: Error statistics over a subset of the gain parameter space for the CBO as obtained via numerical simulation for the linear gyro thermal bias model of Equation 3.7.

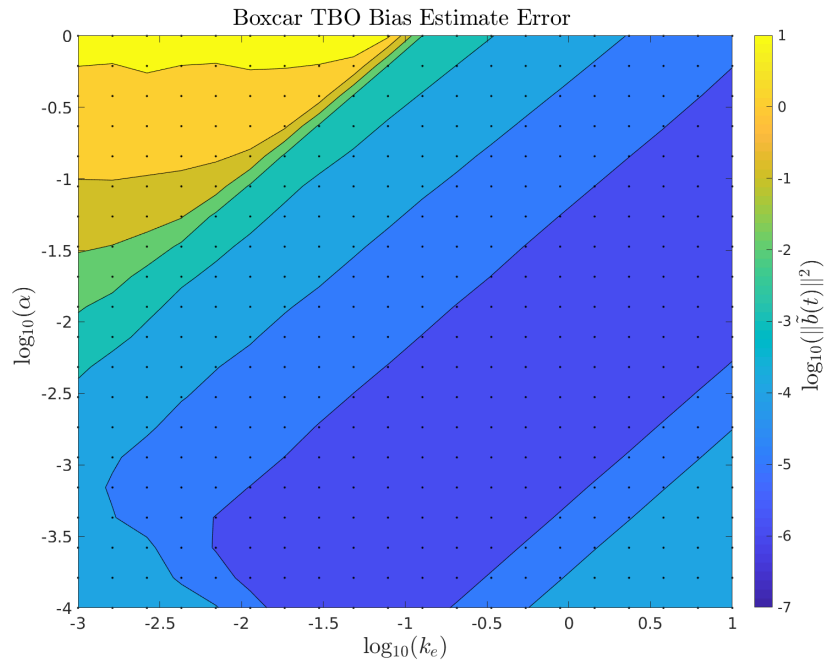
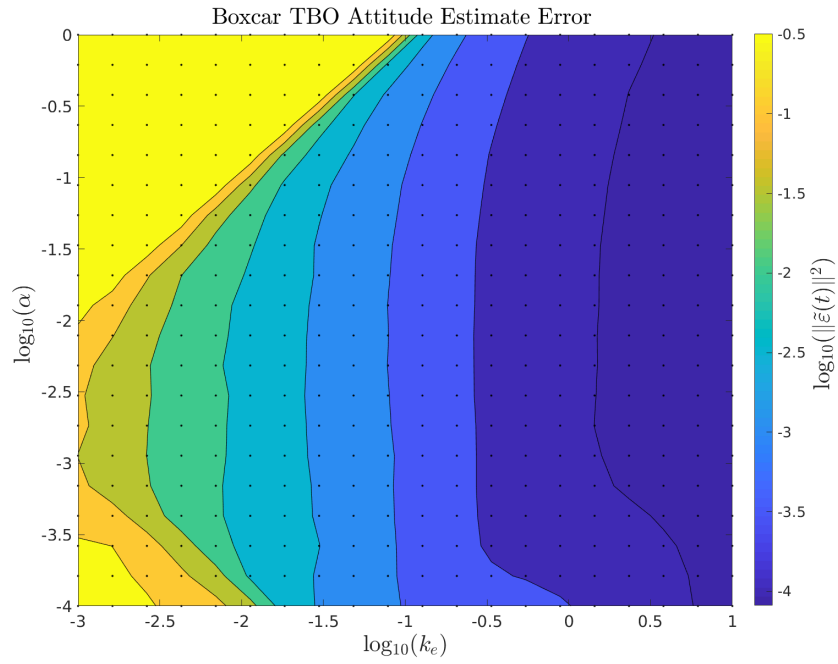


Figure 3.36: Error statistics over a subset of the gain parameter space for the boxcar TBO as obtained via numerical simulation for the linear gyro thermal bias model of Equation 3.7.

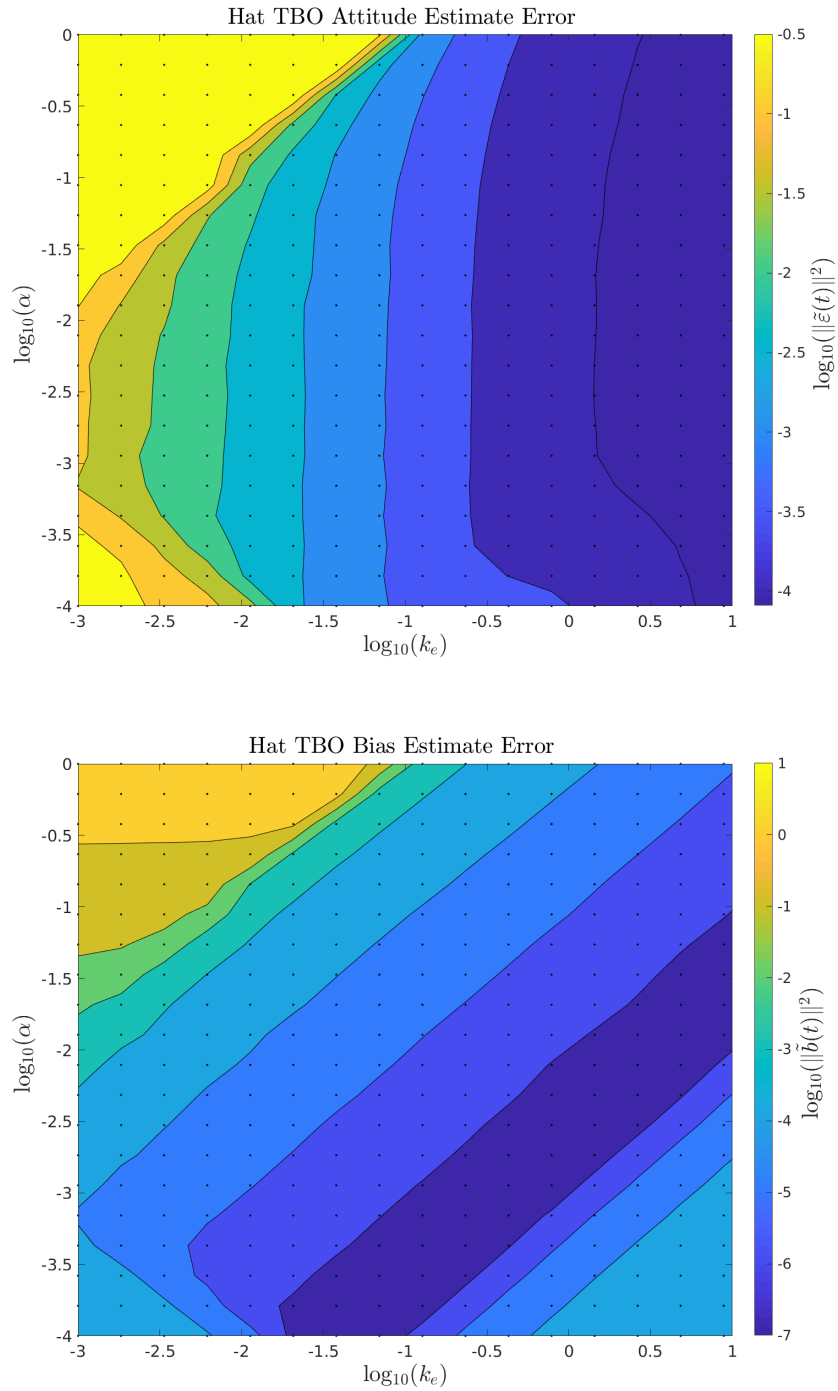


Figure 3.37: Error statistics over a subset of the gain parameter space for the hat TBO as obtained via numerical simulation for the linear gyro thermal bias model of Equation 3.7.

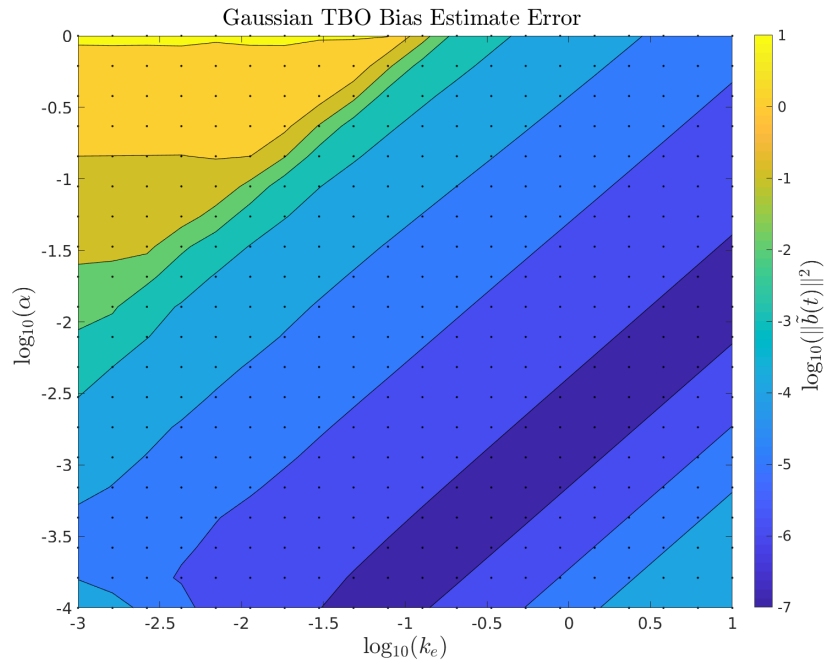
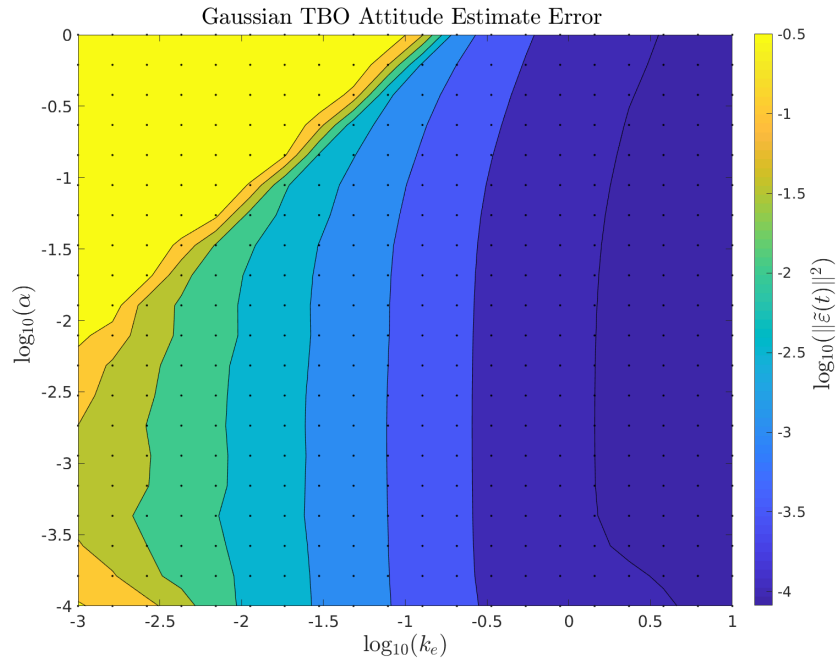


Figure 3.38: Error statistics over a subset of the gain parameter space for the Gaussian TBO as obtained via numerical simulation for the linear gyro thermal bias model of Equation 3.7.

Chapter 4: Attitude Estimation Filter for Noisy Gyro Measurements

A nonlinear attitude estimation filter for angular rate gyro measurements with additive noise and perfect attitude measurements is considered in this chapter. The first section, Section 4.1, presents a formulation of the filter and a derivation of an Itô SDE for its error dynamics. Weak stochastic stability is established and analytic filter performance bounds are found in Section 4.2 using stochastic Lyapunov theory. Section 4.3 uses numerical simulation analysis to demonstrate the validity of the theoretical claims, but the performance bounds are found to be conservative. The next section, Section 4.4, contains a presentation of the Fokker-Planck PDE associated with the error dynamics SDE.

To make further progress on the analysis, the system formulation is reduced to the SO(2) case in Section 4.5. In Section 4.6 the SO(2) case is analyzed using stochastic Lyapunov theory to verify weak stochastic stability and find performance bounds. Section 4.7 includes a comparison of the stochastic Lyapunov performance bounds with numerical simulation, and again the stochastic Lyapunov performance bounds exhibit significant conservatism. A Fokker-Planck analysis in Section 4.8 yields an analytic solution to the stationary Fokker-Planck PDE; the section includes the derivation of analytic expressions for the first two moments of the stationary

probability density. The analytic solution for the ultimate moments are compared to numerical simulation results in Section 4.9. Section 4.10 extrapolates the SO(2) results to provide a heuristic upper bound for the SO(3) case that is tighter than the SO(3) upper bounds generated via the stochastic Lyapunov analysis. Finally, the intuition gained from the SO(2) analysis and the success of the heuristic upper bound are used to solve the Fokker-Planck PDE for the SO(3) case in Section 4.11. The solution is used to compute an analytic expression for the ultimate attitude estimate error mean vector, variance, and covariance matrix. The analytic solution is then compared to numerical simulation realizations in Section 4.12.

4.1 Attitude Filter Formulation in SO(3)

Consider a nonlinear attitude filter given angular rate gyro measurements modeled as

$$\boldsymbol{\omega}_g(t) = \boldsymbol{\omega}(t) + \sigma_w \mathbf{n}_w(t) \quad (4.1)$$

where $\boldsymbol{\omega}_g(t)$ is the gyro measurement at time t , $\boldsymbol{\omega}(t)$ is the true vehicle angular rate at time t , σ_w is a positive scaling constant, and $\mathbf{n}_w(\cdot)$ is a zero mean unit variance Gaussian white noise process.

Further assume that the filter has access to perfect (noise free) attitude measurements $\mathbf{q}_m(t)$ of the vehicle attitude $\mathbf{q}(t)$

$$\mathbf{q}_m(t) = \mathbf{q}(t) = \begin{bmatrix} \boldsymbol{\varepsilon}(t) \\ \eta(t) \end{bmatrix} = \begin{bmatrix} \varepsilon_x(t) \\ \varepsilon_y(t) \\ \varepsilon_z(t) \\ \eta(t) \end{bmatrix} \quad (4.2)$$

The vehicle attitude $\mathbf{q}(t)$ evolves according to the usual kinematics equation

$$\dot{\mathbf{q}}(t) = \frac{1}{2} \boldsymbol{\omega}(t) \otimes \mathbf{q}(t)$$

The nonlinear attitude filter is given by the equation

$$\dot{\hat{\mathbf{q}}}(t) = \frac{1}{2} \left\{ R(\tilde{\mathbf{q}}^{-1}(t)) \left[\boldsymbol{\omega}_g(t) + k_e \tilde{\eta}(t) \tilde{\boldsymbol{\varepsilon}}(t) \right] \right\} \otimes \hat{\mathbf{q}}(t) \quad (4.3)$$

where $k_e > 0$ is a filter (estimator) gain parameter and $\hat{\mathbf{q}}(t)$ is the filter's estimate of the vehicle attitude. The rotation parameterized by $\tilde{\mathbf{q}}(t)$ is the filter's attitude

estimate error, given by

$$\tilde{\mathbf{q}}(t) = \begin{bmatrix} \tilde{\boldsymbol{\varepsilon}}(t) \\ \tilde{\eta}(t) \end{bmatrix} = \mathbf{q}(t) \otimes \hat{\mathbf{q}}^{-1}(t) \quad (4.4)$$

which is available in real time for the filter to use since the attitude measurements are assumed to be noise free. The rotation $R(\tilde{\mathbf{q}}^{-1}(t))$ resolves the angular velocity terms in the filter's reference frame.

The attitude filter dynamics given by Equation 4.3 can be combined with the quaternion error kinematics of Equation 2.71 and the measurement models of Equations 4.1 and 4.2 to find the filter's attitude estimate error dynamics as a Langevin form differential equation:

$$\begin{aligned} \dot{\tilde{\mathbf{q}}}(t) &= \frac{1}{2} \left\{ \boldsymbol{\omega}(t) - R(\tilde{\mathbf{q}}(t)) R(\tilde{\mathbf{q}}^{-1}(t)) \left[\boldsymbol{\omega}(t) + \sigma_w \mathbf{n}_w(t) + k_e \tilde{\eta}(t) \tilde{\boldsymbol{\varepsilon}}(t) \right] \right\} \otimes \tilde{\mathbf{q}}(t) \\ &= \frac{1}{2} \left\{ -k_e \tilde{\eta}(t) \tilde{\boldsymbol{\varepsilon}}(t) - \sigma_w \mathbf{n}_w(t) \right\} \otimes \tilde{\mathbf{q}}(t) \\ &= \begin{bmatrix} -\frac{1}{2} k_e \tilde{\eta}^2(t) \tilde{\boldsymbol{\varepsilon}}(t) \\ \frac{1}{2} k_e \tilde{\eta}(t) \tilde{\boldsymbol{\varepsilon}}^T(t) \tilde{\boldsymbol{\varepsilon}}(t) \end{bmatrix} + \begin{bmatrix} -\frac{1}{2} \left\{ \tilde{\eta}(t) I + [\tilde{\boldsymbol{\varepsilon}}(t) \times] \right\} \sigma_w \\ \frac{1}{2} \tilde{\boldsymbol{\varepsilon}}^T(t) \sigma_w \end{bmatrix} \mathbf{n}_w(t) \end{aligned} \quad (4.5)$$

Note that the filter's attitude estimate error dynamics are independent of the vehicle's angular rate $\boldsymbol{\omega}(t)$.

As explained in Section 2.1.3, the Langevin form error dynamics differential equation 4.5 are interpreted as a Stratonovich SDE. Converting to an Itô SDE results

in the following

$$\begin{aligned}
d\tilde{\mathbf{x}}(t) &= \begin{bmatrix} d\tilde{\boldsymbol{\varepsilon}}(t) \\ d\tilde{\eta}(t) \end{bmatrix} \\
&= \begin{bmatrix} -\frac{1}{2}k_e\tilde{\eta}^2(t)\tilde{\boldsymbol{\varepsilon}}(t) - \frac{3}{8}\sigma_w^2\tilde{\boldsymbol{\varepsilon}}(t) \\ \frac{1}{2}k_e\tilde{\eta}(t)\tilde{\boldsymbol{\varepsilon}}^T(t)\tilde{\boldsymbol{\varepsilon}}(t) - \frac{3}{8}\sigma_w^2\tilde{\eta}(t) \end{bmatrix} dt + \begin{bmatrix} -\frac{1}{2}\left\{\tilde{\eta}(t)I + [\tilde{\boldsymbol{\varepsilon}}(t) \times]\right\}\sigma_w \\ \frac{1}{2}\tilde{\boldsymbol{\varepsilon}}^T(t)\sigma_w \end{bmatrix} d\boldsymbol{\beta}_w(t) \\
&= \mathbf{f}\left(\tilde{\mathbf{x}}(t)\right)dt + G\left(\tilde{\mathbf{x}}(t)\right)d\boldsymbol{\beta}_w(t) \tag{4.6}
\end{aligned}$$

Note that when $k_e = 0$, the homogeneous dynamics of Itô SDE 4.6 are linear.

Choukroun [13] used this fact to show, in this particular case with no feedback, that

$$\lim_{t \rightarrow \infty} E\left[\tilde{\mathbf{q}}(t)\tilde{\mathbf{q}}^T(t)\right] = \frac{1}{4}I \tag{4.7}$$

and hence

$$\lim_{t \rightarrow \infty} E\left[\tilde{\boldsymbol{\varepsilon}}^T(t)\tilde{\boldsymbol{\varepsilon}}(t)\right] = \frac{3}{4} \tag{4.8}$$

However, in the case of feedback (when $k_e > 0$) the homogeneous dynamics are nonlinear and the techniques used by Choukroun do not apply.

4.2 Stochastic Lyapunov Analysis in SO(3)

In this section, weak stochastic stability of the Itô error SDE 4.6 is demonstrated and attitude filter performance bounds are obtained using stochastic Lyapunov theory.

Theorem 4.2.1. *The attitude estimate error dynamics of the Itô SDE 4.6 are weakly stochastically stable. Further, the attitude estimate error has the ultimate bound*

$$\lim_{t \rightarrow \infty} E \left[\tilde{\boldsymbol{\epsilon}}^T(t) \tilde{\boldsymbol{\epsilon}}(t) \right] \leq \frac{3}{4} \quad (4.9)$$

which is valid for any filter gain $k_e \geq 0$.

Proof. Choose as a Lyapunov function $V(t) = \tilde{\boldsymbol{\epsilon}}^T(t) \tilde{\boldsymbol{\epsilon}}(t)$. Then application of the differential generator to the Lyapunov function with respect to the Itô SDE 4.6 yields

$$\begin{aligned} \mathcal{L}V(t) &= \left(\frac{\partial V}{\partial \tilde{\boldsymbol{x}}} \right)^T \mathbf{f}(\tilde{\boldsymbol{x}}(t)) + \frac{1}{2} \text{tr} \left\{ G^T(\tilde{\boldsymbol{x}}(t)) \frac{\partial^2 V}{\partial \tilde{\boldsymbol{x}}^2} G(\tilde{\boldsymbol{x}}(t)) \right\} \\ &= -k_e \tilde{\eta}^2(t) \tilde{\boldsymbol{\epsilon}}^T(t) \tilde{\boldsymbol{\epsilon}}(t) - \sigma_w^2 \tilde{\boldsymbol{\epsilon}}^T(t) \tilde{\boldsymbol{\epsilon}}(t) + \frac{3}{4} \sigma_w^2 \end{aligned} \quad (4.10)$$

$$\leq -\sigma_w^2 \tilde{\boldsymbol{\epsilon}}^T(t) \tilde{\boldsymbol{\epsilon}}(t) + \frac{3}{4} \sigma_w^2 \quad (4.11)$$

Zakai's stability theorem (Theorem 2.1.4) implies the system is weakly stochastically stable.

Zakai's ultimate moment bound theorem (Theorem 2.1.5) implies

$$\lim_{t \rightarrow \infty} E \left[\sigma_w^2 \tilde{\boldsymbol{\epsilon}}^T(t) \tilde{\boldsymbol{\epsilon}}(t) \right] \leq \frac{3}{4} \sigma_w^2 \quad (4.12)$$

Using the fact that the expectation operator is linear, simple algebraic manipulation provides the attitude estimate error ultimate bound.

□

Since application of Theorem 2.1.5 yielded the expectation equality 4.14, one can further deduce a performance *lower* bound.

Corollary 4.2.1.1. *The attitude estimate error dynamics of the Itô SDE 4.6 obey the ultimate **lower** bound*

$$\lim_{t \rightarrow \infty} E \left[\tilde{\mathbf{e}}^T(t) \tilde{\mathbf{e}}(t) \right] \geq \frac{k_e + \sigma_w^2 - \sqrt{k_e^2 + \sigma_w^4 - k_e \sigma_w^2}}{2k_e} \quad (4.13)$$

Proof. Apply Theorem 2.1.5 directly to Equation 4.10 to find

$$\lim_{t \rightarrow \infty} E \left[k_e \tilde{\eta}^2(t) \tilde{\mathbf{e}}^T(t) \tilde{\mathbf{e}}(t) + \sigma_w^2 \tilde{\mathbf{e}}^T(t) \tilde{\mathbf{e}}(t) \right] = \frac{3}{4} \sigma_w^2$$

Using linearity of the expectation operator, the unit quaternion normalization constraint $1 = \tilde{\mathbf{e}}^T(t) \tilde{\mathbf{e}}(t) + \tilde{\eta}^2(t)$, and rearranging results in

$$\begin{aligned} 0 &= \lim_{t \rightarrow \infty} \left\{ E \left[(\tilde{\mathbf{e}}^T(t) \tilde{\mathbf{e}}(t))^2 \right] - \frac{k_e + \sigma_w^2}{k_e} E \left[\tilde{\mathbf{e}}^T(t) \tilde{\mathbf{e}}(t) \right] + \frac{3\sigma_w^2}{4k_e} \right\} \\ &= \lim_{t \rightarrow \infty} \left\{ \left(E \left[\tilde{\mathbf{e}}^T(t) \tilde{\mathbf{e}}(t) \right] \right)^2 + \text{Var} \left[\tilde{\mathbf{e}}^T(t) \tilde{\mathbf{e}}(t) \right] - \frac{k_e + \sigma_w^2}{k_e} E \left[\tilde{\mathbf{e}}^T(t) \tilde{\mathbf{e}}(t) \right] + \frac{3\sigma_w^2}{4k_e} \right\} \end{aligned} \quad (4.14)$$

Combining Equation 4.14 with the fact that $\text{Var} \left[\tilde{\mathbf{e}}^T(t) \tilde{\mathbf{e}}(t) \right] \geq 0$ provides the second order polynomial inequality

$$0 \geq \lim_{t \rightarrow \infty} \left\{ \left(E \left[\tilde{\mathbf{e}}^T(t) \tilde{\mathbf{e}}(t) \right] \right)^2 - \frac{k_e + \sigma_w^2}{k_e} E \left[\tilde{\mathbf{e}}^T(t) \tilde{\mathbf{e}}(t) \right] + \frac{3\sigma_w^2}{4k_e} \right\} \quad (4.15)$$

Solving the polynomial inequality yields the lower ultimate performance bound.

□

This ultimate lower bound matches the ultimate upper bound for small k_e , as seen in the limit

$$\lim_{k_e \rightarrow 0} \frac{k_e + \sigma_w^2 - \sqrt{k_e^2 + \sigma_w^4 - k_e \sigma_w^2}}{2k_e} = \frac{1}{2} + \lim_{k_e \rightarrow 0} \frac{\sigma_w^2 - 2k_e}{4\sqrt{k_e^2 + \sigma_w^4 - k_e \sigma_w^2}} = \frac{3}{4}$$

where the second equality follows from L'Hôpital's rule.

A somewhat tighter upper bound than the one of Theorem 4.2.1 may be deduced by further manipulating Equation 4.10 using an additional assumption.

Corollary 4.2.1.2. *Assuming the underlying probability density of $\tilde{\epsilon}^T(t)\tilde{\epsilon}(t)$ is **unimodal**, the attitude estimate error dynamics of the Itô SDE 4.6 obey the ultimate upper bound*

$$\lim_{t \rightarrow \infty} E \left[\tilde{\epsilon}^T(t)\tilde{\epsilon}(t) \right] \leq \frac{k_e + \sigma_w^2 - \sqrt{\frac{5}{9}k_e^2 + \sigma_w^4 - k_e \sigma_w^2}}{2k_e} \quad (4.16)$$

Proof. As the expression $\tilde{\epsilon}^T(t)\tilde{\epsilon}(t)$ is itself a random variable, the definition of variance provides

$$\text{Var} \left[\tilde{\epsilon}^T(t)\tilde{\epsilon}(t) \right] = E \left[\left(\tilde{\epsilon}^T(t)\tilde{\epsilon}(t) \right)^2 \right] - \left(E \left[\tilde{\epsilon}^T(t)\tilde{\epsilon}(t) \right] \right)^2 \geq 0$$

Combining with Equation 4.14 yields

$$0 \leq \lim_{t \rightarrow \infty} \left\{ \left(E \left[\tilde{\epsilon}^T(t)\tilde{\epsilon}(t) \right] \right)^2 - \frac{k_e + \sigma_w^2}{k_e} E \left[\tilde{\epsilon}^T(t)\tilde{\epsilon}(t) \right] + \left(\frac{3\sigma_w^2}{4k_e} + \sup \text{Var} \left[\tilde{\epsilon}^T(t)\tilde{\epsilon}(t) \right] \right) \right\} \quad (4.17)$$

For a random variable z restricted to the interval $a \leq z \leq b$ with a unimodal distribution, the Jacobson Inequality [36] is given as

$$\text{Var}[z] \leq \frac{(b-a)^2}{9}$$

If the underlying probability density of $\tilde{\boldsymbol{\varepsilon}}^T(t)\tilde{\boldsymbol{\varepsilon}}(t)$ is assumed to be unimodal and recognizing that $0 \leq \tilde{\boldsymbol{\varepsilon}}^T(t)\tilde{\boldsymbol{\varepsilon}}(t) \leq 1$, the Jacobson Inequality for the system provides

$$\sup Var \left[\tilde{\boldsymbol{\varepsilon}}^T(t)\tilde{\boldsymbol{\varepsilon}}(t) \right] \leq \frac{1}{9} \quad (4.18)$$

Substituting the variance bound into Inequality 4.17 results in a second order polynomial inequality in $E \left[\tilde{\boldsymbol{\varepsilon}}^T(t)\tilde{\boldsymbol{\varepsilon}}(t) \right]$:

$$0 \leq \lim_{t \rightarrow \infty} \left\{ \left(E \left[\tilde{\boldsymbol{\varepsilon}}^T(t)\tilde{\boldsymbol{\varepsilon}}(t) \right] \right)^2 - \frac{k_e + \sigma_w^2}{k_e} E \left[\tilde{\boldsymbol{\varepsilon}}^T(t)\tilde{\boldsymbol{\varepsilon}}(t) \right] + \left(\frac{3\sigma_w^2}{4k_e} + \frac{1}{9} \right) \right\} \quad (4.19)$$

Solving the polynomial inequality yields the final result.

□

This new ultimate upper bound matches the prior ultimate upper bound for small k_e , as seen in the limit

$$\lim_{k_e \rightarrow 0} \frac{k_e + \sigma_w^2 - \sqrt{\frac{5}{9}k_e^2 + \sigma_w^4 - k_e\sigma_w^2}}{2k_e} = \frac{3}{4}$$

However, the new ultimate upper bound approaches a different limit for large k_e , specifically

$$\lim_{k_e \rightarrow \infty} \frac{k_e + \sigma_w^2 - \sqrt{\frac{5}{9}k_e^2 + \sigma_w^4 - k_e\sigma_w^2}}{2k_e} = \frac{1}{2} - \frac{\sqrt{5}}{6} \approx 0.127$$

which is independent of the filter gain k_e and the gyro noise parameter σ_w .

4.3 Numerical Simulation of SO(3) Stochastic Lyapunov Bounds

Numerical simulations of the SO(3) attitude filter's Itô SDE error dynamics of Equation 4.6 were performed for a variety of system parameters. The Kloeden-Platen Explicit Weak 2.0 numerical integration scheme discussed in Section 2.2.3 was used. For each simulation realization, a time step size of $\Delta t = 0.1$ was used for a total of 10^8 simulation steps. At the end of a simulation realization, the last 10^7 simulation steps were used to compute the ergodic mean of the filter attitude estimate error $\tilde{\epsilon}^T(t)\tilde{\epsilon}(t)$, which is denoted $\text{Mean}_{t_i \in T_{ss}} \left[\tilde{\epsilon}^T(t_i)\tilde{\epsilon}(t_i) \right]$. An ensemble of 7 realizations were simulated for each choice of system parameters; the ensemble mean of the ergodic means was then computed: $\text{Mean}_{sims} \left[\text{Mean}_{t_i \in T_{ss}} \left[\tilde{\epsilon}^T(t_i)\tilde{\epsilon}(t_i) \right] \right]$.

A gallery of plots of the filter attitude estimate errors are included in Figure 4.1. A magenta dot represents the ensemble mean of the ergodic means. The stochastic Lyapunov bounds of the previous section are also drawn on the plots, with the upper bound from Theorem 4.2.1 in red, the lower bound of Corollary 4.2.1.1 in blue, and the upper bound of Corollary 4.2.1.2 in yellow.

All three bounds correctly envelope the ensemble of numerical realizations. The ultimate performance bound of Theorem 4.2.1 is neither dependent on the filter gain k_e nor the noise scaling parameter σ_w . While the value $\frac{3}{4}$ does bound the ensemble of the means of the realizations of $mean(\|\tilde{\epsilon}(t)\|^2)$, the bound becomes more conservative as k_e increases. The ultimate upper bound of Corollary 4.2.1.2 does bow at the same transition region where the numerical realizations first start to drop, but the upper bound quickly levels off and grows increasingly conservative as k_e

increases. The lower ultimate bound is slightly conservative in the transition region, but consistently tracks the overall shape of the numerical simulation performance. Of all the stochastic Lyapunov bounds considered in this chapter, this is the only bound to suitably capture the filter performance for large gain k_e .

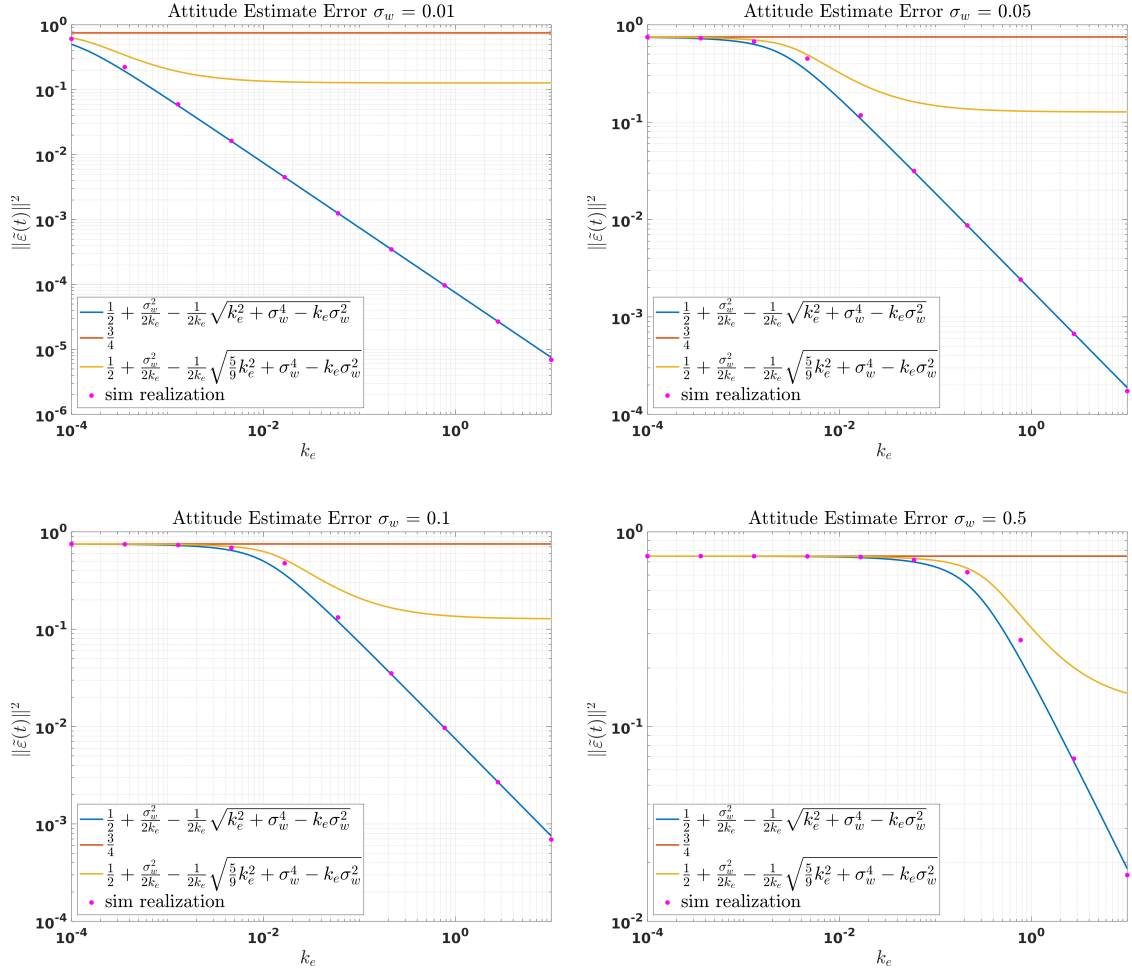


Figure 4.1: Comparison of simulation realizations of attitude estimate errors of the SO(3) error dynamics Itô SDE of Equation 4.6 to the stochastic Lyapunov upper bound from Theorem 4.2.1 in red, the lower bound of Corollary 4.2.1.1 in blue, and the upper bound of Corollary 4.2.1.2 in yellow.

4.4 Fokker-Planck PDE in SO(3)

Let $p = p(\tilde{\mathbf{q}}(t), t) = p(\tilde{\boldsymbol{\varepsilon}}(t), \tilde{\eta}(t), t) = p(\tilde{\varepsilon}_x(t), \tilde{\varepsilon}_y(t), \tilde{\varepsilon}_z(t), \tilde{\eta}(t), t)$ be the joint probability density for the attitude filter error $\tilde{\mathbf{q}}(t)$. The Fokker-Planck partial differential equation associated with the attitude filter error dynamics Itô SDE 4.6 is given by

$$\begin{aligned}
\frac{\partial p}{\partial t} &= - \sum_{i=1}^4 \frac{\partial}{\partial \tilde{q}_i} \left[f_i(\tilde{\mathbf{q}}(t)) p(\tilde{\mathbf{q}}(t), t) \right] + \frac{1}{2} \sum_{i,j=1}^4 \frac{\partial^2}{\partial \tilde{q}_i \partial \tilde{q}_j} \left[\left\{ G(\tilde{\mathbf{q}}(t)) G^T(\tilde{\mathbf{q}}(t)) \right\}_{i,j} p(\tilde{\mathbf{q}}(t), t) \right] \\
&= k_e \left(2\tilde{\eta}^2(t) - \frac{1}{2} \right) p(\tilde{\mathbf{q}}(t), t) - \left(\frac{1}{2} k_e (1 - \tilde{\eta}^2(t)) + \frac{3}{8} \sigma_w^2 \right) \tilde{\eta}(t) \frac{\partial p}{\partial \tilde{\eta}} \\
&\quad + \left(\frac{1}{2} k_e \tilde{\eta}^2(t) - \frac{3}{8} \sigma_w^2 \right) \left(\tilde{\varepsilon}_x(t) \frac{\partial p}{\partial \tilde{\varepsilon}_x} + \tilde{\varepsilon}_y(t) \frac{\partial p}{\partial \tilde{\varepsilon}_y} + \tilde{\varepsilon}_z(t) \frac{\partial p}{\partial \tilde{\varepsilon}_z} \right) \\
&\quad - \frac{\sigma_w^2}{4} \left(\tilde{\varepsilon}_x(t) \tilde{\varepsilon}_y(t) \frac{\partial^2 p}{\partial \tilde{\varepsilon}_x \partial \tilde{\varepsilon}_y} + \tilde{\varepsilon}_x(t) \tilde{\varepsilon}_z(t) \frac{\partial^2 p}{\partial \tilde{\varepsilon}_x \partial \tilde{\varepsilon}_z} + \tilde{\varepsilon}_x(t) \tilde{\eta}(t) \frac{\partial^2 p}{\partial \tilde{\varepsilon}_x \partial \tilde{\eta}} \right. \\
&\quad \quad \left. + \tilde{\varepsilon}_y(t) \tilde{\varepsilon}_z(t) \frac{\partial^2 p}{\partial \tilde{\varepsilon}_y \partial \tilde{\varepsilon}_z} + \tilde{\varepsilon}_y(t) \tilde{\eta}(t) \frac{\partial^2 p}{\partial \tilde{\varepsilon}_y \partial \tilde{\eta}} + \tilde{\varepsilon}_z(t) \tilde{\eta}(t) \frac{\partial^2 p}{\partial \tilde{\varepsilon}_z \partial \tilde{\eta}} \right) \\
&\quad + \frac{\sigma_w^2}{8} \left((1 - \tilde{\varepsilon}_x^2(t)) \frac{\partial^2 p}{\partial \tilde{\varepsilon}_x^2} + (1 - \tilde{\varepsilon}_y^2(t)) \frac{\partial^2 p}{\partial \tilde{\varepsilon}_y^2} + (1 - \tilde{\varepsilon}_z^2(t)) \frac{\partial^2 p}{\partial \tilde{\varepsilon}_z^2} + (1 - \tilde{\eta}^2(t)) \frac{\partial^2 p}{\partial \tilde{\eta}^2} \right)
\end{aligned} \tag{4.20}$$

Since Theorem 4.2.1 proved the attitude filter error dynamics Itô SDE 4.6 is weakly stochastically stable, the joint probability density $p(\tilde{\mathbf{q}}(t), t)$ ultimately approaches a stationary density $p_s(\tilde{\mathbf{q}})$

$$p_s = p_s(\tilde{\mathbf{q}}) = \lim_{t \rightarrow \infty} p(\tilde{\mathbf{q}}(t), t) \tag{4.21}$$

which obeys the stationary Fokker-Planck PDE

$$\begin{aligned}
0 = & k_e \left(2\tilde{\eta}^2 - \frac{1}{2} \right) p_s - \left(\frac{1}{2} k_e (1 - \tilde{\eta}^2) + \frac{3}{8} \sigma_w^2 \right) \tilde{\eta} \frac{\partial p_s}{\partial \tilde{\eta}} \\
& + \left(\frac{1}{2} k_e \tilde{\eta}^2 - \frac{3}{8} \sigma_w^2 \right) \left(\tilde{\varepsilon}_x \frac{\partial p_s}{\partial \tilde{\varepsilon}_x} + \tilde{\varepsilon}_y \frac{\partial p_s}{\partial \tilde{\varepsilon}_y} + \tilde{\varepsilon}_z \frac{\partial p_s}{\partial \tilde{\varepsilon}_z} \right) \\
& - \frac{\sigma_w^2}{4} \left(\tilde{\varepsilon}_x \tilde{\varepsilon}_y \frac{\partial^2 p_s}{\partial \tilde{\varepsilon}_x \partial \tilde{\varepsilon}_y} + \tilde{\varepsilon}_x \tilde{\varepsilon}_z \frac{\partial^2 p_s}{\partial \tilde{\varepsilon}_x \partial \tilde{\varepsilon}_z} + \tilde{\varepsilon}_x \tilde{\eta} \frac{\partial^2 p_s}{\partial \tilde{\varepsilon}_x \partial \tilde{\eta}} \right. \\
& \quad \left. + \tilde{\varepsilon}_y \tilde{\varepsilon}_z \frac{\partial^2 p_s}{\partial \tilde{\varepsilon}_y \partial \tilde{\varepsilon}_z} + \tilde{\varepsilon}_y \tilde{\eta} \frac{\partial^2 p_s}{\partial \tilde{\varepsilon}_y \partial \tilde{\eta}} + \tilde{\varepsilon}_z \tilde{\eta} \frac{\partial^2 p_s}{\partial \tilde{\varepsilon}_z \partial \tilde{\eta}} \right) \\
& + \frac{\sigma_w^2}{8} \left((1 - \tilde{\varepsilon}_x^2) \frac{\partial^2 p_s}{\partial \tilde{\varepsilon}_x^2} + (1 - \tilde{\varepsilon}_y^2) \frac{\partial^2 p_s}{\partial \tilde{\varepsilon}_y^2} + (1 - \tilde{\varepsilon}_z^2) \frac{\partial^2 p_s}{\partial \tilde{\varepsilon}_z^2} + (1 - \tilde{\eta}^2) \frac{\partial^2 p_s}{\partial \tilde{\eta}^2} \right)
\end{aligned} \tag{4.22}$$

At this point the solution to the stationary Fokker-Planck PDE [4.22](#) may not be immediately obvious. First, the system will be reduced to the SO(2) case to gain a deeper understanding of the problem. The SO(2) analysis will result in a stationary Fokker-Planck PDE with a known analytic solution as will be shown in [Section 4.8](#). The intuition gained from the SO(2) case will suggest a solution for the full SO(3) case, which is revisited in [Section 4.11](#).

4.5 Attitude Filter Formulation in SO(2)

In this section, the attitude filter dynamical model is reduced to the single axis case of SO(2). In following sections, the reduced model will be shown to yield tractable analysis results that can provide insight into the full SO(3) case.

As explained in Section 2.3.2, the SO(3) dynamical model may be reduced to the SO(2) case by simply zeroing out the y and z components of all vector quantities. Equivalently, the vector quantities in the SO(3) case reduce to scalar quantities, and SO(3) unit quaternions comprised of four elements reduce to SO(2) unit quaternions with two elements.

The SO(3) Langevin form error dynamics of Equation 4.5 reduce in the SO(2) case to

$$\begin{aligned}\dot{\tilde{\mathbf{q}}}(t) &= \frac{1}{2} \left\{ -\sigma_w n_w(t) - k_e \tilde{\eta}(t) \tilde{\varepsilon}(t) \right\} \otimes \tilde{\mathbf{q}}(t) \\ &= \begin{bmatrix} -\frac{1}{2} k_e \tilde{\eta}^2(t) \tilde{\varepsilon}(t) \\ \frac{1}{2} k_e \tilde{\eta}(t) \tilde{\varepsilon}^2(t) \end{bmatrix} + \begin{bmatrix} -\frac{1}{2} \tilde{\eta}(t) \sigma_w \\ \frac{1}{2} \tilde{\varepsilon}(t) \sigma_w \end{bmatrix} n_w(t) \end{aligned} \quad (4.23)$$

As explained in Section 2.1.3, the Langevin form error dynamics differential equation 4.23 is interpreted as a Stratonovich SDE. Converting to Itô form yields

$$\begin{aligned}d\tilde{\mathbf{x}}(t) &= \begin{bmatrix} d\tilde{\varepsilon}(t) \\ d\tilde{\eta}(t) \end{bmatrix} \\ &= \begin{bmatrix} -\frac{1}{2} k_e \tilde{\eta}^2(t) \tilde{\varepsilon}(t) - \frac{1}{8} \sigma_w^2 \tilde{\varepsilon}(t) \\ \frac{1}{2} k_e \tilde{\eta}(t) \tilde{\varepsilon}^2(t) - \frac{1}{8} \sigma_w^2 \tilde{\eta}(t) \end{bmatrix} dt + \begin{bmatrix} -\frac{1}{2} \tilde{\eta}(t) \sigma_w \\ \frac{1}{2} \tilde{\varepsilon}(t) \sigma_w \end{bmatrix} d\beta_w(t) \\ &= \mathbf{f}(\tilde{\mathbf{x}}(t)) dt + G(\tilde{\mathbf{x}}(t)) d\beta(t) \end{aligned} \quad (4.24)$$

The attitude filter error dynamics of Equation 4.23 can equivalently be written in the SO(2) Euler Axis/Angle parameterization (as explained in Section 2.3.2) as

$$\begin{aligned}\dot{\tilde{\phi}}(t) &= -k_e \tilde{\eta}(t) \tilde{\varepsilon}(t) - \sigma_w n_w(t) \\ &= -\frac{1}{2} k_e \sin\left(\tilde{\phi}(t)\right) - \sigma_w n_w(t)\end{aligned}\tag{4.25}$$

which is immediately in Langevin form. Conversion to an Itô SDE is trivial as the diffusion matrix $G(\tilde{\phi}(t)) = -\sigma_w$ is independent of the state $\tilde{\phi}(t)$:

$$d\tilde{\phi}(t) = -\frac{1}{2} k_e \sin\left(\tilde{\phi}(t)\right) dt - \sigma_w d\beta_w(t)\tag{4.26}$$

Note of course that SDEs 4.24 and 4.26 describe the same system. One can verify, for example, by taking the Itô derivative (given in Equation 2.16) of $\tilde{\varepsilon}(t) = a(t) \sin\left(\frac{\tilde{\phi}(t)}{2}\right)$ and $\tilde{\eta}(t) = \cos\left(\frac{\tilde{\phi}(t)}{2}\right)$ with respect to the Itô SDE 4.26 and the trivial SO(2) Euler axis SDE $d\tilde{a}(t) = 0$ to recover the Itô SDE 4.24 and vice-versa.

4.6 Stochastic Lyapunov Analysis in SO(2)

In this section a stochastic Lyapunov stability analysis of the SO(2) Itô SDE 4.24 is conducted and performance bounds are established. The analysis in this section is the SO(2) analog of the SO(3) analysis of Section 4.2.

Theorem 4.6.1. *The attitude error dynamics of the Itô SDE 4.24 are weakly stochastically stable. Further, the attitude estimate error has the ultimate bound*

$$\lim_{t \rightarrow \infty} E[\tilde{\varepsilon}^2(t)] \leq \frac{1}{2} \quad (4.27)$$

which is valid for all $k_e \geq 0$.

Proof. Choose as a Lyapunov function $V(t) = \tilde{\varepsilon}^2(t)$. Then application of the differential generator to the Lyapunov function with respect to the Itô SDE 4.24 yields

$$\begin{aligned} \mathcal{L}V(t) &= \left(\frac{\partial V}{\partial \tilde{\mathbf{x}}} \right)^T \mathbf{f}(\tilde{\mathbf{x}}(t)) + \frac{1}{2} \text{tr} \left\{ G^T(\tilde{\mathbf{x}}(t)) \frac{\partial^2 V}{\partial \tilde{\mathbf{x}}^2} G(\tilde{\mathbf{x}}(t)) \right\} \\ &= -k_e \tilde{\eta}^2(t) \tilde{\varepsilon}^2(t) - \frac{1}{4} \sigma_w^2 \tilde{\varepsilon}^2(t) + \frac{1}{4} \sigma_w^2 \tilde{\eta}^2(t) \\ &= -k_e \tilde{\eta}^2(t) \tilde{\varepsilon}^2(t) - \frac{1}{2} \sigma_w^2 \tilde{\varepsilon}^2(t) + \frac{1}{4} \sigma_w^2 \end{aligned} \quad (4.28)$$

$$\leq -\frac{1}{2} \sigma_w^2 \tilde{\varepsilon}^2(t) + \frac{1}{4} \sigma_w^2 \quad (4.29)$$

Zakai's stability theorem (Theorem 2.1.4) implies the system is weakly stochastically stable.

Application of Zakai's ultimate moment theorem, Theorem 2.1.5, yields

$$\lim_{t \rightarrow \infty} E \left[\frac{1}{2} \sigma_w^2 \tilde{\varepsilon}^2(t) \right] \leq \frac{1}{4} \sigma_w^2 \quad (4.30)$$

Using the fact that the expectation operator is linear, simple algebraic manipulation provides the attitude estimate error ultimate bound.

□

As in the SO(3) case, this upper bound is a constant and does not capture the performance improvement once the filter gain k_e is large enough to mitigate the influence of the gyro noise. Also as in the SO(3) case, it is possible to find an ultimate **lower** bound on $E[\tilde{\varepsilon}^2(t)]$.

Corollary 4.6.1.1. *The attitude error dynamics of the Itô SDE 4.24 obey the ultimate **lower** bound*

$$\lim_{t \rightarrow \infty} E[\tilde{\varepsilon}^2(t)] \geq \frac{1}{2} + \frac{\sigma_w^2}{4k_e} - \frac{1}{2} \sqrt{1 + \frac{\sigma_w^4}{4k_e^2}} \quad (4.31)$$

Proof. Apply Theorem 2.1.5 directly to Equation 4.28 to find

$$\lim_{t \rightarrow \infty} E\left[k_e \tilde{\eta}^2(t) \tilde{\varepsilon}^2(t) + \frac{1}{2} \sigma_w^2 \tilde{\varepsilon}^2(t)\right] = \frac{1}{4} \sigma_w^2 \quad (4.32)$$

Using linearity of the expectation operator, the unit quaternion norm constraint $\tilde{\varepsilon}^2(t) + \tilde{\eta}^2(t) = 1$, and rearranging results in

$$\begin{aligned} 0 &= \lim_{t \rightarrow \infty} \left\{ E[\tilde{\varepsilon}^4(t)] - \left(1 + \frac{\sigma_w^2}{k_e}\right) E[\tilde{\varepsilon}^2(t)] + \frac{\sigma_w^2}{4k_e} \right\} \\ &= \lim_{t \rightarrow \infty} \left\{ \left(E[\tilde{\varepsilon}^2(t)]\right)^2 + Var[\tilde{\varepsilon}^2(t)] - \left(1 + \frac{\sigma_w^2}{k_e}\right) E[\tilde{\varepsilon}^2(t)] + \frac{\sigma_w^2}{4k_e} \right\} \end{aligned} \quad (4.33)$$

Combining Equation 4.36 with the fact that $Var[\tilde{\varepsilon}^2(t)] \geq 0$ results in the second order polynomial inequality

$$\begin{aligned} 0 &= \lim_{t \rightarrow \infty} \left\{ \left(E[\tilde{\varepsilon}^2(t)]\right)^2 + Var[\tilde{\varepsilon}^2(t)] - \left(1 + \frac{\sigma_w^2}{k_e}\right) E[\tilde{\varepsilon}^2(t)] + \frac{\sigma_w^2}{4k_e} \right\} \\ &\geq \lim_{t \rightarrow \infty} \left\{ \left(E[\tilde{\varepsilon}^2(t)]\right)^2 - \left(1 + \frac{\sigma_w^2}{k_e}\right) E[\tilde{\varepsilon}^2(t)] + \frac{\sigma_w^2}{4k_e} \right\} \end{aligned} \quad (4.34)$$

Solving the polynomial inequality yields the lower ultimate bound.

□

As in the SO(3) case, if the underlying probability density of $\tilde{\varepsilon}^2(t)$ is assumed to be unimodal, the Jacobson inequality can be used to find a tighter ultimate upper bound.

Corollary 4.6.1.2. *If the underlying probability density of $\tilde{\varepsilon}^2(t)$ is **unimodal**, the attitude estimate error dynamics of the Itô SDE 4.24 obey the ultimate upper bound*

$$\lim_{t \rightarrow \infty} E[\tilde{\varepsilon}^2(t)] \leq \frac{1}{2} + \frac{\sigma_w^2}{4k_e} - \frac{1}{2} \sqrt{\frac{5}{9} + \frac{\sigma_w^4}{4k_e^2}} \quad (4.35)$$

Proof. From Equation 4.36 it is clear that

$$\begin{aligned} 0 &= \lim_{t \rightarrow \infty} \left\{ \left(E[\tilde{\varepsilon}^2(t)] \right)^2 + Var[\tilde{\varepsilon}^2(t)] - \left(1 + \frac{\sigma_w^2}{k_e} \right) E[\tilde{\varepsilon}^2(t)] + \frac{\sigma_w^2}{4k_e} \right\} \quad (4.36) \\ &\leq \lim_{t \rightarrow \infty} \left\{ \left(E[\tilde{\varepsilon}^2(t)] \right)^2 - \left(1 + \frac{\sigma_w^2}{k_e} \right) E[\tilde{\varepsilon}^2(t)] + \left(\frac{\sigma_w^2}{4k_e} + \sup Var[\tilde{\varepsilon}^2(t)] \right) \right\} \quad (4.37) \end{aligned}$$

If one assumes the underlying probability density of $\tilde{\varepsilon}^2(t)$ is unimodal and recognizing that $0 \leq \tilde{\varepsilon}^2(t) \leq 1$, the Jacobson Inequality [36] for this system provides

$$\sup Var[\tilde{\varepsilon}^2(t)] \leq \frac{1}{9} \quad (4.38)$$

Substituting the variance bound into Inequality 4.37 results in a second order polynomial inequality in $E[\tilde{\varepsilon}^2(t)]$:

$$0 \leq \lim_{t \rightarrow \infty} \left\{ \left(E[\tilde{\varepsilon}^2(t)] \right)^2 - \left(1 + \frac{\sigma_w^2}{k_e} \right) E[\tilde{\varepsilon}^2(t)] + \left(\frac{\sigma_w^2}{4k_e} + \frac{1}{9} \right) \right\} \quad (4.39)$$

Solving the polynomial inequality yields the final result.

□

This new ultimate upper bound from Corollary 4.6.1.2 matches the upper bound from Theorem 4.6.1 for small k_e as seen in the limit:

$$\lim_{k_e \rightarrow 0} \frac{1}{2} + \frac{\sigma_w^2}{4k_e} - \frac{1}{2} \sqrt{\frac{5}{9} + \frac{\sigma_w^4}{4k_e^2}} = \frac{1}{2} \quad (4.40)$$

For large k_e the upper bound from Corollary 4.6.1.2 has the high gain limit

$$\lim_{k_e \rightarrow \infty} \frac{1}{2} + \frac{\sigma_w^2}{4k_e} - \frac{1}{2} \sqrt{\frac{5}{9} + \frac{\sigma_w^4}{4k_e^2}} = \frac{1}{2} \left(1 - \sqrt{\frac{5}{9}} \right) = \frac{1}{2} - \frac{\sqrt{5}}{6} \approx 0.127 \quad (4.41)$$

which is precisely the same high gain limit as in the SO(3) case.

4.7 Numerical Simulation of Stochastic SO(2) Lyapunov Bounds

Numerical simulations of the SO(2) attitude filter's Itô SDE error dynamics of Equation 4.24 were performed for a variety of system parameters. The Kloeden-Platen Explicit Weak 2.0 numerical integration scheme discussed in Section 2.2.3 was used. For each simulation realization, a time step size of $\Delta t = 0.1$ was used for a total of 10^8 simulation steps. At the end of a simulation realization, the last 10^7 simulation steps were used to compute the empirical ergodic mean of the filter attitude estimate error $\tilde{\varepsilon}^2(t)$. An ensemble of 7 realizations were simulated for each choice of system parameters; as before, the ensemble mean of the ergodic means was then computed.

A gallery of plots of the filter attitude estimate errors are included in Figure 4.2. A magenta dot indicates the ensemble mean of the ergodic means. The stochastic Lyapunov bounds of the previous section are also drawn on the plots, with the upper bound from Theorem 4.6.1 in red, the lower bound of Corollary 4.6.1.1 in blue, and the upper bound of Corollary 4.6.1.2 in yellow. As in the SO(3) case, all the stochastic Lyapunov bounds do correctly envelope the ensemble of the simulation realizations. The ultimate upper bound from Theorem 4.6.1, which is independent of any system parameters, is increasingly conservative for large k_e but does tightly match the numerical simulation data for small k_e . The ultimate upper bound of Corollary 4.6.1.2 bends at the transition region in the numerical simulation data but levels off, growing increasingly conservative, for large k_e . The ultimate lower bound of Corollary 4.6.1.1 most closely bounds the numerical data.

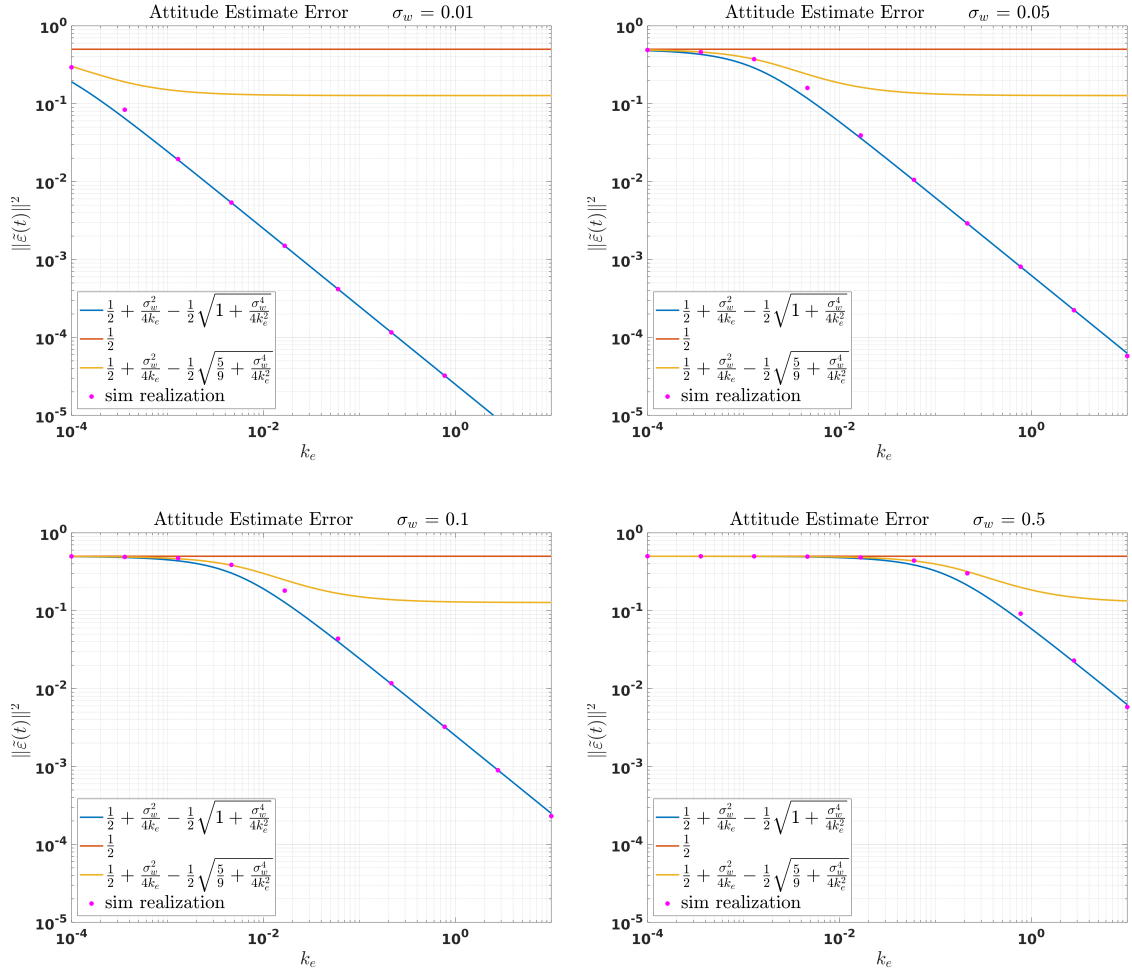


Figure 4.2: Comparison of simulation realizations of attitude estimate errors of the SO(2) error dynamics Itô SDE of Equation 4.24 to the stochastic Lyapunov upper bound from Theorem 4.6.1 in red, the lower bound of Corollary 4.6.1.1 in blue, and the upper bound of Corollary 4.6.1.2 in yellow.

4.8 Fokker-Planck Analysis in SO(2)

Let $p = p(\tilde{\phi}(t), t)$ be the joint probability density for the attitude filter error $\tilde{\phi}(t)$. The Fokker-Planck PDE associated with the attitude filter error dynamics Itô SDE 4.26 is given by

$$\begin{aligned} \frac{\partial p}{\partial t} &= - \sum_{i=1}^1 \frac{\partial}{\partial \tilde{q}_i} \left[f_i(\tilde{\mathbf{q}}(t)) p(\tilde{\mathbf{q}}(t), t) \right] + \frac{1}{2} \sum_{i,j=1}^1 \frac{\partial^2}{\partial \tilde{q}_i \partial \tilde{q}_j} \left[\left\{ G(\tilde{\mathbf{q}}(t)) G^T(\tilde{\mathbf{q}}(t)) \right\}_{i,j} p(\tilde{\mathbf{q}}(t), t) \right] \\ &= \frac{1}{2} k_e \cos(\tilde{\phi}(t)) p(\tilde{\phi}(t), t) + \frac{1}{2} k_e \sin(\tilde{\phi}(t)) \frac{\partial p}{\partial \tilde{\phi}} + \frac{1}{2} \sigma_w^2 \frac{\partial^2 p}{\partial \tilde{\phi}^2} \end{aligned} \quad (4.42)$$

Theorem 4.6.1 showed the attitude filter error dynamics of the Itô SDE 4.24 are weakly stochastically stable. As explained in Section 4.5 the Itô SDE 4.26 is an equivalent parameterization of the Itô SDE 4.24 (as they both describe the same underlying system) and thus the Itô SDE 4.26 is also weakly stochastically stable. For further verification, one can form the SO(2) Fokker-Planck PDE in the SO(2) quaternion parameterization and use the usual change of variables formula (along with the unit quaternion norm constraint $\tilde{\varepsilon}^2(t) + \tilde{\eta}^2(t) = 1$ and the equivalent Euler axis norm constraint $\tilde{a}(t) = 1$) to arrive at the Fokker-Planck PDE 4.42.

Thus the joint probability density function $p(\tilde{\phi}(t), t)$ ultimately approaches a stationary probability density function

$$p_s = p_s(\tilde{\phi}) = \lim_{t \rightarrow \infty} p(\tilde{\phi}(t), t)$$

which is the solution to the stationary Fokker-Planck PDE

$$0 = \frac{1}{2} k_e \cos(\tilde{\phi}) p_s(\tilde{\phi}) + \frac{1}{2} k_e \sin(\tilde{\phi}) \frac{\partial p_s}{\partial \tilde{\phi}} + \frac{1}{2} \sigma_w^2 \frac{\partial^2 p_s}{\partial \tilde{\phi}^2} \quad (4.43)$$

The SO(2) stationary Fokker-Planck PDE, which is actually an ODE, is tractable.

An exact solution is given in the following theorem.

Theorem 4.8.1. *The stationary Fokker-Planck PDE of Equation 4.43 is solved by the von Mises probability density function*

$$p_s(\tilde{\phi}) = \frac{1}{N} \exp \left\{ \frac{k_e}{\sigma_w^2} \cos(\tilde{\phi}) \right\} \quad (4.44)$$

where the normalization constant N is given by

$$N = \int_{-2\pi}^{2\pi} \exp \left\{ \frac{k_e}{\sigma_w^2} \cos(\tilde{\phi}) \right\} d\tilde{\phi} = 4\pi I_0 \left(\frac{k_e}{\sigma_w^2} \right)$$

and $I_0(x)$ is the 0th order modified Bessel function of the first kind.

Proof. The stationary Fokker-Planck PDE of Equation 4.43 is not solved by the wrapped normal distribution, the wrapped Cauchy distribution, the wrapped exponential distribution, or the cardioid distribution [53, 60, 61]. Consider instead the von Mises probability density function of the form

$$p_s(\tilde{\phi}) = \frac{1}{N} \exp \left\{ \kappa \cos(\tilde{\phi}) \right\} \quad (4.45)$$

where the normalization constant N is a positive scalar and the concentration parameter κ is a non-negative scalar.

Substituting the PDF of Equation 4.45 into the right hand side of the PDE 4.43 yields the expression

$$\left\{ \frac{1}{2} \cos(\tilde{\phi}) (k_e - \sigma_w^2 \kappa) + \frac{1}{2} \sin^2(\tilde{\phi}) (\sigma_w^2 \kappa^2 - k_e \kappa) \right\} \frac{1}{N} \exp \left\{ \kappa \cos(\tilde{\phi}) \right\}$$

which is zero for all possible $\tilde{\phi}$ if and only if $\kappa = \frac{k_e}{\sigma_w^2}$.

Thus $p_s(\tilde{\phi}) = \frac{1}{N} \exp\left\{\frac{k_e}{\sigma_w^2} \cos(\tilde{\phi})\right\}$ solves the stationary Fokker-Planck PDE with the to be determined scaling constant N .

The scaling constant N may be recovered by enforcing the probability density normalization constraint

$$\int_{-2\pi}^{2\pi} p_s(\tilde{\phi}) d\tilde{\phi} = 1$$

Noting that the modified Bessel function of first kind is given in integral form [28] as

$$I_\nu(x) = \frac{1}{\pi} \int_0^\pi \cos(\nu\gamma) e^{x \cos(\gamma)} d\gamma - \frac{\sin(\nu\pi)}{\pi} \int_0^\infty e^{-\cosh(t) - \nu t} dt \quad (4.46)$$

the normalization constant can be found as

$$\begin{aligned} N &= \int_{-2\pi}^{2\pi} \exp\left\{\frac{k_e}{\sigma_w^2} \cos(\tilde{\phi})\right\} d\tilde{\phi} \\ &= 2 \int_{-\pi}^{\pi} \exp\left\{\frac{k_e}{\sigma_w^2} \cos(\tilde{\phi})\right\} d\tilde{\phi} \\ &= 4 \int_0^\pi \exp\left\{\frac{k_e}{\sigma_w^2} \cos(\tilde{\phi})\right\} d\tilde{\phi} \\ &= 4\pi I_0\left(\frac{k_e}{\sigma_w^2}\right) \end{aligned}$$

where the second equality holds because the integrand is periodic with period 2π and the third equality holds because the integrand is even.

□

The analytic solution to the stationary Fokker-Planck PDE allows for the computation of ultimate statistics of the filter's attitude estimate error. The following corollary shows that the SO(2) attitude estimation filter of this chapter is an (ultimately) unbiased estimator.

Corollary 4.8.1.1. *The error dynamics of the Itô SDE 4.24 have the ultimate mean*

$$\lim_{t \rightarrow \infty} E[\tilde{\varepsilon}(t)] = 0 \quad (4.47)$$

Proof. Compute the expectation using the probability density function from Theorem 4.8.1

$$\begin{aligned} \lim_{t \rightarrow \infty} E[\tilde{\varepsilon}(t)] &= \frac{1}{N} \int_{-2\pi}^{2\pi} \tilde{\varepsilon} \exp \left\{ \frac{k_e}{\sigma_w^2} \cos(\tilde{\phi}) \right\} d\tilde{\phi} \\ &= \frac{1}{N} \int_{-2\pi}^{2\pi} \sin\left(\frac{\tilde{\phi}}{2}\right) \exp \left\{ \frac{k_e}{\sigma_w^2} \cos(\tilde{\phi}) \right\} d\tilde{\phi} \end{aligned}$$

Note that $\sin(\cdot)$ is an odd function but $e^{\cos(\cdot)}$ is an even function, so the integrand is an odd function. The integral of an odd function over a symmetric interval about the origin is zero.

□

The next corollary allows one to analytically compute the ultimate noncentral second moment of the system. Since the ultimate mean was found to be zero in the previous corollary, the ultimate noncentral second moment given below is also the ultimate variance (also known as the ultimate central moment).

Corollary 4.8.1.2. *The error dynamics of the Itô SDE 4.24 are such that*

$$\lim_{t \rightarrow \infty} E[\tilde{\varepsilon}^2(t)] = \frac{1}{2} \left(1 - \frac{I_1\left(\frac{k_e}{\sigma_w^2}\right)}{I_0\left(\frac{k_e}{\sigma_w^2}\right)} \right) \quad (4.48)$$

where $I_0(x)$ and $I_1(x)$ are the 0th and 1st order modified Bessel functions of the first kind respectively.

Proof. Compute the expectation using the probability density function from Theorem 4.8.1

$$\begin{aligned}
\lim_{t \rightarrow \infty} E[\tilde{\varepsilon}^2(t)] &= \frac{1}{N} \int_{-2\pi}^{2\pi} \tilde{\varepsilon}^2 \exp \left\{ \frac{k_e}{\sigma_w^2} \cos(\tilde{\phi}) \right\} d\tilde{\phi} \\
&= \frac{1}{N} \int_{-2\pi}^{2\pi} \sin^2 \left(\frac{\tilde{\phi}}{2} \right) \exp \left\{ \frac{k_e}{\sigma_w^2} \cos(\tilde{\phi}) \right\} d\tilde{\phi} \\
&= \frac{1}{2N} \int_{-2\pi}^{2\pi} \exp \left\{ \frac{k_e}{\sigma_w^2} \cos(\tilde{\phi}) \right\} d\tilde{\phi} - \frac{1}{2N} \int_{-2\pi}^{2\pi} \cos(\tilde{\phi}) \exp \left\{ \frac{k_e}{\sigma_w^2} \cos(\tilde{\phi}) \right\} d\tilde{\phi} \\
&= \frac{N}{2N} - \frac{2}{N} \int_0^\pi \cos(\tilde{\phi}) \exp \left\{ \frac{k_e}{\sigma_w^2} \cos(\tilde{\phi}) \right\} d\tilde{\phi} \\
&= \frac{2\pi I_0 \left(\frac{k_e}{\sigma_w^2} \right) - 2\pi I_1 \left(\frac{k_e}{\sigma_w^2} \right)}{4\pi I_0 \left(\frac{k_e}{\sigma_w^2} \right)} \\
&= \frac{1}{2} \left(1 - \frac{I_1 \left(\frac{k_e}{\sigma_w^2} \right)}{I_0 \left(\frac{k_e}{\sigma_w^2} \right)} \right)
\end{aligned}$$

where the integral form of the modified Bessel function of the first kind, as stated in Equation 4.46, was used. □

4.9 Numerical Simulation of Stochastic SO(2) Analytic Results

Figure 4.3 shows the probability density function computed from an ensemble of 100 realizations for four different gyro noise levels. The von Mises PDF of Equation 4.44 is also drawn in both plots and is in exact agreement with the numerical data. The top plot depicts the PDFs in SO(2) quaternion space; note that the data is restricted to the unit circle in $(\tilde{\varepsilon}, \tilde{\eta})$ space which is a great circle of the unit quaternion hypersphere. The peaks in the PDF correspond to the $\tilde{\eta} = 1$ and $\tilde{\eta} = -1$ “poles” on the unit quaternion hypersphere. The bottom plot shows the same PDFs in Euler angle space, “unwrapping” the data for a two dimensional plot and confirming the peaks (at $\tilde{\phi} = 0$ and $\tilde{\phi} = \pm 2\pi$) have the same height. Note that the PDF is bimodal and symmetric with period 2π . This is to be expected as there is a 2-to-1 covering from quaternions to rotations; specifically, $\tilde{\mathbf{q}}$ and $-\tilde{\mathbf{q}}$ encode the same rotation.

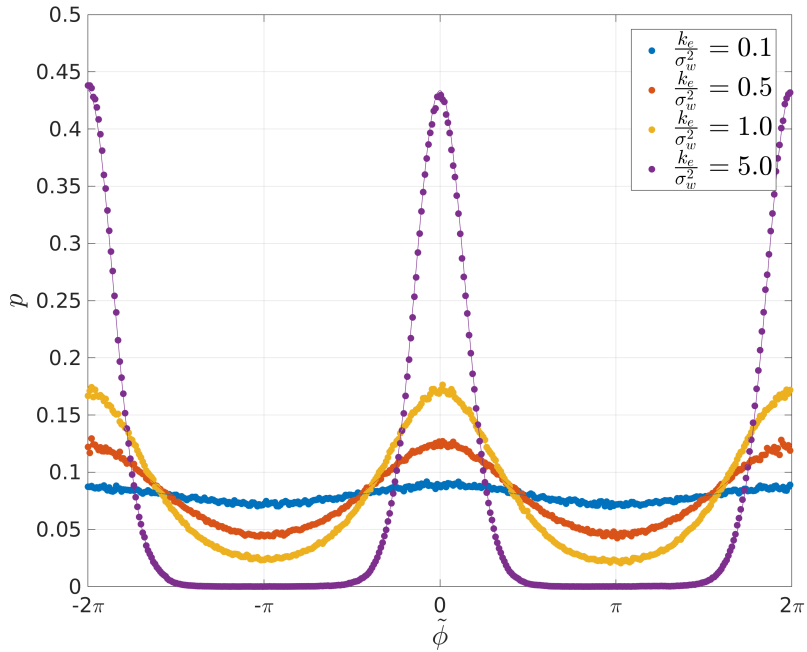
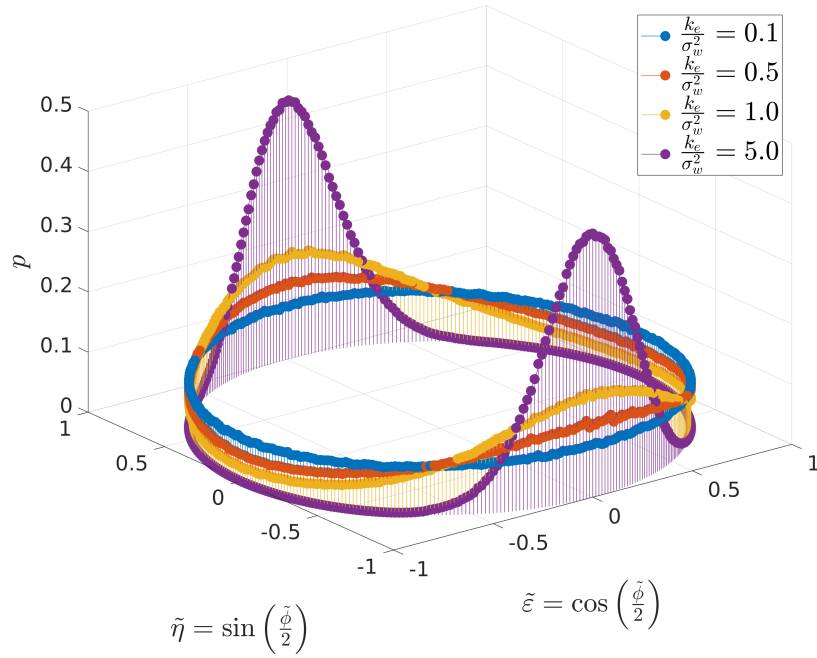


Figure 4.3: PDFs for the Itô SDE 4.24 computed from an ensemble of 100 realizations for four gyro noise levels agree with the von Mises PDF of Equation 4.44; depicted in SO(2) quaternion space (top) and Euler angle space (bottom).

Consider again the numerical simulations of the SO(2) attitude filter's Itô SDE error dynamics of Equation 4.24 first discussed in Section 4.7. Figure 4.4 compares the analytic ultimate variance of Corollary 4.8.1.2 to numerical simulation realizations. There is excellent agreement between the numerical simulation results with the analytic ultimate variance for all sampled values of the system parameters. Note that as Theorem 4.8.1 shows that the ultimate PDF of the underlying system is parameterized by the ratio $\frac{k_e}{\sigma_w^2}$, and consequently the ultimate variance $\lim_{t \rightarrow \infty} E[\tilde{\varepsilon}^2(t)]$ of Corollary 4.8.1.2 is parameterized by the same ratio, a plot of the ultimate variance as a function of k_e is merely shifted horizontally when σ_w changes which correctly matches the numerical simulation results in Figure 4.4.

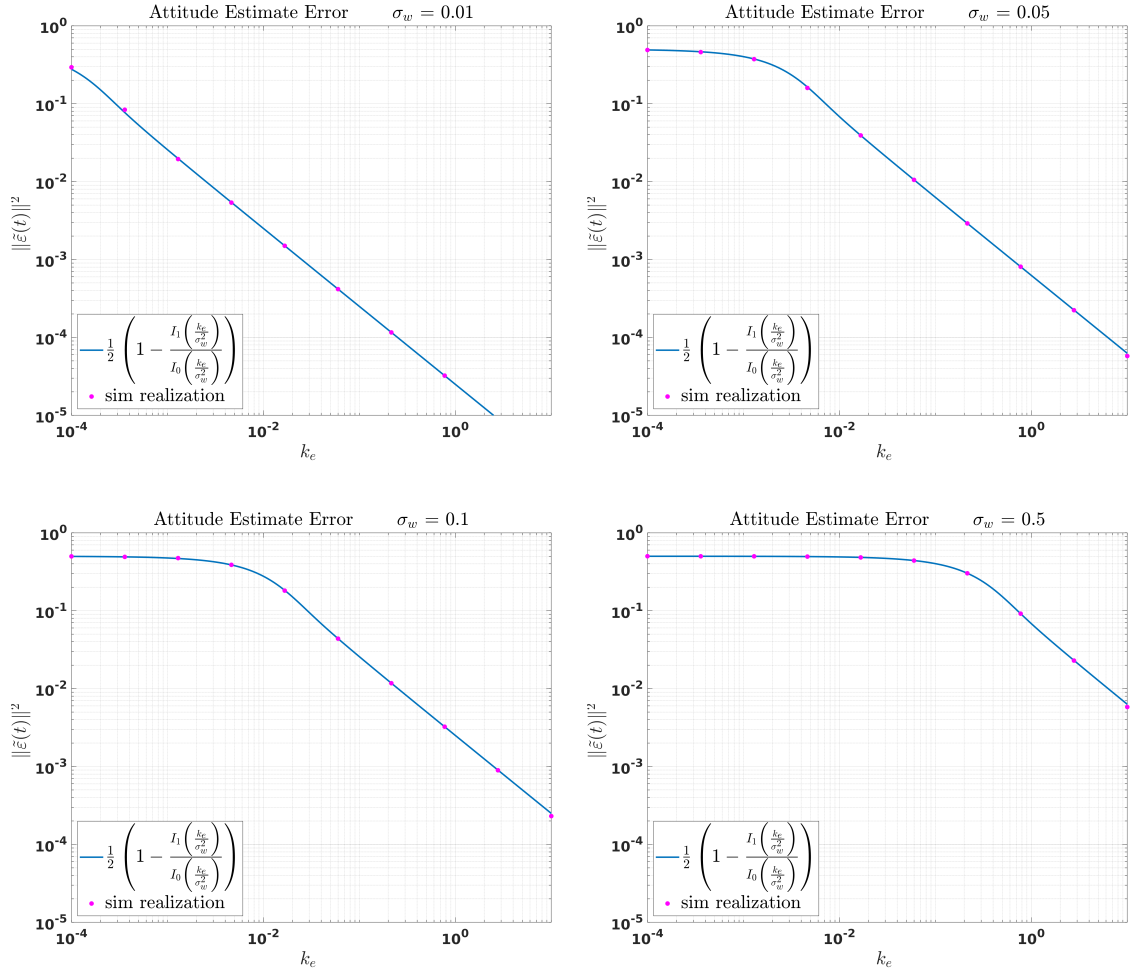


Figure 4.4: Comparison of simulation realizations of attitude estimate errors of the SO(2) error dynamics Itô SDE of Equation 4.24 to the ultimate variance given by the analytic solution from Corollary 4.8.1.2.

4.10 An SO(3) Upper Bound

This section explores possible ultimate upper bounds on $\tilde{\boldsymbol{\varepsilon}}^T(t)\tilde{\boldsymbol{\varepsilon}}(t)$ for the SO(3) case by extrapolating the ultimate upper bound for $\tilde{\boldsymbol{\varepsilon}}^2(t)$ for the SO(2) case given in Corollary 4.8.1.2. The factor of $\frac{1}{2}$ in Equation 4.48 is rescaled to $\frac{3}{4}$ so the SO(3) bound matches the low filter gain limit seen in all the bounds of Section 4.2 as well as the low filter gain limit apparent in the numerical simulation results of Section 4.3. The general form of the notional bound is assumed to have the same structure as that of Equation 4.48, but as the SO(3) case is driven by three independent noise sources the notional bound is assumed to be parameterized by $\frac{k_e}{\xi\sigma_w^2}$ where the positive scaling constant ξ is to be determined. This results in the following proposed SO(3) ultimate upper bound

$$\text{bound}\left(\xi, \frac{k_e}{\sigma_w^2}\right) = \frac{3}{4} \left(1 - \frac{I_1\left(\frac{k_e}{\xi\sigma_w^2}\right)}{I_0\left(\frac{k_e}{\xi\sigma_w^2}\right)}\right) \quad (4.49)$$

Figure 4.5 contains a gallery of the proposed upper bound for various choices of ξ are superimposed on plots of the numerical simulation realizations of the SO(3) attitude filter's error first presented in Section 4.3. In all cases considered, the choice of $\xi = 3$ in the expression of Equation 4.49 bound the simulation realizations; however, smaller choices of ξ do not bound all simulation data.

The choice of $\xi = 3$ can be understood as an upper bound in the following thought experiment. The variance of a random walk process in three dimensions driven by three independent noise sources each acting on a single axis can be upper bounded by the variance of a single dimensional random walk process driven by

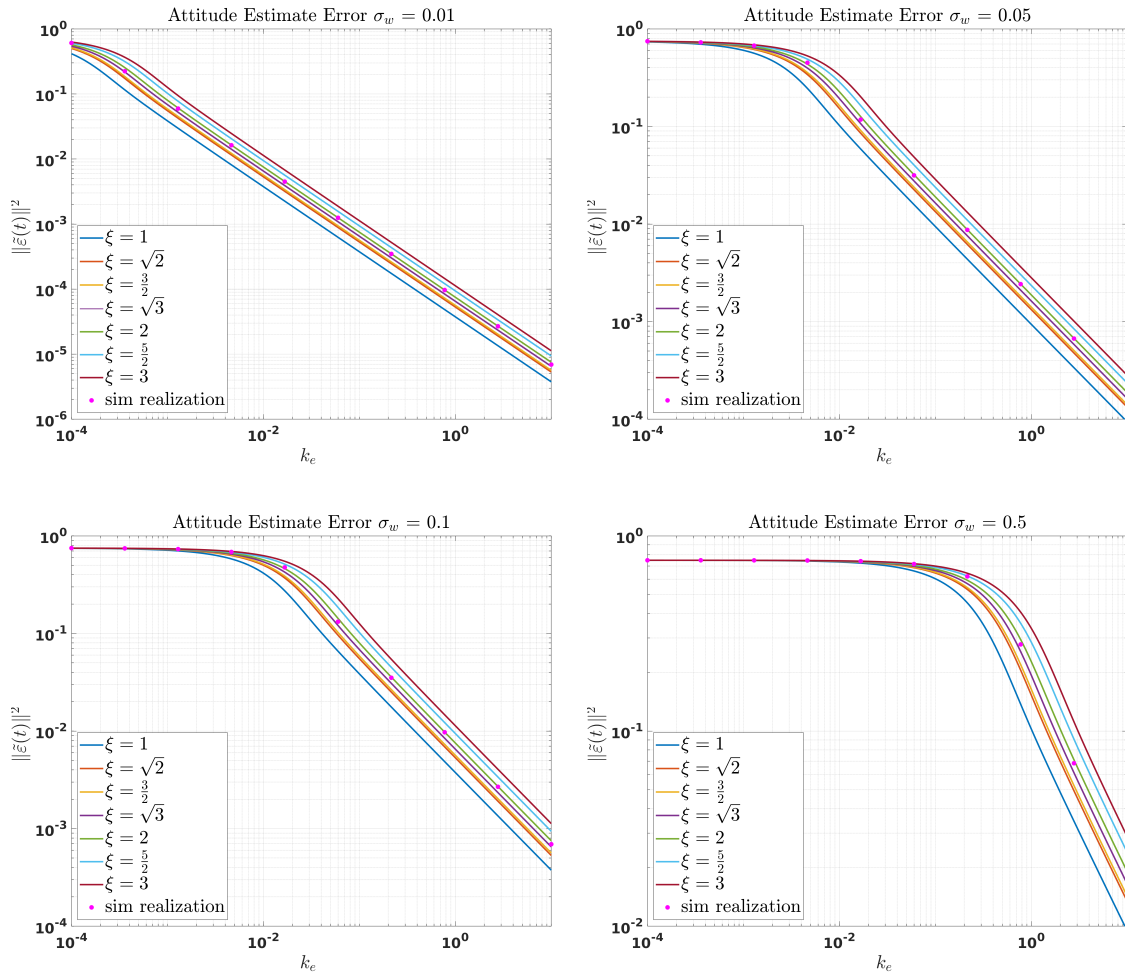


Figure 4.5: Comparison of simulation realizations of the attitude estimate error and the notional bound of Equation 4.49 for several choices of ξ and for various gyro measurement noise levels .

the same three independent noise sources each acting on the single axis. In other words, focusing the noise energy of all noise sources along a single physical dimension maximizes the potential for constructive and destructive interference. Of course, in the $SO(3)$ case considered in this chapter, the energy of any noise source is restricted to a gyro measurement channel; since gyro measurement axes are orthogonal the measurement noise sources will never “align” and the choice of $\xi = 3$ is thus an

upper bound.

Following the above logic, the SO(3) attitude estimate variance may be upper bounded by the attitude estimate variance of the SO(2) attitude filter when driven by three independent noise sources. Assuming the three independent noise sources each have the same variance σ_w^2 , the ultimate attitude estimate error variance is equivalent to that of the SO(2) attitude filter when driven by a single noise of noise variance $3\sigma_w^2$, yielding the heuristic upper bound

$$\lim_{t \rightarrow \infty} E \left[\tilde{\boldsymbol{\epsilon}}^T(t) \tilde{\boldsymbol{\epsilon}}(t) \right] \leq \frac{3}{4} \left(1 - \frac{I_1 \left(\frac{k_e}{3\sigma_w^2} \right)}{I_0 \left(\frac{k_e}{3\sigma_w^2} \right)} \right) \quad (4.50)$$

The upper bound is drawn again for clarity in the plots of Figure 4.6.

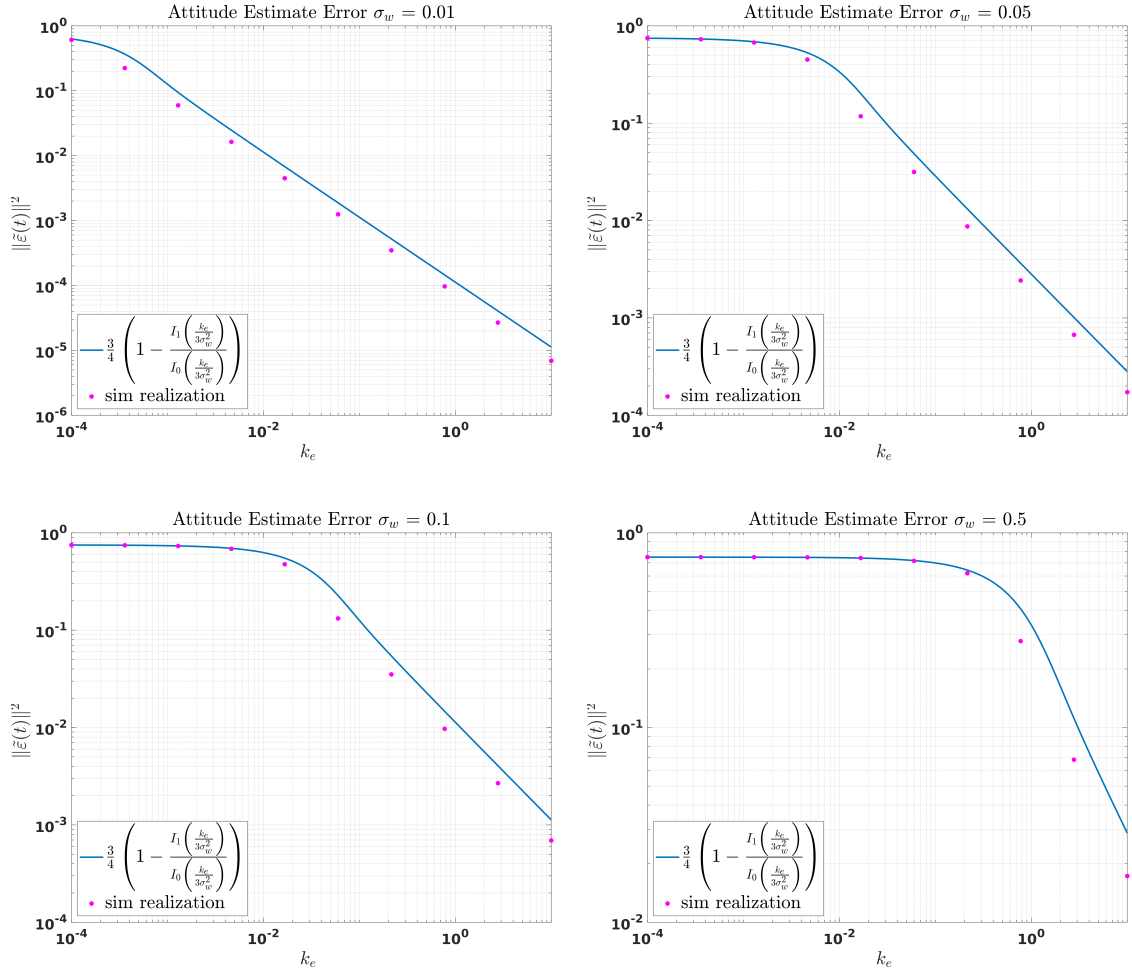


Figure 4.6: Comparison of simulation realizations of the SO(3) attitude estimate error for the Itô SDE 4.6 and the ultimate upper bound of Equation 4.50 for various gyro measurement noise levels .

4.11 Exact Solution to the Stationary SO(3) Fokker-Planck PDE

In this section, the understanding gained from the SO(2) analysis and its SO(3) extrapolation are used to identify a possible distribution for the SO(3) case. This distribution is then shown to indeed solve the SO(3) stationary Fokker-Planck PDE. The solution is used to find an analytical expression for the ultimate attitude estimate error which will be compared to numerical simulation data in the following section.

Given the success of the von Mises distribution in the SO(2) case, it is natural to look for generalizations for the SO(3) case. The Bingham distribution [8] is a distribution on the $d - 1$ unit hypersphere in \mathbb{R}^d ; its probability density function has the form

$$p(\mathbf{x}) = \frac{1}{N} \exp \left\{ \mathbf{x}^T M Z M^T \mathbf{x} \right\} \quad (4.51)$$

where $M \in \mathbb{R}^{d \times d}$ is an orthogonal matrix, $Z \in \mathbb{R}^{d \times d}$ is a negative semidefinite diagonal matrix, and $\mathbf{x} \in \mathbb{R}^d$ is such that $\|\mathbf{x}\| = 1$ [48]. The quadratic form in the exponential of the Bingham probability density function guarantee this distribution antipodally symmetric [60], meaning $p(\mathbf{x}) = p(-\mathbf{x})$. This is a necessary property for a PDF to be meaningful for an orientation distribution as \mathbf{q} and $-\mathbf{q}$ encode the same rotation. For certain choices of parameters, the two dimensional Bingham distribution reduces to the von Mises distribution on the unit circle [48]. The Bingham distribution has been used to represent the assumed probability distribution for quaternions in a Bayesian filter by Glover and Kaelbling [27] and in a recursive filter implementation by Kurz et al [48], as well as being used in texture analysis and

crystallography [47]. A special case of the Bingham distribution, called the Bipolar Bingham distribution by Kunze and Schaeben [47], has the form

$$p_s(\tilde{\phi}) = \frac{1}{N} \exp \left\{ \lambda \cos(\tilde{\phi}) \right\} = \frac{1}{N} \exp \left\{ \lambda(2\tilde{\eta}^2 - 1) \right\} \quad (4.52)$$

which is identical in structure to the von Mises probability density function that solved the SO(2) case. This form is equivalent to the general Bingham PDF with $M = I$ and $Z = \text{diag}(-\lambda, -\lambda, -\lambda, \lambda)$ and noting by the unit quaternion normalization constraint $1 = \tilde{\varepsilon}_x^2 + \tilde{\varepsilon}_y^2 + \tilde{\varepsilon}_z^2 + \tilde{\eta}^2$. The next theorem shows that the Bipolar Bingham distribution solves the SO(3) stationary Fokker-Planck PDE.

Theorem 4.11.1. *The stationary distribution for the attitude estimate error dynamics of the Itô SDE 4.6 is given by the Bipolar Bingham probability density function*

$$p_s(\tilde{\phi}) = \frac{1}{N} \exp \left\{ \frac{k_e}{\sigma_w^2} \cos(\tilde{\phi}) \right\} \quad (4.53)$$

where the normalization constant N is

$$N = \pi^2 I_0 \left(\frac{k_e}{\sigma_w^2} \right) - \pi^2 I_1 \left(\frac{k_e}{\sigma_w^2} \right)$$

and $I_0(x)$ and $I_1(x)$ are the 0th and 1st order modified Bessel functions of the first kind.

Proof. By definition $\tilde{\eta} = \cos\left(\frac{\tilde{\phi}}{2}\right)$, so $\tilde{\eta}^2 = \cos^2\left(\frac{\tilde{\phi}}{2}\right) = \frac{1}{2} \left(1 + \cos\left(\tilde{\phi}\right)\right)$. Substituting into the Bipolar Bingham PDF of Equation 4.52 yields

$$p_s(\tilde{\mathbf{q}}) = \frac{1}{N} \exp \left\{ \lambda(2\tilde{\eta}^2 - 1) \right\} \quad (4.54)$$

Taking partial derivatives as appropriate and substituting into the right hand side of the SO(3) stationary Fokker-Planck PDE 4.22 yields

$$\left\{ -\frac{1}{2}(k_e - \sigma_w^2 \lambda) + 2(1 - \lambda)(k_e - \lambda \sigma_w^2) \tilde{\eta}^2 + 2\lambda(k_e - \lambda \sigma_w^2) \tilde{\eta}^4 \right\} p_s$$

which is zero for all possible $\tilde{\mathbf{q}}$ if and only if $\lambda = \frac{k_e}{\sigma_w^2}$.

Thus $p_s(\tilde{\phi}) = \frac{1}{N} \exp \left\{ \frac{k_e}{\sigma_w^2} \cos \left(\tilde{\phi} \right) \right\}$ solves the stationary Fokker-Planck PDE with the to be determined scaling constant N .

The scaling constant N may be recovered by enforcing the probability density normalization constraint. Note that in the SO(2) case, the normalization constant found in Theorem 4.8.1 was computed by integrating over the circle of unit radius, so the differential element was a section of arc (again with unit radius). To find the normalization constant here, the integration must be done over the surface of the unit quaternion hypersphere which can be performed in hyperspherical coordinates; [47] provides such a parameterization for unit quaternions as

$$\tilde{\mathbf{q}} = \begin{bmatrix} \tilde{\boldsymbol{\varepsilon}} \\ \tilde{\eta} \end{bmatrix} = \begin{bmatrix} \tilde{\mathbf{a}} \sin \left(\frac{\tilde{\phi}}{2} \right) \\ \cos \left(\frac{\tilde{\phi}}{2} \right) \end{bmatrix} = \begin{bmatrix} \tilde{\varepsilon}_x \\ \tilde{\varepsilon}_y \\ \tilde{\varepsilon}_z \\ \tilde{\eta} \end{bmatrix} = \begin{bmatrix} \tilde{r} \sin(\tilde{\theta}) \cos(\tilde{\psi}) \sin \left(\frac{\tilde{\phi}}{2} \right) \\ \tilde{r} \sin(\tilde{\theta}) \sin(\tilde{\psi}) \sin \left(\frac{\tilde{\phi}}{2} \right) \\ \tilde{r} \cos(\tilde{\theta}) \sin \left(\frac{\tilde{\phi}}{2} \right) \\ \tilde{r} \cos \left(\frac{\tilde{\phi}}{2} \right) \end{bmatrix} \quad (4.55)$$

where the final parameterization utilizes hyper-spherical coordinates with radius $\tilde{r} = 1$. Essentially, the hyper-spherical coordinate parameterization is the Euler axis and angle formulation with the Euler axis expressed in (traditional) spherical coordinates $\tilde{\mathbf{a}} = [\sin(\tilde{\theta}) \cos(\tilde{\psi}) \ \sin(\tilde{\theta}) \sin(\tilde{\psi}) \ \cos(\tilde{\theta})]^T$ with polar angle $\tilde{\theta} \in [0, \pi]$ and azimuth angle $\tilde{\psi} \in [0, 2\pi]$.

The differential surface element for this manifold is given in [47] as

$$\frac{1}{2} \sin^2 \left(\frac{\tilde{\phi}}{2} \right) \sin(\tilde{\theta}) d\tilde{\phi} d\tilde{\theta} d\tilde{\psi}$$

so the normalization constant can be found by computing

$$\begin{aligned} N &= \int_{\tilde{\psi}=0}^{2\pi} \int_{\tilde{\theta}=0}^{\pi} \int_{\tilde{\phi}=0}^{\pi} \exp \left\{ \frac{k_e}{\sigma_w^2} \cos(\tilde{\phi}) \right\} \frac{1}{2} \sin^2 \left(\frac{\tilde{\phi}}{2} \right) \sin(\tilde{\theta}) d\tilde{\phi} d\tilde{\theta} d\tilde{\psi} \\ &= \frac{1}{2} \int_0^{2\pi} d\tilde{\psi} \int_0^{\pi} \sin(\tilde{\theta}) d\tilde{\theta} \int_0^{\pi} \sin^2 \left(\frac{\tilde{\phi}}{2} \right) \exp \left\{ \frac{k_e}{\sigma_w^2} \cos(\tilde{\phi}) \right\} d\tilde{\phi} \\ &= 2\pi \int_0^{\pi} \left(\frac{1}{2} - \frac{1}{2} \cos(\tilde{\phi}) \right) \exp \left\{ \frac{k_e}{\sigma_w^2} \cos(\tilde{\phi}) \right\} d\tilde{\phi} \\ &= \pi^2 I_0 \left(\frac{k_e}{\sigma_w^2} \right) - \pi^2 I_1 \left(\frac{k_e}{\sigma_w^2} \right) \end{aligned}$$

recognizing the integral form [5]

$$I_n(z) = \frac{1}{\pi} \int_0^{\pi} \cos(nx) \exp \left\{ z \cos(x) \right\} dx \quad \forall n \in \mathbb{N} \quad (4.56)$$

as the n^{th} order modified Bessel function of the first kind. □

In the Bayesian filter work by Glover and Kaelbling [27] and the recursive filter implementation by Kurz et al [48], the underlying probability distribution was assumed to be given by a Bingham distribution. Motivations for this assumption were given as its natural representation of quaternions, its relationship to the Gaussian distribution, and a maximum entropy property [59]. The above theorem formally proves that the attitude estimate error state for the filter of Equation 4.3 actually does asymptotically converge to a Bingham distribution.

Now that the stationary Fokker-Planck PDE is known to be solved by the Bipolar Bingham distribution of Equation 4.53, the PDF can be used to find analytic

expressions for various stationary statistics of the process. The following corollary shows the filter is ultimately an unbiased estimator.

Corollary 4.11.1.1. *The error dynamics of the Itô SDE 4.6 have zero stationary mean:*

$$\lim_{t \rightarrow \infty} E[\tilde{\boldsymbol{\varepsilon}}(t)] = \mathbf{0}$$

Proof. Using the hyperspherical parameterization for the unit quaternion from Equation 4.55, each element of the stationary mean vector may be computed in turn by taking the expectation on the unit quaternion hypersphere as

$$\lim_{t \rightarrow \infty} E[\tilde{\boldsymbol{\varepsilon}}(t)] = \begin{bmatrix} m_x \\ m_y \\ m_z \end{bmatrix}$$

where

$$\begin{aligned} m_x &= \frac{1}{N} \int_{\tilde{\psi}=0}^{2\pi} \int_{\tilde{\theta}=0}^{\pi} \int_{\tilde{\phi}=0}^{\pi} \tilde{r} \sin(\tilde{\theta}) \cos(\tilde{\psi}) \sin\left(\frac{\tilde{\phi}}{2}\right) \\ &\quad \times \exp\left\{\frac{k_e}{\sigma_w^2} \cos(\tilde{\phi})\right\} \frac{1}{2} \sin^2\left(\frac{\tilde{\phi}}{2}\right) \sin(\tilde{\theta}) d\tilde{\phi} d\tilde{\theta} d\tilde{\psi} \\ &= \frac{1}{2N} \int_0^{2\pi} \cos(\tilde{\psi}) d\tilde{\psi} \int_0^{\pi} \sin^2(\tilde{\theta}) d\tilde{\theta} \int_0^{\pi} \sin^3\left(\frac{\tilde{\phi}}{2}\right) \exp\left\{\frac{k_e}{\sigma_w^2} \cos(\tilde{\phi})\right\} d\tilde{\phi} \\ &= 0 \end{aligned}$$

and

$$\begin{aligned}
m_y &= \frac{1}{N} \int_{\tilde{\psi}=0}^{2\pi} \int_{\tilde{\theta}=0}^{\pi} \int_{\tilde{\phi}=0}^{\pi} \tilde{r} \sin(\tilde{\theta}) \sin(\tilde{\psi}) \sin\left(\frac{\tilde{\phi}}{2}\right) \\
&\quad \times \exp\left\{\frac{k_e}{\sigma_w^2} \cos(\tilde{\phi})\right\} \frac{1}{2} \sin^2\left(\frac{\tilde{\phi}}{2}\right) \sin(\tilde{\theta}) d\tilde{\phi} d\tilde{\theta} d\tilde{\psi} \\
&= \frac{1}{2N} \int_0^{2\pi} \sin(\tilde{\psi}) d\tilde{\psi} \int_0^{\pi} \sin^2(\tilde{\theta}) d\tilde{\theta} \int_0^{\pi} \sin^3\left(\frac{\tilde{\phi}}{2}\right) \exp\left\{\frac{k_e}{\sigma_w^2} \cos(\tilde{\phi})\right\} d\tilde{\phi} \\
&= 0
\end{aligned}$$

and

$$\begin{aligned}
m_z &= \frac{1}{N} \int_{\tilde{\psi}=0}^{2\pi} \int_{\tilde{\theta}=0}^{\pi} \int_{\tilde{\phi}=0}^{\pi} \tilde{r} \cos(\tilde{\theta}) \sin\left(\frac{\tilde{\phi}}{2}\right) \\
&\quad \times \exp\left\{\frac{k_e}{\sigma_w^2} \cos(\tilde{\phi})\right\} \frac{1}{2} \sin^2\left(\frac{\tilde{\phi}}{2}\right) \sin(\tilde{\theta}) d\tilde{\phi} d\tilde{\theta} d\tilde{\psi} \\
&= \frac{1}{2N} \int_0^{2\pi} d\tilde{\psi} \int_0^{\pi} \sin(\tilde{\theta}) \cos(\tilde{\theta}) d\tilde{\theta} \int_0^{\pi} \sin^3\left(\frac{\tilde{\phi}}{2}\right) \exp\left\{\frac{k_e}{\sigma_w^2} \cos(\tilde{\phi})\right\} d\tilde{\phi} \\
&= 0
\end{aligned}$$

□

The next corollary develops an analytic expression for the ultimate noncentral second moment $\lim_{t \rightarrow \infty} E[\tilde{\boldsymbol{\varepsilon}}^T(t)\tilde{\boldsymbol{\varepsilon}}(t)]$, which was only upper and lower bounded in the analysis of Section 4.2 and heuristically bounded in the analysis of Section 4.10. Note that as the ultimate mean was found to be zero, the ultimate noncentral second moment is also the ultimate variance (the ultimate central second moment). The ultimate variance is a function of the **ratio** of $\frac{k_e}{\sigma_w^2}$.

Corollary 4.11.1.2. *The error dynamics of the Itô SDE 4.6 are such that*

$$\lim_{t \rightarrow \infty} E[\tilde{\boldsymbol{\varepsilon}}^T(t)\tilde{\boldsymbol{\varepsilon}}(t)] = \frac{3I_0\left(\frac{k_e}{\sigma_w^2}\right) - 4I_1\left(\frac{k_e}{\sigma_w^2}\right) + I_2\left(\frac{k_e}{\sigma_w^2}\right)}{4\left(I_0\left(\frac{k_e}{\sigma_w^2}\right) - I_1\left(\frac{k_e}{\sigma_w^2}\right)\right)} \quad (4.57)$$

where $I_n(x)$ is the n^{th} order modified Bessel function of the first kind.

Proof. Recall from Section 2.3.1 that $\tilde{\boldsymbol{\varepsilon}}(t) = \tilde{\boldsymbol{\alpha}}(t) \sin\left(\frac{\tilde{\phi}(t)}{2}\right)$.

Noting that by construction $\tilde{\boldsymbol{\alpha}}^T(t)\tilde{\boldsymbol{\alpha}}(t) = 1 \forall t$, the expectation can be computed using the probability density function from Theorem 4.11.1 and integrating on the manifold:

$$\begin{aligned}
\lim_{t \rightarrow \infty} E[\tilde{\boldsymbol{\varepsilon}}^T(t)\tilde{\boldsymbol{\varepsilon}}(t)] &= \frac{1}{N} \int_{\tilde{\psi}=0}^{2\pi} \int_{\tilde{\theta}=0}^{\pi} \int_{\tilde{\phi}=0}^{\pi} \sin^2\left(\frac{\tilde{\phi}}{2}\right) \exp\left\{\frac{k_e}{\sigma_w^2} \cos(\tilde{\phi})\right\} \\
&\quad \times \frac{1}{2} \sin^2\left(\frac{\tilde{\phi}}{2}\right) \sin(\tilde{\theta}) d\tilde{\phi} d\tilde{\theta} d\tilde{\psi} \\
&= \frac{1}{2N} \int_0^{2\pi} d\tilde{\psi} \int_0^{\pi} \sin(\tilde{\theta}) d\tilde{\theta} \int_0^{\pi} \sin^4\left(\frac{\tilde{\phi}}{2}\right) \exp\left\{\frac{k_e}{\sigma_w^2} \cos(\tilde{\phi})\right\} d\tilde{\phi} \\
&= \frac{2\pi}{N} \int_0^{\pi} \left(\frac{3}{8} - \frac{1}{2} \cos(\tilde{\phi}) + \frac{1}{2} \cos(2\tilde{\phi})\right) \exp\left\{\frac{k_e}{\sigma_w^2} \cos(\tilde{\phi})\right\} d\tilde{\phi} \\
&= \frac{2\pi}{\pi^2 \left(I_0\left(\frac{k_e}{\sigma_w^2}\right) - I_1\left(\frac{k_e}{\sigma_w^2}\right)\right)} \left[\frac{3\pi}{8} I_0\left(\frac{k_e}{\sigma_w^2}\right) - \frac{\pi}{2} I_1\left(\frac{k_e}{\sigma_w^2}\right) + \frac{\pi}{8} I_2\left(\frac{k_e}{\sigma_w^2}\right) \right] \\
&= \frac{3I_0\left(\frac{k_e}{\sigma_w^2}\right) - 4I_1\left(\frac{k_e}{\sigma_w^2}\right) + I_2\left(\frac{k_e}{\sigma_w^2}\right)}{4 \left(I_0\left(\frac{k_e}{\sigma_w^2}\right) - I_1\left(\frac{k_e}{\sigma_w^2}\right)\right)}
\end{aligned}$$

□

The ultimate covariance matrix can similarly be found as shown in the following corollary.

Corollary 4.11.1.3. *The error dynamics of the Itô SDE 4.6 have the ultimate covariance matrix*

$$\lim_{t \rightarrow \infty} E[\tilde{\boldsymbol{q}}(t)\tilde{\boldsymbol{q}}^T(t)] = \text{diag}\left(\frac{\nu}{3}, \frac{\nu}{3}, \frac{\nu}{3}, 1 - \nu\right) \quad (4.58)$$

where

$$\nu \left(\frac{k_e}{\sigma_w^2}\right) = \frac{3I_0\left(\frac{k_e}{\sigma_w^2}\right) - 4I_1\left(\frac{k_e}{\sigma_w^2}\right) + I_2\left(\frac{k_e}{\sigma_w^2}\right)}{4 \left(I_0\left(\frac{k_e}{\sigma_w^2}\right) - I_1\left(\frac{k_e}{\sigma_w^2}\right)\right)} = \lim_{t \rightarrow \infty} E[\tilde{\boldsymbol{\varepsilon}}^T(t)\tilde{\boldsymbol{\varepsilon}}(t)]$$

Proof. As in Corollary 4.11.1.1, the hyperspherical parameterization for the unit quaternion from Equation 4.55 can be used to find each element of the stationary covariance matrix by computing in turn the expectation on the unit quaternion hypersphere for

$$\begin{aligned} \lim_{t \rightarrow \infty} E[\tilde{\mathbf{q}}(t)\tilde{\mathbf{q}}^T(t)] &= \lim_{t \rightarrow \infty} \begin{bmatrix} \tilde{\varepsilon}_x^2(t) & \tilde{\varepsilon}_x(t)\tilde{\varepsilon}_y(t) & \tilde{\varepsilon}_x(t)\tilde{\varepsilon}_z(t) & \tilde{\varepsilon}_x(t)\tilde{\eta}(t) \\ \tilde{\varepsilon}_x(t)\tilde{\varepsilon}_y(t) & \tilde{\varepsilon}_y^2(t) & \tilde{\varepsilon}_y(t)\tilde{\varepsilon}_z(t) & \tilde{\varepsilon}_y(t)\tilde{\eta}(t) \\ \tilde{\varepsilon}_x(t)\tilde{\varepsilon}_z(t) & \tilde{\varepsilon}_y(t)\tilde{\varepsilon}_z(t) & \tilde{\varepsilon}_z^2(t) & \tilde{\varepsilon}_z(t)\tilde{\eta}(t) \\ \tilde{\varepsilon}_x(t)\tilde{\eta}(t) & \tilde{\varepsilon}_y(t)\tilde{\eta}(t) & \tilde{\varepsilon}_z(t)\tilde{\eta}(t) & \tilde{\eta}^2(t) \end{bmatrix} \\ &= \begin{bmatrix} c_{xx} & c_{xy} & c_{xz} & c_{xs} \\ c_{xy} & c_{yy} & c_{yz} & c_{ys} \\ c_{xz} & c_{yz} & c_{zz} & c_{zs} \\ c_{xs} & c_{ys} & c_{zs} & c_{ss} \end{bmatrix} \end{aligned}$$

Noting $\tilde{r} = 1 \forall t$, the diagonal elements are computed as

$$\begin{aligned} c_{xx} &= \frac{1}{N} \int_{\tilde{\psi}=0}^{2\pi} \int_{\tilde{\theta}=0}^{\pi} \int_{\tilde{\phi}=0}^{\pi} \tilde{r}^2 \sin^2(\tilde{\theta}) \cos^2(\tilde{\psi}) \sin^2\left(\frac{\tilde{\phi}}{2}\right) \\ &\quad \times \exp\left\{\frac{k_e}{\sigma_w^2} \cos(\tilde{\phi})\right\} \frac{1}{2} \sin^2\left(\frac{\tilde{\phi}}{2}\right) \sin(\tilde{\theta}) d\tilde{\phi} d\tilde{\theta} d\tilde{\psi} \\ &= \frac{1}{2N} \int_0^{2\pi} \cos^2(\tilde{\psi}) d\tilde{\psi} \int_0^{\pi} \sin^3(\tilde{\theta}) d\tilde{\theta} \int_0^{\pi} \sin^4\left(\frac{\tilde{\phi}}{2}\right) \exp\left\{\frac{k_e}{\sigma_w^2} \cos(\tilde{\phi})\right\} d\tilde{\phi} \\ &= \frac{1}{2} \frac{1}{\pi^2 \left(I_0\left(\frac{k_e}{\sigma_w^2}\right) - I_1\left(\frac{k_e}{\sigma_w^2}\right)\right)} \frac{\pi}{1} \frac{4}{3} \left[\frac{3\pi}{8} I_0\left(\frac{k_e}{\sigma_w^2}\right) - \frac{\pi}{2} I_1\left(\frac{k_e}{\sigma_w^2}\right) + \frac{\pi}{8} I_2\left(\frac{k_e}{\sigma_w^2}\right) \right] \\ &= \frac{3I_0\left(\frac{k_e}{\sigma_w^2}\right) - 4I_1\left(\frac{k_e}{\sigma_w^2}\right) + I_2\left(\frac{k_e}{\sigma_w^2}\right)}{3 \cdot 4 \left(I_0\left(\frac{k_e}{\sigma_w^2}\right) - I_1\left(\frac{k_e}{\sigma_w^2}\right)\right)} = \frac{\nu\left(\frac{k_e}{\sigma_w^2}\right)}{3} \end{aligned}$$

$$\begin{aligned}
c_{yy} &= \frac{1}{N} \int_{\tilde{\psi}=0}^{2\pi} \int_{\tilde{\theta}=0}^{\pi} \int_{\tilde{\phi}=0}^{\pi} \tilde{r}^2 \sin^2(\tilde{\theta}) \sin^2(\tilde{\psi}) \sin^2\left(\frac{\tilde{\phi}}{2}\right) \\
&\quad \times \exp\left\{\frac{k_e}{\sigma_w^2} \cos(\tilde{\phi})\right\} \frac{1}{2} \sin^2\left(\frac{\tilde{\phi}}{2}\right) \sin(\tilde{\theta}) d\tilde{\phi} d\tilde{\theta} d\tilde{\psi} \\
&= \frac{1}{2N} \int_0^{2\pi} \sin^2(\tilde{\psi}) d\tilde{\psi} \int_0^{\pi} \sin^3(\tilde{\theta}) d\tilde{\theta} \int_0^{\pi} \sin^4\left(\frac{\tilde{\phi}}{2}\right) \exp\left\{\frac{k_e}{\sigma_w^2} \cos(\tilde{\phi})\right\} d\tilde{\phi} \\
&= \frac{1}{2} \frac{1}{\pi^2 \left(I_0\left(\frac{k_e}{\sigma_w^2}\right) - I_1\left(\frac{k_e}{\sigma_w^2}\right)\right)} \frac{\pi}{1} \frac{4}{3} \left[\frac{3\pi}{8} I_0\left(\frac{k_e}{\sigma_w^2}\right) - \frac{\pi}{2} I_1\left(\frac{k_e}{\sigma_w^2}\right) + \frac{\pi}{8} I_2\left(\frac{k_e}{\sigma_w^2}\right) \right] \\
&= \frac{3I_0\left(\frac{k_e}{\sigma_w^2}\right) - 4I_1\left(\frac{k_e}{\sigma_w^2}\right) + I_2\left(\frac{k_e}{\sigma_w^2}\right)}{3 \cdot 4 \left(I_0\left(\frac{k_e}{\sigma_w^2}\right) - I_1\left(\frac{k_e}{\sigma_w^2}\right)\right)} = \frac{\nu\left(\frac{k_e}{\sigma_w^2}\right)}{3}
\end{aligned}$$

$$\begin{aligned}
c_{zz} &= \frac{1}{N} \int_{\tilde{\psi}=0}^{2\pi} \int_{\tilde{\theta}=0}^{\pi} \int_{\tilde{\phi}=0}^{\pi} \tilde{r}^2 \cos^2(\tilde{\theta}) \sin^2\left(\frac{\tilde{\phi}}{2}\right) \\
&\quad \times \exp\left\{\frac{k_e}{\sigma_w^2} \cos(\tilde{\phi})\right\} \frac{1}{2} \sin^2\left(\frac{\tilde{\phi}}{2}\right) \sin(\tilde{\theta}) d\tilde{\phi} d\tilde{\theta} d\tilde{\psi} \\
&= \frac{1}{2N} \int_0^{2\pi} d\tilde{\psi} \int_0^{\pi} \sin(\tilde{\theta}) \cos^2(\tilde{\theta}) d\tilde{\theta} \int_0^{\pi} \sin^4\left(\frac{\tilde{\phi}}{2}\right) \exp\left\{\frac{k_e}{\sigma_w^2} \cos(\tilde{\phi})\right\} d\tilde{\phi} \\
&= \frac{1}{2} \frac{1}{\pi^2 \left(I_0\left(\frac{k_e}{\sigma_w^2}\right) - I_1\left(\frac{k_e}{\sigma_w^2}\right)\right)} \frac{2\pi}{1} \frac{2}{3} \left[\frac{3\pi}{8} I_0\left(\frac{k_e}{\sigma_w^2}\right) - \frac{\pi}{2} I_1\left(\frac{k_e}{\sigma_w^2}\right) + \frac{\pi}{8} I_2\left(\frac{k_e}{\sigma_w^2}\right) \right] \\
&= \frac{3I_0\left(\frac{k_e}{\sigma_w^2}\right) - 4I_1\left(\frac{k_e}{\sigma_w^2}\right) + I_2\left(\frac{k_e}{\sigma_w^2}\right)}{3 \cdot 4 \left(I_0\left(\frac{k_e}{\sigma_w^2}\right) - I_1\left(\frac{k_e}{\sigma_w^2}\right)\right)} = \frac{\nu\left(\frac{k_e}{\sigma_w^2}\right)}{3}
\end{aligned}$$

$$\begin{aligned}
c_{ss} &= \frac{1}{N} \int_{\tilde{\psi}=0}^{2\pi} \int_{\tilde{\theta}=0}^{\pi} \int_{\tilde{\phi}=0}^{\pi} \tilde{r}^2 \cos^2 \left(\frac{\tilde{\phi}}{2} \right) \\
&\quad \times \exp \left\{ \frac{k_e}{\sigma_w^2} \cos \left(\tilde{\phi} \right) \right\} \frac{1}{2} \sin^2 \left(\frac{\tilde{\phi}}{2} \right) \sin \left(\tilde{\theta} \right) d\tilde{\phi} d\tilde{\theta} d\tilde{\psi} \\
&= \frac{1}{2N} \int_0^{2\pi} d\tilde{\psi} \int_0^{\pi} \sin \left(\tilde{\theta} \right) d\tilde{\theta} \int_0^{\pi} \cos^2 \left(\frac{\tilde{\phi}}{2} \right) \sin^2 \left(\frac{\tilde{\phi}}{2} \right) \exp \left\{ \frac{k_e}{\sigma_w^2} \cos \left(\tilde{\phi} \right) \right\} d\tilde{\phi} \\
&= \frac{1}{2N} \frac{2\pi}{1} \frac{2}{1} \int_0^{\pi} \frac{1}{2} \left(1 + \cos \left(\tilde{\phi} \right) \right) \frac{1}{2} \left(1 - \cos \left(\tilde{\phi} \right) \right) \exp \left\{ \frac{k_e}{\sigma_w^2} \cos \left(\tilde{\phi} \right) \right\} d\tilde{\phi} \\
&= \frac{\pi}{2N} \int_0^{\pi} \left(1 - \cos^2 \left(\tilde{\phi} \right) \right) \exp \left\{ \frac{k_e}{\sigma_w^2} \cos \left(\tilde{\phi} \right) \right\} d\tilde{\phi} \\
&= \frac{\pi}{2N} \left(\frac{1}{2} - \frac{1}{2} \cos \left(2\tilde{\phi} \right) \right) \exp \left\{ \frac{k_e}{\sigma_w^2} \cos \left(\tilde{\phi} \right) \right\} d\tilde{\phi} \\
&= \frac{\pi}{4} \frac{\pi I_0 \left(\frac{k_e}{\sigma_w^2} \right) - \pi I_2 \left(\frac{k_e}{\sigma_w^2} \right)}{\pi^2 I_0 \left(\frac{k_e}{\sigma_w^2} \right) - \pi^2 I_1 \left(\frac{k_e}{\sigma_w^2} \right)} \\
&= \frac{I_0 \left(\frac{k_e}{\sigma_w^2} \right) - I_2 \left(\frac{k_e}{\sigma_w^2} \right)}{4I_0 \left(\frac{k_e}{\sigma_w^2} \right) - 4I_1 \left(\frac{k_e}{\sigma_w^2} \right)} = 1 - \nu \left(\frac{k_e}{\sigma_w^2} \right)
\end{aligned}$$

The off diagonal elements of the ultimate covariance matrix are all zero:

$$\begin{aligned}
c_{xy} &= \frac{1}{N} \int_{\tilde{\psi}=0}^{2\pi} \int_{\tilde{\theta}=0}^{\pi} \int_{\tilde{\phi}=0}^{\pi} \tilde{r}^2 \sin^2 \left(\tilde{\theta} \right) \sin \left(\tilde{\psi} \right) \cos \left(\tilde{\psi} \right) \sin^2 \left(\frac{\tilde{\phi}}{2} \right) \\
&\quad \times \exp \left\{ \frac{k_e}{\sigma_w^2} \cos \left(\tilde{\phi} \right) \right\} \frac{1}{2} \sin^2 \left(\frac{\tilde{\phi}}{2} \right) \sin \left(\tilde{\theta} \right) d\tilde{\phi} d\tilde{\theta} d\tilde{\psi} \\
&= \frac{1}{2N} \int_0^{2\pi} \sin \left(\tilde{\psi} \right) \cos \left(\tilde{\psi} \right) d\tilde{\psi} \int_0^{\pi} \sin^3 \left(\tilde{\theta} \right) d\tilde{\theta} \int_0^{\pi} \sin^4 \left(\frac{\tilde{\phi}}{2} \right) \exp \left\{ \frac{k_e}{\sigma_w^2} \cos \left(\tilde{\phi} \right) \right\} d\tilde{\phi} \\
&= 0
\end{aligned}$$

$$\begin{aligned}
c_{xz} &= \frac{1}{N} \int_{\tilde{\psi}=0}^{2\pi} \int_{\tilde{\theta}=0}^{\pi} \int_{\tilde{\phi}=0}^{\pi} \tilde{r}^2 \sin(\tilde{\theta}) \cos(\tilde{\theta}) \cos(\tilde{\psi}) \sin^2\left(\frac{\tilde{\phi}}{2}\right) \\
&\quad \times \exp\left\{\frac{k_e}{\sigma_w^2} \cos(\tilde{\phi})\right\} \frac{1}{2} \sin^2\left(\frac{\tilde{\phi}}{2}\right) \sin(\tilde{\theta}) d\tilde{\phi} d\tilde{\theta} d\tilde{\psi} \\
&= \frac{1}{2N} \int_0^{2\pi} \cos(\tilde{\psi}) d\tilde{\psi} \int_0^{\pi} \sin^2(\tilde{\theta}) \cos(\tilde{\theta}) d\tilde{\theta} \int_0^{\pi} \sin^4\left(\frac{\tilde{\phi}}{2}\right) \exp\left\{\frac{k_e}{\sigma_w^2} \cos(\tilde{\phi})\right\} d\tilde{\phi} \\
&= 0
\end{aligned}$$

$$\begin{aligned}
c_{xs} &= \frac{1}{N} \int_{\tilde{\psi}=0}^{2\pi} \int_{\tilde{\theta}=0}^{\pi} \int_{\tilde{\phi}=0}^{\pi} \tilde{r}^2 \sin(\tilde{\theta}) \cos(\tilde{\psi}) \sin\left(\frac{\tilde{\phi}}{2}\right) \cos\left(\frac{\tilde{\phi}}{2}\right) \\
&\quad \times \exp\left\{\frac{k_e}{\sigma_w^2} \cos(\tilde{\phi})\right\} \frac{1}{2} \sin^2\left(\frac{\tilde{\phi}}{2}\right) \sin(\tilde{\theta}) d\tilde{\phi} d\tilde{\theta} d\tilde{\psi} \\
&= \frac{1}{2N} \int_0^{2\pi} \cos(\tilde{\psi}) d\tilde{\psi} \int_0^{\pi} \sin^2(\tilde{\theta}) d\tilde{\theta} \int_0^{\pi} \sin^3\left(\frac{\tilde{\phi}}{2}\right) \cos\left(\frac{\tilde{\phi}}{2}\right) \exp\left\{\frac{k_e}{\sigma_w^2} \cos(\tilde{\phi})\right\} d\tilde{\phi} \\
&= 0
\end{aligned}$$

$$\begin{aligned}
c_{yz} &= \frac{1}{N} \int_{\tilde{\psi}=0}^{2\pi} \int_{\tilde{\theta}=0}^{\pi} \int_{\tilde{\phi}=0}^{\pi} \tilde{r}^2 \sin(\tilde{\theta}) \cos(\tilde{\theta}) \sin(\tilde{\psi}) \sin^2\left(\frac{\tilde{\phi}}{2}\right) \\
&\quad \times \exp\left\{\frac{k_e}{\sigma_w^2} \cos(\tilde{\phi})\right\} \frac{1}{2} \sin^2\left(\frac{\tilde{\phi}}{2}\right) \sin(\tilde{\theta}) d\tilde{\phi} d\tilde{\theta} d\tilde{\psi} \\
&= \frac{1}{2N} \int_0^{2\pi} \sin(\tilde{\psi}) d\tilde{\psi} \int_0^{\pi} \sin^2(\tilde{\theta}) \cos(\tilde{\theta}) d\tilde{\theta} \int_0^{\pi} \sin^4\left(\frac{\tilde{\phi}}{2}\right) \exp\left\{\frac{k_e}{\sigma_w^2} \cos(\tilde{\phi})\right\} d\tilde{\phi} \\
&= 0
\end{aligned}$$

$$\begin{aligned}
c_{ys} &= \frac{1}{N} \int_{\tilde{\psi}=0}^{2\pi} \int_{\tilde{\theta}=0}^{\pi} \int_{\tilde{\phi}=0}^{\pi} \tilde{r}^2 \sin(\tilde{\theta}) \sin(\tilde{\psi}) \sin\left(\frac{\tilde{\phi}}{2}\right) \cos\left(\frac{\tilde{\phi}}{2}\right) \\
&\quad \times \exp\left\{\frac{k_e}{\sigma_w^2} \cos(\tilde{\phi})\right\} \frac{1}{2} \sin^2\left(\frac{\tilde{\phi}}{2}\right) \sin(\tilde{\theta}) d\tilde{\phi} d\tilde{\theta} d\tilde{\psi} \\
&= \frac{1}{2N} \int_0^{2\pi} \sin(\tilde{\psi}) d\tilde{\psi} \int_0^{\pi} \sin^2(\tilde{\theta}) d\tilde{\theta} \int_0^{\pi} \sin^3\left(\frac{\tilde{\phi}}{2}\right) \cos\left(\frac{\tilde{\phi}}{2}\right) \exp\left\{\frac{k_e}{\sigma_w^2} \cos(\tilde{\phi})\right\} d\tilde{\phi} \\
&= 0
\end{aligned}$$

$$\begin{aligned}
c_{zs} &= \frac{1}{N} \int_{\tilde{\psi}=0}^{2\pi} \int_{\tilde{\theta}=0}^{\pi} \int_{\tilde{\phi}=0}^{\pi} \tilde{r}^2 \cos(\tilde{\theta}) \sin\left(\frac{\tilde{\phi}}{2}\right) \cos\left(\frac{\tilde{\phi}}{2}\right) \\
&\quad \times \exp\left\{\frac{k_e}{\sigma_w^2} \cos(\tilde{\phi})\right\} \frac{1}{2} \sin^2\left(\frac{\tilde{\phi}}{2}\right) \sin(\tilde{\theta}) d\tilde{\phi} d\tilde{\theta} d\tilde{\psi} \\
&= \frac{1}{2N} \int_0^{2\pi} d\tilde{\psi} \int_0^{\pi} \sin(\tilde{\theta}) \cos(\tilde{\theta}) d\tilde{\theta} \int_0^{\pi} \sin^3\left(\frac{\tilde{\phi}}{2}\right) \cos\left(\frac{\tilde{\phi}}{2}\right) \exp\left\{\frac{k_e}{\sigma_w^2} \cos(\tilde{\phi})\right\} d\tilde{\phi} \\
&= 0
\end{aligned}$$

□

Corollary 4.11.1.3 provides several insights for this system. First, the states are ultimately uncorrelated for any filter gain k_e and gyro noise σ_w . Next, the ultimate covariance matrix is parameterized by the **ratio** of $\frac{k_e}{\sigma_w^2}$ as was the ultimate scalar ultimate variance as found in Corollary 4.11.1.2. Finally, in the no feedback case (when $k_e = 0$), then $\nu(0) = \frac{3}{4}$ and $\lim_{t \rightarrow \infty} E[\tilde{\mathbf{q}}(t)\tilde{\mathbf{q}}^T(t)] = \frac{1}{4}I$. This calculation agrees with the value given in Choukroun [13] who studied the no feedback case. Note however that Choukroun's technique only found the ultimate covariance. Theorem 4.11.1 provides the actual distribution, which in the no feedback case reduces

to a **uniform** distribution on the unit quaternion hypersphere.

4.12 Numerical Simulation of Stochastic SO(3) Analytic Results

The numerical simulation realizations of the SO(3) attitude filter's estimate error first presented in Section 4.3 are depicted again in the gallery of Figure 4.7, now with the analytic ultimate attitude estimate error of Equation 4.57 superimposed. The analytic result exactly matches the numerical simulation data in all cases considered.

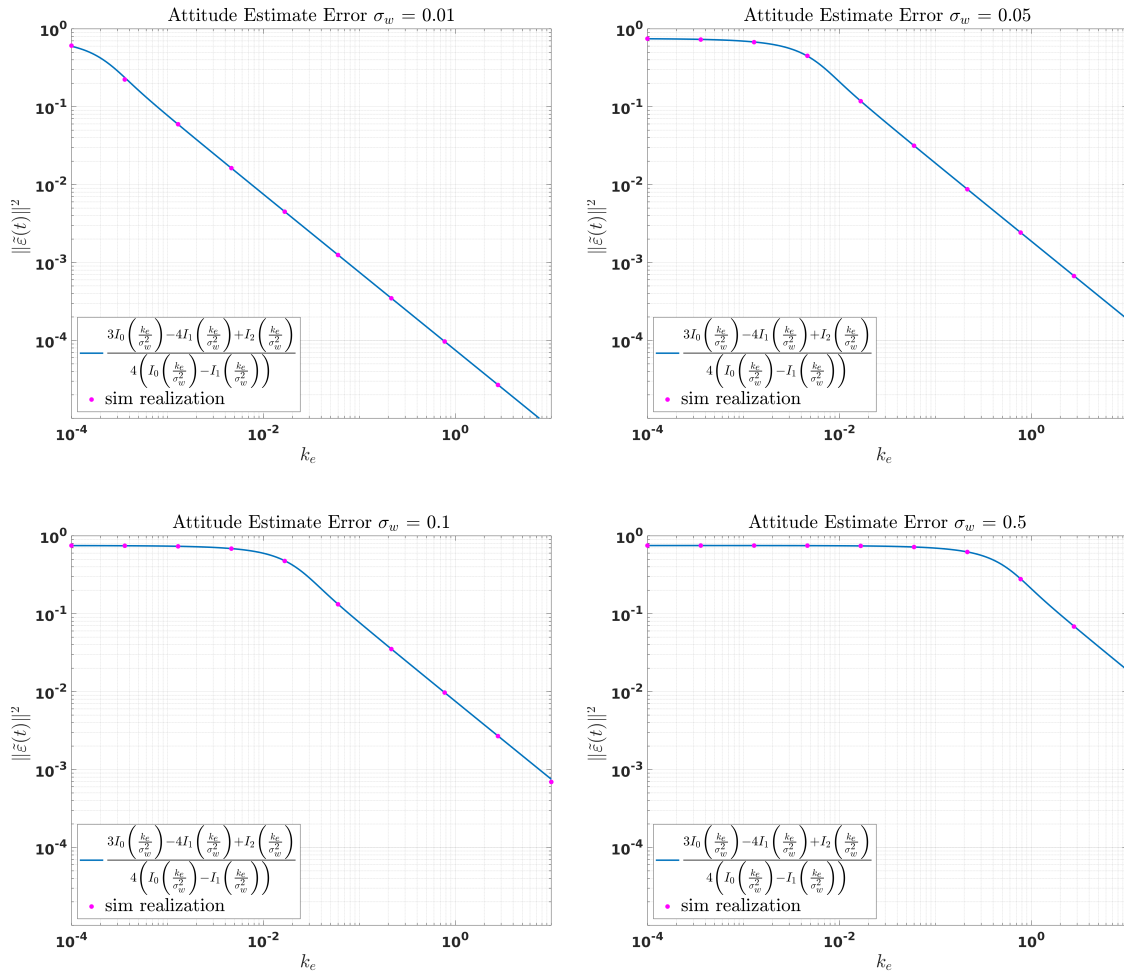


Figure 4.7: The analytic ultimate attitude estimate error of Equation 4.57 exactly matches simulation realizations of the SO(3) attitude estimate error for the Itô SDE 4.6.

Chapter 5: Gyro Bias Filter for Gyro with Constant Bias and Additive Noise

In this chapter, the analysis of the previous chapter, which considered gyro additive noise, is extended by also including constant gyro bias. The filter state is augmented to include a gyro bias estimate which is driven by an adaptation law of the observer from [95,101]. As in Chapter 4, the attitude measurements are assumed to be perfect.

Section 5.1 presents the measurement models considered, the formulation of the attitude filter, and culminates with the derivation of an Itô SDE for the system error dynamics. The following Section 5.2 uses an appeal to the converse Lyapunov theorem by leveraging the GES result of the deterministic observer of [95] to demonstrate the filter is weakly stochastically stable. As the explicit form of the Lyapunov function is not provided via the converse Lyapunov theorem, Zakai's Ultimate Moment Bound Theorem 2.1.5 cannot be invoked to bound system performance. Section 5.3 develops the Fokker-Planck PDE associated with the filter error dynamics.

The system is then reduced to the $SO(2)$ case in Section 5.4 to gain more insight into the filter error dynamics. The $SO(2)$ stationary Fokker-Planck PDE

again proves to be tractable in Section 5.5, yielding analytic expressions for the ultimate attitude estimate error mean and variance as well as the ultimate gyro bias estimate error mean and variance. These results are verified via simulation analysis in Section 5.6. Similar to Section 4.10, Section 5.7 provides bounds for the ultimate attitude estimate error mean and variance as well as the ultimate gyro bias estimate error mean and variance for the SO(3) gyro constant bias filter by extrapolating the SO(2) results of Section 5.5. Finally, the intuition gained from the SO(2) analysis and the success of the heuristic upper bound are used to solve the Fokker-Planck PDE for the SO(3) case in Section 5.8 which is subsequently used to find analytic expressions for various ultimate statistics. The analytic expressions for filter ultimate statistics are then compared to numerical simulation realizations in Section 5.9.

5.1 Gyro Bias Filter Formulation in SO(3)

In this section, the angular rate gyro measurements are modeled as having a constant bias \mathbf{b} as well as additive noise

$$\boldsymbol{\omega}_g(t) = \boldsymbol{\omega}(t) + \mathbf{b} + \sigma_w \mathbf{n}_w(t) \quad (5.1)$$

where, as before, $\boldsymbol{\omega}_g(t)$ is the gyro measurement at time t , $\boldsymbol{\omega}(t)$ is the true vehicle angular rate at time t , σ_w is a positive scaling constant, and $\mathbf{n}_w(\cdot)$ is a zero mean unit variance Gaussian white noise process. As the bias is assumed to be constant, $\dot{\mathbf{b}}(t) = 0$.

Further assume that the filter has access to perfect (noise free) attitude measurements $\mathbf{q}_m(t)$ of the vehicle attitude $\mathbf{q}(t)$

$$\mathbf{q}_m(t) = \mathbf{q}(t) = \begin{bmatrix} \boldsymbol{\varepsilon}(t) \\ \eta(t) \end{bmatrix} = \begin{bmatrix} \varepsilon_x(t) \\ \varepsilon_y(t) \\ \varepsilon_z(t) \\ \eta(t) \end{bmatrix} \quad (5.2)$$

The vehicle attitude $\mathbf{q}(t)$ evolves according to the usual kinematics equation

$$\dot{\mathbf{q}}(t) = \frac{1}{2} \boldsymbol{\omega}(t) \otimes \mathbf{q}(t)$$

Consider a nonlinear adaptive gyro bias filter based on the observer from [95]

$$\begin{aligned} \dot{\hat{\mathbf{q}}}(t) &= \frac{1}{2} \left\{ R(\tilde{\mathbf{q}}^{-1}(t)) \left[\boldsymbol{\omega}_g(t) - \hat{\mathbf{b}}(t) + k_e \tilde{\eta}(t) \tilde{\boldsymbol{\varepsilon}}(t) \right] \right\} \otimes \hat{\mathbf{q}}(t) \\ \dot{\hat{\mathbf{b}}}(t) &= -\alpha \tilde{\eta}(t) \tilde{\boldsymbol{\varepsilon}}(t) \end{aligned} \quad (5.3)$$

where $\alpha > 0$ is the filter adaptation gain parameter and $\hat{\mathbf{b}}(t)$ is the filter's estimate at time t of the gyro bias \mathbf{b} . The filter's bias estimate error $\tilde{\mathbf{b}}(t)$ is given as

$$\tilde{\mathbf{b}}(t) = \mathbf{b} - \hat{\mathbf{b}}(t) \quad (5.4)$$

The filter uses its bias estimate in the filter kinematic equation to attempt to correct for the true bias in the gyro measurement. As before, $k_e > 0$ is a filter (estimator) gain parameter and $\hat{\mathbf{q}}(t)$ is the filter's estimate of the vehicle attitude. The rotation parameterized by $\tilde{\mathbf{q}}(t)$ is the filter's attitude estimate error, given by

$$\tilde{\mathbf{q}}(t) = \begin{bmatrix} \tilde{\boldsymbol{\varepsilon}}(t) \\ \tilde{\boldsymbol{\eta}}(t) \end{bmatrix} = \mathbf{q}(t) \otimes \hat{\mathbf{q}}^{-1}(t) \quad (5.5)$$

which is available in real time for the filter to use since the attitude measurements are assumed to be noise free. The rotation $R(\tilde{\mathbf{q}}^{-1}(t))$ resolves the angular velocity terms in the filter's reference frame.

The attitude filter dynamics given by Equation 5.3 can be combined with the quaternion error kinematics of Equation 2.71 and the measurement models of Equations 5.1 and 5.2 to find the filter's estimate error dynamics as a Langevin form differential equation:

$$\begin{aligned}
\dot{\hat{\mathbf{x}}}(t) &= \begin{bmatrix} \dot{\hat{\mathbf{q}}}(t) \\ \dot{\hat{\mathbf{b}}}(t) \end{bmatrix} = \begin{bmatrix} \dot{\tilde{\boldsymbol{\varepsilon}}}(t) \\ \dot{\tilde{\eta}}(t) \\ \dot{\tilde{\mathbf{b}}}(t) \end{bmatrix} \\
&= \begin{bmatrix} \frac{1}{2} \left\{ \boldsymbol{\omega}(t) - \boldsymbol{\omega}(t) - \mathbf{b} - \sigma_w \mathbf{n}_w(t) + \hat{\mathbf{b}}(t) - k_e \tilde{\eta}(t) \tilde{\boldsymbol{\varepsilon}}(t) \right\} \otimes \tilde{\mathbf{q}}(t) \\ \alpha \tilde{\eta}(t) \tilde{\boldsymbol{\varepsilon}}(t) \end{bmatrix} \\
&= \begin{bmatrix} \frac{1}{2} \left\{ -k_e \tilde{\eta}(t) \tilde{\boldsymbol{\varepsilon}}(t) - \tilde{\mathbf{b}}(t) - \sigma_w \mathbf{n}_w(t) \right\} \otimes \tilde{\mathbf{q}}(t) \\ \alpha \tilde{\eta}(t) \tilde{\boldsymbol{\varepsilon}}(t) \end{bmatrix} \\
&= \begin{bmatrix} -\frac{1}{2} k_e \tilde{\eta}^2(t) \tilde{\boldsymbol{\varepsilon}}(t) - \frac{1}{2} \left\{ \tilde{\eta}(t) I + [\tilde{\boldsymbol{\varepsilon}}(t) \times] \right\} \tilde{\mathbf{b}}(t) \\ \frac{1}{2} k_e \tilde{\eta}(t) \tilde{\boldsymbol{\varepsilon}}^T(t) \tilde{\boldsymbol{\varepsilon}}(t) + \frac{1}{2} \tilde{\boldsymbol{\varepsilon}}^T(t) \tilde{\mathbf{b}}(t) \\ \alpha \tilde{\eta}(t) \tilde{\boldsymbol{\varepsilon}}(t) \end{bmatrix} + \begin{bmatrix} -\frac{1}{2} \left\{ \tilde{\eta}(t) I + [\tilde{\boldsymbol{\varepsilon}}(t) \times] \right\} \sigma_w \\ \frac{1}{2} \tilde{\boldsymbol{\varepsilon}}^T(t) \sigma_w \\ 0 \end{bmatrix} \mathbf{n}_w(t)
\end{aligned} \tag{5.6}$$

As explained in Section 2.1.3, the Langevin form error dynamics differential equation 5.6 are interpreted as a Stratonovich SDE. Converting to an Itô SDE results

in the following

$$\begin{aligned}
d\tilde{\mathbf{x}}(t) &= \begin{bmatrix} d\tilde{\mathbf{q}}(t) \\ d\tilde{\mathbf{b}}(t) \end{bmatrix} = \begin{bmatrix} d\tilde{\boldsymbol{\varepsilon}}(t) \\ d\tilde{\eta}(t) \\ d\tilde{\mathbf{b}}(t) \end{bmatrix} \\
&= \begin{bmatrix} -\frac{1}{2}k_e\tilde{\eta}^2(t)\tilde{\boldsymbol{\varepsilon}}(t) - \frac{1}{2}\left\{\tilde{\eta}(t)I + [\tilde{\boldsymbol{\varepsilon}}(t) \times]\right\}\tilde{\mathbf{b}}(t) - \frac{3}{8}\sigma_w^2\tilde{\boldsymbol{\varepsilon}}(t) \\ \frac{1}{2}k_e\tilde{\eta}(t)\tilde{\boldsymbol{\varepsilon}}^T(t)\tilde{\boldsymbol{\varepsilon}}(t) + \frac{1}{2}\tilde{\boldsymbol{\varepsilon}}^T(t)\tilde{\mathbf{b}}(t) - \frac{3}{8}\sigma_w^2\tilde{\eta}(t) \\ \alpha\tilde{\eta}(t)\tilde{\boldsymbol{\varepsilon}}(t) \end{bmatrix} dt \\
&\quad + \begin{bmatrix} -\frac{1}{2}\left\{\tilde{\eta}(t)I + [\tilde{\boldsymbol{\varepsilon}}(t) \times]\right\}\sigma_w \\ \frac{1}{2}\tilde{\boldsymbol{\varepsilon}}^T(t)\sigma_w \\ 0 \end{bmatrix} d\boldsymbol{\beta}_w(t) \\
&= \mathbf{f}\left(\tilde{\mathbf{x}}(t)\right)dt + G\left(\tilde{\mathbf{x}}(t)\right)d\boldsymbol{\beta}_w(t) \tag{5.7}
\end{aligned}$$

5.2 Stochastic Stability Analysis in SO(3)

A tractable analysis demonstrating weak stochastic stability of the gyro constant bias filter's error dynamics of Itô SDE 5.7 does not appear to be as straightforward as the stability analysis for the filters of Chapters 4 and 5. An explanation will be given in this section; however, a conclusion of weak stochastic stability is reached by leveraging analysis of the deterministic case and an appeal to a converse Lyapunov theorem.

A Lyapunov function that allows one to determine weak stochastic stability for the error dynamics of the Itô SDE 5.7 using Zakai's stability result of Theorem 2.1.4 has eluded the author. Consider a simple augmentation of the Lyapunov function that proved successful in Section 4.2

$$V(\tilde{\mathbf{x}}(t)) = \frac{1}{2}\tilde{\boldsymbol{\varepsilon}}^T(t)\tilde{\boldsymbol{\varepsilon}}(t) + \frac{1}{4\alpha}\tilde{\mathbf{b}}^T(t)\tilde{\mathbf{b}}(t) \quad (5.8)$$

Application of the differential generator with respect to the Itô SDE 5.7 yields

$$\begin{aligned} \mathcal{L}V(\tilde{\mathbf{x}}(t)) &= \left(\frac{\partial V}{\partial \tilde{\mathbf{x}}}\right)^T \mathbf{f}(\tilde{\mathbf{x}}(t)) + \frac{1}{2} \text{tr} \left\{ G^T(\tilde{\mathbf{x}}(t)) \frac{\partial^2 V}{\partial \tilde{\mathbf{x}}^2} G(\tilde{\mathbf{x}}(t)) \right\} \\ &= -\frac{1}{2}k_e\tilde{\eta}^2(t)\tilde{\boldsymbol{\varepsilon}}^T(t)\tilde{\boldsymbol{\varepsilon}}(t) - \frac{1}{2}\sigma_w^2\tilde{\boldsymbol{\varepsilon}}^T(t)\tilde{\boldsymbol{\varepsilon}}(t) + \frac{3}{8}\sigma_w^2 \end{aligned} \quad (5.9)$$

Note that while $\mathcal{L}V$ is negative for sufficiently large attitude estimate error, it is completely unaffected by the bias estimate error state. Zakai's Stability Theorem 2.1.4 requires $\mathcal{L}V$ to be negative definite for any $\|\tilde{\mathbf{x}}\| > R_0$ (for some appropriate choice of finite R_0) to conclude weak stochastic stability. Thus the Lyapunov function of Equation 5.8 does not meet the conditions of Zakai's theorem; however,

Zakai’s Stability Theorem does **not** necessarily conclude that the system of Itô SDE 5.7 is **not** weakly stochastically stable. It could very well be the case that another Lyapunov function does meet the conditions of Zakai’s Stability Theorem.

This situation is frequently encountered in deterministic adaptive estimation and control theory [32]. In the deterministic version of the error dynamics for this filter (when $\sigma_w = 0$) the Lyapunov function of Equation 5.8 encounters a similar issue, \dot{V} is only negative semidefinite. The invariance principle of LaSalle for autonomous systems, or the lemma by Barbalat for nonautonomous systems, can be used [42] to show that the system is still stable in the deterministic case. There are nonautonomous stochastic extensions of LaSalle’s Theorem [15, 57, 86]; however the versions cited all require $\mathcal{L}V$ to be upper bounded [15] or ultimately upper bounded [57, 86] by a negative semidefinite function. The positive constant $\frac{3}{8}\sigma_w^2$ at the end of $\mathcal{L}V$ of Equation 5.9 prevents the Lyapunov function of 5.8 from satisfying the conditions of the cited stochastic extensions of LaSalle’s Theorem.

Fortunately a much stronger stability result for a deterministic version of the gyro constant bias filter, referred to here as a constant bias observer, is available due to Thienel and Sanner [95]. In addition to merely showing the the constant bias observer is stable via Barbalat’s Lemma, they were able to prove the observer is Globally Exponentially Stable (GES). The fact that the observer’s estimate errors go to zero is intuitively obvious; a bias estimate error would corrupt the observer’s attitude kinematics which would in turn lead to an attitude estimate error, but attitude estimate errors are used to drive the bias adaptation law to correct the bias estimate. The proof behind this intuition is not obvious; it was conducted via

a time varying observability analysis that effectively demonstrated persistency of excitation of the error states. Thienel and Sanner were able to conclude that not only do $\tilde{\mathbf{e}}(t)$ and $\tilde{\mathbf{b}}(t)$ go to zero, but the convergence is exponentially fast.

As the deterministic observer's error dynamics are GES, the Converse Lyapunov Theorem 2.1.3 may be employed to demonstrate existence of a Lyapunov function with the property

$$\frac{\partial V}{\partial \tilde{\mathbf{x}}} \mathbf{f}_{lang}(\tilde{\mathbf{x}}(t)) \leq -c_3 \|\tilde{\mathbf{x}}\|^2 \quad (5.10)$$

where

$$\mathbf{f}_{lang}(\tilde{\mathbf{x}}(t)) = \begin{bmatrix} -\frac{1}{2}k_e \tilde{\eta}^2(t) \tilde{\mathbf{e}}(t) - \frac{1}{2} \left\{ \tilde{\eta}(t) I + [\tilde{\mathbf{e}}(t) \times] \right\} \tilde{\mathbf{b}}(t) \\ \frac{1}{2}k_e \tilde{\eta}(t) \tilde{\mathbf{e}}^T(t) \tilde{\mathbf{e}}(t) + \frac{1}{2} \tilde{\mathbf{e}}^T(t) \tilde{\mathbf{b}}(t) \\ \alpha \tilde{\eta}(t) \tilde{\mathbf{e}}(t) \end{bmatrix} \quad (5.11)$$

Equation 5.10 implies that the Stratonovich to Itô conversion term

$$\frac{1}{2} \sum_j \frac{\partial \mathbf{g}_j}{\partial \tilde{\mathbf{x}}} \mathbf{g}_j = \mathbf{f}_{conv}(\tilde{\mathbf{x}}(t)) = \begin{bmatrix} -\frac{3}{8} \sigma_w^2 \tilde{\mathbf{e}}(t) \\ -\frac{3}{8} \sigma_w^2 \tilde{\eta}(t) \\ \mathbf{0} \end{bmatrix}$$

is such that

$$\frac{\partial V}{\partial \tilde{\mathbf{x}}} \mathbf{f}_{conv}(\tilde{\mathbf{x}}(t)) \leq -c_3 \|\tilde{\mathbf{x}}\|^2$$

Provided the additional assumption that $\frac{\partial^2 V}{\partial \tilde{\mathbf{x}}^2}$ is bounded, this Lyapunov function satisfies the conditions of Zakai's Stability Theorem 2.1.4 and the gyro constant bias filter's error dynamics of Itô SDE 5.7 are weakly stochastically stable. Note that the explicit form of this Lyapunov function remains unknown and thus can not be used with Zakai's Ultimate Moment Bound Theorem 2.1.5 to provide a quantitative performance bound.

5.3 Fokker-Planck PDE in SO(3)

Let

$$\begin{aligned} p &= p\left(\tilde{\mathbf{q}}(t), \tilde{\mathbf{b}}(t), t\right) = p\left(\tilde{\boldsymbol{\varepsilon}}(t), \tilde{\eta}(t), \tilde{\mathbf{b}}(t), t\right) \\ &= p\left(\tilde{\varepsilon}_x(t), \tilde{\varepsilon}_y(t), \tilde{\varepsilon}_z(t), \tilde{\eta}(t), \tilde{b}_x(t), \tilde{b}_y(t), \tilde{b}_z(t), t\right) \end{aligned}$$

be the joint probability density for the attitude estimate error $\tilde{\mathbf{q}}(t)$ and gyro bias estimate error $\tilde{\mathbf{b}}(t)$. The Fokker-Planck PDE associated with the gyro bias filter error dynamics Itô SDE 5.7 is given by

$$\begin{aligned} \frac{\partial p}{\partial t} &= k_e \left(2\tilde{\eta}^2(t) - \frac{1}{2} \right) p - \left(\frac{1}{2} k_e (1 - \tilde{\eta}^2(t)) \tilde{\eta}(t) + \frac{3}{8} \sigma_w^2 \tilde{\eta}(t) + \frac{1}{2} \tilde{\boldsymbol{\varepsilon}}^T(t) \tilde{\mathbf{b}}(t) \right) \frac{\partial p}{\partial \tilde{\eta}} \\ &+ \frac{1}{2} \left\{ \left(k_e \tilde{\eta}^2(t) - \frac{3}{4} \sigma_w^2 \right) \tilde{\varepsilon}_x(t) + \tilde{\eta}(t) \tilde{b}_x(t) - \tilde{\varepsilon}_z(t) \tilde{b}_y(t) + \tilde{\varepsilon}_y(t) \tilde{b}_z(t) \right\} \frac{\partial p}{\partial \tilde{\varepsilon}_x} \\ &+ \frac{1}{2} \left\{ \left(k_e \tilde{\eta}^2(t) - \frac{3}{4} \sigma_w^2 \right) \tilde{\varepsilon}_y(t) + \tilde{\eta}(t) \tilde{b}_y(t) - \tilde{\varepsilon}_x(t) \tilde{b}_z(t) + \tilde{\varepsilon}_z(t) \tilde{b}_x(t) \right\} \frac{\partial p}{\partial \tilde{\varepsilon}_y} \\ &+ \frac{1}{2} \left\{ \left(k_e \tilde{\eta}^2(t) - \frac{3}{4} \sigma_w^2 \right) \tilde{\varepsilon}_z(t) + \tilde{\eta}(t) \tilde{b}_z(t) - \tilde{\varepsilon}_y(t) \tilde{b}_x(t) + \tilde{\varepsilon}_x(t) \tilde{b}_y(t) \right\} \frac{\partial p}{\partial \tilde{\varepsilon}_z} \\ &- \frac{\sigma_w^2}{4} \left(\tilde{\varepsilon}_x(t) \tilde{\varepsilon}_y(t) \frac{\partial^2 p}{\partial \tilde{\varepsilon}_x \partial \tilde{\varepsilon}_y} + \tilde{\varepsilon}_x(t) \tilde{\varepsilon}_z(t) \frac{\partial^2 p}{\partial \tilde{\varepsilon}_x \partial \tilde{\varepsilon}_z} + \tilde{\varepsilon}_y(t) \tilde{\varepsilon}_z(t) \frac{\partial^2 p}{\partial \tilde{\varepsilon}_y \partial \tilde{\varepsilon}_z} \right. \\ &\quad \left. + \tilde{\varepsilon}_y(t) \tilde{\varepsilon}_z(t) \frac{\partial^2 p}{\partial \tilde{\varepsilon}_y \partial \tilde{\varepsilon}_z} + \tilde{\varepsilon}_y(t) \tilde{\eta}(t) \frac{\partial^2 p}{\partial \tilde{\varepsilon}_y \partial \tilde{\eta}} + \tilde{\varepsilon}_z(t) \tilde{\eta}(t) \frac{\partial^2 p}{\partial \tilde{\varepsilon}_z \partial \tilde{\eta}} \right) \\ &+ \frac{\sigma_w^2}{8} \left((1 - \tilde{\varepsilon}_x^2(t)) \frac{\partial^2 p}{\partial \tilde{\varepsilon}_x^2} + (1 - \tilde{\varepsilon}_y^2(t)) \frac{\partial^2 p}{\partial \tilde{\varepsilon}_y^2} + (1 - \tilde{\varepsilon}_z^2(t)) \frac{\partial^2 p}{\partial \tilde{\varepsilon}_z^2} + (1 - \tilde{\eta}^2(t)) \frac{\partial^2 p}{\partial \tilde{\eta}^2} \right) \\ &- \alpha \tilde{\eta}(t) \left(\tilde{\varepsilon}_x(t) \frac{\partial p}{\partial \tilde{b}_x} + \tilde{\varepsilon}_y(t) \frac{\partial p}{\partial \tilde{b}_y} + \tilde{\varepsilon}_z(t) \frac{\partial p}{\partial \tilde{b}_z} \right) \end{aligned} \quad (5.12)$$

which is the same PDE as Equation 4.20 with additional terms associated with the gyro bias estimation error highlighted in red.

Since the gyro bias filter error dynamics Itô SDE 5.7 were shown to be weakly stochastically stable in Section 5.2, the joint probability density $p\left(\tilde{\mathbf{q}}(t), \tilde{\mathbf{b}}(t), t\right)$ ul-

timately approaches a stationary density $p_s(\tilde{\mathbf{q}}, \tilde{\mathbf{b}})$

$$p_s = p_s(\tilde{\mathbf{q}}, \tilde{\mathbf{b}}) = \lim_{t \rightarrow \infty} p(\tilde{\mathbf{q}}(t), \tilde{\mathbf{b}}(t), t) \quad (5.13)$$

which obeys the stationary Fokker-Planck PDE

$$\begin{aligned} 0 = & k_e \left(2\tilde{\eta}^2 - \frac{1}{2} \right) p_s - \left(\frac{1}{2} k_e (1 - \tilde{\eta}^2) \tilde{\eta} + \frac{3}{8} \sigma_w^2 \tilde{\eta} + \frac{1}{2} \tilde{\boldsymbol{\varepsilon}}^T \tilde{\mathbf{b}} \right) \frac{\partial p_s}{\partial \tilde{\eta}} \\ & + \frac{1}{2} \left\{ \left(k_e \tilde{\eta}^2 - \frac{3}{4} \sigma_w^2 \right) \tilde{\varepsilon}_x + \tilde{\eta} \tilde{b}_x - \tilde{\varepsilon}_z \tilde{b}_y + \tilde{\varepsilon}_y \tilde{b}_z \right\} \frac{\partial p_s}{\partial \tilde{\varepsilon}_x} \\ & + \frac{1}{2} \left\{ \left(k_e \tilde{\eta}^2 - \frac{3}{4} \sigma_w^2 \right) \tilde{\varepsilon}_y + \tilde{\eta} \tilde{b}_y - \tilde{\varepsilon}_x \tilde{b}_z + \tilde{\varepsilon}_z \tilde{b}_x \right\} \frac{\partial p_s}{\partial \tilde{\varepsilon}_y} \\ & + \frac{1}{2} \left\{ \left(k_e \tilde{\eta}^2 - \frac{3}{4} \sigma_w^2 \right) \tilde{\varepsilon}_z + \tilde{\eta} \tilde{b}_z - \tilde{\varepsilon}_y \tilde{b}_x + \tilde{\varepsilon}_x \tilde{b}_y \right\} \frac{\partial p_s}{\partial \tilde{\varepsilon}_z} \\ & - \frac{\sigma_w^2}{4} \left(\tilde{\varepsilon}_x \tilde{\varepsilon}_y \frac{\partial^2 p_s}{\partial \tilde{\varepsilon}_x \partial \tilde{\varepsilon}_y} + \tilde{\varepsilon}_x \tilde{\varepsilon}_z \frac{\partial^2 p_s}{\partial \tilde{\varepsilon}_x \partial \tilde{\varepsilon}_z} + \tilde{\varepsilon}_x \tilde{\eta} \frac{\partial^2 p_s}{\partial \tilde{\varepsilon}_x \partial \tilde{\eta}} \right. \\ & \quad \left. + \tilde{\varepsilon}_y \tilde{\varepsilon}_z \frac{\partial^2 p_s}{\partial \tilde{\varepsilon}_y \partial \tilde{\varepsilon}_z} + \tilde{\varepsilon}_y \tilde{\eta} \frac{\partial^2 p_s}{\partial \tilde{\varepsilon}_y \partial \tilde{\eta}} + \tilde{\varepsilon}_z \tilde{\eta} \frac{\partial^2 p_s}{\partial \tilde{\varepsilon}_z \partial \tilde{\eta}} \right) \\ & + \frac{\sigma_w^2}{8} \left((1 - \tilde{\varepsilon}_x^2) \frac{\partial^2 p_s}{\partial \tilde{\varepsilon}_x^2} + (1 - \tilde{\varepsilon}_y^2) \frac{\partial^2 p_s}{\partial \tilde{\varepsilon}_y^2} + (1 - \tilde{\varepsilon}_z^2) \frac{\partial^2 p_s}{\partial \tilde{\varepsilon}_z^2} + (1 - \tilde{\eta}^2) \frac{\partial^2 p_s}{\partial \tilde{\eta}^2} \right) \\ & - \alpha \tilde{\eta} \left(\tilde{\varepsilon}_x \frac{\partial p_s}{\partial \tilde{b}_x} + \tilde{\varepsilon}_y \frac{\partial p_s}{\partial \tilde{b}_y} + \tilde{\varepsilon}_z \frac{\partial p_s}{\partial \tilde{b}_z} \right) \end{aligned} \quad (5.14)$$

which is similar to the stationary Fokker-Planck PDE of Equation 4.22 with new terms highlighted in red.

The solution to the stationary Fokker-Planck PDE 5.14 may not be clear at this point. First, the system will be reduced to the SO(2) case to gain a deeper understanding of the problem. The SO(2) analysis will result in a stationary Fokker-Planck PDE with a known analytic solution as will be shown in Section 5.5. The intuition gained from the SO(2) case will suggest a solution for the full SO(3) case, which is revisited in Section 5.8.

5.4 Attitude Filter Formulation in SO(2)

In this section, the gyro bias filter dynamical model is reduced to the single axis case of SO(2). In following sections, the reduced model will provide tractable analytic results that can provide insight into the full SO(3) case.

As explained in Section 2.3.2, the SO(3) dynamical model may be reduced to the SO(2) case by simply zeroing out the y and z components of all vector quantities. Equivalently, the vector quantities in the SO(3) case reduce to scalar quantities, and SO(3) unit quaternions comprised of 4 elements reduce to SO(2) unit quaternions with two elements.

The SO(3) Langevin form error dynamics of Equation 5.6 reduce in the SO(2) case to

$$\begin{aligned}
 \dot{\hat{\mathbf{x}}}(t) &= \begin{bmatrix} \dot{\hat{\mathbf{q}}}(t) \\ \dot{\hat{\mathbf{b}}}(t) \end{bmatrix} = \begin{bmatrix} \dot{\tilde{\varepsilon}}(t) \\ \dot{\tilde{\eta}}(t) \\ \dot{\tilde{\mathbf{b}}}(t) \end{bmatrix} \\
 &= \begin{bmatrix} \frac{1}{2} \left\{ -k_e \tilde{\eta}(t) \tilde{\varepsilon}(t) - \tilde{\mathbf{b}}(t) - \sigma_w n_w(t) \right\} \otimes \tilde{\mathbf{q}}(t) \\ \alpha \tilde{\eta}(t) \tilde{\varepsilon}(t) \end{bmatrix} \\
 &= \begin{bmatrix} -\frac{1}{2} k_e \tilde{\eta}^2(t) \tilde{\varepsilon}(t) - \frac{1}{2} \tilde{\eta}(t) \tilde{\mathbf{b}}(t) \\ \frac{1}{2} k_e \tilde{\eta}(t) \tilde{\varepsilon}^2(t) + \frac{1}{2} \tilde{\varepsilon}(t) \tilde{\mathbf{b}}(t) \\ \alpha \tilde{\eta}(t) \tilde{\varepsilon}(t) \end{bmatrix} + \begin{bmatrix} -\frac{1}{2} \tilde{\eta}(t) \sigma_w \\ \frac{1}{2} \tilde{\varepsilon}(t) \sigma_w \\ 0 \end{bmatrix} n_w(t) \quad (5.15)
 \end{aligned}$$

As explained in Section 2.1.3, the Langevin form error dynamics differential

equation 5.15 is interpreted as a Stratonovich SDE. Converting to Itô form yields

$$\begin{aligned}
d\tilde{\mathbf{x}}(t) &= \begin{bmatrix} d\tilde{\mathbf{q}}(t) \\ d\tilde{b}(t) \end{bmatrix} = \begin{bmatrix} d\tilde{\varepsilon}(t) \\ d\tilde{\eta}(t) \\ d\tilde{b}(t) \end{bmatrix} \\
&= \begin{bmatrix} -\frac{1}{2}k_e\tilde{\eta}^2(t)\tilde{\varepsilon}(t) - \frac{1}{2}\tilde{\eta}(t)\tilde{b}(t) - \frac{1}{8}\sigma_w^2\tilde{\varepsilon}(t) \\ \frac{1}{2}k_e\tilde{\eta}(t)\tilde{\varepsilon}^2(t) + \frac{1}{2}\tilde{\varepsilon}(t)\tilde{b}(t) - \frac{1}{8}\sigma_w^2\tilde{\eta}(t) \\ \alpha\tilde{\eta}(t)\tilde{\varepsilon}(t) \end{bmatrix} dt + \begin{bmatrix} -\frac{1}{2}\tilde{\eta}(t)\sigma_w \\ \frac{1}{2}\tilde{\varepsilon}(t)\sigma_w \\ 0 \end{bmatrix} d\beta_w(t) \\
&= \mathbf{f}(\tilde{\mathbf{x}}(t))dt + G(\tilde{\mathbf{x}}(t))d\beta_w(t) \tag{5.16}
\end{aligned}$$

The attitude filter error dynamics of Equation 5.15 can equivalently be written in the SO(2) Euler Axis/Angle parameterization (as explained in Section 2.3.2). Let

$$\tilde{\mathbf{q}} = \begin{bmatrix} \tilde{\varepsilon} \\ \tilde{\eta} \end{bmatrix} = \begin{bmatrix} \sin\left(\frac{\tilde{\phi}}{2}\right) \\ \cos\left(\frac{\tilde{\phi}}{2}\right) \end{bmatrix}$$

Then the SO(2) Euler Axis/Angle parameterization of the filter error dynamics is given as

$$\begin{aligned}
\dot{\tilde{\mathbf{y}}}(t) &= \begin{bmatrix} \dot{\tilde{\phi}}(t) \\ \dot{\tilde{b}}(t) \end{bmatrix} = \begin{bmatrix} -k_e\tilde{\eta}(t)\tilde{\varepsilon}(t) - \tilde{b}(t) - \sigma_w n_w(t) \\ \alpha\tilde{\eta}(t)\tilde{\varepsilon}(t) \end{bmatrix} \\
&= \begin{bmatrix} -\frac{1}{2}k_e \sin\left(\frac{\tilde{\phi}(t)}{2}\right) - \tilde{b}(t) \\ \frac{1}{2}\alpha \sin\left(\frac{\tilde{\phi}(t)}{2}\right) \end{bmatrix} + \begin{bmatrix} -\sigma_w \\ 0 \end{bmatrix} n_w(t) \tag{5.17}
\end{aligned}$$

which is immediately in Langevin form. Conversion to an Itô SDE is trivial as the

diffusion matrix $\begin{bmatrix} -\sigma_w & 0 \end{bmatrix}^T$ is independent of the state:

$$\begin{aligned}
 d\tilde{\mathbf{y}}(t) &= \begin{bmatrix} d\tilde{\phi}(t) \\ d\tilde{b}(t) \end{bmatrix} \\
 &= \begin{bmatrix} -\frac{1}{2}k_\epsilon \sin(\tilde{\phi}(t)) - \tilde{b}(t) \\ \frac{1}{2}\alpha \sin(\tilde{\phi}(t)) \end{bmatrix} dt + \begin{bmatrix} -\sigma_w \\ 0 \end{bmatrix} d\beta_w(t) \\
 &= \mathbf{f}(\tilde{\mathbf{y}}(t))dt + G(\tilde{\mathbf{y}}(t))d\beta(t)
 \end{aligned} \tag{5.18}$$

5.5 Fokker-Planck Analysis in SO(2)

In this section the stationary Fokker-Planck PDE is derived and directly solved for the Gyro Constant Bias Filter. The solution is subsequently used to find analytic ultimate expectations for the filter's attitude estimate error mean, attitude estimate error variance, the gyro bias estimate error mean, and the gyro bias estimate error variance.

Let $p = p(\tilde{\mathbf{y}}(t), t) = p(\tilde{\phi}(t), \tilde{b}(t), t)$ be the joint probability density for the SO(2) Gyro Constant Bias Filter estimate error states. Then the Fokker-Planck PDE associated with the Itô SDE 5.18 is given by

$$\begin{aligned} \frac{\partial p}{\partial t} &= - \sum_{i=1}^2 \frac{\partial}{\partial \tilde{y}_i} \left[f_i(\tilde{\mathbf{y}}(t)) p(\tilde{\mathbf{y}}(t), t) \right] + \frac{1}{2} \sum_{i,j=1}^2 \frac{\partial^2}{\partial \tilde{y}_i \partial \tilde{y}_j} \left[\left\{ G(\tilde{\mathbf{y}}(t)) G^T(\tilde{\mathbf{y}}(t)) \right\}_{i,j} p(\tilde{\mathbf{y}}(t), t) \right] \\ &= \frac{1}{2} k_e \cos(\tilde{\phi}(t)) p(\tilde{\mathbf{y}}(t), t) + \left(\frac{1}{2} k_e \sin(\tilde{\phi}(t)) + \tilde{b}(t) \right) \frac{\partial p}{\partial \tilde{\phi}} \\ &\quad - \frac{1}{2} \alpha \sin(\tilde{\phi}(t)) \frac{\partial p}{\partial \tilde{b}} + \frac{1}{2} \sigma_w^2 \frac{\partial^2 p}{\partial \tilde{\phi}^2} \end{aligned} \quad (5.19)$$

Note that as the bias estimate error is not directly driven by the noise process, the bottom entry of G is zero in Equation 5.18. Thus there is no $\frac{\partial^2 p}{\partial \tilde{b}^2}$ term in the Fokker-Planck PDE.

The SO(2) Gyro Constant Bias Filter is weakly stochastically stable as the full SO(3) version was shown to be so via a converse Lyapunov theorem in Section 5.2. Thus the joint probability density function $p(\tilde{\phi}(t), \tilde{b}(t), t)$ ultimately approaches a stationary probability density function

$$p_s = p_s(\tilde{\phi}, \tilde{b}) = \lim_{t \rightarrow \infty} p(\tilde{\phi}(t), \tilde{b}(t), t)$$

which is a solution to the stationary Fokker-Planck PDE

$$0 = k_e \cos(\tilde{\phi}) p_s(\tilde{\phi}, \tilde{b}) + (k_e \sin(\tilde{\phi}) + 2\tilde{b}) \frac{\partial p_s}{\partial \tilde{\phi}} - \alpha \sin(\tilde{\phi}) \frac{\partial p_s}{\partial \tilde{b}} + \sigma_w^2 \frac{\partial^2 p_s}{\partial \tilde{\phi}^2} \quad (5.20)$$

The stationary Fokker-Planck PDE is solved in the following theorem.

Theorem 5.5.1. *The stationary Fokker-Planck PDE of Equation 5.20 is solved by the probability density function*

$$p_s(\tilde{\phi}, \tilde{b}) = \frac{1}{4\pi I_0\left(\frac{k_e}{\sigma_w^2}\right)} \exp\left\{\frac{k_e}{\sigma_w^2} \cos(\tilde{\phi})\right\} \frac{1}{\sqrt{\frac{\pi\alpha\sigma_w^2}{k_e}}} \exp\left\{-\frac{k_e}{\alpha\sigma_w^2} \tilde{b}^2\right\} \quad (5.21)$$

where $I_0(x)$ is the 0th order modified Bessel function of the first kind.

Proof. Note that as $\tilde{\phi}(t) \in (-2\pi, 2\pi)$ and $\tilde{b}(t) \in \mathbb{R}$, the domain of the filter's estimate error state covers the surface of an infinitely long cylinder. So, check to see if the cylindrical probability density function of Mardia and Sutton [62] is a solution to the stationary Fokker-Planck PDE of Equation 5.20. Mardia and Sutton's probability density function is of the form

$$p_s(\tilde{\phi}, \tilde{b}) = \frac{1}{N} \exp\left\{\kappa \cos(\tilde{\phi}) + \nu \tilde{b}^2\right\}$$

where the normalization constant N is a positive scalar, the concentration parameter κ is a non-negative scalar, and ν is a scalar.

Substituting the probability density function into the right hand side of PDE 5.20 yields the expression

$$\left\{ (k_e - \sigma_w^2 \kappa) \cos(\tilde{\phi}) - \kappa (k_e - \sigma_w^2 \kappa) \sin^2(\tilde{\phi}) - 2(\kappa - \alpha\nu) \tilde{b} \sin(\tilde{\phi}) \right\} p_s(\tilde{\phi}, \tilde{b})$$

which is zero for all possible $(\tilde{\phi}, \tilde{b})$ if and only if $\kappa = \frac{k_e}{\sigma_w^2}$ and $\nu = \frac{-k_e}{\alpha\sigma_w^2}$. Thus the solution to the stationary Fokker-Planck PDE is given by

$$p_s(\tilde{\phi}, \tilde{b}) = \frac{1}{N} \exp \left\{ \frac{k_e}{\sigma_w^2} \cos(\tilde{\phi}) - \frac{k_e}{\alpha\sigma_w^2} \tilde{b}^2 \right\} \quad (5.22)$$

The scaling constant N may be recovered by enforcing the probability density normalization constraint

$$\int_{-2\pi}^{2\pi} \int_{-\infty}^{\infty} p_s(\tilde{\phi}, \tilde{b}) d\tilde{b} d\tilde{\phi} = 1$$

Substituting in the probability density function of Equation 5.22 and rearranging results in

$$\begin{aligned} N &= \int_{-2\pi}^{2\pi} \int_{-\infty}^{\infty} \exp \left\{ \frac{k_e}{\sigma_w^2} \cos(\tilde{\phi}) - \frac{k_e}{\alpha\sigma_w^2} \tilde{b}^2 \right\} d\tilde{b} d\tilde{\phi} \\ &= \int_{-2\pi}^{2\pi} \exp \left\{ \frac{k_e}{\sigma_w^2} \cos(\tilde{\phi}) \right\} d\tilde{\phi} \int_{-\infty}^{\infty} \exp \left\{ -\frac{k_e}{\alpha\sigma_w^2} \tilde{b}^2 \right\} d\tilde{b} \end{aligned} \quad (5.23)$$

The first integral of Equation 5.23 was solved in the proof of Theorem 4.8.1 as

$$\int_{-2\pi}^{2\pi} \exp \left\{ \frac{k_e}{\sigma_w^2} \cos(\tilde{\phi}) \right\} d\tilde{\phi} = 4\pi I_0 \left(\frac{k_e}{\sigma_w^2} \right)$$

where $I_0(x)$ is the 0th order modified Bessel function of the first kind. Since the exponential function is such that for all positive scalars a

$$\int_{-\infty}^{\infty} \exp \left\{ -\frac{1}{a} x^2 \right\} dx = \sqrt{\pi a}$$

the second integral in Equation 5.23 evaluates to

$$\int_{-\infty}^{\infty} \exp \left\{ -\frac{k_e}{\alpha\sigma_w^2} \tilde{b}^2 \right\} d\tilde{b} = \sqrt{\frac{\pi\alpha\sigma_w^2}{k_e}}$$

Combining yields the normalization constant.

□

Observe that the stationary probability density function is such that (ultimately) \tilde{b} and $\tilde{\phi}$ are independent. By inspection, the ultimate marginal distribution for $\tilde{\phi}$ is distributed according to a von Mises probability distribution with zero mean and concentration parameter $\frac{k_e}{\sigma_w^2}$. Using the nonlinear relationship $\tilde{\varepsilon}(t) = \sin\left(\frac{\tilde{\phi}(t)}{2}\right)$ one can find ultimate statistics for $\tilde{\varepsilon}(t)$. First it is shown that the ultimate attitude estimate error is unbiased.

Corollary 5.5.1.1. *The error dynamics of the Itô SDE 5.16 have the ultimate mean*

$$\lim_{t \rightarrow \infty} E\left[\tilde{\varepsilon}(t)\right] = 0$$

Proof. Compute the ultimate expectation using the stationary probability density function of Theorem 5.5.1

$$\begin{aligned} \lim_{t \rightarrow \infty} E\left[\tilde{\varepsilon}(t)\right] &= \int_{-2\pi}^{2\pi} \int_{-\infty}^{\infty} \tilde{\varepsilon} p_s(\tilde{\phi}, \tilde{b}) d\tilde{b} d\tilde{\phi} \\ &= \int_{-2\pi}^{2\pi} \int_{-\infty}^{\infty} \sin\left(\frac{\tilde{\phi}}{2}\right) p_s(\tilde{\phi}, \tilde{b}) d\tilde{b} d\tilde{\phi} \\ &= \frac{1}{4\pi I_0\left(\frac{k_e}{\sigma_w^2}\right)} \int_{-2\pi}^{2\pi} \sin\left(\frac{\tilde{\phi}}{2}\right) \exp\left\{\frac{k_e}{\sigma_w^2} \cos(\tilde{\phi})\right\} d\tilde{\phi} \\ &\quad \times \frac{1}{\sqrt{\frac{\pi \alpha \sigma_w^2}{k_e}}} \int_{-\infty}^{\infty} \exp\left\{-\frac{k_e}{\alpha \sigma_w^2} \tilde{b}^2\right\} d\tilde{b} \\ &= \frac{1}{4\pi I_0\left(\frac{k_e}{\sigma_w^2}\right)} \int_{-2\pi}^{2\pi} \sin\left(\frac{\tilde{\phi}}{2}\right) \exp\left\{\frac{k_e}{\sigma_w^2} \cos(\tilde{\phi})\right\} d\tilde{\phi} \end{aligned}$$

Note that $\sin(\cdot)$ is an odd function but $e^{\cos(\cdot)}$ is an even function, so the integrand is an odd function. The integral of an odd function over a symmetric interval about the origin is zero.

□

The following corollary shows the computation of the ultimate noncentral second moment of the attitude estimate error. Since the ultimate mean was found to be zero, the ultimate noncentral second moment is equivalent to the ultimate variance. The ultimate attitude estimate error variance is precisely the same as in Section 4.8.1.2 when there was no bias in the gyro model.

Corollary 5.5.1.2. *The error dynamics of the Itô SDE 5.16 have the ultimate variance*

$$\lim_{t \rightarrow \infty} E \left[\tilde{\varepsilon}^2(t) \right] = \frac{1}{2} \left(1 - \frac{I_1 \left(\frac{k_e}{\sigma_w^2} \right)}{I_0 \left(\frac{k_e}{\sigma_w^2} \right)} \right)$$

Proof. Compute the ultimate expectation using the stationary probability density function of Theorem 5.5.1

$$\begin{aligned} \lim_{t \rightarrow \infty} E \left[\tilde{\varepsilon}^2(t) \right] &= \int_{-2\pi}^{2\pi} \int_{-\infty}^{\infty} \tilde{\varepsilon}^2 p_s(\tilde{\phi}, \tilde{b}) d\tilde{b} d\tilde{\phi} \\ &= \frac{1}{N} \int_{-2\pi}^{2\pi} \int_{-\infty}^{\infty} \sin^2 \left(\frac{\tilde{\phi}}{2} \right) \exp \left\{ \frac{k_e}{\sigma_w^2} \cos(\tilde{\phi}) - \frac{k_e}{\alpha \sigma_w^2} \tilde{b}^2 \right\} d\tilde{b} d\tilde{\phi} \\ &= \frac{1}{4\pi I_0 \left(\frac{k_e}{\sigma_w^2} \right)} \int_{-2\pi}^{2\pi} \sin^2 \left(\frac{\tilde{\phi}}{2} \right) \exp \left\{ \frac{k_e}{\sigma_w^2} \cos(\tilde{\phi}) \right\} d\tilde{\phi} \end{aligned}$$

which was solved in Corollary 4.8.1.2.

□

By inspection of the ultimate joint probability density function of Theorem 5.5.1, it can be seen that \tilde{b} is ultimately distributed according to a Gaussian distribution with zero mean

$$\lim_{t \rightarrow \infty} E \left[\tilde{b}(t) \right] = 0 \tag{5.24}$$

and variance

$$\lim_{t \rightarrow \infty} E \left[\tilde{b}^2(t) \right] = \frac{\alpha \sigma_w^2}{2k_e} \quad (5.25)$$

Since the ultimate mean of both the attitude estimate error and the gyro bias estimate error are zero, the filter is an (ultimately) unbiased estimator. While the random variables $\tilde{\phi}(t)$ and $\tilde{b}(t)$ are ultimately independent of one another, the ultimate variance of the gyro bias estimate error is inversely proportional to the tracking gain k_e while being proportional to the adaptation gain α and the gyro noise scaling parameter σ_w^2 .

Note that this analysis is of the *stationary* Fokker-Planck PDE. As the gyro bias is modeled as a constant, in the infinite time limit a larger adaptation gain does not help as the gyro bias estimate has already conceivably “learned” the gyro bias. From this analysis perspective, the adaptation gain merely lets gyro noise corrupt the gyro bias estimate and should be set as small as possible. Of course this analysis says nothing about the transient performance of the filter when the adaptation law attempts to estimate the gyro bias in the first place.

5.6 Numerical Simulation of Stochastic SO(2) Analytic Results

Two numerical simulations of the SO(2) Gyro Constant Bias Filter's Itô SDE error dynamics of Equation 5.16 were performed for a variety of system parameters. The Kloeden-Platen Explicit Weak 2.0 numerical integration scheme discussed in Section 2.2.3 was used. For each simulation realization, a time step size of $\Delta t = 0.1$ was used for a total of 10^8 simulation steps. At the end of a simulation realization, the last 10^7 simulation steps were used to compute the ergodic mean of the filter attitude estimate error $\tilde{\varepsilon}^2(t)$ and the filter bias estimate error $\tilde{b}^2(t)$. Ensembles of 7 realizations were performed for each choice of system parameters, and the ensemble mean of the ergodic means are reported in the figures below as magenta dots; the attitude estimate errors are computed as $\text{Mean}_{sims} \left[\text{Mean}_{t_i \in T_{ss}} \left[\tilde{\varepsilon}^2(t_i) \right] \right]$ and the bias estimate errors are computed as $\text{Mean}_{sims} \left[\text{Mean}_{t_i \in T_{ss}} \left[\tilde{b}^2(t_i) \right] \right]$.

The first simulation study varied the filter tracking gain k_e across a range of values. A gallery of plots of the filter attitude estimate errors are included in Figure 5.1, a gallery of plots of the filter bias estimate errors for the same simulations are included in Figure 5.2. The numerical results, shown in magenta dots, are compared to plots of the ultimate attitude estimate error variance of Corollary 5.5.1.2 and the ultimate gyro bias estimate error variance of Equation 5.25 respectively which are drawn in blue lines.

As predicted by the analytic solutions for the ultimate attitude estimate error variance of Corollary 5.5.1.2 and the ultimate gyro bias estimate error variance of Equation 5.25, decreasing the gyro noise value σ_w shifts the performance curve

for $\tilde{\varepsilon}^2$ left and the performance curve for \tilde{b}^2 down. Increasing the adaptation gain α increases the bias estimate error variance curve while having no impact on the ultimate attitude estimate error variance curve.

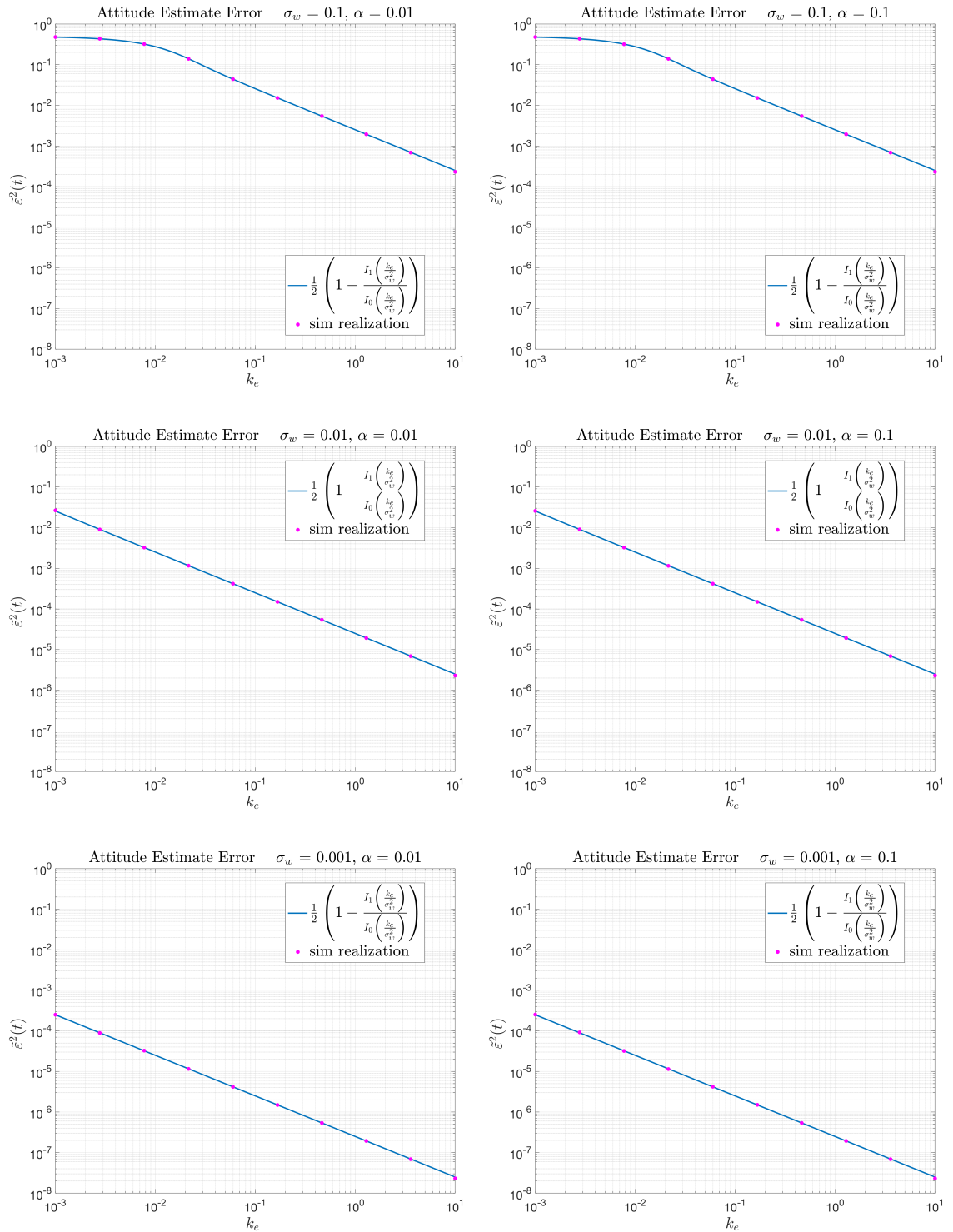


Figure 5.1: Comparison of the ultimate attitude estimate error variance of Corollary

5.5.1.2 to simulation realizations for a range of values of the tracking gain

k_e .

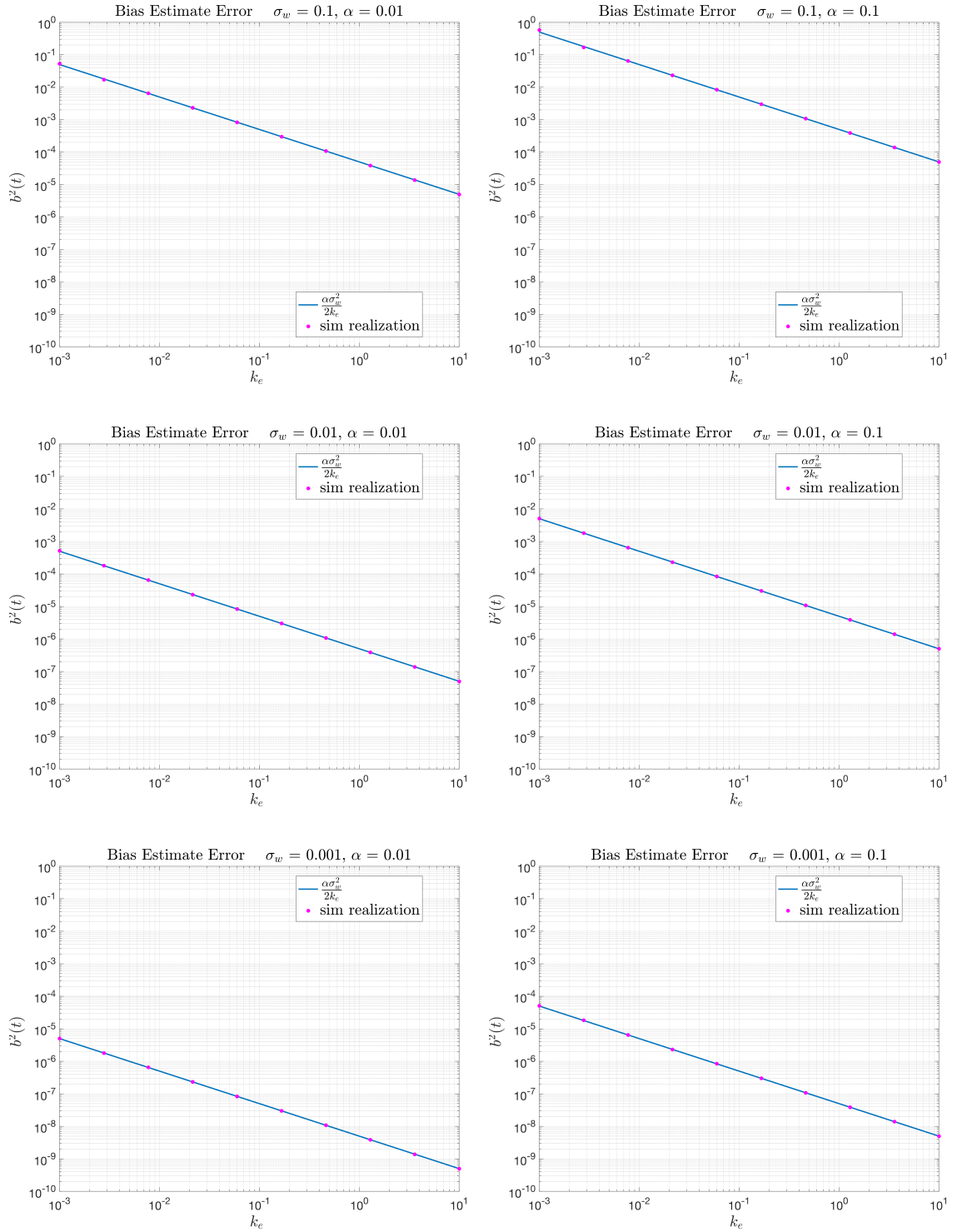


Figure 5.2: Comparison of the ultimate gyro bias estimate error variance of Equation 5.25 to simulation realizations for a range of values of the tracking gain k_e .

The second simulation study varied the filter's bias adaptation gain α across a range of values. A gallery of plots of the filter attitude estimate errors are included in Figure 5.3, a gallery of plots of the filter bias estimate errors for the same simulations are included in Figure 5.4. The numerical results, shown in magenta dots, are compared to plots of the ultimate attitude estimate error variance of Corollary 5.5.1.2 and the ultimate gyro bias estimate error variance of Equation 5.25 respectively which are drawn in blue lines.

As the form of the ultimate attitude estimate error variance of Corollary 5.5.1.2 predicts, the ultimate attitude estimate error variance is completely unaffected by variation of the adaptation gain parameter. The ultimate gyro bias estimate error variance of Equation 5.25 captures the trend seen in the numerical data that an increase in the adaptation gain parameter increases the bias estimate error variance.

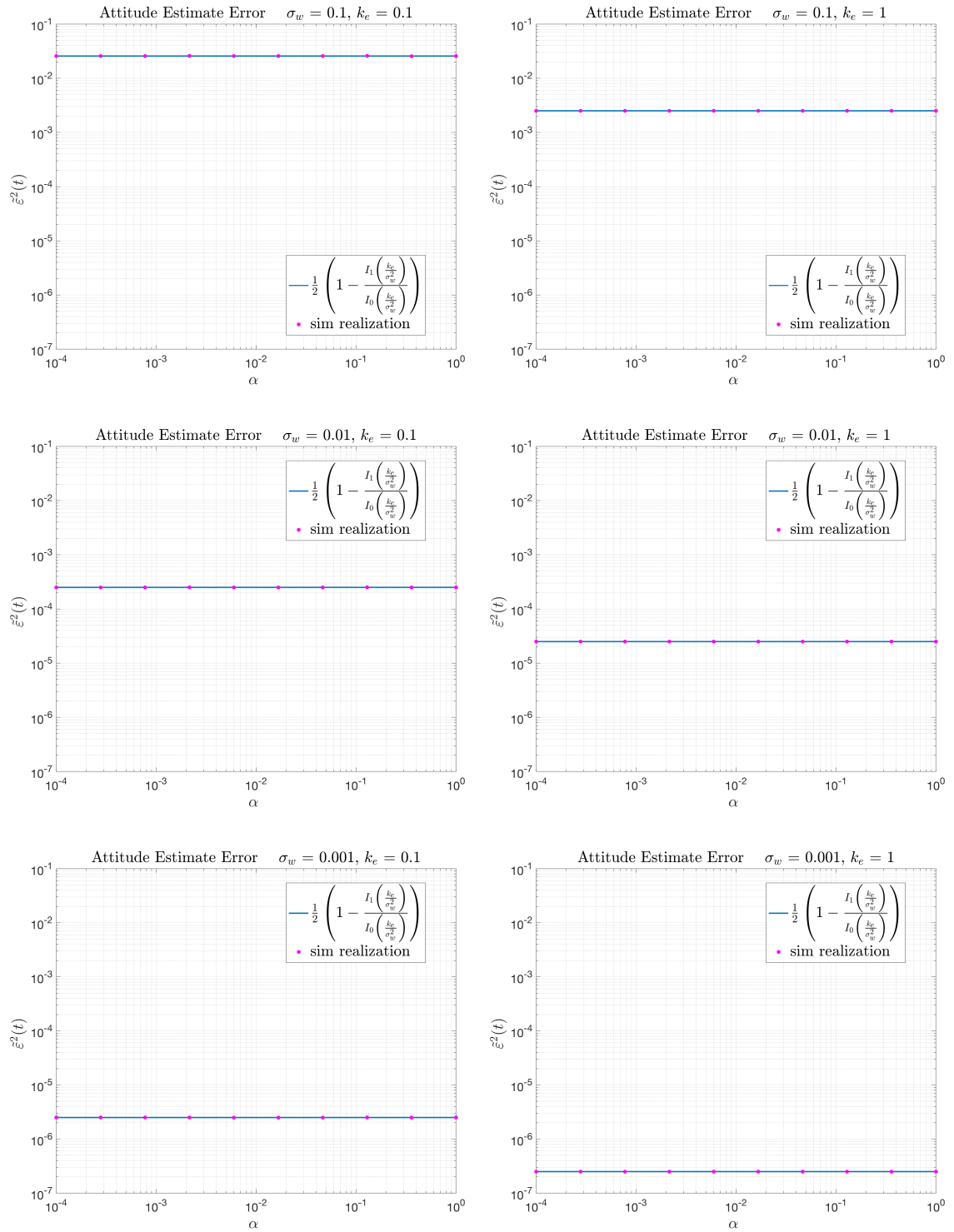


Figure 5.3: Comparison of the ultimate attitude estimate error variance of Corollary

5.5.1.2 to simulation realizations for a range of values of the adaptation gain

α .

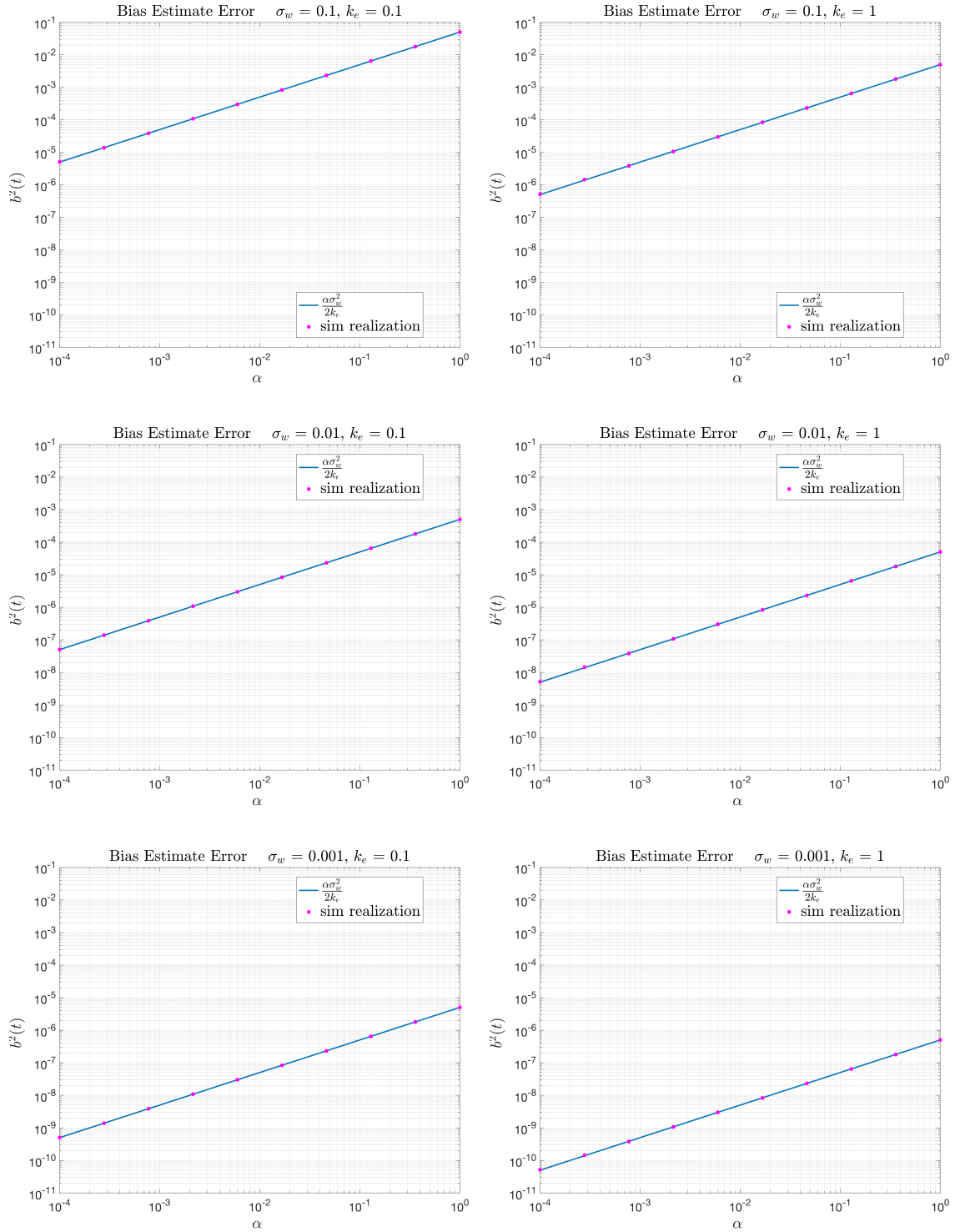


Figure 5.4: Comparison of the ultimate gyro bias estimate error variance of Equation 5.25 to simulation realizations for a range of values of the adaptation gain α .

5.7 An SO(3) Upper Bound

Following the same approach as that of Section 4.10 , this section extrapolates upper bounds for the stationary statistics of the SO(3) filter from the analytic solutions of the SO(2) case.

The SO(3) ultimate attitude estimate error variance bound is assumed to have the form of the SO(2) ultimate attitude estimate error variance from Corollary 5.5.1.2, but as before is rescaled to account for the low filter gain limit seen in the previous chapters. The proposed SO(3) ultimate upper bound is given by

$$\text{bound} \left(\xi, \frac{k_e}{\sigma_w^2} \right) = \frac{3}{4} \left(1 - \frac{I_1 \left(\frac{k_e}{\xi \sigma_w^2} \right)}{I_0 \left(\frac{k_e}{\xi \sigma_w^2} \right)} \right) \quad (5.26)$$

Similarly, the ultimate bias estimate error variance bound is assumed to have the same form as Equation 5.25 but with the same scaling parameter acting on the gyro variance σ_w^2

$$\text{bound} \left(\xi, \frac{k_e}{\sigma_w^2} \right) = \frac{\xi \alpha \sigma_w^2}{2k_e} \quad (5.27)$$

Numerical simulations of the Itô SDE 5.7 were performed to evaluate the notional bounds. As before, the Kloeden-Platen Explicit Weak 2.0 numerical integration scheme discussed in Section 2.2.3 was used. For each simulation realization, a time step size of $\Delta t = 0.1$ was used for a total of 10^7 simulation steps. At the end of a simulation realization, the last 10^6 simulation steps were used to compute the ergodic mean of the filter attitude estimate error $\tilde{\boldsymbol{\epsilon}}^T(t)\tilde{\boldsymbol{\epsilon}}(t)$ and the filter bias estimate error $\tilde{\boldsymbol{b}}^T(t)\tilde{\boldsymbol{b}}(t)$. Ensembles of 7 realizations were performed for each choice of system parameters, and the ensemble mean of the ergodic means

are reported in the figures below as magenta dots; the attitude estimate errors are computed as $\text{Mean}_{sim_s} \left[\text{Mean}_{t_i \in T_{ss}} \left[\tilde{\boldsymbol{\varepsilon}}^T(t_i) \tilde{\boldsymbol{\varepsilon}}(t_i) \right] \right]$ and the bias estimate errors are computed as $\text{Mean}_{sim_s} \left[\text{Mean}_{t_i \in T_{ss}} \left[\tilde{\boldsymbol{b}}^T(t_i) \tilde{\boldsymbol{b}}(t_i) \right] \right]$.

Figure 5.5 contains a gallery of the proposed upper bound for the stationary attitude estimate error variance of Equation 5.26 for various choices of ξ superimposed on plots of the numerical simulation realizations for a range of tracking gain parameters k_e . Figure 5.6 similarly contains a gallery of the proposed upper bound for the stationary gyro bias estimate error variance of Equation 5.27 for the corresponding choices of ξ for the range of tracking gain parameters k_e . In all cases considered, the choice of $\xi = 3$ in the expression of Equation 5.26 and 5.27 bound the simulation realizations; however, smaller choices of ξ do not.

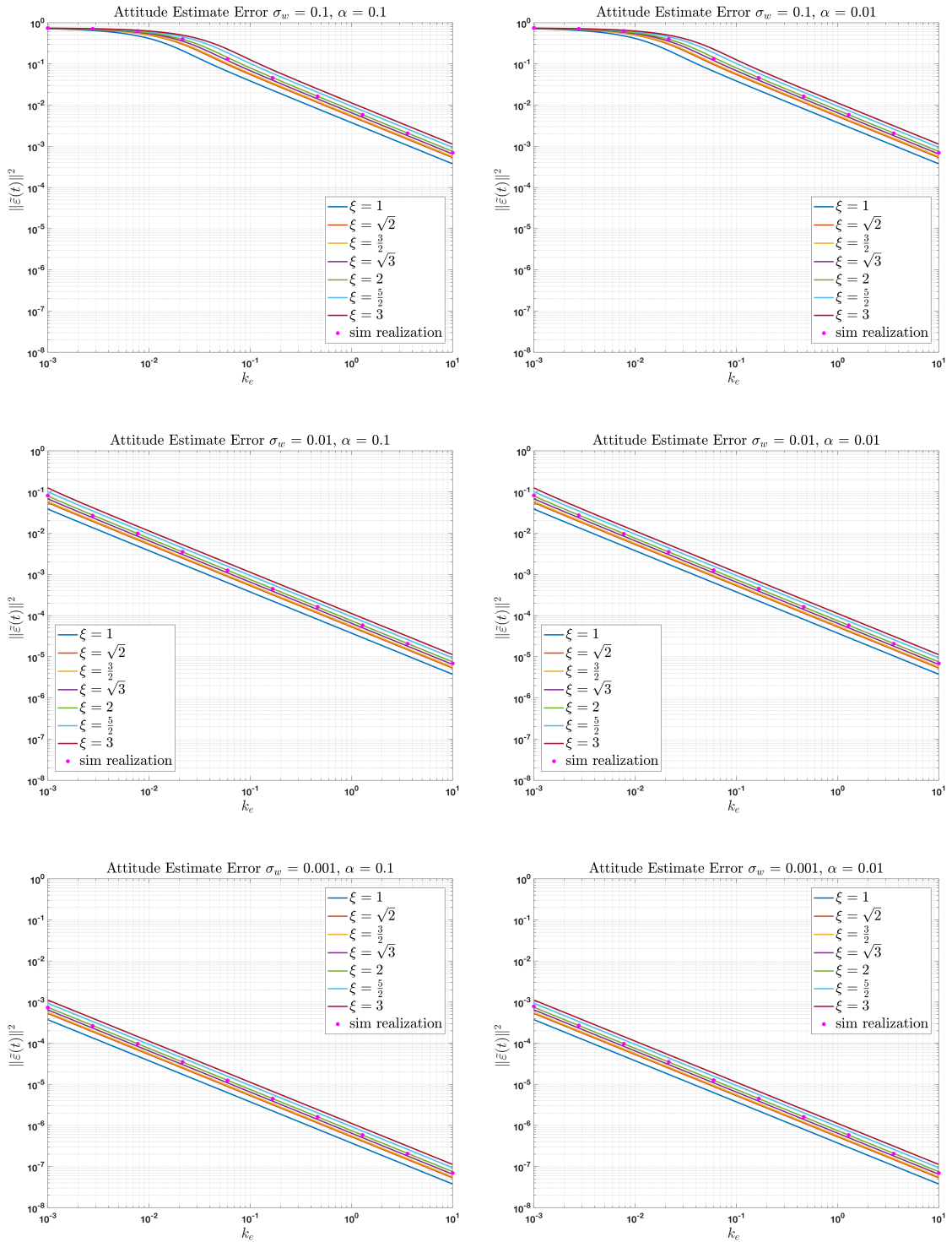


Figure 5.5: Comparison of simulation realizations of the attitude estimate error variance and the notional bound of Equation 5.26 for several choices of ξ over a range of tracking gains k_e .

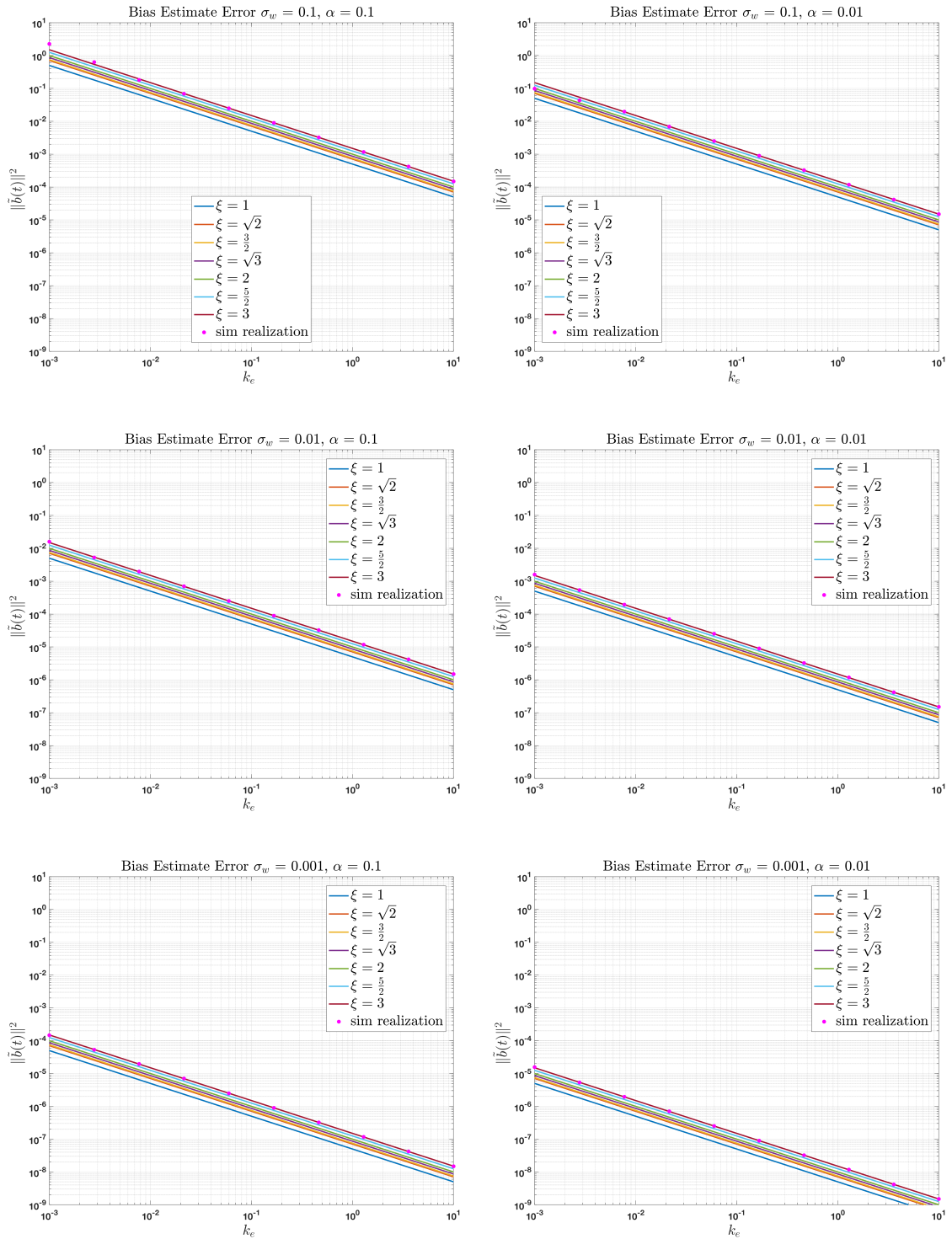


Figure 5.6: Comparison of simulation realizations of the bias estimate error variance and the notional bound of Equation 5.26 for several choices of ξ over a range of tracking gains k_e .

A second numerical simulation study was performed to verify that the choice of adaptation gain α had no impact on the ultimate attitude estimate variance and to evaluate the ultimate bias estimate notional bounds. Figure 5.7 contains a gallery of the proposed upper bound for the stationary attitude estimate error variance of Equation 5.26 for various choices of ξ . The numerical simulation data confirms the attitude estimate error is independent of the choice of α . Figure 5.6 similarly contains a gallery of the proposed upper bound for the stationary gyro bias estimate error variance of Equation 5.27 for the corresponding choices of ξ . As before, the choice of $\xi = 3$ in the expression of Equation 5.26 and 5.27 bound the simulation realizations; however, smaller choices of ξ do not.

Thus the simulation data suggest the ultimate upper bounds of

$$\lim_{t \rightarrow \infty} E[\tilde{\boldsymbol{\epsilon}}^T(t)\tilde{\boldsymbol{\epsilon}}(t)] \leq \frac{3}{4} \left(1 - \frac{I_1\left(\frac{k_e}{3\sigma_w^2}\right)}{I_0\left(\frac{k_e}{3\sigma_w^2}\right)} \right) \quad (5.28)$$

and

$$\lim_{t \rightarrow \infty} E[\tilde{\boldsymbol{\epsilon}}^T(t)\tilde{\boldsymbol{\epsilon}}(t)] \leq \frac{3\alpha\sigma_w^2}{2k_e} \quad (5.29)$$

which, for clarity, are drawn in the gallery of Figure 5.9 for the ultimate attitude estimate error variance bound of Equation 5.28 and Figure 5.10 for the ultimate bias estimate error variance bound of Equation 5.29 for a range of tracking gain parameters k_e . The bounds are drawn for a variety of adaptation gain parameters α in the gallery of Figure 5.11 for the ultimate attitude estimate error and the gallery of Figure 5.12 for the ultimate bias estimate error.

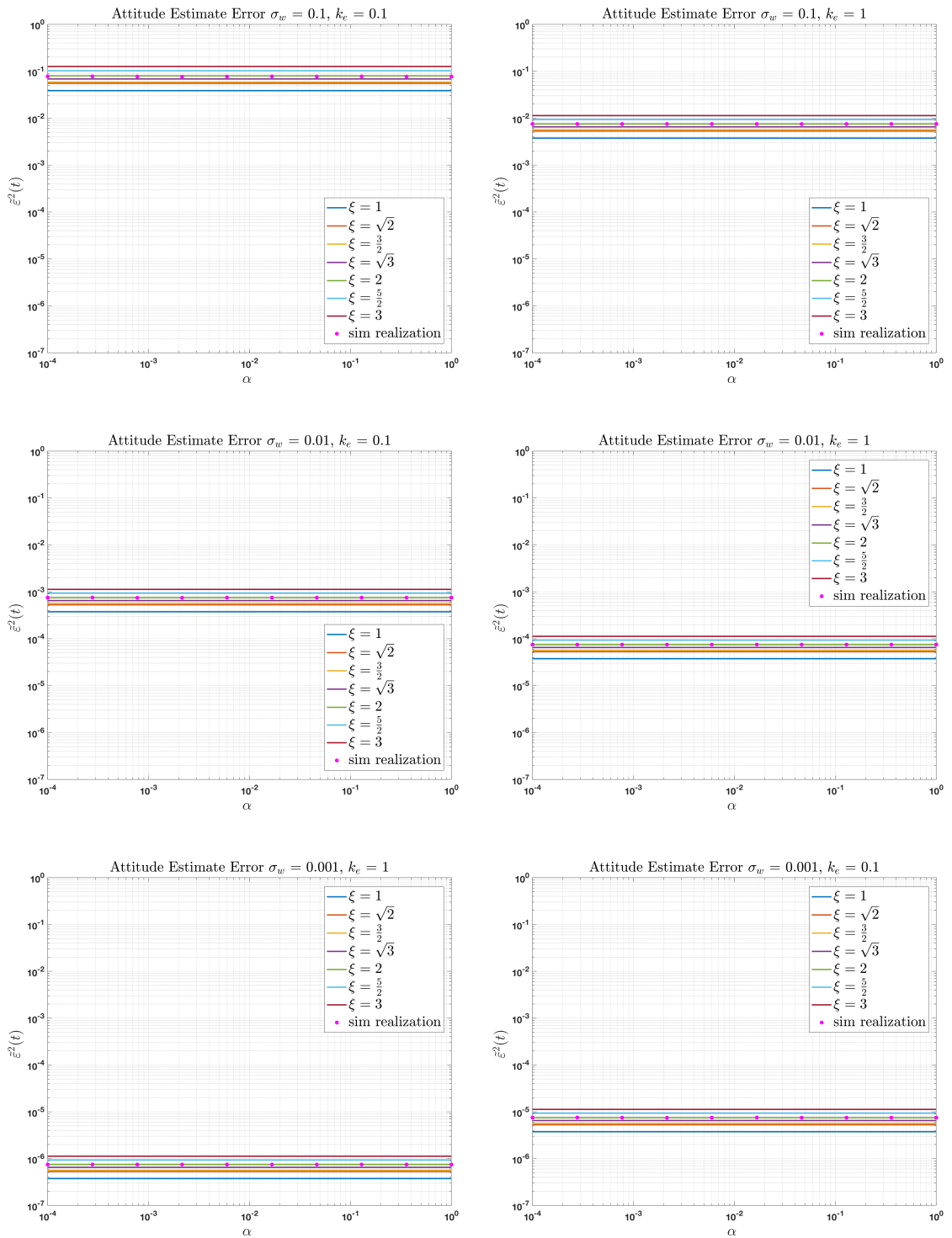


Figure 5.7: Comparison of simulation realizations of the attitude estimate error variance and the notional bound of Equation 5.26 for several choices of ξ over a range of adaptation gains α .

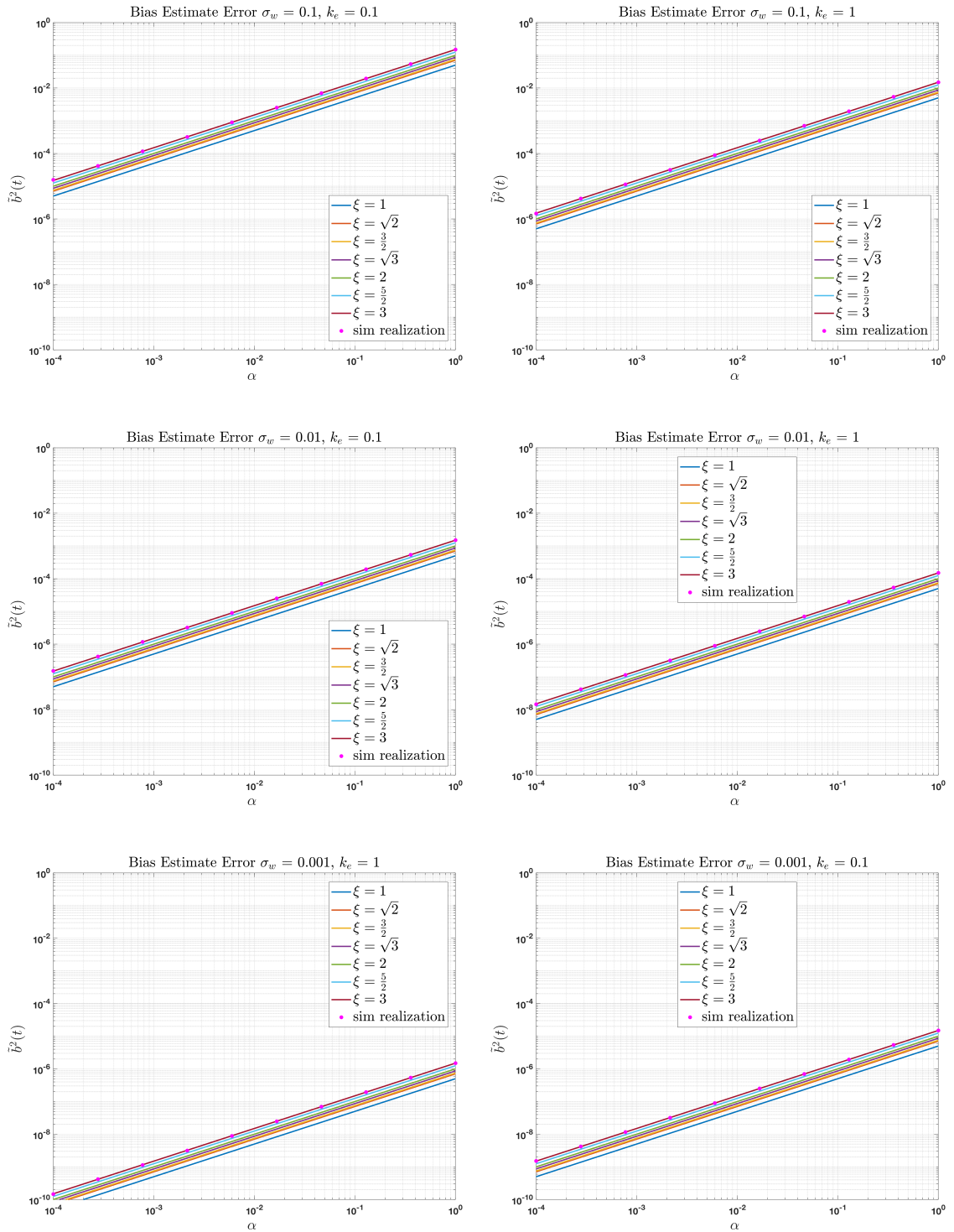


Figure 5.8: Comparison of simulation realizations of the bias estimate error variance and the notional bound of Equation 5.26 for several choices of ξ over a range of adaptation gains α .

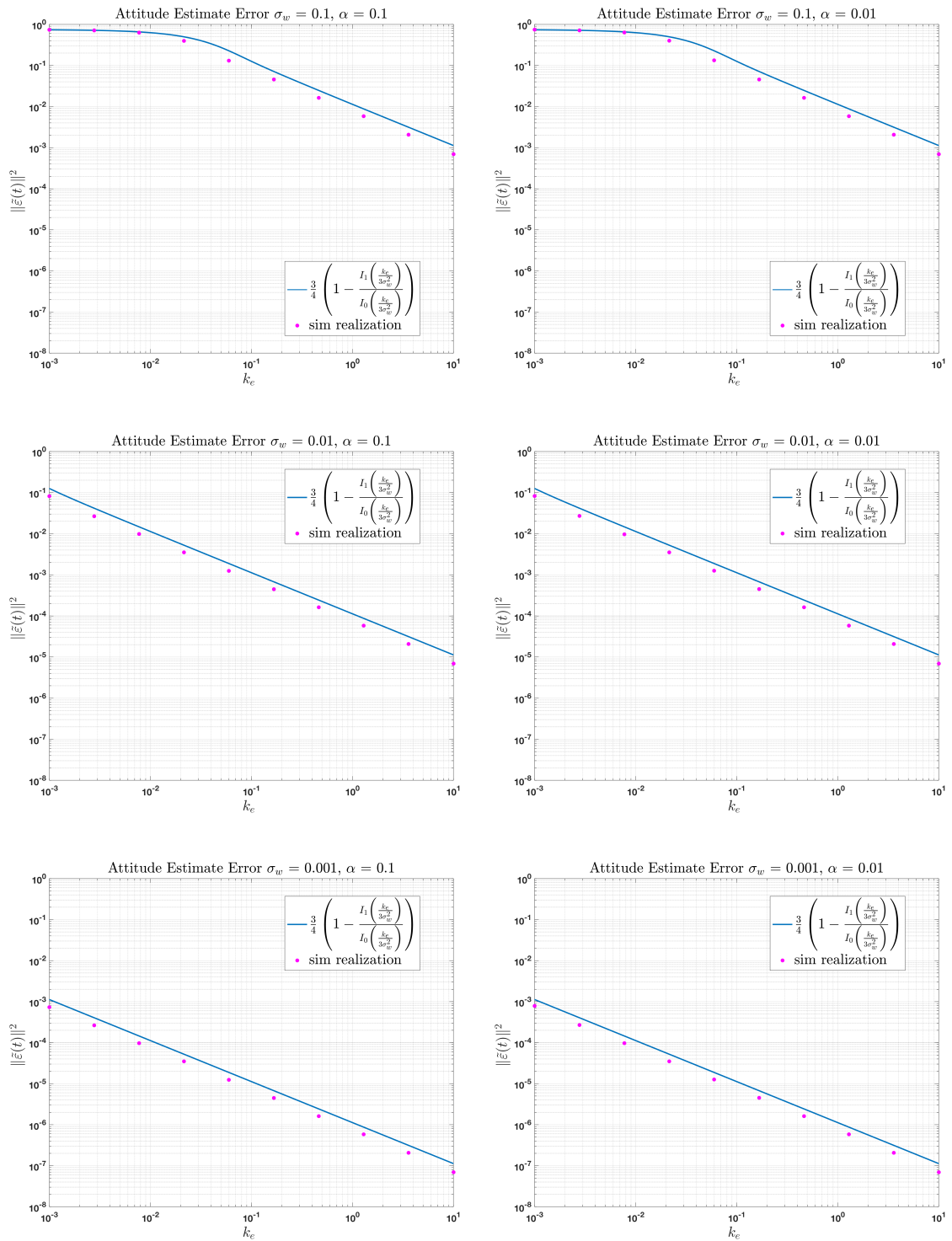


Figure 5.9: Comparison of simulation realizations of the attitude estimate error variance and the notional bound of Equation 5.28 for a range of tracking gain parameters k_e .

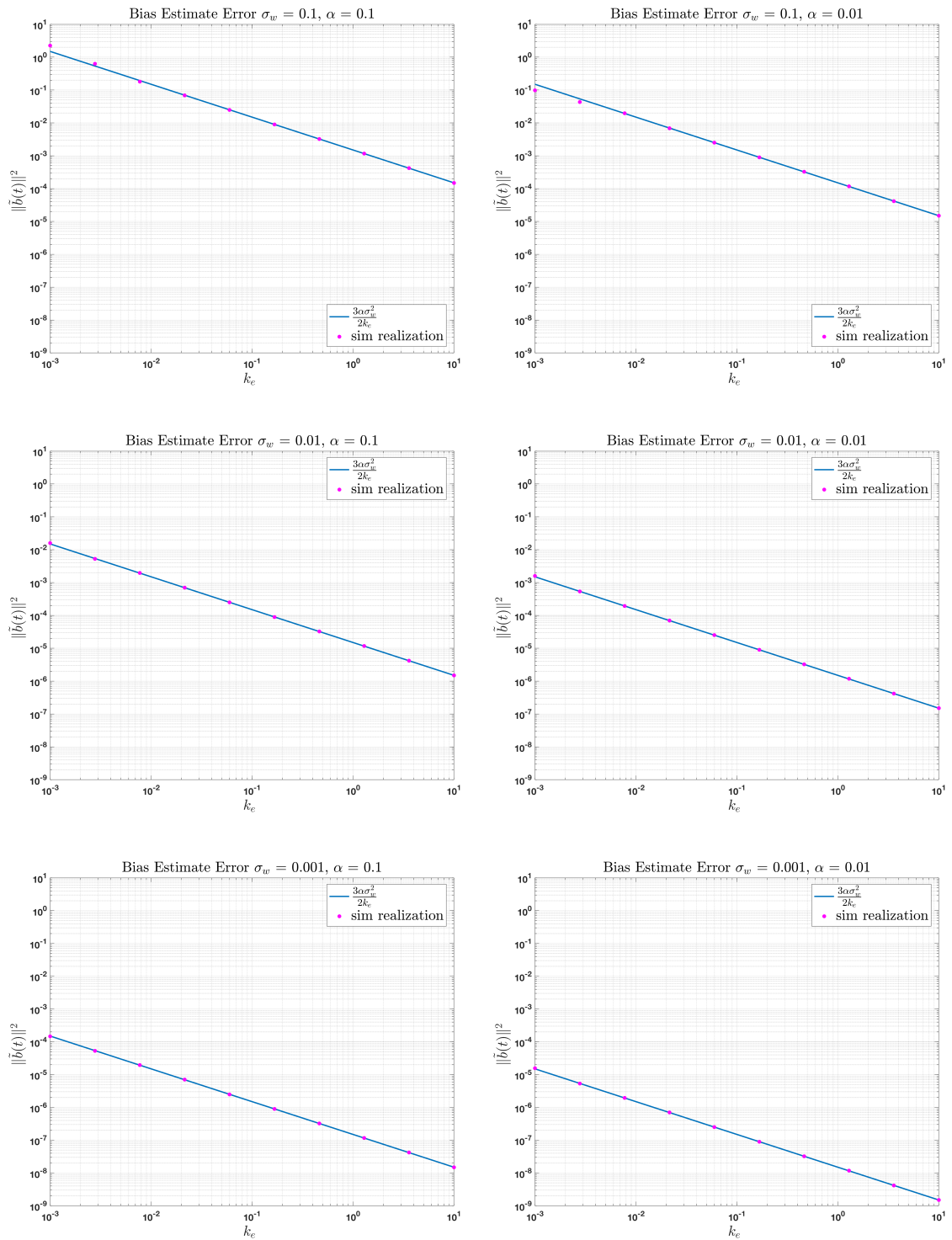


Figure 5.10: Comparison of simulation realizations of the bias estimate error variance and the notional bound of Equation 5.29 for a range of tracking gain parameters k_e .

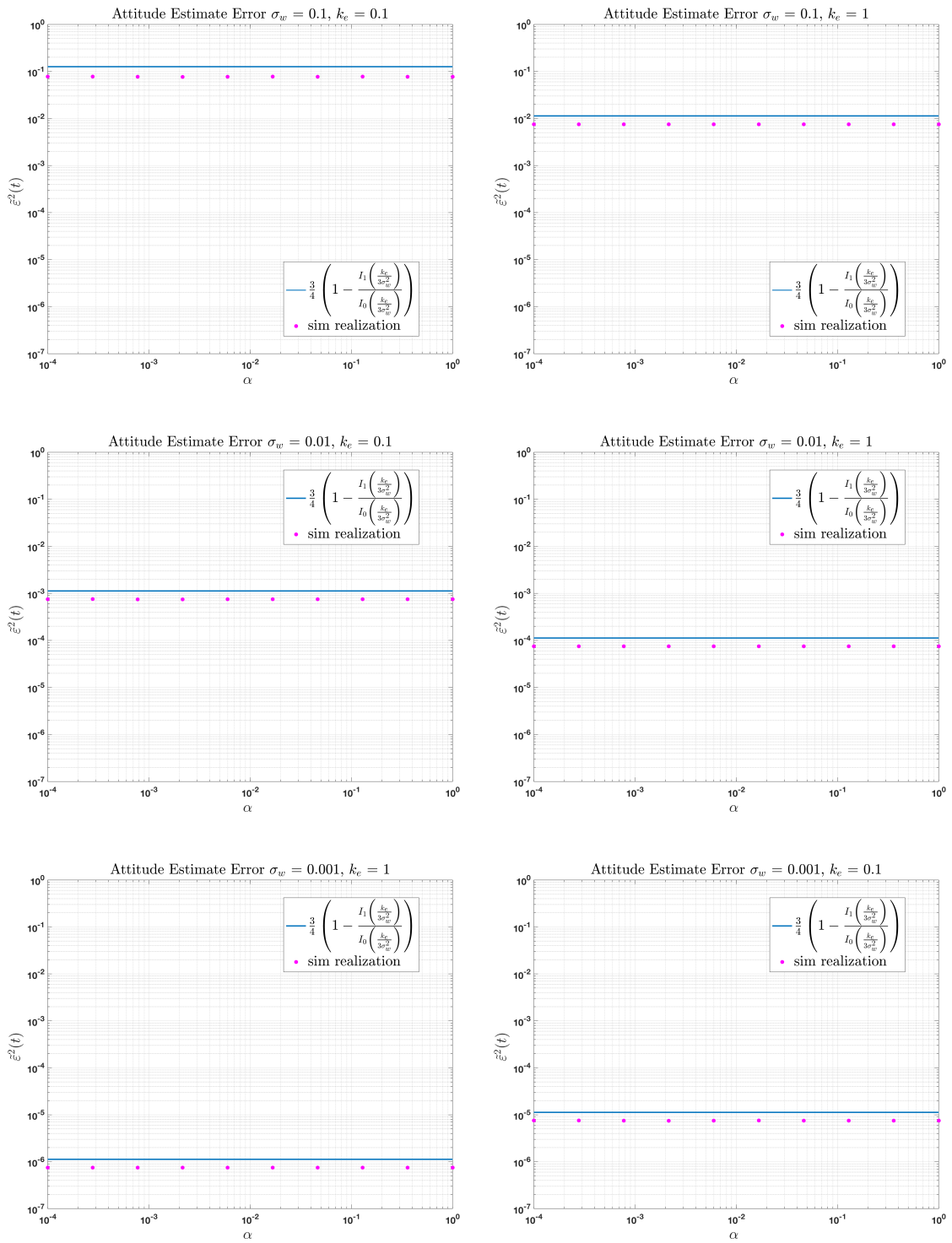


Figure 5.11: Comparison of simulation realizations of the attitude estimate error variance and the notional bound of Equation 5.28 for a range of adaptation gain parameters α .

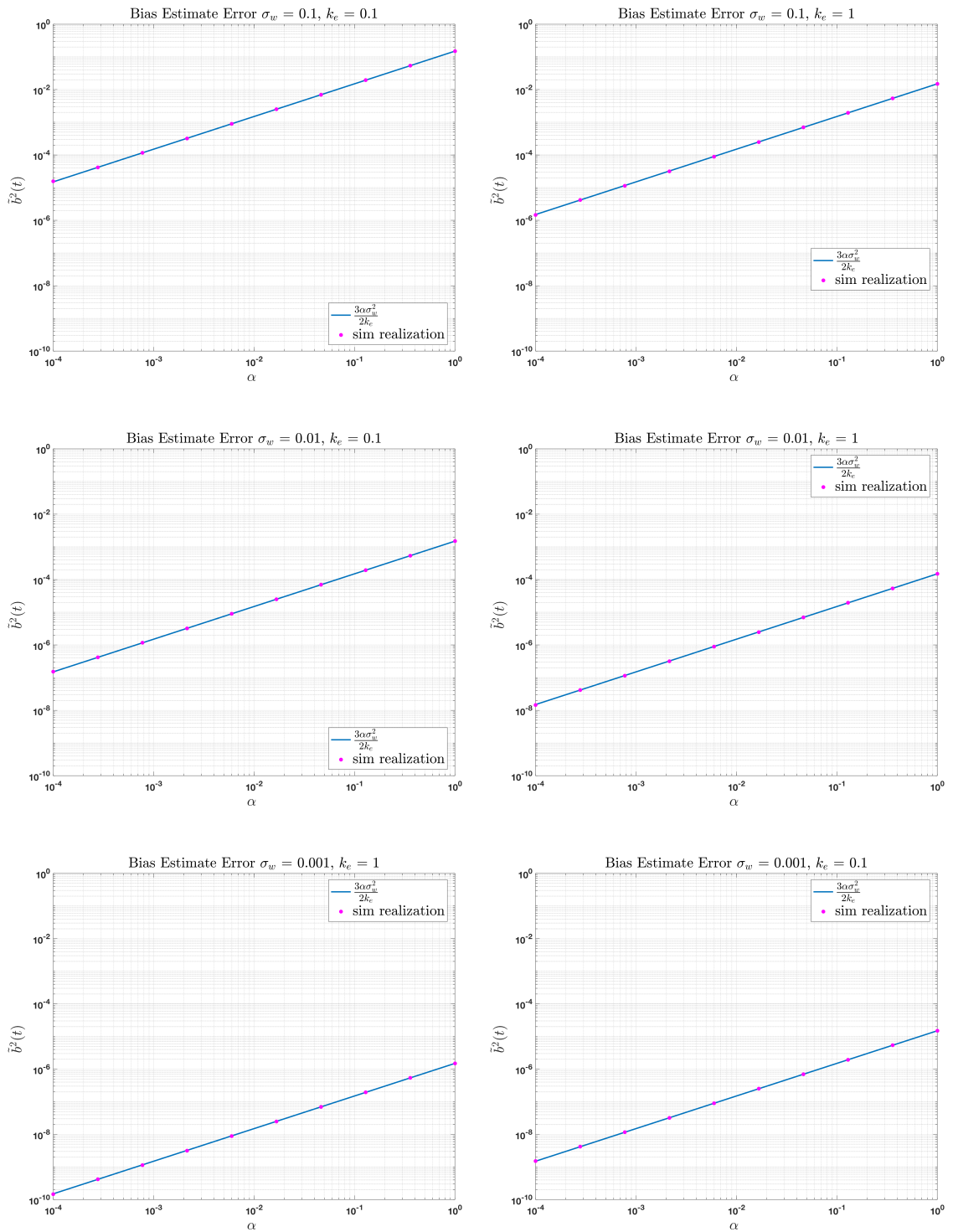


Figure 5.12: Comparison of simulation realizations of the bias estimate error variance and the notional bound of Equation 5.29 for a range of adaptation gain parameters α .

5.8 Exact Solution to the Stationary SO(3) Fokker-Planck PDE

In this section, the understanding gained from the SO(2) analysis and its SO(3) extrapolation, as well as the solution to the SO(2) and SO(3) stationary Fokker-Planck PDEs for the gyro noise case studied in the previous chapter, are used to identify a possible distribution for the SO(3) case. This distribution is then shown to indeed solve the SO(3) stationary Fokker-Planck PDE. The solution is used to find an analytical expression for the ultimate attitude estimate error and ultimate bias estimate error which will be compared to numerical simulation data in the following section.

In Chapter 4, the attitude estimation filter for gyro measurements with additive noise was studied. In particular, the stationary Fokker-Planck PDE was shown to be solved by a von Mises PDF in the SO(2) case in Section 4.8 and a bipolar Bingham PDF in the SO(3) case in Section 4.11. In Section 5.5, the stationary Fokker-Planck PDE for the gyro measurements with additive noise and constant bias in the SO(2) case was shown to be solved by a joint PDF consisting of an independent von Mises distribution and a Gaussian distribution. The following theorem shows the pattern continues; that the SO(3) stationary Fokker-Planck PDE is indeed solved by a joint PDF consisting of an independent bipolar Bingham distribution and a multivariate Gaussian.

Theorem 5.8.1. *The stationary distribution for the filter error dynamics of the Itô SDE 5.7 is given by the joint PDF with a Bipolar Bingham PDF and multivariate*

Gaussian PDF

$$p_s(\tilde{\mathbf{q}}, \tilde{\mathbf{b}}) = \frac{1}{N_q} \exp \left\{ \frac{k_e}{\sigma_w^2} (2\tilde{\eta}^2 - 1) \right\} \frac{1}{N_b} \exp \left\{ -\frac{k_e}{\alpha\sigma_w^2} \tilde{\mathbf{b}}^T \tilde{\mathbf{b}} \right\} \quad (5.30)$$

where the normalization constant N_q is given by

$$N_q = \pi^2 I_0 \left(\frac{k_e}{\sigma_w^2} \right) - \pi^2 I_1 \left(\frac{k_e}{\sigma_w^2} \right)$$

and the normalization constant N_b is given by

$$N_b = \sqrt{\frac{\pi^3 \alpha^3 \sigma_w^6}{k_e^3}}$$

Proof. Per the reasoning given above, consider the jointly independent PDF that is a bipolar Bingham distribution in the attitude estimate error and a multivariate Gaussian in the bias estimate error

$$p_s(\tilde{\mathbf{q}}, \tilde{\mathbf{b}}) = \frac{1}{N_q} \exp \left\{ \lambda (2\tilde{\eta}^2 - 1) \right\} \frac{1}{N_b} \exp \left\{ \gamma \tilde{\mathbf{b}}^T \tilde{\mathbf{b}} \right\}$$

Taking partial derivatives as appropriate and substituting into the right hand side of the SO(3) stationary Fokker-Planck PDE 5.14 yields

$$\left\{ -\frac{1}{2}(k_e - \sigma_w^2 \lambda) + 2(1 - \lambda)(k_e - \lambda \sigma_w^2) \tilde{\eta}^2 + 2\lambda(k_e - \lambda \sigma_w^2) \tilde{\eta}^4 - 2\tilde{\eta} \tilde{\boldsymbol{\varepsilon}}^T \tilde{\mathbf{b}} (\alpha \gamma + \lambda) \right\} p_s$$

which is zero for all possible $\tilde{\mathbf{q}}$ and $\tilde{\mathbf{b}}$ if and only if $\lambda = \frac{k_e}{\sigma_w^2}$ and $\gamma = -\frac{k_e}{\alpha \sigma_w^2}$.

The scaling constants N_q and N_b may be recovered by enforcing the probability density normalization constraints on the marginal PDFs. The normalization constant for the bipolar Bingham marginal PDF was found in Theorem 4.11.1 to be

$$N_q = \pi^2 I_0 \left(\frac{k_e}{\sigma_w^2} \right) - \pi^2 I_1 \left(\frac{k_e}{\sigma_w^2} \right)$$

Similarly, the normalization constant for the multivariate Gaussian marginal PDF is given as

$$\begin{aligned}
N_b &= \int_{-\infty}^{\infty} \int_{-\infty}^{\infty} \int_{-\infty}^{\infty} \exp \left\{ -\frac{k_e}{\alpha \sigma_w^2} \left(\tilde{b}_x^2 + \tilde{b}_y^2 + \tilde{b}_z^2 \right) \right\} d\tilde{b}_x d\tilde{b}_y d\tilde{b}_z \\
&= \int_{-\infty}^{\infty} \exp \left\{ -\frac{k_e}{\alpha \sigma_w^2} \tilde{b}_x^2 \right\} d\tilde{b}_x \int_{-\infty}^{\infty} \exp \left\{ -\frac{k_e}{\alpha \sigma_w^2} \tilde{b}_y^2 \right\} d\tilde{b}_y \int_{-\infty}^{\infty} \exp \left\{ -\frac{k_e}{\alpha \sigma_w^2} \tilde{b}_z^2 \right\} d\tilde{b}_z \\
&= \sqrt{\frac{\pi \alpha \sigma_w^2}{k_e}} \sqrt{\frac{\pi \alpha \sigma_w^2}{k_e}} \sqrt{\frac{\pi \alpha \sigma_w^2}{k_e}} = \sqrt{\frac{\pi^3 \alpha^3 \sigma_w^6}{k_e^3}} \tag{5.31}
\end{aligned}$$

where the Gaussian integral

$$\int_{-\infty}^{\infty} e^{-ax^2} dx = \sqrt{\frac{\pi}{a}} \quad \forall a > 0$$

was used. □

Theorem 5.8.1 shows the ultimate PDF 5.30 that satisfies the stationary Fokker-Planck PDE 5.14 is jointly independent. Specifically, it consists of a bipolar Bingham distribution in the attitude estimate error $\tilde{\mathbf{q}}$ which is independent of the multivariate Gaussian in the bias estimate error $\tilde{\mathbf{b}}$. Thus the ultimate statistics for the attitude estimate error have zero mean as shown in Corollary 4.11.1.1, the variance as given in Corollary 4.11.1.2, and the covariance matrix as found in Corollary 4.11.1.3. Similarly, the ultimate statistics for the bias estimate error can be computed with the associated marginal PDF. Since the marginal PDF is a simple uncorrelated multivariate Gaussian, the ultimate statistics are merely stated here.

The ultimate bias estimate error has the mean

$$\lim_{t \rightarrow \infty} E[\tilde{\mathbf{b}}(t)] = \mathbf{0} \tag{5.32}$$

the ultimate variance

$$\lim_{t \rightarrow \infty} E[\tilde{\mathbf{b}}^T(t)\tilde{\mathbf{b}}(t)] = \frac{3\alpha\sigma_w^2}{2k_e} \quad (5.33)$$

and the ultimate covariance matrix

$$\lim_{t \rightarrow \infty} E[\tilde{\mathbf{b}}(t)\tilde{\mathbf{b}}^T(t)] = \frac{\alpha\sigma_w^2}{2k_e} I \quad (5.34)$$

where the I (without a subscript) is the 3×3 identity matrix.

Note that, as in Chapter 4, the ultimate attitude estimate error statistics depend on the ratio of $\frac{k_e}{\sigma_w^2}$; however, they are completely independent of the gyro bias adaptation gain α .

While the bias estimate error is (ultimately) independent of the attitude estimate error, the gyro bias estimate error is ultimately parameterized by the ratio of $\frac{\alpha\sigma_w^2}{k_e}$. Thus increasing (or decreasing) both the filter tracking gain k_e and the adaptation gain α by the same amount will have no impact on the bias estimation error in the infinite time limit.

5.9 Numerical Simulation of Stochastic SO(3) Analytic Results

Consider again the simulations reported in Section 5.6. The first simulation study investigates filter performance as the tracking gain k_e is varied. The attitude estimate error numerical simulation statistics are repeated in Figure 5.13 with the analytic solution using the bipolar Bingham marginal of the PDF 5.30 to compute the expected attitude estimate error. The analytic solution exactly matches the numerical simulation data. The bias estimate error numerical simulation statistics are repeated in Figure 5.14 with the analytic solution for the variance from Equation 5.33 superimposed. The analytic solution matches the numerical simulation data exactly except for the smallest two tracking gain points in the $\sigma_w = 0.1$ case, which is possibly due to the simulation realizations not fully reaching steady state. The slopes of all data are -1 on the log-log plot, which agrees with the ultimate variance being inversely proportional to the tracking gain k_e .

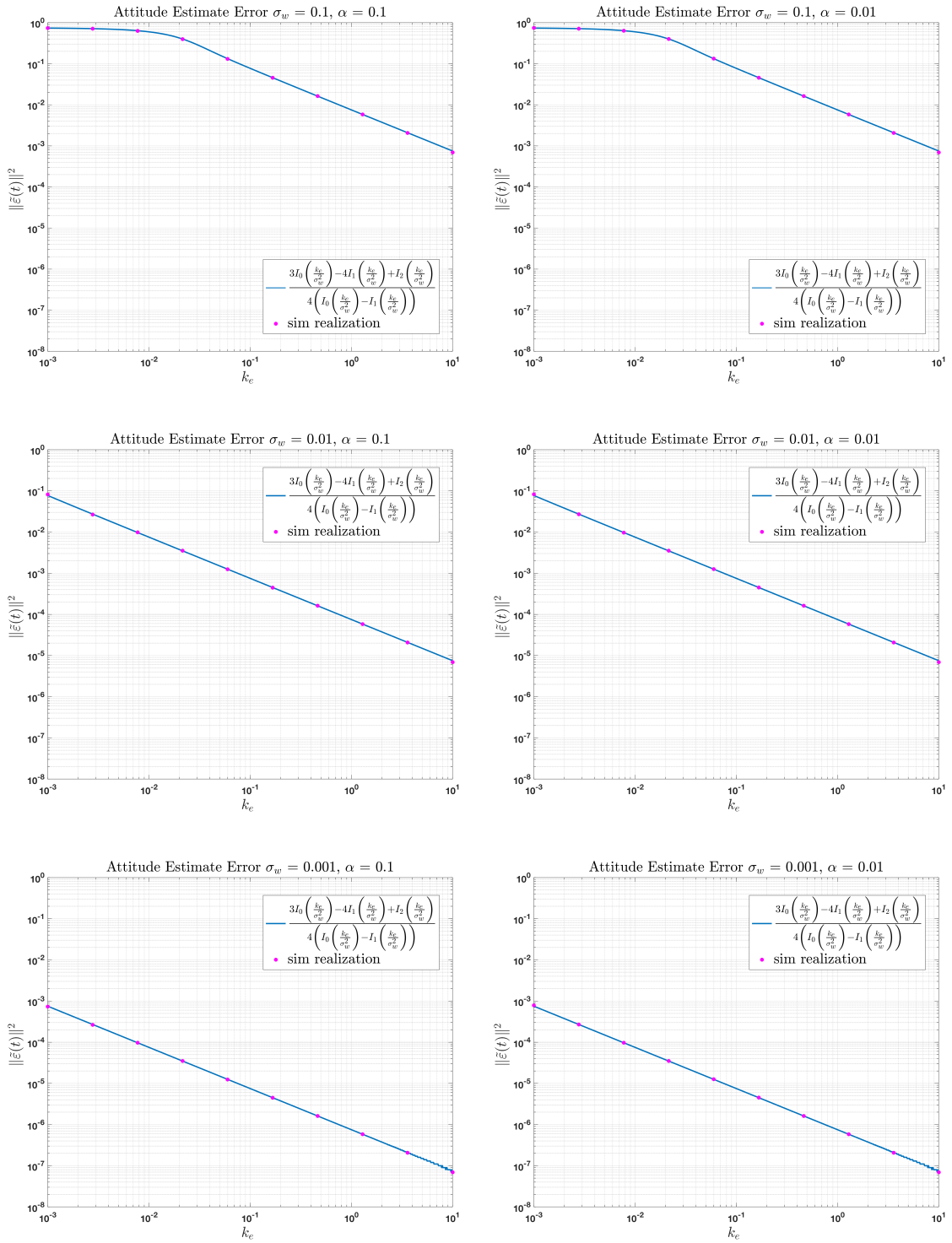


Figure 5.13: Comparison of simulation realizations of the attitude estimate error variance with the analytic solution for a range of tracking gain parameters k_e .

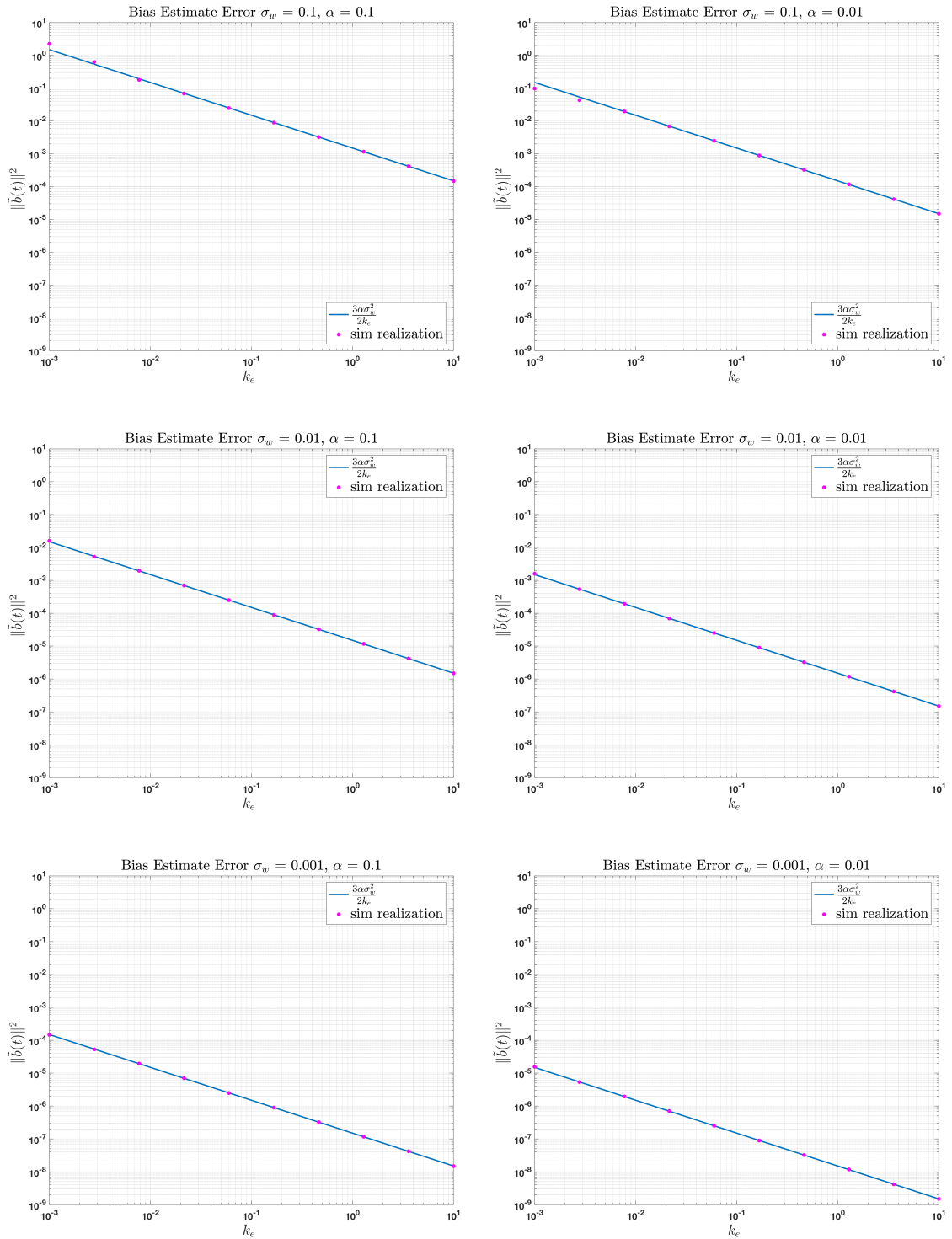


Figure 5.14: Comparison of simulation realizations of the bias estimate error variance with the analytic solution for a range of tracking gain parameters k_e .

The second simulation study examines filter performance as the adaptation gain α is varied. The attitude estimate error numerical simulation statistics are repeated in Figure 5.15 with the analytic solution using the bipolar Bingham marginal of the PDF 5.30 to compute the expected attitude estimate error. The analytic solution exactly matches the numerical simulation data, and clearly show that variation of the adaptation gain α has no impact on the ultimate attitude estimate error variance. The bias estimate error numerical simulation statistics are repeated in Figure 5.16 with the analytic solution for the variance from Equation 5.33 superimposed. The analytic solution matches the numerical simulation data exactly. The slopes of all data are +1 on the log-log plot, which agrees with the ultimate variance being directly proportional to the adaptation gain α .

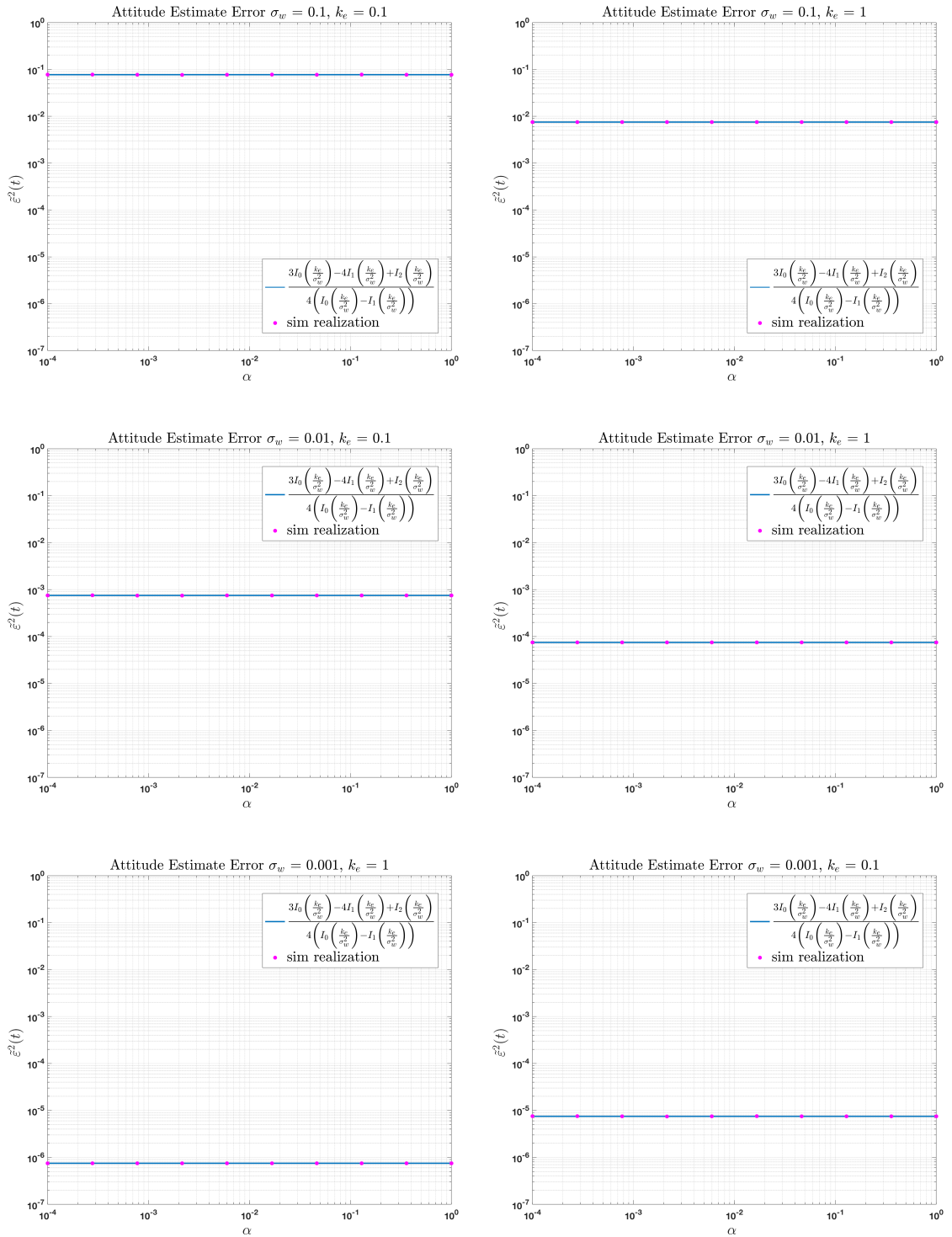


Figure 5.15: Comparison of simulation realizations of the attitude estimate error variance with the analytic solution for a range of adaptation gain parameters α .

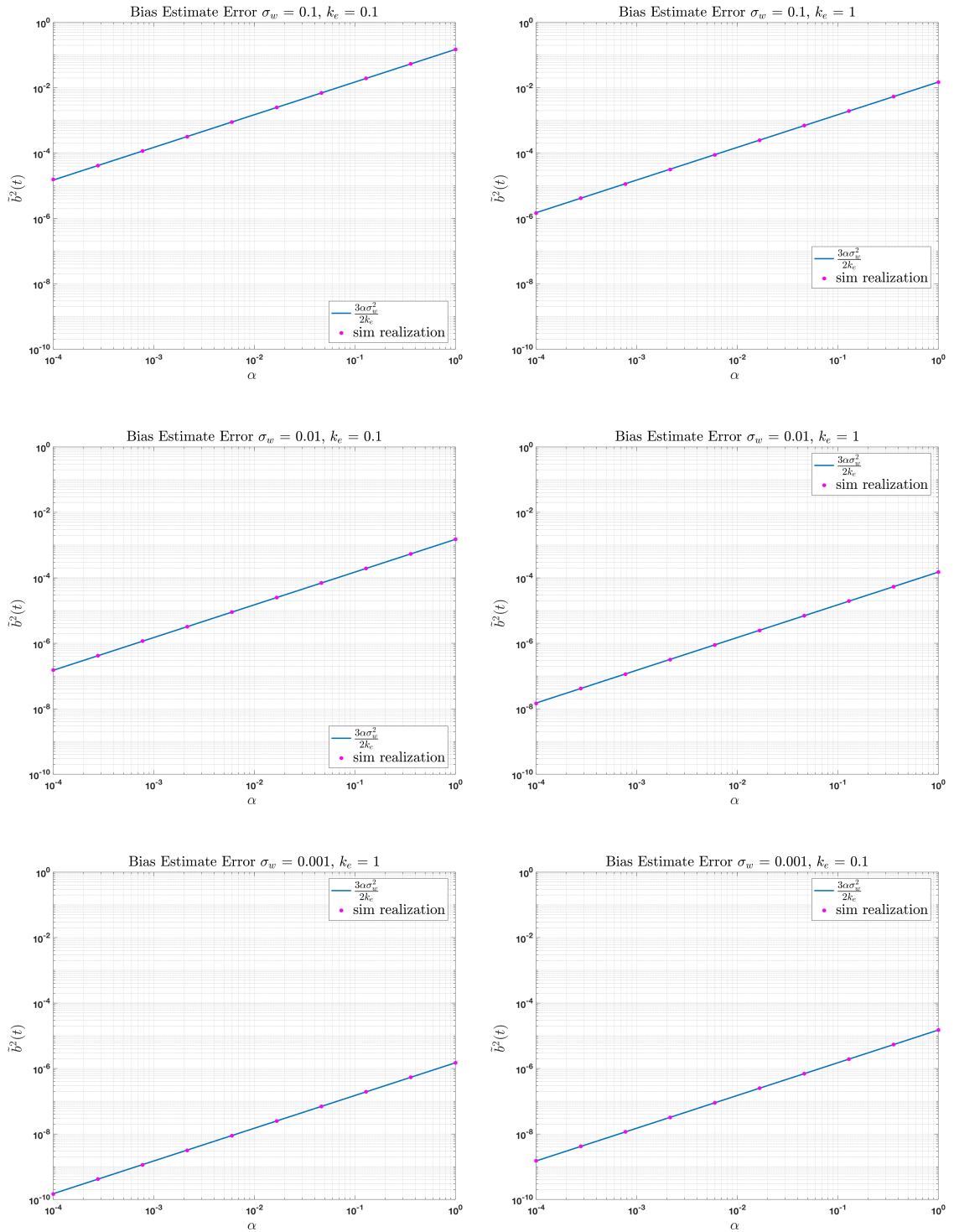


Figure 5.16: Comparison of simulation realizations of the bias estimate error variance with the analytic solution for a range of adaptation gain parameters α .

Chapter 6: Attitude Measurement Noise

This chapter extends the analysis of Chapters 4 and 5 by considering attitude measurement noise. Section 6.1 introduces a measurement noise model that obeys the quaternion norm constraint and will be used throughout the chapter. Specifically, the Itô SDE for the attitude noise filter of Chapter 4 is used to provide a continuous time process whose ultimate noise density is a bipolar Bingham distribution which can be specified to model an attitude measurement sensor.

Section 6.2 extends the gyro additive noise measurement model analysis of Chapter 4 by also including the attitude measurement noise model of Section 6.1. An Itô SDE for the filter state is formulated and augmented by the attitude measurement process noise model in Section 6.2.1 to provide a complete mathematical description of the system. Section 6.2.2 uses a stochastic Lyapunov analysis to find conditions needed to ensure weak stochastic stability of the $SO(3)$ system as well as stochastic Lyapunov performance bounds, which are then examined numerically in Section 6.2.3. The system is then reduced to the $SO(2)$ case in Section 6.2.4. The $SO(2)$ stationary Fokker-Planck PDE again proves to be tractable in Section 6.2.7, yielding analytic expressions for the ultimate attitude estimate error mean and variance which are verified via simulation analysis in Section 6.2.8. Similar to Sections

4.10 and 5.7, Section 6.2.9 provides bounds for the ultimate attitude estimate error mean and variance for the SO(3) case by extrapolating the SO(2) results of Section 6.2.7.

Section 6.3 extends the analysis of Section 6.2 by further including the gyro constant bias as in Chapter 5. Similar to the analysis of Section 5.5, a Fokker-Planck analysis of the reduced system in SO(2) finds that a particular extension of the stationary probability density function from Section 6.2 can be made to asymptotically approach a solution to the stationary Fokker-Planck PDE of this Section. The asymptotic solution to the SO(2) stationary Fokker-Planck PDE for this system is then used to find analytic expressions for the ultimate attitude estimate error variance as well as the ultimate gyro bias estimate error mean and variance. The results are verified via numerical simulation. Bounds for the filter's ultimate attitude estimate error variance as well as the filter's ultimate gyro bias estimate error mean and variance in the SO(3) case are provided by extrapolating the SO(2) results.

6.1 Quaternion Measurement Noise Model

This section develops a quaternion measurement noise process suitable for modeling attitude measurement noise. The measurement noise model will be used in the remaining sections of this chapter.

The general form of the nonlinear attitude estimation dynamics considered in this thesis is given by

$$\dot{\hat{\mathbf{q}}}(t) = \frac{1}{2} \left\{ R(\tilde{\mathbf{q}}^{-1}(t)) \left[\boldsymbol{\omega}_g(t) + k_e \tilde{\eta}(t) \tilde{\boldsymbol{\varepsilon}}(t) \right] \right\} \otimes \hat{\mathbf{q}}(t)$$

which depends on the attitude estimate error

$$\tilde{\mathbf{q}}(t) = \begin{bmatrix} \tilde{\boldsymbol{\varepsilon}}(t) \\ \tilde{\eta}(t) \end{bmatrix} = \mathbf{q}(t) \otimes \hat{\mathbf{q}}^{-1}(t)$$

The true attitude estimate error was assumed to be available to the estimator in Chapters 4 and 5 as the attitude measurements were assumed perfect in those chapters.

This chapter considers the case of attitude measurement noise, so the estimators no longer have direct access to the true attitude $\mathbf{q}(t)$; instead, in this chapter the estimators will only have access to a noise corrupted version

$$\mathbf{q}_m(t) = \begin{bmatrix} \boldsymbol{\varepsilon}_m(t) \\ \eta_m(t) \end{bmatrix} = \check{\mathbf{q}}^{-1}(t) \otimes \mathbf{q}(t) \quad (6.1)$$

where $\check{\mathbf{q}}(t)$ is “quaternion noise”. Thus the true attitude estimate error $\tilde{\mathbf{q}}(t)$ will no longer be available to the estimation algorithms. The estimators will now have to

use the noise corrupted attitude estimate error

$$\begin{aligned}
\tilde{\mathbf{q}}_m(t) &= \begin{bmatrix} \tilde{\boldsymbol{\varepsilon}}_m(t) \\ \tilde{\boldsymbol{\eta}}_m(t) \end{bmatrix} \\
&= \mathbf{q}_m(t) \otimes \hat{\mathbf{q}}^{-1}(t) \\
&= \check{\mathbf{q}}^{-1}(t) \otimes \mathbf{q}(t) \otimes \hat{\mathbf{q}}^{-1}(t) \\
&= \check{\mathbf{q}}^{-1}(t) \otimes \tilde{\mathbf{q}}(t)
\end{aligned}$$

The theoretical tools used in this thesis assume the error dynamics under consideration may be formulated as an Itô SDE; namely that the error dynamics are affine in the driving noise, and further that the driving noise is zero mean and normally distributed. The construction of a continuous time quaternion measurement noise model that is restricted to the unit quaternion hypersphere and is affine in the driving noise does not appear to exist in the literature. A common attitude measurement model [64, 66] is given by

$$\mathbf{q}_m(t) = \delta\mathbf{q}\left(\sigma_m \mathbf{n}_m(t)\right) \otimes \mathbf{q}(t)$$

where $\delta\mathbf{q}\left(\cdot\right)$ is a unit quaternion parameterized by a small angle $\sigma_m \mathbf{n}_m(\cdot)$ where $\mathbf{n}_m(\cdot)$ is a zero mean unit variance Gaussian white noise process in \mathbb{R}^3 . Various parameterization choices for the mapping $\delta\mathbf{q}\left(\cdot\right)$ exist [64] (such as Gibbs parameters, modified Rodrigues parameters, the rotation vector, or even Euler angles), however all are highly nonlinear functions of their input arguments and thus these attitude measurement models can not be expressed as an affine function of the driving noise. As this common model can not be expressed as an affine function of the

driving noise, the model can not be written as an Itô SDE and thus none of the stochastic Lyapunov analysis techniques of Section 2.1.4, nor the stochastic numerical integration methods of Section 2.2, are applicable. Another approach, used by Choukroun [13], is given as

$$d\mathbf{q}_m(t) = \mathbf{q}(t)dt + \sigma_q \mathbf{n}_q(t)$$

where the driving noise is modeled by $\mathbf{n}_q(\cdot)$, a zero mean unit variance Gaussian white noise process in \mathbb{R}^4 . Note that this model does not restrict the quaternion measurements to have unit norm which in turn means they *do not parameterize a rotation*. As the normalization operation is also highly nonlinear, enforcing the normalization constraint would similarly prevent this model from being written as an Itô SDE.

Note that the analysis of Chapter 4 did, however, identify a continuous time quaternion process that was restricted to the unit quaternion hypersphere and was affine in the driving noise (and thus an Itô SDE). Rearranging the attitude measurement model of Equation 6.1 to solve for the noise quaternion yields

$$\check{\mathbf{q}}(t) = \mathbf{q}(t) \otimes \mathbf{q}_m^{-1}(t) \tag{6.2}$$

which is precisely the form of the attitude estimate error computation used in Equation 4.4. Thus the attitude filter dynamics of Equation 4.3 can be used here to provide a SDE to serve as the dynamical model for the quaternion noise and all the results of Chapter 4 may be leveraged to understand the properties of the model. With this choice, attitude measurement evolves according to the Langevin form

differential equation

$$\dot{\mathbf{q}}_m(t) = \frac{1}{2} \left\{ R(\check{\mathbf{q}}^{-1}(t)) [\boldsymbol{\omega}(t) + \sigma_m \mathbf{n}_m(t) + k_m \check{\eta}(t) \check{\boldsymbol{\varepsilon}}(t)] \right\} \otimes \mathbf{q}_m(t) \quad (6.3)$$

where k_m and σ_m are positive scalars that parameterize the attitude measurement noise statistics and $\mathbf{n}_m(\cdot)$ is a collection of independent identically distributed zero mean unit variance Gaussian white noise processes independent of gyro noise $\mathbf{n}_w(\cdot)$.

The attitude measurement noise error dynamics are given by

$$\begin{aligned} \dot{\check{\mathbf{q}}}(t) &= \frac{1}{2} \left\{ -k_m \check{\eta}(t) \check{\boldsymbol{\varepsilon}}(t) - \sigma_m \mathbf{n}_m(t) \right\} \otimes \check{\mathbf{q}}(t) \\ &= \begin{bmatrix} -\frac{1}{2} k_m \check{\eta}^2(t) \check{\boldsymbol{\varepsilon}}(t) \\ \frac{1}{2} k_m \check{\eta}(t) \check{\boldsymbol{\varepsilon}}^T(t) \check{\boldsymbol{\varepsilon}}(t) \end{bmatrix} + \begin{bmatrix} -\frac{1}{2} \left\{ \check{\eta}(t) I + [\check{\boldsymbol{\varepsilon}}(t) \times] \right\} \sigma_m \\ \frac{1}{2} \check{\boldsymbol{\varepsilon}}^T(t) \sigma_m \end{bmatrix} \mathbf{n}_m(t) \end{aligned} \quad (6.4)$$

The attitude measurement noise model of Equation 6.4 can be viewed in this context as a coloring filter. The model is driven by the unbounded white noise process $\mathbf{n}_m(\cdot)$ but the attitude measurement noise state $\check{\mathbf{q}}(t)$ remains on the unit quaternion hypersphere.

Again note the error dynamics share precisely the same structure as the error dynamics of the previous chapter's filter of Equation 4.5; the results of Section 4.11 imply that the quaternion noise model asymptotically approaches a stationary density given by a bipolar Bingham distribution that is parameterized by the ratio $\frac{k_m}{\sigma_m^2}$. Specifically, the attitude measurement noise has ultimate mean

$$\lim_{t \rightarrow \infty} E[\check{\boldsymbol{\varepsilon}}(t)] = \mathbf{0}$$

the ultimate variance

$$\nu \left(\frac{k_m}{\sigma_m^2} \right) = \lim_{t \rightarrow \infty} E[\check{\boldsymbol{\varepsilon}}^T(t) \check{\boldsymbol{\varepsilon}}(t)] = \frac{3I_0 \left(\frac{k_m}{\sigma_m^2} \right) - 4I_1 \left(\frac{k_m}{\sigma_m^2} \right) + I_2 \left(\frac{k_m}{\sigma_m^2} \right)}{4 \left(I_0 \left(\frac{k_m}{\sigma_m^2} \right) - I_1 \left(\frac{k_m}{\sigma_m^2} \right) \right)}$$

and ultimate covariance matrix

$$\lim_{t \rightarrow \infty} E[\check{\mathbf{q}}(t)\check{\mathbf{q}}^T(t)] = \text{diag} \left(\frac{1}{3}\nu \left(\frac{k_m}{\sigma_m^2} \right), \frac{1}{3}\nu \left(\frac{k_m}{\sigma_m^2} \right), \frac{1}{3}\nu \left(\frac{k_m}{\sigma_m^2} \right), 1 - \nu \left(\frac{k_m}{\sigma_m^2} \right) \right)$$

6.2 Attitude Estimation Filter for Gyro Additive Noise and Attitude Measurement Noise

This section extends the gyro additive noise measurement model analysis of Chapter 4 by also including attitude measurement noise. Section 6.2.1 presents the filter formulation and noise models, culminating in an Itô SDE for the system error dynamics. The next section, Section 6.2.2, contains a stochastic Lyapunov analysis that derives conditions needed to ensure weak stochastic stability of the $SO(3)$ system as well as stochastic Lyapunov performance bounds. Section 6.2.3 includes a numerical simulation analysis of the $SO(3)$ error dynamics.

The system is then reduced to the $SO(2)$ case in Section 6.2.4. The $SO(2)$ stationary Fokker-Planck PDE again proves to be tractable in Section 6.2.7, yielding analytic expressions for the ultimate attitude estimate error mean and variance. These results are verified via simulation analysis in Section 6.2.8. Similar to Sections 4.10 and 5.7, Section 6.2.9 provides bounds for the ultimate attitude estimate error mean and variance for the $SO(3)$ case by extrapolating the $SO(2)$ results of Section 6.2.7.

6.2.1 Filter Formulation in SO(3)

This subsection develops a formulation for the attitude estimation filter with gyro additive noise and attitude measurement noise. The attitude measurement model is given in Section 6.1.

The angular rate gyro measurement model is the same as in Chapter 4, which is repeated here for convenience

$$\boldsymbol{\omega}_g(t) = \boldsymbol{\omega}(t) + \sigma_w \mathbf{n}_w(t) \quad (6.5)$$

where $\boldsymbol{\omega}_g(t)$ is the gyro measurement of the true vehicle angular rate $\boldsymbol{\omega}(t)$ at time t , σ_w is a positive scaling constant, and $\mathbf{n}_w(\cdot)$ is a zero mean unit variance Gaussian white noise process.

As explained in Section 6.1, if the filter had access to the true attitude, it could use the filter attitude estimate error $\tilde{\mathbf{q}}(t) = \begin{bmatrix} \tilde{\boldsymbol{\epsilon}}(t) \\ \tilde{\boldsymbol{\eta}}(t) \end{bmatrix} = \mathbf{q}(t) \otimes \hat{\mathbf{q}}^{-1}(t)$ to drive its kinematics as in Equation 4.3; however, in this chapter the filter only has access to attitude measurements corrupted by noise. Thus the filter kinematics equation is given as

$$\dot{\hat{\mathbf{q}}}(t) = \frac{1}{2} \left\{ R(\tilde{\mathbf{q}}_m^{-1}(t)) \left[\boldsymbol{\omega}_g(t) + k_e \tilde{\boldsymbol{\eta}}_m(t) \tilde{\boldsymbol{\epsilon}}_m(t) \right] \right\} \otimes \hat{\mathbf{q}}(t) \quad (6.6)$$

which is driven by

$$\begin{aligned}
\tilde{\mathbf{q}}_m(t) &= \begin{bmatrix} \tilde{\boldsymbol{\epsilon}}_m(t) \\ \tilde{\eta}_m(t) \end{bmatrix} = \mathbf{q}_m(t) \otimes \hat{\mathbf{q}}^{-1}(t) \\
&= \check{\mathbf{q}}^{-1}(t) \otimes \mathbf{q}(t) \otimes \hat{\mathbf{q}}^{-1}(t) \\
&= \check{\mathbf{q}}^{-1}(t) \otimes \tilde{\mathbf{q}}(t)
\end{aligned}$$

Expanding the expression $\tilde{\eta}_m(t)\tilde{\boldsymbol{\epsilon}}_m(t)$ yields

$$\tilde{\eta}_m(t)\tilde{\boldsymbol{\epsilon}}_m(t) = \left(\check{\eta}(t)\tilde{\eta} + \check{\boldsymbol{\epsilon}}^T(t)\tilde{\boldsymbol{\epsilon}}(t) \right) \begin{bmatrix} -\tilde{\eta}(t)\check{\boldsymbol{\epsilon}}(t) + \check{\eta}(t)\tilde{\boldsymbol{\epsilon}}(t) + \check{\boldsymbol{\epsilon}}(t) \times \tilde{\boldsymbol{\epsilon}}(t) \end{bmatrix} \quad (6.7)$$

which simplifies to $\tilde{\eta}(t)\tilde{\boldsymbol{\epsilon}}(t)$ when there is no attitude noise, i.e. when $\check{\mathbf{q}}^T(t) = [\check{\boldsymbol{\epsilon}}^T(t) \quad \check{\eta}(t)] = [0 \ 0 \ 0 \ \pm 1]^T$.

The attitude filter dynamics given by Equation 6.6 can be combined with the quaternion error kinematics of Equation 2.71 and the gyro measurement model from Equation 6.5 to find the filter's attitude estimate error dynamics

$$\begin{aligned}
\dot{\tilde{\mathbf{q}}}(t) &= \frac{1}{2} \left\{ \boldsymbol{\omega}(t) - R(\tilde{\mathbf{q}}(t))R(\tilde{\mathbf{q}}_m^{-1}(t)) \left[\boldsymbol{\omega}_g(t) + k_e \tilde{\eta}_m(t)\tilde{\boldsymbol{\epsilon}}_m(t) \right] \right\} \otimes \tilde{\mathbf{q}}(t) \\
&= \frac{1}{2} \left\{ \boldsymbol{\omega}(t) - R(\tilde{\mathbf{q}}(t))R(\tilde{\mathbf{q}}^{-1}(t))R(\check{\mathbf{q}}(t)) \left[\boldsymbol{\omega}(t) + \sigma_w \mathbf{n}_w(t) + k_e \tilde{\eta}_m(t)\tilde{\boldsymbol{\epsilon}}_m(t) \right] \right\} \otimes \tilde{\mathbf{q}}(t) \\
&= \frac{1}{2} \left\{ \left[I - R(\check{\mathbf{q}}(t)) \right] \boldsymbol{\omega}(t) - R(\check{\mathbf{q}}(t)) \left[k_e \tilde{\eta}_m(t)\tilde{\boldsymbol{\epsilon}}_m(t) + \sigma_w \mathbf{n}_w(t) \right] \right\} \otimes \tilde{\mathbf{q}}(t) \quad (6.8)
\end{aligned}$$

which is not independent of the vehicle's angular rate $\boldsymbol{\omega}(t)$. This is in contrast to the filter attitude estimate error dynamics of Equation 4.5 in the perfect attitude measurement case. Since the attitude filter in this chapter must rely on noise corrupted attitude measurements, it is not able to perfectly resolve the filter's angular rate estimate in the appropriate frame.

Combining the attitude noise model error dynamics of Equation 6.4, the filter attitude estimate error dynamics of Equation 6.8, and suppressing function of time notation for brevity, the Langevin form error dynamics are found as

$$\begin{aligned}
 \begin{bmatrix} \dot{\tilde{\mathbf{e}}} \\ \dot{\tilde{\eta}} \\ \dot{\tilde{\mathbf{e}}} \\ \dot{\tilde{\eta}} \end{bmatrix} &= \begin{bmatrix} -\frac{1}{2}k_m\check{\eta}^2\check{\tilde{\mathbf{e}}} \\ \frac{1}{2}k_m\check{\eta}\check{\tilde{\mathbf{e}}}^T\check{\tilde{\mathbf{e}}} \\ \frac{1}{2}\left[\check{\eta}I + [\check{\tilde{\mathbf{e}}}\times]\right]\left[I - R(\check{\mathbf{q}})\right]\boldsymbol{\omega} - \frac{1}{2}k_e\left[\check{\eta}I + [\check{\tilde{\mathbf{e}}}\times]\right]R(\check{\mathbf{q}})\check{\eta}_m\check{\tilde{\mathbf{e}}}_m \\ -\frac{1}{2}\check{\tilde{\mathbf{e}}}^T\left[I - R(\check{\mathbf{q}})\right]\boldsymbol{\omega} + \frac{1}{2}k_e\check{\tilde{\mathbf{e}}}^TR(\check{\mathbf{q}})\check{\eta}_m\check{\tilde{\mathbf{e}}}_m \end{bmatrix} \\
 &+ \begin{bmatrix} -\frac{1}{2}\left[\check{\eta}I + [\check{\tilde{\mathbf{e}}}\times]\right]\sigma_m & 0 \\ \frac{1}{2}\check{\tilde{\mathbf{e}}}^T\sigma_m & 0 \\ 0 & -\frac{1}{2}\left[\check{\eta}I + [\check{\tilde{\mathbf{e}}}\times]\right]R(\check{\mathbf{q}})\sigma_w \\ 0 & \frac{1}{2}\check{\tilde{\mathbf{e}}}^TR(\check{\mathbf{q}})\sigma_w \end{bmatrix} \begin{bmatrix} \mathbf{n}_m \\ \mathbf{n}_w \end{bmatrix} \quad (6.9)
 \end{aligned}$$

where $\check{\eta}_m\check{\tilde{\mathbf{e}}}_m$ is expanded in Equation 6.7.

As discussed in Section 2.1.3, the Langevin form error dynamics differential equation 6.9 is interpreted as a Stratonovich SDE. Converting to an Itô SDE results

in the following

$$\begin{aligned}
\begin{bmatrix} d\check{\boldsymbol{\varepsilon}} \\ d\check{\eta} \\ d\check{\boldsymbol{\varepsilon}} \\ d\check{\eta} \end{bmatrix} &= \begin{bmatrix} -\frac{1}{2}k_m\check{\eta}^2\check{\boldsymbol{\varepsilon}} - \frac{3}{8}\sigma_m^2\check{\boldsymbol{\varepsilon}} \\ \frac{1}{2}k_m\check{\eta}\check{\boldsymbol{\varepsilon}}^T\check{\boldsymbol{\varepsilon}} - \frac{3}{8}\sigma_m^2\check{\eta} \\ \frac{1}{2}[\check{\eta}I + [\check{\boldsymbol{\varepsilon}} \times]] [I - R(\check{\boldsymbol{q}})] \boldsymbol{\omega} - \frac{1}{2}k_e [\check{\eta}I + [\check{\boldsymbol{\varepsilon}} \times]] R(\check{\boldsymbol{q}}) \check{\eta}_m \check{\boldsymbol{\varepsilon}}_m - \frac{3}{8}\sigma_w^2 \check{\boldsymbol{\varepsilon}} \\ -\frac{1}{2}\check{\boldsymbol{\varepsilon}}^T [I - R(\check{\boldsymbol{q}})] \boldsymbol{\omega} + \frac{1}{2}k_e \check{\boldsymbol{\varepsilon}}^T R(\check{\boldsymbol{q}}) \check{\eta}_m \check{\boldsymbol{\varepsilon}}_m - \frac{3}{8}\sigma_w^2 \check{\eta} \end{bmatrix} dt \\
&+ \begin{bmatrix} -\frac{1}{2}[\check{\eta}I + [\check{\boldsymbol{\varepsilon}} \times]] \sigma_m & 0 \\ \frac{1}{2}\check{\boldsymbol{\varepsilon}}^T \sigma_m & 0 \\ 0 & -\frac{1}{2}[\check{\eta}I + [\check{\boldsymbol{\varepsilon}} \times]] R(\check{\boldsymbol{q}}) \sigma_w \\ 0 & \frac{1}{2}\check{\boldsymbol{\varepsilon}}^T R(\check{\boldsymbol{q}}) \sigma_w \end{bmatrix} \begin{bmatrix} d\boldsymbol{\beta}_m \\ d\boldsymbol{\beta}_w \end{bmatrix} \\
&= \boldsymbol{f}(\tilde{\boldsymbol{x}}) dt + G(\tilde{\boldsymbol{x}}) d\boldsymbol{\beta} \tag{6.10}
\end{aligned}$$

where $\tilde{\boldsymbol{x}}^T = [\check{\boldsymbol{\varepsilon}}^T \quad \check{\eta} \quad \check{\boldsymbol{\varepsilon}}^T \quad \check{\eta}]$.

6.2.2 Stochastic Lyapunov Analysis in SO(3)

In this section, stochastic Lyapunov theory is used to show the Itô error SDE 6.10 is weakly stochastically stable provided the vehicle angular rate is bounded. A generalized moment ultimate bound for the attitude filter is found which can be used as a performance metric. An ultimate bound for $\tilde{\boldsymbol{\epsilon}}^T(t)\tilde{\boldsymbol{\epsilon}}(t)$ is also established.

Theorem 6.2.1. *The attitude error dynamics of the Itô SDE 6.10 are weakly stochastically stable provided the vehicle angular rate is bounded, $\|\boldsymbol{\omega}(t)\| < \omega_{max} < \infty \quad \forall t$. Further, the attitude error dynamics are such that*

$$\begin{aligned} \lim_{t \rightarrow \infty} E & \left[k_m \check{\eta}^2(t) \check{\boldsymbol{\epsilon}}^T(t) \check{\boldsymbol{\epsilon}}(t) + \sigma_m^2 \check{\boldsymbol{\epsilon}}^T(t) \check{\boldsymbol{\epsilon}}(t) + \sigma_w^2 \tilde{\boldsymbol{\epsilon}}^T(t) \tilde{\boldsymbol{\epsilon}}(t) \right. \\ & + k_e \tilde{\eta}^2(t) \tilde{\boldsymbol{\epsilon}}^T(t) \tilde{\boldsymbol{\epsilon}}(t) \left(\check{\boldsymbol{\epsilon}}^T(t) \tilde{\boldsymbol{\epsilon}}(t) \right)^2 + k_e \tilde{\eta}^2(t) \check{\eta}^4(t) \tilde{\boldsymbol{\epsilon}}^T(t) \tilde{\boldsymbol{\epsilon}}(t) \\ & \left. + k_e \check{\eta}^2(t) \tilde{\eta}^2(t) \|\check{\boldsymbol{\epsilon}}(t) \times \tilde{\boldsymbol{\epsilon}}(t)\|^2 + k_e \check{\eta}^2(t) \tilde{\eta}^2(t) \left(\check{\boldsymbol{\epsilon}}^T(t) \tilde{\boldsymbol{\epsilon}}(t) \right)^2 \right] \\ & \leq 5k_e + 2\omega_{max} + \frac{3}{4}\sigma_m^2 + \frac{3}{4}\sigma_w^2 \end{aligned} \quad (6.11)$$

Proof. Choose as a Lyapunov function

$$V(t) = \frac{1}{2} \check{\boldsymbol{\epsilon}}^T(t) \check{\boldsymbol{\epsilon}}(t) + \frac{1}{2} \tilde{\boldsymbol{\epsilon}}^T(t) \tilde{\boldsymbol{\epsilon}}(t)$$

Application of the differential generator to the Lyapunov function with respect to the Itô SDE 6.10 is computed according to

$$\mathcal{L}V(t) = \left(\frac{\partial V}{\partial \tilde{\boldsymbol{x}}} \right)^T \mathbf{f}(\tilde{\boldsymbol{x}}(t)) + \frac{1}{2} \text{tr} \left\{ G^T(\tilde{\boldsymbol{x}}(t)) \frac{\partial^2 V}{\partial \tilde{\boldsymbol{x}}^2} G(\tilde{\boldsymbol{x}}(t)) \right\}$$

which is rather involved for this system, so each term is computed in sequence.

Suppressing function of time notation for clarity, the first term is found as

$$\begin{aligned}
\left(\frac{\partial V}{\partial \tilde{\mathbf{x}}}\right)^T \mathbf{f}(\tilde{\mathbf{x}}) &= -\frac{1}{2}k_m \tilde{\eta}^2 \check{\boldsymbol{\epsilon}}^T \check{\boldsymbol{\epsilon}} - \frac{3}{8}\sigma_m^2 \check{\boldsymbol{\epsilon}}^T \check{\boldsymbol{\epsilon}} - \frac{3}{8}\sigma_w^2 \check{\boldsymbol{\epsilon}}^T \check{\boldsymbol{\epsilon}} \\
&\quad + \frac{1}{2}\tilde{\boldsymbol{\epsilon}}^T \left[\tilde{\eta} I + [\tilde{\boldsymbol{\epsilon}} \times] \right] \left[I - R(\check{\mathbf{q}}) \right] \boldsymbol{\omega} \\
&\quad - \frac{1}{2}k_e \check{\boldsymbol{\epsilon}}^T \left[\tilde{\eta} I + [\tilde{\boldsymbol{\epsilon}} \times] \right] R(\check{\mathbf{q}}) (\tilde{\eta} \tilde{\boldsymbol{\eta}} + \check{\boldsymbol{\epsilon}}^T \tilde{\boldsymbol{\epsilon}}) \left[-\tilde{\eta} \check{\boldsymbol{\epsilon}} + \tilde{\eta} \tilde{\boldsymbol{\epsilon}} + \check{\boldsymbol{\epsilon}} \times \tilde{\boldsymbol{\epsilon}} \right] \\
&= -\frac{1}{2}k_m \tilde{\eta}^2 \check{\boldsymbol{\epsilon}}^T \check{\boldsymbol{\epsilon}} - \frac{3}{8}\sigma_m^2 \check{\boldsymbol{\epsilon}}^T \check{\boldsymbol{\epsilon}} - \frac{3}{8}\sigma_w^2 \check{\boldsymbol{\epsilon}}^T \check{\boldsymbol{\epsilon}} \\
&\quad + \frac{1}{2}\tilde{\eta} \tilde{\boldsymbol{\epsilon}}^T \left[I - R(\check{\mathbf{q}}) \right] \boldsymbol{\omega} \\
&\quad - \frac{1}{2}k_e (\tilde{\eta} \tilde{\boldsymbol{\eta}} + \check{\boldsymbol{\epsilon}}^T \tilde{\boldsymbol{\epsilon}}) \tilde{\eta} \check{\boldsymbol{\epsilon}}^T R(\check{\mathbf{q}}) \left[-\tilde{\eta} \check{\boldsymbol{\epsilon}} + \tilde{\eta} \tilde{\boldsymbol{\epsilon}} + \check{\boldsymbol{\epsilon}} \times \tilde{\boldsymbol{\epsilon}} \right]
\end{aligned}$$

where the second equality holds since $\tilde{\boldsymbol{\epsilon}}^T [\tilde{\boldsymbol{\epsilon}} \times] = \mathbf{0}^T$.

To compute the trace term, first note by the cyclic property of the trace operator

$$\text{tr} \left\{ G^T \frac{\partial^2 V}{\partial \tilde{\mathbf{x}}^2} G \right\} = \text{tr} \left\{ G G^T \frac{\partial^2 V}{\partial \tilde{\mathbf{x}}^2} \right\}$$

Using the rotation matrix property $R(\check{\mathbf{q}}) R^T(\check{\mathbf{q}}) = I$, the expression evaluates as

$$\frac{1}{2} \text{tr} \left\{ G^T \frac{\partial^2 V}{\partial \tilde{\mathbf{x}}^2} G \right\} = \frac{3}{8}\sigma_m^2 \tilde{\eta}^2 + \frac{1}{4}\sigma_m^2 \check{\boldsymbol{\epsilon}}^T \check{\boldsymbol{\epsilon}} + \frac{3}{8}\sigma_w^2 \tilde{\eta}^2 + \frac{1}{4}\sigma_w^2 \check{\boldsymbol{\epsilon}}^T \check{\boldsymbol{\epsilon}}$$

Combining the two terms and using the quaternion normalization constraints

$\tilde{\eta}^2 + \check{\boldsymbol{\epsilon}}^T \check{\boldsymbol{\epsilon}} = 1$ and $\tilde{\eta}^2 + \tilde{\boldsymbol{\epsilon}}^T \tilde{\boldsymbol{\epsilon}} = 1$ yields

$$\begin{aligned}
\mathcal{L}V &= -\frac{1}{2}k_m \tilde{\eta}^2 \check{\boldsymbol{\epsilon}}^T \check{\boldsymbol{\epsilon}} - \frac{1}{2}\sigma_m^2 \check{\boldsymbol{\epsilon}}^T \check{\boldsymbol{\epsilon}} - \frac{1}{2}\sigma_w^2 \check{\boldsymbol{\epsilon}}^T \check{\boldsymbol{\epsilon}} \\
&\quad - \frac{1}{2}k_e (\tilde{\eta} \tilde{\boldsymbol{\eta}} + \check{\boldsymbol{\epsilon}}^T \tilde{\boldsymbol{\epsilon}}) \tilde{\eta} R(\check{\mathbf{q}}) \left[-\tilde{\eta} \check{\boldsymbol{\epsilon}} + \tilde{\eta} \tilde{\boldsymbol{\epsilon}} + \check{\boldsymbol{\epsilon}} \times \tilde{\boldsymbol{\epsilon}} \right] \\
&\quad + \frac{1}{2}\tilde{\eta} \tilde{\boldsymbol{\epsilon}}^T \left[I - R(\check{\mathbf{q}}) \right] \boldsymbol{\omega} + \frac{3}{8}\sigma_m^2 + \frac{3}{8}\sigma_w^2
\end{aligned}$$

Expanding out the fourth term's rotation matrix $R(\check{\mathbf{q}})$ in terms of $\check{\boldsymbol{\epsilon}}$ and $\tilde{\eta}$ according

to Equation 2.64 and simplifying leads to

$$\begin{aligned}
\mathcal{L}V &= -\frac{1}{2}k_m\check{\eta}^2\check{\epsilon}^T\check{\epsilon} - \frac{1}{2}\sigma_m^2\check{\epsilon}^T\check{\epsilon} - \frac{1}{2}\sigma_w^2\check{\epsilon}^T\check{\epsilon} \\
&\quad - \frac{1}{2}k_e(\check{\eta}\check{\eta} + \check{\epsilon}^T\check{\epsilon})\check{\eta}\left(-\check{\eta}\check{\epsilon}^T\check{\epsilon} + \check{\eta}^3\check{\epsilon}^T\check{\epsilon} + \check{\eta}\|\check{\epsilon} \times \check{\epsilon}\|^2 + \check{\eta}(\check{\epsilon}^T\check{\epsilon})^2\right) \\
&\quad + \frac{1}{2}\check{\eta}\check{\epsilon}^T\left[I - R(\check{q})\right]\omega + \frac{3}{8}\sigma_m^2 + \frac{3}{8}\sigma_w^2 \\
&= -\frac{1}{2}k_m\check{\eta}^2\check{\epsilon}^T\check{\epsilon} - \frac{1}{2}\sigma_m^2\check{\epsilon}^T\check{\epsilon} - \frac{1}{2}\sigma_w^2\check{\epsilon}^T\check{\epsilon} \\
&\quad - \frac{1}{2}k_e\check{\eta}^2\check{\epsilon}^T\check{\epsilon}(\check{\epsilon}^T\check{\epsilon})^2 - \frac{1}{2}k_e\check{\eta}^2\check{\eta}^4\check{\epsilon}^T\check{\epsilon} - \frac{1}{2}k_e\check{\eta}^2\check{\eta}^2\|\check{\epsilon} \times \check{\epsilon}\|^2 - \frac{1}{2}k_e\check{\eta}^2\check{\eta}^2(\check{\epsilon}^T\check{\epsilon})^2 \\
&\quad + \frac{1}{2}k_e\check{\eta}\check{\eta}^3\check{\epsilon}^T\check{\epsilon} + \frac{1}{2}k_e(\check{\epsilon}^T\check{\epsilon})^2 - \frac{1}{2}k_e\check{\eta}\check{\eta}^3\check{\epsilon}^T\check{\epsilon}\check{\epsilon}^T\check{\epsilon} - \frac{1}{2}k_e\check{\eta}\check{\eta}\check{\epsilon}^T\check{\epsilon}\|\check{\epsilon} \times \check{\epsilon}\|^2 - \frac{1}{2}k_e\check{\eta}\check{\eta}(\check{\epsilon}^T\check{\epsilon})^3 \\
&\quad + \frac{1}{2}\check{\eta}\check{\epsilon}^T\left[I - R(\check{q})\right]\omega + \frac{3}{8}\sigma_m^2 + \frac{3}{8}\sigma_w^2
\end{aligned}$$

Noting that $\|I - R(\check{q})\| = \sqrt{\lambda_{\max}[4(\check{\epsilon}^T\check{\epsilon}I - \check{\epsilon}\check{\epsilon}^T)]} = 2\|\check{\epsilon}\|$ and using $|\check{\eta}| \leq 1$

and $|\check{\eta}| \leq 1$, $\mathcal{L}V$ can be bound as

$$\begin{aligned}
\mathcal{L}V &\leq -\frac{1}{2}k_m\check{\eta}^2\check{\epsilon}^T\check{\epsilon} - \frac{1}{2}\sigma_m^2\check{\epsilon}^T\check{\epsilon} - \frac{1}{2}\sigma_w^2\check{\epsilon}^T\check{\epsilon} \\
&\quad - \frac{1}{2}k_e\check{\eta}^2\check{\epsilon}^T\check{\epsilon}(\check{\epsilon}^T\check{\epsilon})^2 - \frac{1}{2}k_e\check{\eta}^2\check{\eta}^4\check{\epsilon}^T\check{\epsilon} - \frac{1}{2}k_e\check{\eta}^2\check{\eta}^2\|\check{\epsilon} \times \check{\epsilon}\|^2 - \frac{1}{2}k_e\check{\eta}^2\check{\eta}^2(\check{\epsilon}^T\check{\epsilon})^2 \\
&\quad + \frac{1}{2}k_e\|\check{\epsilon}\|\|\check{\epsilon}\| + \frac{1}{2}k_e\|\check{\epsilon}\|^2\|\check{\epsilon}\|^2 + \frac{1}{2}k_e\|\check{\epsilon}\|\|\check{\epsilon}\|^3 + \frac{1}{2}k_e\|\check{\epsilon}\|\|\check{\epsilon}\|\|\check{\epsilon} \times \check{\epsilon}\|^2 \\
&\quad + \frac{1}{2}k_e\|\check{\epsilon}\|^3\|\check{\epsilon}\|^3 + \|\check{\epsilon}\|\|\check{\epsilon}\|\|\omega\| + \frac{3}{8}\sigma_m^2 + \frac{3}{8}\sigma_w^2 \\
&\leq -\frac{1}{2}k_m\check{\eta}^2\check{\epsilon}^T\check{\epsilon} - \frac{1}{2}\sigma_m^2\check{\epsilon}^T\check{\epsilon} - \frac{1}{2}\sigma_w^2\check{\epsilon}^T\check{\epsilon} \\
&\quad - \frac{1}{2}k_e\check{\eta}^2\check{\epsilon}^T\check{\epsilon}(\check{\epsilon}^T\check{\epsilon})^2 - \frac{1}{2}k_e\check{\eta}^2\check{\eta}^4\check{\epsilon}^T\check{\epsilon} - \frac{1}{2}k_e\check{\eta}^2\check{\eta}^2\|\check{\epsilon} \times \check{\epsilon}\|^2 - \frac{1}{2}k_e\check{\eta}^2\check{\eta}^2(\check{\epsilon}^T\check{\epsilon})^2 \\
&\quad + \frac{5}{2}k_e + \omega_{\max} + \frac{3}{8}\sigma_m^2 + \frac{3}{8}\sigma_w^2 \tag{6.12}
\end{aligned}$$

where to find the second inequality $\|\check{\epsilon}\| \leq 1$, $\|\check{\epsilon}\| \leq 1$, and $\|\omega\| \leq \omega_{\max}$ were used.

Zakai's stability theorem (Theorem 2.1.4) implies the system is weakly stochastically stable. Further, Zakai's ultimate moment bound theorem (Theorem 2.1.5) directly yields the ultimate expectation.

□

The generalized moment ultimate bound of Equation 6.11 can be further refined to yield an ultimate bound for $\tilde{\epsilon}^T(t)\tilde{\epsilon}(t)$.

Corollary 6.2.1.1. *The attitude error dynamics of the Itô SDE 6.10 are such that*

$$\lim_{t \rightarrow \infty} E[\tilde{\epsilon}^T(t)\tilde{\epsilon}(t)] \leq 9\frac{k_e}{\sigma_w^2} + 2\frac{1}{\sigma_w^2}\omega_{max} + \frac{3}{4} \quad (6.13)$$

Proof. Bounding the cross-coupling terms of Equation 6.12 yields

$$\begin{aligned} \mathcal{L}V &\leq -\frac{1}{2}k_m\check{\eta}^2\check{\epsilon}^T\check{\epsilon} - \frac{1}{2}\sigma_m^2\check{\epsilon}^T\check{\epsilon} - \frac{1}{2}\sigma_w^2\tilde{\epsilon}^T\tilde{\epsilon} \\ &\quad + \frac{1}{2}k_e|\check{\eta}|^2\|\tilde{\epsilon}\|^4\|\check{\epsilon}\|^2 + \frac{1}{2}k_e|\check{\eta}|^2|\check{\eta}|^4\|\tilde{\epsilon}\|^2 + \frac{1}{2}k_e|\check{\eta}|^2|\check{\eta}|^2\|\check{\epsilon}\|^2\|\tilde{\epsilon}\|^2 + \frac{1}{2}k_e|\check{\eta}|^2|\check{\eta}|^2\|\check{\epsilon}\|^2\|\tilde{\epsilon}\|^2 \\ &\quad + \frac{5}{2}k_e + \omega_{max} + \frac{3}{8}\sigma_m^2 + \frac{3}{8}\sigma_w^2 \\ &\leq -\frac{1}{2}k_m\check{\eta}^2\check{\epsilon}^T\check{\epsilon} - \frac{1}{2}\sigma_m^2\check{\epsilon}^T\check{\epsilon} - \frac{1}{2}\sigma_w^2\tilde{\epsilon}^T\tilde{\epsilon} + \frac{9}{2}k_e + \omega_{max} + \frac{3}{8}\sigma_m^2 + \frac{3}{8}\sigma_w^2 \end{aligned}$$

where the last inequality follows from the norm constraint on unit quaternions.

Application of Zakai's ultimate moment bound theorem (Theorem 2.1.5) results in

$$\lim_{t \rightarrow \infty} E[k_m\check{\eta}^2\check{\epsilon}^T\check{\epsilon} + \sigma_m^2\check{\epsilon}^T\check{\epsilon} + \sigma_w^2\tilde{\epsilon}^T\tilde{\epsilon}] \leq 9k_e + 2\omega_{max} + \frac{3}{4}\sigma_m^2 + \frac{3}{4}\sigma_w^2$$

Using the linearity property of the expectation operator and rearranging leads to

$$\begin{aligned} \lim_{t \rightarrow \infty} E[\tilde{\epsilon}^T\tilde{\epsilon}] &\leq 9\frac{k_e}{\sigma_w^2} + 2\frac{1}{\sigma_w^2}\omega_{max} + \frac{3}{4}\frac{\sigma_m^2}{\sigma_w^2} + \frac{3}{4} \\ &\quad - \frac{k_m}{\sigma_w^2} \lim_{t \rightarrow \infty} E[\check{\eta}^2\check{\epsilon}^T\check{\epsilon}] - \frac{\sigma_m^2}{\sigma_w^2} \lim_{t \rightarrow \infty} E[\check{\epsilon}^T\check{\epsilon}] \\ &= 9\frac{k_e}{\sigma_w^2} + 2\frac{1}{\sigma_w^2}\omega_{max} + \frac{3}{4}\frac{\sigma_m^2}{\sigma_w^2} + \frac{3}{4} \\ &\quad - \frac{k_m + \sigma_m^2}{\sigma_w^2} \lim_{t \rightarrow \infty} E[\check{\epsilon}^T\check{\epsilon}] + \frac{k_m}{\sigma_w^2} \lim_{t \rightarrow \infty} E[(\check{\epsilon}^T\check{\epsilon})^2] \end{aligned} \quad (6.14)$$

where the last line holds from the norm constraint on unit quaternions.

From Chapter 4, Equation 4.15 provides a bound on $\lim_{t \rightarrow \infty} E[(\check{\boldsymbol{\varepsilon}}^T \check{\boldsymbol{\varepsilon}})^2]$, specifically

$$\lim_{t \rightarrow \infty} E[(\check{\boldsymbol{\varepsilon}}^T \check{\boldsymbol{\varepsilon}})^2] \leq \frac{k_m + \sigma_m^2}{k_m} \lim_{t \rightarrow \infty} E[\check{\boldsymbol{\varepsilon}}^T \check{\boldsymbol{\varepsilon}}] - \frac{3 \sigma_m^2}{4 k_m}$$

Combining with Equation 6.14 results in

$$\begin{aligned} \lim_{t \rightarrow \infty} E[\check{\boldsymbol{\varepsilon}}^T \check{\boldsymbol{\varepsilon}}] &\leq 9 \frac{k_e}{\sigma_w^2} + 2 \frac{1}{\sigma_w^2} \omega_{max} + \frac{3 \sigma_m^2}{4 \sigma_w^2} + \frac{3}{4} \\ &\quad + \left(\frac{k_m}{\sigma_w^2} \frac{k_m + \sigma_m^2}{k_m} - \frac{k_m + \sigma_m^2}{\sigma_w^2} \right) \lim_{t \rightarrow \infty} E[\check{\boldsymbol{\varepsilon}}^T \check{\boldsymbol{\varepsilon}}] - \frac{3 \sigma_m^2 k_m}{4 k_m \sigma_w^2} \\ &= 9 \frac{k_e}{\sigma_w^2} + 2 \frac{1}{\sigma_w^2} \omega_{max} + \frac{3}{4} \end{aligned}$$

□

The bound on $\tilde{\boldsymbol{\varepsilon}}^T(t) \tilde{\boldsymbol{\varepsilon}}(t)$ can be larger than one which suggests significant conservatism since $\tilde{\boldsymbol{q}}$ is a unit quaternion and thus $\tilde{\boldsymbol{\varepsilon}}^T(t) \tilde{\boldsymbol{\varepsilon}}(t) \leq 1 \forall t$. It is important to note that Equation 6.13 is merely **an** ultimate upper bound and not necessarily the **least** ultimate upper bound. The first term in the ultimate upper bound arose as the sign indefinite terms and cross coupling terms between $\check{\boldsymbol{q}}(t)$ and $\tilde{\boldsymbol{q}}(t)$ in $\mathcal{L}V$ were bounded in the proof. The observation that the ultimate bound on $\tilde{\boldsymbol{\varepsilon}}^T(t) \tilde{\boldsymbol{\varepsilon}}(t)$ is proportional to the filter gain k_e may be an artifact of the choice of Lyapunov function or the analysis techniques used. Of course from inspection of the filter equations, if the filter gain k_e is set very large the filter kinematic equation will be dominated by the feedback term and the filter's estimate will follow the attitude measurement noise.

Additionally, according to the second term on the right hand side of Equation

6.13, the ultimate upper bound on $\tilde{\boldsymbol{\epsilon}}^T(t)\tilde{\boldsymbol{\epsilon}}(t)$ is proportional to the vehicle angular rate. This term arose from the $\left[I - R(\check{\boldsymbol{q}}(t))\right]\boldsymbol{\omega}(t)$ terms in the system dynamics. From Chapter 4, the ultimate PDF for the attitude noise error dynamics are given by a bipolar Bingham distribution with zero mean, or in symbols $\lim_{t \rightarrow \infty} E[\check{\boldsymbol{\epsilon}}(t)] = \mathbf{0}$, so it is possible that in the mean the vehicle angular rate plays no part in the ultimate attitude estimate error. Similar to the observation of the previous paragraph, the fact that the ultimate upper bound on $\tilde{\boldsymbol{\epsilon}}^T(t)\tilde{\boldsymbol{\epsilon}}(t)$ is proportional to the vehicle angular rate may be an artifact of the choice of Lyapunov function or the analysis techniques used.

6.2.3 Numerical Simulation of SO(3) Stochastic Lyapunov Bounds

Numerical simulations of the attitude filter's Itô SDE error dynamics of Equation 6.10 were performed for a variety of system parameters. The Kloeden-Platen Explicit Weak 2.0 numerical integration scheme discussed in Section 2.2.3 was used. For each simulation realization, a time step size of $\Delta t = 0.001$ was used for a total of 10^7 simulation steps. At the end of a simulation realization, the last 10^6 simulation steps were used to compute the empirical mean of the generalized moment of Equation 6.11

$$\begin{aligned} \text{mean}_{t \in T_{ss}} & \left[k_m \check{\eta}^2(t) \check{\boldsymbol{\epsilon}}^T(t) \check{\boldsymbol{\epsilon}}(t) + \sigma_m^2 \check{\boldsymbol{\epsilon}}^T(t) \check{\boldsymbol{\epsilon}}(t) + \sigma_w^2 \check{\boldsymbol{\epsilon}}^T(t) \check{\boldsymbol{\epsilon}}(t) \right. \\ & + k_e \check{\eta}^2(t) \check{\boldsymbol{\epsilon}}^T(t) \check{\boldsymbol{\epsilon}}(t) \left(\check{\boldsymbol{\epsilon}}^T(t) \check{\boldsymbol{\epsilon}}(t) \right)^2 + k_e \check{\eta}^2(t) \check{\eta}^4(t) \check{\boldsymbol{\epsilon}}^T(t) \check{\boldsymbol{\epsilon}}(t) \\ & \left. + k_e \check{\eta}^2(t) \check{\eta}^2(t) \|\check{\boldsymbol{\epsilon}}(t) \times \check{\boldsymbol{\epsilon}}(t)\|^2 + k_e \check{\eta}^2(t) \check{\eta}^2(t) \left(\check{\boldsymbol{\epsilon}}^T(t) \check{\boldsymbol{\epsilon}}(t) \right)^2 \right] \end{aligned}$$

and statistics for the numerical realizations of the filter attitude estimate error

$$\text{Mean}_{sims} \left[\text{Mean}_{t_i \in T_{ss}} \left[\check{\boldsymbol{\epsilon}}^T(t_i) \check{\boldsymbol{\epsilon}}(t_i) \right] \right]$$

A gallery of plots of the generalized moment of Equation 6.11 are included in Figure 6.1 for a spin stabilized spacecraft and in Figure 6.2 for an inertially fixed spacecraft. In each plot, a magenta dot represents a single simulation realization. The blue line in each plot is the generalized moment upper bound from Equation 6.11. The generalized moment upper bound does appear to bound the ensemble of simulation realizations for all simulated cases, however the upper bound grows increasingly conservative for large filter gains. Despite the bound being proportional

to the vehicle angular rate, the numerical simulation realizations from the spinning case appear to be of similar magnitude to the inertially fixed case.

A gallery of plots of the filter attitude estimate errors are included in Figure 6.3 for a spin stabilized spacecraft and in Figure 6.4 for an inertially fixed spacecraft. As before, a magenta dot represents a single simulation realization. The blue line in each plot is the stochastic Lyapunov upper bound from Equation 6.13. The stochastic Lyapunov upper bound also upper bounds the ensemble of simulation realizations, but similar to the general moment bound the stochastic Lyapunov upper bound on the attitude estimate errors grows increasingly conservative for large filter gain k_e . The stochastic Lyapunov bounds are clearly unsuitable for filter performance characterization.

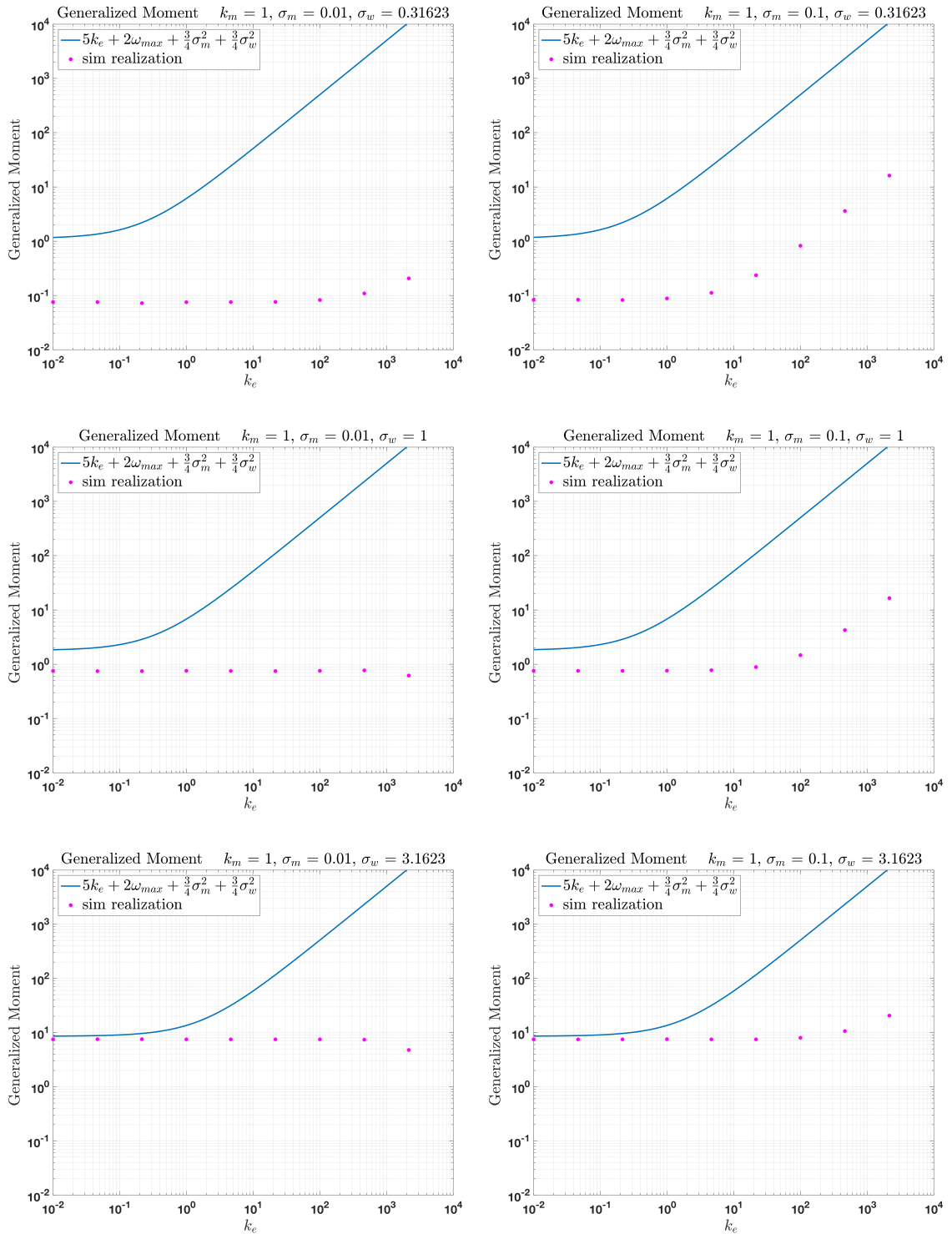


Figure 6.1: Comparison of simulation realizations of the general moment of Equation 6.11 and the associated bound for the case of a vehicle spinning at 5 revolutions per minute about the vehicle body's $[1 \ 2 \ 3]^T$ axis.

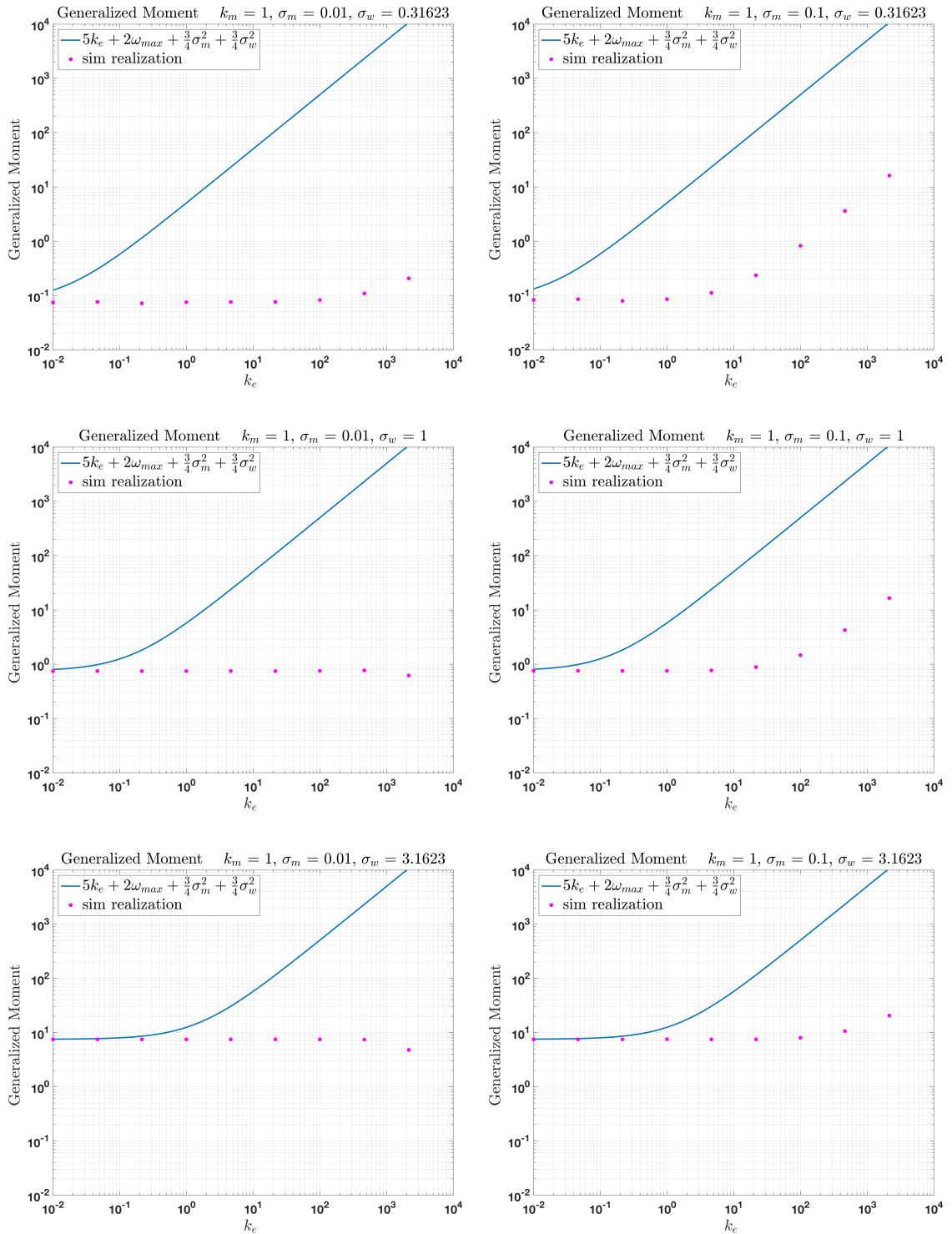


Figure 6.2: Comparison of simulation realizations of the general moment of Equation 6.11 and the associated bound for the case of a vehicle inertially fixed (not spinning).

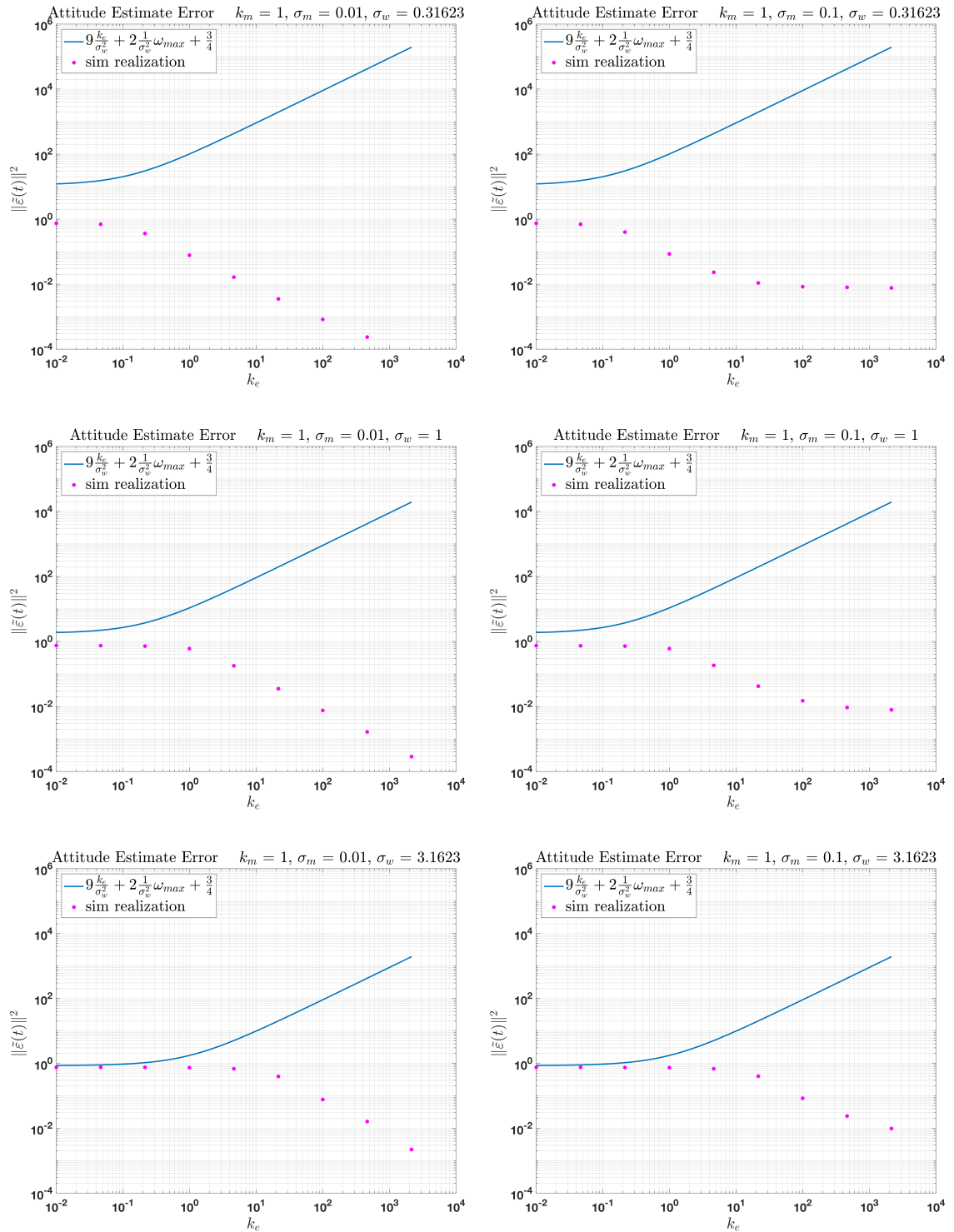


Figure 6.3: Comparison of simulation realizations of the attitude estimate error and the bound of Equation 6.13 for the case of a vehicle spinning at 5 revolutions per minute about the vehicle body's $[1 \ 2 \ 3]^T$ axis.

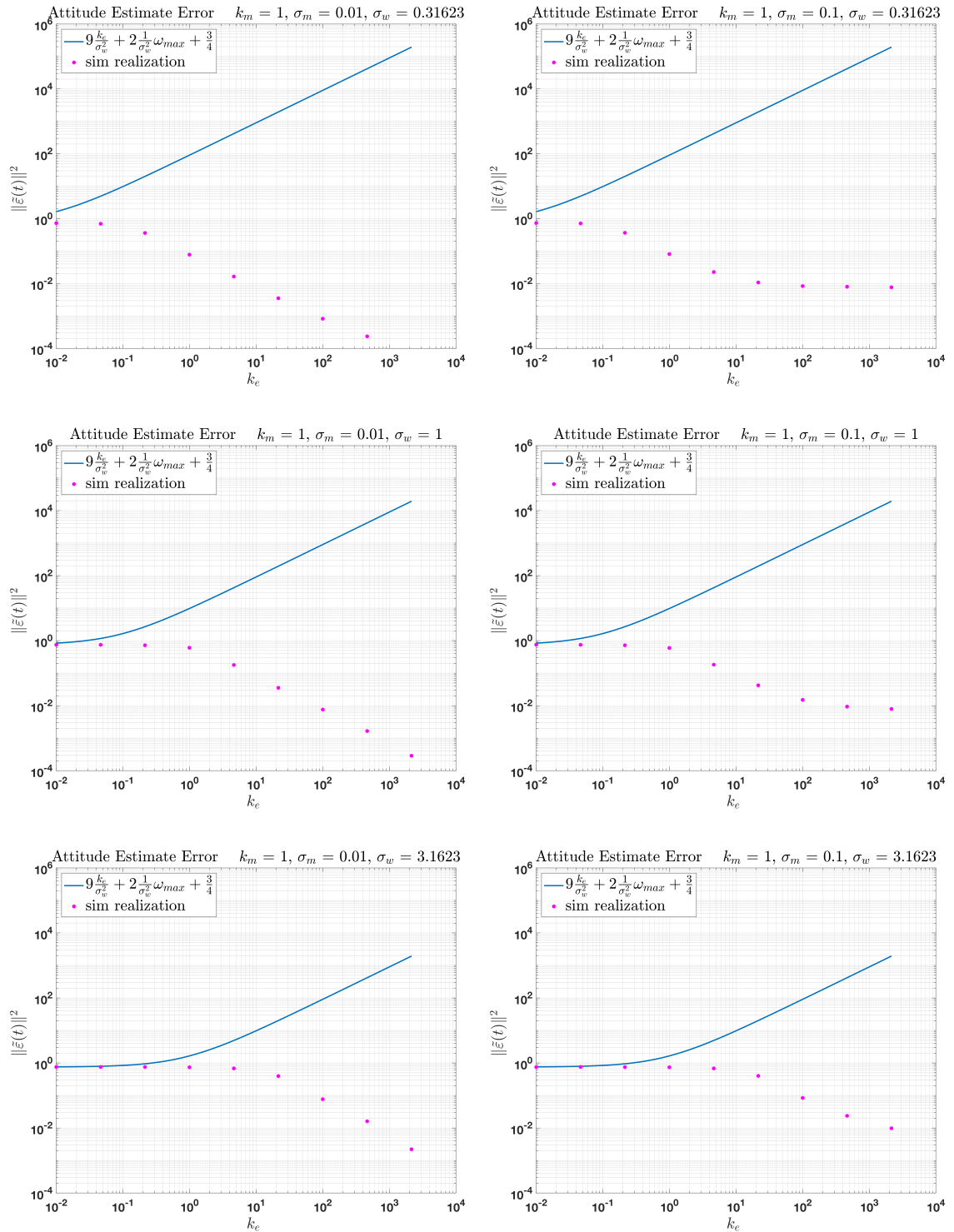


Figure 6.4: Comparison of simulation realizations of the attitude estimate error and the bound of Equation 6.13 for the case of a vehicle inertially fixed (not spinning).

6.2.4 Filter Formulation in SO(2)

In this section, the attitude filter dynamical model is reduced to the single axis case of SO(2). In following sections, the reduced model will provide tractable analytic results that can provide insight into the full SO(3) case.

As explained in Section 2.3.2, the SO(3) dynamical model may be reduced to the SO(2) case by simply zeroing out the y and z components of all vector quantities. Equivalently, the vector quantities in the SO(3) case reduce to scalar quantities, and SO(3) unit quaternions comprised of 4 elements reduce to SO(2) unit quaternions with two elements.

The SO(3) Langevin form error dynamics of Equation 6.9 reduce in the SO(2) case to

$$\begin{aligned} \dot{\tilde{\mathbf{x}}} &= \begin{bmatrix} \dot{\tilde{\mathbf{q}}} \\ \dot{\tilde{\mathbf{q}}} \end{bmatrix} = \begin{bmatrix} \dot{\tilde{\sigma}} \\ \dot{\tilde{\eta}} \\ \dot{\tilde{\varepsilon}} \\ \dot{\tilde{\eta}} \end{bmatrix} \\ &= \begin{bmatrix} -\frac{1}{2}k_m\check{\eta}^2\check{\varepsilon} \\ \frac{1}{2}k_m\check{\eta}\check{\varepsilon}^2 \\ -\frac{1}{2}k_e\check{\eta}(\check{\eta}\check{\eta} + \check{\varepsilon}\check{\varepsilon})(-\check{\eta}\check{\varepsilon} + \check{\eta}\check{\varepsilon}) \\ \frac{1}{2}k_e\check{\varepsilon}(\check{\eta}\check{\eta} + \check{\varepsilon}\check{\varepsilon})(-\check{\eta}\check{\varepsilon} + \check{\eta}\check{\varepsilon}) \end{bmatrix} + \begin{bmatrix} -\frac{1}{2}\check{\eta}\sigma_m & 0 \\ \frac{1}{2}\check{\varepsilon}\sigma_m & 0 \\ 0 & -\frac{1}{2}\check{\eta}\sigma_w \\ 0 & \frac{1}{2}\check{\varepsilon}\sigma_w \end{bmatrix} \begin{bmatrix} n_m \\ n_w \end{bmatrix} \end{aligned} \quad (6.15)$$

where again the function of time notation has been suppressed for brevity. Note that, as derived in Section 2.3.2, the angular rate driving the attitude error kinematics in SO(2) do not depend on any rotation matrices as SO(2) rotation matrices are

trivially $R = 1$. Thus the $\left[I - R(\check{\mathbf{q}}(t)) \right] \boldsymbol{\omega}(t)$ term from the SO(3) case vanishes in the reduced SO(2) case.

As explained in Section 2.1.3, the Langevin form error dynamics differential equation 4.23 is interpreted as a Stratonovich SDE. Converting to Itô form yields

$$\begin{aligned}
d\tilde{\mathbf{x}} &= \begin{bmatrix} d\check{\mathbf{q}} \\ d\tilde{\mathbf{q}} \end{bmatrix} = \begin{bmatrix} d\check{\varepsilon} \\ d\check{\eta} \\ d\check{\varepsilon} \\ d\check{\eta} \end{bmatrix} \\
&= \begin{bmatrix} -\frac{1}{2}k_m\check{\eta}^2\check{\varepsilon} - \frac{1}{8}\sigma_m^2\check{\varepsilon} \\ \frac{1}{2}k_m\check{\eta}\check{\varepsilon}^2 - \frac{1}{8}\sigma_m^2\check{\eta} \\ -\frac{1}{2}k_e\check{\eta}(\check{\eta}\check{\eta} + \check{\varepsilon}\check{\varepsilon})\left(-\check{\eta}\check{\varepsilon} + \check{\eta}\check{\varepsilon}\right) - \frac{1}{8}\sigma_w^2\check{\varepsilon} \\ \frac{1}{2}k_e\check{\varepsilon}(\check{\eta}\check{\eta} + \check{\varepsilon}\check{\varepsilon})\left(-\check{\eta}\check{\varepsilon} + \check{\eta}\check{\varepsilon}\right) - \frac{1}{8}\sigma_w^2\check{\eta} \end{bmatrix} dt + \begin{bmatrix} -\frac{1}{2}\check{\eta}\sigma_m & 0 \\ \frac{1}{2}\check{\varepsilon}\sigma_m & 0 \\ 0 & -\frac{1}{2}\check{\eta}\sigma_w \\ 0 & \frac{1}{2}\check{\varepsilon}\sigma_w \end{bmatrix} \begin{bmatrix} d\beta_m \\ d\beta_w \end{bmatrix} \\
&= \mathbf{f}(\tilde{\mathbf{x}})dt + G(\tilde{\mathbf{x}})d\boldsymbol{\beta} \tag{6.16}
\end{aligned}$$

The attitude filter error dynamics of Equation 6.15 can equivalently be written in the SO(2) Euler Axis/Angle parameterization (as explained in Section 2.3.2). Let

$$\check{\mathbf{q}} = \begin{bmatrix} \check{\varepsilon} \\ \check{\eta} \end{bmatrix} = \begin{bmatrix} \sin\left(\frac{\check{\phi}}{2}\right) \\ \cos\left(\frac{\check{\phi}}{2}\right) \end{bmatrix} \quad \tilde{\mathbf{q}} = \begin{bmatrix} \check{\varepsilon} \\ \check{\eta} \end{bmatrix} = \begin{bmatrix} \sin\left(\frac{\tilde{\phi}}{2}\right) \\ \cos\left(\frac{\tilde{\phi}}{2}\right) \end{bmatrix}$$

Then the SO(2) Euler Axis/Angle parameterization of the filter error dynamics is

given as

$$\begin{aligned}
\dot{\tilde{\mathbf{y}}} &= \begin{bmatrix} \dot{\check{\phi}} \\ \dot{\check{\phi}} \end{bmatrix} = \begin{bmatrix} -k_m \check{\eta} \check{\varepsilon} \\ -k_e (\check{\eta} \check{\eta} + \check{\varepsilon} \check{\varepsilon}) (-\check{\eta} \check{\varepsilon} + \check{\eta} \check{\varepsilon}) \end{bmatrix} + \begin{bmatrix} -\sigma_m & 0 \\ 0 & -\sigma_w \end{bmatrix} \begin{bmatrix} n_m \\ n_w \end{bmatrix} \\
&= \begin{bmatrix} -\frac{1}{2} k_m \sin(\check{\phi}) \\ -\frac{1}{2} k_e \sin(\check{\phi} - \check{\phi}) \end{bmatrix} + \begin{bmatrix} -\sigma_m & 0 \\ 0 & -\sigma_w \end{bmatrix} \begin{bmatrix} n_m \\ n_w \end{bmatrix}
\end{aligned} \tag{6.17}$$

which is immediately in Langevin form. Conversion to an Itô SDE is trivial as the diffusion matrix is independent of the state:

$$\begin{aligned}
d\tilde{\mathbf{y}} &= \begin{bmatrix} d\check{\phi} \\ d\check{\phi} \end{bmatrix} = \begin{bmatrix} -\frac{1}{2} k_m \sin(\check{\phi}) \\ -\frac{1}{2} k_e \sin(\check{\phi} - \check{\phi}) \end{bmatrix} dt + \begin{bmatrix} -\sigma_m & 0 \\ 0 & -\sigma_w \end{bmatrix} \begin{bmatrix} d\beta_m \\ d\beta_w \end{bmatrix} \\
&= \mathbf{f}(\tilde{\mathbf{y}})dt + G(\tilde{\mathbf{y}})d\boldsymbol{\beta}
\end{aligned} \tag{6.18}$$

6.2.5 Stochastic Lyapunov Analysis in SO(2)

In this section weak stochastic stability of the SO(2) Itô SDE 6.16 is established via stochastic Lyapunov theory. A number of performance bounds are also found.

Theorem 6.2.2. *The attitude error dynamics of the Itô SDE 6.16 are weakly stochastically stable. Further,*

$$\lim_{t \rightarrow \infty} E \left[\tilde{\varepsilon}^2(t) \right] \leq \frac{1}{2} + \frac{k_e}{\sigma_w^2} \quad (6.19)$$

Proof. Note that the dynamics governing the attitude measurement noise states $\check{\varepsilon}(t)$ and $\check{\eta}(t)$ are decoupled from the dynamics of the filter's attitude estimate error states $\tilde{\varepsilon}(t)$ and $\tilde{\eta}(t)$. Further, the dynamics governing the attitude measurement states have (by construction) the same form as those of the SO(2) Itô SDE from the previous chapter given in Equation 4.24. Thus the attitude measurement noise states are weakly stochastically stable as shown in Theorem 4.6.1 and the attitude measurement noise Euler angle has the ultimate probability density given in Theorem 4.44.

To show weak stochastic stability of the filter's attitude estimate error states, choose the Lyapunov function $V = \frac{1}{2}\tilde{\varepsilon}^2$. Application of the differential generator with respect to the Itô SDE 6.16 yields

$$\mathcal{L}V = -\frac{1}{2}k_e\tilde{\eta}^2\tilde{\varepsilon}^2 - \frac{1}{4}\sigma_w^2\tilde{\varepsilon}^2 + \frac{1}{8}\sigma_w^2 + \frac{1}{2}k_e\left(\check{\eta}\check{\varepsilon}\tilde{\eta}\tilde{\varepsilon}(2\tilde{\eta}^2 - 1) + 2\check{\varepsilon}^2\tilde{\eta}^2\tilde{\varepsilon}^2\right) \quad (6.20)$$

Observe that the final term, $\frac{1}{2}k_e\left(\check{\eta}\check{\varepsilon}\tilde{\eta}\tilde{\varepsilon}(2\tilde{\eta}^2 - 1) + 2\check{\varepsilon}^2\tilde{\eta}^2\tilde{\varepsilon}^2\right)$, is upper and lower bounded as all of its components are bounded by the norm constraint on unit quater-

nions. Specifically, using the norm constraint one can find

$$-\frac{1}{16} \leq \check{\eta} \tilde{\varepsilon} \tilde{\eta} \tilde{\varepsilon} (2\tilde{\eta}^2 - 1) + 2\tilde{\varepsilon}^2 \tilde{\eta}^2 \tilde{\varepsilon}^2 \leq \frac{1}{2} \quad (6.21)$$

Combining the bound on this term with Equation 6.20 yields

$$\begin{aligned} \mathcal{L}V &\leq -\frac{1}{2}k_e \tilde{\eta}^2 \tilde{\varepsilon}^2 - \frac{1}{4}\sigma_w^2 \tilde{\varepsilon}^2 + \frac{1}{8}\sigma_w^2 + \frac{1}{4}k_e \\ &\leq -\frac{1}{4}\sigma_w^2 \tilde{\varepsilon}^2 + \frac{1}{8}\sigma_w^2 + \frac{1}{4}k_e \end{aligned} \quad (6.22)$$

Zakai's stability theorem (Theorem 2.1.4) implies the system is weakly stochastically stable.

Application of Zakai's ultimate moment bound theorem (Theorem 2.1.5) implies

$$\lim_{t \rightarrow \infty} E \left[\frac{1}{4} \sigma_w^2 \tilde{\varepsilon}^2(t) \right] \leq \frac{1}{8} \sigma_w^2 + \frac{1}{4} k_e$$

Linearity of the expectation operator and algebraic manipulation yields the final result.

□

Again observe the curious result that the ultimate bound on $\tilde{\varepsilon}^2(t)$ is proportional to the filter gain k_e and inversely proportional to the square of the gyro noise parameter σ_w which was seen in the SO(3) case. As before, it is important to note that Equation 6.19 is merely **an** ultimate upper bound and not necessarily the **least** ultimate upper bound. The observation that the ultimate bound on $\tilde{\varepsilon}^2(t)$ is proportional to the filter gain k_e may be an artifact of the analysis techniques used.

Zakai's ultimate moment bound theorem (Theorem 2.1.5) provides a means of finding an ultimate moment upper bound, specifically if $\mathcal{L}V \leq k - L(\mathbf{x})$ then

$\lim_{t \rightarrow \infty} E[L(\mathbf{x})] \leq k$. As can be seen from Zakai's proof [114], the equalities hold: if $\mathcal{L}V = k - L(\mathbf{x})$ then $\lim_{t \rightarrow \infty} E[L(\mathbf{x})] = k$. If it can be assumed that the ultimate moment bound theorem can be used for finding ultimate moment lower bounds, meaning if $\mathcal{L}V \geq k - L(\mathbf{x})$ then $\lim_{t \rightarrow \infty} E[L(\mathbf{x})] \geq k$, a lower bound can be found for the system of SDE 6.16.

Corollary 6.2.2.1. *Assume Zakai's ultimate moment bound theorem (Theorem 2.1.5) provides a means of finding an ultimate moment lower bound in the following way: if $\mathcal{L}V = k - L(\mathbf{x})$ then $\lim_{t \rightarrow \infty} E[L(\mathbf{x})] = k$. Then the attitude error dynamics of the Itô SDE 6.16 are such that*

$$\lim_{t \rightarrow \infty} E[\tilde{\varepsilon}^2(t)] \geq \frac{1}{2} + \frac{\sigma_w^2}{4k_e} - \frac{1}{2} \sqrt{\frac{5}{4} + \frac{\sigma_w^4}{4k_e^2}} \quad (6.23)$$

Proof. Using the bound $-\frac{1}{16} \leq \check{\eta}\tilde{\varepsilon}\tilde{\eta}\tilde{\varepsilon}(2\tilde{\eta}^2 - 1) + 2\tilde{\varepsilon}^2\tilde{\eta}^2\tilde{\varepsilon}^2$ from Equation 6.21, a lower bound for Equation 6.20 can be found as

$$\mathcal{L}V \geq -\frac{1}{2}k_e\tilde{\eta}^2\tilde{\varepsilon}^2 - \frac{1}{4}\sigma_w^2\tilde{\varepsilon}^2 + \frac{1}{8}\sigma_w^2 - \frac{1}{32}k_e \quad (6.24)$$

Using the assumed version of Zakai's ultimate moment bound theorem (Theorem 2.1.5) for ultimate lower bounds results in

$$\lim_{t \rightarrow \infty} E\left[\frac{1}{2}k_e\tilde{\eta}^2\tilde{\varepsilon}^2 + \frac{1}{4}\sigma_w^2\tilde{\varepsilon}^2\right] \geq \frac{1}{8}\sigma_w^2 - \frac{1}{32}k_e$$

Rearranging and using the quaternion norm constraint $\tilde{\varepsilon}^2 + \tilde{\eta}^2 = 1$ leads to

$$0 \geq \lim_{t \rightarrow \infty} E[\tilde{\varepsilon}^4] - \left(1 + \frac{\sigma_w^2}{2k_e}\right) \lim_{t \rightarrow \infty} E[\tilde{\varepsilon}^2] + \frac{\sigma_w^2}{4k_e} - \frac{1}{16}$$

Using the definition of variance, $Var[\tilde{\varepsilon}^2] = E[\tilde{\varepsilon}^4] - \left(E[\tilde{\varepsilon}^2]\right)^2 \geq 0$, one finds

$$\begin{aligned} 0 &\geq \lim_{t \rightarrow \infty} \left(E[\varepsilon^2]\right)^2 - \left(1 + \frac{\sigma_w^2}{2k_e}\right) \lim_{t \rightarrow \infty} E[\varepsilon^2] + \frac{\sigma_w^2}{4k_e} - \frac{1}{16} + \lim_{t \rightarrow \infty} Var[\tilde{\varepsilon}^2] \\ &\geq \lim_{t \rightarrow \infty} \left(E[\varepsilon^2]\right)^2 - \left(1 + \frac{\sigma_w^2}{2k_e}\right) \lim_{t \rightarrow \infty} E[\varepsilon^2] + \frac{\sigma_w^2}{4k_e} - \frac{1}{16} \end{aligned}$$

Solving the polynomial inequality yields the final result. □

If the underlying probability density of $\tilde{\varepsilon}^2(t)$ is assumed to be unimodal, the Jacobson inequality can be used to find a tighter ultimate upper bound than the one of Theorem 6.2.2.

Corollary 6.2.2.2. *Assuming the underlying probability density of $\tilde{\varepsilon}^2(t)$ is unimodal, the attitude estimate error dynamics of the Itô SDE 6.16 obey the ultimate upper bound*

$$\lim_{t \rightarrow \infty} E[\tilde{\varepsilon}^2(t)] \leq \frac{1}{2} + \frac{\sigma_w^2}{4k_e} - \frac{1}{2} \sqrt{\frac{\sigma_w^4}{4k_e^2} - \frac{13}{9}} \quad (6.25)$$

Proof. Apply Zakai's ultimate moment bound theorem (Theorem 2.1.5) directly to Equation 6.22 to find

$$\lim_{t \rightarrow \infty} E\left[\frac{1}{2}k_e\tilde{\eta}^2\tilde{\varepsilon}^2 + \frac{1}{4}\sigma_w^2\tilde{\varepsilon}^2\right] \leq \frac{1}{8}\sigma_w^2 + \frac{1}{4}k_e$$

Using $\tilde{\eta}^2 = 1 - \tilde{\varepsilon}^2$, the definition of variance $Var[\tilde{\varepsilon}^2] = E[\tilde{\varepsilon}^4] - \left(E[\tilde{\varepsilon}^2]\right)^2$, and rearranging, yields

$$0 \leq \lim_{t \rightarrow \infty} \left(E[\tilde{\varepsilon}^2]\right)^2 - \left(1 + \frac{\sigma_w^2}{2k_e}\right) \lim_{t \rightarrow \infty} E[\tilde{\varepsilon}^2] + \frac{\sigma_w^2}{4k_e} + \frac{1}{2} + \lim_{t \rightarrow \infty} Var[\tilde{\varepsilon}^2]$$

As $a = 0 \leq \tilde{\varepsilon}^2 \leq 1 = b$, Jacobson's Inequality guarantees $Var[\tilde{\varepsilon}^2] \leq \frac{(b-a)^2}{9} = \frac{1}{9}$.

Combining with the above leads to the polynomial inequality

$$0 \leq \lim_{t \rightarrow \infty} \left(E[\tilde{\varepsilon}^2] \right)^2 - \left(1 + \frac{\sigma_w^2}{2k_e} \right) \lim_{t \rightarrow \infty} E[\tilde{\varepsilon}^2] + \frac{\sigma_w^2}{4k_e} + \frac{11}{18}$$

Solving the polynomial inequality yields the final result. □

While the previous corollary used an upper bound on the term $\frac{1}{2}k_e \left(\check{\eta} \check{\eta} \tilde{\varepsilon} (2\check{\eta}^2 - 1) + 2\check{\varepsilon}^2 \check{\eta}^2 \tilde{\varepsilon}^2 \right)$, it is possible to separate the cross coupled terms using Young's inequality and bounding the attitude noise states given that their ultimate probability density function is known. This line of analysis results in the following corollary.

Corollary 6.2.2.3. *Assuming the underlying probability density of $\tilde{\varepsilon}^2(t)$ is unimodal, the attitude estimate error dynamics of the Itô SDE 6.16 obey the ultimate upper bound*

$$\lim_{t \rightarrow \infty} E[\tilde{\varepsilon}^2(t)] \leq \frac{1}{2} + \frac{\sigma_w^2}{2k_e} - \frac{1}{2} \sqrt{\frac{\sigma_w^4}{k_e^2} - 12 \lim_{t \rightarrow \infty} E[\check{\eta}^2(t) \tilde{\varepsilon}^2(t)] - 8 \lim_{t \rightarrow \infty} E[\check{\varepsilon}^4(t)]} - \frac{51}{81} \quad (6.26)$$

where

$$\lim_{t \rightarrow \infty} E[\check{\eta}^2(t) \tilde{\varepsilon}^2(t)] = \frac{1}{4} \frac{I_1\left(\frac{k_m}{\sigma_m^2}\right)}{\frac{k_m}{\sigma_m^2} I_0\left(\frac{k_m}{\sigma_m^2}\right)}$$

and

$$\lim_{t \rightarrow \infty} E[\check{\varepsilon}^4(t)] = \frac{1}{2} \left(1 - \frac{1 + 2\frac{k_m}{\sigma_m^2} I_1\left(\frac{k_m}{\sigma_m^2}\right)}{2\frac{k_m}{\sigma_m^2} I_0\left(\frac{k_m}{\sigma_m^2}\right)} \right)$$

Proof. Apply Young's Inequality, $ab \leq \frac{a^2}{2} + \frac{b^2}{2}$, to Equation 6.20 to find

$$\begin{aligned} \mathcal{LV} &\leq -\frac{1}{4}k_e \check{\eta}^2 \tilde{\varepsilon}^2 - \frac{1}{4}\sigma_w^2 \tilde{\varepsilon}^2 + \frac{1}{8}\sigma_w^2 + \frac{3}{4}k_e \check{\eta}^2 \tilde{\varepsilon}^2 + \frac{1}{2}k_e \check{\varepsilon}^4 + \frac{1}{2}k_e \check{\eta}^6 \tilde{\varepsilon}^2 + \frac{1}{2}k_e \check{\eta}^4 \tilde{\varepsilon}^4 \\ &\leq -\frac{1}{4}k_e \check{\eta}^2 \tilde{\varepsilon}^2 - \frac{1}{4}\sigma_w^2 \tilde{\varepsilon}^2 + \frac{1}{8}\sigma_w^2 + \frac{3}{4}k_e \check{\eta}^2 \tilde{\varepsilon}^2 + \frac{1}{2}k_e \check{\varepsilon}^4 + \frac{6}{81}k_e \end{aligned}$$

where the last line holds since $0 \leq \tilde{\eta}^6 \tilde{\varepsilon}^2 + \tilde{\eta}^4 \tilde{\varepsilon}^4 \leq \frac{12}{81}$ which follows from $1 = \tilde{\varepsilon}^2 + \tilde{\eta}^2$.

Application of Zakai's ultimate moment bound theorem (Theorem 2.1.5) yields

$$\lim_{t \rightarrow \infty} E \left[\frac{1}{4} k_e \tilde{\eta}^2 \tilde{\varepsilon}^2 + \frac{1}{4} \sigma_w^2 \tilde{\varepsilon}^2 \right] \leq \frac{1}{8} \sigma_w^2 + \frac{3}{4} k_e \lim_{t \rightarrow \infty} E \left[\check{\eta}^2 \check{\varepsilon}^2 \right] + \frac{1}{2} k_e \lim_{t \rightarrow \infty} E \left[\check{\varepsilon}^4 \right] + \frac{6}{81} k_e$$

Rearranging and using the definition of variance yields

$$\begin{aligned} 0 \leq \lim_{t \rightarrow \infty} \left(E \left[\tilde{\varepsilon}^2 \right] \right)^2 - \left(1 + \frac{\sigma_w^2}{k_e} \right) \lim_{t \rightarrow \infty} E \left[\varepsilon^2 \right] + \frac{\sigma_w^2}{2k_e} \\ + 3 \lim_{t \rightarrow \infty} E \left[\check{\eta}^2 \check{\varepsilon}^2 \right] + 2 \lim_{t \rightarrow \infty} E \left[\check{\varepsilon}^4 \right] + \frac{24}{81} + \lim_{t \rightarrow \infty} Var \left[\tilde{\varepsilon}^2 \right] \end{aligned}$$

Using Jacobson's Inequality, $Var \left[\tilde{\varepsilon}^2 \right] \leq \frac{(b-a)^2}{9} = \frac{1}{9}$ for $a = 0 \leq \tilde{\varepsilon}^2 \leq 1 = b$, leads to

$$0 \leq \lim_{t \rightarrow \infty} \left(E \left[\tilde{\varepsilon}^2 \right] \right)^2 - \left(1 + \frac{\sigma_w^2}{k_e} \right) \lim_{t \rightarrow \infty} E \left[\varepsilon^2 \right] + \frac{\sigma_w^2}{2k_e} + 3 \lim_{t \rightarrow \infty} E \left[\check{\eta}^2 \check{\varepsilon}^2 \right] + 2 \lim_{t \rightarrow \infty} E \left[\check{\varepsilon}^4 \right] + \frac{35}{81}$$

Solving the polynomial inequality provides the final result.

Note that, as explained in the proof of Theorem 6.2.2, the attitude measurement noise states are weakly stochastically stable as shown in Theorem 4.6.1 and the attitude measurement noise Euler angle $\check{\phi}$ has the ultimate probability density given in Theorem 4.44, specifically

$$p_s(\check{\phi}) = \frac{1}{4\pi I_0 \left(\frac{k_m}{\sigma_m^2} \right)} \exp \left\{ \frac{k_m}{\sigma_m^2} \cos \left(\check{\phi} \right) \right\}$$

Using the relations $\check{\varepsilon} = \sin \left(\frac{\check{\phi}}{2} \right)$ and $\check{\eta} = \sin \left(\frac{\check{\phi}}{2} \right)$ and the ultimate probability density one can compute $\lim_{t \rightarrow \infty} E \left[\check{\eta}^2 \check{\varepsilon}^2 \right]$ and $\lim_{t \rightarrow \infty} E \left[\check{\varepsilon}^4 \right]$ as follows

$$\begin{aligned} \lim_{t \rightarrow \infty} E \left[\check{\eta}^2(t) \check{\varepsilon}^2(t) \right] &= \frac{1}{4\pi I_0 \left(\frac{k_m}{\sigma_m^2} \right)} \int_{-2\pi}^{2\pi} \sin^2 \left(\frac{\check{\phi}}{2} \right) \cos^2 \left(\frac{\check{\phi}}{2} \right) \exp \left\{ \frac{k_m}{\sigma_m^2} \cos \left(\check{\phi} \right) \right\} d\check{\phi} \\ &= \frac{1}{16\pi I_0 \left(\frac{k_m}{\sigma_m^2} \right)} \int_{-2\pi}^{2\pi} \sin^2 \left(\check{\phi} \right) \exp \left\{ \frac{k_m}{\sigma_m^2} \cos \left(\check{\phi} \right) \right\} d\check{\phi} \\ &= \frac{1}{4} \frac{I_1 \left(\frac{k_m}{\sigma_m^2} \right)}{\frac{k_m}{\sigma_m^2} I_0 \left(\frac{k_m}{\sigma_m^2} \right)} \end{aligned}$$

and

$$\begin{aligned}
\lim_{t \rightarrow \infty} E[\check{\varepsilon}^4(t)] &= \frac{1}{4\pi I_0\left(\frac{k_m}{\sigma_m^2}\right)} \int_{-2\pi}^{2\pi} \sin^4\left(\frac{\check{\phi}}{2}\right) \exp\left\{\frac{k_m}{\sigma_m^2} \cos(\check{\phi})\right\} d\check{\phi} \\
&= \frac{1}{4\pi I_0\left(\frac{k_m}{\sigma_m^2}\right)} \left[\frac{1}{4} \int_{-2\pi}^{2\pi} \exp\left\{\frac{k_m}{\sigma_m^2} \cos(\check{\phi})\right\} d\check{\phi} \right. \\
&\quad - \frac{1}{2} \int_{-2\pi}^{2\pi} \cos(\check{\phi}) \exp\left\{\frac{k_m}{\sigma_m^2} \cos(\check{\phi})\right\} d\check{\phi} \\
&\quad \left. + \frac{1}{4} \int_{-2\pi}^{2\pi} \cos^2(\check{\phi}) \exp\left\{\frac{k_m}{\sigma_m^2} \cos(\check{\phi})\right\} d\check{\phi} \right] \\
&= \frac{1}{4\pi I_0\left(\frac{k_m}{\sigma_m^2}\right)} \left[\pi I_0\left(\frac{k_m}{\sigma_m^2}\right) - 2\pi I_1\left(\frac{k_m}{\sigma_m^2}\right) \right. \\
&\quad \left. + \left(\frac{\pi}{\frac{k_m}{\sigma_m^2}} I_1\left(\frac{k_m}{\sigma_m^2}\right) + \pi I_2\left(\frac{k_m}{\sigma_m^2}\right) \right) \right] \\
&= \frac{1}{4I_0\left(\frac{k_m}{\sigma_m^2}\right)} \left[I_0\left(\frac{k_m}{\sigma_m^2}\right) - 2I_1\left(\frac{k_m}{\sigma_m^2}\right) \right. \\
&\quad \left. + \frac{1}{\frac{k_m}{\sigma_m^2}} I_1\left(\frac{k_m}{\sigma_m^2}\right) + I_0\left(\frac{k_m}{\sigma_m^2}\right) - \frac{2}{\frac{k_m}{\sigma_m^2}} I_1\left(\frac{k_m}{\sigma_m^2}\right) \right] \\
&= \frac{1}{2} \left(1 - \frac{1 + 2\frac{k_m}{\sigma_m^2} I_1\left(\frac{k_m}{\sigma_m^2}\right)}{2\frac{k_m}{\sigma_m^2} I_0\left(\frac{k_m}{\sigma_m^2}\right)} \right)
\end{aligned}$$

where the Bessel function recurrence identity $I_\nu(x) = I_{\nu-2}(x) - \frac{2(\nu-1)}{x} I_{\nu-1}(x)$ was used.

□

6.2.6 Numerical Simulation Verification of Stochastic SO(2) Lyapunov Bounds

Numerical simulations of the SO(2) attitude filter's Itô SDE error dynamics of Equation 6.16 were performed for a variety of system parameters. The Kloeden-Platen Explicit Weak 2.0 numerical integration scheme discussed in Section 2.2.3 was used. For each simulation realization, a time step size of $\Delta t = 0.001$ was used for a total of 10^8 simulation steps. At the end of a simulation realization, the last 10^7 simulation steps were used to compute the empirical mean of the filter attitude estimate error $\tilde{\varepsilon}^2(t)$.

A gallery of plots of the filter attitude estimate errors are included in Figure 6.5. As before, a magenta dot represents a single simulation realization. The stochastic Lyapunov bounds of the previous section are also drawn on the plots, with the upper bound of Equation 6.19 in blue, the lower bound of Equation 6.23 in red, and the upper bound of Equation 6.25 in yellow. As in the SO(3) case, the stochastic Lyapunov bounds do correctly envelope the ensemble of numerical realizations, but the bounds grow conservative for large filter gain k_e and are insufficient for filter performance characterization. In contrast to the SO(3) case, the SO(2) stochastic Lyapunov bounds are tight in the small filter gain regime when the attitude estimate state is essentially a random walk process.

In order to compute the stochastic Lyapunov upper bound of Equation 6.25, $\lim_{t \rightarrow \infty} E \left[\dot{\eta}^2(t) \tilde{\varepsilon}^2(t) \right]$ and $\lim_{t \rightarrow \infty} E \left[\tilde{\varepsilon}^4(t) \right]$ must be evaluated. While analytic expressions of these ultimate expectations were given in terms of the modified Bessel

functions of the first kind, they can still be difficult to evaluate using standard analysis software. For example, for the attitude noise level $\frac{k_m}{\sigma_m^2} = 10000$, Mathematica yields $I_0(10000) \approx 3.513 * 10^{4340}$ while MATLAB returns **Inf**. Standard numerical tools such as MATLAB use 64 bit floating point numbers, which can encode numbers with exponents as high as 10^{308} or low as 10^{-308} , but this is not sufficient for evaluating the upper bound of Equation 6.25. Mathematica was used to evaluate the bound, while MATLAB was used for loading the simulation results from file and creating plots.

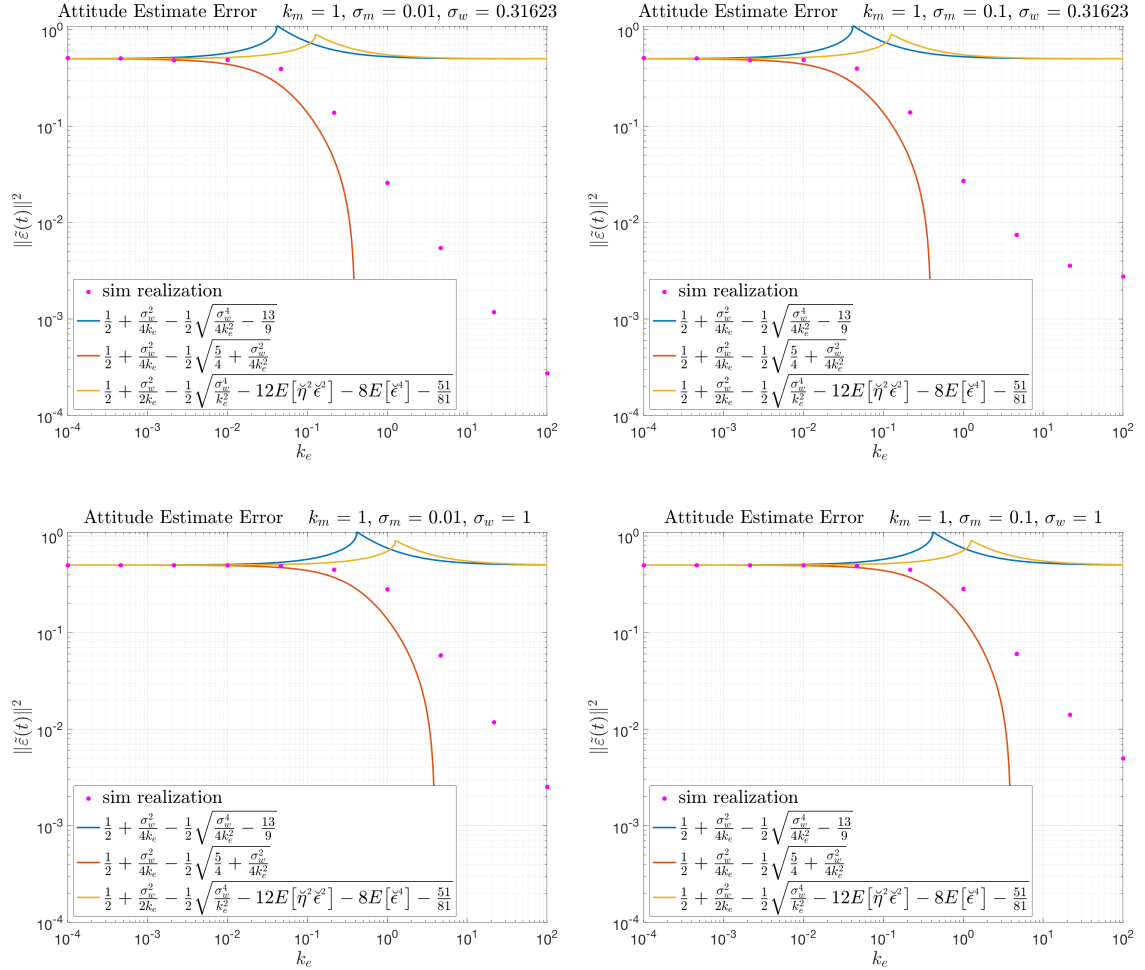


Figure 6.5: Comparison of simulation realizations of attitude estimate errors of the SO(2) error dynamics Itô SDE of Equation 6.16 to the stochastic Lyapunov upper bound of Equation 6.19 in blue, the stochastic Lyapunov lower bound of Equation 6.23 in red, and the stochastic Lyapunov upper bound of Equation 6.25 in yellow.

6.2.7 Fokker-Planck Analysis in SO(2)

This section presents a Fokker-Planck analysis of the SO(2) attitude filter. As the system was shown to be weakly stochastically stable, the joint probability density for the system will ultimately approach the solution to the stationary Fokker-Planck PDE. In this section, the stationary Fokker-Planck PDE is derived and a probability density function that asymptotically approaches the solution to the stationary Fokker-Planck PDE is found. The asymptotic solution is subsequently used to find stationary statistics for the system states.

Let $p = p(\tilde{\mathbf{y}}(t), t) = p(\tilde{\phi}(t), \check{\phi}(t), t)$ be the joint probability density function for the filter attitude estimate error $\tilde{\phi}(t)$ and the attitude measurement noise error $\check{\phi}(t)$. The Fokker-Planck PDE associated with the attitude filter error dynamics Itô SDE 6.18 is given by

$$\begin{aligned}
\frac{\partial p}{\partial t} &= - \sum_{i=1}^2 \frac{\partial}{\partial \tilde{y}_i} \left[f_i(\tilde{\mathbf{y}}(t)) p(\tilde{\mathbf{y}}(t), t) \right] + \frac{1}{2} \sum_{i,j=1}^2 \frac{\partial^2}{\partial \tilde{y}_i \partial \tilde{y}_j} \left[\left\{ G(\tilde{\mathbf{y}}(t)) G^T(\tilde{\mathbf{y}}(t)) \right\}_{i,j} p(\tilde{\mathbf{y}}(t), t) \right] \\
&= \frac{1}{2} \left(k_m \cos(\tilde{\phi}(t)) + k_e \cos(\tilde{\phi}(t) - \check{\phi}(t)) \right) p(\tilde{\mathbf{y}}(t), t) \\
&\quad + \frac{1}{2} k_m \sin(\check{\phi}(t)) \frac{\partial p}{\partial \check{\phi}} + \frac{1}{2} k_e \sin(\tilde{\phi}(t) - \check{\phi}(t)) \frac{\partial p}{\partial \tilde{\phi}} \\
&\quad + \frac{1}{2} \sigma_m^2 \frac{\partial^2 p}{\partial \check{\phi}^2} + \frac{1}{2} \sigma_w^2 \frac{\partial^2 p}{\partial \tilde{\phi}^2}
\end{aligned} \tag{6.27}$$

The underlying system was shown to be weakly stochastically stable in Theorem 6.2.2, thus the joint probability density function $p(\tilde{\phi}(t), \check{\phi}(t), t)$ ultimately approaches a stationary joint probability density function

$$p_s = p_s(\tilde{\mathbf{y}}) = p_s(\tilde{\phi}, \check{\phi}) = \lim_{t \rightarrow \infty} p(\tilde{\phi}(t), \check{\phi}(t), t)$$

The stationary joint probability density function solves the stationary Fokker-Planck PDE

$$0 = \frac{1}{2} \left(k_m \cos(\tilde{\phi}) + k_e \cos(\tilde{\phi} - \check{\phi}) \right) p_s + \frac{1}{2} k_m \sin(\check{\phi}) \frac{\partial p_s}{\partial \check{\phi}} + \frac{1}{2} k_e \sin(\tilde{\phi} - \check{\phi}) \frac{\partial p_s}{\partial \tilde{\phi}} + \frac{1}{2} \sigma_m^2 \frac{\partial^2 p_s}{\partial \check{\phi}^2} + \frac{1}{2} \sigma_w^2 \frac{\partial^2 p_s}{\partial \tilde{\phi}^2} \quad (6.28)$$

The next theorem presents a probability density function that asymptotically approaches the stationary probability density function p_s .

Theorem 6.2.3. *The solution joint probability density function $p_s(\tilde{\phi}, \check{\phi})$ of the stationary Fokker-Planck PDE of Equation 6.28 is such that*

$$p_s(\tilde{\phi}, \check{\phi}) = \lim_{\substack{\sigma_m \rightarrow 0 \\ \frac{k_m}{\sigma_m^2} \text{ constant}}} p_a(\tilde{\phi}, \check{\phi})$$

where $p_a(\tilde{\phi}, \check{\phi})$ is the bivariate von Mises PDF given as

$$p_a(\tilde{\phi}, \check{\phi}) = \frac{1}{N} \exp \left\{ \frac{k_m}{\sigma_m^2} \cos(\check{\phi}) + \frac{k_e}{\sigma_m^2 + \sigma_w^2} \cos(\tilde{\phi} - \check{\phi}) \right\} \quad (6.29)$$

with the normalization constant

$$N = 16\pi^2 I_0 \left(\frac{k_e}{\sigma_m^2 + \sigma_w^2} \right) I_0 \left(\frac{k_m}{\sigma_m^2} \right)$$

where $I_0(x)$ is the 0th order modified Bessel function of the first kind.

Proof. Consider the bivariate von Mises (BVM) distribution [49, 60] which is, in general, specified as

$$p_a(\tilde{\phi}, \check{\phi}) = \frac{1}{N} \exp \left\{ \kappa_1 \cos(\check{\phi} - \mu_1) + \kappa_2 \cos(\tilde{\phi} - \mu_2) + \left[\cos(\check{\phi} - \mu_1) \quad \sin(\check{\phi} - \mu_1) \right] C \begin{bmatrix} \cos(\tilde{\phi} - \mu_2) \\ \sin(\tilde{\phi} - \mu_2) \end{bmatrix} \right\}$$

where N is a normalization constant, κ_1 and κ_2 are real-valued scaling parameters, and C is a 2x2 real constant matrix. In general there are no requirements on C ; it may be full rank, singular, zero, negative definite, positive definite, or sign indefinite.

As noted in Theorem 6.2.2, the attitude measurement noise states (\check{q} in the quaternion parameterization, $\check{\phi}$ in the Euler Axis/Angle parameterization) are decoupled from the filter attitude estimate error states but not vice-versa. The stationary probability density function for the attitude measurement noise states was found in the Euler Axis/Angle parameterization in Theorem 4.8.1. This in turn implies the marginal probability density of the solution p_s to the stationary Fokker-Planck PDE of Equation 6.28 must be such that

$$\int p_s(\check{\phi}, \check{\phi}) d\check{\phi} = \frac{1}{4\pi I_0\left(\frac{k_m}{\sigma_m^2}\right)} \exp\left\{\frac{k_m}{\sigma_m^2} \cos(\check{\phi})\right\} \quad (6.30)$$

Therefore $\kappa_1 = \frac{k_m}{\sigma_m^2}$ and $\mu_1 = 0$. Since all the trigonometric terms in the stationary Fokker-Planck PDE have zero phase, one can further conclude that $\mu_2 = 0$.

As explained in [49, 60], the bivariate von Mises distribution may have the von Mises marginal distribution of Equation 6.30 if and only if precisely one of the

following sets of conditions holds: $C = 0$, $\kappa_2 = 0$ and $C = c \begin{bmatrix} -1 & 1 \\ 1 & 1 \end{bmatrix}$, $\kappa_2 = 0$ and $C = c \begin{bmatrix} 1 & -1 \\ 1 & 1 \end{bmatrix}$, $\kappa_2 = 0$ and $C = c \begin{bmatrix} 1 & 1 \\ -1 & 1 \end{bmatrix}$, $\kappa_2 = 0$ and $C = c \begin{bmatrix} 1 & 1 \\ 1 & -1 \end{bmatrix}$, $\kappa_2 = 0$ and $C = c \begin{bmatrix} 0 & 1 \\ 1 & 0 \end{bmatrix}$, or $\kappa_2 = 0$ and $C = c \begin{bmatrix} 1 & 0 \\ 0 & 1 \end{bmatrix}$. The first six of the seven possibilities do not satisfy the stationary Fokker-Planck PDE of Equation 6.28. Substituting the

last possibility into the Fokker-Planck PDE results in

$$0 = \left\{ \left(k_e - c(\sigma_m^2 + \sigma_w^2) \right) \left(\cos(\check{\phi} - \tilde{\phi}) - c \sin^2(\check{\phi} - \tilde{\phi}) \right) - ck_m \sin(\check{\phi}) \sin(\check{\phi} - \tilde{\phi}) \right\} p_s$$

Choosing $c = \frac{k_e}{\sigma_m^2 + \sigma_w^2}$, the above equation becomes

$$\begin{aligned} 0 &= \left\{ \frac{k_e k_m}{\sigma_m^2 + \sigma_w^2} \sin(\check{\phi}) \sin(\check{\phi} - \tilde{\phi}) \right\} p_s \\ &= \left\{ \frac{k_e \frac{k_m}{\sigma_m^2}}{1 + \frac{\sigma_w^2}{\sigma_m^2}} \sin(\check{\phi}) \sin(\check{\phi} - \tilde{\phi}) \right\} p_s \end{aligned} \quad (6.31)$$

which does not hold for all possible $\tilde{\phi}$ and $\check{\phi}$ so this is not a solution. Note however that the right hand side of Equation 6.31 asymptotically approaches 0 for any possible $\tilde{\phi}$ and $\check{\phi}$ when σ_m goes to zero while the ratio $\frac{k_m}{\sigma_m^2}$ is held constant. The attitude measurement noise density of Equation 6.30 is parameterized by the ratio $\frac{k_m}{\sigma_m^2}$, so as long as k_m is made small enough to maintain the ratio $\frac{k_m}{\sigma_m^2}$ the parameter σ_m may be made arbitrarily small without altering the ultimate statistics of the attitude measurement noise.

Thus

$$p_a(\tilde{\phi}, \check{\phi}) = \frac{1}{N} \exp \left\{ \frac{k_m}{\sigma_m^2} \cos(\check{\phi}) + \frac{k_e}{\sigma_m^2 + \sigma_w^2} \cos(\tilde{\phi} - \check{\phi}) \right\} \quad (6.32)$$

asymptotically approaches the solution to the stationary Fokker-Planck PDE of Equation 6.28 in the sense that

$$\lim_{\substack{\sigma_m \rightarrow 0 \\ \frac{k_m}{\sigma_m^2} \text{ constant}}} p_a(\tilde{\phi}, \check{\phi}) = p_s(\tilde{\phi}, \check{\phi})$$

The scaling constant N may be recovered by enforcing the probability density normalization constraint

$$\int_{-2\pi}^{2\pi} \int_{-2\pi}^{2\pi} p_a(\tilde{\phi}, \check{\phi}) d\tilde{\phi} d\check{\phi} = 1$$

Substituting in the probability density function of Equation 6.32 and rearranging yields

$$\begin{aligned}
N &= \int_{-2\pi}^{2\pi} \int_{-2\pi}^{2\pi} \exp \left\{ \frac{k_m}{\sigma_m^2} \cos(\check{\phi}) + \frac{k_e}{\sigma_m^2 + \sigma_w^2} \cos(\tilde{\phi} - \check{\phi}) \right\} d\tilde{\phi} d\check{\phi} \\
&= \int_{-2\pi}^{2\pi} \exp \left\{ \frac{k_m}{\sigma_m^2} \cos(\check{\phi}) \right\} \int_{-2\pi}^{2\pi} \exp \left\{ \frac{k_e}{\sigma_m^2 + \sigma_w^2} \cos(\tilde{\phi} - \check{\phi}) \right\} d\tilde{\phi} d\check{\phi} \quad (6.33)
\end{aligned}$$

Observe that $\exp \left\{ \frac{k_e}{\sigma_m^2 + \sigma_w^2} \cos(\tilde{\phi} - \check{\phi}) \right\}$ is 2π periodic with phase $\check{\phi}$, so

$$\int_{-2\pi}^{2\pi} \exp \left\{ \frac{k_e}{\sigma_m^2 + \sigma_w^2} \cos(\tilde{\phi} - \check{\phi}) \right\} d\tilde{\phi} = \int_{-2\pi}^{2\pi} \exp \left\{ \frac{k_e}{\sigma_m^2 + \sigma_w^2} \cos(\tilde{\phi}) \right\} d\tilde{\phi}$$

The modified Bessel function of first kind is given in integral form as

$$I_\nu(x) = \frac{1}{\pi} \int_0^\pi \cos(\nu\gamma) e^{x \cos(\gamma)} d\gamma - \frac{\sin(\nu\pi)}{\pi} \int_0^\infty e^{-\cosh(t) - \nu t} dt \quad (6.34)$$

Then

$$\begin{aligned}
&\int_{-2\pi}^{2\pi} \exp \left\{ \frac{k_e}{\sigma_m^2 + \sigma_w^2} \cos(\tilde{\phi}) \right\} d\tilde{\phi} \\
&= 2 \int_{-\pi}^{\pi} \exp \left\{ \frac{k_e}{\sigma_m^2 + \sigma_w^2} \cos(\tilde{\phi}) \right\} d\tilde{\phi} \\
&= 4 \int_0^\pi \exp \left\{ \frac{k_e}{\sigma_m^2 + \sigma_w^2} \cos(\tilde{\phi}) \right\} d\tilde{\phi} \\
&= 4\pi I_0 \left(\frac{k_e}{\sigma_m^2 + \sigma_w^2} \right) \quad (6.35)
\end{aligned}$$

where the first equality holds because the integrand is periodic with period 2π and the second equality holds because the integrand is even.

Substituting back into Equation 6.33 results in

$$\begin{aligned}
N &= 4\pi I_0 \left(\frac{k_e}{\sigma_m^2 + \sigma_w^2} \right) \int_{-2\pi}^{2\pi} \exp \left\{ \frac{k_m}{\sigma_m^2} \cos(\check{\phi}) \right\} d\check{\phi} \\
&= 16\pi^2 I_0 \left(\frac{k_e}{\sigma_m^2 + \sigma_w^2} \right) I_0 \left(\frac{k_m}{\sigma_m^2} \right) \quad (6.36)
\end{aligned}$$

where again the facts that the integrand is periodic with period 2π and is even were used.

□

The bivariate von Mises (BVM) probability density function of Equation 6.29 asymptotically approaches the solution to the stationary Fokker-Planck PDE of Equation 6.28 as $\sigma_m \rightarrow 0$ while the ratio $\frac{k_m}{\sigma_m^2}$ is held constant, meaning $k_m \rightarrow 0$ at the same rate $\sigma_m^2 \rightarrow 0$. The attitude measurement noise density of Equation 6.30 is parameterized by the ratio $\frac{k_m}{\sigma_m^2}$ so the ultimate statistics for the attitude measurement noise given in Corollary 4.8.1.1 and Corollary 4.8.1.2 are unaffected. However it is unclear as to whether there is some consequence to entirely parameterizing the attitude measurement noise process via the ratio $\frac{k_m}{\sigma_m^2}$. The measurement noise PDF of Equation 6.30 does not provide information about the autocorrelation of the attitude measurement noise process, which could be parameterized by some different function of k_m and σ_m^2 . Despite the potential loss of generality in parameterizing the von Mises PDF of Equation 6.30 via the ratio $\frac{k_m}{\sigma_m^2}$, the BVM PDF of Equation 6.29 can be used to compute ultimate statistics of the filter attitude estimate error as shown in the next corollary.

Corollary 6.2.3.1. *The error dynamics of the Itô SDE 6.18 are such that*

$$\lim_{t \rightarrow \infty} E[\tilde{\varepsilon}^2(t)] = \frac{1}{2} \left(1 - \frac{I_1\left(\frac{k_e}{\sigma_w^2}\right) I_1\left(\frac{k_m}{\sigma_m^2}\right)}{I_0\left(\frac{k_e}{\sigma_w^2}\right) I_0\left(\frac{k_m}{\sigma_m^2}\right)} \right) \quad (6.37)$$

where $I_0(x)$ and $I_1(x)$ are the 0th and 1st order modified Bessel functions of the first kind respectively.

Proof. Compute the expectation using the probability density function from Theorem 6.2.3

$$\begin{aligned}
& \lim_{t \rightarrow \infty} E[\tilde{\varepsilon}^2(t)] \\
&= \lim_{\substack{\sigma_m \rightarrow 0 \\ \frac{k_m}{\sigma_m^2} \text{ constant}}} \frac{1}{N} \int_{-2\pi}^{2\pi} \int_{-2\pi}^{2\pi} \tilde{\varepsilon}^2 \exp \left\{ \frac{k_m}{\sigma_m^2} \cos(\check{\phi}) + \frac{k_e}{\sigma_m^2 + \sigma_w^2} \cos(\tilde{\phi} - \check{\phi}) \right\} d\tilde{\phi} d\check{\phi} \\
&= \lim_{\substack{\sigma_m \rightarrow 0 \\ \frac{k_m}{\sigma_m^2} \text{ constant}}} \frac{1}{N} \int_{-2\pi}^{2\pi} \int_{-2\pi}^{2\pi} \sin^2\left(\frac{\tilde{\phi}}{2}\right) \exp \left\{ \frac{k_m}{\sigma_m^2} \cos(\check{\phi}) + \frac{k_e}{\sigma_m^2 + \sigma_w^2} \cos(\tilde{\phi} - \check{\phi}) \right\} d\tilde{\phi} d\check{\phi} \\
&= \lim_{\substack{\sigma_m \rightarrow 0 \\ \frac{k_m}{\sigma_m^2} \text{ constant}}} \frac{1}{2N} \int_{-2\pi}^{2\pi} \int_{-2\pi}^{2\pi} \exp \left\{ \frac{k_m}{\sigma_m^2} \cos(\check{\phi}) + \frac{k_e}{\sigma_m^2 + \sigma_w^2} \cos(\tilde{\phi} - \check{\phi}) \right\} d\tilde{\phi} d\check{\phi} \\
&\quad - \frac{1}{2N} \lim_{\substack{\sigma_m \rightarrow 0 \\ \frac{k_m}{\sigma_m^2} \text{ constant}}} \int_{-2\pi}^{2\pi} \int_{-2\pi}^{2\pi} \cos(\tilde{\phi}) \exp \left\{ \frac{k_m}{\sigma_m^2} \cos(\check{\phi}) + \frac{k_e}{\sigma_m^2 + \sigma_w^2} \cos(\tilde{\phi} - \check{\phi}) \right\} d\tilde{\phi} d\check{\phi} \\
&= \frac{1}{2} - \frac{1}{2N} \lim_{\substack{\sigma_m \rightarrow 0 \\ \frac{k_m}{\sigma_m^2} \text{ constant}}} \left[\int_{-2\pi}^{2\pi} \exp \left\{ \frac{k_m}{\sigma_m^2} \cos(\check{\phi}) \right\} \int_{-2\pi}^{2\pi} \cos(\tilde{\phi}) \exp \left\{ \frac{k_e}{\sigma_m^2 + \sigma_w^2} \cos(\tilde{\phi} - \check{\phi}) \right\} d\tilde{\phi} d\check{\phi} \right]
\end{aligned}$$

The $\tilde{\phi}$ integral can be found in Mathematica [108] as

$$\int_{-2\pi}^{2\pi} \cos(\tilde{\phi}) \exp \left\{ \frac{k_e}{\sigma_m^2 + \sigma_w^2} \cos(\tilde{\phi} - \check{\phi}) \right\} d\tilde{\phi} = 4\pi I_1 \left(\frac{k_e}{\sigma_m^2 + \sigma_w^2} \right) \cos(\check{\phi})$$

Substituting into the above yields

$$\begin{aligned}
\lim_{t \rightarrow \infty} E[\tilde{\varepsilon}^2(t)] &= \frac{1}{2} - \lim_{\substack{\sigma_m \rightarrow 0 \\ \frac{k_m}{\sigma_m^2} \text{ constant}}} \frac{4\pi I_1 \left(\frac{k_e}{\sigma_m^2 + \sigma_w^2} \right)}{2N} \int_{-2\pi}^{2\pi} \cos(\check{\phi}) \exp \left\{ \frac{k_m}{\sigma_m^2} \cos(\check{\phi}) \right\} d\check{\phi} \\
&= \frac{1}{2} - \lim_{\substack{\sigma_m \rightarrow 0 \\ \frac{k_m}{\sigma_m^2} \text{ constant}}} \frac{16\pi^2 I_1 \left(\frac{k_e}{\sigma_m^2 + \sigma_w^2} \right) I_1 \left(\frac{k_m}{\sigma_m^2} \right)}{2N} \\
&= \lim_{\substack{\sigma_m \rightarrow 0 \\ \frac{k_m}{\sigma_m^2} \text{ constant}}} \frac{1}{2} \left(1 - \frac{I_1 \left(\frac{k_e}{\sigma_m^2 + \sigma_w^2} \right) I_1 \left(\frac{k_m}{\sigma_m^2} \right)}{I_0 \left(\frac{k_e}{\sigma_m^2 + \sigma_w^2} \right) I_0 \left(\frac{k_m}{\sigma_m^2} \right)} \right)
\end{aligned}$$

Now hold the ratio $\frac{k_m}{\sigma_m^2} = \gamma$ fixed but let $\sigma_m \rightarrow \infty$:

$$\begin{aligned}
\lim_{t \rightarrow \infty} E \left[\tilde{\varepsilon}^2(t) \right] &= \lim_{\substack{\sigma_m \rightarrow 0 \\ \frac{k_m}{\sigma_m^2} \text{ constant}}} \frac{1}{2} \left(1 - \frac{I_1 \left(\frac{k_e}{\sigma_m^2 + \sigma_w^2} \right) I_1 \left(\frac{k_m}{\sigma_m^2} \right)}{I_0 \left(\frac{k_e}{\sigma_m^2 + \sigma_w^2} \right) I_0 \left(\frac{k_m}{\sigma_m^2} \right)} \right) \\
&= \lim_{\sigma_m \rightarrow 0} \frac{1}{2} \left(1 - \frac{I_1 \left(\frac{k_e}{\sigma_m^2 + \sigma_w^2} \right) I_1 (\gamma)}{I_0 \left(\frac{k_e}{\sigma_m^2 + \sigma_w^2} \right) I_0 (\gamma)} \right) \\
&= \frac{1}{2} \left(1 - \frac{I_1 \left(\frac{k_e}{\sigma_m^2 + \sigma_w^2} \right) I_1 (\gamma)}{I_0 \left(\frac{k_e}{\sigma_m^2 + \sigma_w^2} \right) I_0 (\gamma)} \right) \\
&= \frac{1}{2} \left(1 - \frac{I_1 \left(\frac{k_e}{\sigma_w^2} \right) I_1 \left(\frac{k_m}{\sigma_m^2} \right)}{I_0 \left(\frac{k_e}{\sigma_w^2} \right) I_0 \left(\frac{k_m}{\sigma_m^2} \right)} \right) \tag{6.38}
\end{aligned}$$

□

6.2.8 Numerical Simulation of Stochastic SO(2) Analytic Results

Consider again the simulations of the SO(2) attitude filter's Itô SDE error dynamics of Equation 6.16 previously discussed in Section 6.2.6. In the proof of Corollary 6.2.3.1, $\lim_{t \rightarrow \infty} E[\tilde{\varepsilon}^2(t)]$ was shown to be such that

$$\lim_{t \rightarrow \infty} E[\tilde{\varepsilon}^2(t)] = \lim_{\sigma_m \rightarrow 0} \frac{1}{2} \left(1 - \frac{I_1\left(\frac{k_e}{\sigma_m^2 + \sigma_w^2}\right) I_1(\gamma)}{I_0\left(\frac{k_e}{\sigma_m^2 + \sigma_w^2}\right) I_0(\gamma)} \right) \quad (6.39)$$

where $\gamma = \frac{k_m}{\sigma_m^2}$ is held constant. The gallery in Figure 6.6 shows plots of the right hand side of Equation 6.39 for a logarithmic sequence of σ_m approaching zero (while holding the ratio $\gamma = \frac{k_m}{\sigma_m^2}$ constant) overlaid on the mean simulation realizations of $\tilde{\varepsilon}^2(t)$. In each set of simulation realizations considered, the analytic ultimate expectation of $\tilde{\varepsilon}^2(t)$ converges to the simulation results as $\sigma_m \rightarrow 0$. The gallery is repeated in Figure 6.7 with the $\sigma_m \rightarrow 0$ limit used for the ultimate expectation.

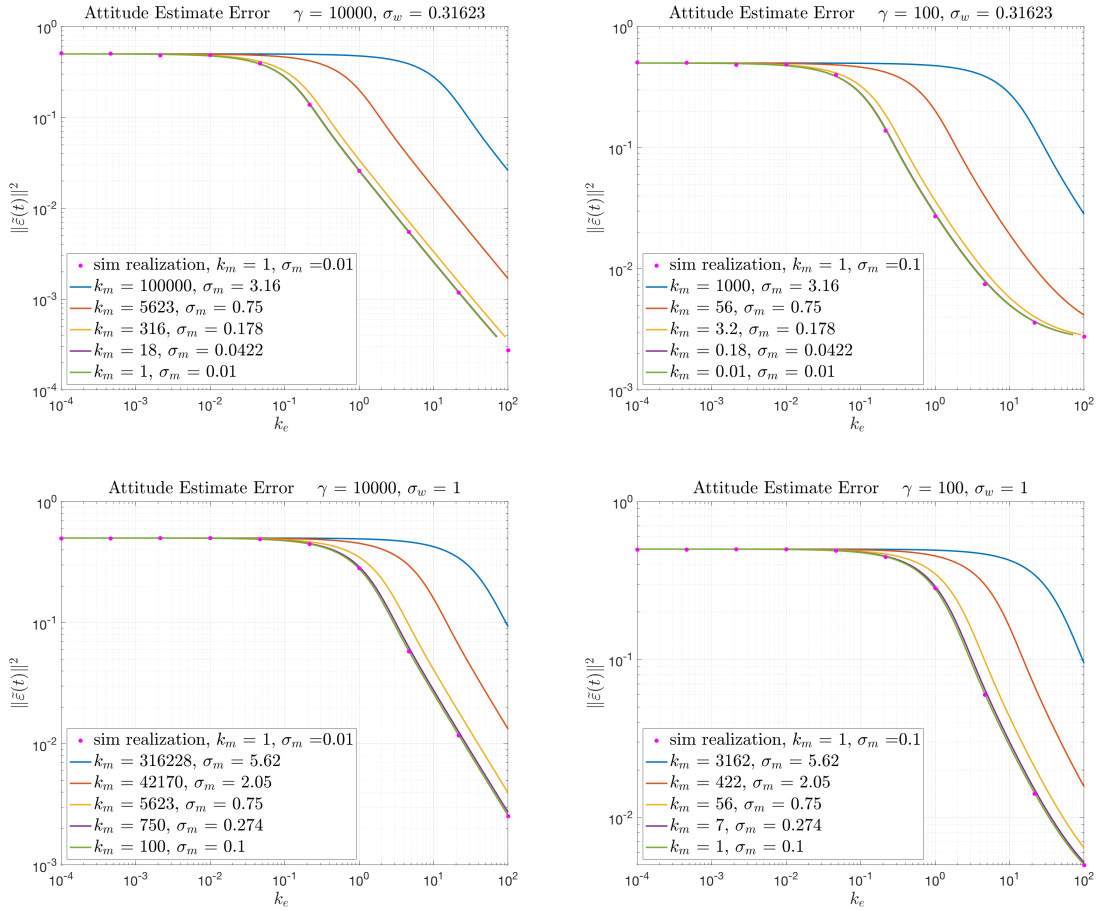


Figure 6.6: The analytic ultimate expectation of $\tilde{\varepsilon}(t)$, provided in Equation 6.39, converges to simulation realizations of attitude estimate errors of the SO(2) error dynamics Itô SDE of Equation 6.16 as $\gamma \rightarrow 0$.

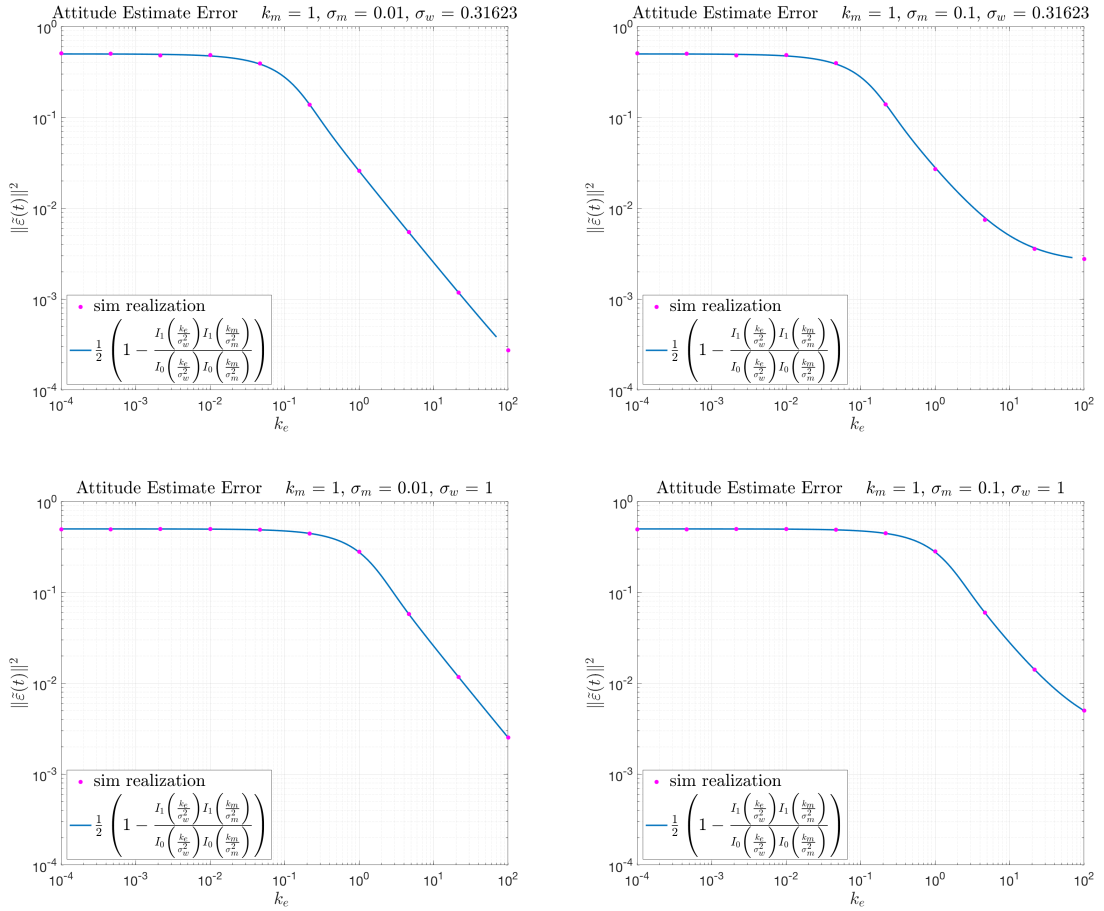


Figure 6.7: The analytic ultimate expectation of Corollary 6.2.3.1 matches the simulation realizations of attitude estimate errors of the SO(2) error dynamics Itô SDE of Equation 6.16.

As further evidence to corroborate the result that the ultimate attitude estimate error is a function of the ratio of $\gamma = \frac{k_m}{\sigma_m^2}$ as in Corollary 6.2.3.1, several sets of simulations were performed. Each of the plots in Figure 6.8 consists of simulations with the same ratio $\gamma = \frac{k_m}{\sigma_m^2}$, but each plot has distinct values of σ_m (and thus also k_m). The analytic ultimate attitude estimate error performance curve from Corollary 6.2.3.1 is compared to simulation realizations for a range of tracking gains k_e in each plot. The performance curves, both from the analytic expression and the simulation results, have the same shape in each plot since they all have the same ratio γ .

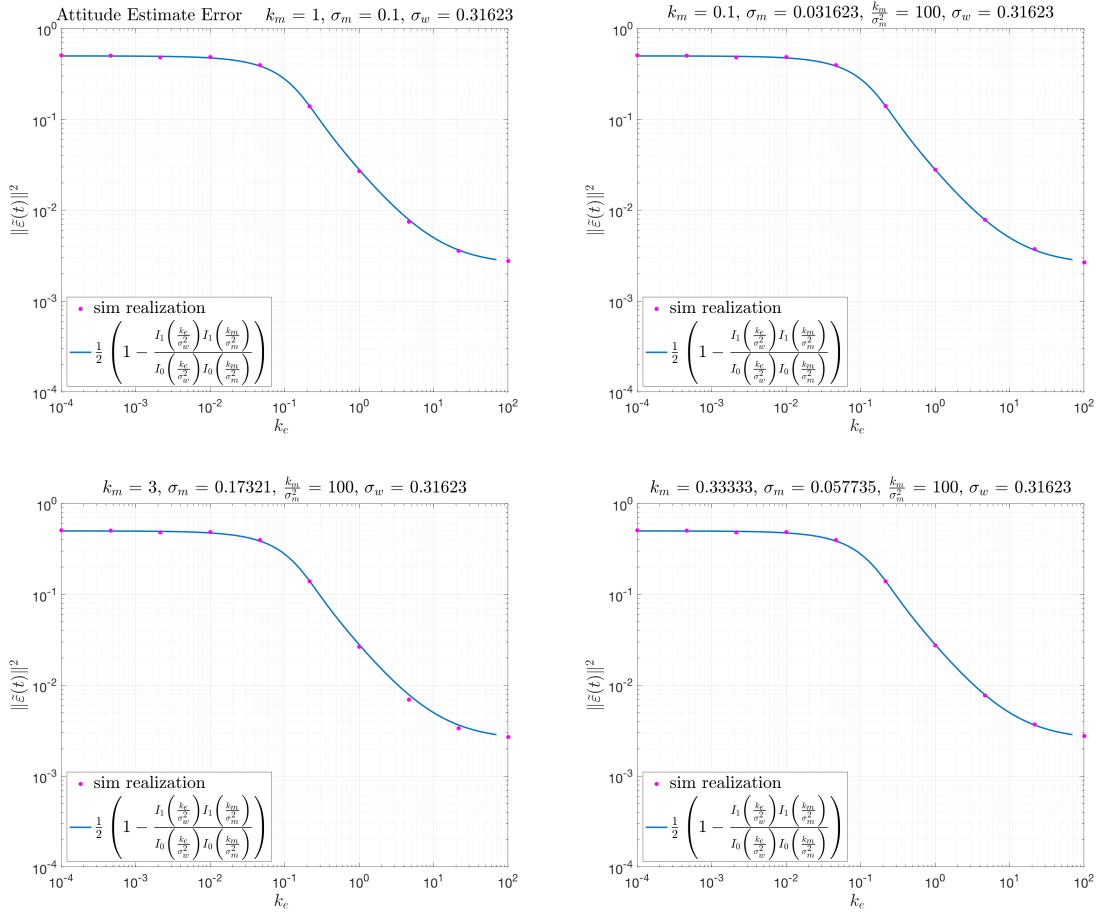


Figure 6.8: Varying the individual values of k_m and σ_m^2 while holding the ratio $\frac{k_m}{\sigma_m}$ constant yields the same performance curve from both the analytic expectation of Corollary 6.2.3.1 and the simulation realizations.

Plots of the ultimate expectation from Corollary 6.2.3.1 for various attitude measurement noise levels $\frac{\sigma_m^2}{k_m}$ are shown in Figure 6.9. As the attitude measurement noise level $\frac{\sigma_m^2}{k_m}$ is reduced (as $\frac{k_m}{\sigma_m^2}$ increases), the high filter gain k_e limit of $\lim_{t \rightarrow \infty} E[\tilde{\varepsilon}^2(t)]$ decreases. This result agrees with intuition since, given the structure of the filter, larger gains force the filter states to track the attitude measurements more closely. In the low gain limit, the filter is unable to incorporate attitude measurement information in its state estimate faster than the state estimate randomly walks due to gyro measurement noise.

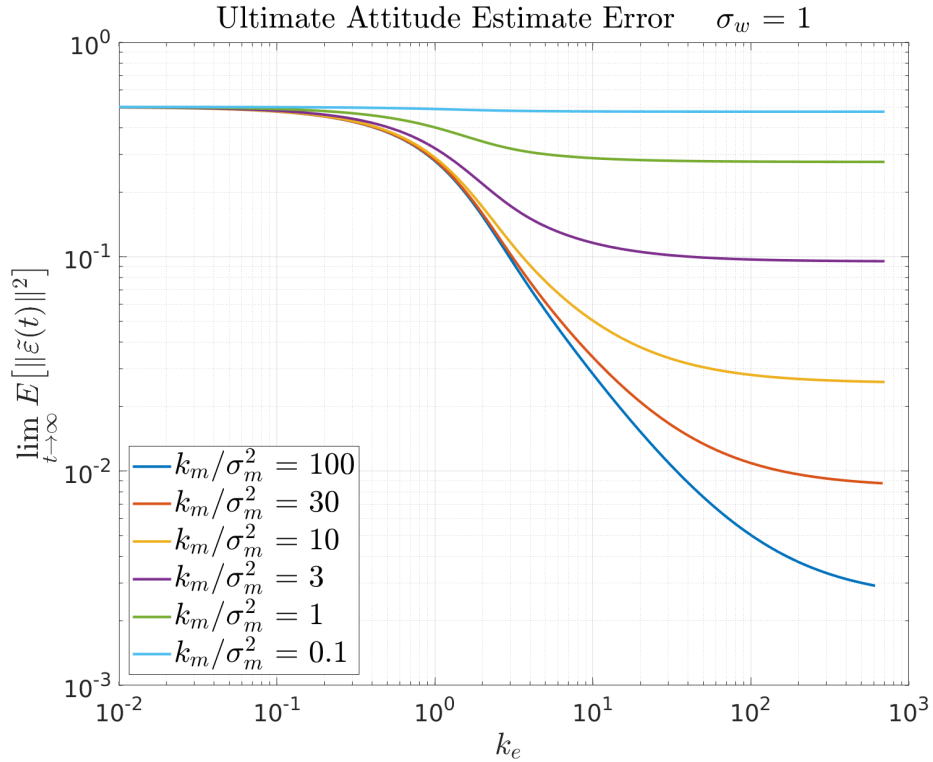


Figure 6.9: Plots of the ultimate expectation from Corollary 6.2.3.1 for various attitude measurement noise levels $\frac{\sigma_m^2}{k_m}$; as the attitude measurement noise level $\frac{\sigma_m^2}{k_m}$ decreases (as $\frac{k_m}{\sigma_m^2}$ increases), the high filter gain limit of the attitude estimate errors decrease.

Plots of the ultimate expectation from Corollary 6.2.3.1 for various gyro measurement noise levels σ_w are shown in Figure 6.10. As the gyro measurement noise increases, the filter gain must increase to allow attitude measurement information to significantly improve the state estimate. Conversely, as the gyro measurement noise decreases, the filter gain allows the state estimates to track the attitude measurements more quickly. Thus the effect of changing the gyro measurement noise parameter σ_w is to simply shift the plot of the ultimate expectation from Corollary 6.2.3.1 horizontally.

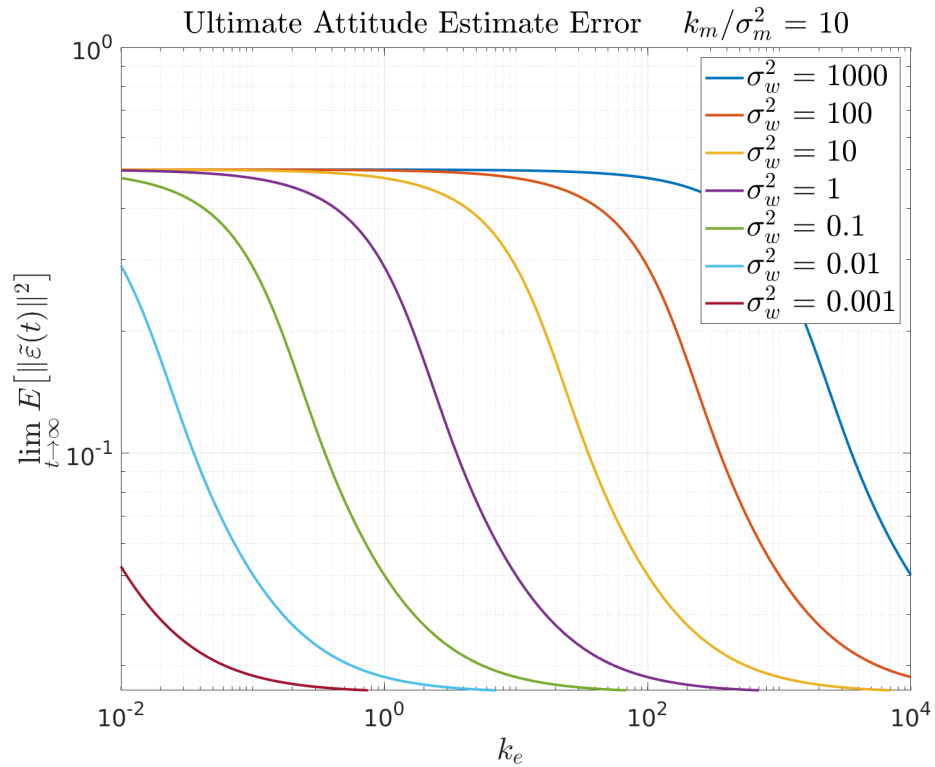


Figure 6.10: Plots of the ultimate expectation from Corollary 6.2.3.1 for various angular measurement noise levels σ_w . The effect of increasing σ_w is to shift the filter's attitude estimate performance curve to the right.

The plots in Figures 6.9 and 6.10 show that the ultimate attitude estimate error variance $\lim_{t \rightarrow \infty} E[\tilde{\varepsilon}^2(t)]$ approaches the ultimate attitude measurement noise variance $\lim_{t \rightarrow \infty} E[\tilde{\varepsilon}^2(t)]$ in the high filter gain limit, when $k_e \rightarrow \infty$. One might expect this result as the filter's feedback term $k_e \tilde{\eta}_m \tilde{\varepsilon}_m$ compares the filter attitude estimate to the attitude measurement. As the filter gain k_e is increased, the feedback term forces the filter to track the attitude measurements more closely.

This phenomena can be further understood by investigating a linear time invariant (LTI) system analogous to the nonlinear attitude filter. Consider the simple LTI kinematics equation for translation

$$\dot{x}(t) = v(t) \tag{6.40}$$

where $x(t)$ is position at time t and $v(t)$ is velocity at time t . Assume two types of measurements of the system state are continuously available. The first measurement is from a velocity sensor with the measurement model

$$v_m(t) = v(t) + \sigma_v w_v(t) \tag{6.41}$$

which produces measurements $v_m(t)$ of the true velocity $v(t)$, but the measurement is perturbed by additive unbounded noise generated by the zero mean Gaussian white noise process $w_v(\cdot)$ and $\sigma_v > 0$ is a scaling constant. The velocity sensor is analogous to the angular rate gyro. The second measurement comes from a position sensor with the measurement model

$$\begin{aligned} x_m(t) &= x(t) + n(t) \\ n(t) &= -\lambda n(t) + \sigma_n w_n(t) \end{aligned} \tag{6.42}$$

where the measurements $x_m(t)$ of the true position $x(t)$ at time t are corrupted by the non-white noise $n(t)$. The non-white noise process is given as a First Order Gauss Markov (FOGM) process with correlation time $\frac{1}{\lambda} > 0$ and driving noise density $\sigma_n > 0$. The driving process noise $w_n(\cdot)$ is a zero mean unit variance Gaussian which is independent of $w_v(\cdot)$.

A translation filter for the velocity measurements of Equation 6.41 and the position measurements of Equation 6.42 can be formulated as

$$\begin{aligned}\dot{\hat{x}}(t) &= v_m(t) + k_e (x_m(t) - \hat{x}(t)) \\ &= v(t) + k_e (x(t) - \hat{x}(t) + n(t)) + \sigma_v w_v(t)\end{aligned}\tag{6.43}$$

with tracking gain $k_e > 0$ as a scalar. The filter of Equation 6.43 is a translational analog of the nonlinear attitude estimation filter of Section 6.2.1; the velocity sensor measurement is used to (imperfectly) propagate the filter kinematic equation, and a feedback term $k_e (x_m(t) - \hat{x}(t))$ is used to drive the position estimate $\hat{x}(t)$ towards the position measurement $x_m(t)$.

Defining the LTI filter's translational estimate error as $\tilde{x}(t) = x(t) - \hat{x}(t)$, the estimate error dynamics are then

$$\begin{aligned}\dot{\tilde{x}}(t) &= \dot{x}(t) - \dot{\hat{x}}(t) \\ &= v(t) - v(t) - k_e (x(t) - \hat{x}(t) + n(t)) + \sigma_v w_v(t) \\ &= -k_e \tilde{x}(t) - k_e n(t) - \sigma_v w_v(t)\end{aligned}$$

Augmenting the estimate error dynamics with the FOGM process dynamics yields

the filter error dynamics

$$\begin{aligned}\dot{\mathbf{x}}(t) &= \begin{bmatrix} \dot{n}(t) \\ \dot{\tilde{x}}(t) \end{bmatrix} = \begin{bmatrix} -\lambda & 0 \\ -k_e & -k_e \end{bmatrix} \begin{bmatrix} n(t) \\ \tilde{x}(t) \end{bmatrix} + \begin{bmatrix} \sigma_n & 0 \\ 0 & -\sigma_v \end{bmatrix} \begin{bmatrix} w_n(t) \\ w_v(t) \end{bmatrix} \\ &= F\mathbf{x}(t) + G\mathbf{w}(t)\end{aligned}\tag{6.44}$$

The filter error dynamics of Equation 6.44 constitute an LTI system. As $\lambda > 0$ and $k_e > 0$ by construction, the matrix F is Hurwitz. As discussed in Section 2.1.4.1, the LTI system with Hurwitz dynamics matrix F has a covariance matrix $P(t) = E[\mathbf{x}(t)\mathbf{x}^T(t)]$ that approaches a stationary covariance matrix $P_s = \lim_{t \rightarrow \infty} E[\mathbf{x}(t)\mathbf{x}^T(t)]$ that satisfies the covariance Lyapunov equation

$$0 = FP_s + P_sF^T + GG^T$$

Denoting

$$P_s = \begin{bmatrix} p_{n,n} & p_{n,x} \\ p_{n,x} & p_{x,x} \end{bmatrix} = \lim_{t \rightarrow \infty} E[\mathbf{x}(t)\mathbf{x}^T(t)]$$

and solving the covariance Lyapunov equation yields

$$\begin{aligned}p_{n,n} &= \lim_{t \rightarrow \infty} E[n^2(t)] = \frac{\sigma_n^2}{2\lambda} \\ p_{n,x} &= \lim_{t \rightarrow \infty} E[n(t)x(t)] = -\frac{k_e}{\lambda + k_e} \frac{\sigma_n^2}{2\lambda} \\ p_{x,x} &= \lim_{t \rightarrow \infty} E[x^2(t)] = \frac{\sigma_v^2}{2k_e} + \frac{k_e}{\lambda + k_e} \frac{\sigma_n^2}{2\lambda}\end{aligned}\tag{6.45}$$

The translational position estimate error variance $p_{x,x}$ is composed of two terms: the first term describes the contribution of the velocity sensor noise density σ_v to the estimate error variance, while the second describes the contribution of the non-white position measurement noise density σ_n . For infinitely large tracking gain k_e ,

the contribution of the velocity sensor noise vanishes; however, the contribution from the position measurement noise remains. This result can be further corroborated by examining the structure of the filter dynamics of Equation 6.43. The filter tracking gain k_e essentially acts as a weighting coefficient balancing contributions to the filter dynamics between the filter translation kinematic model and position measurement feedback. For a small tracking gain k_e the filter dynamics $\dot{\hat{x}}(t)$ are principally given by the filter's translational kinematic model driven by the velocity measurement. For a large tracking gain k_e the filter dynamics $\dot{\hat{x}}(t)$ are principally driven by the estimate error term $e_x(t) = x_m(t) - \hat{x}(t)$.

The above analysis in the LTI case is analogous to that of the nonlinear attitude filter. For large tracking gain k_e , the ultimate attitude estimate error variance $\lim_{t \rightarrow \infty} E[\tilde{\varepsilon}^2(t)]$ approaches the ultimate attitude measurement noise variance $\lim_{t \rightarrow \infty} E[\varepsilon^2(t)]$. From the construction of the nonlinear attitude filter, the tracking gain k_e acts as a weighting coefficient balancing contributions to the filter dynamics between the filter attitude kinematic model and attitude measurement feedback. For a small tracking gain k_e the filter dynamics $\dot{\hat{\mathbf{q}}}(t)$ are principally given by the filter's attitude kinematic model driven by the gyro measurement. For a large tracking gain k_e the filter dynamics $\dot{\hat{\mathbf{q}}}(t)$ are principally driven by the attitude estimate error term $e(t) = \tilde{\eta}_m(t)\tilde{\varepsilon}_m(t)$ which compares the filter attitude estimate $\hat{\mathbf{q}}(t)$ with the attitude measurement $\mathbf{q}_m(t)$.

6.2.9 SO(3) Bound Extrapolated from SO(2) Analytic Solution

Following the same approach as that of Section 4.10, this section extrapolates an upper bound for the ultimate expectation of the SO(3) filter's attitude estimate errors from the analytic solution of the ultimate expectation of the SO(2) filter's attitude estimate errors given in Corollary 6.2.3.1. The factor of $\frac{1}{2}$ in Equation 6.37 is rescaled to $\frac{3}{4}$ so the SO(3) bound matches the low filter gain limit seen in the numerical simulation results. Next, various choices of noise level scaling ξ are used in the expression

$$\text{bound} \left(\xi, \frac{k_e}{\sigma_w^2}, \frac{k_m}{\sigma_m^2} \right) = \frac{3}{4} \left(1 - \frac{I_1 \left(\frac{k_e}{\xi \sigma_w^2} \right) I_1 \left(\frac{k_m}{\xi \sigma_m^2} \right)}{I_0 \left(\frac{k_e}{\xi \sigma_w^2} \right) I_0 \left(\frac{k_m}{\xi \sigma_m^2} \right)} \right) \quad (6.46)$$

The notional bound with various choices of ξ is superimposed on plots of the numerical simulations of the SO(3) Itô SDE 6.10 for the case of a spinning vehicle in the gallery of Figure 6.11 and an inertially fixed vehicle in Figure 6.12.

In all cases considered, the choice of $\xi = 3$ in the expression of Equation 6.46 bound the simulation realizations. Again this agrees with the logic considered in Section 4.10, that the variance of a random walk process in three dimensions driven by independent noise sources along each axis is upper bounded by the variance of a random walk process in one dimension with the three independent noise sources each acting on the single axis. Focusing all the noise energy along a single physical dimension maximizes the potential for constructive and destructive interference. This is an upper bound as the noise channels in the SO(3) case represent actual sensor hardware noise which are physically restricted to independent axes. Thus

the heuristic upper bound for the SO(3) case is given here as

$$\lim_{t \rightarrow \infty} E \left[\tilde{\boldsymbol{\epsilon}}^T(t) \tilde{\boldsymbol{\epsilon}}(t) \right] \leq \frac{3}{4} \left(1 - \frac{I_1 \left(\frac{k_e}{3\sigma_w^2} \right) I_1 \left(\frac{k_m}{3\sigma_m^2} \right)}{I_0 \left(\frac{k_e}{3\sigma_w^2} \right) I_0 \left(\frac{k_m}{3\sigma_m^2} \right)} \right) \quad (6.47)$$

The upper bound is drawn again for clarity for the case of a spinning vehicle in the gallery of Figure 6.13 and an inertially fixed vehicle in Figure 6.14.

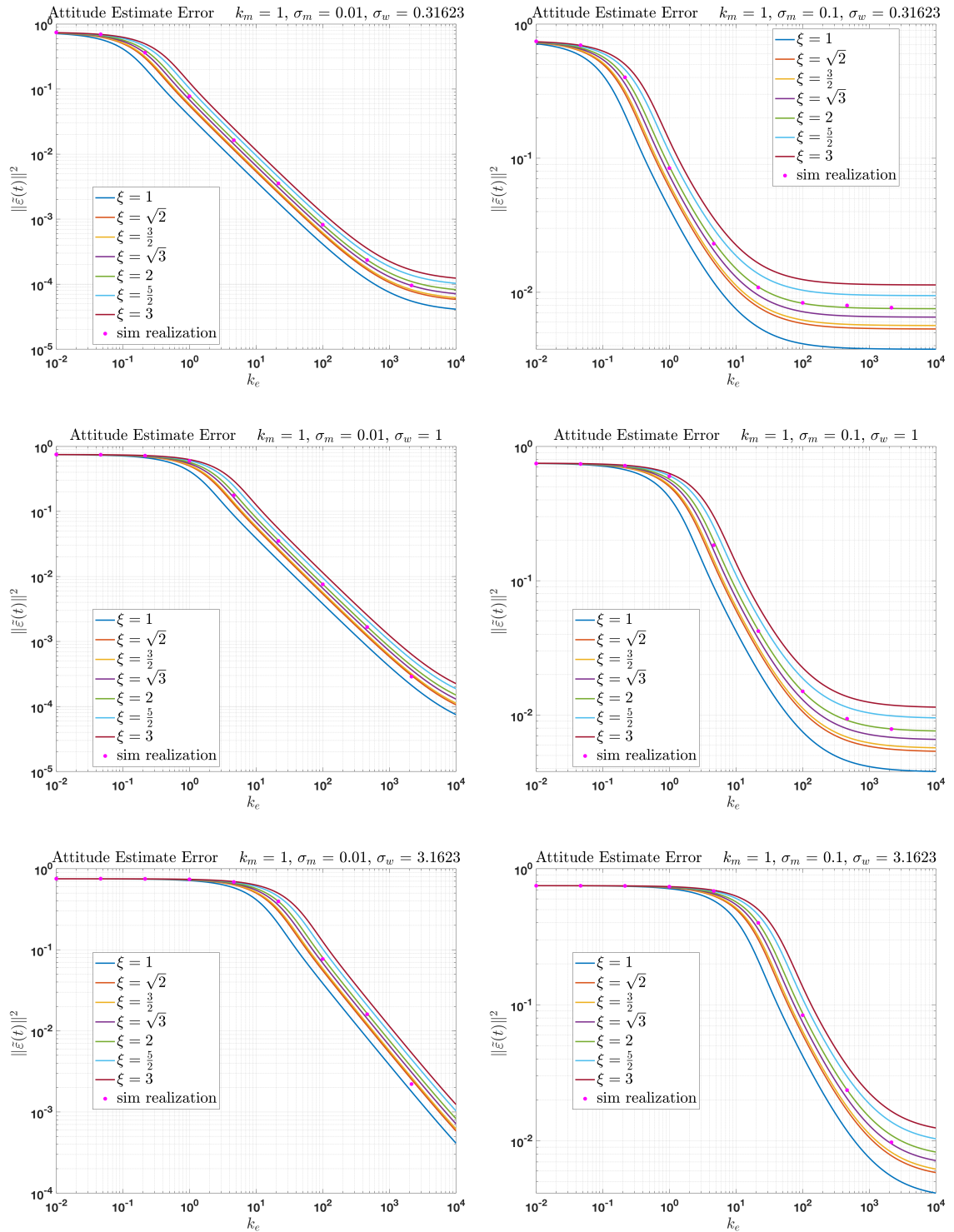


Figure 6.11: Comparison of simulation realizations of the attitude estimate error and the notional bound of Equation 6.46 for several choices of ξ and for the case of a vehicle spinning at 5 revolutions per minute about the vehicle body's $[1 \ 2 \ 3]^T$ axis.

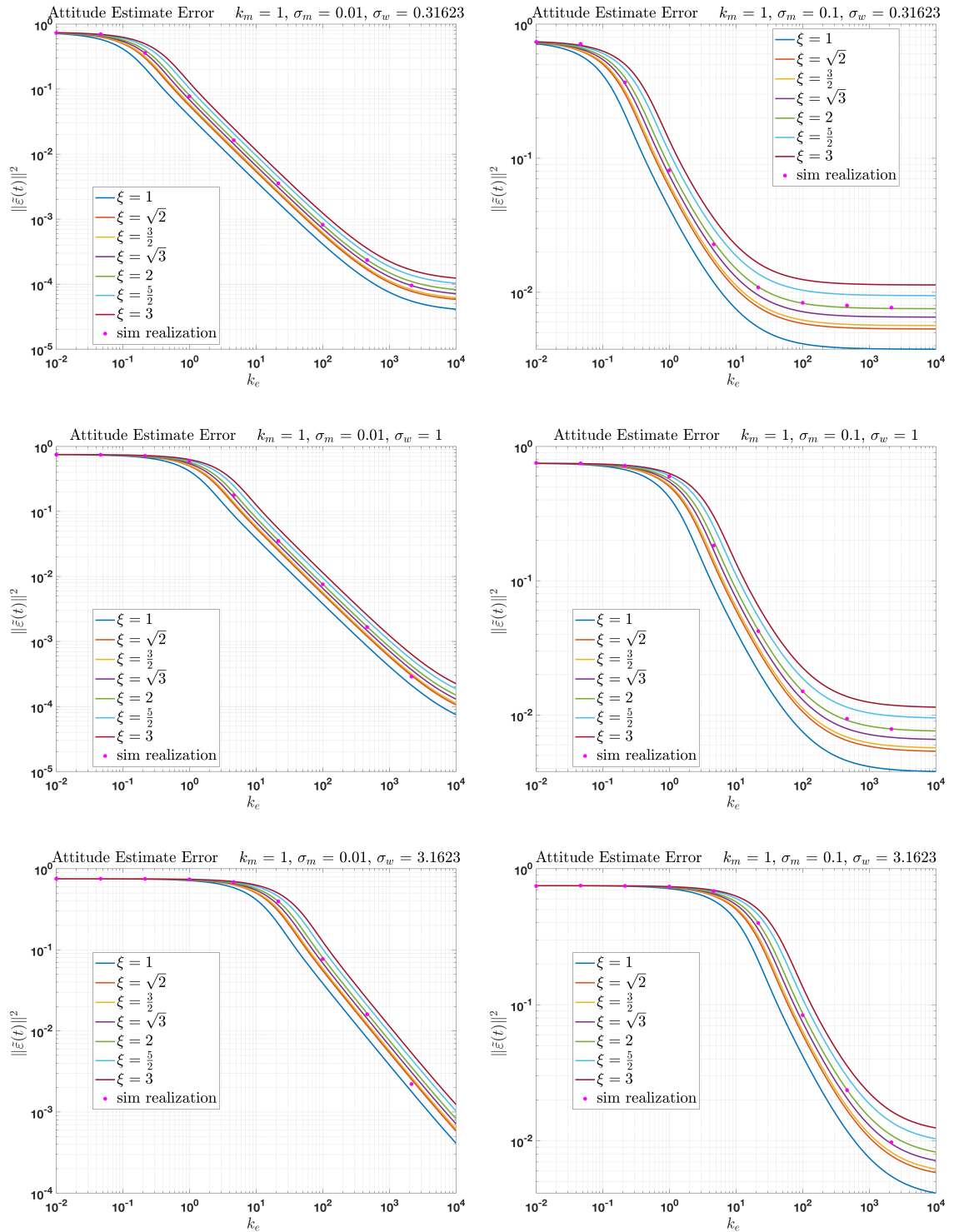


Figure 6.12: Comparison of simulation realizations of the attitude estimate error and the notional bound of Equation 6.46 for several choices of ξ and for the case of a vehicle inertially fixed (not spinning).

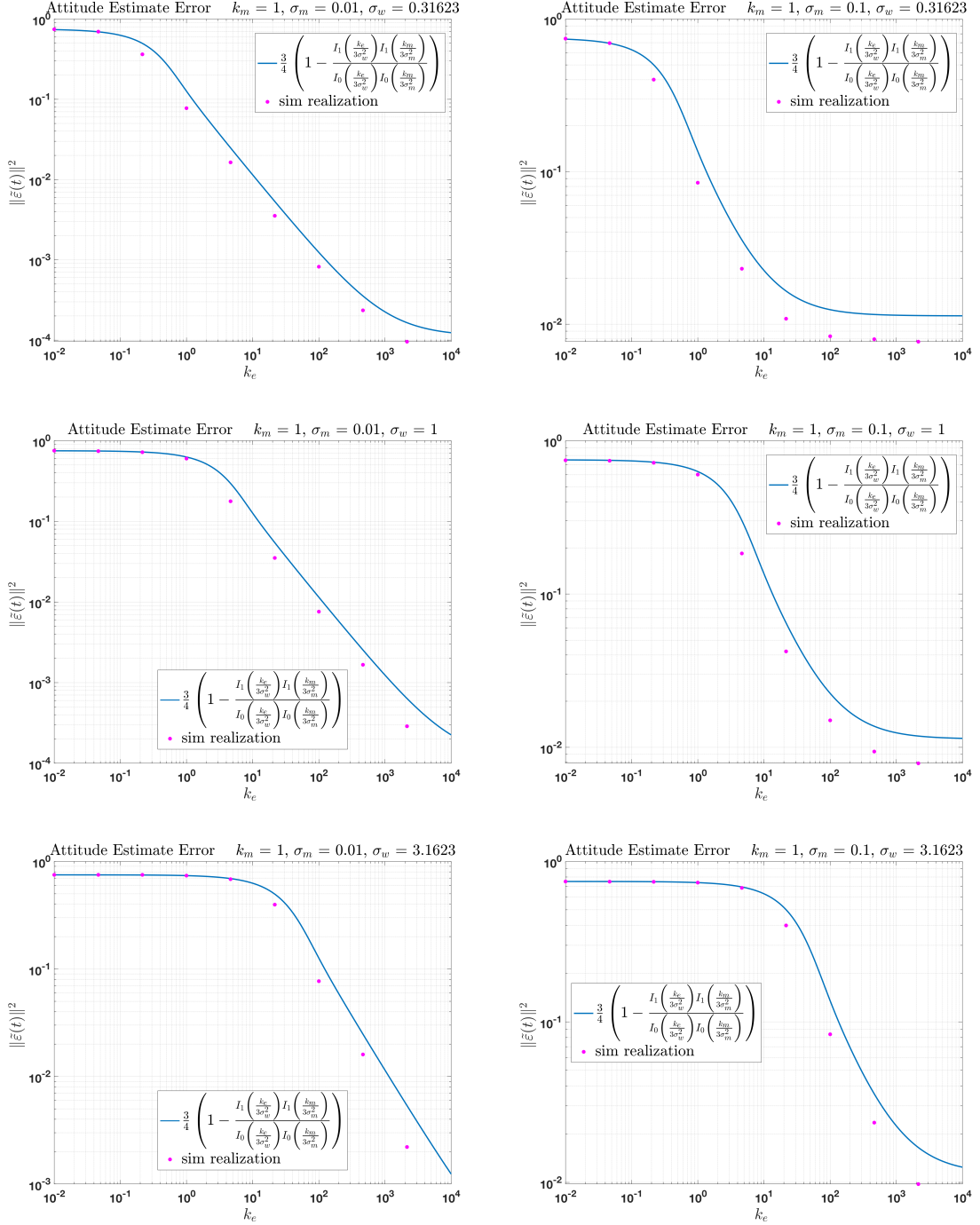


Figure 6.13: Comparison of simulation realizations of the attitude estimate error and the heuristic bound of Equation 6.47 for the case of a vehicle spinning at 5 revolutions per minute about the vehicle body's $[1 \ 2 \ 3]^T$ axis.

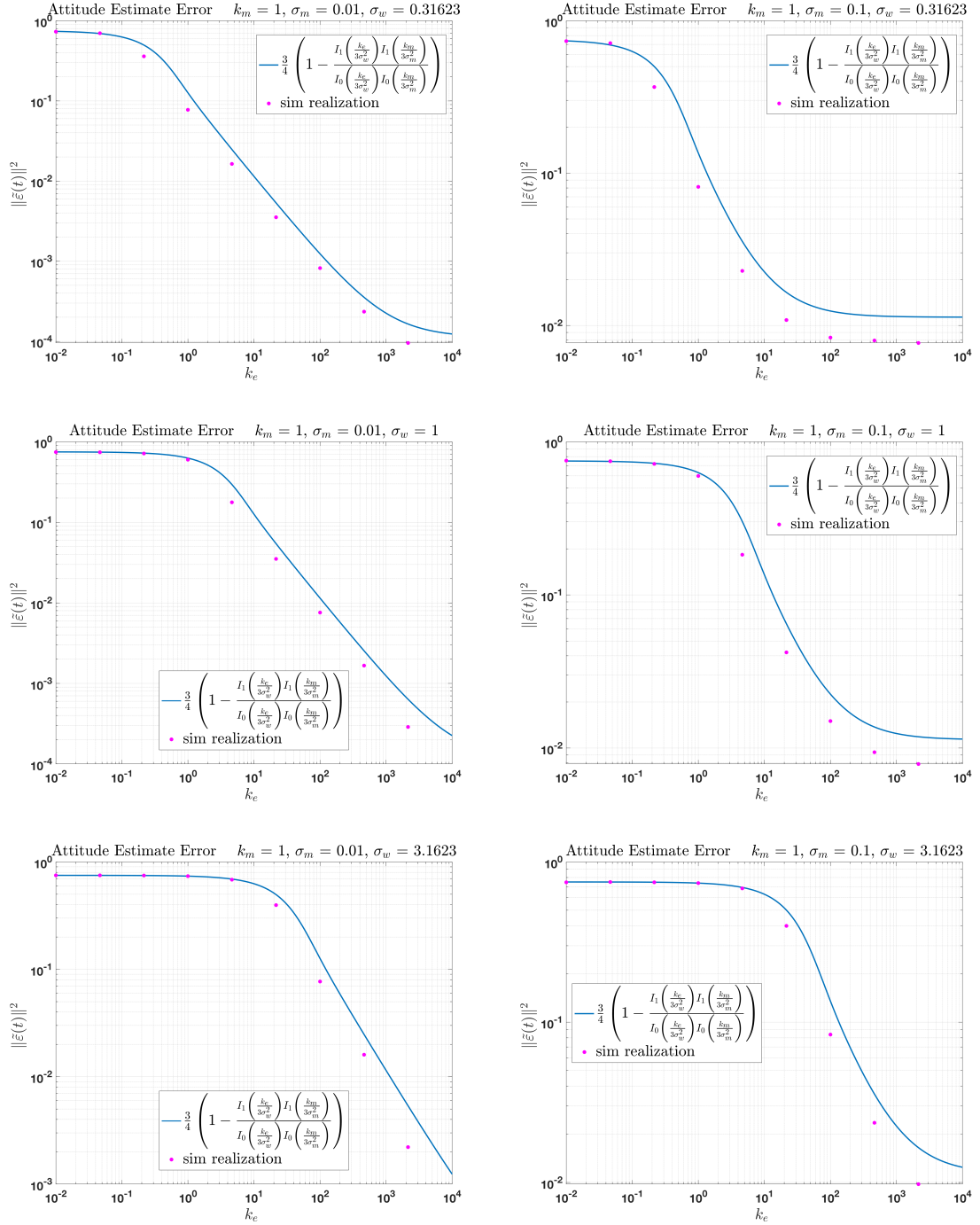


Figure 6.14: Comparison of simulation realizations of the attitude estimate error and the heuristic bound of Equation 6.47 for the case of a vehicle inertially fixed (not spinning).

6.3 Gyro Constant Bias Filter for Gyro Additive Noise and Attitude Measurement Noise

This section considers the inclusion of attitude measurement noise in the gyro constant bias estimation problem. Specifically, the gyro constant bias estimation filter studied in Chapter 5 is now assumed to have the attitude measurement noise model of Section 6.1.

Section 6.3.1 presents the measurement models considered, the formulation of the attitude filter, and culminates with the derivation of an Itô SDE for the system error dynamics. While the constant gyro bias filter was able to utilize the converse Lyapunov theorem to find a Lyapunov function suitable to demonstrate weak stochastic stability in Section 5.2, the converse Lyapunov theorem does not apply to the filter error dynamics augmented with the quaternion measurement noise model; a Fokker-Planck analysis is pursued under the **assumption** that the filter error dynamics are stable. The system is reduced to the $SO(2)$ case in Section 6.3.2 to first gain insight.

Similar to the attitude estimation filter with attitude measurement noise studied in Section 6.2, an asymptotic solution to the $SO(2)$ stationary Fokker-Planck PDE is found in Section 6.3.3. The asymptotic solution is subsequently used to find analytic expressions for the ultimate attitude estimate error variance as well as the ultimate gyro bias estimate error mean and variance. These results are verified via simulation analysis in Section 6.3.4. Similar to Sections 4.10, 5.7, and 6.2.9, Section

6.3.5 provides bounds for the ultimate attitude estimate error variance as well as the ultimate gyro bias estimate error variance for the $SO(3)$ case by extrapolating the $SO(2)$ results of Section 6.3.3 .

6.3.1 Gyro Constant Bias Filter Formulation in SO(3)

As in Section 5.1, the angular rate gyro measurements are modeled as having a constant bias \mathbf{b} as well as additive noise

$$\boldsymbol{\omega}_g(t) = \boldsymbol{\omega}(t) + \mathbf{b} + \sigma_w \mathbf{n}_w(t) \quad (6.48)$$

where, as before, $\boldsymbol{\omega}_g(t)$ is the gyro measurement at time t , $\boldsymbol{\omega}(t)$ is the true vehicle angular rate at time t , σ_w is a positive scaling constant, and $\mathbf{n}_w(\cdot)$ is a zero mean unit variance Gaussian white noise process. As the bias is assumed to be constant, $\dot{\mathbf{b}}(t) = 0$.

The attitude measurement $\mathbf{q}_m(t)$, possibly from a quaternion output star tracker, is modeled here as a noise corrupted version of the true vehicle attitude $\mathbf{q}(t)$ as presented in Section 6.1

$$\mathbf{q}_m(t) = \check{\mathbf{q}}^{-1}(t) \otimes \mathbf{q}(t) \quad (6.49)$$

where $\check{\mathbf{q}}(\cdot)$ is a quaternion noise process. The attitude measurement evolves according to Equation 6.3 repeated here for convenience

$$\dot{\mathbf{q}}_m(t) = \frac{1}{2} \left\{ R \left(\check{\mathbf{q}}^{-1}(t) \right) \left[\boldsymbol{\omega}(t) + \sigma_m \mathbf{n}_m(t) + k_m \check{\eta}(t) \check{\boldsymbol{\epsilon}}(t) \right] \right\} \otimes \mathbf{q}_m(t) \quad (6.50)$$

where k_m and σ_m are positive scalars that parameterize the attitude measurement noise statistics, $\mathbf{n}_m(\cdot)$ is a collection of independent identically distributed zero mean unit variance Gaussian white noise processes independent of $\mathbf{n}_w(\cdot)$, and $\check{\mathbf{q}}(t)$ compares the attitude measurement noise process to the true vehicle attitude

$$\check{\mathbf{q}}(t) = \mathbf{q}(t) \otimes \mathbf{q}_m^{-1}(t) = \begin{bmatrix} \check{\boldsymbol{\epsilon}}(t) \\ \check{\eta}(t) \end{bmatrix} \quad (6.51)$$

The attitude measurement noise error dynamics are given in Equation 6.4.

In Chapter 5 the gyro constant bias filter had access to the true attitude in real time; it could use the filter attitude estimate error $\tilde{\mathbf{q}}(t) = \begin{bmatrix} \tilde{\boldsymbol{\epsilon}}(t) \\ \tilde{\eta}(t) \end{bmatrix} = \mathbf{q}(t) \otimes \hat{\mathbf{q}}^{-1}(t)$ to drive its kinematics as in Equation 5.3. In this chapter, however, the filter is restricted to using attitude measurements corrupted by noise. Thus in this section the filter equations are given as

$$\begin{aligned} \dot{\hat{\mathbf{q}}}(t) &= \frac{1}{2} \left\{ R(\tilde{\mathbf{q}}_m^{-1}(t)) \left[\boldsymbol{\omega}_g(t) - \hat{\mathbf{b}}(t) + k_e \tilde{\eta}_m(t) \tilde{\boldsymbol{\epsilon}}_m(t) \right] \right\} \otimes \hat{\mathbf{q}}(t) \\ \dot{\hat{\mathbf{b}}}(t) &= -\alpha \tilde{\eta}_m(t) \tilde{\boldsymbol{\epsilon}}_m(t) \end{aligned} \quad (6.52)$$

which is driven by the noise corrupted attitude estimate error

$$\begin{aligned} \tilde{\mathbf{q}}_m(t) &= \begin{bmatrix} \tilde{\boldsymbol{\epsilon}}_m(t) \\ \tilde{\eta}_m(t) \end{bmatrix} = \mathbf{q}_m(t) \otimes \hat{\mathbf{q}}^{-1}(t) \\ &= \check{\mathbf{q}}^{-1}(t) \otimes \mathbf{q}(t) \otimes \hat{\mathbf{q}}^{-1}(t) \\ &= \check{\mathbf{q}}^{-1}(t) \otimes \tilde{\mathbf{q}}(t) \end{aligned} \quad (6.53)$$

The expression $\tilde{\eta}_m(t) \tilde{\boldsymbol{\epsilon}}_m(t)$ is expanded in terms of $\tilde{\boldsymbol{\epsilon}}(t)$, $\tilde{\eta}(t)$, $\check{\boldsymbol{\epsilon}}(t)$, and $\check{\eta}(t)$ in Equation 6.7. As before, $k_e > 0$ is a filter (estimator) gain parameter, $\hat{\mathbf{q}}(t)$ is the filter's estimate of the vehicle attitude $\mathbf{q}(t)$ at time t , $\alpha > 0$ is the filter adaptation gain parameter, and $\hat{\mathbf{b}}(t)$ is the filter's estimate at time t of the gyro bias \mathbf{b} .

The filter's bias estimate error $\tilde{\mathbf{b}}(t)$ is given as

$$\tilde{\mathbf{b}}(t) = \mathbf{b} - \hat{\mathbf{b}}(t) \quad (6.54)$$

The filter uses its bias estimate in the filter kinematic equation to attempt to correct for the true bias in the gyro measurement. Since the gyro bias is assumed to be

constant, $\dot{\hat{\mathbf{b}}}(t) = 0$, the bias estimate error dynamics are simply

$$\dot{\tilde{\mathbf{b}}}(t) = \alpha \tilde{\eta}_m(t) \tilde{\boldsymbol{\varepsilon}}_m(t) \quad (6.55)$$

The attitude estimate dynamics in Equation 6.52 can be combined with the quaternion error kinematics of Equation 2.71 and the gyro measurement model from Equation 6.48 to find the filter's attitude estimate error dynamics. Suppressing function of time notation for brevity, the attitude estimate error dynamics are found to be

$$\begin{aligned} \dot{\tilde{\mathbf{q}}} &= \frac{1}{2} \left\{ \boldsymbol{\omega} - R(\tilde{\mathbf{q}}) R(\tilde{\mathbf{q}}_m^{-1}) \left[\boldsymbol{\omega}_g - \hat{\mathbf{b}} + k_e \tilde{\eta}_m \tilde{\boldsymbol{\varepsilon}}_m \right] \right\} \otimes \tilde{\mathbf{q}} \\ &= \frac{1}{2} \left\{ \boldsymbol{\omega} - R(\tilde{\mathbf{q}}) R(\tilde{\mathbf{q}}^{-1}) R(\check{\mathbf{q}}) \left[\boldsymbol{\omega} + \mathbf{b} + \sigma_w \mathbf{n}_w - \hat{\mathbf{b}} + k_e \tilde{\eta}_m \tilde{\boldsymbol{\varepsilon}}_m \right] \right\} \otimes \tilde{\mathbf{q}} \\ &= \frac{1}{2} \left\{ \left[I - R(\check{\mathbf{q}}) \right] \boldsymbol{\omega} - R(\check{\mathbf{q}}) \left[k_e \tilde{\eta}_m \tilde{\boldsymbol{\varepsilon}}_m + \tilde{\mathbf{b}} + \sigma_w \mathbf{n}_w \right] \right\} \otimes \tilde{\mathbf{q}} \end{aligned} \quad (6.56)$$

Just as in Section 6.2.1, the attitude measurement noise prevents the filter from being able to perfectly resolve its angular rate estimate in the appropriate frame. A consequence is that the vehicle angular rate $\boldsymbol{\omega}$ appears explicitly in the attitude estimate error dynamics. As before, when the attitude noise is zero ($\check{\mathbf{q}} = \mathbf{q}_{Identity}$), the $\left[I - R(\check{\mathbf{q}}) \right] \boldsymbol{\omega}$ term vanishes and $\tilde{\eta}_m \tilde{\boldsymbol{\varepsilon}}_m$ simplifies to $\tilde{\eta} \tilde{\boldsymbol{\varepsilon}}$.

Combining the attitude noise model error dynamics of Equation 6.4, the filter attitude estimate error dynamics of Equation 6.56, and the bias estimate error

dynamics of Equation 6.55 leads to the Langevin form filter error dynamics

$$\begin{aligned}
\dot{\hat{\mathbf{x}}} &= \begin{bmatrix} \dot{\check{\mathbf{q}}} \\ \dot{\check{\mathbf{q}}} \\ \dot{\check{\mathbf{b}}} \end{bmatrix} = \begin{bmatrix} \dot{\check{\boldsymbol{\varepsilon}}} \\ \dot{\check{\eta}} \\ \dot{\check{\boldsymbol{\varepsilon}}} \\ \dot{\check{\eta}} \\ \dot{\check{\mathbf{b}}} \end{bmatrix} \\
&= \begin{bmatrix} -\frac{1}{2}k_m\check{\eta}^2\check{\boldsymbol{\varepsilon}} \\ \frac{1}{2}k_m\check{\eta}\check{\boldsymbol{\varepsilon}}^T\check{\boldsymbol{\varepsilon}} \\ \frac{1}{2}[\check{\eta}I + [\check{\boldsymbol{\varepsilon}} \times]] [I - R(\check{\mathbf{q}})] \boldsymbol{\omega} - \frac{1}{2}[\check{\eta}I + [\check{\boldsymbol{\varepsilon}} \times]] R(\check{\mathbf{q}}) [k_e\tilde{\eta}_m\tilde{\boldsymbol{\varepsilon}}_m + \tilde{\mathbf{b}}] \\ -\frac{1}{2}\check{\boldsymbol{\varepsilon}}^T [I - R(\check{\mathbf{q}})] \boldsymbol{\omega} + \frac{1}{2}\check{\boldsymbol{\varepsilon}}^T R(\check{\mathbf{q}}) [k_e\tilde{\eta}_m\tilde{\boldsymbol{\varepsilon}}_m + \tilde{\mathbf{b}}] \\ \alpha\tilde{\eta}_m\tilde{\boldsymbol{\varepsilon}}_m \end{bmatrix} \\
&+ \begin{bmatrix} -\frac{1}{2}[\check{\eta}I + [\check{\boldsymbol{\varepsilon}} \times]] \sigma_m & 0 \\ \frac{1}{2}\check{\boldsymbol{\varepsilon}}^T \sigma_m & 0 \\ 0 & -\frac{1}{2}[\check{\eta}I + [\check{\boldsymbol{\varepsilon}} \times]] R(\check{\mathbf{q}}) \sigma_w \\ 0 & \frac{1}{2}\check{\boldsymbol{\varepsilon}}^T R(\check{\mathbf{q}}) \sigma_w \\ 0 & 0 \end{bmatrix} \begin{bmatrix} \mathbf{n}_m \\ \mathbf{n}_w \end{bmatrix} \quad (6.57)
\end{aligned}$$

where $\tilde{\eta}_m\tilde{\boldsymbol{\varepsilon}}_m$ is expanded in Equation 6.7.

As discussed in Section 2.1.3, the Langevin form error dynamics differential equation 6.57 is interpreted as a Stratonovich SDE. Converting to an Itô SDE results

in the following

$$\begin{aligned}
d\tilde{\mathbf{x}} &= \begin{bmatrix} d\check{\mathbf{q}} \\ d\tilde{\mathbf{q}} \\ d\tilde{\mathbf{b}} \end{bmatrix} = \begin{bmatrix} d\check{\boldsymbol{\varepsilon}} \\ d\check{\eta} \\ d\tilde{\boldsymbol{\varepsilon}} \\ d\tilde{\eta} \\ d\tilde{\mathbf{b}} \end{bmatrix} \\
&= \begin{bmatrix} -\frac{1}{2}k_m\check{\eta}^2\check{\boldsymbol{\varepsilon}} - \frac{3}{8}\sigma_m^2\check{\boldsymbol{\varepsilon}} \\ \frac{1}{2}k_m\check{\eta}\check{\boldsymbol{\varepsilon}}^T\check{\boldsymbol{\varepsilon}} - \frac{3}{8}\sigma_m^2\check{\eta} \\ \frac{1}{2}[\tilde{\eta}I + [\tilde{\boldsymbol{\varepsilon}} \times]] [I - R(\check{\mathbf{q}})] \boldsymbol{\omega} - \frac{1}{2}[\tilde{\eta}I + [\tilde{\boldsymbol{\varepsilon}} \times]] R(\check{\mathbf{q}}) [k_e\tilde{\eta}_m\tilde{\boldsymbol{\varepsilon}}_m + \tilde{\mathbf{b}}] - \frac{3}{8}\sigma_w^2\tilde{\boldsymbol{\varepsilon}} \\ -\frac{1}{2}\tilde{\boldsymbol{\varepsilon}}^T [I - R(\check{\mathbf{q}})] \boldsymbol{\omega} + \frac{1}{2}\tilde{\boldsymbol{\varepsilon}}^T R(\check{\mathbf{q}}) [k_e\tilde{\eta}_m\tilde{\boldsymbol{\varepsilon}}_m + \tilde{\mathbf{b}}] - \frac{3}{8}\sigma_w^2\tilde{\eta} \\ \alpha\tilde{\eta}_m\tilde{\boldsymbol{\varepsilon}}_m \end{bmatrix} dt \\
&\quad + \begin{bmatrix} -\frac{1}{2}[\check{\eta}I + [\check{\boldsymbol{\varepsilon}} \times]] \sigma_m & 0 \\ \frac{1}{2}\check{\boldsymbol{\varepsilon}}^T \sigma_m & 0 \\ 0 & -\frac{1}{2}[\tilde{\eta}I + [\tilde{\boldsymbol{\varepsilon}} \times]] R(\check{\mathbf{q}}) \sigma_w \\ 0 & \frac{1}{2}\tilde{\boldsymbol{\varepsilon}}^T R(\check{\mathbf{q}}) \sigma_w \\ 0 & 0 \end{bmatrix} \begin{bmatrix} d\boldsymbol{\beta}_m \\ d\boldsymbol{\beta}_w \end{bmatrix} \\
&= \mathbf{f}(\tilde{\mathbf{x}})dt + G(\tilde{\mathbf{x}})d\boldsymbol{\beta} \tag{6.58}
\end{aligned}$$

Note that the converse Lyapunov theorem can not be invoked here as in Section 5.2. Here, the attitude estimate error states and the measurement error states mix in the nonlinear function $\tilde{\eta}_m(t)\tilde{\boldsymbol{\varepsilon}}_m(t)$ of Equation 6.7. While the quaternion measurement error dynamics of Equation 6.4 were shown to be weakly stochastically stable in Section 4.2.1 and the noise-free attitude measurement gyro constant bias

observer of Chapter 5 was shown to be weakly stochastically stable in Section 5.2, there is no guarantee that providing the state of one weakly stochastically stable system as an input into another weakly stochastically stable system results in a combination that is weakly stochastically stable. Even in the deterministic nonlinear case there is no guarantee of a separation principle as discussed in Thienel and Sanner [95].

Instead, the analysis in the remainder of this chapter assumes the error dynamics are weakly stochastically stable. The analysis will proceed with an investigation of the stationary Fokker-Planck PDE and any results obtained will be corroborated via comparison to statistics from numerical simulation realizations.

6.3.2 Gyro Constant Bias Filter Formulation in SO(2)

As in the attitude estimation filter for gyro additive noise and attitude measurement noise case studied in Section 6.2, the author has not yet been able to solve the Fokker-Planck PDE for the full SO(3) case. The SO(2) case, however, will be shown to have a tractable solution. In this section the attitude filter dynamical model will be reduced to the SO(2) case to enable the Fokker-Planck analysis in the following section.

As explained in Section 2.3.2, the SO(3) dynamical model may be reduced to the SO(2) case by simply zeroing out the y and z components of all vector quantities. Equivalently, the vector quantities in the SO(3) case reduce to scalar quantities, and SO(3) unit quaternions comprised of four elements reduce to SO(2) unit quaternions with two elements.

The SO(3) Langevin form error dynamics of Equation 5.6 reduce in the SO(2) case to

$$\dot{\mathbf{x}} = \begin{bmatrix} \dot{\tilde{\mathbf{q}}} \\ \dot{\tilde{\mathbf{q}}} \\ \dot{\tilde{\mathbf{b}}} \end{bmatrix} = \begin{bmatrix} \dot{\tilde{\epsilon}} \\ \dot{\tilde{\eta}} \\ \dot{\tilde{\epsilon}} \\ \dot{\tilde{\eta}} \\ \dot{\tilde{\mathbf{b}}} \end{bmatrix} = \begin{bmatrix} -\frac{1}{2}k_m\tilde{\eta}^2\tilde{\epsilon} \\ \frac{1}{2}k_m\tilde{\eta}\tilde{\epsilon}^2 \\ -\frac{1}{2}k_e\tilde{\eta}\tilde{\eta}_m\tilde{\epsilon}_m - \frac{1}{2}\tilde{\eta}\tilde{\mathbf{b}} \\ \frac{1}{2}k_e\tilde{\epsilon}\tilde{\eta}_m\tilde{\epsilon}_m + \frac{1}{2}\tilde{\epsilon}\tilde{\mathbf{b}} \\ \alpha\tilde{\eta}_m\tilde{\epsilon}_m \end{bmatrix} + \begin{bmatrix} -\frac{1}{2}\tilde{\eta}\sigma_m & 0 \\ \frac{1}{2}\tilde{\epsilon}\sigma_m & 0 \\ 0 & -\frac{1}{2}\tilde{\eta}\sigma_w \\ 0 & \frac{1}{2}\tilde{\epsilon}\sigma_w \\ 0 & 0 \end{bmatrix} \begin{bmatrix} n_m \\ n_w \end{bmatrix} \quad (6.59)$$

where again the function of time notation has been suppressed for brevity. In the SO(2) case the feedback term is given by

$$\tilde{\eta}_m\tilde{\epsilon}_m = (\tilde{\eta}\tilde{\eta} + \tilde{\epsilon}\tilde{\epsilon})(\tilde{\eta}\tilde{\epsilon} - \tilde{\eta}\tilde{\epsilon}) \quad (6.60)$$

As explained in Section 2.1.3, the Langevin form error dynamics differential equation 6.59 is interpreted as a Stratonovich SDE. Converting to Itô form yields

$$\begin{aligned}
d\tilde{\mathbf{x}} &= \begin{bmatrix} d\check{\mathbf{q}} \\ d\tilde{\mathbf{q}} \\ d\tilde{\mathbf{b}} \end{bmatrix} = \begin{bmatrix} d\check{\varepsilon} \\ d\check{\eta} \\ d\tilde{\varepsilon} \\ d\tilde{\eta} \\ d\tilde{\mathbf{b}} \end{bmatrix} \\
&= \begin{bmatrix} -\frac{1}{2}k_m\check{\eta}^2\check{\varepsilon} - \frac{1}{8}\sigma_m^2\check{\varepsilon} \\ \frac{1}{2}k_m\check{\eta}\check{\varepsilon}^2 - \frac{1}{8}\sigma_m^2\check{\eta} \\ -\frac{1}{2}k_e\tilde{\eta}\tilde{\eta}_m\tilde{\varepsilon}_m - \frac{1}{2}\tilde{\eta}\tilde{\mathbf{b}} - \frac{1}{8}\sigma_w^2\tilde{\varepsilon} \\ \frac{1}{2}k_e\tilde{\varepsilon}\tilde{\eta}_m\tilde{\varepsilon}_m + \frac{1}{2}\tilde{\varepsilon}\tilde{\mathbf{b}} - \frac{1}{8}\sigma_w^2\tilde{\eta} \\ \alpha\tilde{\eta}_m\tilde{\varepsilon}_m \end{bmatrix} dt + \begin{bmatrix} -\frac{1}{2}\check{\eta}\sigma_m & 0 \\ \frac{1}{2}\check{\varepsilon}\sigma_m & 0 \\ 0 & -\frac{1}{2}\tilde{\eta}\sigma_w \\ 0 & \frac{1}{2}\tilde{\varepsilon}\sigma_w \\ 0 & 0 \end{bmatrix} \begin{bmatrix} d\beta_m \\ d\beta_w \end{bmatrix} \quad (6.61)
\end{aligned}$$

The attitude filter error dynamics of Equation 6.59 can equivalently be written in the SO(2) Euler Axis/Angle parameterization (as explained in Section 2.3.2). Let

$$\check{\mathbf{q}} = \begin{bmatrix} \check{\varepsilon} \\ \check{\eta} \end{bmatrix} = \begin{bmatrix} \sin\left(\frac{\check{\phi}}{2}\right) \\ \cos\left(\frac{\check{\phi}}{2}\right) \end{bmatrix} \quad \tilde{\mathbf{q}} = \begin{bmatrix} \tilde{\varepsilon} \\ \tilde{\eta} \end{bmatrix} = \begin{bmatrix} \sin\left(\frac{\tilde{\phi}}{2}\right) \\ \cos\left(\frac{\tilde{\phi}}{2}\right) \end{bmatrix}$$

Then the SO(2) Euler Axis/Angle parameterization of the filter error dynamics is

given as

$$\begin{aligned}
\dot{\tilde{\mathbf{y}}} &= \begin{bmatrix} \dot{\check{\phi}} \\ \dot{\tilde{\phi}} \\ \dot{\tilde{b}} \end{bmatrix} = \begin{bmatrix} -k_m \check{\eta} \check{\varepsilon} \\ -k_e (\check{\eta} \tilde{\eta} + \check{\varepsilon} \tilde{\varepsilon}) (\check{\eta} \tilde{\varepsilon} - \tilde{\eta} \check{\varepsilon}) - \tilde{b} \\ \alpha (\check{\eta} \tilde{\eta} + \check{\varepsilon} \tilde{\varepsilon}) (\check{\eta} \tilde{\varepsilon} - \tilde{\eta} \check{\varepsilon}) \end{bmatrix} + \begin{bmatrix} -\sigma_m & 0 \\ 0 & -\sigma_w \\ 0 & 0 \end{bmatrix} \begin{bmatrix} n_m \\ n_w \end{bmatrix} \\
&= \begin{bmatrix} -\frac{1}{2} k_m \sin(\check{\phi}) \\ -\frac{1}{2} k_e \sin(\tilde{\phi} - \check{\phi}) - \tilde{b} \\ \frac{1}{2} \alpha \sin(\tilde{\phi} - \check{\phi}) \end{bmatrix} + \begin{bmatrix} -\sigma_m & 0 \\ 0 & -\sigma_w \\ 0 & 0 \end{bmatrix} \begin{bmatrix} n_m \\ n_w \end{bmatrix} \tag{6.62}
\end{aligned}$$

which is immediately in Langevin form. Conversion to an Itô SDE is trivial as the diffusion matrix is independent of the state :

$$\begin{aligned}
d\tilde{\mathbf{y}} &= \begin{bmatrix} d\check{\phi} \\ d\tilde{\phi} \\ d\tilde{b} \end{bmatrix} = \begin{bmatrix} -\frac{1}{2} k_m \sin(\check{\phi}) \\ -\frac{1}{2} k_e \sin(\tilde{\phi} - \check{\phi}) - \tilde{b} \\ \frac{1}{2} \alpha \sin(\tilde{\phi} - \check{\phi}) \end{bmatrix} dt + \begin{bmatrix} -\sigma_m & 0 \\ 0 & -\sigma_w \\ 0 & 0 \end{bmatrix} \begin{bmatrix} d\beta_m \\ d\beta_w \end{bmatrix} \\
&= \mathbf{f}(\tilde{\mathbf{y}})dt + G(\tilde{\mathbf{y}})d\boldsymbol{\beta} \tag{6.63}
\end{aligned}$$

6.3.3 Fokker-Planck Analysis in SO(2)

This section presents a Fokker-Planck analysis of the SO(2) attitude filter. Assuming the SO(2) attitude filter error dynamics of Itô SDE 6.61 are weakly stochastically stable, the joint probability density for the system will ultimately approach the solution to the stationary Fokker-Planck PDE. In this section, the stationary Fokker-Planck PDE is derived and a probability density function that asymptotically approaches the solution to the stationary Fokker-Planck PDE is found. The asymptotic solution is subsequently used to find stationary statistics for the system states.

Let $p = p(\tilde{\mathbf{y}}(t), t) = p(\tilde{\phi}(t), \check{\phi}(t), \tilde{b}(t), t)$ be the joint probability density function for the filter attitude estimate error $\tilde{\phi}(t)$, the attitude measurement noise error $\check{\phi}(t)$, and the bias estimate error $\tilde{b}(t)$. Then the Fokker-Planck PDE associated with the attitude filter error dynamics Itô SDE 6.63 is given by

$$\begin{aligned}
\frac{\partial p}{\partial t} &= - \sum_{i=1}^3 \frac{\partial}{\partial \tilde{y}_i} \left[f_i(\tilde{\mathbf{y}}(t)) p(\tilde{\mathbf{y}}(t), t) \right] + \frac{1}{2} \sum_{i,j=1}^3 \frac{\partial^2}{\partial \tilde{y}_i \partial \tilde{y}_j} \left[\left\{ G(\tilde{\mathbf{y}}(t)) G^T(\tilde{\mathbf{y}}(t)) \right\}_{i,j} p(\tilde{\mathbf{y}}(t), t) \right] \\
&= \frac{1}{2} \left[k_m \cos(\tilde{\phi}(t)) + k_e \cos(\tilde{\phi}(t) - \check{\phi}(t)) \right] p(\tilde{\mathbf{y}}(t), t) \\
&\quad + \frac{1}{2} k_m \sin(\check{\phi}(t)) \frac{\partial p}{\partial \check{\phi}} + \left[\frac{1}{2} k_e \sin(\tilde{\phi}(t) - \check{\phi}(t)) + \tilde{b}(t) \right] \frac{\partial p}{\partial \tilde{\phi}} \\
&\quad - \frac{1}{2} \alpha \sin(\tilde{\phi}(t) - \check{\phi}(t)) \frac{\partial p}{\partial \tilde{b}} + \frac{1}{2} \sigma_m^2 \frac{\partial^2 p}{\partial \check{\phi}^2} + \frac{1}{2} \sigma_w^2 \frac{\partial^2 p}{\partial \tilde{\phi}^2}
\end{aligned} \tag{6.64}$$

Assuming the underlying system is weakly stochastically stable, the joint probability density function $p(\tilde{\phi}(t), \check{\phi}(t), \tilde{b}(t), t)$ ultimately approaches a stationary joint

probability density function

$$p_s = p_s(\tilde{\mathbf{y}}) = p_s(\tilde{\phi}, \check{\phi}, \tilde{b}) = \lim_{t \rightarrow \infty} p(\tilde{\phi}(t), \check{\phi}(t), \tilde{b}(t), t)$$

The stationary joint probability density function solves the stationary Fokker-Planck PDE

$$0 = \left[k_m \cos(\tilde{\phi}) + k_e \cos(\tilde{\phi} - \check{\phi}) \right] p_s + k_m \sin(\check{\phi}) \frac{\partial p_s}{\partial \check{\phi}} + \left[k_e \sin(\tilde{\phi} - \check{\phi}) + 2\tilde{b} \right] \frac{\partial p_s}{\partial \tilde{\phi}} - \alpha \sin(\tilde{\phi} - \check{\phi}) \frac{\partial p_s}{\partial \tilde{b}} + \sigma_m^2 \frac{\partial^2 p_s}{\partial \check{\phi}^2} + \sigma_w^2 \frac{\partial^2 p_s}{\partial \tilde{\phi}^2} \quad (6.65)$$

The next theorem presents a probability density function that asymptotically approaches the stationary probability density function p_s .

Theorem 6.3.1. *The solution joint probability density function $p_s(\tilde{\phi}, \check{\phi}, \tilde{b})$ of the stationary Fokker-Planck PDE of Equation 6.65 is such that*

$$p_s(\tilde{\phi}, \check{\phi}, \tilde{b}) = \lim_{\substack{\sigma_m \rightarrow 0 \\ \frac{k_m}{\sigma_m^2} \text{ constant}}} p_a(\tilde{\phi}, \check{\phi}, \tilde{b})$$

where

$$p_a(\tilde{\phi}, \check{\phi}, \tilde{b}) = \frac{1}{N} \exp \left\{ \frac{k_m}{\sigma_m^2} \cos(\check{\phi}) + \frac{k_e}{\sigma_m^2 + \sigma_w^2} \cos(\tilde{\phi} - \check{\phi}) - \frac{k_e}{\alpha(\sigma_w^2 + \sigma_m^2)} \tilde{b}^2 \right\} \quad (6.66)$$

with the normalization constant

$$N = 16\pi^2 I_0 \left(\frac{k_e}{\sigma_m^2 + \sigma_w^2} \right) I_0 \left(\frac{k_m}{\sigma_m^2} \right) \sqrt{\frac{\pi\alpha(\sigma_w^2 + \sigma_m^2)}{k_e}}$$

where $I_0(x)$ is the 0th order modified Bessel function of the first kind.

Proof. Recalling that the attitude measurement noise stationary Fokker-Planck PDE was asymptotically solved by a bivariate von Mises distribution in Theorem 6.2.3 and

the gyro constant bias stationary Fokker-Planck PDE was solved by the cylindrical probability density function of Mardia and Sutton [62] in Theorem 5.5.1, consider the following joint distribution that is a combination of the forms of the mentioned PDFs

$$p_a(\tilde{\phi}, \tilde{b}) = \frac{1}{N} \exp \left\{ \kappa \cos(\tilde{\phi}) + \lambda \cos(\tilde{\phi} - \check{\phi}) + \nu \tilde{b}^2 \right\}$$

where the normalization constant N is a positive scalar, the concentration parameters κ and λ are non-negative scalars, and ν is a scalar.

Substituting the probability density function into the right hand side of PDE 6.65 yields the expression

$$\begin{aligned} 0 = & \left\{ \left(k_m - \kappa \sigma_m^2 \right) \cos(\check{\phi}) + \left(k_e - \kappa(\sigma_m^2 + \sigma_w^2) \right) \left(\cos(\tilde{\phi} - \check{\phi}) - \kappa \sin^2(\tilde{\phi} - \check{\phi}) \right) \right. \\ & - \kappa \left(k_m - \kappa \sigma_m^2 \right) \sin^2(\check{\phi}) + \lambda \left(k_m - 2\kappa \sigma_m^2 \right) \sin(\check{\phi}) \sin(\tilde{\phi} - \check{\phi}) \\ & \left. - 2(\lambda + \nu \alpha) \tilde{b} \sin(\tilde{\phi} - \check{\phi}) \right\} p_a \end{aligned}$$

Choosing $\kappa = \frac{k_m}{\sigma_m^2}$, $\lambda = \frac{k_e}{\sigma_m^2 + \sigma_w^2}$, and $\nu = -\frac{\lambda}{\alpha} = -\frac{k_e}{\alpha(\sigma_m^2 + \sigma_w^2)}$ and substituting into the above equation results in

$$\begin{aligned} 0 &= \frac{k_e k_m}{\sigma_m^2 + \sigma_w^2} \sin(\check{\phi}) \sin(\tilde{\phi} - \check{\phi}) p_a \\ &= \frac{k_e \frac{k_m}{\sigma_m^2}}{1 + \frac{\sigma_w^2}{\sigma_m^2}} \sin(\check{\phi}) \sin(\tilde{\phi} - \check{\phi}) p_a \end{aligned} \quad (6.67)$$

which does not hold for all possible $\tilde{\phi}$ and $\check{\phi}$ so this is not a solution. Note however that the right hand side of Equation 6.67 asymptotically approaches 0 for any possible $\tilde{\phi}$ and $\check{\phi}$ when σ_m goes to zero while the ratio $\frac{k_m}{\sigma_m^2}$ is held constant. As discussed in the proof of Theorem 6.2.3, the attitude measurement noise density is parameterized by the **ratio** of $\frac{k_m}{\sigma_m^2}$; as long as k_m is made small enough to maintain

the ratio $\frac{k_m}{\sigma_m^2}$ the parameter σ_m may be made arbitrarily small without altering the ultimate statistics of the attitude measurement noise.

Thus

$$p_a(\tilde{\phi}, \check{\phi}, \tilde{b}) = \frac{1}{N} \exp \left\{ \frac{k_m}{\sigma_m^2} \cos(\check{\phi}) + \frac{k_e}{\sigma_m^2 + \sigma_w^2} \cos(\tilde{\phi} - \check{\phi}) - \frac{k_e}{\alpha(\sigma_m^2 + \sigma_w^2)} \tilde{b}^2 \right\} \quad (6.68)$$

asymptotically approaches the solution to the stationary Fokker-Planck PDE of Equation 6.65 in the sense that

$$\lim_{\substack{\sigma_m \rightarrow 0 \\ \frac{k_m}{\sigma_m^2} \text{ constant}}} p_a(\tilde{\phi}, \check{\phi}, \tilde{b}) = p_s(\tilde{\phi}, \check{\phi}, \tilde{b})$$

The scaling constant N may be recovered by enforcing the probability density normalization constraint

$$\int_{-2\pi}^{2\pi} \int_{-2\pi}^{2\pi} \int_{-\infty}^{\infty} p_a(\tilde{\phi}, \check{\phi}, \tilde{b}) d\tilde{b} d\tilde{\phi} d\check{\phi} = 1$$

Substituting in the probability density function of Equation 6.68 and rearranging results in

$$\begin{aligned} N &= \int_{-2\pi}^{2\pi} \int_{-2\pi}^{2\pi} \int_{-\infty}^{\infty} \exp \left\{ \frac{k_m}{\sigma_m^2} \cos(\check{\phi}) \right. \\ &\quad \left. + \frac{k_e}{\sigma_m^2 + \sigma_w^2} \cos(\tilde{\phi} - \check{\phi}) - \frac{k_e}{\alpha(\sigma_m^2 + \sigma_w^2)} \tilde{b}^2 \right\} d\tilde{b} d\tilde{\phi} d\check{\phi} \\ &= \int_{-2\pi}^{2\pi} \int_{-2\pi}^{2\pi} \exp \left\{ \frac{k_m}{\sigma_m^2} \cos(\check{\phi}) + \frac{k_e}{\sigma_m^2 + \sigma_w^2} \cos(\tilde{\phi} - \check{\phi}) \right\} d\tilde{\phi} d\check{\phi} \\ &\quad \times \int_{-\infty}^{\infty} \exp \left\{ -\frac{k_e}{\alpha(\sigma_m^2 + \sigma_w^2)} \tilde{b}^2 \right\} d\tilde{b} \end{aligned} \quad (6.69)$$

In the proof of Theorem 6.2.3, the double integral of Equation 6.69 was found

to be

$$\begin{aligned} & \int_{-2\pi}^{2\pi} \int_{-2\pi}^{2\pi} \exp \left\{ \frac{k_m}{\sigma_m^2} \cos(\check{\phi}) + \frac{k_e}{\sigma_m^2 + \sigma_w^2} \cos(\tilde{\phi} - \check{\phi}) \right\} d\tilde{\phi} d\check{\phi} \\ &= 16\pi^2 I_0 \left(\frac{k_e}{\sigma_m^2 + \sigma_w^2} \right) I_0 \left(\frac{k_m}{\sigma_m^2} \right) \end{aligned}$$

where $I_0(x)$ is the 0th order modified Bessel function of the first kind. Since the exponential function is such that for all positive scalars a

$$\int_{-\infty}^{\infty} \exp \left\{ -\frac{1}{a} x^2 \right\} dx = \sqrt{\pi a}$$

the second integral in Equation 6.69 evaluates to

$$\int_{-\infty}^{\infty} \exp \left\{ -\frac{k_e}{\alpha(\sigma_m^2 + \sigma_w^2)} \tilde{b}^2 \right\} d\tilde{b} = \sqrt{\frac{\pi \alpha (\sigma_m^2 + \sigma_w^2)}{k_e}}$$

Combining yields the normalization constant.

□

Similar to the discussion in Section 6.2.7, the asymptotic solution to the stationary Fokker-Planck PDE of Theorem 6.3.1 asymptotically approaches the solution to the stationary Fokker-Planck PDE of Equation 6.65 as $\sigma_m \rightarrow 0$ while the ratio $\frac{k_m}{\sigma_m^2}$ is held constant, meaning $k_m \rightarrow 0$ at the same rate $\sigma_m^2 \rightarrow 0$. The attitude measurement noise density is parameterized by the ratio $\frac{k_m}{\sigma_m^2}$ so the ultimate statistics for the attitude measurement noise given in Corollary 4.8.1.1 and Corollary 4.8.1.2 are unaffected, but the attitude measurement noise density says nothing about the autocorrelation of the attitude measurement noise process. Despite the potential loss of generality in parameterizing the attitude measurement noise PDF via the ratio $\frac{k_m}{\sigma_m^2}$, the asymptotic solution of Theorem 6.3.1 can be used to compute ultimate

statistics of the filter attitude estimate error and the filter bias estimate error which will be shown in the remainder of this section.

Corollary 6.3.1.1. *The error dynamics of the Itô SDE 6.63 are such that*

$$\lim_{t \rightarrow \infty} E \left[\tilde{\varepsilon}^2(t) \right] = \frac{1}{2} \left(1 - \frac{I_1 \left(\frac{k_e}{\sigma_w^2} \right) I_1 \left(\frac{k_m}{\sigma_m^2} \right)}{I_0 \left(\frac{k_e}{\sigma_w^2} \right) I_0 \left(\frac{k_m}{\sigma_m^2} \right)} \right) \quad (6.70)$$

Proof. Compute the expectation using the probability density function from Theorem 6.3.1

$$\begin{aligned} & \lim_{\substack{\sigma_m \rightarrow 0 \\ \frac{k_m}{\sigma_m^2} \text{ constant}}} \lim_{t \rightarrow \infty} E \left[\tilde{\varepsilon}^2(t) \right] \\ &= \lim_{\substack{\sigma_m \rightarrow 0 \\ \frac{k_m}{\sigma_m^2} \text{ constant}}} \frac{1}{N} \int_{-2\pi}^{2\pi} \int_{-2\pi}^{2\pi} \int_{-\infty}^{\infty} \tilde{\varepsilon}^2 \exp \left\{ \frac{k_m}{\sigma_m^2} \cos(\check{\phi}) \right. \\ & \quad \left. + \frac{k_e}{\sigma_m^2 + \sigma_w^2} \cos(\tilde{\phi} - \check{\phi}) - \frac{k_e}{\alpha(\sigma_m^2 + \sigma_w^2)} \tilde{b}^2 \right\} d\tilde{b} d\tilde{\phi} d\check{\phi} \\ &= \lim_{\substack{\sigma_m \rightarrow 0 \\ \frac{k_m}{\sigma_m^2} \text{ constant}}} \frac{1}{16\pi^2 I_0 \left(\frac{k_e}{\sigma_m^2 + \sigma_w^2} \right) I_0 \left(\frac{k_m}{\sigma_m^2} \right)} \\ & \quad \times \int_{-2\pi}^{2\pi} \int_{-2\pi}^{2\pi} \sin^2 \left(\frac{\tilde{\phi}}{2} \right) \exp \left\{ \frac{k_m}{\sigma_m^2} \cos(\check{\phi}) + \frac{k_e}{\sigma_m^2 + \sigma_w^2} \cos(\tilde{\phi} - \check{\phi}) \right\} d\tilde{\phi} d\check{\phi} \end{aligned}$$

which was solved in Corollary 6.2.3.1. \square

By inspection of the ultimate joint probability density function of Theorem 6.3.1, it can be seen that \tilde{b} is ultimately distributed according to a Gaussian distribution with zero mean

$$\lim_{t \rightarrow \infty} E \left[\tilde{b}(t) \right] = 0$$

and variance

$$\lim_{t \rightarrow \infty} E \left[\tilde{b}^2(t) \right] = \frac{\alpha \sigma_w^2}{2k_e} \quad (6.71)$$

6.3.4 Numerical Simulation of Stochastic SO(2) Analytic Results

Two numerical simulations of the SO(2) filter's Itô SDE error dynamics of Equation 6.61 were performed for a variety of system parameters. The Kloeden-Platen Explicit Weak 2.0 numerical integration scheme discussed in Section 2.2.3 was used. For each simulation realization, a time step size of $\Delta t = 0.1$ was used for a total of 10^8 simulation steps. At the end of a simulation realization, the last 10^7 simulation steps were used to compute the empirical mean of the filter attitude estimate error $\tilde{\varepsilon}^2(t)$ and the filter bias estimate error $\tilde{b}^2(t)$.

The first simulation study varied the filter tracking gain k_e across a range of values. A gallery of plots of the filter attitude estimate errors are included in Figure 6.15, a gallery of plots of the filter bias estimate errors for the same simulations are included in Figure 6.16. The numerical results, shown in magenta dots, are compared to plots of the ultimate attitude estimate error variance of Corollary 6.3.1.1 and the ultimate gyro bias estimate error variance of Equation 6.71 respectively which are drawn in blue lines.

The analytic ultimate expectations are in good agreement with the numerical simulation realizations with a few exceptions. In the top two attitude estimate error variance plots of Figure 6.15, the ultimate expectation differs from the numerical realizations when the ultimate expectation curve flattens out horizontally (near $k_e = 1$). Other than these discrepancies, the numerical data matches the overall trends predicted by the analytic ultimate expectations: the attitude estimate error variance curve shifts horizontally with σ_w , the high k_e limit of the attitude esti-

mate error variance decreases with decreased attitude measurement noise density (increased $\frac{k_m}{\sigma_m^2}$), and the bias estimate error variance curve shifts vertically with σ_w . Similarly, the bias estimate error simulation realizations are in good agreement with the analytic expectation; the negative unit slope on the log-log plots are indicative of the analytic result that the bias estimate error is inversely proportional to the tracking gain k_e .

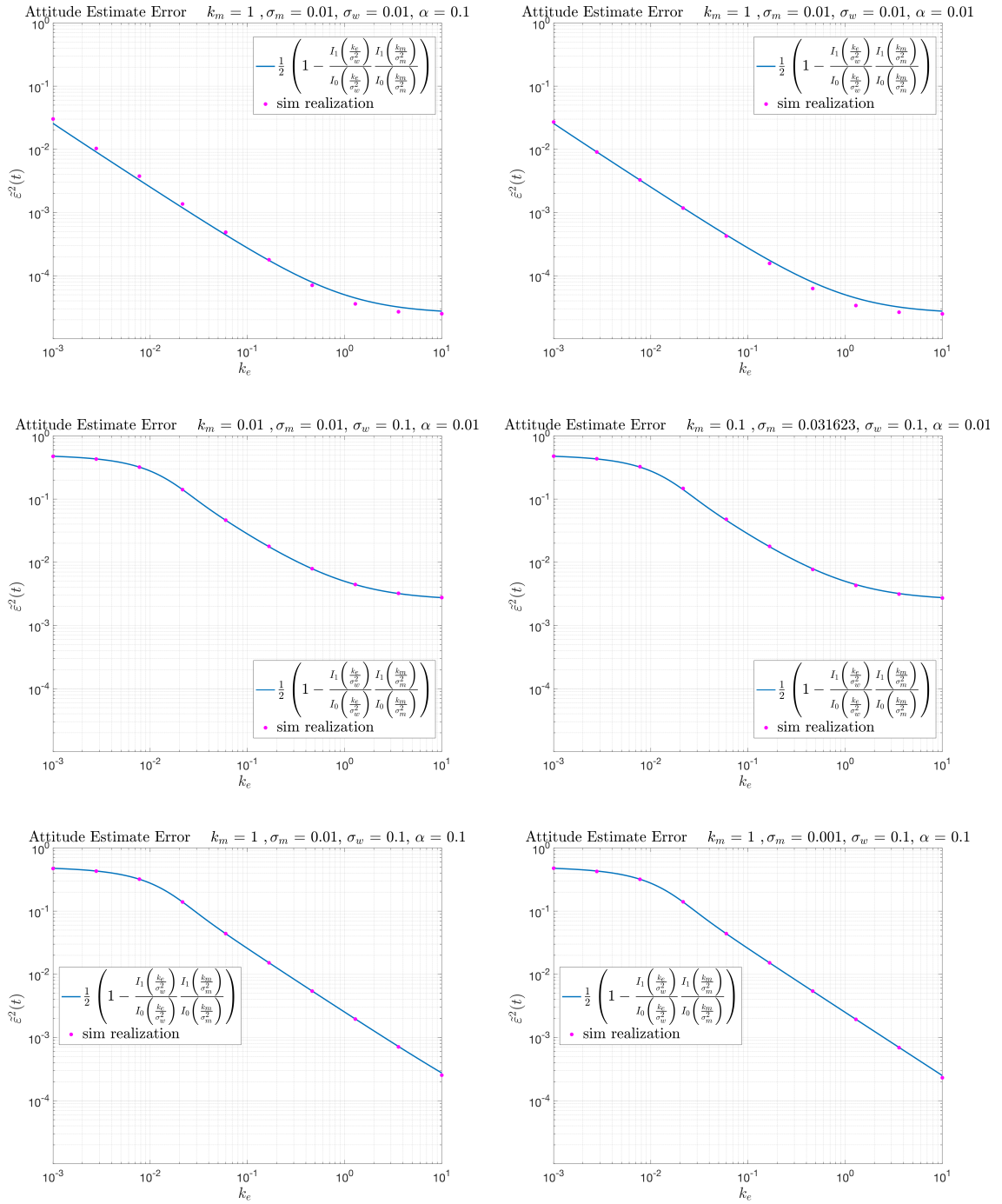


Figure 6.15: Comparison of the ultimate attitude estimate error variance of Corollary 6.3.1.1 to simulation realizations for a range of values of the tracking gain k_e .

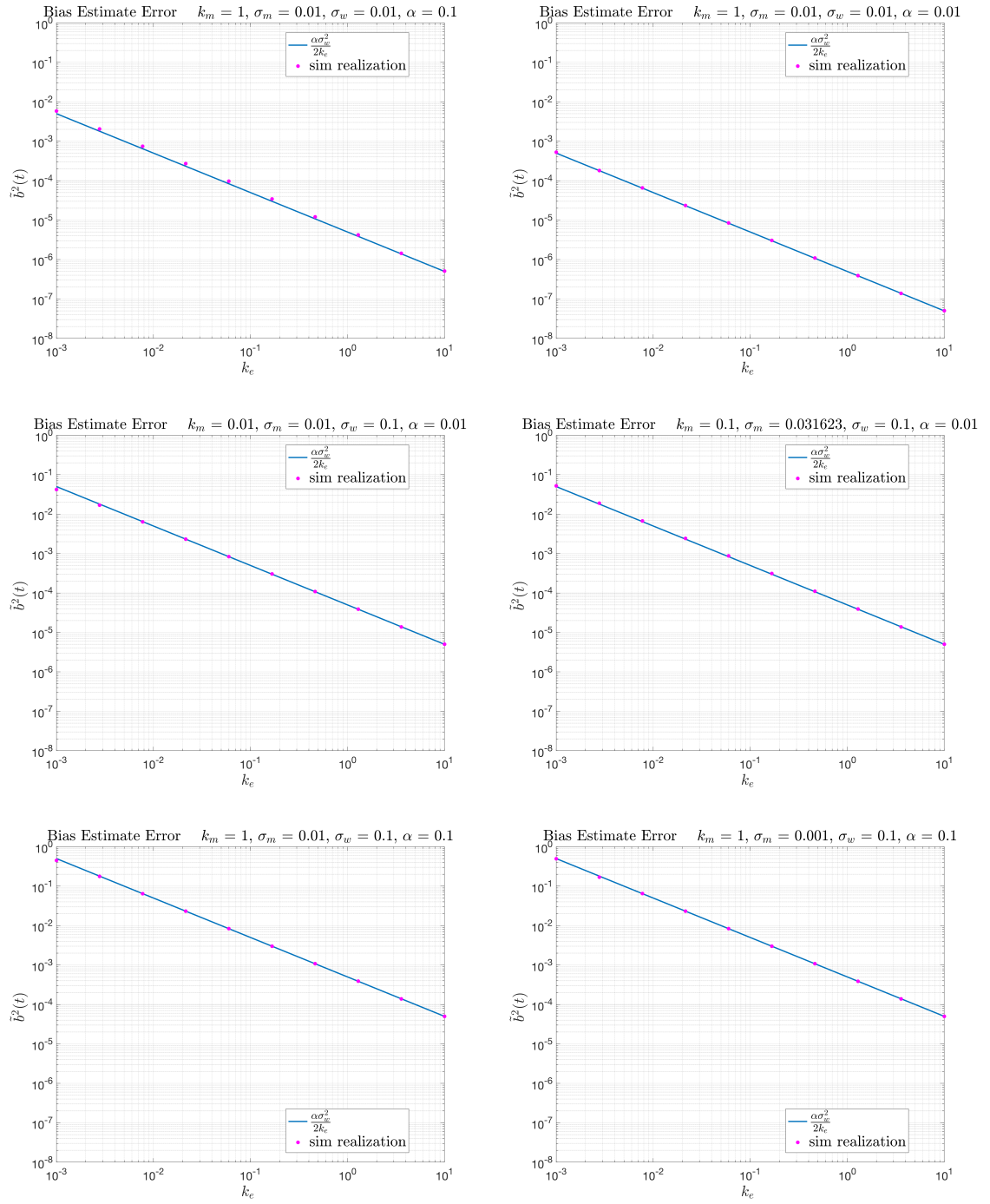


Figure 6.16: Comparison of the ultimate gyro bias estimate error variance of Equation 6.71 to simulation realizations for a range of values of the tracking gain k_e .

The second simulation study varied the filter's bias adaptation gain α across a range of values. A gallery of plots of the filter attitude estimate errors are included in Figure 6.17, a gallery of plots of the filter bias estimate errors for the same simulations are included in Figure 6.18. The numerical results, shown in magenta dots, are compared to plots of the ultimate attitude estimate error variance of Corollary 6.3.1.1 and the ultimate gyro bias estimate error variance of Equation 6.71 respectively which are drawn in blue lines.

The numerical simulation realizations agree with the analytic ultimate expectations. The attitude estimate error variance is unaffected by changing the adaptation gain α . The linear relationship between the ultimate bias estimate error variance and the adaptation gain is apparent in the data as well.

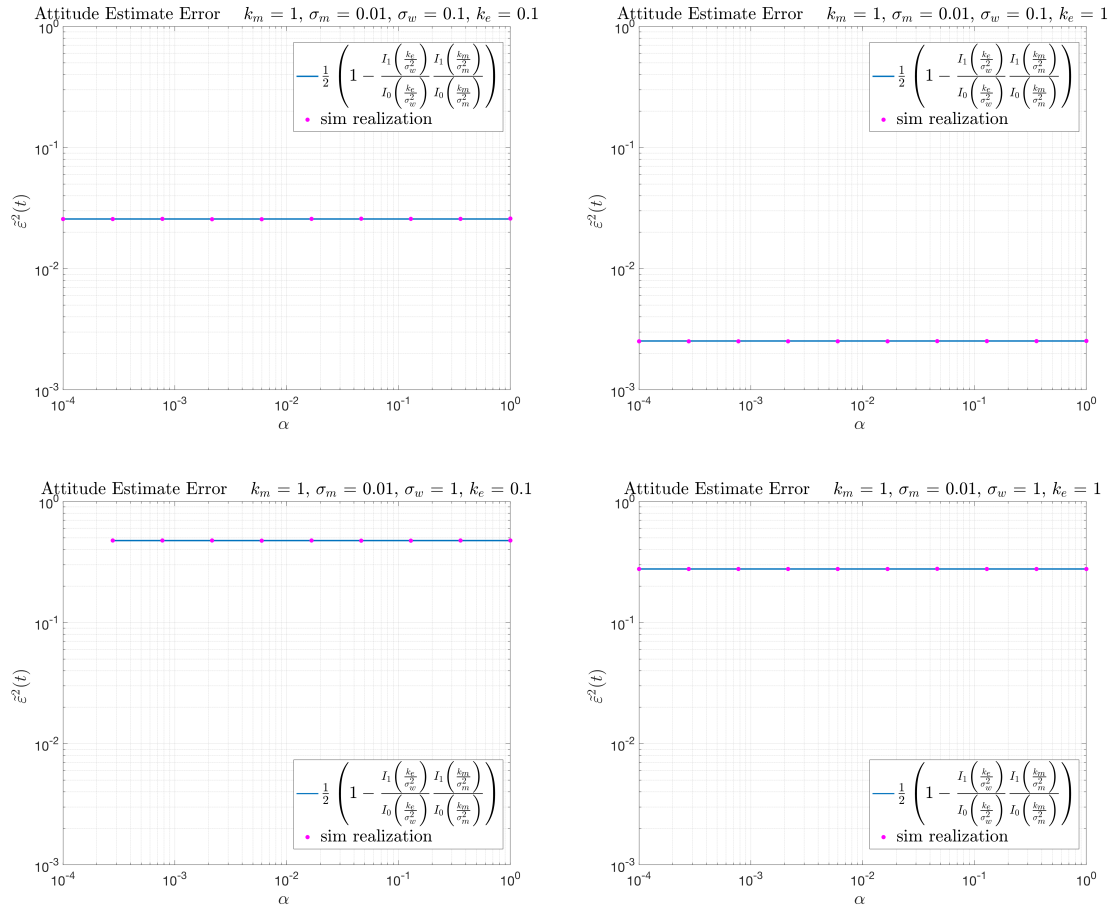


Figure 6.17: Comparison of the ultimate attitude estimate error variance of Corollary 6.3.1.1 to simulation realizations for a range of values of the adaptation gain α .

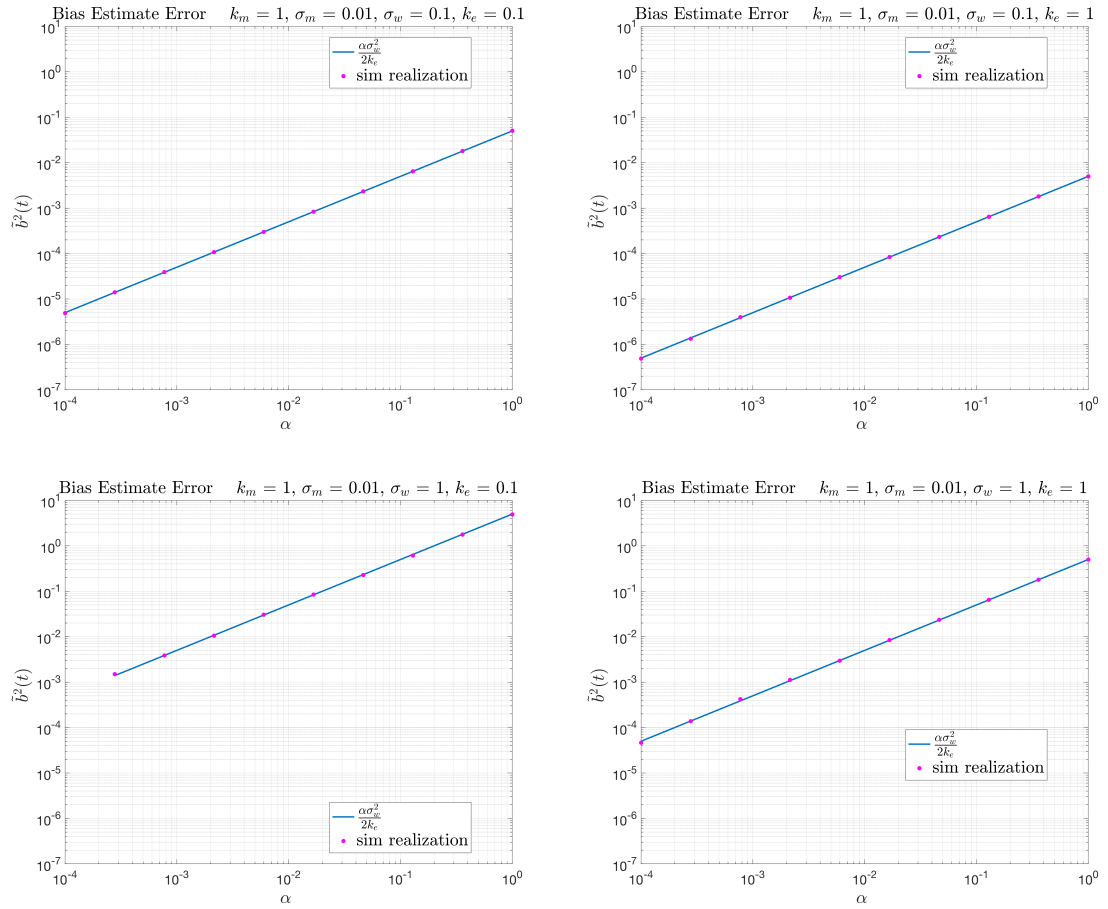


Figure 6.18: Comparison of the ultimate gyro bias estimate error variance of Equation 6.71 to simulation realizations for a range of values of the adaptation gain α .

6.3.5 SO(3) Bound Extrapolated from SO(2) Analytic Solution

Following the same approach as that of Section 4.10, 5.7, and 6.2.9, this section extrapolates upper bounds for the stationary statistics of the SO(3) filter from the analytic solutions of the SO(2) case.

The SO(3) ultimate attitude estimate error variance bound is assumed to have the form of the SO(2) ultimate attitude estimate error variance from Corollary 6.3.1.1, but as before is rescaled to account for the low filter gain limit seen in the previous chapters. The proposed SO(3) ultimate upper bound is given by

$$\text{bound} \left(\xi, \frac{k_e}{\sigma_w^2}, \frac{k_m}{\sigma_m^2} \right) = \frac{3}{4} \left(1 - \frac{I_1 \left(\frac{k_e}{\xi \sigma_w^2} \right) I_1 \left(\frac{k_m}{\xi \sigma_m^2} \right)}{I_0 \left(\frac{k_e}{\xi \sigma_w^2} \right) I_0 \left(\frac{k_m}{\xi \sigma_m^2} \right)} \right) \quad (6.72)$$

Similarly, the ultimate bias estimate error variance bound is assumed to have the same form as Equation 6.71 but with the same scaling parameter acting on the gyro variance σ_w^2

$$\text{bound} \left(\xi, \frac{k_e}{\sigma_w^2} \right) = \frac{\xi \alpha \sigma_w^2}{2k_e} \quad (6.73)$$

A number of numerical simulations of the Itô SDE 6.58 were performed to evaluate the notional bounds. The Kloeden-Platen Explicit Weak 2.0 numerical integration scheme discussed in Section 2.2.3 was used. For each simulation realization, a time step size of $\Delta t = 0.1$ was used for a total of 10^7 simulation steps. At the end of a simulation realization, the last 10^6 simulation steps were used to compute the ergodic mean of the filter attitude estimate error $\tilde{\boldsymbol{\varepsilon}}^T(t)\tilde{\boldsymbol{\varepsilon}}(t)$ and the filter bias estimate error $\tilde{\boldsymbol{b}}^T(t)\tilde{\boldsymbol{b}}(t)$. Finally, ensembles of seven ergodic means were computed for a final statistic for each set of simulation parameters k_e , σ_w , k_m , and σ_m .

Four simulation studies in total were conducted. First the vehicle was simulated as having no inertial rate; the analytic and simulation statistics are considered for a range of tracking gains k_e in Figures 6.19 and 6.20. Next, a range of tracking gains k_e were considered for a spinning vehicle in Figures 6.21 and 6.22. Then a range of adaptation gains α were considered for an inertially fixed vehicle in Figures 6.23 and 6.24. Finally, a range of adaptation gains α were considered for a spinning vehicle in Figures 6.25 and 6.26. In all cases considered, the choice of $\xi = 3$ in the expression of Equation 6.72 bound the simulation realizations; however, smaller choices of ξ do not bound all simulation data.

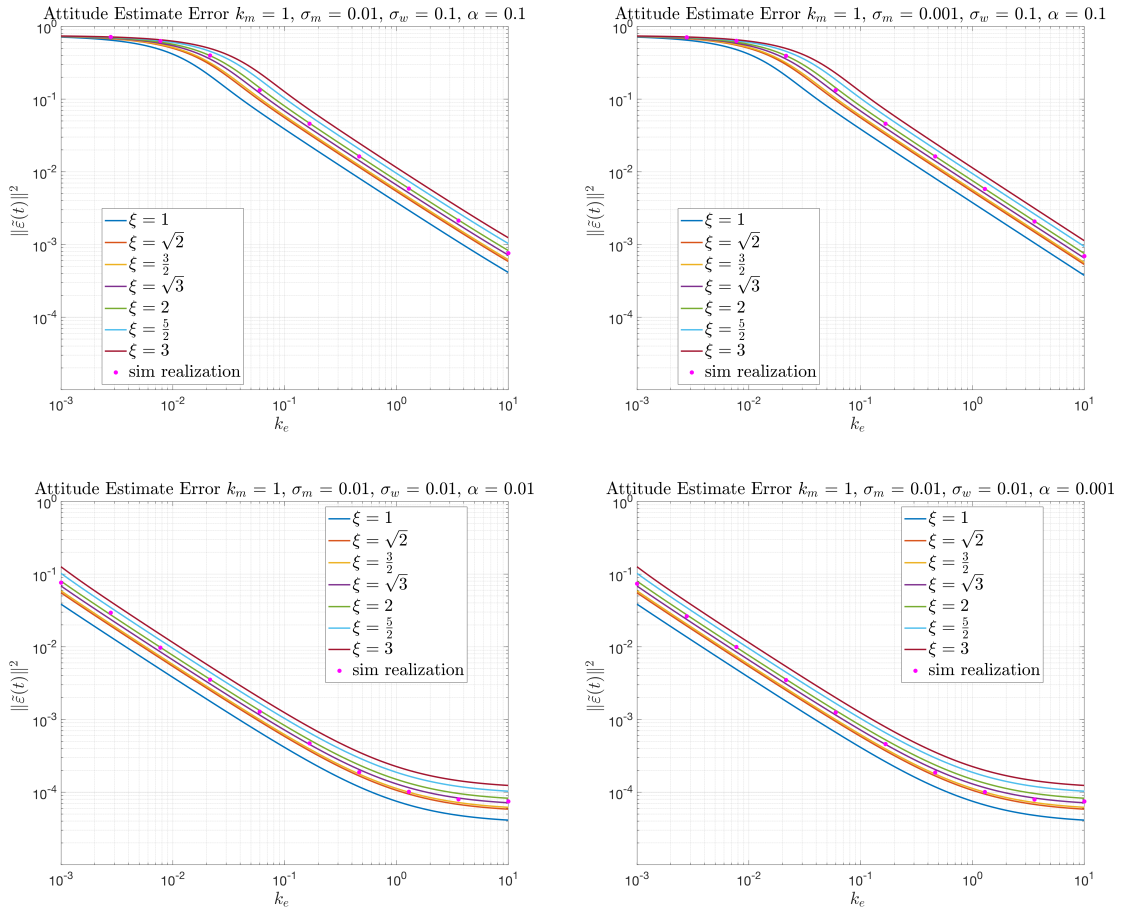


Figure 6.19: Comparison of simulation realizations of the attitude estimate error variance and the notional bound of Equation 6.72 for several choices of ξ for a range of tracking gains k_e for an inertially fixed vehicle (not spinning).

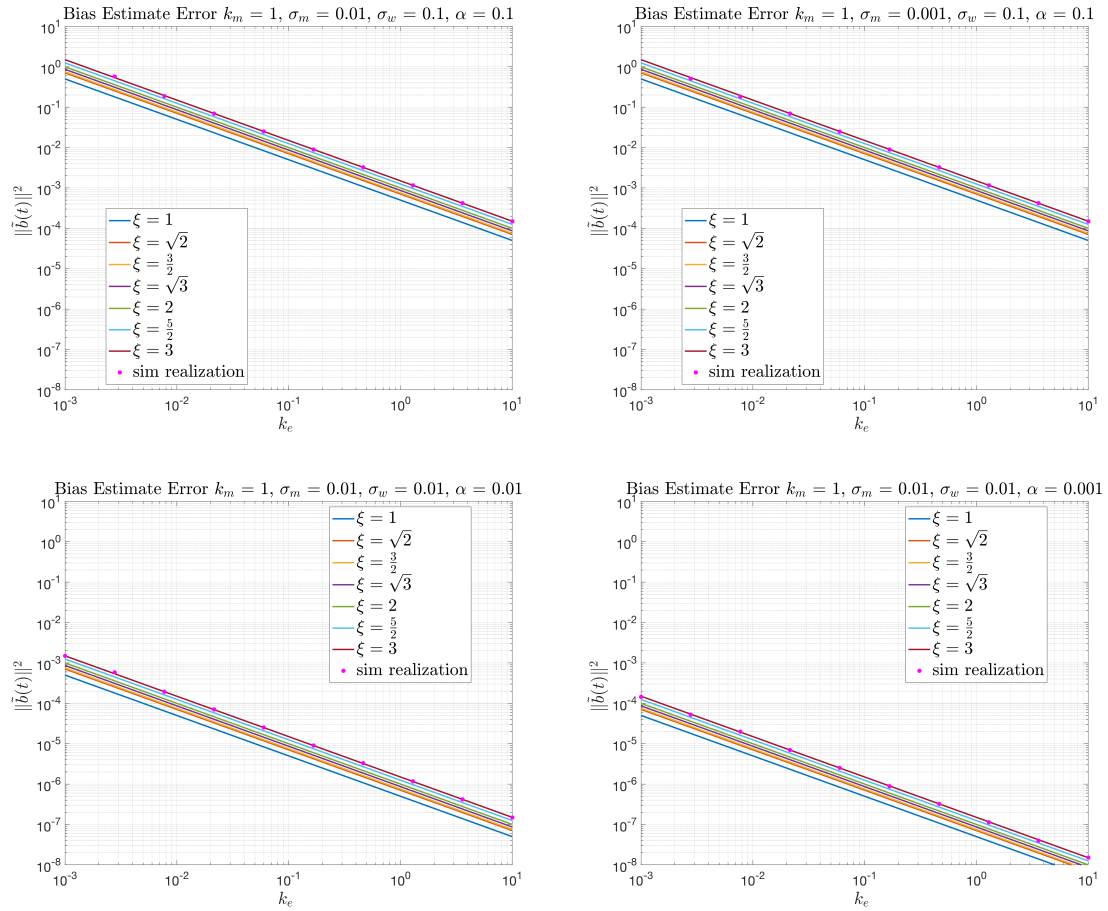


Figure 6.20: Comparison of simulation realizations of the bias estimate error variance and the notional bound of Equation 6.73 for several choices of ξ for a range of tracking gains k_e for an inertially fixed vehicle (not spinning).

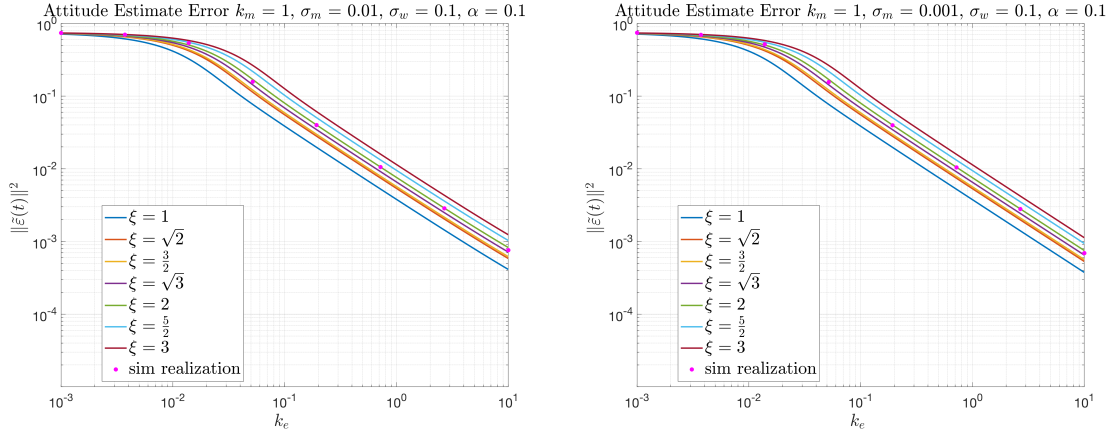


Figure 6.21: Comparison of simulation realizations of the attitude estimate error variance and the notional bound of Equation 6.72 for several choices of ξ for a range of tracking gains k_e for a vehicle spinning at 5 revolutions per minute about the vehicle body's $[1 \ 2 \ 3]^T$ axis.

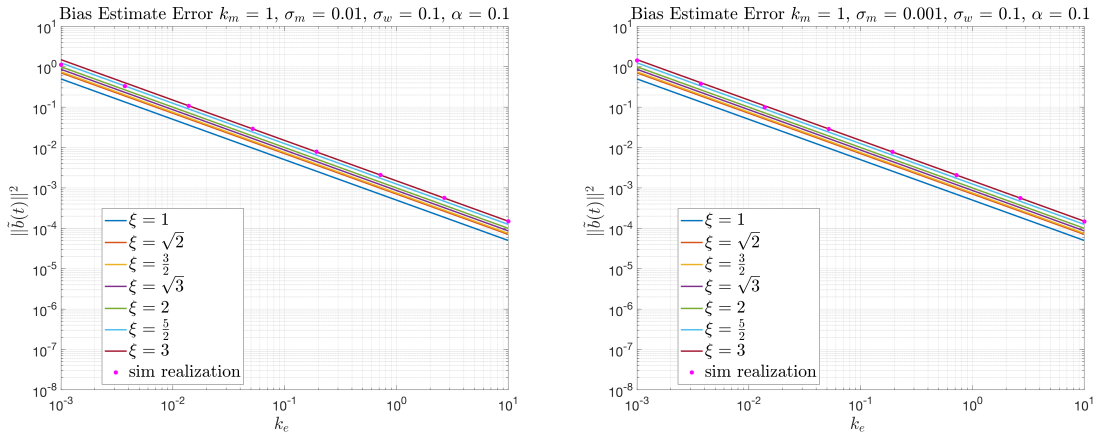


Figure 6.22: Comparison of simulation realizations of the bias estimate error variance and the notional bound of Equation 6.73 for several choices of ξ for a range of tracking gains k_e for a vehicle spinning at 5 revolutions per minute about the vehicle body's $[1 \ 2 \ 3]^T$ axis.

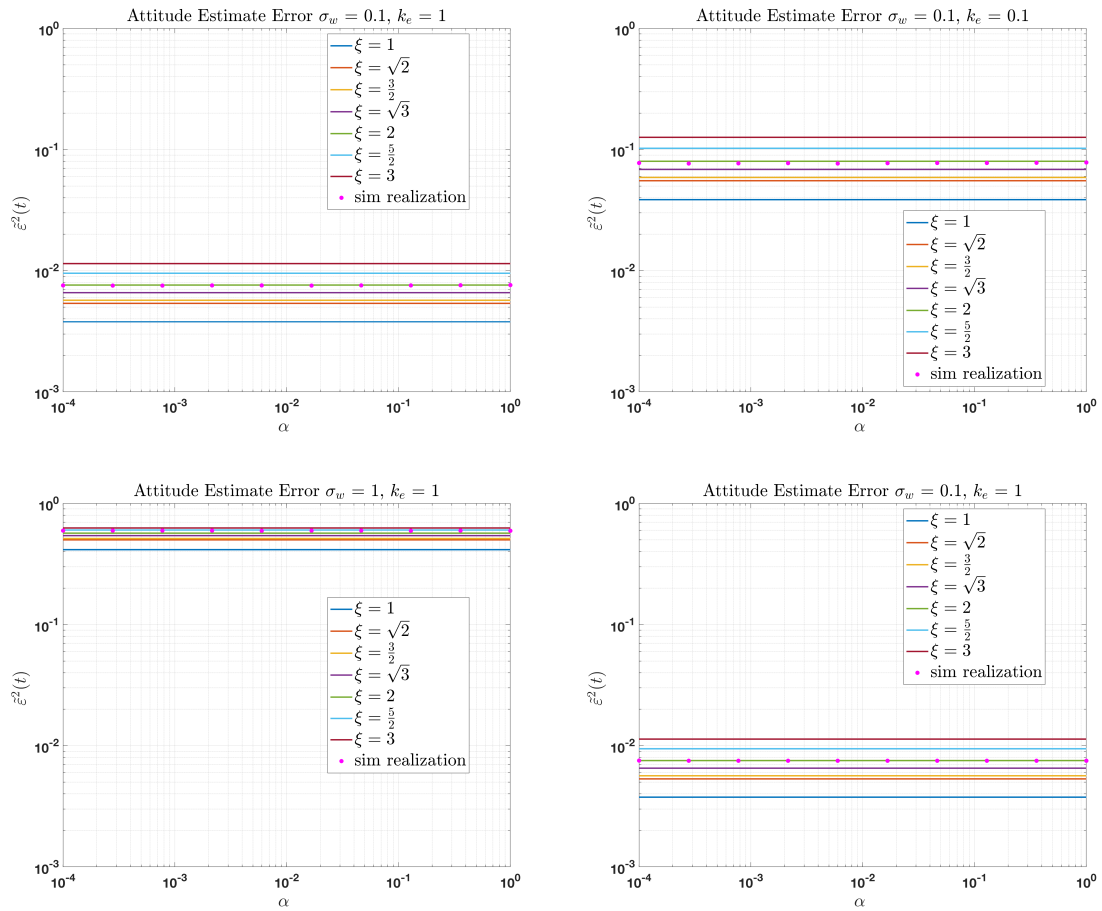


Figure 6.23: Comparison of simulation realizations of the attitude estimate error variance and the notional bound of Equation 6.72 for several choices of ξ for a range of adaptation gains α for an inertially fixed vehicle (not spinning).

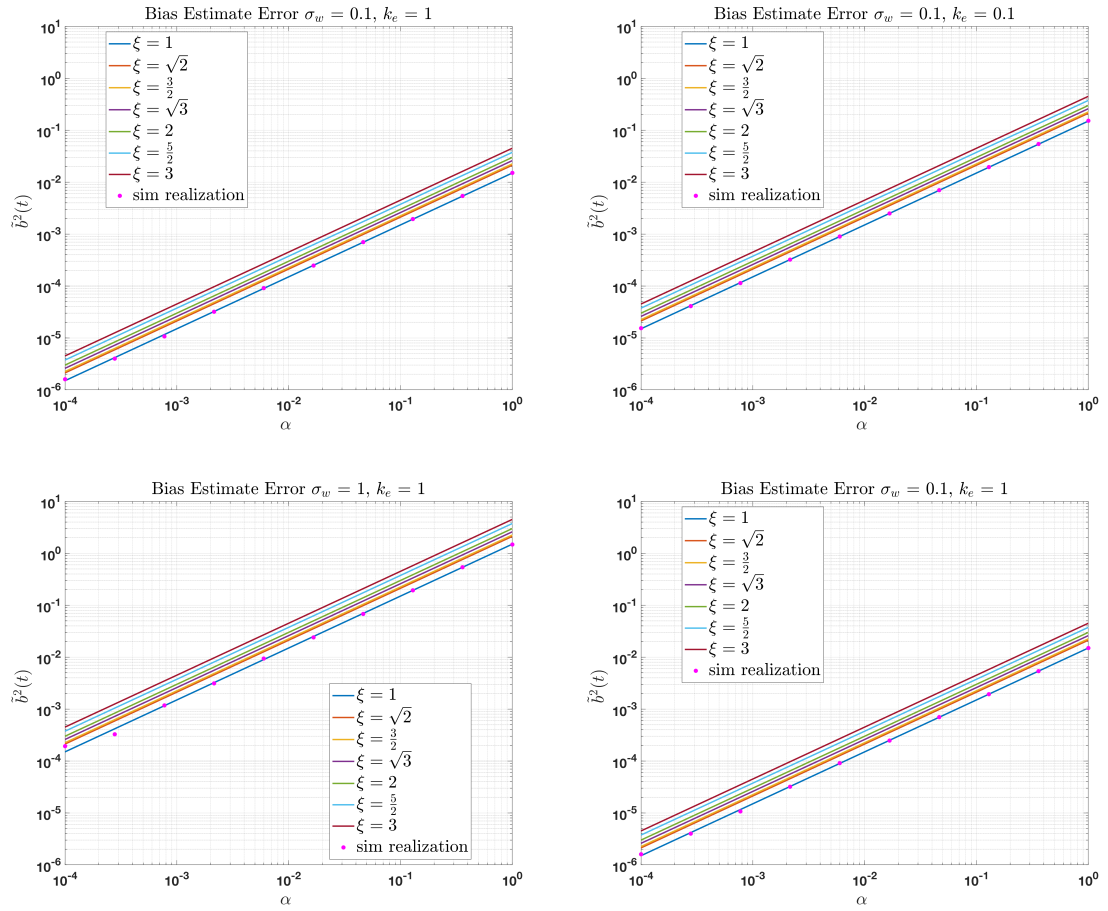


Figure 6.24: Comparison of simulation realizations of the bias estimate error variance and the notional bound of Equation 6.73 for several choices of ξ for a range of adaptation gains α for an inertially fixed vehicle (not spinning).

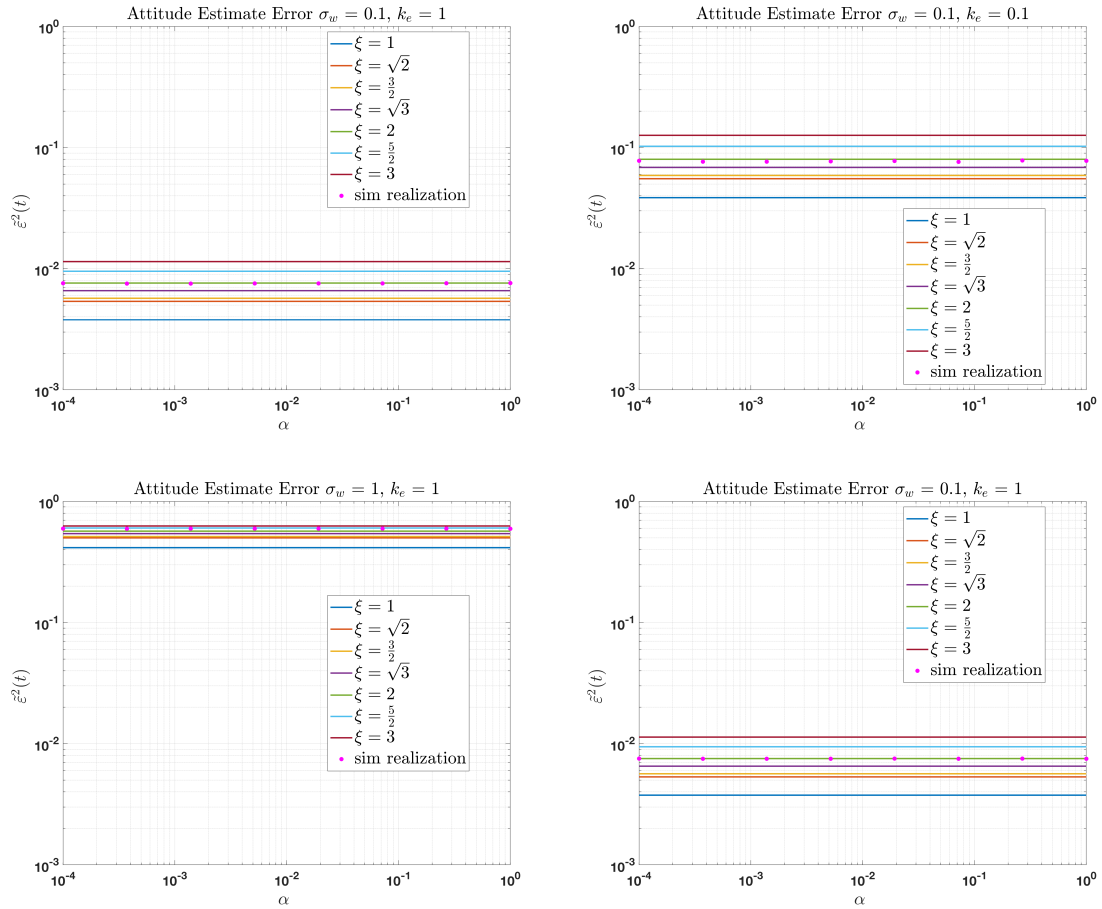


Figure 6.25: Comparison of simulation realizations of the attitude estimate error variance and the notional bound of Equation 6.72 for several choices of ξ for a range of adaptation gains α for a vehicle spinning at 5 revolutions per minute about the vehicle body's $[1 \ 2 \ 3]^T$ axis.

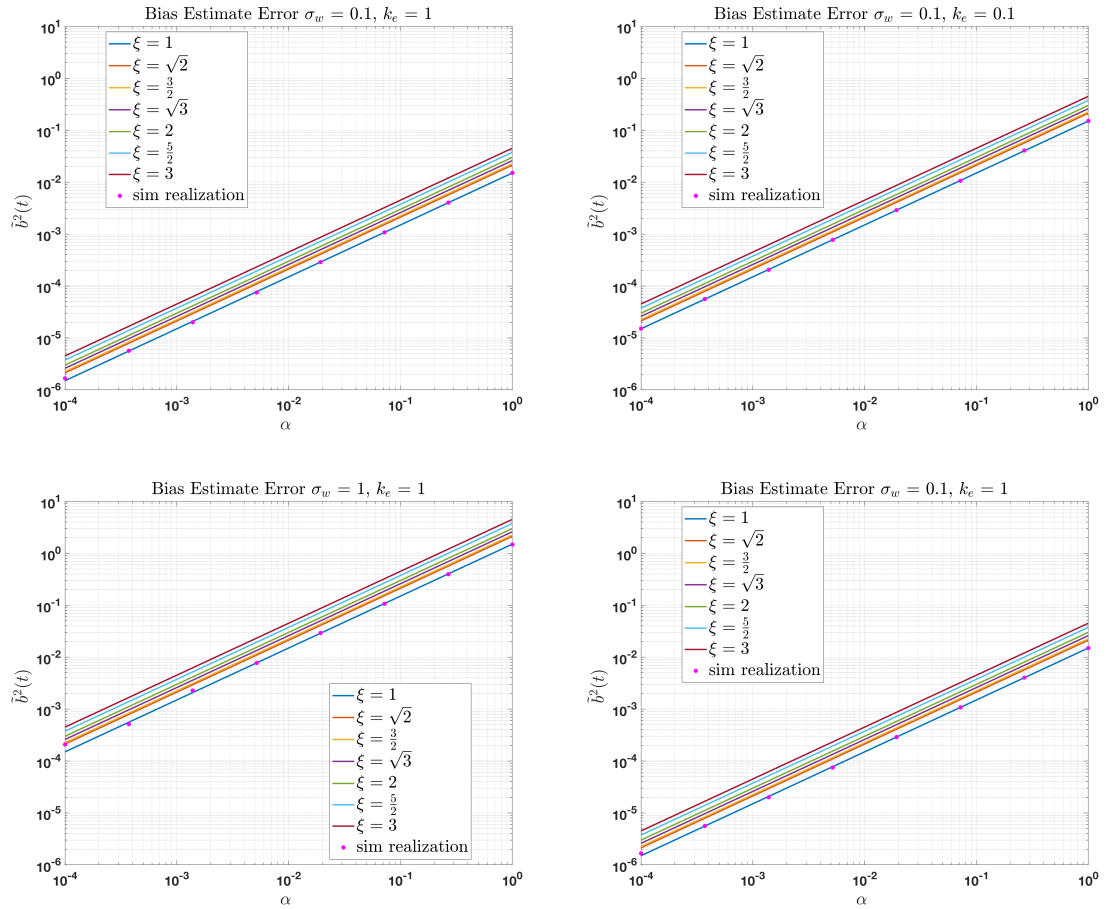


Figure 6.26: Comparison of simulation realizations of the bias estimate error variance and the notional bound of Equation 6.73 for several choices of ξ for a range of adaptation gains α for a vehicle spinning at 5 revolutions per minute about the vehicle body's $[1 \ 2 \ 3]^T$ axis.

Thus the simulation data suggest the ultimate upper bounds of

$$\lim_{t \rightarrow \infty} E[\tilde{\boldsymbol{\epsilon}}^T(t)\tilde{\boldsymbol{\epsilon}}(t)] \leq \frac{3}{4} \left(1 - \frac{I_1\left(\frac{k_e}{3\sigma_w^2}\right) I_1\left(\frac{k_m}{3\sigma_m^2}\right)}{I_0\left(\frac{k_e}{3\sigma_w^2}\right) I_0\left(\frac{k_m}{3\sigma_m^2}\right)} \right) \quad (6.74)$$

and

$$\lim_{t \rightarrow \infty} E[\tilde{\boldsymbol{\epsilon}}^T(t)\tilde{\boldsymbol{\epsilon}}(t)] \leq \frac{3\alpha\sigma_w^2}{2k_e} \quad (6.75)$$

bound the ultimate expectations for the attitude estimate error and the bias estimate error respectively. For clarity, the bounds are drawn in the following figures.

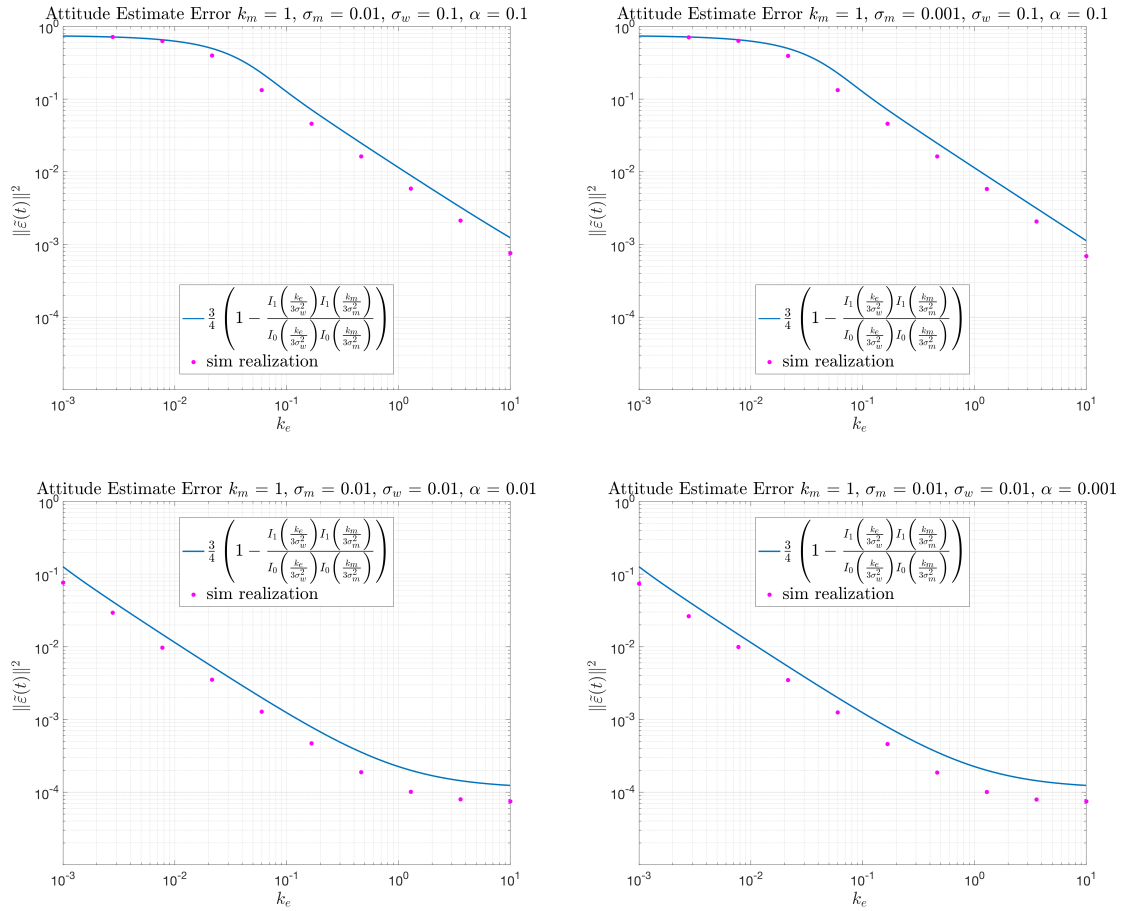


Figure 6.27: Comparison of simulation realizations of the attitude estimate error variance and the notional bound of Equation 6.74 for a range of tracking gains k_e for an inertially fixed vehicle (not spinning).

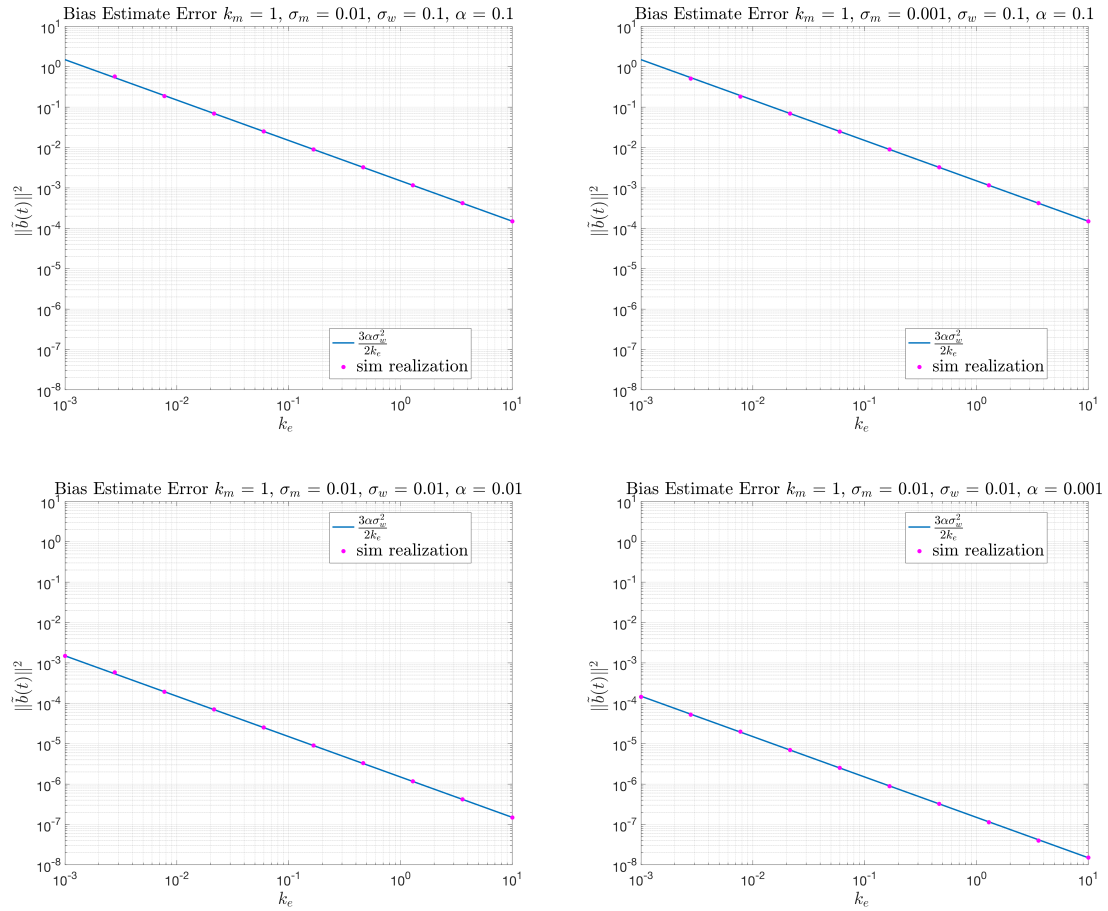


Figure 6.28: Comparison of simulation realizations of the bias estimate error variance and the notional bound of Equation 6.73 for a range of tracking gains k_e for an inertially fixed vehicle (not spinning).

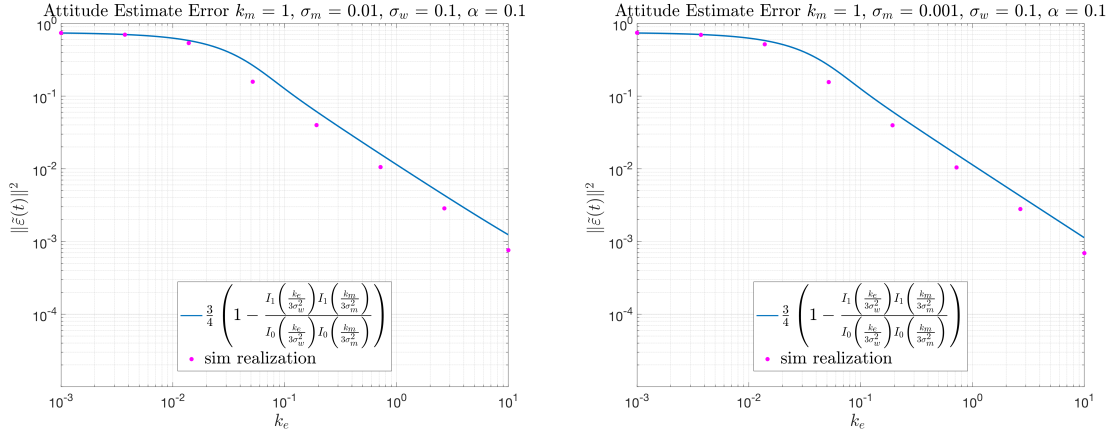


Figure 6.29: Comparison of simulation realizations of the bias estimate error variance and the notional bound of Equation 6.75 for a range of tracking gains k_e for a vehicle spinning at 5 revolutions per minute about the vehicle body's $[1 \ 2 \ 3]^T$ axis.

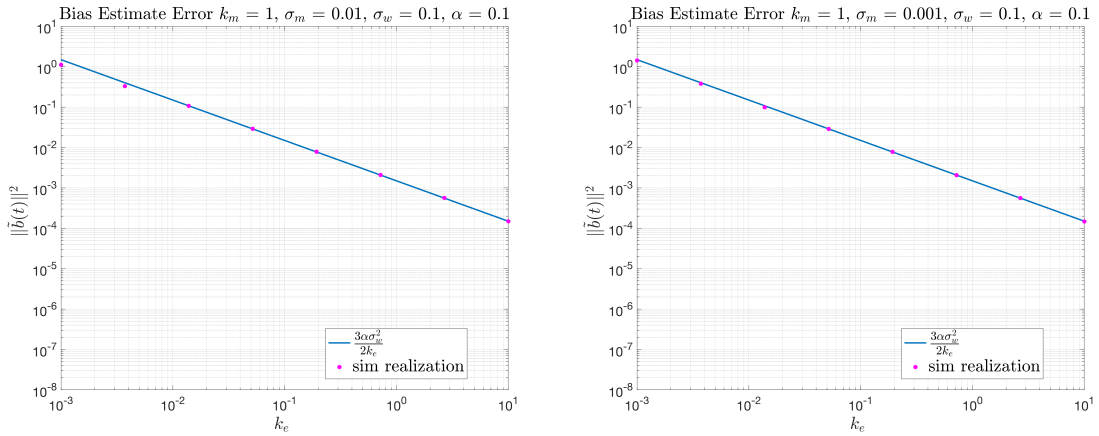


Figure 6.30: Comparison of simulation realizations of the bias estimate error variance and the notional bound of Equation 6.75 for a range of tracking gains k_e for a vehicle spinning at 5 revolutions per minute about the vehicle body's $[1 \ 2 \ 3]^T$ axis.

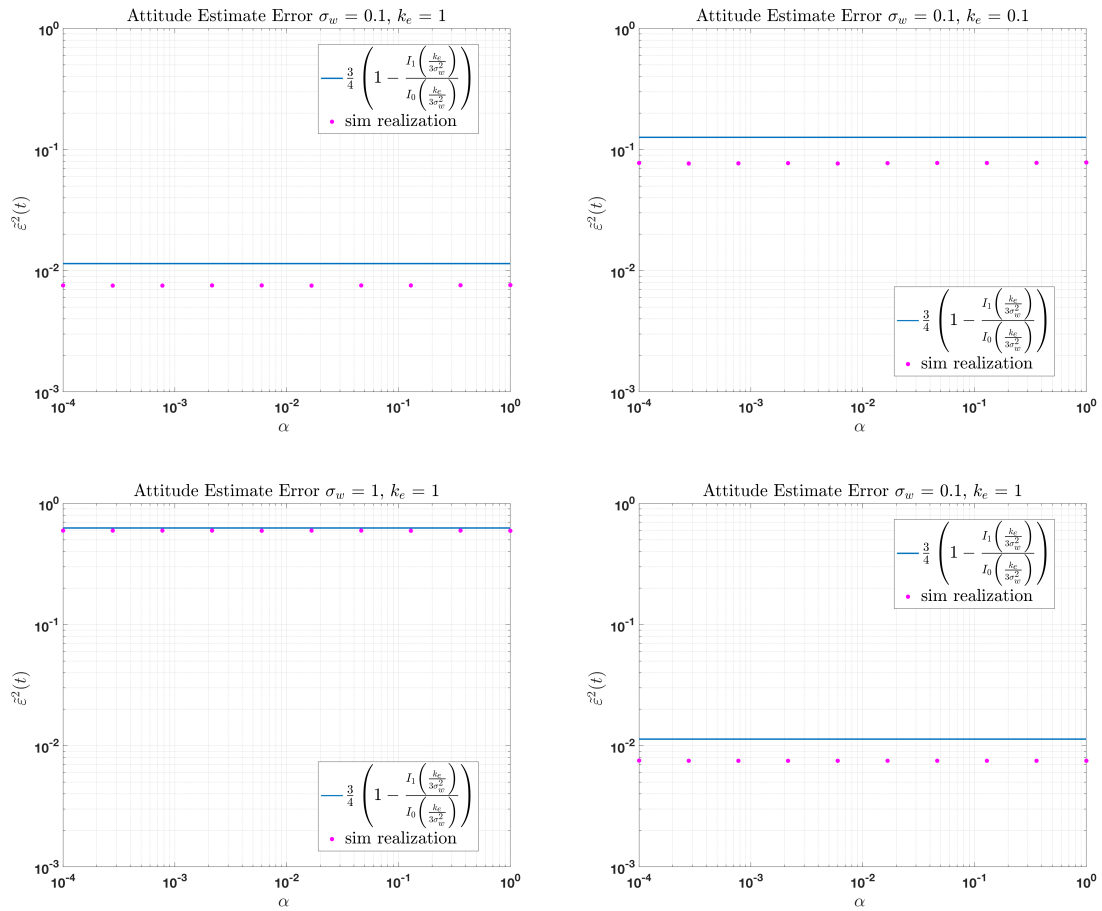


Figure 6.31: Comparison of simulation realizations of the attitude estimate error variance and the notional bound of Equation 6.74 for a range of adaptation gains α for an inertially fixed vehicle (not spinning).

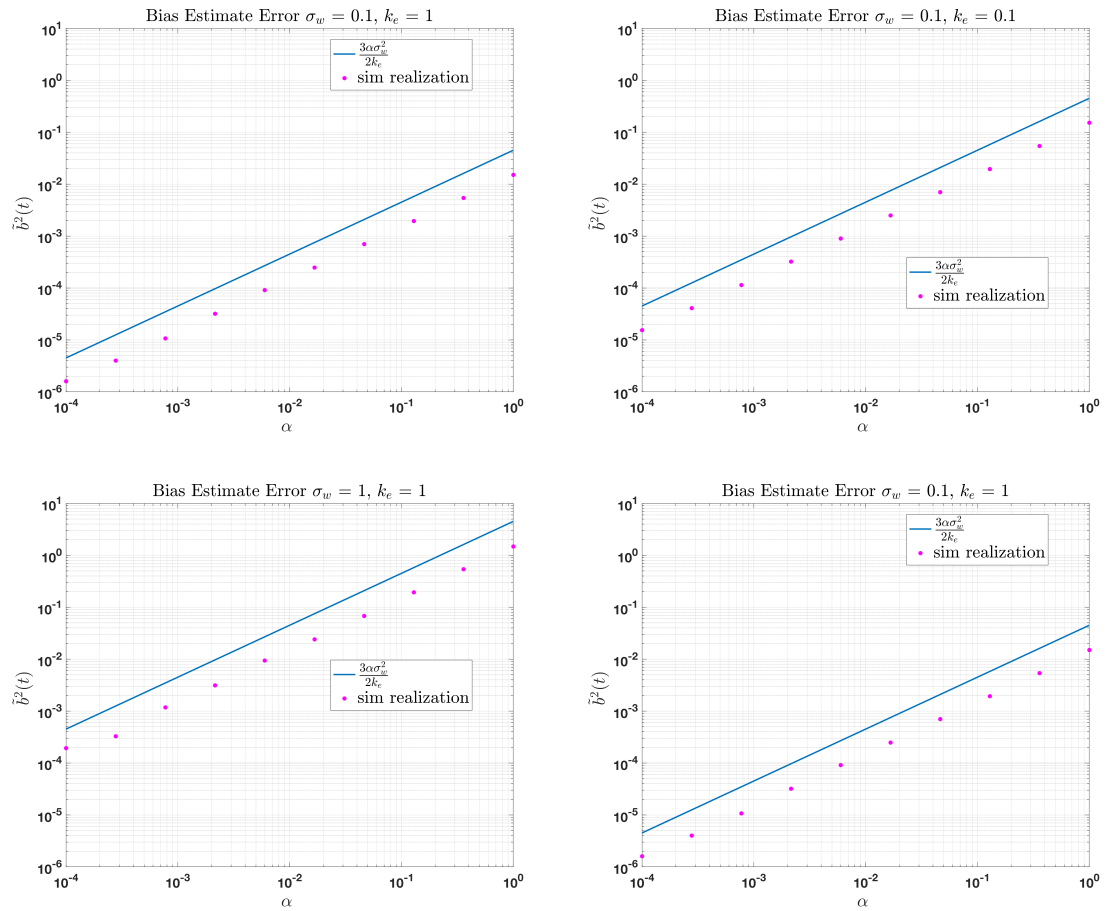


Figure 6.32: Comparison of simulation realizations of the bias estimate error variance and the notional bound of Equation 6.75 for a range of adaptation gains α for an inertially fixed vehicle (not spinning).

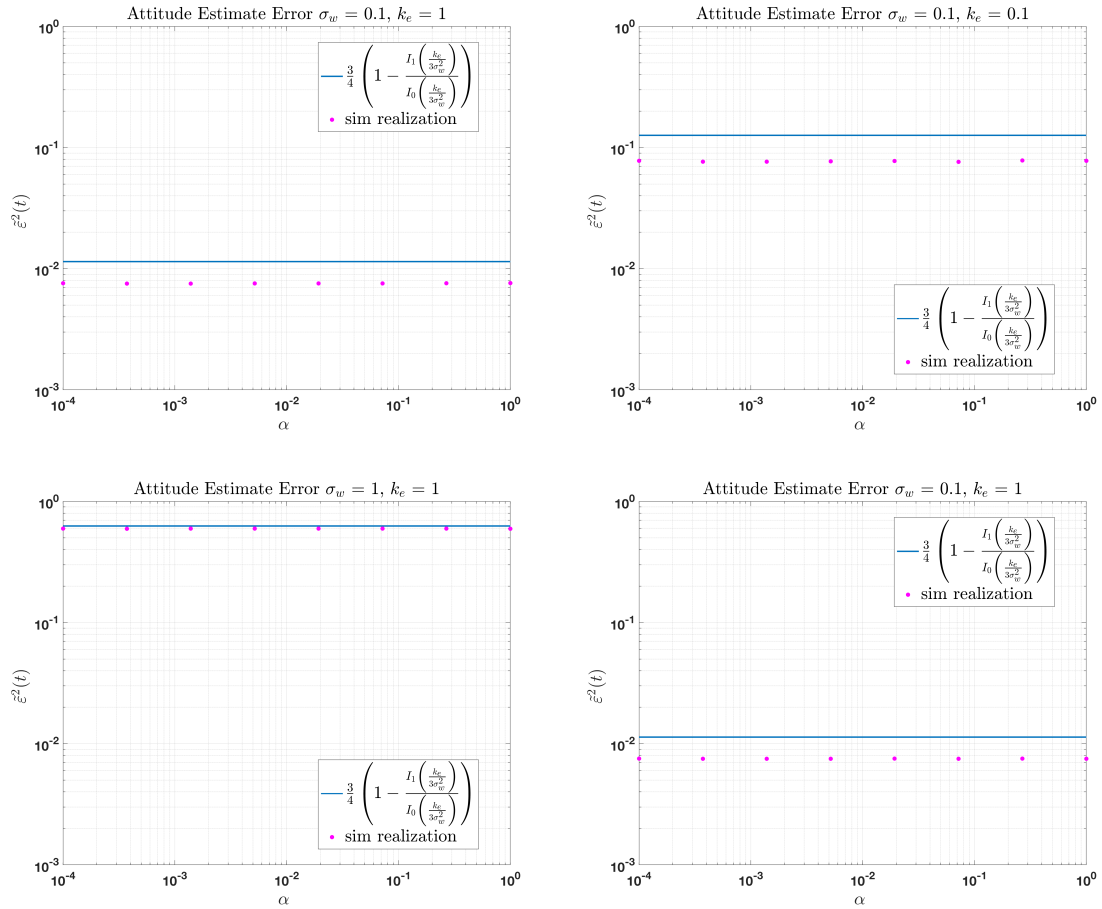


Figure 6.33: Comparison of simulation realizations of the attitude estimate error variance and the notional bound of Equation 6.74 for a range of adaptation gains α for a vehicle spinning at 5 revolutions per minute about the vehicle body's $[1 \ 2 \ 3]^T$ axis.

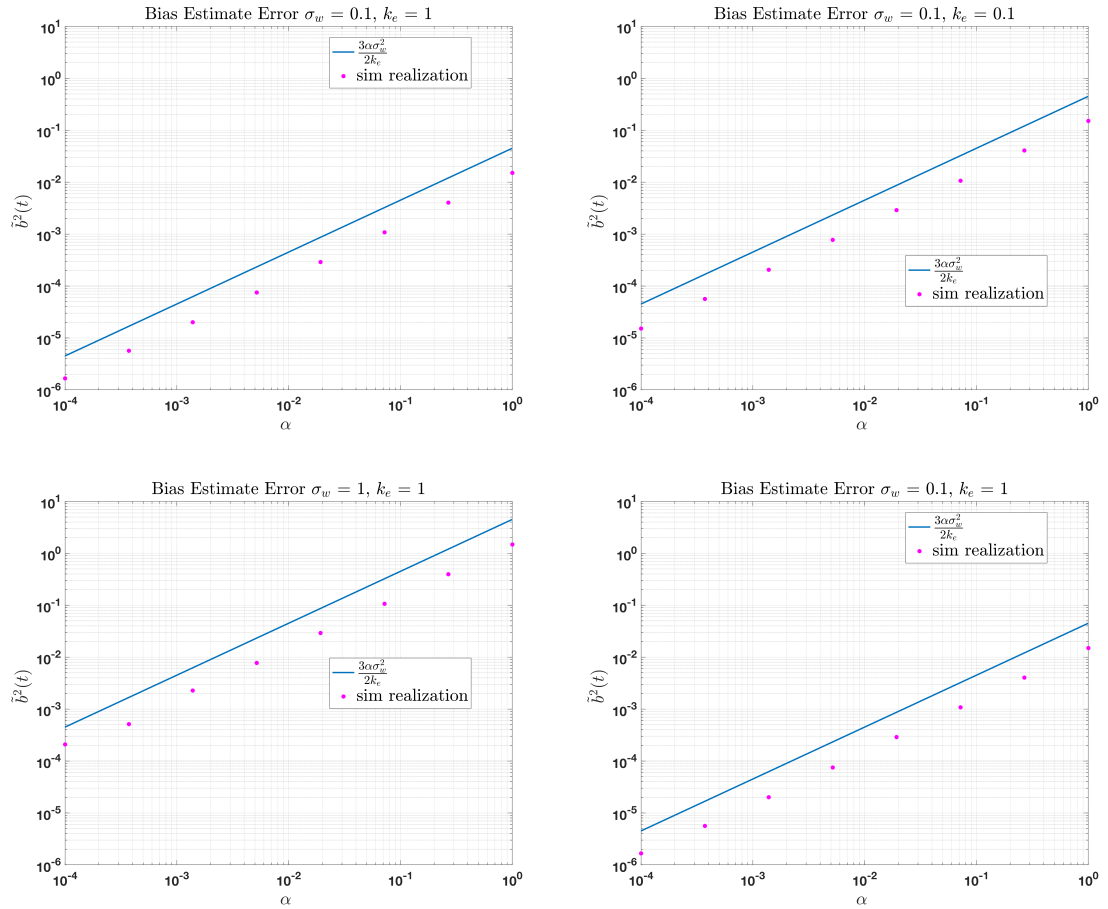


Figure 6.34: Comparison of simulation realizations of the bias estimate error variance and the notional bound of Equation 6.75 for a range of adaptation gains α for a vehicle spinning at 5 revolutions per minute about the vehicle body's $[1 \ 2 \ 3]^T$ axis.

Chapter 7: Future Directions and Concluding Remarks

Attitude estimation systems are critical components of satellite control systems, aircraft autopilots, and underwater vehicle control systems; additionally, they are used extensively for virtual reality devices, fitness tracking equipment, and other applications. The performance of attitude estimation systems is typically driven by the error and noise properties of the sensor measurements. Gyroscopes in particular are known for being corrupted by significant measurement bias error. Nonlinear adaptive state observers are an attractive technique for estimating gyro constant bias in real time onboard applications as in the deterministic setting they have global stability properties, but their stability and performance properties in a rigorous stochastic setting were not previously well understood.

The first part of this thesis provided an extension of a nonlinear adaptive gyro bias observer by introducing additional dynamics to allow for the learning of gyro thermal bias functions of arbitrary shape provided they are sufficiently smooth. Numerical simulation studies were conducted to demonstrate performance in the deterministic case. The stochastic case was then considered by introducing additive unbounded gyro noise and attitude measurement noise by formulating the system dynamics as a formal stochastic differential equation. Observer estimate error per-

formance was examined in the stochastic case by conducting simulation studies at a variety of samples of the parameter space. The computational expense and imprecise nature of the technique provided motivation to find analytic bounds or solutions to observer estimate error as a function of gain parameters and measurement noise specifications.

To gain a formal understanding of the stability and performance properties for this class of nonlinear attitude observers, the simplest case of an attitude observer with additive gyro noise was first considered in detail. Stochastic Lyapunov theory was used to prove the filter is weakly stochastically stable. Bounds on the ultimate error statistics were found and compared to numerical simulation but were shown to be conservative. The weak stochastic stability result allowed for the determination of the analytic solution to the stationary Fokker-Planck PDE; the solution to the stationary Fokker-Planck PDE in the $SO(2)$ case was found to be given by a von Mises distribution and the $SO(3)$ case was solved by a bipolar Bingham distribution. The stationary probability distribution functions were in turn used to derive closed form expressions for stationary statistics which matched numerical simulation results exactly.

Next, constant gyro bias was considered along with gyro additive noise. The gyro constant bias filter was shown to be weakly stochastically stable via an appeal to the converse Lyapunov theorem. Once weak stochastic stability was shown, the stationary Fokker-Planck PDE was investigated. The filter error dynamics were found to converge to a joint distribution that was a von Mises distribution in the attitude estimate error and a Gaussian distribution in the bias estimate error in the

SO(2) case; the SO(3) case had the stationary PDF given as a joint distribution that was a bipolar Bingham distribution in the attitude estimate error and a multivariate Gaussian distribution in the bias estimate error. In both the SO(2) and SO(3) cases the ultimate attitude estimate error and ultimate bias estimate error were found to be independent of each other; the ultimate attitude estimate error statistics were completely independent of the bias estimation error while the ultimate bias estimation error distribution depended on the tracking gain. The stationary probability distribution functions were in turn used to derive closed form expressions for stationary statistics which matched numerical simulation results exactly.

Next, attitude measurement noise was introduced into the analysis. In order to utilize the stochastic Lyapunov analysis theorems and stationary Fokker-Planck analysis approach, the system error dynamics needed to be formulated as an Itô SDE. A process that can be formulated as an Itô SDE and has a known ultimate probability density on the unit quaternion hypersphere was identified as the error dynamics of the attitude estimation filter. Thus to consider an attitude estimation filter with gyro additive noise and quaternion measurement noise, the filter error dynamics were augmented with an additional process to model non-white quaternion noise. The combined system was then shown to be weakly stochastically stable for bounded angular rate. Stochastic Lyapunov theory was further used to find ultimate performance bounds; while the bounds did correctly bound numerical simulation statistics, the performance bounds were not indicative of the simulated filter performance. An asymptotic solution to the stationary Fokker-Planck PDE in SO(2) was found to be given by a bivariate von Mises distribution; ultimate performance

statistics computed from this stationary PDF agreed with numerical simulation results. Ultimate statistics derived from the asymptotic solution to the stationary SO(2) Fokker-Planck PDE were found to agree with numerical simulation realizations. The solution to the SO(3) stationary Fokker-Planck PDE remains unknown to the author, but heuristic bounds were found in the SO(3) case by extrapolating the structure of the analytic expressions for the ultimate expectations from the SO(2) analysis.

Finally, a filter with gyro additive noise, gyro constant bias, and attitude measurement noise was considered. A stochastic stability result was not found, but assuming the system was stochastically stable allowed for the determination of an asymptotic solution to the stationary Fokker-Planck PDE in the SO(2) case. The asymptotic SO(2) solution was found to be a joint PDF that was a bivariate von Mises distribution in the attitude estimate error and attitude measurement noise model, and a Gaussian distribution in the bias estimate error. As before, the ultimate attitude estimate error and attitude noise model states given by the bivariate von Mises were found to be independent of the ultimate bias estimate error. Ultimate statistics derived from the asymptotic solution to the stationary SO(2) Fokker-Planck PDE were found to agree with numerical simulation realizations. The solution to the SO(3) stationary Fokker-Planck PDE remains unknown to the author, but heuristic bounds were found in the SO(3) case by extrapolating the structure of the analytic expressions for the ultimate expectations from the SO(2) analysis.

7.1 Future Directions

The stochastic analysis framework utilized in this thesis can hopefully be used to explore the impact of the many other important measurement phenomena that were not addressed in this thesis. Of course several spots on the Table 1.1 are empty or have less satisfying results. Given that the converse Lyapunov theorem shows that the Gyro Constant Bias Filter with additive gyro noise and perfect attitude measurements of Chapter 5 has an (as yet unidentified by the author) Lyapunov function that does show stochastic stability for that filter, the explicit determination of that Lyapunov function would be useful. In particular, such a Lyapunov function could likely be suitably augmented to demonstrate weak stochastic stability for the Gyro Constant Bias Filter with additive gyro noise and attitude measurement noise examined in Section 6.3; the simulation analysis of that section suggests the filter under those conditions is weakly stochastically stable. Further, an asymptotic solution to the stationary Fokker-Planck PDE in the $SO(2)$ case was found for both filters considered in Chapter 6, but no solution was identified for the full $SO(3)$ versions of those analyses.

The remainder of this chapter outlines several new directions that might further be considered with the stochastic analysis tools and strategies demonstrated in this thesis.

7.1.1 Non-axis-symmetric Gyro Additive Noise

The gyro additive measurement noise model considered in this thesis was axis symmetric and uncorrelated. Specifically, the gyro additive noise $\mathbf{n}_w(t)$ was assumed to obey $E[\mathbf{n}_w(t)\mathbf{n}_w^T(\tau)] = \sigma_w^2 I \delta(t - \tau)$. In the case of an attitude estimation filter with gyro additive noise and perfect attitude measurements as studied in Chapter 4, the solution to the stationary Fokker-Planck PDE was shown to be given as a special case of the Bingham distribution, the bipolar Bingham distribution, which was

$$p_s(\tilde{\mathbf{q}}) = \frac{1}{N} \exp \left\{ \frac{k_e}{\sigma_w^2} (2\tilde{\eta}^2 - 1) \right\}$$

It was noted in Section 4.11 that the above bipolar Bingham distribution is equivalent to the general Bingham distribution

$$p_s(\tilde{\mathbf{q}}) = \frac{1}{N} \exp \{ \tilde{\mathbf{q}}^T M Z M^T \tilde{\mathbf{q}} \}$$

for $M = I$ and $Z = \text{diag} \left(-\frac{k_e}{\sigma_w^2}, -\frac{k_e}{\sigma_w^2}, -\frac{k_e}{\sigma_w^2}, \frac{k_e}{\sigma_w^2} \right) = \frac{k_e}{\sigma_w^2} \text{diag}(-1, -1, -1, 1)$.

A more general gyro additive noise model is $E[\mathbf{n}_w(t)\mathbf{n}_w^T(\tau)] = \Sigma_w \delta(t - \tau)$ where Σ_w is a symmetric positive definite matrix. This more general model allows for the noise density of each gyro sensing axis to differ from the others, as well as allowing for the consideration of cross-coupling in the measurement noise. While the more general noise model might lead to a more involved stationary Fokker-Planck PDE in the SO(3) case, it seems natural to expect the solution might be given by a Bingham distribution with $M \neq I$ and $Z \neq \frac{k_e}{\sigma_w^2} \text{diag}(-1, -1, -1, 1)$. A possibility that matches the form of the axis-symmetric solution would be when Z is a function

of $k_e \Sigma_w^{-1}$.

7.1.2 Gyro Random Walk Bias

An important gyro measurement model is one with gyro additive noise and random walk bias, given as

$$\begin{aligned}\boldsymbol{\omega}_g(t) &= \boldsymbol{\omega}(t) + \mathbf{b}(t) + \sigma_w \mathbf{n}_w(t) \\ \dot{\mathbf{b}}(t) &= \sigma_b \mathbf{n}_b(t)\end{aligned}\tag{7.1}$$

where $\mathbf{n}_b(\cdot)$ is a zero mean unit variance Gaussian white noise process independent of $\mathbf{n}_w(t)$ and σ_b is a positive scalar. This model is utilized in the widely used MEKF [51, 64]. A gyro random walk bias can be used to model deterministic error sources that might be difficult to quantify such as fluctuations in gyro operating temperature or variation in the provided electrical power. Gyro random walk bias can also be used as a simple model to attempt to account for more complicated stochastic noise sources such as flicker noise and sinusoidal noise.

Extending the SO(2) gyro constant bias filter error dynamics Itô SDE to model gyro random walk bias in the SO(2) case leads

$$\begin{aligned}d\tilde{\mathbf{y}}(t) &= \begin{bmatrix} d\tilde{\phi}(t) \\ d\tilde{\mathbf{b}}(t) \end{bmatrix} \\ &= \begin{bmatrix} -\frac{1}{2}k_e \sin(\tilde{\phi}(t)) - \tilde{\mathbf{b}}(t) \\ \frac{1}{2}\alpha \sin(\tilde{\phi}(t)) \end{bmatrix} dt + \begin{bmatrix} -\sigma_w & 0 \\ 0 & \sigma_b \end{bmatrix} \begin{bmatrix} d\beta_w(t) \\ d\beta_b(t) \end{bmatrix} \\ &= \mathbf{f}(\tilde{\mathbf{y}}(t))dt + Gd\boldsymbol{\beta}(t)\end{aligned}$$

which differs from the Itô SDE 5.18 of Section 5.4 by an additional Brownian motion noise process and a larger diffusion matrix G which now has full rank.

Let $p = p(\tilde{\mathbf{y}}(t), t) = p(\tilde{\phi}(t), \tilde{b}(t), t)$ be the joint probability density for the SO(2) Gyro Random Walk Bias Filter estimate error states. Assuming the system is weakly stochastically stable, then $\lim_{t \rightarrow \infty} p(\tilde{\mathbf{y}}(t), t) = p_s(\tilde{\phi}, \tilde{b})$ where $p_s = p_s(\tilde{\phi}, \tilde{b})$ solves the stationary Fokker-Planck PDE for the system. Similar to the development in Section 5.5, the stationary Fokker-Planck PDE can be found as

$$0 = k_e \cos(\tilde{\phi}) p_s + \left(k_e \sin(\tilde{\phi}) + 2\tilde{b}\right) \frac{\partial p_s}{\partial \tilde{\phi}} - \alpha \sin(\tilde{\phi}) \frac{\partial p_s}{\partial \tilde{b}} + \sigma_w^2 \frac{\partial^2 p_s}{\partial \tilde{\phi}^2} + \sigma_b^2 \frac{\partial^2 p_s}{\partial \tilde{b}^2}$$

which differs from the Gyro Constant Bias Filter's SO(2) stationary Fokker-Planck PDE by the additional term $\sigma_b^2 \frac{\partial^2 p_s}{\partial \tilde{b}^2}$.

The similarity between the stationary Fokker-Planck PDE in SO(2) for the Gyro Constant Bias Filter and the Gyro Random Walk Bias Filter suggest the solutions to the stationary Fokker-Planck PDEs may be similar as well. Note that the analysis of this section assumes the error dynamics for the Gyro Random Walk Bias Filter are weakly stochastically stable. Weak stochastic stability for the Gyro Constant Bias Filter was established in Section 5.2 via an appeal to the converse Lyapunov theorem as the explicit form of a Lyapunov function that satisfies the conditions of the Zakai Stability Theorem 2.1.4 were not found in this thesis; a similar appeal could be used for the Gyro Random Walk Bias Filter.

7.1.3 Augment Attitude Estimation Filter State to Estimate Non-White Attitude Measurement Noise

Chapter 6 considered attitude measurement noise. In order to formulate the system dynamics as an Itô SDE, the attitude measurements were modeled as corrupting the true attitude by quaternion noise. The quaternion noise was generated as the output of a continuous process driven by Gaussian white noise as described in Section 6.1. An interesting consequence of using a continuous process driven by white noise is that the resulting quaternion noise, while constrained to the unit quaternion hypersphere, is not white.

The analysis in Section 6.2 showed that in the high filter gain limit (as $k_e \rightarrow \infty$), the attitude estimate error is ultimately limited by the attitude measurement noise density. A discussion at the end of Section 6.2.8 used a linear time invariant (LTI) analog to clarify the issue. The analogous LTI system was given by the translational kinematics

$$\dot{x}(t) = v(t)$$

A velocity sensor, the translational analog of an angular rate gyro, was assumed to provide velocity measurements perturbed by unbounded additive white noise

$$v_m(t) = v(t) + \sigma_v w_v(t)$$

Further, a translational position sensor was considered with the measurement model

$$x_m(t) = x(t) + n(t)$$

where the process $n(\cdot)$ is non-white noise given by a First Order Gauss Markov (FOGM) process

$$\dot{n}(t) = -\lambda n(t) + \sigma_n w_n(t)$$

An LTI analog of the nonlinear attitude filter for this system was given as the translational position filter

$$\dot{\hat{x}}(t) = v_m(t) + k_e(x_m(t) - \hat{x}(t))$$

The LTI translational position filter used the velocity measurement to propagate its kinematic model. The feedback term $e_m(t) = x_m(t) - \hat{x}(t)$ was used to drive the translation estimate $x(t)$ towards the translation measurement $x_m(t)$. Since the noise process $n(t)$ is non-white, its mean process $E[n(t)]$ is in general nonzero; the consequence of the non-white position noise is that the mean of the feedback term is non-zero even if the position estimate $\hat{x}(t)$ matches the true position $x(t)$. However, it might be possible to reduce the impact of this noise by augmenting the filter state to estimate not only the true system state $x(t)$ but also estimate the non-white noise; thus the filter would have an estimate $\hat{x}(t)$ of the state and an estimate $\hat{n}(t)$ of the non-white noise. The filter could then use the feedback term $e_{m2}(t) = x_m(t) - (\hat{x}(t) + \hat{n}(t))$ which will be nonzero when either $\hat{x}(t)$ or $\hat{n}(t)$ have error. The augmented filter could be implemented as

$$\dot{\hat{x}}(t) = v_m(t) + k_e e_{m2}(t)$$

$$\dot{\hat{n}}(t) = -\lambda \hat{n}(t) - k_n e_{m2}(t)$$

The details of how to incorporate these ideas in a quaternion estimation algorithm may not be immediately apparent, but in the deterministic case Thienel [94,

Chapter 5] was able to augment a gyro bias observer with a gyro alignment observer in a quaternion formulation. Specifically, the nonlinear attitude filter of Chapter 6 would need its state to be augmented by an estimate $\hat{\mathbf{q}}(t)$ of the quaternion noise $\check{\mathbf{q}}(t)$.

The feedback term for the attitude filter would then need to be appropriately modified. In Chapter 6 the feedback term was computed as $k_e \tilde{\eta}_m(t) \tilde{\boldsymbol{\varepsilon}}_m(t)$ where

$$\begin{aligned} \tilde{\mathbf{q}}_m(t) &= \begin{bmatrix} \tilde{\boldsymbol{\varepsilon}}_m(t) \\ \tilde{\eta}_m(t) \end{bmatrix} = \mathbf{q}_m(t) \otimes \hat{\mathbf{q}}^{-1}(t) \\ &= \check{\mathbf{q}}^{-1}(t) \otimes \mathbf{q}(t) \otimes \hat{\mathbf{q}}^{-1}(t) \\ &= \check{\mathbf{q}}^{-1}(t) \otimes \tilde{\mathbf{q}}(t) \end{aligned}$$

compared the attitude measurement $\mathbf{q}_m(t)$ with the attitude estimate $\hat{\mathbf{q}}(t)$. The feedback term was based on the comparison $\tilde{\mathbf{q}}_m(t)$ which was a noise corrupted version of the attitude estimate error $\tilde{\mathbf{q}}(t)$.

This section proposes augmenting the filter state with an estimate $\hat{\check{\mathbf{q}}}(t)$ of the non-white attitude measurement noise $\check{\mathbf{q}}(t)$ which can be used to compute the augmented feedback term

$$\begin{aligned} \tilde{\mathbf{q}}_{m2}(t) &= \begin{bmatrix} \tilde{\boldsymbol{\varepsilon}}_{m2}(t) \\ \tilde{\eta}_{m2}(t) \end{bmatrix} = \hat{\check{\mathbf{q}}}(t) \otimes \mathbf{q}_m(t) \otimes \hat{\mathbf{q}}^{-1}(t) \\ &= \hat{\check{\mathbf{q}}}(t) \otimes \check{\mathbf{q}}^{-1}(t) \otimes \mathbf{q}(t) \otimes \hat{\mathbf{q}}^{-1}(t) \\ &= \check{\check{\mathbf{q}}}^{-1}(t) \otimes \tilde{\mathbf{q}}(t) \end{aligned}$$

The feedback term would then be used to drive the filter's attitude estimate quaternion kinematics $\dot{\hat{\mathbf{q}}}(t)$ as well as the filter's quaternion measurement noise model $\dot{\check{\mathbf{q}}}(t)$.

7.1.4 Closed Loop Attitude Control Analysis

Another important area that could benefit from the techniques of this thesis is the closed-loop attitude control problem. Consider the attitude control problem for a rigid body vehicle (such as a satellite or an aerial vehicle with negligible drag) with the dynamics

$$H\dot{\boldsymbol{\omega}}(t) + [\boldsymbol{\omega}(t) \times]H\boldsymbol{\omega}(t) = \boldsymbol{\tau} = \mathbf{u}_{nom}(t)$$

where H is the system inertia matrix, $\boldsymbol{\omega}(t)$ is the vehicle angular rate, and $\boldsymbol{\tau}$ are torques acting on the system. Egeland and Godhavn [17] propose the nonlinear attitude tracking controller

$$\mathbf{u}_{nom}(t) = -K\mathbf{s}(t) + H\dot{\boldsymbol{\omega}}_{ref}(t) + [\boldsymbol{\omega}_{ref}(t) \times]H\boldsymbol{\omega}(t)$$

where the controller attitude error $\tilde{\mathbf{q}}(t) = \begin{bmatrix} \tilde{\boldsymbol{\epsilon}}(t) \\ \tilde{\boldsymbol{\eta}}(t) \end{bmatrix} = \mathbf{q}(t) \otimes \mathbf{q}_d^{-1}(t)$ compares the error between the true attitude $\mathbf{q}(t)$ and desired attitude $\mathbf{q}_d(t)$ at time t , the angular rate tracking error is given by $\tilde{\boldsymbol{\omega}}(t) = \boldsymbol{\omega}(t) - R(\tilde{\mathbf{q}}(t))\boldsymbol{\omega}_d(t)$ compares the true angular rate with the desired angular rate $\boldsymbol{\omega}_d(t)$, $\boldsymbol{\omega}_{ref}(t) = R(\tilde{\mathbf{q}}(t))\boldsymbol{\omega}_d(t) - \lambda\tilde{\boldsymbol{\epsilon}}(t)$, the composite tracking error metric $\mathbf{s}(t) = \tilde{\boldsymbol{\omega}}(t) + \lambda\tilde{\boldsymbol{\epsilon}}(t)$ relatively weights the attitude and rate tracking error via the scalar $\lambda > 0$, and the matrix $K > 0$ consists of controller gains. They show the tracking controller is globally asymptotically stable and is able to track arbitrarily rapid slews. By setting $\dot{\boldsymbol{\omega}}_d(t) = \boldsymbol{\omega}_d(t) = \mathbf{0}$, the controller simplifies to the celebrated PD quaternion feedback regulator of Wie, Weiss, and Arapostathis [106].

Now assume the controller no longer has access to the true vehicle attitude; instead it is given gyro measurements perturbed by additive gyro noise

$$\boldsymbol{\omega}_g(t) = \boldsymbol{\omega}(t) + \sigma_w \mathbf{n}_w(t)$$

and the dynamics are perturbed by random disturbance torques (such as aerodynamic torques, solar radiation pressure, or fuel slosh for a satellite) according to

$$H\dot{\boldsymbol{\omega}}(t) + [\boldsymbol{\omega}(t) \times]H\boldsymbol{\omega}(t) = \boldsymbol{\tau} = \mathbf{u}_{meas}(t) + \sigma_d \mathbf{n}_d(t)$$

where $\sigma_w > 0$, $\sigma_d > 0$, and $\mathbf{n}_w(t)$ and $\mathbf{n}_d(t)$ are independent zero mean Gaussian white noise processes. The closed-loop error dynamics can then be found as the Itô SDE

$$\begin{aligned} d\mathbf{s}(t) &= \left\{ H^{-1} \left[(H\boldsymbol{\omega}(t)) \times \right] \mathbf{s}(t) - H^{-1}K\mathbf{s}(t) \right\} dt \\ &\quad + \begin{bmatrix} H^{-1}\Delta(\tilde{\mathbf{q}}(t), \boldsymbol{\omega}_d(t))\sigma_w & H^{-1}\sigma_d \end{bmatrix} \begin{bmatrix} d\boldsymbol{\beta}_w(t) \\ d\boldsymbol{\beta}_d(t) \end{bmatrix} \\ &= \mathbf{f}(\mathbf{s}(t))dt + G(\mathbf{s}(t))d\boldsymbol{\beta}(t) \end{aligned} \tag{7.2}$$

where

$$\Delta(\tilde{\mathbf{q}}(t), \boldsymbol{\omega}_d(t)) = H[\boldsymbol{\omega}_d(t) \times] + [\boldsymbol{\omega}_{ref}(t) \times]H - \frac{1}{2}\lambda H(\tilde{\eta}(t)I + [\tilde{\boldsymbol{\epsilon}}(t) \times]) - K$$

Note that the desired angular acceleration $\dot{\boldsymbol{\omega}}_d(t)$ does not appear in the error dynamics as the inertia matrix is assumed to be known and the controller has access to perfect attitude measurements.

In the axis symmetric case where $K = kI$, $H = hI$, and $h, k > 0$ the following theorem shows the closed-loop system is weakly stochastically stable provided the desired angular rate is bounded.

Theorem 7.1.1. *In the axis symmetric case, the closed loop attitude tracking error dynamics of the Itô SDE 7.2 are weakly stochastically stable provided $\omega_{max} = \sup_t \|\boldsymbol{\omega}_d(t)\|$. Further,*

$$\lim_{t \rightarrow \infty} E[\mathbf{s}^T(t)\mathbf{s}(t)] \leq \left(4\sigma_w^2 h \omega_{max}^2 + 6\sigma_w^2 \lambda h \omega_{max} + \frac{9}{4}\sigma_w^2 \lambda^2 h + \frac{3}{2}\sigma_d^2 \frac{1}{h} \right) \frac{1}{k} + \frac{3}{2}\sigma_w^2 \lambda + \frac{3}{2}\sigma_w^2 \frac{1}{h} k \quad (7.3)$$

Proof. Choose the Lyapunov function $V(t) = \frac{1}{2}\mathbf{s}^T(t)H\mathbf{s}(t)$. Application of the differential generator yields

$$\begin{aligned} \mathcal{L}V(t) &= \left(\frac{\partial V}{\partial \mathbf{s}} \right)^T \mathbf{f}(\mathbf{s}(t)) + \frac{1}{2} \text{tr} \left\{ G^T(\mathbf{s}(t)) \frac{\partial^2 V}{\partial \mathbf{s}^2} G(\mathbf{s}(t)) \right\} \\ &= -\mathbf{s}(t)K\mathbf{s}(t) + \frac{1}{2}\sigma_w^2 \text{tr}(\Delta^T H^{-1} \Delta) + \frac{1}{2}\sigma_d^2 \text{tr}(H^{-1}) \end{aligned}$$

Invoking the axis symmetric simplification and algebraic manipulation lead to

$$\begin{aligned} \mathcal{L}V(t) &\leq -k\mathbf{s}^T(t)\mathbf{s}(t) + 4\sigma_w^2 h \omega_{max}^2 + 6\sigma_w^2 \lambda h \omega_{max} \\ &\quad + \frac{9}{4}\sigma_w^2 \lambda^2 h + \frac{3}{2}\sigma_w^2 \lambda k + \frac{3}{2}\sigma_w^2 \frac{1}{h} k^2 + \frac{3}{2}\sigma_d^2 \frac{1}{h} \end{aligned}$$

Thus the error dynamics are weakly stochastically stable via the Zakai Stability Theorem 2.1.4. Further, application of the Zakai Ultimate Moment Bound Theorem 2.1.5 and dividing by k yields the ultimate error statistic.

□

The result agrees well with intuition. If the controller gain k is too small, the controller is overwhelmed by disturbance torques. If the controller gain is too large, the controller admits too much gyro measurement noise. Additionally, the bound provides criteria to optimize the controller gain given system parameters noise specifications.

Optimizing the ultimate error upper bound of Equation 7.3 for the controller gain results in

$$k_{opt} = \sqrt{\frac{8}{3}h^2\omega_{max}^2 + 4\lambda h^2\omega_{max} + \frac{3}{2}\lambda^2 h^2 + \frac{\sigma_d^2}{\sigma_w^2}}$$

Numerical simulations of the Itô SDE 7.2 for a sample of controller gain k are shown in Figure 7.1. The dashed line superimposed on the plot is the ultimate error upper bound of Equation 7.3. The controller gain that optimizes the ultimate error upper bound for the given system parameters is drawn as a circle.

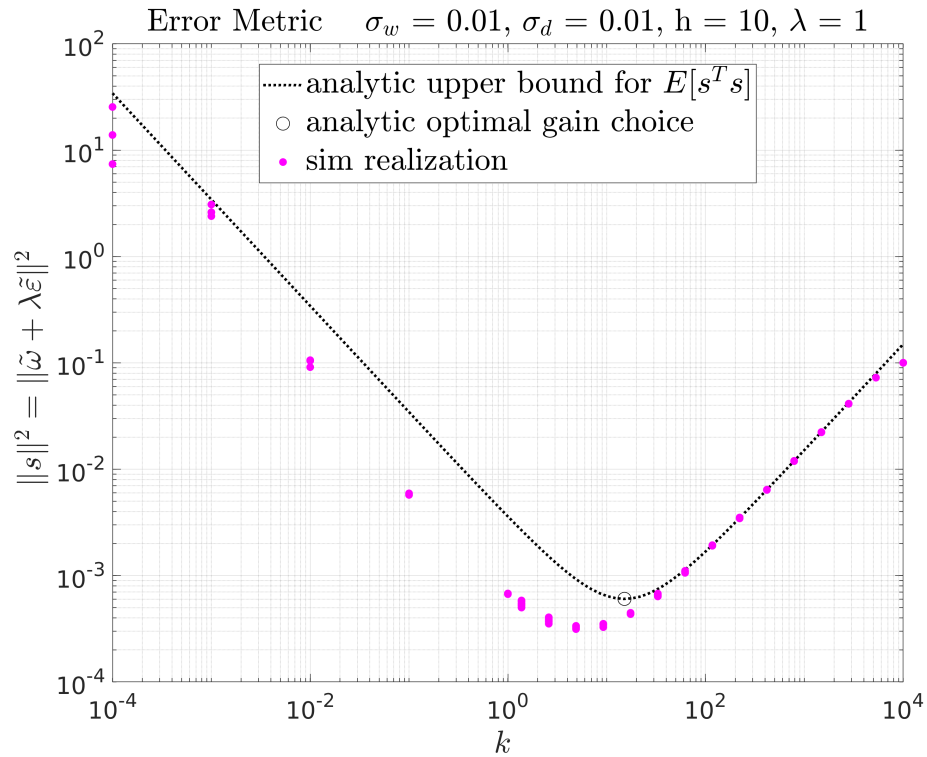


Figure 7.1: Comparison of numerical simulations of the closed-loop attitude controller error Itô SDE 7.2 with the ultimate error upper bound of Equation 7.3.

Unfortunately the minimum of the stochastic Lyapunov bound does not match the minimum in the numerical simulation data. A recurring theme throughout

Chapters 4, 5, and 6 is that the stochastic Lyapunov bounds have been conservative compared to numerical simulation and the Fokker-Planck solutions (when available). As before, the error in the Lyapunov bound may be an artifact of the Lyapunov function chosen or bounding techniques used in the proof; different Lyapunov function choices may provide a better bound. Note the challenge that might be involved in conducting a Fokker-Planck analysis of the system as the error dynamics are a function of the (time varying) desired angular rate $\omega_d(t)$.

A direction for further investigation is to consider the closed-loop feedback control problem where a state observer provides attitude and rate estimates for use by the controller in a certainty equivalence fashion. The deterministic case was studied by Thienel [94] and Thienel and Sanner [95] for a class of nonlinear adaptive gyro observers with this same control law. They found that that the separation principle, which does not in general hold for nonlinear systems, does hold for the Thienel and Sanner gyro constant bias observer and the Egeland and Godhavn controller closed loop system. Does the situation hold in the stochastic setting?

7.2 Final Remarks

The driving goal of this thesis was to address practical concerns in the use of nonlinear state estimation strategies for attitude estimation applications.

The first contribution toward this goal was the extension of a Gyro Constant Bias Observer to account for a physically significant deterministic error source of gyro bias, that of bias variation as a function of gyro operating temperature. Modification of the Gyro Constant Bias Observer adaptation law to update a gyro thermal bias function approximation was able to mitigate the impact of gyro thermal bias in the deterministic case. Use of simulation analysis to understand performance and select gains in the stochastic case proved troubling due to the extensive computational cost; further, the simulation analysis provided no guarantee of stability in the stochastic setting with unbounded additive gyro noise.

The remainder of the thesis investigated nonlinear state estimation strategies in a formal stochastic setting. Four measurement configurations (and the corresponding filter formulation) were considered: gyro additive noise, gyro additive noise and constant gyro bias, gyro additive noise and attitude measurement noise, and finally gyro additive noise, constant gyro bias, and attitude measurement noise. Stochastic Lyapunov theory was used to establish that the nonlinear filters were weakly stochastically stable for every configuration considered with the exception of the filter with attitude measurement noise, gyro additive noise, and gyro bias. Further, stochastic Lyapunov theory was used to find bounds on the stationary statistics of the filters when no attitude measurement noise was present, but these

results were often very conservative compared to numerical simulation.

The most precise results from this thesis were found by using a hybrid analysis approach: first stochastic Lyapunov theory was used to determine the system under consideration was weakly stochastically stable, then the stability result could be used to simplify the corresponding Fokker-Planck PDE to the simpler stationary Fokker-Planck PDE. For the single rotation axis (motion on $SO(2)$) setting, exact or asymptotic solutions were found for the stationary Fokker-Planck PDE for all four nonlinear filters considered. For the gyro additive noise case, the exact solution to the full $SO(3)$ stationary Fokker-Planck PDE was found to be given by a bipolar Bingham distribution which allowed for the precise calculation of stationary statistics. The filter dynamics for the gyro additive noise case were later used as a process model for quaternion measurement noise, which had a known stationary distribution given by the bipolar Bingham distribution from the prior analysis. The exact solution to the full $SO(3)$ stationary Fokker-Planck PDE for the gyro additive noise and gyro constant bias case was found to be given by a joint bipolar Bingham and multivariate Gaussian distribution. The exact solution to the full $SO(3)$ stationary Fokker-Planck PDE was not found in this thesis for the attitude measurement noise cases, but heuristic bounds for stationary $SO(3)$ statistics were found by extrapolating the $SO(2)$ analytic results and rescaling based on simulation realizations.

The stochastic stability tools and approach to the Fokker-Planck analysis are readily extensible to other nonlinear attitude estimation filters and measurement models as detailed in the Future Directions Section [7.1](#). Further, the analysis

paradigm may be of use to other estimation and control problems beyond the domain of attitude estimation.

In summary, a deterministic extension to the nonlinear gyro bias filter was formulated to account for a common type of gyro deterministic error source. Then various types of measurement noise were considered in a formal stochastic setting. Stability results were obtained for several important system models. The exact $SO(3)$ stationary distributions were found for the attitude estimation filter and gyro constant bias filter. The analysis techniques utilized in this thesis provide a promising approach to obtain more results for other important attitude estimation filters.

Bibliography

- [1] BLAS - Basic Linear Algebra Subprograms. <http://www.netlib.org/blas/>.
- [2] GSL - GNU Scientific Library. <https://www.gnu.org/software/gsl/>.
- [3] LAPACK Linear Algebra PACKage. <http://www.netlib.org/lapack/>.
- [4] MATIO - MATLAB MAT File I/O Library. <https://github.com/telehan/libmatio>.
- [5] Milton Abramowitz and Irene Stegun. Handbook of Mathematical Functions. *National Bureau of Standards Applied Mathematics Series*, 55:589–626, 1972.
- [6] Priyanka Aggarwal, Zainab Syed, and Naser El-Sheimy. Thermal Calibration of Low Cost MEMS Sensors for Land Vehicle Navigation System. In *Vehicle Technology Conference, 2008. VTC Spring 2008. IEEE*, pages 2859–2863. IEEE, 2008.
- [7] Jan K. Bekkeng. Calibration of a Novel MEMS Inertial Reference Unit. *IEEE Transactions on Instrumentation and Measurement*, 58(6):1967–1974, 2009.
- [8] Christopher Bingham. An Antipodally Symmetric Distribution on the Sphere. *The Annals of Statistics*, pages 1201–1225, 1974.
- [9] Robert G. Brown and Patrick Y.C. Hwang. *Introduction to Random Signals and Applied Kalman Filtering*. John Wiley and Sons, New York, NY, 3rd edition, 1997.
- [10] Ovidiu Calin. *An Informal Introduction to Stochastic Calculus with Applications*. World Scientific, 2015.
- [11] Chi-Tsong Chen. *Linear System Theory and Design*. Oxford University Press, Inc., 1995.

- [12] Yang Cheng and John Crassidis. Particle Filtering for Sequential Spacecraft Attitude Estimation. In *AIAA Guidance, Navigation, and Control Conference and Exhibit*, page 5337, 2004.
- [13] Daniel Choukroun. Novel Stochastic Modeling and Filtering of the Attitude Quaternion. *The Journal of the Astronautical Sciences*, 57(1-2):167–189, 2009.
- [14] John L Crassidis and F Landis Markley. Unscented Filtering for Spacecraft Attitude Estimation. *Journal of Guidance, Control, and Dynamics*, 26(4):536–542, 2003.
- [15] Hua Deng, Miroslav Krstic, and Ruth J Williams. Stabilization of Stochastic Nonlinear Systems Driven by Noise of Unknown Covariance. *IEEE Transactions on automatic control*, 46(8):1237–1253, 2001.
- [16] Joseph L Doob. *Stochastic Processes*, volume 7. Wiley New York, 1953.
- [17] O. Egeland and J.-M. Godhavn. Passivity-Based Adaptive Attitude Control of a Rigid Spacecraft. *Automatic Control, IEEE Transactions on*, 39(4):842–846, 1994.
- [18] James Lawrence Farrell. Attitude Determination by Kalman Filtering. Technical report, NASA CR-598, 1964.
- [19] James Lawrence Farrell. Attitude Determination by Kalman Filtering. *Automatica*, 6(3):419–430, 1970.
- [20] R.L. Farrenkopf. Analytic Steady-state Accuracy Solutions for Two Common Spacecraft Attitude Estimators. *Journal of Guidance, Control, and Dynamics*, 1(4):282–284, 1978.
- [21] O.-E. Fjellstad and Thor I. Fossen. Singularity-Free Tracking of Unmanned Underwater Vehicles in 6 DOF. In *Decision and Control, 1994., Proceedings of the 33rd IEEE Conference on*, volume 2, pages 1128–1133. IEEE, 1994.
- [22] Adriaan Daniël Fokker. Die mittlere Energie rotierender elektrischer Dipole im Strahlungsfeld. *Annalen der Physik*, 348(5):810–820, 1914.
- [23] Thor I Fossen. *Guidance and Control of Ocean Vehicles*, volume 199. Wiley New York, 1994.
- [24] Eric Foxlin. Pedestrian Tracking with Shoe-mounted Inertial Sensors. *IEEE Computer graphics and applications*, 25(6):38–46, 2005.
- [25] Joseph M. Galante and Robert M. Sanner. A Nonlinear Adaptive Filter for Gyro Thermal Bias Error Cancellation. In *AIAA Guidance, Navigation, and Control Conference*, 2012.
- [26] Crispin Gardiner. *Stochastic Methods: A Handbook for the Natural and Social Sciences*. Springer-Verlag, 4 edition, 2009.

- [27] Jared Glover and Leslie Pack Kaelbling. Tracking 3-D Rotations with the Quaternion Bingham Filter. *MIT CSAIL Technical Report*, 2013.
- [28] Izrail Solomonovich Gradshteyn and Iosif Moiseevich Ryzhik. *Table of Integrals, Series, and Products*. Academic press, 2014.
- [29] Farid Gulmammadov. Analysis, Modeling and Compensation of Bias Drift in MEMS Inertial Sensors. In *Recent Advances in Space Technologies, 2009. RAST'09. 4th International Conference on*, pages 591–596. IEEE, 2009.
- [30] William Rowan Hamilton. *Elements of Quaternions*. Longmans, Green, & Company, 1866.
- [31] Peter Hughes. *Spacecraft Attitude Dynamics*. Courier Dover Publications, 2012.
- [32] Petros A Ioannou and Jing Sun. *Robust Adaptive Control*, volume 1. PTR Prentice-Hall Upper Saddle River, NJ, 1996.
- [33] Kiyoshi Itô. Stochastic Integral. *Proceedings of the Imperial Academy*, 20:519–524, 1944.
- [34] Kiyoshi Itô. *On Stochastic Differential Equations*, volume 4. American Mathematical Soc., 1951.
- [35] Kiyosi Itô. Multiple Wiener Integral. *Journal of the Mathematical Society of Japan*, 3(1):157–169, 1951.
- [36] Harold I. Jacobson. The Maximum Variance of Restricted Unimodal Distributions. *The Annals of Mathematical Statistics*, 40(5):1746–1752, 1969.
- [37] Andrew H. Jazwinski. *Stochastic Processes and Filtering Theory*. Courier Dover Publications, 2007.
- [38] Fang Jiancheng and Li Jianli. Integrated Model and Compensation of Thermal Errors of Silicon Microelectromechanical Gyroscope. *IEEE Transactions on Instrumentation and Measurement*, 58(9):2923–2930, 2009.
- [39] Rudolph Emil Kalman. A New Approach to Linear Filtering and Prediction Problems. *Journal of Basic Engineering*, 82(1):35–45, 1960.
- [40] Ioannis Karatzas and Steven Shreve. *Brownian Motion and Stochastic Calculus*, volume 113. Springer Science & Business Media, 2012.
- [41] D. Keymeulen, C. Peay, K. Yee, and D.L. Li. Effect of Temperature on MEMS Vibratory Rate Gyroscope. In *Aerospace Conference, 2005 IEEE*, pages 1–6. IEEE, 2005.
- [42] Hassan K. Khalil. *Nonlinear Systems*, volume 3. Prentice hall Upper Saddle River, 2002.

- [43] Rafail Khasminskii. *Stochastic Stability of Differential Equations*, volume 66. Springer Science & Business Media, 2 edition, 2011. Originally published in Russian in 1969.
- [44] Fima C Klebaner. *Introduction to Stochastic Calculus with Applications*, volume 57. World Scientific, 2005.
- [45] Peter Eris Kloeden, Eckhard Platen, and Henri Schurz. *Numerical Solution of SDE Through Computer Experiments*. Springer Science & Business Media, 2012.
- [46] Andrei Kolmogoroff. Über die analytischen Methoden in der Wahrscheinlichkeitsrechnung. *Mathematische Annalen*, 104(1):415–458, 1931.
- [47] Karsten Kunze and Helmut Schaeben. The Bingham Distribution of Quaternions and its Spherical Radon Transform in Texture Analysis. *Mathematical Geology*, 36(8):917–943, 2004.
- [48] Gerhard Kurz, Igor Gilitschenski, Simon Julier, and Uwe D Hanebeck. Recursive Estimation of Orientation Based on the Bingham Distribution. In *Information Fusion (FUSION), 2013 16th International Conference on*, pages 1487–1494. IEEE, 2013.
- [49] Gerhard Kurz and Uwe D. Hanebeck. Toroidal Information Fusion Based on the Bivariate von Mises Distribution. In *Multisensor Fusion and Integration for Intelligent Systems (MFI), 2015 IEEE International Conference on*, pages 309–315. IEEE, 2015.
- [50] Jean Bernard Lasserre. *An Introduction to Polynomial and Semi-Algebraic Optimization*, volume 52. Cambridge University Press, 2015.
- [51] Ern J Lefferts, F. Landis Markley, and Malcolm D Shuster. Kalman Filtering for Spacecraft Attitude Estimation. *Journal of Guidance, Control, and Dynamics*, 5(5):417–429, 1982.
- [52] Jason Leggett. Optimal Stochastic Nonlinear Control of Spacecraft Angular Velocity. In *47th AIAA Aerospace Sciences Meeting Including The New Horizons Forum and Aerospace Exposition*, pages 5–8, 2009.
- [53] Christophe Ley and Thomas Verdebout. *Modern Directional Statistics*. CRC Press, 2017.
- [54] Kristina Lundquist. A Comparative Study of Stochastic and Deterministic Population Models. UMEA University, 2011.
- [55] Fabricio Anicio de Magalhaes, Giuseppe Vannozzi, Giorgio Gatta, and Silvia Fantozzi. Wearable Inertial Sensors in Swimming Motion Analysis: a Systematic Review. *Journal of sports sciences*, 33(7):732–745, 2015.

- [56] Robert Mahony, Tarek Hamel, and Jean-Michel Pflimlin. Nonlinear Complementary Filters on the Special Orthogonal Group. *Automatic Control, IEEE Transactions on*, 53(5):1203–1218, 2008.
- [57] Xuerong Mao. Stochastic Versions of the LaSalle Theorem. *Journal of Differential Equations*, 153(1):175–195, 1999.
- [58] Xuerong Mao. *Stochastic Differential Equations and Applications*. Elsevier, 2007.
- [59] Kanti V Mardia. Characterizations of Directional Distributions. In *A Modern Course on Statistical Distributions in Scientific Work*, pages 365–385. Springer, 1975.
- [60] Kanti V Mardia. Statistics of Directional Data. *Journal of the Royal Statistical Society. Series B (Methodological)*, pages 349–393, 1975.
- [61] Kanti V Mardia. *Statistics of Directional Data*. Academic press, 2014.
- [62] Kanti V Mardia and T.W. Sutton. A Model for Cylindrical Variables with Applications. *Journal of the Royal Statistical Society. Series B (Methodological)*, pages 229–233, 1978.
- [63] João Luís Marins, Xiaoping Yun, Eric R Bachmann, Robert B McGhee, and Michael J Zyda. An Extended Kalman Filter for Quaternion-based Orientation Estimation using MARG Sensors. In *Intelligent Robots and Systems, 2001. Proceedings. 2001 IEEE/RSJ International Conference on*, volume 4, pages 2003–2011. IEEE, 2001.
- [64] F. Landis Markley. Attitude Error Representations for Kalman Filtering. *Journal of Guidance, Control, and Dynamics*, 26(2):311–317, 2003.
- [65] F. Landis Markley. Unit Quaternion from Rotation Matrix. *Journal of Guidance, Control, and Dynamics*, 31(2):440–442, 2008.
- [66] F. Landis Markley and John L. Crassidis. *Fundamentals of Spacecraft Attitude Determination and Control*. Springer, 2014.
- [67] Peter S. Maybeck. *Stochastic Models, Estimation, and Control*, volume 2. Academic press, 1982.
- [68] Peter S. Maybeck. *Stochastic Models, Estimation, and Control*, volume 1. Academic press, 1982.
- [69] John D. McLean, Stanley F. Schmidt, and Leonard A. McGee. Optimal Filtering and Linear Prediction applied to a Midcourse Navigation System for the Circumlunar Mission. Technical report, NASA TN D 1208, 1962.
- [70] W. Moon and J.S. Wettlaufer. On the Interpretation of Stratonovich Calculus. *New Journal of Physics*, 16(5):055017, 2014.

- [71] Richard E. Mortensen. Mathematical Problems of Modeling Stochastic Non-linear Dynamic Systems. *Journal of statistical physics*, 1(2):271–296, 1969.
- [72] Bernt Øksendal. *Stochastic Differential Equations*. Springer, 2003.
- [73] Yaakov Oshman and Avishy Carmi. Adaptive Estimation of Spacecraft Attitude from Vector Observations Using a Quaternion Particle Filter. *Advances in the Astronautical Sciences*, 122:229–245, 2006.
- [74] D.C. Paulson, D.B. Jackson, and C.D. Brown. SPARS Algorithms and Simulation Results. In *Proceedings of the Symposium on Spacecraft Attitude Determination*, volume 1, pages 293–316, 1969.
- [75] M. Planck. ber einen Satz der statischen Dynamik und seine Erweiterung in der Quantentheorie. *Akad. Wiss. Phys. Math. Kl*, 324, 1917.
- [76] J.E. Potter and W.E. Vander Velde. Optimum Mixing of Gyroscope and Star Tracker Data. *Journal of Spacecraft and Rockets*, 5:536–540, 1968.
- [77] Michael James David Powell. *Approximation Theory and Methods*. Cambridge university press, 1981.
- [78] Igor P. Prikhodko, Alexander A. Trusov, and Andrei M. Shkel. Compensation of Drifts in High-Q MEMS Gyroscopes using Temperature Self-Sensing. *Sensors and Actuators A: Physical*, 201:517–524, 2013.
- [79] Albert E. Sabroff. Advanced Spacecraft Stabilization and Control Techniques. *Journal of Spacecraft and Rockets*, 5(12):1377–1393, 1968.
- [80] S. Salcudean. A Globally Convergent Angular Velocity Observer for Rigid Body Motion. *Automatic Control, IEEE Transactions on*, 36(12):1493–1497, 1991.
- [81] Robert M. Sanner and Jean-Jacques E. Slotine. Gaussian Networks for Direct Adaptive Control. *IEEE Transactions on Neural Networks*, 3(6):837–863, 1992.
- [82] Stanley F. Schmidt. Application of State-space Methods to Navigation Problems. In *Advances in Control Systems*, volume 3, pages 293–340. Elsevier, 1966.
- [83] Stanley F. Schmidt. The Kalman filter-Its Recognition and Development for Aerospace Applications. *Journal of Guidance, Control, and Dynamics*, 4(1):4–7, 1981.
- [84] Bob Schutz, Byron Tapley, and George H. Born. *Statistical Orbit Determination*. Academic Press, 2004.
- [85] Sensoror. STIM300 Inertia Measurement Unit Datasheet, August 2013. TS1524 rev. 12.

- [86] Yi Shen, Qi Luo, and Xuerong Mao. The Improved LaSalle-Type Theorems for Stochastic Functional Differential Equations. *Journal of Mathematical Analysis and Applications*, 318(1):134–154, 2006.
- [87] John Smythe, Frank Moss, Peter V.E. McClintock, and Douglas Clarkson. Itô versus Stratonovich Revisited. *Physics Letters A*, 97(3):95–98, 1983.
- [88] T.K. Soboleva and A.B. Pleasants. Population Growth as a Nonlinear Stochastic Process. *Mathematical and Computer Modelling*, 38(11-13):1437–1442, 2003.
- [89] I.M. Sokolov. Itô, Stratonovich, Hänggi and all the Rest: The Thermodynamics of Interpretation. *Chemical Physics*, 375(2-3):359–363, 2010.
- [90] Josef Stoer and Roland Bulirsch. *Introduction to Numerical Analysis*, volume 12. Springer Science & Business Media, 2013.
- [91] Ruslan L. Stratonovich. A New Representation for Stochastic Integrals and Equations. *SIAM Journal on Control*, 4(2):362–371, 1966.
- [92] Ruslan L. Stratonovich. *Topics in the Theory of Random Noise*, volume 2. CRC Press, 1967.
- [93] M. Tenenbaum and H. Pollard. *Ordinary Differential Equations: an Elementary Textbook for Students of Mathematics, Engineering, and the Sciences*, 1985.
- [94] Julie K. Thienel. *Nonlinear Observer/Controller Designs for Spacecraft Attitude Control Systems with Uncalibrated Gyros*. PhD thesis, University of Maryland, 2004.
- [95] Julie K. Thienel and Robert M. Sanner. A Coupled Nonlinear Spacecraft Attitude Controller and Observer with an Unknown Constant Gyro Bias and Gyro Noise. *Automatic Control, IEEE Transactions on*, 48(11):2011–2015, 2003.
- [96] Uffe Høgsbro Thygesen. *A Survey of Lyapunov Techniques for Stochastic Differential Equations*. IMM, Department of Mathematical Modelling, Technical University of Denmark, 1997.
- [97] N.F. Toda, J.L. Heiss, and F.H. Schlee. SPARS: The System, Algorithms, and Test Results. In *Proceedings of the Symposium on Spacecraft Attitude Determination, Aerospace Corp. Rept. TR-0066 (6306)-12*, volume 1, pages 361–370, 1969.
- [98] Nicolaas Godfried Van Kampen. Itô versus Stratonovich. *Journal of Statistical Physics*, 24(1):175–187, 1981.

- [99] Nicolaas Godfried Van Kampen. The Validity of Nonlinear Langevin Equations. *Journal of Statistical Physics*, 25(3):431–442, 1981.
- [100] Nicolaas Godfried Van Kampen. *Stochastic Processes in Physics and Chemistry*, volume 1. Elsevier, 1992.
- [101] Bjørnar Vik, Anton Shiriaev, and Thor I Fossen. Nonlinear Observer Design for Integration of DGPS and INS. In *New Directions in Nonlinear Observer Design*, pages 135–159. Springer, 1999.
- [102] Wernher Von Braun and Frederick I. Ordway III. *History of Rocketry and Space Travel*. Crowell Publishing. New York City, NY, 1975.
- [103] James R. Wertz. *Spacecraft Attitude Determination and Control*. Kluwer Academic Publishers, Boston, MA, 1978.
- [104] B.J. West, A.R. Bulsara, K. Lindenberg, V. Seshadri, and K.E. Shuler. Stochastic Processes with Non-Additive Fluctuations: I. Itô and Stratonovich Calculus and the Effects of Correlations. *Physica A: Statistical Mechanics and its Applications*, 97(2):211–233, 1979.
- [105] Bong Wie and Peter M. Barba. Quaternion Feedback for Spacecraft Large Angle Maneuvers. *Journal of Guidance, Control, and Dynamics*, 8(3):360–365, 1985.
- [106] Bong Wie, H. Weiss, and A. Arapostathis. Quaternion Feedback Regulator for Spacecraft Eigenaxis Rotations. *Journal of Guidance, Control, and Dynamics*, 12(3):375–380, 1989.
- [107] Norbert Wiener. Generalized Harmonic Analysis. *Acta mathematica*, 55(1):117–258, 1930.
- [108] Wolfram Research, Inc. Mathematica 11.2.
- [109] Eugene Wong and Bruce Hajek. *Stochastic Processes in Engineering Systems*. Springer Science & Business Media, 1984.
- [110] Eugene Wong and Moshe Zakai. On the Convergence of Ordinary Integrals to Stochastic Integrals. *The Annals of Mathematical Statistics*, pages 1560–1564, 1965.
- [111] Eugene Wong and Moshe Zakai. On the Relation Between Ordinary and Stochastic Differential Equations. *International Journal of Engineering Science*, 3(2):213–229, 1965.
- [112] W.M. Wonham. A Liapunov Method for the Estimation of Statistical Averages. *Journal of differential equations*, 2(4):365–377, 1966.
- [113] W.M. Wonham. Liapunov Criteria for Weak Stochastic Stability. *Journal of Differential Equations*, 2(2):195–207, 1966.

- [114] Moshe Zakai. A Lyapunov Criterion for the Existence of Stationary Probability Distributions for Systems Perturbed by Noise. *SIAM Journal on Control*, 7(3):390–397, 1969.